

2017年科研汇报年编

2017 Annual Report of Scientific Research

University of Michigan - Shanghai Jiao Tong University Joint Institute



JOINT INSTITUTE
交大密西根学院

Contents

Research Overview of University of Michigan--Shanghai Jiao Tong University Joint Institute	P1
2017 Research Projects and Funding	P3
2017 Patent Applications and Grants	P9
2017 Published Journal Papers Index	P11
Mechanical Engineering	P11
Electrical and Computer Engineering	P14
Material Science and Engineering	P17
Other Disciplines	P18
2017 Published Conference Papers Index	P19
Mechanical Engineering	P19
Electrical and Computer Engineering	P21
Material Science and Engineering	P23
Other Disciplines	P24
2017 Published Journal Papers First Page	P25
Mechanical Engineering	P25
Electrical and Computer Engineering	P74
Material Science and Engineering	P117
Other Disciplines	P140

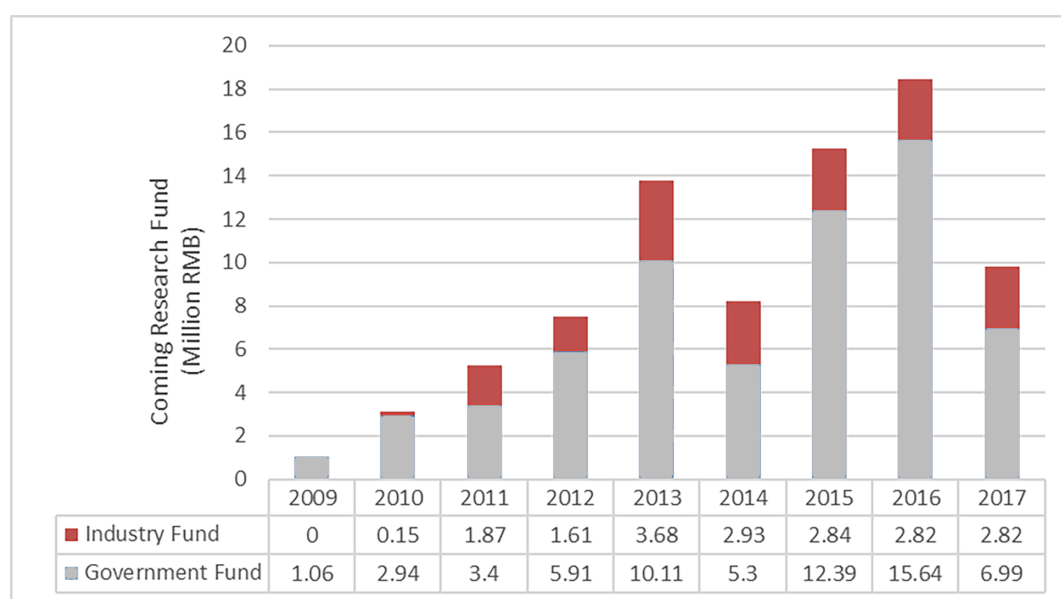
2017 Published Conference Papers First Page	<i>P147</i>
Mechanical Engineering.....	<i>P147</i>
Electrical and Computer Engineering.....	<i>P177</i>
Material Science and Engineering.....	<i>P206</i>
Other Disciplines.....	<i>P212</i>

Research Overview of the University of Michigan--Shanghai Jiao Tong University Joint Institute

Over the past 11 years, the UM-SJTU Joint Institute Joint Institute, founded in 2006 as the strategic global partnership between two top universities in the U.S. and China, has grown to become a top institute with great academic impact and international reputation. It has won many awards for higher education innovation, including the Model of International Education in Shanghai, the Model of China's Higher Education, and the prestigious Andrew Heiskell Award.

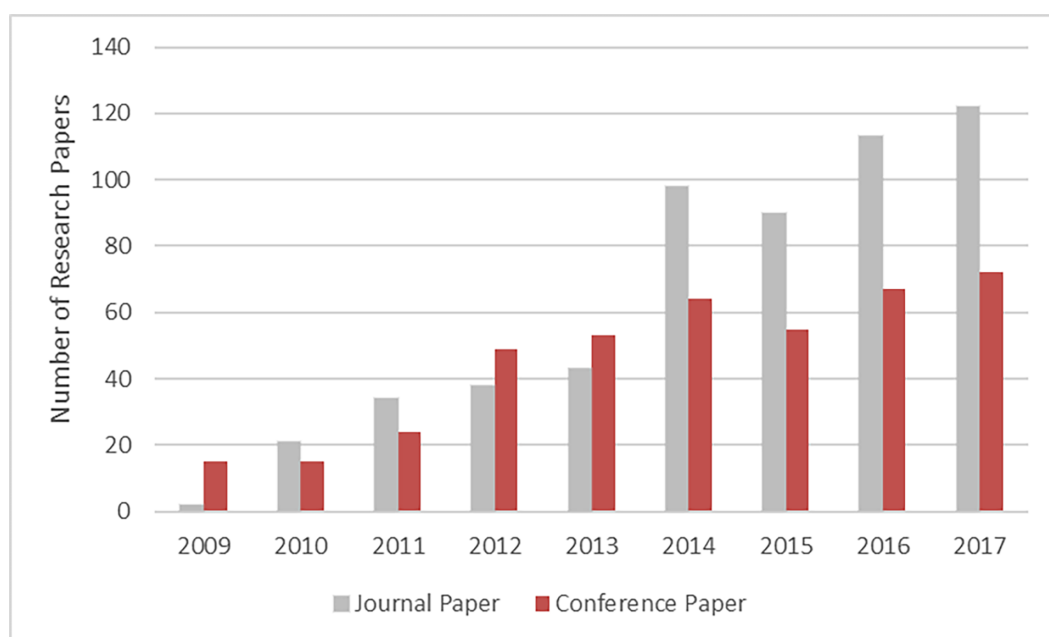
Research is at the core of the Joint Institute's development. Up to the end of 2017, JI has 30 tenured and tenure-track faculty members, who come from world-class universities and research institutes, and 6 faculty members have got tenure appointment. Their research are in 3 disciplines, including 15 faculty in Mechanical Engineering(ME), 11 faculty in Electrical and Computer Engineering(ECE) and 4 faculty in Materials Science Engineering(MSE). The main subjects are as follows: design and manufacturing, dynamics and vibrations, energy and power systems, mechatronics and control, thermo/fluid dynamics under ME area, communication and networking, micro/nano/bio devices, optics and optoelectronics, biomedical technology under ECE area, structure materials, polymer and material fracturing, advanced energy and electronic materials design under MSE area. In order to enhance the cross-disciplinary cooperation between our current faculties from different disciplines, JI holds 3 research centers, i.e., Center of Optics and Optoelectronics (COO), Center of Advanced Computational Engineering and Material Science (CACEMS), Joint Research Center for Smart Connected System on SJTU Minhang campus.

Over the past few years, JI has undertaken a lot of research projects sponsored by Natural Science Foundation of China(NSFC), Ministry of Science and Technology(MOST), State Key Labs, Shanghai Governments, SJTU, and Industry, etc., and achieved lots of R&D achievements. JI also has built broad cooperation relationship with domestic and international universities, research institutes and companies. In 2017, JI boasted 21 funded projects, reaching a total research funding of 8.55 million RMB. The coming funding in 2017 is 9.81 million RMB, including government funding 6.99 million RMB and industry funding 2.82 million RMB.



In 2017, 6 projects were sponsored by NSFC, the total NSFC funding is 2.7 million RMB. Prof. Chien-Pin Chen's research project was funded by Major Research Plan "Fundamental Research on Turbulent Combustion for Engine" Fostering Program of NSFC. Together with the above, both of Prof. Xudong Wang and Sung-liang Chen got the general program of NSFC. Near 40% of the government fund are from NSFC, which shows JI faculty strength on the cut-edged areas. From 2009 to the end of 2017, JI has 51 projects sponsored by NSFC including 22 General Fund projects, 17 Young Scientist Fund projects, 2 Major Research Plan Fostering Fund project, 8 International Young Scientist Fund projects, 1 NSFC International Cooperation Fund project and 1 NSFC Directors' Research Fund project.

In 2017, 194 papers had been published, including 122 journal papers and 72 conference papers. 132 papers were indexed by SCI and 113 papers were indexed by EI. 54 papers were jointly published with international co-authors. As for patent application, there have been 7 patent applications, and 13 granted patents.



In 2017, Prof. Xudong Wang was conferred the prestigious IEEE Grade of Fellow for his extraordinary accomplishments in the field of wireless mesh networks. Prof. Mian Li was appointed as associate editor of the "Journal of Mechanical Design".

2017 Research Projects and Funding

I. 2017 New and On-going Government Research Project

No.	PI.	Project Title	Source/Program	Award Year	Grant No	Total Fund	Duration	Coming fund this year
1	Hua Bao	First-principles investigation of electron-phonon coupling and non-equilibrium conduction	NSFC/General Program	2016	51676121	702,000	2017.1 - 2020.12	
2	Qianli Chen	Improving the microstructure, optical and electronic properties for perovskite solar cell materials fabricated by spray coating	STCSM/Yangfan Program	2016	16YF1406200	200,000	2016.1 – 2019.5	
3	Sung-Liang Chen	Focusing-free photoacoustic endomicroscopy based on a miniature fiber photoacoustic imaging probe and a mirrored synthetic aperture	NSFC/General Program	2017	61775134	660,000	2018.1 - 2020.12	396,000
4	Sung-Liang Chen	Study of the change of microcirculation by photoacoustic imaging during the treatment of sepsis by mesenchymal stem cells	SJTU/Medical and Engineering Cross Discipline Program	2016		70,000	2016.1 - 2018.12	
5	Sung-Liang Chen	National Youth 1000 Distinguished Scholar Program	Organization Department of the CPC Central Committee	2015		3,000,000	2015.1 - 2017.12	1,000,000
6	Sung-Liang Chen	Large depth-of-field photoacoustic microscopy based on optical millimeter-ring resonators	NSFC/Young Scientist	2014	61405112	260,000	2015.1 - 2017.12	
7	Chien-Pin Chen	Multiphase spray flamelet based turbulent spray combustion research	NSFC/ Major Research Plan "Fundamental research on turbulent combustion for engine" Fostering Program	2017	91741111	600,000	2018.1 - 2020.12	
8	Roberto Dugnani	Characterization of stress field in brittle material by advance multi-scale fractographic analysis	SJTU/ Research Incentive Program of Recruited Overseas Non-Chinese Foreign Faculty	2016		789,000	2016.1 - 2019.12	
9	Yaping Dan	*****	Military Technology Commission	2017		1,000,000	2017.7- 2018.6	500,000
10	Yaping Dan	Plasmon-enhanced graphene mid-infrared photodetectors	Key Laboratory of Infrared Imaging Materials and Detectors CAS	2016		100,000	2017.1 - 2018.12	50,000

11	Yaping Dan(co-PI)	Photon chips and quantum computing by femtosecond laser direct writing	STCSM/Fundamental research	2016		480,000	2016.7 - 2019.6	
12	Yaping Dan	Single dopant manipulation by self-assembly of proteins	SHMEC/Research Innovation Program	2014		80,000	2015.1- 2017.12	
13	Yaping Dan	Surface plasma antenna enhanced bipolar phototransistors based on single germanium nanowires	NSFC/General Program	2013		800,000	2014.1- 2017.12	
14	Morteza Eslamian	Development and fabrication of efficient perovskite solar cells by novel scalable techniques	SJTU/ Research Incentive Program of Recruited Overseas Non-Chinese Foreign Faculty	2016		600,000	2016.1 - 2018.12	
15	Morteza Eslamian	Fundamental study on the structure and the fabrication of thin film planar perovskite solar cells by ultrasonic spray coating	NSFC/International Young Scientist	2015	51550110 229	410,000	2016.1 - 2017.12	140,000
16	Morteza Eslamian	Oriental Scholar	SHMEC&SJTU	2014		600,000	2015.1 - 2017.12	
17	Bin Guan	Single atom doping of silicon by self-assembly of macromolecules	NSFC/Young Scientist	2015	21503135	252,000		84,000
18	Yunlong Guo	Study on a rapid and highly controllable method for ultra stable polymer anti-reflective coating	NSFC/General Program	2015	21574083	780,000	2016.1 - 2019.12	195,000
19	Yunlong Guo	National Youth 1000 Distinguished Scholar Program	Organization Department of the CPC Central Committee	2015		2,000,000	2015.1 - 2017.12	600,000
20	Chong Han	Channel modeling simulation platform development and characteristic analysis for wireless communications in the terahertz band	NSFC/Young Scientist	2017	61701300	260,000	2018.1- 2020.12	156,000
21	Chong Han	Ultra-massive MIMO system design for terahertz wireless communications	STCSM/Yangfan	2017	17YF1409 900	200,000	2017.7- 2020.6	200,000
22	Chong Han	Cloud internet-of-things (CIoT) enabled smart healthcare for after-delivery recover	SJTU/Medical and Engineering Cross Discipline Program	2017	YG2017Q N17	40,000	2018.1- 2020.12	
23	Peisen Huang	An active optical encoder based on flat panel display technology	NSFC/General Program	2013	51375310	950,000	2014.1- 2017.12	
24	Shane Johnson	Region Specific Plan Tar Soft Tissue Multiscale Viscoelastic Modeling And Experimental Validations With Developed Shear Sensor	NSFC/International Young Scientist	2017	51750410 692	300,000	2018.1 - 2019.12	
25	Shane Johnson	3D Reconfigurable Surfacing Shaping System for Composite Material Manufacturing	SJTU/ Research Incentive Program of Recruited Overseas Non-Chinese Foreign Faculty	2016		800,000	2016.1- 2019.12	

26	Shane Johnson	Research on the development of the pathology and bio-mechanical mechanism for foot and ankle joint inversion for osteoarthritis patients	SJTU/Medical and Engineering Cross Discipline Program	2016		95,000	2017.1-2019.12	
27	Shane Johnson	Constitutive multi-scale region specific modeling of the plantar soft tissue	NSFC/International Young Scientist	2015	51550110233	402,800	2016.1-2017.12	135,600
28	Shane Johnson	Biomechanical study of the Plantar Aponeurosis and development of orthoses with tunable stiffness based on finite element modeling and gait analysis	NSFC/ Young Scientist	2015	51505282	252,000	2016.1-2018.12	84,000
29	Jaehyung Ju	Thermo-mechanically programmable metamaterials	STCSM/SHNSF	2017	17ZR1414700	200,000	2017.5-2020.4	200,000
30	Jaehyung Ju	Programmable Mechanical Metamaterials	SJTU/ Research Incentive Program of Recruited Overseas Non-Chinese Foreign Faculty	2017		1,000,000	2017.1-2021.12	600,000
31	Mian Li	Research on Multi-objective Multidisciplinary Collaborative Optimization for Decision Making on Manufacturing Tolerances of Complex Engineering Systems	NSFC/General Program	2013	51375302	710,000	2014.1-2017.12	
32	Yong Long	Ultra-Low Dose CT Image Reconstruction Based on Big Data Priors	SJTU/UM-SJTU Joint Research Fund	2015		621,000	2015.9-2017.8	
33	Yong Long	Enabling fast low-dose CT imaging using model-based image reconstruction	STCSM/Pujiang Talent Program	2015	15PJ1403900	200,000	2015.7-2017.6	
34	Yong Long	Development and research of key technology of the optical navigation and 3D ultrasound imaging assisted craniomaxillofacial puncture robot	SJTU/Medical and Engineering Cross Discipline Program	2015		60,000	2016.1-2018.12	60,000
35	Yong Long	Multi-material decomposition using reconstruction methods for low-dose dual-energy CT	NSFC/ Young Scientist	2015	61501292	252,000	2016.1-2018.12	84,000
36	Chengbin Ma	Optimized power distribution in megahertz multiple-receiver wireless power transfer systems	STCSM/SH-NSF	2016	16ZR1416300	200,000	2016.1-2018.12	
37	Weikang Qian	Design and synthesis of combinational circuits for approximate computing	NSFC/General Program	2015	61574089	696,000	2016.1-2019.12	87,000
38	Weikang Qian co PI	The Design of Stochastic Gate and the Application of Stochastic Gate-Based Architecture in Machine Learning	NSFC/General Program	2014		400,000	2015.1-2018.12	
39	Yanfeng Shen	Self-sensing and health monitoring of piezoelectric composite structures using liquid metal electrodes	NSFC/ Young Scientist	2016	51605284	240,000	2017.1-2019.12	

40	Yongxing Shen	National Youth 1000 Distinguished Scholar Program	Organization Department of the CPC Central Committee	2015		2,000,000	2015.1- 2017.12	600,000
41	Yongxing Shen	A multi-scale numerical simulation method to predict hydraulic fractures based on universal meshes and phase-field modeling	NSFC/ Young Scientist	2014	11402146	280,000	2015.1- 2017.12	
42	Teh Kwee Yan	Investigating cycle-to-cycle variation of fuel spray momentum flux	NSFC/International Young Scientist	2016	51650110 493	391,200	2017.1- 2018.12	
43	Wenjie Wan	Non-hermitian Optics in high-Q microcavities	MOST 2016 National Key Research and Development Program "Quantum Control and Quantum Information" Key Special	2016	2016YFA 0302500	4,980,000	2016.7- 2021.6.	
44	Wenjie Wan	Self-referenced Optical Comb and Low-noise Microwave Generation in Microcavities	NSFC/General Program	2016	11674228	808,400	2017.1- 2020.12	
45	Wenjie Wan	SERS Gas Sensor Based on Nanoimprint Technology for Atmospheric Surveillance	SCTSM "Innovation activity plan" international cooperation program	2015	15220721 400	300,000	2015.9- 2018.8.	
46	Wenjie Wan	All optical modulation by coherent perfect absorption	NSFC/General program	2014	61475100	780,000	2015.1- 2018.12	195,000
47	Wenjie Wan	All-optical modulation based on coherent perfect absorber	SCTSM "Innovation activity plan" basic research program	2014	14JC1402 900	500,000	2014.9- 2017.8.	
48	Lipo Wang	Lagrangian turbulence: numerical studies and marine experimental applications	NSFC/CNRS international cooperation program	2016	11611130 099	150,000	2016.1- 2018.12	
49	Lipo Wang	Study of the flame-flow nonlocal interaction and the relevant fundamental physics	NSFC/ Major Research Plan "Fundamental research on turbulent combustion for engine" Fostering Program	2014	91441116	800,000	2015.1- 2017.12	
50	Xudong Wang	Research on mmwave-based hybrid mesh networking for 5G ultra-dense cellular networks	NSFC/General Program	2017	61771312	620,000	2018.1- 2021.12	372,000
51	Huimin Wen	Ordered and controllable doping of dendrimer-like boron polymers on silicon surface	NSFC/ Young Scientist	2017	B0313/21 703140	260,000	2018.1- 2020.12	156,000
52	Huimin Wen	Single-Atom Boron Doping in Silicon by Self-Assembled Macromolecular Monolayer	China Postdoctoral Science Foundation /General program	2016	2016M60 1582	50,000	2016.12 - 2017.12	50,000
53	Jigang Wu	Optical coherence tomography - photoacoustic dual-modality endoscopic imaging technique for atherosclerosis diagnosis	"863" Program/Young Scientist	2014	2015AA0 20944	1,180,000	2015.1- 2017.12	150,000
54	Jigang Wu	Optical coherence tomography - photoacoustic dual-modality	SH "863" Program matching fund	2016	16801912 5	118,000	2015.1- 2017.12	35,000

		endoscopic imaging technique for atherosclerosis diagnosis						
55	Tian Yang	Research on new type of optical fiber sensing technique applied to a second screening	SJTU/Medical and Engineering Cross Discipline Program/General program	2016		80,000	2017.1-2019.12	80,000
56	Tian Yang	Reproducible measurement of single molecule Raman scattering: experiment and physics	NSFC/General Program	2015	11574207	856,000	2016.1-2019.12	219,000
57	Yunlong Zan	High-dimensional reconstruction algorithm in cardiac dynamic SPECT imaging	China Postdoctoral Science Foundation /General program	2017	2017M611572	50,000	2017.7-2018.9.	50,000
58	Qiang Zhang	Effect of Relative Casing Motion in Transonic Condition	NSFC/General Program	2013	51376127	800,000	2014.1-2017.12	
59	Jun Zhang	Theoretical analysis and experimental implementation for precise metrology by using quantum control	State Key Laboratory of Precision Spectroscopy (East China Normal University)	2016		75,000	2016.1-2017.12	
60	Jun Zhang	Quantum system identification and parameter estimation with their applications	NSFC/General Program	2016	61673264	758,800	2017.1-2020.12	
61	Hong Zhu	Hybrid Perovskite Design based on High-throughput Calculations for Photovoltaic Applications	STCSM/Yangfan Program	2016	16YF1406000	200,000	2016.6-2019.5.	
62	Hong Zhu	High-throughput computational Materials Design for Layered Ternary Compounds with "Phonon Glass-Electron Crystal" Features	NSFC/ Young Scientist	2016	51602196	236,000	2017.1-2019.12	
63		NSFC indirect cost	NSFC	2017				512,080
		Total				37,535,200		6,990,680

II. 2017 New and On-going Industry Research Project

No.	PI	Project Title	Source	Award Year	Total Funding (RMB)	Duration	Coming fund this year
1	Hua Bao	Thermoelectric Cooling Applied to Generator Circuit Breaker	Alstom Grid Technology Center Co. Ltd	2016	450,000	2016.5-2018.4	-
2	Hua Bao	First-principles investigations on the dielectric properties of typical materials	Beijing Institute of environmental characteristics	2015	200,000	2015.11-2017.10	-
3	Qianli Chen	Graphene/PEDOT:PSS nanocomposite transparent conductive thin films based on polarizers	Shenzhen Shengbo Photoelectric Technology Co., Ltd.	2016	300,000	2015.3-2018.3	100,000

4	Yaping Dan	Microfabrication of nanoscale chemical gas sensors	Xi'an Jiao Tong University	2016	40,000	2017.1-2017.12	40,000
5	David Hung	Spray Characterization for Gasoline Direct Injection Engines	Nissan Mortor Co.,Ltd	2017	303,638	2017.1-2017.3	303,638
6	David Hung	Research on the design of timing chain guided plate using new material	ASAHI KASEI Plastics (Shanghai) Co., Ltd	2015	600,000	2015.6-2018.6	150,000
7	David Hung	General Motors	Spray Impingement Characterization of Delphi Fuel Injectors in Chamber and Flow Field Investigation in SIDI Optical Engine	2016	676,470	2016.1-2016.12	377,383.5
8	Mian Li	Structural Design and data processing development for dynamic charge dust meter	Beijing Palmay Technology Ltd.	2017	50,000	2017.4-2017.6	25,000
9	Mian Li	Probabilistic design method and tool development for gas turbine components	Siemens AG	2017	800,000	2017.4-2021.3	-
10	Chengbin Ma	Battery management system engineering service Phase I	United Automotive Electronic Systems Co., Ltd	2017	38,868	2017.3-2017.7	-
11	Chengbin Ma	Cooperation project of high frequency magnetic resonance mobile phone radio technology	Hua Wei Tech Co. ,Ltd	2017	684,250	2017.4-2018.4	493,344
12	Chengbin Ma	Research on vehicle-mounted wireless charging module	United Automotive Electronic Systems Co., Ltd	2017	203,562	2016.12-2019.12	-
13	Chengbin Ma	Cooperation project of automatic driving test target system	Hua Wei Tech Co. ,Ltd	2017	442,900	2017.2-2017.7	303,850
14	Chengbin Ma	Battery and Ultra Capacitor Hybrid Energy System of Vehicle by Simulation and Experimental Validation	Nippon Chemi-con, Corporation Japan.	2016	65,069	2016.4-2017.3	59,590
15	Chengbin Ma	Battery Management System for A Large-scale Lithium-ion Battery Pack	Beijing Jiao Tong University	2015	200,000	2015.11-2016.11	40,000
16	Chengbin Ma	Dynamic Control and Energy Management of an In-wheel-motor Electric Vehicle	Chongqing Changan Industry(Group) Co., Ltd	2013	72,386.5		72,386.5
17	Xudong Wang	IAB technology research	Hua Wei Tech Co. ,Ltd	2017	500,000	2017.12-2018.11	
18	Xudong Wang	Dubai big data technology cooperation project	Huawei Terminal (Dongguan) Co., Ltd.	2017	340,000	2017.4-2018.12	102,000
19	Xudong Wang	Research on key technologies of informatization and security strategies for internet plus power system reform	State Grid/Shanghai Municipal Electric Power Company	2016	450,000	2016.9-2017.6	300,000
20	Xudong Wang	Research on mesh networking architecture and dynamic routing mechanism for ultra-dense networks	Hua Wei Tech Co. ,Ltd	2016	370,000	2017.1-2017.12	114,330
21	Xudong Wang	Research on key technologies of high efficient networking in wireless networks	Hua Wei Tech Co. ,Ltd	2015	300,000	2016.1-2016.12	123,600

22	Xudong Wang	Scalable full duplex communication system	Hua Wei Tech Co. ,Ltd	2015	298,000	2015.4-2016.9	214,240
	Total				6,235,144		2,819,362

2017 Patent Applications and Grants

I. Applied Patents

No.	Patent Name	Application Code	Inventor
1	A droplet generator device with multi-excited vibration	CN201710013299.8	Lingxun Kong, Penghui Ge, Jian he, Xue Dong
2	Method for holographic microscopy imaging based on digital interpolation and phase iteration	CN201710371165.3	Jigang Wu, Zhaodong Feng, Mingjun Wang
3	A dual mode endoscope with optical coherence tomography and photoacoustic imaging	CN201710364571.7	Jigang Wu, Songliang Chen
4	Orthoses with continuously tunable arch height	CN201710662074.5	ShaneJohnson, Haihua Ou, Zesshan Qaiser, Liping Kang
5	Optical fibre sensor and sound wave detection application method therefor	WOCN17100770	Tian Yang, Xin Zhou
6	Optical fiber sensor and sound wave detecting application method	PCTJT170204	Tian Yang, Xin Zhou
7	Metal micro-nano structure and fiber with metal micro-nano structure at the end-facet	PCT/CN2017/100772	Tian Yang, Xin Zhou

II. Granted Patents

No.	Patent Name	Application Code	Inventor
1	A dual layer radiative cooling nanocoating and the fabrication method	CN201510846914.4	Hua Bao, Cheng Yan, Changyin Zhao, Boxiang Wang
2	Thermal Insolation device assembly with Phase Change material	CN201620545766.2	Shane Johnson, Liping Kang
3	Method for producing Ni base single crystal superalloy parts by laser cladding Technology	CN201410840290.0	Zhaoyang Liu, Huan Qi
4	Method and device for controlling tissue growth during laser cladding single crystal alloy	CN201510118939.2	Zhaoyang Liu, Huan Qi

5	Data uploading for mobile terminals based on wireless mesh networks	CN201310606833.8	Xudong Wang, Yuhang Zhang
6	An analog self-interference cancellation design for multiple input and multiple output full duplex wireless communications	CN201310750505.5	Aimin Tang, Xudong Wang
7	Random analog network coding for wireless networks	CN201410628246.3	Xudong Wang, Wenguang Mao
8	One type of separable endoscope	CN201610023766.0	Jigang Wu, Jie Wang
9	A modular flexible manipulator system with high redundancy and multiple degrees of freedom	CN201610227400.5	Kai Xu, Xiangyang Zhu, Zhixiong Yang, Huan Liu, Zhijun Zhu, liangliang Han
10	Handheld unfoldable single port laparoscope	CN201410857406.1	Kai Xu, Zhengcheng Dai, Bo Feng, Jiangran Zhao, Zhixiong Yang, Wukun Mei, Minhua Zheng
11	A label-free optical sensor on fiber end facet based on single-mode to multi-mode fiber mode matching coupler	CN201310182823.6	Tian Yang, Xiaolong He
12	Multi-channel fiber based label-free bio-sensing system	CN201410766162.6	Tian Yang, Xiaolong He
13	Medium access control for a wireless LAN with full duplex AP and half duplex stations	CN201410429421.6	Xudong Wang, Aimin Tang

2017 Published Journal Papers

Mechanical Engineering

- [1] **Bao Hua**, Yan Chen, Wang Boxiang, Fang Xing, Zhao C. Y., Ruan Xiulin, "Double-layer nanoparticle-based coatings for efficient terrestrial radiative cooling", *Solar Energy Materials and Solar Cells*, vol. 168, 78-84, 2017.P25
- [2] Wang Zhongyong, Tong Zhen, Ye Qinxian, Hu Hang, Nie Xiao, Yan Chen, Shang Wen, Song Chengyi, Wu Jianbo, Wang Jun, **Bao Hua**, Tao Peng, Deng Tao, "Dynamic tuning of optical absorbers for accelerated solar-thermal energy storage", *Nature Communications*, vol. 8 (1): 1478, 2017.P26
- [3] Xie Han, Gu Xiaokun, **Bao Hua**, "Effect of the accuracy of interatomic force constants on the prediction of lattice thermal conductivity", *Computational Materials Science*, vol. 138, 368-376, 2017.P27
- [4] Rong Qingyuan, Shao Cheng, **Bao Hua**, "Molecular dynamics study of the interfacial thermal conductance of multi-walled carbon nanotubes and van der Waals force induced deformation", *Journal of Applied Physics*, vol. 121(5): 054302, 2017.P28
- [5] Cheng Shao, Qingyuan Rong, Ming Hu, **Hua Bao**, "Probing phonon-surface interaction by wave-packet simulation: Effect of roughness and morphology", *Journal of Applied Physics*, vol. 122, 155104, 2017.P29
- [6] Fang Xing, Zhao Changying, **Bao Hua**, "Selection of materials for perfect absorption in layered absorbers with ultrathin films", *Journal of Engineering Thermophysics*, vol. 38, 1282-1287, 2017.P30
- [7] Cheng Shao, Xiaoxiang Yu, Nuo Yang, Yanan Yue, and **Hua Bao**, "A review of thermal transport in low-dimensional materials under external perturbation: effect of strain, substrate, and clustering", *Nanoscale and Microscale Thermophysical Engineering*, 21, 1-36, 2017.P31
- [8] Han Shilei and **Bauchau Olivier A**, "Nonlinear, three-dimensional beam theory for dynamic analysis", *Multibody System Dynamics*, vol. 41(2): 173-200, 2017.P32
- [9] Wang Qiaoling and **Chen C P**, "Simulated kinetics and chemical and physical properties of a four component diesel surrogate fuel", *Energy and Fuels*, vol. 31(12): 13190–13197, 2017.P33
- [10] Ying Kongqing, Tian Ran, Zhou Jie, Li Hua, **Dugnani Roberto**, Lu Yanyan, Duan Huanan, Guo Yiping, Liu Hezhou, "A three dimensional sulfur/reduced graphene oxide with embedded carbon nanotubes composite as a binder-free, free-standing cathode for lithium-sulfur batteries", *RSC Advances*, vol. 7, 43483-43490, 2017.P34
- [11] Zhang Chunmei, Li Hua, Zhuo Zhangzhi, **Dugnani Roberto**, Xue Wenchao, Zhou Yong, Chen Yujie, Liu Hezhou, "Characterization of the damping and mechanical properties of a novel (ZnSnO₃/PVDF)@PPy nanofibers/EP composite", *RSC Advances*, vol. 7, 37130-37138, 2017.P35
- [12] Zhou Jie, Li Hua, Tian Ran, **Dugnani Roberto**, Lu Huiyuan, Chen Yujie, Guo Yiping, Duan Huanan, Liu Hezhou, "Fabricating fast triggered electroactive shape memory graphite/silvernano-wires/epoxy resin composite from polymer template", *Scientific Reports*, vol. 7, 2017.P36
- [13] Zhang Chunmei, Li Hua, Zhuo Zhangzhi, **Dugnani Roberto**, Sun Chongyang, Chen Yujie, Liu Hezhou, "Facile fabrication of ultra-light and highly resilient PU/RGO foams for microwave absorption", *RSC Advances*, vol. 7, 41321-41329, 2017.P37
- [14] Zhuang Y, Kopsaftopoulos F, **Dugnani R**, Chang FK, "Integrity monitoring of adhesively bonded joints via an electromechanical impedance-based approach", *Structural Health Monitoring*, 1475921717732331, 2017.P38

- [15] **Dugnani R**, Chang FK, "Analytical model of lap-joint adhesive with embedded piezoelectric transducer for weak bond detection", *J. of Intelligent Material Systems and Structures*, vol. 28(1), 124-140, 2017.P39
- [16] Zhou J, Chen YJ, Li H, **Dugnani R**, Du Q, Liu H, Ur H, Kang H, Liu H, "Facile synthesis of three-dimensional lightweight nitrogen-doped graphene aerogel with excellent electromagnetic wave absorption properties", *Journal of Material Science*, 53(6): 4067-4077, 2018.P40
- [17] **Dugnani, Roberto**, "Residual stress in ion-exchanged silicate glass: An analytical solution", *Journal of Non-Crystalline Solids*, vol. 471, 368-378, 2017.P41
- [18] Wu Shengqi, Xu Min, **Hung David L. S.**, Pan Hujie, "Effects of nozzle configuration on internal flow and primary jet breakup of flash boiling fuel sprays", *International Journal of Heat and Mass Transfer*, vol. 110, 730-738, 2017.P42
- [19] Yang Jie, Xu Min, **Hung David L. S.**, Wu Qiang, Dong Xue, "Influence of swirl ratio on fuel distribution and cyclic variation under flash boiling conditions in a spark ignition direct injection gasoline engine", *Energy Conversion and Management*, vol. 138, 565-576, 2017.P43
- [20] Wu Shengqi, Xu Min, **Hung David L. S.**, Pan Hujie, "In-nozzle flow investigation of flash boiling fuel sprays", *Applied Thermal Engineering*, vol. 117, 644-651, 2017.P44
- [21] Ge Penghui, **Hung David L. S.**, "Investigation of cycle-to-cycle variation of in-cylinder engine swirl flow fields using quadruple proper orthogonal decomposition", *Journal of Engineering for Gas Turbines and Power-Transactions of the ASME*, vol. 139, 2017.P45
- [22] Qaiser Zeeshan, Kang Liping, **Johnson Shane**, "Design of a bioinspired tunable stiffness robotic foot", *Mechanism and Machine Theory*, vol. 110, 1-15, 2017.P46
- [23] Lan Shouren, Cui Chaoyi, Liu Xin, **Johnson S.**, Su Jialiang, Chen Benzhi, Wang Lisheng, "Separation and visualization of arteries and heart in 3D computed tomography angiography images", *Journal of Shanghai Jiaotong University (Science)*, vol. 22, 1-9, 2017.P47
- [24] Ou H., Qaiser Z., Kang L., **Johnson S.**, "Experimental and computational analysis of orthotic medial longitudinal arch support height", *Footwear Science*, vol. 9 (sup1): S1-S2, 2017.P48
- [25] S. Yoo, M.S. Uddin, H. Heo, **J. Ju**, S.-J. Choi, "Thermoviscoelastic modeling of a nonpneumatic tire with a lattice spoke", *proc. IMechE Part D: Journal of Automobile Engineering*, 231(2):241-252, 2017.P49
- [26] M.S. Uddin **and J. Ju**, "Enhanced coarse-graining of thermoplastic polyurethane elastomer for multiscale modeling", *Transactions of the ASME: Journal of Engineering Materials and Technology*, 139(1):011001, 2017.P50
- [27] Swenson Carolyn W., Smith Tovia M., **Luo Jiajia**, Kolenic Giselle E., Ashton-Miller James A., DeLancey John O., "Intraoperative cervix location and apical support stiffness in women with and without pelvic organ prolapse", *American Journal of Obstetrics and Gynecology*, vol. 216, 2017.P51
- [28] Beek Av, **Li M**, Ren C, "Heuristics-enhanced model fusion considering incomplete data using kriging models," *Journal of Mechanical Design*, 140(2): 021403, 2018.P52
- [29] Ma J., Kremer G.E.O. and **Li M.**, "A key components-based heuristic modular product design approach to reduce product assembly cost", *International Journal on Interactive Design and Manufacturing*, 1-11, 2017.P53
- [30] Xi Jiaqi, Shentu Lifeng, Hu Jikang, **Li Mian**, "Automated surface inspection for steel products using computer vision approach", *Applied Optics*, vol. 56, 184-192, 2017.P54

- [31] Zheng Ruixiang, **Li Mian**, Wang Zhaoguang, Zhang Qiang, "Control of blow-down wind tunnel using combined extended kalman and nonlinear predictive filters", *Journal of Fluids Engineering-Transactions of the ASME*, vol. 139, 2017.P55
- [32] Zhang, Jizhou; Qiu, Yu; **Li, Mian**; Xu, Min, "Sequential multi-objective optimization for lubrication system of gasoline engines with bilevel optimization structure", *Journal of Mechanical Design*, vol. 139(4): 041401, 2017.P56
- [33] Wang Zhaozhao, Peng Linfa, Lin Zhongqin, **Ni Jun**, Yi Peiyun, Lai Xinmin, He Xiaolong, Lei, Zeyu, "Flexible semiconductor technologies with nanoholes-provided high areal coverages and their application in plasmonic-enhanced thin film photovoltaics", *Scientific Reports*, vol. 7 (1): 13155, 2017.P57
- [34] Liu Chunguang, Cooley Christopher G., **Parker Robert G.**, "Parametric instability of spinning elastic rings excited by fluctuating space-fixed stiffnesses", *Journal of Sound and Vibration*, 400, 533-549, 2017.P58
- [35] Zhang Mengyang, **Shen Yanfeng**, Xiao Li, Qu Wenzhong, "Application of subharmonic resonance for the detection of bolted joint looseness", *Nonlinear Dynamics*, vol. 88, 1643-1653, 2017.P59
- [36] Bhuiyan Y.M, **Shen Yanfeng**, Giurgiutiu V., "Interaction of lamb waves with rivet hole cracks from multiple directions", *Proceedings of the Institution of Mechanical Engineers, Part C: Journal of Mechanical Engineering Science*, Vol. 231(16), 2974-2987, 2017.P60
- [37] **Shen Yanfeng.**, Cesnik C.E.S., "Modeling of nonlinear interactions between guided waves and fatigue cracks using local interaction simulation approach", *Ultrasonics*, vol. 74, 106, 2017.P61
- [38] Chiaramonte Maurizio M., **Shen Yongxing**, Lew Adrian J., "Mapped finite element methods: High-order approximations of problems on domains with cracks and corners", *International Journal for Numerical Methods in Engineering*, vol. 111, 864-900, 2017.P62
- [39] **Shen Yongxing**, Wu Can, Wan Yang, "Universal meshes for a branched crack", *Finite elements in Analysis and Design*, vol. 129, 53-62, 2017.P63
- [40] W. Yan, Y. Qian, W. Ma, B. Zhou, **Yongxing. Shen**, Feng Lin. "Modeling and experimental validation of electron beam selective melting process", *Engineering* 3(5) (2017) 701—707, 2017.P64
- [41] Shibo Gu, **Lipo Wang, David L. S. Hung**, "Instability evolution of the viscous elliptic liquid jet in the Rayleigh regime", *Physical Review E* 95, 063112 , 2017.P65
- [42] Ma H, Zhang Q., He L, Wang Z, **Wang L.**, "Cooling injection effect on a transonic squealer tip - part i: experimental heat transfer results and CFD validation", *Journal of Engineering for Gas Turbines and Power*, vol. 139(5): 052506, 2017.P66
- [43] Ma H, Zhang Q, He L, Wang Z, **Wang L.**, "Cooling injection effect on a transonic squealer tip - part ii: analysis of aerothermal interaction physics", *Journal of Engineering for Gas Turbines and Power*, vol. 139(5): 052507, 2017.P67
- [44] Huang Yongxiang, **Wang Lipo**, Schmitt F. G., Zheng Xiaobo, Jiang Nan, Liu Yulu, "Extremal-point density of scaling processes: From fractional Brownian motion to turbulence in one dimension", *Physical Review E*, vol. 96 (1): 012215, 2017.P68
- [45] **Wang Lipo**, Huang Yongxiang, "Intrinsic flow structure and multifractality in two-dimensional bacterial turbulence", *Physical Review E*, vol. 95 (5): 052215, 2017.P69
- [46] Lin ZhiLiang, **Wang Lipo**, Liao ShiJun, "On the origin of intrinsic randomness of Rayleigh-Benard turbulence", *Science China-Physics Mechanics & Astronomy*, vol. 60 (1): 014712, 2017.P70

- [47] Chakraborty Nilanjan, **Wang Lipo**, Konstantinou Ilias, Klein Markus, "Vorticity statistics based on velocity and density-weighted velocity in premixed reactive turbulence", *Journal of Turbulence*, vol. 18, 825-853, 2017.P71
- [48] **Wang Lipo**, "Analysis of the filtered non-premixed turbulent flame", *Combustion and Flame*, 175: 259-269, 2017.P72
- [49] Zhong Fangpan, Zhou Chao, Ma H, **Zhang Q.**, "Heat transfer of winglet tips in a transonic turbine cascade", *Journal of Engineering for Gas Turbines and Power*, vol. 139 (1): 012605, 2017.P73

Electrical and Computer Engineering

- [50] Li Guangyao, Guo Zhendong, **Chen Sung-Liang**, "Miniature all-optical probe for large synthetic aperture photoacoustic-ultrasound imaging", *Optics Express*, vol. 25, 25023-25035, 2017.P74
- [51] Cai De, Li Zhongfei, Li Yao, Guo Zhendong, **Chen Sung-Liang**, "Photoacoustic microscopy in vivo using synthetic-aperture focusing technique combined with three-dimensional deconvolution", *Optics Express*, vol. 25, 1421-1434, 2017.P75
- [52] **Chen Sung-Liang**, "Review of laser-generated ultrasound transmitters and their applications to all-optical ultrasound transducers and imaging", *Applied Sciences-Basel*, vol. 7 (1): 25, 2017.P76
- [53] Cai De, Li Guangyao, Xia Dongqing, Li Zhongfei, Guo Zhendong, **Chen Sung-Liang**, "Synthetic aperture focusing technique for photoacoustic endoscopy", *Optics Express*, vol. 25, 20162-20171, 2017.P77
- [54] Du Sichao, Lu Wei, Ali Ayaz, Zhao Pei, Shehzad Khurram, Guo Hongwei, Ma Lingling, Liu Xuemei, Pi Xiaodong, Wang Peng, Fang Hehai, Xu Zhen, Gao Chao, **Dan Yaping**, Tan Pingheng, et al, "A broadband fluorographene photodetector", *Advanced Materials*, vol. 29(22), 2017.P78
- [55] Wan Xia, Xu Yang, Guo Hongwei, Shehzad Khurram, Ali Ayaz, Liu Yuan, Yang Jianyi, Dai Daoxin, Lin Cheng-Te, Liu Liwei, Cheng Hung-Chieh, Wang Fengqiu, Wang Xiaomu, Lu Hai, Hu Weida, Pi Xiaodong, **Dan Yaping**, Luo Jikui, et al, "A self-powered high-performance graphene/silicon ultraviolet photodetector with ultra-shallow junction: breaking the limit of silicon?", *NPJ 2D Materials and Applications*, vol. 1 (1): 4, 2017.P79
- [56] Zhao Xingyan, **Dan Yaping**, "A silicon nanowire heater and thermometer", *Applied Physics Letters*, vol. 111 (4): 043504, 2017.P80
- [57] Wu Haigang, Guan Bin, Sun Yingri, Zhu Yiping, **Dan Yaping**, "Controlled doping by self-assembled dendrimer-like macromolecules", *Scientific Reports*, vol. 7 : 41299, 2017.P81
- [58] Wu Haigang, Li Ke, Gao Xuejiao, **Dan Yaping**, "Phosphorus ionization in silicon doped by self-assembled macromolecular monolayers", *AIP Advances*, vol. 7 (10): 105310, 2017.P82
- [59] **C. Han**, I. F. Akyildiz, and W. H. Gerstacker, "Timing acquisition and error analysis for pulse-based terahertz band wireless systems", *IEEE Transactions on Vehicular Technology*, vol. 66(11), 10102-10113, 2017.P83
- [60] **Han Chong**, Tong Wenqian, Yao Xin-Wei, "MA-ADM: A memory-assisted angular-division-multiplexing MAC protocol in Terahertz communication networks", *NANO Communication Networks*, vol. 13, 51-59, 2017.P84

- [61] Yao Xin-Wei, Wang Chao-Chao, Wang Wan-Liang, **Han Chong**, "Stochastic geometry analysis of interference and coverage in Terahertz networks", *NANO Communication Networks*, vol. 13, 9-19, 2017.P85
- [62] **Han Chong**, Akyildiz Ian F., "Three-dimensional end-to-end modeling and analysis for graphene-enabled terahertz band communications", *IEEE Transactions on Vehicular Technology*, vol. 66, 5626-5634, 2017.P86
- [63] Zan Yunlong, **Long Yong**, Chen Kewei, Li Biao, Huang Qiu, Gullberg Grant T., "Design of a short nonuniform acquisition protocol for quantitative analysis in dynamic cardiac SPECT imaging-a retrospective I-123-MIBG animal study", *Medical Physics*, vol. 44, 3639-3649, 2017.P87
- [64] Xuechang Zheng, Zening Lu, Ravishankar S., **Yong Long**, Fessler J.A., "Low dose CT image reconstruction with learned sparsifying transform [arXiv]", *arXiv*, 1-5, 2017.P88
- [65] Xue Yi, Ruan Ruoshui, Hu Xiuhua, Kuang Yu, Wang Jing, **Long Yong**, Niu Tianye, "Statistical image-domain multimaterial decomposition for dual-energy CT", *Medical Physics*, vol. 44, 886-901, 2017.P89
- [66] Fu Minfan, Yin He, Liu Ming, Wang Yong, **Ma Chengbin**, "A 6.78 MHz multiple-receiver wireless power transfer system with constant output voltage and optimum efficiency", *IEEE Transactions on Power Electronics*, 2017.P90
- [67] Liu Ming, Liu Shuangke, **Ma Chengbin**, "A high-efficiency/output power and low-noise megahertz wireless power transfer system over a wide range of mutual inductance", *IEEE Transactions on Microwave Theory and Techniques*, vol. 65, 4317-4325, 2017.P91
- [68] Liu Ming, Qiao Yue, Liu Shuangke, **Ma Chengbin**, "Analysis and design of a robust class E-2 DC-DC converter for megahertz wireless power transfer", *IEEE Transactions on Power Electronics*, vol. 32, 2835-2845, 2017.P92
- [69] Liu Ming, Zhao Chen, Song Jibin, **Ma Chengbin**, "Battery charging profile-based parameter design of a 6.78-MHz class E-2 wireless charging system", *IEEE Transactions on Industrial Electronics*, vol. 64, 6169-6178, 2017.P93
- [70] Song Jibin, Liu Ming, **Ma Chengbin**, "Efficiency optimization and power distribution design of a megahertz multi-receiver wireless power transfer system", *2017 IEEE PELS Workshop on Emerging Technologies - Wireless Power Transfer (WOW)*, 54-58, 2017.P94
- [71] Liu Ming, Fu Minfan, **Ma Chengbin**, "Low-harmonic-contents and high-efficiency class e full-wave current-driven rectifier for megahertz wireless power transfer systems", *IEEE Transactions on Power Electronics*, vol. 32, 1198-1209, 2017.P95
- [72] Fu Minfan, Yin He, **Ma Chengbin**, "Megahertz multiple-receiver wireless power transfer systems with power flow management and maximum efficiency point tracking", *IEEE Transactions on Microwave Theory and Techniques*, vol. 65, 4285-4293, 2017.P96
- [73] S. Liu, M. Liu, S. Yang, C. Ma, X. Zhu, "A novel design methodology for high-efficiency current-mode and voltage-mode class-e power amplifiers in wireless power transfer systems", *IEEE Transactions on Power Electronics*, vol. 32(6): 4514-4523, 2017.P97
- [74] Liu Shuangke, Liu Ming, Han Songyang, **Zhu Xinen**, **Ma Chengbin**, "Tunable class E² DC-DC converter with high efficiency and stable output power for 6.78 MHz wireless power transfer", *IEEE Transactions on Power Electronics*, 2017.P98
- [75] Hu Junjun, Li Zhijing, Yang Meng, Huang Zixin, **Qian Weikang**, "A high-accuracy approximate adder with correct sign calculation", *Integration, the VLSI Journal*, 2017.P99

- [76] Najafi M. Hassan, Li Peng, Lilja David J., **Qian Weikang**, Bazargan Kia, Riedel, Marc, "A reconfigurable architecture with sequential logic-based stochastic computing", *ACM Journal on Emerging Technologies in Computing Systems*, vol. 13, 2017.P100
- [77] Ryu Byunghoon, Nam Hongsuk, Oh Bo-Ram, Song Yujing, Chen Pengyu, Park Younggeun, **Wan Wenjie**, Kurabayashi Katsuo, Liang Xiaogan, "Cyclewise operation of printed MoS₂ transistor biosensors for rapid biomolecule quantification at femtomolar levels", *ACS Sensors*, vol. 2, 274-281, 2017.P101
- [78] Cao Jianjun, Shen Dongyi, Zheng Yuanlin, Feng Yaming, Kong Yan, **Wan Wenjie**, "Femtosecond OPO based on MgO:PPLN synchronously pumped by a 532 nm fiber laser", *Laser Physics*, vol. 27(5): 055402, 2017.P102
- [79] Suo Yaji, Feng Yaming, Xu Da-xiao, **Wan Wenjie**, "Optical velocimeter by second order correlation", *Laser Physics*, vol. 27 (6): 065602, 2017.P103
- [80] Cao Jianjun, Kong Yan, Gao Shumei, **Wan Wenjie**, "Subwavelength imaging by a nonlinear negative refraction lens through four wave mixing", *Optics Express*, vol. 25, 24272-24280, 2017.P104
- [81] Kwon Younggap, **Wang Xudong**, Hwang Taewon, "A Game with randomly distributed eavesdroppers in wireless ad hoc networks: A Secrecy EE Perspective", *IEEE Transactions on Vehicular Technology*, vol. 66(11): 9916-9930, 2017.P105
- [82] **Wang Xudong**, Pi Yibo, Tang Aimin, "Scheduling of electric vehicle charging via multi-server fair queueing", *IEEE Transactions on Parallel and Distributed Systems*, vol. 28, 3298-3312, 2017.P106
- [83] A. Tang, **X. Wang**, and C. Zhang, "Cooperative Full Duplex Device to Device Communication Underlying Cellular Networks," *IEEE Transactions on Wireless Communications*, Volume 16, no. 12, Pages 7800-7815. Dec. 2017.P107
- [84] Feng Shaodong, Wang Mingjun, **Wu Jigang**, "Enhanced resolution for amplitude object in lensless inline holographic microscope with grating illumination", *Optical Engineering*, vol. 56(9): 093107, 2017.P108
- [85] Feng Shaodong, Wang Mingjun, **Wu Jigang**, "Enhanced resolution in lensless in-line holographic microscope by data interpolation and iterative reconstruction", *Optics Communications*, vol. 402, 104-108, 2017.P109
- [86] Wang Mingjun, Feng Shaodong, **Wu Jigang**, "Multilayer pixel super-resolution lensless in-line holographic microscope with random sample movement", *Scientific Reports*, vol. 7 (1): 12791, 2017.P110
- [87] Feng Shaodong, **Wu Jigang**, "Resolution enhancement method for lensless in-line holographic microscope with spatially-extended light source", *Optics Express*, vol. 25, 24735-24744, 2017.P111
- [88] Lei Zeyu, Zhou Xin, Yang Jie, He Xiaolong, Wang Yalin, **Yang Tian**, "Second-order distributed-feedback surface plasmon resonator for single-mode fiber end-facet biosensing", *Applied Physics Letters*, vol. 110 (17): 171107, 2017.P112
- [89] Zeyu Lei, **Tian Yang**, "Converting state of polarization with a miniaturized metasurface device," *Photonics Technology Letters*, 29, 615, 2017.P113
- [90] Wang Yuanlong, Dong Daoyi, Qi Bo, **Zhang Jun**, Petersen Ian R, Yonezawa Hidehiro, "A quantum hamiltonian identification algorithm: computational complexity and error analysis", *IEEE Transactions on Automatic Control*, 2017.P114
- [91] Sarovar Mohan, **Zhang Jun**, Zeng Lishan, "Reliability of analog quantum simulation", *EPJ Quantum Technology*, vol. 4 (1): 1, 2017.P115

- [92] Liu Shuangke, Zhu Lei, Allibert Frederic, Radu Ionut, **Zhu Xinen**, Lu Yumin, "Physical models of planar spiral inductor integrated on the high-resistivity and trap-rich silicon-on-insulator substrates", *IEEE Transactions on Electron Devices*, vol. 64, 2775-2781, 2017.P116

Material Science and Engineering

- [93] Peremanuele Canepa, **Shou-Hang Bo**, Gopalakrishnan Sai Gautam, Baris Key, William D. Richards, Tan Shi, Yaosen Tian, Yan Wang, Juchuan Li & Gerbrand Ceder, "High magnesium mobility in ternary spinel chalcogenides", *Nature communications*, 8(1): 1759, 2017.P117
- [94] **Q. Chen**, A. Braun, "Protons and the hydrogen economy", *MRS Energy & Sustainability: A Review Journal* 4, E14, 2017.P118
- [95] Braun Artur, **Chen Qianli**, "Experimental neutron scattering evidence for proton polaron in hydrated metal oxide proton conductors", *Nature Communications*, vol. 8:15830, 2017.P119
- [96] Habibi Mehran, Rahimzadeh Amin, Bennouna Inas, **Eslamian Morteza**, "Defect-free large-area (25 cm(2)) light absorbing perovskite thin films made by spray coating", *Coatings*, vol. 7 (3): 42, 2017.P120
- [97] **Eslamian Morteza**, Soltani-Kordshuli Firuze, "Development of multiple-droplet drop-casting method for the fabrication of coatings and thin solid films", *Journal of Coatings Technology and Research*, 1-10, 2017.P121
- [98] Wang Qin, Chueh Chu-Chen, Zhao Ting, Cheng Jiaqi, **Eslamian Morteza**, Choy Wallace C. H., Jen Alex K. Y., "Effects of self-assembled monolayer modification of nickel oxide nanoparticles layer on the performance and application of inverted perovskite solar cells", *Chemsuschem*, vol. 10, 3794-3803, 2017.P122
- [99] **Eslamian Morteza**, "Excitation by acoustic vibration as an effective tool for improving the characteristics of the solution-processed coatings and thin films", *Progress in Organic Coatings*, 113, 60-73, 2017.P123
- [100] Rahimzadeh Amin, **Eslamian Morteza**, "Experimental study on the evaporation of sessile droplets excited by vertical and horizontal ultrasonic vibration", *International Journal of Heat and Mass Transfer*, vol. 114, 786-795, 2017.P124
- [101] Soltani-Kordshuli Firuze, **Eslamian Morteza**, "Impact dynamics and deposition of pristine and graphene-doped PEDOT:PSS polymeric droplets on stationary and vibrating substrates", *Experimental Thermal and Fluid Science*, vol. 89, 238-248, 2017.P125
- [102] **Eslamian Morteza**, "Inorganic and organic solution-processed thin film devices", *NANO-MICRO Letters*, vol. 9(1): 3, 2017.P126
- [103] Rahimzadeh Amin, **Eslamian Morteza**, "On evaporation of thin liquid films subjected to ultrasonic substrate vibration", *International Communications in Heat and Mass Transfer*, vol. 83, 15-22, 2017.P127
- [104] Habibi Mehran, Ahmadian-Yazdi Mohammad-Reza, **Eslamian Morteza**, "Optimization of spray coating for the fabrication of sequentially deposited planar perovskite solar cells", *Journal of Photonics for Energy*, vol. 7 (2): 022003, 2017.P128

- [105] Zabihi Fatemeh, Ahmadian-Yazdi Mohammad-Reza, **Eslamian Morteza**, "Photocatalytic Graphene-TiO₂ thin films fabricated by low-temperature ultrasonic vibration-assisted spin and spray coating in a sol-gel process", *Catalysts*, vol. 7(5): 136, 2017.P129
- [106] Rahimzadeh Amin, **Eslamian Morteza**, "Stability of thin liquid films subjected to ultrasonic vibration and characteristics of the resulting thin solid films", *Chemical Engineering Science*, vol. 158, 587-598, 2017.P130
- [107] Q. Wang, F. Lin, C C. Chueh, T. Zhao, **M. Eslamian**, A. K.Y. Jen, "Enhancing efficiency of perovskite solar cells by reducing defects through imidazolium cation incorporation", *Materials Today Energy*, 2017.P131
- [108] F. Zabihi, **M. Eslamian**, "Low-cost transparent graphene electrodes made by ultrasonic substrate vibration-assisted spray coating (SVASC) for thin film devices", *Graphene Technology*, 2(1-2): 1-11, 2017.P132
- [109] Ur Rehman H., Chen Y., Hedenqvist M.S., Li H., Xue W., **Guo Y.**, Guo Y., Duan H., and Liu H. "Self-healing shape memory PUPCL copolymer with high cycle life," *Advanced Functional Materials* (IF = 12.12), 1704109, 2017.P133
- [110] Ma Mingchao, Xue Tianju, Chen Shenyue, **Guo Yunlong**, Chen Yujie, Liu Hezhou, "Features of structural relaxation in diblock copolymers", *Polymer Testing*, vol. 60, 1-5, 2017.P134
- [111] Cui Yanguang, Xie Dongyue, Yu Ping, **Guo Yunlong**, Rong Yonghua, Zhu Guozhen, Wen Mao, "Formation of iron hydride in α -Fe under dislocation strain field and its effect on dislocation interaction", *Computational Materials Science*, vol. 141, 254-259, 2018.P135
- [112] Cui Yanguang, **Guo Yunlong**, Li Yangxin, Wan Jianfeng, Zhang Jihua, Rong Yonghua, Chen Nailu, Wang Dong, Wang Yunzhi, "Origin of the modulus anomaly over a wide temperature range of Mn_{0.70}Fe_{0.25}Cu_{0.05} alloy", *Computational Materials Science*, vol. 140, 89-94, 2017.P136
- [113] Chowdhury Mithun, **Guo Yunlong**, Wang Yucheng, Merling Weston L., Mangalara Jayachandra H., Simmons David S., Priestley Rodney D., "Spatially distributed rheological properties in confined polymers by noncontact shear", *Journal of Physical Chemistry Letters*, vol. 8, 1229-1234, 2017.P137
- [114] Liu Yang, Gu Xin, Qi Wen, **Zhu Hong**, Shan Hao, Chen Wenlong, Tao Peng, Song Chengyi, Shang Wen, Deng Tao, Wu Jianbo, "Enhancing the photocatalytic hydrogen evolution performance of a metal/semiconductor catalyst through modulation of the schottky barrier height by controlling the orientation of the interface", *ACS Applied Materials & Interfaces*, vol. 9, 12494-12500, 2017.P138
- [115] ZM Gibbs, F Ricci, G Li, **H Zhu**, K Persson, G Ceder, G Hautier, A Jain, and G. Jeffrey Snyder, "Effective mass and Fermi surface complexity factor from ab initio band structure calculations", *npj Computational Materials*, 3(1): 8, 2017.P139

Other Disciplines

- [116] **Clancy R F**, "Making the case for political anthropology: Understanding and addressing the backlash against liberalism", *Identity and Difference: Contemporary Debates on the Self*, 129-152, 2016.P140
- [117] F. Khatun, J. U. Palas and **P.Ray**, "Using the UTAUT model to analyse cloud-based mHealth service for primary care", *Digital Medicine*, vol 3, Issue 2, 2017.P141

- [118] M. Ashraf, N. Hasan, L.Lewis, R. Hasan and **P.Ray**, "A systematic literature review of the application of information communication technology (ICT) for the visually impaired", *the International Journal of Disability Management*, vol. 11, 2017.P142
- [119] A. Bakshi, A. Talaei-Khoei, **P.Ray** and T. Solvoll, "PoDMan: policy deviation management", *Australasian Journal of Information Systems*, vol. 21, 2017.P143
- [120] J. U. Palas, M. Asdhraf and **P.Ray**, "Financing universal health coverage: a systematic survey", *The International Technology Management Review*, vol. 6, No. 4, 133-148, 2017.P144
- [121] **Pradeep Ray**, Junhua Li, Arni Ariani and Vasvi Shah, "Tablet-based well-being check for the elderly: development and evaluation of usability and acceptability", *JMIR Human Factors*, 4(2):e12, 2017. ...P145
- [122] Md Mahfuz Ashraf, Mohammed Abdur Razzaque, Siaw-Teng Liaw, **Pradeep Kumar Ray**, Md Rashadul Hasan, "Social business as an entrepreneurship model in emerging economy: Systematic review and case study", *Management Decision*, <https://doi.org/10.1108/MD-04-2017-0343>, 2017.P146

2017 Published Conference Papers

Mechanical Engineering

- [1] Wang Qiaoling and **Chen C P**, "Simulation of single diesel droplet evaporation and combustion process with a unified diesel surrogate", *ILASS-Americas 29th Annual Conference on Liquid Atomization and Spray Systems*, 2017.P147
- [2] Zhao Bolin and **Chen C P**, "Modeling of cavitation induced fuel atomization and breakup processes", *American Society of Mechanical Engineers, Fluids Engineering Division (Publication) FEDSM*, vol. 2, 2017.P148
- [3] Penghui Ge, Fengnian Zhao, **David L.S. Hung**, Hujie Pan, Min Xu, "Distortion mapping correction of in-cylinder flow field measurements through optical liner using gaussian optics model", *SAE Paper 2017-01-0615, 2017 SAE World Congress and Exhibition*, 2017.P149
- [4] Hujie Pan, Min Xu, Xue Dong, **David L.S. Hung**, Huijia Lv, Tang-Wei Kuo, Ronald O. Grover, Scott E. Parrish, "Experimental investigation of fuel film characteristics of ethanol impinging spray at ultra-low temperature," *SAE Paper 2017-01-0851, 2017 SAE World Congress and Exhibition*, 2017.P150
- [5] Jingjing Cao, Min Xu, **Hung David L.S.**, Hujie Pan, Xue Dong, "Uncertainty quantification of spray wall impingement simulation", *COMODIA 2017 - 9th International Conference on Modeling and Diagnostics for Advanced Engine Systems*, 2017.P151
- [6] Fengnian Zhao, Penghui Ge, Hanyang Zhuang, **David L.S. Hung**, "Analysis of crank-angle-resolved vortex characteristics under high swirl condition in a spark-ignition direct-injection engine", *Paper No. ICEF2017-3574, Proceedings of the ASME 2017 Internal Combustion Fall Technical Conference*, 15-18, 2017.P152
- [7] Hujie Pan, Di Xiao, Min Xu, **David L.S. Hung**, Xue Dong, "Transient structure and footprint of iso-octane impinging spray under room and low temperature", *ILASS-Asia 2017*, Oct. 18-21, 2017.P153
- [8] Zhe Sun, Xue Dong, Peng Yin, Tianyun Li, **David L.S. Hung**, Min Xu, "Validation of spray evaporation model via simultaneous measurements of liquid and vapor concentration of a single plume spray", *ILASS-Asia 2017*, Oct. 18-21, 2017.P154

- [9] Qinglin Xu, Min Xu, **David L.S. Hung**, Tianyun Li, Xue Dong, "Suppressed prompt atomization of flash-boiling spray by elevating injection pressure", *ILASS-Asia 2017*, Oct. 18-21, 2017.P155
- [10] Li Shen, Kwee-Yan Teh, Penghui Ge, Yusheng Wang, **David L.S. Hung**, "Detecting outliers in crank angle resolved engine flow field datasets for proper orthogonal decomposition analysis", *2017 SAE World Congress and Exhibition*, SAE Paper 2017-01-0612, 2017.P156
- [11] Qinglin Xu, Min Xu, **David Hung**, Shengqi Wu, Xue Dong, Hiroaki Ochiai, Zhisong Zhao, Caixia Wang, Kaiyue Jin, "Diesel spray characterization at ultra-high injection pressure of denso 250 mpa common rail fuel injection system", *2017 SAE World Congress and Exhibition*, SAE Paper 2017-01-0821, 2017.P157
- [12] Qaiser Zeeshan, Kang Liping and **Johnson S.**, "Concentric helical axial spring tunable stiffness mechanism: analytical modeling, design optimization and experimental validation", *ASME Proceedings of the 41st Robotics Conference IDETC/CIE 2017*, DETC2017-67677, 2017.P158
- [13] **Johnson S.**, Van Beek Anton, Qaiser Zeeshan, Kang Liping, "Optimization for large or linear tunable stiffness control with a concentric circular tapered beam design", *ASME Proceedings of the 41st Robotics Conference IDETC/CIE 2017*, DETC2017-67346, 2017.P159
- [14] Su J., **Johnson S.**, "Rapid development of a finite element model of the foot and ankle from CT section scan data", *Congress of the International Society of Biomechanics*, June 22-27, 2017.
- [15] Ou H., Qaiser Z., Kang L., **Johnson S.**, "Adjustable medial longitudinal arch height foot orthoses and biomechanical significance", *Congress of the International Society of Biomechanics*, June 22-27, 2017.
- [16] Cui and **J. Ju**, "2D motion structures of n-fold rotational symmetry, in proceedings of the ASME international mechanical engineering congress and exposition", *IMECE*, 70854, 2017.P160
- [17] Z. Yuan and **J. Ju**, "Tunable triangular cellular structures by pneumatic control of dual channel actuators", *In Proceedings of the ASME International Mechanical Engineering Congress and Exposition, IMECE*, 70858, 2017.P161
- [18] M.S. Uddin and **J. Ju**, "Understanding the shape memory behavior of thermoplastic polyurethane elastomers with coarse grained molecular dynamics simulations", *MRS Advances*, 2(6): 375-380, 2017.P162
- [19] Zhang Y.J., and **M. Li**, "Robust optimization with parameter and model uncertainties using gaussian processes with limited samples," *IDETC/CIE 2017, ASME 2017 International Design Engineering Technical Conferences & Computers and Information in Engineering Conference*, 2017.P163
- [20] Zhou J.H., T.T. Xia, **M. Li** and M. Xu, "A normalized circle intersection method for bi-objective optimization programming", *IDETC/CIE 2017, ASME 2017 International Design Engineering Technical Conferences & Computers and Information in Engineering Conference*, 2017.P164
- [21] Zhang J.Z., Zhou J.H., **M. Li** and M. Xu, "Multi-objective tolerance optimization considering friction loss for internal combustion engines", *SAE 2017 World Congress*, 2017.P165
- [22] **Shen Yanfeng**, Cesnik Carlos E. S., "Efficient modeling of nonlinear scattering of ultrasonic guided waves from fatigue cracks using local interaction simulation approach", *Proceedings of the ASME International Mechanical Engineering Congress and Exposition*, vol. 9, 2017.P166
- [23] **Shen Yanfeng** and JunZhen Wang, "Guided Wave Generation and Propagation in Piezoelectric Composite Plates for Establishing Structural Self-awareness", *Structural Health Monitoring 2017: Real-Time*

- [24] **Shen Yanfeng**, "Numerical investigation of nonlinear interactions between multimodal guided waves and delamination in composite structures", *Health Monitoring of Structural and Biological Systems 2017*, 10170, 2017.P168
- [25] **Shen Yanfeng**, Wang Junfang, Ni Yi-Qing, "Structural health monitoring of high-speed railways using ultrasonic guided waves", *Structural Health Monitoring 2017: Real-Time Material State Awareness and Data-Driven Safety Assurance - Proceedings of the 11th International Workshop on Structural Health Monitoring*, vol. 2, 2927-2934, 2017.P169
- [26] **Shen Y**, "An efficient modeling strategy for linear and nonlinear guided wave propagation in complex structures", *CCTAM-2017*, August 13-16, 2017.P170
- [27] Shen L., **Teh K.**, Ge P., Wang Y. et al., "Detecting outliers in crank angle resolved engine flow field datasets for proper orthogonal decomposition analysis," *SAE Technical Paper*, 2017.P171
- [28] **Kwee-Yan Teh**, Penghui Ge, **David L.S. Hung**, "Cycle-to-cycle variation of in-cylinder tumble flow by moment normalization", *SAE Powertrain Fuels and Lubes Meeting*, SAE Paper No. 2017-01-2214, 2017.P172
- [29] P. Zhao, **L. Wang**, N. Chakraborty, "Flame-wall interaction in premixed reactive turbulence", *26th International Colloquium on the Dynamics of Explosions and Reactive Systems*, 2017.P173
- [30] Hongmei Jiang, Qiang Zhang, Li He, Shaopeng Lu, **Lipo Wang**, Jinfang Teng, "Experimental evidence of temperature ratio effect on turbine blade tip heat transfe", *Turbo Expo*, 2017.P174
- [31] Jiang Hongmei, He Li, **Zhang Qiang**, Wang Lipo, "On scaling method to investigate high-speed over-tip-leakage flow at low-speed condition", *Proceedings of the ASME Turbo Expo: Turbine Technical Conference and Exposition*, 2017.P175
- [32] Zhu D., Lu S., Ma H., **Zhang Q.**, Teng J., "Rotating effect on transonic squealer tip cooling performance", *Proceedings of the ASME Turbo Expo: Turbine Technical Conference and Exposition*, vol. 5A, 2017.P176

Electrical and Computer Engineering

- [33] Cai De, Li Zhongfei, Li Yao, Guo Zhendong, **Chen Sung-Liang**, "Combined synthetic aperture focusing technique and three-dimensional deconvolution for resolution enhancement in photoacoustic microscopy", *Photons Plus Ultrasound: Imaging and Sensing 2017*, vol. 10064, 2017.P177
- [34] Zhou Xin, Cai De, He Xiaolong, **Chen Sung-Liang**, Wang Xueding, **Yang Tian**, "Ultrasound detection with surface plasmon resonance on fiber end-facet", *Optics InfoBase Conference Papers*, 1-2, 2017.P178
- [35] **Chong Han**, Wenqian Tong, Xinyi Wu, "A memory-assisted MAC protocol with angular-division-multiplexing in terahertz networks", *2017 IEEE International Conference on Communications (ICC)*, 1-6, 2017.P179
- [36] C. C. Wang, X. W. Yao, W. L. Wang, and **C. Han**, "Interference and coverage analysis for terahertz band communication in nanonetworks", *IEEE Globecom*, 2017.P180

- [37] S. Nie, C. **Han**, and I. F. Akyildiz, "A three-dimensional time-varying channel model for 5G wireless communication systems", *IEEE VTC Fall*, 2017.P181
- [38] W. Tong, and C. **Han**, "MRA-MAC: a multi-radio assisted medium access control in terahertz communication networks", *IEEE Global Communications Conference (GLOBECOM)*, 2017.P182
- [39] Xie Xiaobin, McGaffin Madison G., **Long Yong**, Tessler Jeffrey A., Wen Minhua, Lin James, "Accelerating separable footprint (SF) forward and back projection on GPU", *Medical Imaging 2017: PHYSICS OF MEDICAL IMAGING*, vol. 10132, 2017.P183
- [40] I. Y. Chun, X. Zheng, **Y. Long**, and J. A. Fessler, "Sparse-view X-ray CT reconstruction using L1 regularization with learned sparsifying transform", *In Proc. Intl. Mtg. on Fully 3D Image Recon. in Rad. and Nuc. Med*, 115-119, 2017.P184
- [41] X. Zheng, S. Ravishankar, **Y. Long**, and J. A. Fessler. Union of learned sparsifying transforms based low-dose 3D CT image reconstruction. *In Proc. Intl. Mtg. on Fully 3D Image Recon. in Rad. and Nuc. Med*, 69-72, 2017.P185
- [42] Q. Ding, T. Niu, X. Zhang and **Y. Long**, "Image-domain multi-material decomposition for dual-energy CT via total nuclear norm and L0 norm", *In Proc. Intl. Mtg. on Fully 3D Image Recon. in Rad. and Nuc. Med*, 69-72, 2017.P186
- [43] S. Ye, S. Ravishankar, **Y. Long**, and J. A. Fessler, "Adaptive sparse modeling and shifted-Poisson likelihood based approach for low-dose CT image reconstruction", *In Proc. IEEE Wkshp. Machine Learning for Signal Proc.*, 154-159, 2017.P187
- [44] Songyang Han, He Yin, Alsabbagh A., **Chengbin Ma**, "A flexible distributed approach to energy management of an isolated microgrid", *2017 IEEE 26th International Symposium on Industrial Electronics (ISIE). Proceedings*, 2063-8, 2017.P188
- [45] Yandong Wang, He Yin, Songyang Han, Alsabbagh A., **Chengbin Ma**, "A novel switched capacitor circuit for battery cell balancing speed improvement", *2017 IEEE 26th International Symposium on Industrial Electronics (ISIE). Proceedings*, 1977-82, 2017.P189
- [46] Fu Xinhong, Liu Ming, Tang Zefan, **Ma Chengbin**, "Design procedure of a class E2DC-DC converter for megahertz wireless power transfer based on a compact class e current-driven rectifier", *IEEE International Symposium on Industrial Electronics*, 694-699, 2017.P190
- [47] Siyu Peng, Ming Liu, Zefan Tang, **Chengbin Ma**, "Optimal design of megahertz wireless power transfer systems for biomedical implants", *Industrial Electronics (ISIE), 2017 IEEE 26th International Symposium on. IEEE*, 2017.P191
- [48] C. Zhao, H. Yin, C. **Ma**, "Two-level energy management strategy for a fuel cell-battery-ultracapacitor hybrid system", *the 42nd Annual Conference of the IEEE Industrial Electronics Society*, Oct. 23-26, 2016.P192
- [49] H. Yin, C. Zhao, C. **Ma**, "A decentralized energy management for a multiple energy system with fault tolerance analysis", *the 42nd Annual Conference of the IEEE Industrial Electronics Society*, Oct. 23-26, 2017.P193
- [50] Wu Yi, Shen Chuyu, Jia Yi, **Qian Weikang**, "Approximate logic synthesis for FPGA by wire removal and local function change", *2017 22ND ASIA and South Pacific Design Automation Conference (ASP-DAC)*, 163-169, 2017.P194

- [51] Yue Yao, Shuyang Huang, Chen Wang, Yi Wu, and **Weikang Qian**, "Approximate disjoint bi-decomposition and its application to approximate logic synthesis," to appear in *Proceedings of the 35th IEEE International Conference on Computer Design (ICCD)*, 2017.P195
- [52] Meng Yang, John Hayes, Deliang Fan, and **Weikang Qian**, "Design of accurate stochastic number generators with noisy emerging devices for stochastic computing", *2017 IEEE/ACM International Conference on Computer-Aided Design (ICCAD)*, 2017.P196
- [53] Meng Yang and **Weikang Qian**, "Design of reliable stochastic number generators using emerging devices for stochastic computing", *2017 International Workshop on Logic and Synthesis (IWLS)*, 52-59, 2017.P197
- [54] Zheng Yuanlin, Qin Tian, Yang Jianfan, Ge Li, **Wan Wenjie**, "Observation of transient nonlinear dynamics of optical frequency comb in a microcavity", *Optics InfoBase Conference Papers*, vol Part F54-NLO, 2017.P198
- [55] Feng Shaocong, Wang Mingjun, **Wu Jigang**, "Digital in-line holographic microscope based on the grating illumination with improved resolution by interpolation", *Holography, Diffractive Optics, and Applications VII*, 10022, 2017.P199
- [56] Feng Shaocong, Wang Mingjun, **Wu Jigang**, "Iterative holographic reconstruction based on the grating illumination with improved resolution by interpolation", *Optics InfoBase Conference Papers*, vol. Part F43-CLEO_AT. 2017.P200
- [57] Wang Mingjun, Feng Shaocong, **Wu Jigang**, "Pixel super-resolution in digital in-line holography", *Holography, Diffractive Optics, and Applications VII*, 10022, 2017.P201
- [58] Wang Xiaodan, Yi Hui, **Yang Tian**, "Efficient four-wave mixing in loaded nanoscale plasmonic hotspots", *Optics InfoBase Conference Papers*, vol. Part F54-NLO, 2017.P202
- [59] **Tian Yang**, Jing Long, Xiaodan Wang, "Stepwise quantum phonon pumping in surface-enhanced raman scattering," *OSA Nonlinear Optics Topical Meeting*, 2733153, 2017.P203
- [60] Xin Zhou, De Cai, Xiaolong He, Sung-Liang Chen, Xueding Wang, **Tian Yang**, "Ultrasound detection with surface plasmon resonance on fiber end-facet", *Conference on Lasers and Electro-Optics*, 1-2, 2017.P204
- [61] Yuanlong Wang, Daoyi Dong, Ian R. Petersen, **Jun Zhang**, "An approximation algorithm for Quantum Hamiltonian Identification with Complexity Analysis", *IFAC Congress*, July 9-14, 2017.P205

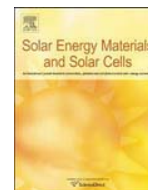
Material Science and Engineering

- [62] Braun Artur, **Chen Qianli**, "Swiss team discovers how protons move through fuel cell", *Fuel Cells Bulletin*, vol. 2017(6):14, 2017.P206
- [63] M. Habibi, **M. Eslamian**, "Role of the fabrication technique in the stability of CH₃NH₃PbI₃ perovskite thin films", *33th European photovoltaic solar energy conference and exhibition*, 2017.P207

- [64] A. Rahimzadeh, **M. Eslamian**, "Evaporation of DMF sessile drops on stationary and vibrating substrates", *13TH International Conference HEFAT*, pp. 387-392, 2017.P208
- [65] F. Zabihi, **M. Eslamian**, "Ultrasonic assisted solution deposition of graphene based nano-composite thin films; highly functional component for opto-electrical devices", *International Research Conference on Sustainable Energy, Engineering, Materials and Environment*, 2017.P209
- [66] J. Huang, Z. Yuan, S. Gao, J. Liao, **M. Eslamian**, "Observation of the coating process in spray coating", *29th Annual Conference on Liquid Atomization and Spray Systems (ILASS-Americas)*, May 15-18, 2017.P210
- [67] **M. Eslamian**, F. Zabihi, A. Rahimzadeh, Q. Wang, Y. Xie, "Ultrasonic vibration imposed on thin liquid solution films as an effective tool for improved characteristics of ensuing thin solid films", *American Physical Society (APS) March Meeting*, Abstract: A35.00013, March 13-17, 2017.P211

Other Disciplines

- [68] **Clancy Rockwell Franklin**, Sessford Joanna Ruth, An Longfei and Ge Yan, "Which factors are correlated with engineering students' expectations of ethical issues?", *ASEE Annual Conference and Exposition, Conference Proceedings*, 2017.P212
- [69] **P.Ray** and C. Zhang, "Role of entrepreneurship in universal health coverage (UHC) using mHealth", *Proceedings of the IEEE Technology and Engineering Management Society Conference*, 2017.P213
- [70] ST Liaw, A. Marcelo, P. Narsimhan, M. Ashraf and **P.Ray**, "Global eHealth, Social Business and Citizen Engagement: a Natural Convergence?", *Proceedings of the MedInfo2017 Conference*, 2017.P214
- [71] Y. Jahan, M. Rahman, **P. Ray** and M. Moryama, "Patient-physician communication by using mobile technology in developing countries", *Asian Hospital and Healthcare Management*, Issue 36, 2017. ...P215
- [72] **Zheng Gang, Yang Yanchun**, "A successful joint venture for international engineering education", *ASEE Annual Conference and Exposition, Conference Proceedings*, 2017.P216



Double-layer nanoparticle-based coatings for efficient terrestrial radiative cooling



Hua Bao^{a,*}, Chen Yan^a, Boxiang Wang^b, Xing Fang^b, C.Y. Zhao^b, Xiulin Ruan^c

^a University of Michigan-Shanghai Jiao Tong University Joint Institute, Shanghai Jiao Tong University, Shanghai 200240, China

^b Institute of Engineering Thermophysics, School of Mechanical Engineering, Shanghai Jiao Tong University, Shanghai 200240, China

^c School of Mechanical Engineering and Birk Nanotechnology Center, Purdue University, West Lafayette, IN 47907, United States

ARTICLE INFO

Keywords:

Radiative cooling
Particle embedded coatings
Multiple scattering
Selective radiative property

ABSTRACT

One passive cooling approach is pumping energy to outer space through thermal radiation. Such a radiative cooling mechanism widely exists in nature and is important to maintain the temperature of the earth. However, natural materials generally have poor radiative cooling efficiency. To better utilize the radiative cooling for thermal management applications, the surface should be designed to have a high reflectivity in the solar spectrum and high emissivity in the "sky window" region (8–13 μm in wavelength). In this work, we propose and demonstrate a highly scalable nanoparticle-based double-layer coating to achieve such selective radiative properties. Double-layer coatings consisting of a top reflective layer with high solar albedo and a bottom emissive layer are achieved by properly designed TiO_2 , SiO_2 , and SiC nanoparticles. These coatings were fabricated on both low- and high-emissivity substrates and their spectral radiative properties were characterized. The coating composed of TiO_2 and SiO_2 on a reflective substrate has excellent selective emission property for radiative cooling purpose. Under dry air conditions and assuming non-radiative heat transfer coefficient $h_c = 4 \text{ W/m}^2 \text{ K}$, $\text{TiO}_2 + \text{SiO}_2$ and $\text{TiO}_2 + \text{SiC}$ can theoretically achieve about 17 °C below ambient at night and 5 °C below ambient under direct solar radiation (AM1.5). On-site measurements have also been conducted. Under direct solar irradiation, significant temperature reduction was observed for both aluminum and black substrate after the coating was applied. At nighttime, radiative cooling effect can cool the surface to a few degrees below ambient temperature. Although the theoretical cooling under dry weather condition is not observed, the experiment results can be well explained by theoretical calculations with the consideration of high humidity and non-radiative heat transfer. This nanoparticle-based approach can be easily applied to large area, which is a significant step of achieving large scale application of the radiative cooling technology.

1. Introduction

Radiative heat pumping to outer space is an important mechanism to maintain the temperature of the earth. The efficiency of radiative cooling depends on the spectral emissivity of the surface of an object. If surface emissivity can be tuned to enhance the efficiency of radiative cooling, it could be an important passive cooling approach and widely applied to thermal management of buildings [1], electronics heat dissipation [2] and cooling of solar cells [3]. Radiative cooling relies on the fact that the atmosphere transmits about 87% of the outgoing radiation from the earth in the "sky window" region (8–13 μm in wavelength) [4]. It is possible for the surface to exchange heat with the cold outer space through the "sky window". The surfaces, which emit strongly in this wavelength region and reflect strongly beyond this region, experience an imbalance of outgoing and incoming thermal

radiation and achieve lower steady-state temperature than the ambient.

It is a common practice to apply coatings on the material surface to modify its thermal radiative properties. Recent researches on radiative cooling coatings can be divided into two categories: daytime radiative cooling and nighttime radiative cooling, and the latter neglects solar radiation. To achieve nighttime cooling, the spectrally selective coatings should emit strongly in "sky window" region. Early investigations rely on bulk and thin film materials with an intrinsic emissive peak in "sky window" region to achieve radiative cooling. Granqvist and Hjortsberg [5] evaporated SiO film on Al substrate which can theoretically achieve 40 °C below ambient temperature (assuming $T_a = 21 \text{ °C}$) by neglecting non-radiative heat transfer. Although a single emission peak was observed, the average emittance in "sky window" regime was only 43%. Diatezua et al. [6] deposited three silicon oxynitride multi-layers onto aluminum-coated glass substrate to obtain wide absorption

* Corresponding author.

E-mail address: hua.bao@sjtu.edu.cn (H. Bao).

<http://dx.doi.org/10.1016/j.solmat.2017.04.020>

Received 1 November 2016; Received in revised form 23 February 2017; Accepted 10 April 2017

Available online 26 April 2017




0927-0248/ © 2017 Elsevier B.V. All rights reserved.

ARTICLE

DOI: 10.1038/s41467-017-01618-w

OPEN

Dynamic tuning of optical absorbers for accelerated solar-thermal energy storage

Zhongyong Wang¹, Zhen Tong², Qinxian Ye¹, Hang Hu¹, Xiao Nie¹, Chen Yan², Wen Shang¹ , Chengyi Song¹, Jianbo Wu¹, Jun Wang³, Hua Bao², Peng Tao¹  & Tao Deng¹ 

Currently, solar-thermal energy storage within phase-change materials relies on adding high thermal-conductivity fillers to improve the thermal-diffusion-based charging rate, which often leads to limited enhancement of charging speed and sacrificed energy storage capacity. Here we report the exploration of a magnetically enhanced photon-transport-based charging approach, which enables the dynamic tuning of the distribution of optical absorbers dispersed within phase-change materials, to simultaneously achieve fast charging rates, large phase-change enthalpy, and high solar-thermal energy conversion efficiency. Compared with conventional thermal charging, the optical charging strategy improves the charging rate by more than 270% and triples the amount of overall stored thermal energy. This superior performance results from the distinct step-by-step photon-transport charging mechanism and the increased latent heat storage through magnetic manipulation of the dynamic distribution of optical absorbers.

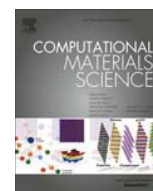
¹ State Key Laboratory of Metal Matrix Composites, School of Materials Science and Engineering, Shanghai Jiao Tong University, Shanghai 200240, China.

² University of Michigan-Shanghai Jiao Tong University Joint Institute, Shanghai Jiao Tong University, Shanghai 200240, China. ³ A123 Systems Research Center, A123 Systems, LLC, Waltham, MA 02451, USA. Zhongyong Wang, Zhen Tong and Qinxian Ye contributed equally to this work. Correspondence and requests for materials should be addressed to P.T. (email: taopeng@sjtu.edu.cn) or to H.B. (email: hua.bao@sjtu.edu.cn) or to T.D. (email: dengtao@sjtu.edu.cn)



Contents lists available at ScienceDirect

Computational Materials Science

journal homepage: www.elsevier.com/locate/commatsci

Effect of the accuracy of interatomic force constants on the prediction of lattice thermal conductivity

Han Xie^a, Xiaokun Gu^b, Hua Bao^{a,*}^a University of Michigan-Shanghai Jiao Tong University Joint Institute, Shanghai Jiao Tong University, Shanghai 200240, China^b Institute of Engineering Thermophysics, School of Mechanical Engineering, Shanghai Jiao Tong University, Shanghai 200240, China

ARTICLE INFO

Article history:

Received 2 March 2017

Received in revised form 1 June 2017

Accepted 2 June 2017

Available online 16 July 2017

Keywords:

Thermal conductivity

Peierls-Boltzmann transport equation

Interatomic force constants

Grüneisen parameters

ABSTRACT

Solving Peierls-Boltzmann transport equation with interatomic force constants (IFCs) from first-principles calculations has been a widely used method for predicting lattice thermal conductivity of three-dimensional materials. With the increasing research interests in two-dimensional materials, this method is directly applied to them but different works show quite different results. In this work, classical potential was used to investigate the effect of the accuracy of IFCs on the predicted thermal conductivity. Inaccuracies were introduced to the third-order IFCs by generating errors in the input forces. When the force error lies in the typical value of first-principles calculations, the calculated thermal conductivity would be quite different from the benchmark result. It is found that imposing translational invariance conditions cannot always guarantee a better thermal conductivity result. It is also shown that Grüneisen parameters cannot be used as a necessary and sufficient criterion for the accuracy of third-order IFCs in the aspect of predicting thermal conductivity.

© 2017 Elsevier B.V. All rights reserved.

1. Introduction

In crystalline semiconductors and insulators, phonons (*i.e.* lattice vibrations) are the major heat carriers, so the thermal conductivity can be calculated with the knowledge of phonon properties. Recently there are growing interests to predict the lattice thermal conductivity by solving Peierls-Boltzmann transport equation (PBTE), either under single mode relaxation time approximation (SMRTA) or with full iterative solution [1,2]. With interatomic force constants (IFCs) extracted from first-principles calculations as the input, this method has been widely used to calculate the thermal conductivity of three-dimensional (3D) materials [3–26]. The good agreement between these calculated values and measured experimental data proves its accuracy and reliability [3–21].

The discovery of ultrahigh thermal conductivity of graphene [27] has stimulated a growing research interest in the thermal conductivity of two-dimensional (2D) materials. The first-principles PBTE method for predicting thermal conductivity has been directly applied to 2D materials like graphene [28–31], silicene [32–35], phosphorene [36–40], MoS₂ [41–43], borophene [44], *etc.* However, previous calculations show quite different results in different works. For example, the predicted thermal conductivity for black

phosphorene from SMRTA [36–40] at room temperature along armchair direction varies a lot from 5.46 to 33 W/mK, and the result along zigzag direction spans a rather large range between 15.33 and 83.5 W/mK. Similar discrepancy is also observed in the case of MoS₂, whose thermal conductivity at room temperature was predicted from SMRTA to be 83 W/mK by Li et al. [41] as well as Gu and Yang [42]. In comparison, Yan et al. [43] got a result of 35.5 W/mK with the same method. The lack of consistency in the predicted thermal conductivity may arise from using iterative method instead of SMRTA [30,31], imposing translational invariance conditions to third-order IFCs [15,35], different exchange-correlation functionals used in first-principles calculations [45], enforcing a quadratic branch in the dispersion of 2D materials [44], *etc.* In materials where resistive Umklapp scattering processes dominate in the phonon-phonon scattering, both SMRTA and iterative method should give similar results [1,2]. For graphene, iterative method yields a much larger thermal conductivity value than SMRTA because the momentum-conserving normal scattering processes also play an important role in phonon transport [30,31], which has been explained by the hydrodynamic phonon transport at room temperature [46,47]. Regarding the translational invariance conditions (*i.e.* acoustic sum rules), Lindsay et al. [15] demonstrated that imposing it to third-order IFCs would play an important role in determining thermal conductivity. Our previous results for silicene also showed its importance [32,35]. Transla-

* Corresponding author.

E-mail address: hua.bao@sjtu.edu.cn (H. Bao).

Molecular dynamics study of the interfacial thermal conductance of multi-walled carbon nanotubes and van der Waals force induced deformation

Qingyuan Rong,^{a)} Cheng Shao,^{a)} and Hua Bao^{b)}

University of Michigan—Shanghai Jiao Tong University Joint Institute, Shanghai Jiao Tong University, Shanghai 200240, China

(Received 31 August 2016; accepted 17 January 2017; published online 1 February 2017)

Thermal boundary resistance (TBR) plays an important role in the thermal conduction of carbon nanotube (CNT)-based materials and CNT networks (e.g., thin films, arrays, and aerogels). Although individual CNTs have extremely high thermal conductivity, interfacial resistances can dominate the overall resistance and largely influence their thermal performance. Using molecular dynamics simulations, we systematically study the interfacial thermal conductance (ITC, the inverse of TBR) of multi-walled carbon nanotube (MWNT)-substrate interfaces and MWNT-MWNT junctions, and compare the CNT-CNT junctions with graphene-graphene junctions. The results show that for CNTs with the diameter of a few nanometers, the total ITCs first decrease and then stabilize with the increase of the number of walls, mainly due to the changes of mechanical strength and adhesive energy. Increasing the CNT diameter leads to a larger total ITC and it is mainly due to a larger contact area. The area normalized ITC of CNT-CNT junctions increases and then saturates with the number of walls, and it behaves non-monotonically with the diameter. Furthermore, a trapezoidal model of multi-layer graphene-graphene junctions is used to explain the number of wall dependence of ITC. We also find that with the same adhesive energy, total ITCs of CNT-CNT junctions and graphene-graphene junctions are similar, which allows us to roughly estimate ITCs of CNT-CNT junctions without performing numerical simulations. *Published by AIP Publishing.*

[<http://dx.doi.org/10.1063/1.4975032>]

I. INTRODUCTION

Carbon nanotubes are very attractive for a wide range of applications leveraging their unique electrical, thermal, and mechanical properties.¹ For example, the extremely high thermal conductivity of carbon nanotubes (CNTs) makes them the most promising candidates as nanofillers for thermally conductive composites.² The combination of high thermal conductivity and high mechanical compliance makes CNT arrays potential for high-performance thermal interface materials (TIMs).^{3,4} However, in contrast to the ultra-high intrinsic thermal conductivity of free-standing CNTs, it is found that the overall improvement in thermal properties is quite limited when CNTs are integrated in real device applications. For example, experiments have shown that the thermal conductivity of multi-walled carbon nanotubes (MWNT)/epoxy composites increases very modestly as a function of the filler content, and in the case of single-walled CNT (SWNT) composites, the thermal conductivity can be even lower than that of the pristine epoxy.⁵ The performance of the CNT-based TIMs is also below expectation, with the thermal conductance ranging from $\sim 10^3$ to $10^5 \text{ W m}^{-2} \text{ K}^{-1}$,^{6,7} which is even lower than that of some conventional TIMs.⁴

Some studies have been carried out recently to resolve this problem. Gojny *et al.* experimentally evaluated the

influence of the type of CNT and surface-functionalization on the thermal conductivity of CNT/epoxy composites. They attribute the small enhancement in thermal conductivity to the large interfacial area between CNTs and epoxy as well as strong phonon scattering at the interfaces.⁸ Using a transient thermo-reflectance method, Tong *et al.* measured the thermal conductance at vertically aligned CNT array interfaces as well as the thermal conductivity of CNT arrays itself. Their results show that the interface between the free end of CNT tips and the target surface has a relatively small conductance ($\sim 10^5 \text{ W m}^{-2} \text{ K}^{-1}$) and is the dominant resistance.⁹ Moreover, some experiments have measured the thermal conductivities of CNT networks and the values are typically very low, which is mainly due to the large resistance at CNT junctions.^{10–13} Some mesoscopic models are also proposed to model and predict the thermal conductivity of CNT networks, in which the CNT-CNT and CNT-substrate interfacial resistances are the basic inputs to such models.^{14–16} Therefore, it is of great importance to develop a better understanding on the thermal transport at CNT-substrate interfaces and CNT-CNT junctions.

Due to the nature of interfacial thermal transport, atomic level simulations are usually necessary to investigate this effect. For example, through molecular dynamics (MD) simulations, it is found that the conductance at the interface between the vertically aligned SWNT and Si substrate can be enhanced by applying pressure or inserting a graphene layer, mainly due to the enhancement of the contact area and adhesive energy.^{17,18} Considering the free end of CNT tips

^{a)}Q. Rong and C. Shao contributed equally to this work.

^{b)}Author to whom correspondence should be addressed. Electronic mail: hua.bao@sjtu.edu.cn

Probing phonon–surface interaction by wave-packet simulation: Effect of roughness and morphology

Cheng Shao,¹ Qingyuan Rong,¹ Ming Hu,^{2,3} and Hua Bao^{1,a)}

¹University of Michigan–Shanghai Jiao Tong University Joint Institute, Shanghai Jiao Tong University, Shanghai, China

²Institute of Mineral Engineering, Division of Materials Science and Engineering, Faculty of Georesources and Materials Engineering, RWTH Aachen University, Aachen 52064, Germany

³Aachen Institute for Advanced Study in Computational Engineering Science (AICES), RWTH Aachen University, Aachen 52062, Germany

(Received 10 May 2017; accepted 3 October 2017; published online 19 October 2017)

One way to reduce the lattice thermal conductivity of solids is to induce additional phonon–surface scattering through nanostructures. However, the way in which phonons interact with surfaces, especially at the atomic level, is not well understood at present. In this work, we perform two-dimensional atomistic wave-packet simulations to investigate angular-resolved phonon reflection at a surface. Different surface morphologies, including smooth surfaces, periodically rough surfaces, and surfaces with amorphous coatings, are considered. For a smooth surface, mode conversion can occur after reflection, with the resulting wave-packet energy distribution depending on the surface condition and the polarization of the incident phonon. At a periodically rough surface, the reflected wave-packet distribution does not follow the well-known Ziman model but shows a nonmonotonic dependence on the depth of the surface roughness. When an amorphous layer is attached to a smooth surface, the incident wave packet is absorbed by the amorphous region and is then reflected diffusively at the surface. Our results show that the commonly adopted specular-diffusive model is insufficient to describe phonon reflection at a periodically rough surface and that an amorphous layer can induce strong diffusive reflection. This work provides a comprehensive analysis of phonon reflection at different types of surfaces, which is important for better understanding of thermal transport in various nanostructures. *Published by AIP Publishing.*

<https://doi.org/10.1063/1.5008367>

I. INTRODUCTION

Engineering the thermal conductivity of solids has become an important research topic over the past two decades. Efficient thermoelectric materials (i.e., with large figure of merit or ZT) require a low lattice thermal conductivity. A fundamental way to achieve low thermal conductivity is to utilize phonon–surface scattering in nanostructures. Theoretical and experimental investigations of this approach have yielded significant breakthroughs by using various types of nanostructures, including embedded nanoparticles,^{1,2} nanowires,^{3,4} thin films,^{5–8} and porous structures.^{9–12} For example, the thermal conductivity of crystalline $\text{In}_{0.53}\text{Ga}_{0.47}\text{As}$ was lowered beyond the “alloy limit” by embedding ErAs nanoparticles.¹ The thermal conductivities of rough Si nanowires were found to be two orders of magnitude lower than that of their bulk counterpart.⁴ The reduction of thermal conductivity in these examples is attributable mostly to the classical size effect: surfaces can induce additional phonon scattering channels, which limit the phonon mean free path and thus reduce the lattice thermal conductivity.^{13,14} After scattering at a surface, a phonon is assumed to reflect with a specular and a diffuse component.^{13,15} The specular portion of the energy is proportional to the specularity parameter p , while the other part $(1 - p)$ of the energy is diffusely scattered.

In 1955, Ziman proposed an analytical formula (known as Ziman’s formula) to estimate the specularity parameters at surfaces,^{15,16} which was later extended by Soffer¹⁷ to include the angular dependence. Since then, this formula has been applied to describe phonon scattering at surfaces.^{18–22} In other investigations, this specularity parameter was used as a fitting parameter to obtain insights from experimental results.^{23–26} The Boltzmann transport theory predicts that the thermal conductivity of a nanowire should be minimal when the specularity parameter is 0 (i.e., when there is completely diffuse scattering), which is also known as the “Casimir limit.”²⁷ Recent measurements, however, have shown that the thermal conductivity of rough nanowires can be lower than the predicted Casimir limit,⁴ and this has stimulated many recent attempts to develop a new theory going beyond the traditional understanding.^{28–36} Most of these efforts have been based on continuum models, incorporating either the particle-like^{30,31} or the wave-like^{36–38} nature of phonons. Although such work has advanced our understanding of phonon–surface scattering, the way in which atomic-level details of the surface morphology can affect phonon–surface scattering is still an open question.

In this work, we investigate angular-resolved phonon reflection at surfaces using an atomistic wave-packet simulation. This method uses molecular dynamics (MD) to study the atomistic details of phonon–surface scattering and requires no further assumptions other than the interatomic

^{a)}Electronic mail: hua.bao@sjtu.edu.cn

含超薄膜的层状吸收器完全吸收时材料优化选择

方兴¹ 赵长颖¹ 鲍华²

(1. 上海交通大学机械与动力工程学院, 上海 200240;

2. 上海交通大学 上海交通大学密西根学院, 上海 200240)

摘 要 含超薄膜结构的层状吸收器不仅设计加工结构十分简单, 而且保证了优异的吸收性能, 因而获得了越来越多的关注。层状结构实现完全吸收的机理, 可以归结为吸收器在入射界面处导纳与入射空间导纳完全匹配。根据导纳分析理论, 本文发展了一种可直接计算材料最优光学常数的方法, 用于指导层状吸收器的材料优化选择。在不同的吸收基底上实现完全吸收, 研究发现镀膜薄膜的复折射率实部和虚部满足近似的线性关系, 这对层状薄膜吸收器材料选择提供了必要的选择依据。根据导纳轨迹规律, 仅借助导纳轨迹图, 可以快速确定吸收材料的优化光学常数范围, 因此对于估计和快速设计有着良好的参考价值。

关键词 超薄膜; 吸收器; 导纳分析

中图分类号 TK124

文献标识码 A

文章编号 0253-231X(2017)06-1282-06

Selection of Materials for Perfect Absorption in Layered Absorbers with Ultrathin Films

FANG Xing¹ ZHAO Chang-Ying¹ BAO Hua²

(1. School of Mechanical Engineering, Shanghai Jiao Tong University, Shanghai 200240, China;

2. University of Michigan-Shanghai Jiao Tong University Joint Institute, Shanghai Jiao Tong University, Shanghai 200240, China)

Abstract Layered absorbers with ultrathin films are not only easy to design and manufacture, but also have good performance, which have attracted increasing attention. The mechanism of perfect absorption in layered structures can be attributed to the admittance matching between the absorber interface and the incident medium. Based on admittance analysis, the method of directly calculating optimal optical constants of materials is proposed, which can guide the selection of materials in layered absorbers. It is found that optimized materials have a near linear relationship between the real part and the imaginary part of optical constants for various substrates in absorbers. Considering the characteristic of admittance loci, admittance loci diagrams can be employed to fast narrow the region of optimal optical constants, which is helpful for quick engineering designs.

Key words ultrathin film; absorber; admittance analysis

0 引 言

在太阳能集热器、光伏电池、热光伏, 以及光电探测器、传感器等能量收集和探测设备中, 辐射吸收器是最重要的组件之一。为了设计并制备完美的辐射吸收器, 考虑到微纳结构在波长可比拟波段内作用强烈, 通常可通过设计和加工合适的微纳结构来实现可见到红外范围的辐射吸收, 因而大量的微纳结构被提出用于辐射吸收器中。其中, 超材料、等离子体结构就是其中最为关注的结构之一。然而, 超材料和等离子体结构的制备需要复杂的制模、沉积和刻蚀等工艺, 因而难以实现大规模、低成本生

产, 成为制约其推广应用的关键瓶颈。

近年来, 含超薄膜结构的层状结构获得了越来越多的关注^[1-7]。主要原因就是其设计加工十分的简单, 采用普通的镀膜技术即可实现制备。另一方面, 引入了超薄膜后层状吸收器的吸收性能得到了改善, 因而保证了优异的吸收性能。现有的含超薄膜结构的层状吸收器的完全吸收机理可以分成两类, 即考虑传输特性的波理论和考虑能量特性的场理论。例如, 反射分波相位法^[8]以及非对称法布里珀特理论^[9], 就是根据计算反射系数及相位, 提出完全吸

收稿日期: 2016-12-25; 修订日期: 2017-05-14

基金项目: 上海市重点基础研究项目 (No.16JC1403200); 国家自然科学基金 (No.51476097, No.51306111)

作者简介: 方 兴 (1987-), 男, 博士生, 主要从事微纳尺度热辐射研究。通信作者: 赵长颖, 男, 教授, changying.zhao@sjtu.edu.cn

A Review of Thermal Transport in Low-Dimensional Materials Under External Perturbation: Effect of Strain, Substrate, and Clustering

Cheng Shao^a, Xiaoxiang Yu^b, Nuo Yang^b, Yanan Yue^c, and Hua Bao^a

^aUniversity of Michigan–Shanghai Jiao Tong University Joint Institute, Shanghai Jiao Tong University, Shanghai, P.R. China; ^bState Key Laboratory of Coal Combustion, Huazhong University of Science and Technology, Wuhan, P. R. China, and Nano Interface Center for Energy, School of Energy and Power Engineering, Huazhong University of Science and Technology, Wuhan, P. R. China; ^cSchool of Power and Mechanical Engineering, Wuhan University, Wuhan, P. R. China

ABSTRACT

Due to their exceptional electrical, thermal, and optical properties, low-dimensional (LD) materials are very promising for many applications, such as nanoelectronic devices, energy storage, energy conversion, and thermal management. The thermal performance of LD materials is often an important consideration in these applications. Although freestanding LD materials exhibit interesting thermal properties, they are almost never used in such a form. Instead, they are often integrated into a certain environment; for example, in a composite material or on a substrate. Due to the large surface-to-volume ratio of LD materials, the environment usually has a strong impact on the thermal transport properties of these materials. The thermal behavior of the LD materials can be completely different from the freestanding form. The effect of environmental perturbation on thermal transport properties has recently attracted a lot of research interest. In this article, we aim to provide a comprehensive review of how the typical external perturbations, including tensile strain, substrate, and clustering, can affect the thermal transport properties of LD materials. Emphasis will be placed on how these perturbations affect the lattice structure, phonon dispersion, lattice anharmonicity, and thermal conductivity. We will also summarize the achievements and the remaining challenges on this research topic.

ARTICLE HISTORY

Received 6 October 2016
Accepted 20 January 2017

KEYWORDS

Low dimensional materials;
external perturbation; strain;
substrate effects; clustering

Introduction

The emergence of low-dimensional materials in the last few decades has attracted enormous research interest in their structures and electronic [1–3], optical [4–6], and thermal properties [7, 8]. For example, carbon nanotubes (CNTs) and graphene are representative one-dimensional (1D) and two-dimensional (2D) materials to investigate the unique electron and phonon transport properties [7, 8]. The extremely high thermal conductivity of CNTs and graphene make them very promising for thermal management applications, including thermal interface materials [9–11], high thermal conductivity composites [12, 13], and interconnects for electronic devices [14]. Some 1D materials, such as polyethylene (PE) chains and nanofibers, are found to have high thermal conductivity, which suggests that polymers can be a cheap alternative to metals for heat dissipation in electronics and optoelectronics [15, 16]. Other 2D materials, such as molybdenum disulfide (MoS₂), silicene, and phosphorene, are regarded as promising candidates for next-generation semiconductor devices [2, 3,

CONTACT Hua Bao  hua.bao@sjtu.edu.cn  University of Michigan–Shanghai Jiao Tong University Joint Institute, 800 Dong Chuan Road, Shanghai Jiao Tong University, Shanghai 200240, China.

Color versions of one or more of the figures in the article can be found online at www.tandfonline.com/umte.

© 2017 Taylor & Francis

Nonlinear, three-dimensional beam theory for dynamic analysis

Shilei Han¹ · Olivier A. Bauchau²

Received: 13 April 2016 / Accepted: 13 October 2016 / Published online: 10 November 2016
© Springer Science+Business Media Dordrecht 2016

Abstract For beams undergoing large motions but small strains, the displacement field can be decomposed into an arbitrarily large rigid-section motion and a warping field. When applying beam theory to dynamic problems, it is customary to assume that all inertial effects associated with warping are negligible. This paper examines this assumption in details. It is shown that inertial forces affect the beam's dynamic response in two manners: (1) warping motion induces inertial forces directly, and (2) secondary warping arises that alters the beam's constitutive laws. Numerical examples demonstrate the range of validity of the proposed approach for beams made of both homogeneous isotropic and heterogeneous anisotropic materials. For low-frequency warping, it is shown that inertial forces associated with warping and secondary warping resulting from inertial forces are negligible. To examine the dynamic behavior of beams over a wider range of frequencies, their dispersion curves, natural vibration frequencies, and mode shapes are evaluated using both one- and three-dimensional models; good correlation is observed between the two models. Applications of the proposed beam theory to multibody problems are also presented; here again, good correlation is observed between the prediction of beam models and of full three-dimensional analysis.

Keywords Beam · Warping · Inertial forces · Anisotropic

1 Introduction

A beam is defined as a structure having one of its dimensions much larger than the other two. The generally curved axis of the beam is defined along that longer dimension and the cross-section slides along this axis. The cross-section's geometric and physical properties are assumed to be uniform along the beam's span. Numerous components found in flexible

✉ S. Han
shilei.han@outlook.com

¹ University of Michigan–Shanghai Jiao Tong University Joint Institute, Shanghai 200240, China

² Department of Aerospace Engineering, University of Maryland, College Park, Maryland 20742, USA

Simulated Kinetics and Chemical and Physical Properties of a Four-Component Diesel Surrogate Fuel

Qiaoling Wang and C. P. Chen*

University of Michigan–Shanghai Jiao Tong University Joint Institute, Shanghai Jiao Tong University, Shanghai 200240, People's Republic of China

ABSTRACT: Real diesel fuels are mixtures composed of hundreds to thousands of components; thus, developing surrogate fuels composed of a few representative hydrocarbon components is essential for multidimensional computational fluid dynamics spray combustion simulation purposes. Surrogates that can characterize the thermophysical properties and evaporation processes of real fuel are the “physical” surrogates. Surrogates that are able to mimic fuel chemical-kinetics-related properties are viewed as the “chemical” surrogate models. For spray combustion modeling, fuels experience thermophysical (heating and evaporation) and chemical kinetics (ignition and combustion) processes. To model the multiphase spray combustion process, a “unified” diesel surrogate, which can emulate both the physical and chemical (kinetics) properties of the real diesel fuel, is proposed in this study. A group of hydrocarbon species was selected, using an inversed batch distillation methodology, to match the experimental distillation curve of standard diesel blends. For the chemical kinetics target, a detailed reaction mechanism of 352 species with 13 264 reactions was used for gas-phase ignition delay time predictions and a reduced reaction mechanism of 200 species with 6907 reactions was used for laminar flame speed simulations. On the basis of the hydrocarbon class concentrations of typical diesel fuels of normal/isoalkanes, cycloalkanes and aromatics, this study identified the four-component surrogate fuel for diesel fuel as 1,2,4-trimethylbenzene (C_9H_{12}), *trans*-decalin ($C_{10}H_{18}$), heptamethylnonane ($iC_{16}H_{34}$), and *n*-hexadecane ($C_{16}H_{34}$) with mole fraction 0.262:0.065:0.365:0.308. Important thermophysical and chemical targets, including molecular weight, lower heating value, cetane number, hydrogen/carbon mass ratio, density, kinematic viscosity, surface tension, and specific heat, are also predicted using this surrogate. In addition, chemical kinetics characteristics, including ignition delay times as well as laminar flame speeds, are used to validate the proposed surrogate fuel.

1. INTRODUCTION

During the last few decades, diesel engines have become important energy-supplying sources for various industrial sectors, including transportation and manufacturing. Although diesel engines have better combustion and thermal efficiencies when compared to gasoline engines, issues related to emissions and cold starts require further improvement. Engine performance depends highly upon the fuel type and the subsequent fuel atomization, fuel droplet breakup, vaporization, mixing, and combustion processes. Multidimensional computational fluid dynamics (CFD) methods have been routinely used to gain insight of complex phenomena associated with spray combustion involving real transportation fuels. Real diesel fuels are mixtures composed of hundreds to thousands of components; thus, it is not possible to perform real fuel spray combustion simulations, even with high-performance computing. Therefore, in developing surrogate fuels composed of only a few representative hydrocarbon components, it is essential that they mimic the properties of real fuel.

Component selection for surrogate fuels is closely related to the targeted applications. Surrogates that can characterize the thermophysical properties and evaporation processes of real fuel are called “physical” surrogates,¹ and surrogates that are capable of mimicking fuel chemical kinetics-related phenomena (for example, gas-phase ignition delay times, laminar flame speed, etc.) are considered as “chemical” surrogate models.² In the previous research, much emphasis has been put on gas-phase chemical kinetics. Therefore, the suggested surrogates usually focus on a single-phase gas combustion process.

However, some of the chemical surrogates are not able to match physical properties, including fuel volatility or distillation curve, and, thus, are not suitable for characterizing the complex process of droplet heating and evaporation. In many cases, surrogate development and validation studies predict the distillation curve, evaporation process, and chemical kinetics separately. For spray combustion modeling, fuels experience thermophysical (heating and evaporation) and chemical kinetics (ignition and combustion) processes. To model the multiphase spray combustion process, a “unified” diesel surrogate that can emulate the physical, chemical, and combustion (kinetics) properties of the real diesel fuel is highly desirable.

Research activities on developing surrogate diesel fuels have been active for the past few decades. Recent proposed multicomponent-based surrogates are summarized in Table 1. Table 1a summarizes the surrogates based on physical and chemical property predictions, while Table 1b summarizes surrogates focused on chemical kinetics properties of diesel predictions. Luo et al.³ uses a three-component surrogate to simulate ignition delay and combustion phenomenon in a simplified engine. This surrogate, however, shows high discrepancy in physical properties, such as density and C/H mass ratio. Liang et al.⁴ uses two different surrogates for engine

Received: July 6, 2017

Revised: November 8, 2017

Published: November 9, 2017



Cite this: *RSC Adv.*, 2017, 7, 43483

A three dimensional sulfur/reduced graphene oxide with embedded carbon nanotubes composite as a binder-free, free-standing cathode for lithium–sulfur batteries†

Kongqing Ying,^a Ran Tian,^a Jie Zhou,^a Hua Li,^{ID}*^{ab} Roberto Dugnani,^c Yanyan Lu,^d Huanan Duan,^{ID}^a Yiping Guo^{ID}^a and Hezhou Liu^{ab}

Binder-free and free-standing electrodes have been regarded as an attractive and promising structure in lithium–sulfur batteries. In this work we describe how a free-standing sulfur/reduced graphene oxide with embedded carbon nanotubes electrode has been synthesized by a novel, facile and eco-friendly method taking advantage of the solubility difference of polar and nonpolar materials. First, the nonpolar elemental sulfur is dissolved in a weak polar solvent (ethanol) by intensive ultrasonication. During a subsequent heavy polar solvent (deionized water) drop-wise procedure, nano-sized sulfur particles are precipitated from the ethanol and deposited on the dispersed carbon nanotubes and graphene oxide. Noticeably, since ascorbic acid is taken as the reducing agent for graphene oxide at 75 °C, the process produces no toxic byproducts. Besides, the ‘as-designed’ sulfur/reduced graphene oxide with embedded carbon nanotubes displays a unique structure with both the sulfur and carbon nanotubes embedded in the basal plane of reduced graphene oxide. The manufactured electrode is found to exhibit excellent rate capability and cyclability, with the maximum capacity of 1025 mA h g^{−1} observed in the third cycle and a stable capacity of 704 mA h g^{−1} after 100 cycles.

Received 5th July 2017
Accepted 1st September 2017

DOI: 10.1039/c7ra07418b

rsc.li/rsc-advances

Introduction

With the development of portable devices, energy storage devices like rechargeable batteries are in high demand. Currently, in the portable devices' battery systems, lithium-ion batteries (LIBs) play a dominant role due to their high performance and being relatively light weight. But the energy density limits of LIBs cannot fit the increased demand of electric and large-scale vehicles. Researchers are exploring new energy storage devices such as lithium–sulfur batteries (Li–S batteries)¹ and hydrogen storage,² which could replace the commercial lithium-ion batteries due to their abundance and high energy density.

For Li–S batteries cathode, many kinds of carbon could act effectively as electric conductors to enhance the utilization of the insulating sulfur and could also serve as a porous framework to contain redox products.^{3–5} Various researchers have used

different kinds of carbon to improve the property of S/C cathode as a result of the low density, abundance in nature, low cost, among other advantages of Li–S batteries.^{6–9} The volume changes during charging and discharging of S/C cathode could be effectively suppressed because of the combination of the mesoporous carbon.¹⁰ At the same period, carbon nanotubes (CNTs) have been introduced into Li–S batteries system with benefits such as its extremely high conductivity and low density. It has been shown that carbon nanotubes with 155 °C heat treatment did improve cell performance, by both an increase in discharge capacity and an enhancement in cycle life. This also indicated a new stabilization mechanism of sulfur in carbon.^{11–13} Unfortunately the loss of the sulfur cathode material causes significant capacity fading in lithium/sulfur cells which cannot be solved effectively by mesoporous carbon. Therefore, graphene oxide with reactive functional groups has been used to immobilize sulfur and lithium polysulfides *via* chemical approaches. In addition, the mechanism of polysulfide immobilization on defective graphene has also been studied.^{8,14,15}

Regrettably, the cathode materials of the composites mentioned above require the use of binders and aluminum foils as a part of the cell components. Conventionally designed electrodes use either PVDF (polyvinylidene fluoride) or PEO (poly(ethylene glycol)) binders. Moreover, the composites need to be ground into powder and then mixed with carbon black and

^aState Key Laboratory of Metal Matrix Composites, School of Materials Science and Engineering, Shanghai Jiao Tong University, Dongchuan Road No. 800, Shanghai 200240, China. E-mail: lih@sjtu.edu.cn

^bCollaborative Innovation Center for Advanced Ship and Deep-Sea Exploration, Shanghai Jiao Tong University, China

^cUniversity of Michigan-Shanghai Jiao Tong University Joint Institute, China

^dShanghai Petrochemical Academy, Shanghai 201512, China

† Electronic supplementary information (ESI) available. See DOI: 10.1039/c7ra07418b




Cite this: *RSC Adv.*, 2017, 7, 37130

Characterization of the damping and mechanical properties of a novel (ZnSnO₃/PVDF)@PPy nanofibers/EP composite†

Chunmei Zhang,^{‡a} Hua Li,^{‡*ab} Zhangzhi Zhuo,^c Roberto Dugnani,^d Wenchao Xue,^a Yong Zhou,^a Yujie Chen^{*a} and Hezhou Liu^{ab}

In this paper, a novel (ZnSnO₃/PVDF)@PPy nanofiber (ZPPs)/EP composite (ZPPE) was prepared and its damping and mechanical properties were investigated. The morphology and structure of the composites were studied using X-ray diffraction (XRD), scanning electron microscopy (SEM), and energy dispersive spectroscopy (EDS). The damping performance was investigated by dynamic mechanical analysis (DMA), and the results showed that for composite ZPPE-60 (i.e., 60% wt ZnSnO₃), the storage modulus (E'), loss modulus (E'') and loss factor ($\tan \delta$) values at 20 °C and 1 Hz increased respectively by about 195%, 655% and 330% compared with the epoxy matrix due to the piezo-damping effect (external mechanical energy–electrical energy–heat energy) and internal friction effect (from fiber–fiber and fiber–matrix friction). The flexural strength and Shore D hardness were also measured to test the composites' mechanical and wear resistance properties. The results suggested that the fabricated ZPPE composites can be used as good structural damping materials.

Received 6th June 2017

Accepted 18th July 2017

DOI: 10.1039/c7ra06328h

rsc.li/rsc-advances

1. Introduction

Vibrations and noise generated from automobile, construction, manufacturing industries, *etc.*, negatively affect the design lifetime of engineered structures and could also be harmful to human health and safety. The reduction of vibrations and noise in the aerospace and military fields, *etc.*, has also been extensively researched due to its great strategic implications. Therefore the study of vibration and noise reduction is currently very important both in civil and military fields.^{1–7}

Generally, the loss factor ($\tan \delta$) is used to characterize the damping behavior of a material. Materials displaying high $\tan \delta$ values can dissipate external mechanical vibrations and noise into heat more effectively. Polymers are the most widely used damping materials and, in particular epoxy resins have been extensively utilized in civil and military applications due to their high mechanical strength, low volumetric shrinkage, and good curing characteristics.^{8–12} Significant damping for epoxy resin is

usually limited to the temperature range of $T_g \pm 10$ °C, since external mechanical energy is dissipated into heat mainly *via* the friction among macromolecule chains near T_g . However, most applications for damping materials require to be used near room temperature hence it is paramount to improve the damping behavior of epoxy polymer near room temperature.

Piezo-damping composite is a new kind of damping materials which is composed of the piezoelectric phase, electro-conductive phase, and the polymer matrix. For these class of composites, external mechanical energy can be dissipated *via* three routes: the viscoelasticity of the polymer matrix itself, internal friction, and the piezo-damping effect. By introducing the piezoelectric phase and conductive phase into the polymer matrix, some of the energy associated with vibration and acoustic noise transforms into electrical energy through the piezoelectric effect of the piezoelectric ceramics. Subsequently, the generated electrical energy can be dissipated into heat as it flows through the composite's resistive phase. Besides, some mechanical energy is dissipated through friction generated by boundary sliding (filler–filler) and interfacial sliding (filler–matrix).^{13–15} Various piezo-damping materials using epoxy resin or rubber as the polymer matrix have been studied in the past and some promising results have been already reached.^{16–19} Piezoelectric ceramics with perovskite structure are normally used as the piezoelectric phase in the piezo-damping materials due to their efficient ferroelectric properties. Among them, lead-containing piezoelectric ceramics, such as lead zirconate titanate (PZT), are widely used due to their high piezoelectric coefficient (d_{33}). Nonetheless the fabrication of lead-containing piezoelectric ceramics generates toxic by-

^aState Key Laboratory of Metal Matrix Composites, School of Materials Science and Engineering, Shanghai Jiao Tong University, Dongchuan Road No. 800, Shanghai 200240, China. E-mail: lih@sjtu.edu.cn; yujiechen@sjtu.edu.cn

^bCollaborative Innovation Center for Advanced Ship and Deep-Sea Exploration, Shanghai Jiao Tong University, China

^cWuHu State-owned Factory of Machining, Jiujiang District Wanli Village No. 99, WuHu 241000, China

^dUniversity of Michigan-Shanghai Jiao Tong University Joint Institute, China

† Electronic supplementary information (ESI) available. See DOI: 10.1039/c7ra06328h

‡ These authors contributed equally to this work.



SCIENTIFIC REPORTS

OPEN

Fabricating fast triggered electro-active shape memory graphite/silver nanowires/epoxy resin composite from polymer template

Jie Zhou¹, Hua Li^{1,2}, Ran Tian¹, Roberto Dugnani³, Huiyuan Lu¹, Yujie Chen¹, Yiping Guo¹, Huanan Duan¹ & Hezhou Liu^{1,2}

In recent years shape-memory polymers have been under intense investigation due to their unique mechanical, thermal, and electrical properties that could potentially make them extremely valuable in numerous engineering applications. In this manuscript, we report a polymer-template-assisted assembly manufacturing strategy used to fabricate graphite/silver nanowires/epoxy resin (PGSE) composite. In the proposed method, the porous polymer foams work as the skeleton by forming three-dimensional graphite structure, whereas the silver nanowires act as the continuous conductive network. Preliminary testing on hybrid foams after vacuum infusion showed high electrical conductivity and excellent thermal stability. Furthermore, the composites were found to recover their original shape within 60 seconds from the application of a 0.8 V mm^{-1} electric field. Notably, the reported shape-memory polymer composites are manufactured with readily-available raw materials, they are fast to manufacture, and are shape-controlled.

Shape-memory polymers (SMPs) and their composites (SMPCs), can recover their original (or permanent) shape upon exposure to external stimuli¹. There are various types of methods to stimulate the deformation, of which thermal- and electro-responsive are the most common^{2,3}. SMPs have numerous advantages such as being light-weight, inexpensive, and easy to manufacture; additionally they display high deformability, good biodegradability and easy-to-tailor glass transition temperatures compared with shape memory alloys and shape memory ceramics⁴⁻⁷. Therefore, in recent years an increasing number of international researchers have been focusing on the development of the shape memory effect in polymers^{8,9}. Comparing with SMPs, SMPCs have higher strength, higher stiffness, and distinctive physical characteristics determined by the type and amount of added fillers. So many attractive features have already inspired a variety of applications in the fields of aerospace¹⁰, biomedicine¹¹, textiles¹², etc.

Graphite, which has outstanding electrical¹³, mechanical¹⁴, and optical properties¹⁵, has been receiving considerable attention as one of the most promising engineering materials. However, graphite's poor dispersion characteristics have partially limited its application¹⁶. Various methods have been proposed to improve graphite's dispersion, such as for instance chemical exfoliation¹⁷. Unfortunately, graphite oxide synthesized by chemical exfoliation has been found to display abundant defects and chemical moieties^{18,19}, which significantly decrease its electrical conductivity. Even after graphite oxide (GO) is reduced, the reduced graphite oxide (RGO) is still less conductive than pristine graphite²⁰. In addition, aggregation and stacking between individual graphite sheets (driven by the strong π - π interaction) greatly compromise the intrinsically high specific surface area of graphite. Furthermore, the high conductivity of graphite is also largely compromised by the inter-sheet contact resistance. The three-dimensional (3D) graphite structure was deemed to alleviate the aforementioned problems currently hindering the performance of graphite composites. The 3D graphite network is continuous and displays higher conductivity due to increasing inter-sheet junctions. It is believed that developing 3D structures of graphite would

¹State Key Laboratory of Metal Matrix Composites, School of Materials Science and Engineering, Shanghai Jiao Tong University, Shanghai, China. ²Collaborative Innovation Center for Advanced Ship and Deep-Sea Exploration, Shanghai Jiao Tong University, Shanghai, China. ³University of Michigan-Shanghai Jiao Tong University Joint Institute, Shanghai, China. Jie Zhou and Hua Li contributed equally to this work. Correspondence and requests for materials should be addressed to H.L. (email: lih@sjtu.edu.cn) or Y.C. (email: yujiechen@sjtu.edu.cn)


Cite this: *RSC Adv.*, 2017, 7, 41321

Facile fabrication of ultra-light and highly resilient PU/RGO foams for microwave absorption†

Chunmei Zhang,^{‡a} Hua Li,^{‡*ab} Zhangzhi Zhuo,^c Roberto Dugnani,^d Chongyang Sun,^a Yujie Chen^{*a} and Hezhou Liu^{ab}

Using commercial polyurethane foams as templates, PU/RGO foams were prepared by a simple dip-coating method, which is economical and suitable for industrialized production. The formation of RGO was studied using X-ray diffraction (XRD), X-ray photoelectron spectroscopy (XPS), Raman spectroscopy, and scanning electron microscopy (SEM). The microwave absorption properties of the PU/RGO foams were investigated and the results show that for composites with a RGO loading of 31.3 wt%, the minimum reflection loss of the PU/RGO foam can reach -50.8 dB at 12.9 GHz, and the frequency bandwidth at less than -10 dB is from 10.75 to 15.95 GHz at a thickness of 2.5 mm. In addition, the results of cyclic compression tests and twisting experiments indicated that the PU/RGO composite was highly resilient. Moreover, the measured density of the foam material is just approximately 0.027 g cm $^{-3}$ which is considerably smaller compared with most commercial wave-absorbing materials. The fabricated PU/RGO foams can be used as good microwave absorbing commercial cladding materials, with particularly lightweight and highly elastic properties.

Received 15th July 2017
Accepted 14th August 2017

DOI: 10.1039/c7ra07794g

rsc.li/rsc-advances

1. Introduction

Microwave absorbing materials are becoming increasingly important due to the extensive use of wireless communication devices.^{1–3} Microwave absorbing materials with low density, superior mechanical performance, and good wave-absorption ability are in high demand in various fields, such as civil, military and aerospace applications.^{4,5} Graphene is essentially a two-dimensional (2D) sheet composed of sp²-bonded carbon atoms which is extensively researched due to its excellent electrical, thermal, mechanical properties and high specific surface area.^{6–8} Recently graphene has been widely used in applications such as super capacitors,^{9–11} oil absorption materials,^{12–14} sensors,^{15–17} and polymer composites.^{18–21}

Good electrical conductivity is harmful for EM wave absorption according to the impedance match mechanism, and due to the high conductivity, graphene has a strong dielectric loss but a weak attenuation to microwaves. However, chemically reduced graphene oxide (RGO) with residual defects and

functional groups possesses considerably lower conductivity and improved impedance-match characteristics. Wang *et al.*²² found that besides dielectric loss, defect polarization relaxation and functional groups' electronic dipole relaxation were also introduced into RGO, which was beneficial for the improvement of microwave absorbing properties of the material. Recently, graphene-containing materials play an important role in electromagnetic wave absorbers. Zhang *et al.*²³ synthesized RGO/CuS/PVDF composites and with a filler loading of 5 wt%, the maximum loss was -32.7 dB at 10.7 GHz with a thickness of just 2.5 mm. Pan *et al.*²⁴ studied the microwave absorption properties of Fe₃O₄@SiO₂@RGO nanocomposites with a maximum reflection loss up to -26.6 dB at 9.7 GHz and the bandwidth below -10 dB being from 4.4 to 17.3 GHz. Wang *et al.*²⁵ fabricated RGO/Co₃O₄/poly(vinylidene fluoride) composites, and with a filler loading of 10 wt%, the composite showed excellent microwave absorbing properties with reflection loss low to -25.05 dB at 11.6 GHz at a thickness of 4 mm. Guo *et al.*²⁶ prepared rGO@MoS₂/PVDF composites, and the maximum reflection loss can reach -43.1 dB at 14.48 GHz with a filling rate of only 5.0 wt%, and the frequency bandwidth below -10 dB was 3.6–17.8 GHz with a thickness of 1–5 mm. Guo *et al.*²⁷ fabricated rGO@barium titanate/poly(vinylidene fluoride) (PVDF) composite exhibiting the highest reflection coefficients up to -33.2 , -45.3 , -32.9 and -22.8 dB with filler amounts of 10, 15, 20 and 25 wt% at thicknesses of 1–5 mm. Luo *et al.*²⁸ synthesized a ternary composite composed of reduced graphene oxide, Fe₃O₄ porous nanospheres and polyaniline with a reflection loss reaching -29.51 dB at 14.69 GHz. Kowsari *et al.*²⁹ prepared magnetic functional graphene oxide (MFGO)/epoxy

^aState Key Laboratory of Metal Matrix Composites, School of Materials Science and Engineering, Shanghai Jiao Tong University, Dongchuan Road No. 800, Shanghai 200240, China. E-mail: lih@sjtu.edu.cn; yujiechen@sjtu.edu.cn

^bCollaborative Innovation Center for Advanced Ship and Deep-Sea Exploration, Shanghai Jiao Tong University, China

^cWuHu State-Owned Factory of Machining, Jiujiang District Wanli Village No. 99, WuHu 241000, China

^dUniversity of Michigan–Shanghai Jiao Tong University Joint Institute, China

† Electronic supplementary information (ESI) available. See DOI: 10.1039/c7ra07794g

‡ These authors contributed equally to this work.

Integrity monitoring of adhesively bonded joints via an electromechanical impedance-based approach

Yitao Zhuang¹, Fotis Kopsaftopoulos², Roberto Dugnani³
and Fu-Kuo Chang¹

Structural Health Monitoring

1–15

© The Author(s) 2017

Reprints and permissions:

sagepub.co.uk/journalsPermissions.nav

DOI: 10.1177/1475921717732331

journals.sagepub.com/home/shm



Abstract

Monitoring the bondline integrity of adhesively bonded joints is one of the most critical concerns in the design of aircraft structures to date. Due to the lack of confidence on the integrity of the bondline both during fabrication and service, the industry standards and regulations require assembling the primary airframe structure using the inefficient “black-aluminum” approach, that is, drill holes and use fasteners. Furthermore, state-of-the-art non-destructive evaluation and structural health monitoring approaches are not yet able to provide mature solutions on the issue of bondline integrity monitoring. Therefore, the objective of this work is the introduction and feasibility investigation of a novel bondline integrity monitoring method that is based on the use of piezoelectric sensors embedded inside adhesively bonded joints in order to provide an early detection of bondline degradation. The proposed approach incorporates (1) micro-sensors embedded inside the adhesive layer leaving a minimal footprint on the material, (2) numerical and analytical modeling of the electromechanical impedance of the adhesive bondline, and (3) electromechanical impedance-based diagnostic algorithms for monitoring and assessing the bondline integrity. The experimental validation and assessment of the proposed approach is achieved via the design and fabrication of prototype adhesively bonded lap joints with embedded piezoelectric sensors and a series of mechanical tests under various static and dynamic (fatigue) loading conditions. The obtained results demonstrate the potential of the proposed approach in providing increased confidence on the use of adhesively bonded joints for aerospace structures.

Keywords

Adhesively bonded structures, bondline integrity monitoring, electromechanical impedance, finite element model, kissing bond detection, piezoelectric sensors, structural health monitoring

Introduction

In the last decade, significant progress has been made in the development and improvement of methods for the investigation of adhesively bonded joints and structures. Bondline integrity monitoring is still one of the most critical concerns in the design of aircraft and spacecraft structures to date. Although adhesively bonded joints have demonstrated superior properties over mechanically fastened joints, current standards still require the use of fasteners along with the adhesive due to the lack of confidence on monitoring the integrity of bondlines during both the fabrication process and service life. Regardless of the nature of adhesive and adherents, any adhesively bonded system may be considered as a multilayered assembly, in which the adhesive must provide the integrity of the whole

construction. Therefore, potential structural defects of the adhesive can negatively influence the integrity of the bonded joint and decrease the expected strength of the assembly.^{1–3}

The main bondline defects that can impact the quality of the adhesive strength are voids, discontinuities, delaminations, “kissing” bonds, porosity, air bubbles

¹Department of Aeronautics & Astronautics, Stanford University, Stanford, USA

²Department of Mechanical, Aerospace and Nuclear Engineering, Rensselaer Polytechnic Institute, NY, USA


³UM-SJTU Joint Institute (JI), 800 Dongchuan Rd, Shanghai, China

Corresponding author:

Fotis Kopsaftopoulos, Aeronautics & Astronautics Department, Stanford University, Stanford, CA 94305, USA.

Email: kopsaf@rpi.edu

Analytical model of lap-joint adhesive with embedded piezoelectric transducer for weak bond detection

Journal of Intelligent Material Systems and Structures
2017, Vol. 28(1) 124–140
© The Author(s) 2016
Reprints and permissions:
sagepub.co.uk/journalsPermissions.nav
DOI: 10.1177/1045389X16645864
journals.sagepub.com/home/jim


Roberto Dugnani¹ and Fu-Kuo Chang²

Abstract

In recent years, the aerospace and automotive industries experienced a growing interest in the implementation of structural members' bonding using adhesive films. Adhesive joints contribute to manufacturing savings and are advantageous from a structural prospective as they provide a relatively uniform stress distribution at the bonded region, hence reducing local stress concentration. Regretfully, the adhesive bonds' strength is vulnerable to the presence of defects which limits their use for structural purposes. A particularly dangerous class of defects—generically referred to as “kissing bond”—consists of localized imperfections that do not provide adequate bonding between the adherent and the adhesive yet maintaining the two surfaces in contact. Past attempts at detecting kissing bonds using ultrasonics were only marginally successful stressing the need to search for more reliable methods. This article describes a novel, in situ, impedance-based method for bond-line degradation detection during the service life of a structure. The method relies on piezoelectric transducers embedded within the adhesive bond-line and actuated by a low-voltage harmonic signal. The article focuses on deriving an approximate analytical model describing the dynamic behavior of the actuator embedded in the homogeneous bond-line. A study describing the sensitivity of the electro-mechanical response of the transducer to the changes in various bond-line properties and adhesion conditions is also presented.

Keywords

Lap-joint, bond-line, impedance, piezoelectric, sensor, structural health monitoring, adhesive, actuator, Lamb waves, diagnostics, prognostics

Introduction

Structural adhesive bonds have become of great interest to both the automotive and the aeronautic industries due to attractive potential benefits such as uniform stress distribution, light weight, and stress concentration reduction. Regretfully, the assessment of the bonding interface integrity is one of the most challenging problems in quantitative non-destructive evaluation (NDE), and up-to-date, the use of adhesive bonding is limited for the most part to non-structural elements. Currently, the most challenging type of inspection is related to “interface weakness,” which happens when the adhesive and the adherent are in direct physical contact but lack bonding strength. Traditional ultrasonic techniques cannot unequivocally distinguish between a good and a weak interface as acoustic reflections are weakly affected by the strength of the bond.

Various damage detection techniques based on different types of acoustic waves have been described in the literature. Rokhlin and Marom (1986) and Brotherhood et al. (2003) proposed using a

combination of incident and shear waves to detect weak interfaces in bond-lines. The methods exploited the fact that the ultrasonic reflection coefficient at the interface between the adhesive and the adherent is sensitive to boundary imperfections as also shown by Pilarski and Pawlowski (1980). Nagy (1991) reported that the utilization of relatively high-frequency acoustic beams could result in the successful damage detection for normal-beam ultrasonic techniques especially for the case of shear waves. Nonetheless, the practical difficulties in generating and receiving normal incident shear waves led to the development of ultrasonic oblique incidence technique as, for instance, described by Pilarski and Rose (1998). Kühn and Lutsch (1961) and

¹UM-SJTU JI, Shanghai, China

²Stanford University, Stanford, CA, USA


Corresponding author:

Roberto Dugnani, UM-SJTU JI, 800 Dongchuan Rd., Shanghai 200240, China.

Email: roberto.dugnani@sjtu.edu.cn



Facile synthesis of three-dimensional lightweight nitrogen-doped graphene aerogel with excellent electromagnetic wave absorption properties

Jie Zhou¹, Yujie Chen¹, Hua Li^{1,2,*} , Roberto Dugnani³, Qi Du¹, Hafeez UrRehman¹, Hongmei Kang¹, and Hezhou Liu^{1,2}

¹State Key Laboratory of Metal Matrix Composites, School of Materials Science and Engineering, Shanghai Jiao Tong University, Dongchuan Road No. 800, Shanghai 200240, China

²Collaborative Innovation Center for Advanced Ship and Deep-Sea Exploration, Shanghai Jiao Tong University, Shanghai, China

³University of Michigan-Shanghai Jiao Tong University Joint Institute, Shanghai, China

Received: 20 August 2017

Accepted: 17 November 2017

Published online:

27 November 2017

© Springer Science+Business Media, LLC, part of Springer Nature 2017

ABSTRACT

The widespread use of communication facilities and electronic devices has increased the demand for novel high-efficiency and lightweight microwave absorption materials. In this work, we propose using N-doped graphene (NG)/wax composites, where an interconnected 3D graphene network is used as filler in a wax matrix. Nitrogen atoms were substitutionally doped into the graphene lattice by hydrothermal method. It was found that controlling the amount of NG could effectively modulate the electrical properties of graphene. Inspection of the samples prepared showed that to a large extent, the vacuum infusion method effectively retained the graphene intact 3D structure. Samples filled with 3.6 wt% NG exhibited the most prominent microwave absorption properties; the minimum reflection loss registered was 53.25 dB at 13.10 GHz for a sample thickness of 3.3 mm, and the bandwidth of the reflection loss less than 10 dB (90% absorption) can reach up to 8.15 GHz. The result indicates that the nitrogen-doped graphene can greatly improve the dielectric loss of electromagnetic wave absorber. More importantly, the work presented provides the framework for a unique facile approach to manufacture low-cost NG/wax composites with strong electromagnetic wave absorption ability at very low filler loading.

Introduction

With the recent increase in the use of electronic devices and communication facilities, concern has been raised because electromagnetic (EM) pollution

might potentially harm both highly sensitive precision electronic equipment and human health. Electromagnetic wave absorption materials can mitigate or even overcome these mentioned problems by reducing the stray electromagnetic waves [1, 2]. Great

Address correspondence to E-mail: lih@sjtu.edu.cn



Residual stress in ion-exchanged silicate glass: An analytical solution

Roberto Dugnani

University of Michigan - Shanghai Jiao Tong University Joint Institute, 800, Dong Chuan Road, Shanghai 200240, China



ARTICLE INFO

Keywords:

Glass
Silicate
Ion-exchange
Analytical solution
Residual stress
Relaxation

ABSTRACT

The ion-exchanged residual stress profile influences both the strength and the wear-resistance of glass hence its description is of great importance. Currently, residual stress profiles of silicate glasses can only be estimated by numerical time-integration based on the known ionic concentration profile and the expected stress relaxation behavior of the glass. In this work, we derived and validated the constant coefficients analytical solution describing the residual stress profile in single-step ion-exchanged glasses. The proposed solution is based on Sane and Cooper's model and assumed that both the generalized Maxwell stress relaxation function applied and that a constant ionic inter-diffusion coefficient could accurately describe the behavior of the system. Furthermore, an analytical approximation for composition-dependent stress relaxation behavior of the glass was proposed. Examples of how the newly developed analytical description of the stress profile could be fitted through regression analysis to available residual stress data were also presented.

1. Introduction

The ion exchange process occurs when a silicate glass containing mobile cation (e.g., Na^+ , Li^+) is exposed to an environment with high concentration of a different mobile cation (e.g., K^+ , Na^+). Such environment generally consists of a molten salt (e.g., KNO_3 , NaNO_3) at a temperature high enough to overcome the activation energy for the glass inter-diffusion but lower than the strain point of the glass. As the glass sample is immersed in the molten bath, the ions near the surface diffuse out of the glass sample and are substituted by larger ions from the salt bath [1]. Due to the different ionic radii between the diffusing atoms, normally residual compressive stresses are introduced into the glass although tensile stresses would also be theoretical possible through multi-step ion exchange. In binary ion-exchange systems, the exchange cations diffuse at rates proportional to the local ionic fraction of each species. Often times, an inter-diffusion coefficient, \bar{D} , is used to describe the overall ion-exchange diffusion process. Although the inter-diffusion coefficient is a function of both the self-diffusion coefficients and of the local ionic fraction of each species, the Na^+ - K^+ inter-diffusion coefficients in alumino-silicate (ASG) and soda-lime glasses (SLG) has been reported to be nearly constant [2,3]. Gy [4] for instance found that in SLG, the inter-diffusion coefficient at low temperatures (420–460 °C) and short exchange times (72 h) did not vary considerably, especially near the glass surface. The inter-diffusion coefficient is generally assumed to follow an Arrhenius relationship:

$$D = D_0 \exp\left(-\frac{e}{RT}\right) \quad (1)$$

In Eq. (1), D_0 (m^2/s) is a material constant, e (J/mol) the activation energy, R (J/mol·K) the gas constant, and T (K) the absolute temperature of the salt bath. Based on Eq. (1), high salt bath temperatures promote high diffusion rates. At the same time, the high bath temperature induces visco-elastic relaxation in the glass hence reducing the stress build-up magnitude. It follows that both diffusion and relaxation effects need to be carefully accounted for when designing a ion-exchanged residual stress profile.

Knowledge of the residual stress field has great practical interest as the strength of the glass can be linked to both the depth of the compressive layer (DOL) and the maximum surface compressive stress (CS) of glass articles after ion-exchange. In the past, an equation in integral form (Eq. (2)) was put forward by Sane and Cooper [5] in the attempt to describe the residual stress field after ion exchange in a single step exchange bath:

$$\sigma(x, t) = -\frac{B \cdot E}{1 - \nu} \int_0^t R(t - t') \frac{\partial}{\partial t'} C(x, t') dt' \quad (2)$$

The term, $C(x, t)$, stands for the ionic concentration near the surface of the glass. The terms B ($\text{wt}\%^{-1}$), E (Pa), and ν refer to the dilation coefficient, the Young's modulus, and the Poisson ratio of the silicate glass respectively. The equation assumed that the ionic distribution function, $C(x, t)$, the Young's modulus, the Poisson's ratio, the dilation constant, and the stress relaxation function, $R(t)$, were known. Sane and Cooper's equation has been often used in the literature to describe the residual stress profile as for instance in Shen and Green [6], and recently by Seaman et al. [7]. In all cases, the equation had to be solved

E-mail address: roberto.dugnani@sjtu.edu.cn.

<http://dx.doi.org/10.1016/j.jnoncrysol.2017.06.027>

Received 15 April 2017; Received in revised form 11 June 2017; Accepted 19 June 2017

Available online 30 June 2017

0022-3093/ © 2017 Elsevier B.V. All rights reserved.



Contents lists available at ScienceDirect

International Journal of Heat and Mass Transfer

journal homepage: www.elsevier.com/locate/ijhmt

Effects of nozzle configuration on internal flow and primary jet breakup of flash boiling fuel sprays

Shengqi Wu^a, Min Xu^{a,*}, David L.S. Hung^{a,b}, Hujie Pan^a^a School of Mechanical Engineering, Shanghai Jiao Tong University, National Engineering Laboratory of Electronic Control Technology, Shanghai 200240, China^b University of Michigan – SJTU Joint Institute, Shanghai Jiao Tong University, Shanghai 200240, China

ARTICLE INFO

Article history:

Received 29 September 2016

Received in revised form 23 February 2017

Accepted 21 March 2017

Available online 30 March 2017

Keywords:

Flash boiling spray

2D transparent nozzle

Internal flow

Primary jet breakup

Nozzle configuration

ABSTRACT

Fuel spray plays more vital role in governing fuel economy and emission quality of IC engines due to the wide application of direct injection system in automotive engines. High temperature fuel spray, namely flash boiling spray, has been documented to improve fuel atomization and evaporation with less energy consumption compared with high pressure fuel spray. It is because the hot exhaust gas and coolant are two potential energy sources can be used to heat the fuel. Most of existing research works of flash boiling spray focus on investigating the spray behavior outside the nozzle, and limited studies can be found about the in-nozzle superheated flow. In this study, a two-dimensional transparent slit nozzle was designed to reveal the in-nozzle flow under various superheated conditions. Both internal flow and near-nozzle fuel jet were investigated using high-speed backlit imaging technique to acquire a better understanding of the primary breakup process of flash boiling sprays. The slit thickness was 40 μm with well-adjusted nozzle length and inlet corner radius to investigate the effects of nozzle configuration. The ambient pressure ranged from 40 kPa to 190 kPa, and fuel temperature varied from 41 $^{\circ}\text{C}$ to 71 $^{\circ}\text{C}$, which produced a wide range of superheated conditions. N-pentane was chosen as test fluid with an injection pressure of 0.6 MPa. Experimental results showed that the bubbles occurring inside the nozzle near the nozzle exit affected the near-nozzle fuel jet characteristics. Stronger superheated conditions resulted in larger in-nozzle bubbles, which facilitated the jet break-up process significantly. Longer nozzle and nozzle with sharp inlet corner led to larger inner bubble volume fraction and narrower liquid core of near-nozzle fuel jet. In summary, the effects of nozzle configuration on in-nozzle flow and near-nozzle fuel jet were revealed with more fundamental understanding of the primary breakup process of flash boiling sprays.

© 2017 Elsevier Ltd. All rights reserved.

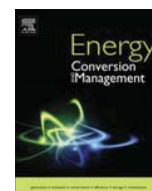
1. Introduction

Flash boiling fuel spray, proven to be highly atomized even at a low injection pressure, is beneficial to improve fuel economy and reduce emissions of IC engines [1–3]. Extensive experimental [4–8] and numerical studies [9–12] can be found about flash boiling fuel spray characteristics. These studies show that flash boiling fuel spray exhibits different atomization and evaporation characteristics from conventional liquid fuel spray, including wider spray structure [4,5], smaller drop sizes [6], faster evaporation [7], and larger momentum transfer to surrounding gas [8]. Superheat degree, which is defined as the difference between fuel temperature and fuel boiling temperature at the ambient pressure condition, has been experimentally demonstrated to govern the flash

boiling characteristics [5]. In addition, it is documented that the nozzle internal flow of flash boiling spray greatly affects the spray atomization quality [13–16]. Nozzle internal flow not only influences the flow characteristics at the nozzle exit, but also plays a vital role in governing fuel spray formation. Park and Lee [13] studied the internal flow and external flow patterns simultaneously under superheated conditions. They showed that bubbles were generated inside the nozzle which controlled the external spray disintegration process outside the nozzle. Günther and Wirth [14] found that evaporation inside the nozzle had a great impact on superheated atomization, and hence on the resulting spray characteristics. Wu et al. [15] also found that fuel already evaporated inside the nozzle near the nozzle exit, and the in-nozzle flash boiling bubbles resulted in faster fuel atomization and influenced the spray structure. All these results indicate that in-nozzle evaporation exists under superheated conditions, and it affects the spray atomization and evaporation.

* Corresponding author.

E-mail addresses: shengqiwu@sjtu.edu.cn (S. Wu), mxu@sjtu.edu.cn (M. Xu).



Influence of swirl ratio on fuel distribution and cyclic variation under flash boiling conditions in a spark ignition direct injection gasoline engine



Jie Yang^a, Min Xu^{a,*}, David L.S. Hung^{a,b}, Qiang Wu^a, Xue Dong^a

^a School of Mechanical Engineering, Shanghai Jiao Tong University, National Engineering Laboratory for Automotive Electronic Control Technology, Shanghai 200240, China

^b University of Michigan-Shanghai Jiao Tong University Joint Institute, Shanghai Jiao Tong University, Shanghai 200240, China

ARTICLE INFO

Article history:

Received 17 November 2016

Received in revised form 4 February 2017

Accepted 9 February 2017

Available online 24 February 2017

Keywords:

Swirl ratio

Fuel distribution

Laser induced fluorescence

Cycle-to-cycle variation

ABSTRACT

One effective way of suppressing the cycle-to-cycle variation in engine is to design a combustion system that is robust to the root causes of engine variation over the entire engine working process. Flash boiling has been demonstrated as an ideal technique to produce stable fuel spray. But the generation of stable intake flow and fuel mixture remains challenging. In this study, to evaluate the capability of enhanced swirl flow to produce repeatable fuel mixture formation, the fuel distribution inside a single cylinder optical engine under two swirl ratios were measured using laser induced fluorescence technique. The swirl ratio was regulated by a swirl control valve installed in one of the intake ports. A 266 nm wavelength laser sheet from a frequency-quadrupled laser was directed into the optical engine through the quartz liner 15 mm below the tip of the spark plug. The fluorescence signal from the polycyclic aromatic hydrocarbon in gasoline was collected by applying a 320–420 nm band pass filter mounted in front of an intensified charge coupled device camera. Test results show that the in-cylinder fuel distribution is strongly influenced by the swirl ratio. Specifically, under high swirl condition, the fuel is mainly concentrated on the left side of the combustion chamber. While under the low swirl flow, fuel is distributed more randomly over the observing plane. This agrees well with the measurements of the stable flame location. Additionally, the cycle-to-cycle variation of the fuel distribution were analyzed. Results show that well organized fuel mixture with lower cycle-to-cycle variation is achieved by enhanced swirl flow.

© 2017 Elsevier Ltd. All rights reserved.

1. Introduction

Spark-ignition direct-injection (SIDI) has become the mainstream technology for the automotive industry due to its improved fuel economy, higher thermal efficiency, more precise air-fuel ratio control and faster transient response [1].

However, the cycle-to-cycle variation (CCV) of engine remains a big concern. It is well known that combustion process does not behave repeatedly for consecutive engine cycles, even under the carefully maintained engine condition due to the turbulent nature of in-cylinder air motion [2]. This leads to substantial CCV of in-cylinder pressure. Variations of engine output such as the indicated mean effective pressure (IMEP) not only results in fluctuations of the engine torque, but also prohibits the engine from operating at its optimal condition, which degrades the drivability and reduces the engine power even more. Moreover, the non-optimal

cycles resulted from partial or unstable combustion will increase the hydrocarbon (HC) emission and fuel consumption.

The root causes for the combustion variations are fairly complicated [1]. Large amount of research has demonstrated that CCV of engine can be attributed to multiple factors such as variation of injection, intake flow and spark discharge [3]. Specifically, needle bouncing and pressure oscillation are the main reason for the variation of injection [4]. The pressure wave fluctuation in the intake runner, resonance and the valve dynamics all contributed to the variation of intake flow [5]. The variation of fuel spray in the engine is strongly influenced by air flow and changes with the operating conditions [6]. Even though the root causes of engine CCV are known, unveiling the mechanism for variation is difficult. Because CCV is also coupled with the in-cylinder turbulence, thereby the control of variation could be more challenging. However, instead of control the sources of variation, designing a combustion system that is robust to the root causes of variation is a viable approach to suppress the CCV of engine output. Numerical study shows that the combustion efficiency could be improved significantly through the

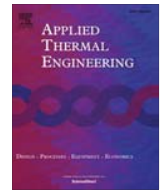
* Corresponding author.

E-mail address: mxu@sjtu.edu.cn (M. Xu).



Contents lists available at ScienceDirect

Applied Thermal Engineering

journal homepage: www.elsevier.com/locate/apthermeng

Research Paper

In-nozzle flow investigation of flash boiling fuel sprays

Shengqi Wu^a, Min Xu^{a,*}, David L.S. Hung^{a,b}, Hujie Pan^a^a School of Mechanical Engineering, Shanghai Jiao Tong University, National Engineering Laboratory of Electronic Control Technology, Shanghai 200240, China^b University of Michigan–SJTU Joint Institute, Shanghai Jiao Tong University, Shanghai 200240, China

HIGHLIGHTS

- Effects of fuel temperature and ambient pressure on in-nozzle flow characteristics are revealed.
- The relationship between in-nozzle flash boiling bubbles and near nozzle fuel jet characteristic is investigated.
- Flash boiling spray characteristics are dominated by in-nozzle fuel evaporation and outside nozzle fuel boiling.

ARTICLE INFO

Article history:

Received 11 September 2016

Revised 18 December 2016

Accepted 23 December 2016

Available online 27 December 2016

Keywords:

Flash boiling spray

2D transparent nozzle

Internal flow

Jet breakup

ABSTRACT

It is widely recognized that a well atomized spray promotes the fuel evaporation in engine cylinder and contributes to higher fuel efficiency and lower exhaust emission. Specifically, higher fuel temperature enhances the fuel spray evaporation due to the superheat phenomenon even at low injection pressure. In this study, both internal flow and near nozzle fuel jet of a two-dimensional transparent nozzle were investigated using high-speed backlit imaging technique to acquire a better understanding of the primary breakup process of flash boiling sprays. The two-dimensional slit transparent nozzle was designed to facilitate the enhanced visualization of bubbles inside the nozzle by squeezing small bubbles and eliminating overlapping bubbles. The ambient pressure ranged from 40 kPa to 190 kPa, and fuel temperature varied from 41 °C to 71 °C, to produce a wide range of superheated conditions. N-pentane was chosen as test fluid with an injection pressure was 0.5 MPa. Experimental results show that the bubbles occurring inside the nozzle near the nozzle exit under flash boiling conditions affect the shape and dynamic behavior of near nozzle fuel jet. It shows that higher fuel temperature and lower ambient pressure increase the inner bubble size and volume fraction, which led to narrower liquid core of near nozzle fuel jet. Inner bubbles facilitate the breakup process of fuel jet significantly. The breakup process of flash boiling spray can be elucidated with more fundamental understanding of bubble behavior inside the nozzle.

© 2017 Elsevier Ltd. All rights reserved.

1. Introduction

Wider adoption of direct-injection system in gasoline engines has made fuel spray more influential to engine performance and emission quality. It is because when the liquid fuel is injected into the combustion chamber directly, it must be atomized quickly to create sufficient evaporation and effective air-fuel mixture formation in a very short time. If the mixture is not well prepared, soot may be generated in rich mixture concentration zones resulted from incomplete combustion of unevaporated fuel in the combustion chamber [1,2]. Thus, it is desirable to achieve a fast evaporating fuel spray to improve fuel economy and to meet the stringent regulations of emission reductions.

It has been reported that flash boiling fuel spray can be highly atomized even at a low injection pressure to improve engine combustion stability, fuel economy, and emission reductions [3–5]. Many researchers have paid extensive attention to characterize the flash boiling fuel sprays, both experimentally [6–9] and numerically [10–13]. Their results show that flash boiling fuel spray exhibits different atomization and evaporation characteristics from conventional liquid fuel spray, including wider spray structure, smaller drop sizes, faster evaporation, and larger momentum transfer to surrounding gas. Although the superheated phenomenon has been studied extensively outside of the nozzle, accurate predictive flash boiling spray model is still unavailable. One main reason is that there should be phase transition inside the nozzle before the fuel is injected, which is not accounted for in most of the relevant spray sub-models. Therefore, many researchers have

* Corresponding author.

E-mail address: mxu@sjtu.edu.cn (M. Xu).

Investigation of Cycle-to-Cycle Variation of In-Cylinder Engine Swirl Flow Fields Using Quadruple Proper Orthogonal Decomposition

Penghui Ge

University of Michigan-Shanghai Jiao Tong
University Joint Institute,
Shanghai Jiao Tong University,
800 Dongchuan Road,
Shanghai 200240, China
e-mail: penghuige@sjtu.edu.cn

David L. S. Hung¹

Mem. ASME
University of Michigan-Shanghai Jiao Tong
University Joint Institute,
Shanghai Jiao Tong University,
800 Dongchuan Road,
Shanghai 200240, China
e-mail: dhung@sjtu.edu.cn

It has been observed that the swirl characteristics of in-cylinder air flow in a spark ignition direct injection (SIDI) engine affect the fuel spray dispersion and flame propagation speed, impacting the fuel mixture formation and combustion process under high swirl conditions. In addition, the cycle-to-cycle variations (CCVs) of swirl flow often degrade the air-fuel mixing and combustion quality in the cylinder. In this study, the 2D flow structure along a swirl plane at 30 mm below the injector tip was recorded using high-speed particle image velocimetry (PIV) in a four-valve optical SIDI engine under high swirl condition. Quadruple proper orthogonal decomposition (POD) was used to investigate the cycle-to-cycle variations of 200 consecutive cycles. The flow fields were analyzed by dividing the swirl plane into four zones along the measured swirl plane according to the positions of intake and exhaust valves in the cylinder head. Experimental results revealed that the coefficient of variation (COV) of the quadruple POD mode coefficients could be used to estimate the cycle-to-cycle variations at a specific crank angle. The dominant structure was represented by the first POD mode in which its kinetic energy could be correlated with the motions of the intake valves. Moreover, higher order flow variations were closely related to the flow stability at different zones. In summary, quadruple POD provides another meaningful way to understand the intake swirl impact on the cycle-to-cycle variations of the in-cylinder flow characteristics in SIDI engine.

[DOI: 10.1115/1.4035628]

1 Introduction

More stricter regulations of engine emission reduction and fuel efficiency improvement have been imposed on carmakers in recent years by governments and regulatory agencies around the world. The implementations of spark ignition direct injection (SIDI) engines have an advantage in achieving better fuel economy and higher power output, as opposed to the conventional port fuel injection engine where liquid fuel is injected into the intake ports [1,2]. This prevalent engine technology requires highly pressurized gasoline to be directly injected into the combustion chamber. In some applications, direct fuel injection technology allows the engine to run at specific combustion modes, such as stratified fuel charge combustion, for improved fuel efficiency with reduced emission level at low load operation.

However, the cycle-to-cycle variations (CCVs) of in-cylinder flow structure have often been linked to certain critical engine issues such as misfires and partial burns [3]. The CCV of engine flow has been studied by many researchers in recent years. An estimate of 10% power output improvement of the engine could be achieved at the same fuel consumption if the CCV would have been eliminated [4].

By virtue of the rapid development of high spatial/temporal laser diagnostic techniques, researchers are able to visualize the full evolution of in-cylinder air flow characteristics of various strokes inside an optical engine [5]. Extensive research studies of CCV have been made over investigating the consecutive flow fields [6–9]. For instance, Sick et al. [6] reviewed various high-

speed diagnostic developments with a focus on application into SIDI engines. They concluded that the identification of random events such as CCV and ignition instabilities had been well progressed by the model and device developments with unprecedented access to the in-cylinder flow. Depending on different levels of swirl motion, the swirl and tumble in-cylinder flow motions could significantly affect the air-fuel mixture formation by dispersing fuel droplets and vapor fully across the cylinder or gathering the droplets at specific cylinder zones, or both. Lee et al. investigated the effects of tumble and swirl flows on combustion performance in a four-valve SIDI engine [10]. Porpatham et al. studied the influence of swirl flow on the emissions and flame propagation of a biogas fuelled SI engine [11]. Both of them concluded that there was a strong relationship between swirl flow patterns and engine performance.

Planar PIV measurements allow researchers to study the instantaneous in-cylinder flow fields and higher order turbulence. As a conventional approach, the Reynolds-averaged Navier–Stokes (RANS) decomposition is often used to separate the cycle average from the cycle fluctuation of the original flow velocities. The cycle average provides the mean flow behavior, and the cycle fluctuating part exhibits a higher order of flow motion related to flow turbulence. However, this kind of decomposition has limitation to resolve the CCV issues quantitatively.

Various studies have been made to investigate the CCV by applying modal filtering to the flow measurement. One popular approach among the analysis methods is the proper orthogonal decomposition (POD). POD is a modal filtering method, which is widely used in fluid flow analysis by separating the overall flow into an average flow structure and a series of fluctuation flow structures according to the energy level. Using this statistical POD method, Chen et al. [12,13] studied the variations of intake air motion and spray structure in a cylinder of running engine

¹Corresponding author.

Contributed by the IC Engine Division of ASME for publication in the JOURNAL OF ENGINEERING FOR GAS TURBINES AND POWER. Manuscript received November 9, 2016; final manuscript received December 7, 2016; published online February 23, 2017. Editor: David Wisler.



Design of a bioinspired tunable stiffness robotic foot



Zeeshan Kaiser^a, Liping Kang^a, Shane Johnson^{a,b,*}

^a Center of Advanced Mechanics, Material and Structures (CAMMS), University of Michigan and Shanghai Jiao Tong University Joint Institute, Shanghai Jiao Tong University, 800 Dongchuan Rd, Shanghai 200240, China

^b State Key Laboratory of Mechanical Systems and Vibrations, Shanghai Jiao Tong University, Shanghai 200240, China

ARTICLE INFO

Keywords:

Tunable stiffness mechanism
Bipedal robots
Parallel robotics
Optimization
Robotic foot

ABSTRACT

The human foot is capable of adapting to various diverse terrains, and this function is due, in part, to the foot's capacity of varying its stiffness in different anatomical regions. The purpose of this study is to develop an adaptable robotic foot by emulating the human foot's arch, horizontal tie (the plantar aponeurosis, midfoot ligaments, etc.), and its ability of varying its stiffness. The robotic foot is designed, analyzed, optimized and fabricated as a semi-circular arch with a horizontal tie consisting of a Tunable Stiffness Mechanism (TSM). The active number of coils in parallel/series configuration of concentric helical springs is changed to control the stiffness of the TSM. The arch stiffness and tunable stiffness range were optimized using the epsilon constraint method. Analytical and finite element modeling results closely match the experimental validation of both the tunable axial stiffness behavior of the TSM and tunable bending stiffness of the robotic foot assembly. The results also show that the TSM is capable of varying the potential energy storage at midstance depending on the load or displacement applied. In conclusion, a robotic foot was developed to adapt to various diverse terrains through varying stiffness and therefore potential energy stored at midstance; the potential energy is then available for an elastic rebound and propulsion in the terminal phase of gait. By implementing proper control algorithms, the proposed tunable stiffness robotic foot is capable of real-time adaptations to changing terrains, which may lead to the design and development of more adaptive industrial and bipedal walking robots.

1. Introduction

Humans modulate the stiffness of their feet, legs and arms to perform a wide range of tasks (running, jumping, climbing, gripping, etc.) [1]. This function is achieved by muscles which are natural actuators possessing tunable force and stiffness control [2]. The human foot varies its stiffness in different anatomical regions to achieve an efficient gait and adaptation to various diverse terrains. A gait cycle can be divided into three distinct phases: force absorption phase (heel strike), midstance, and propulsion phase (toe off). To reduce total mechanical energy during a human gait cycle, a portion of kinetic energy is stored in the Plantar Aponeurosis (PA) and midfoot ligaments as potential energy in the form of elastic strain energy during midstance. This energy is later utilized for elastic rebound in the terminal phase of gait [3]. The human foot is commonly described as an arched beam structure with a horizontal tie [4] as illustrated in Fig. 1. The PA, midfoot ligaments and muscles are represented here as a horizontal tie. In this arch structure, compressive stresses observed at the upper posterior surface and tensile stresses at the plantar surface, and the bending of the arch generates a tensile stretch of the horizontal tie. The stiffness of the horizontal tie affects both the stiffness

* Corresponding author at: Center of Advanced Mechanics, Material and Structures (CAMMS), University of Michigan and Shanghai Jiao Tong University Joint Institute, Shanghai Jiao Tong University, 800 Dongchuan Rd, Shanghai 200240, China.

E-mail addresses: shane.johnson@sjtu.edu.cn (S. Johnson).

<http://dx.doi.org/10.1016/j.mechmachtheory.2016.12.003>

Received 2 August 2016; Received in revised form 9 December 2016; Accepted 15 December 2016

Available online 23 December 2016

0094-114X/ © 2016 Elsevier Ltd. All rights reserved.

Separation and Visualization of Arteries and Heart in 3D Computed Tomography Angiography Images

LAN Shouren¹ (兰守忍), CUI Chaoyi² (崔超毅), LIU Xin³ (刘鑫), JOHNSON Shane⁴
SU Jialiang⁴ (苏佳良), CHEN Benzhi¹ (陈本智), WANG Lisheng^{1*} (王利生)

(1. Department of Automation, Shanghai Jiao Tong University, Shanghai 200240, China; 2. Department of Vascular Surgery, Shanghai Ninth People's Hospital, Shanghai Jiao Tong University School of Medicine, Shanghai 200011, China;

3. Center for Machine Vision and Signal Analysis, University of Oulu, Oulu 90014, Finland;

4. University of Michigan - Shanghai Jiao Tong University Joint Institute, Shanghai 200240, China)

© Shanghai Jiao Tong University and Springer-Verlag Berlin Heidelberg 2017

Abstract: The visualization of arteries and heart usually plays a crucial role in the clinical diagnosis, but researchers face the problems of region selection and mutual occlusion in clinical visualization. Therefore, the arteries and the heart cannot be easily visualized by current visualization methods. To solve the problems, we propose a new framework for arteries and cardiac visualization by combining a priori knowledge and the set operations. Firstly, a suitable region can be easily determined in the transfer function space with a priori knowledge and the visual feedback results. Secondly, the arteries and the heart can be directly extracted by the marked seed point. Finally, the arteries and the heart are separated for solving mutual occlusion through the set operations. This framework can easily solve the mutual occlusion problem in clinical visualization and greatly improve the region selection method in the transfer function space. Its effectiveness has been demonstrated on the basis of many experimental results.

Key words: occlusion removal, multi-atlas, interactive extraction, set operations, volume rendering

CLC number: TP 391.9 **Document code:** A

0 Introduction

Volume rendering^[1-2] is an important visualization tool. It is especially useful in medical imaging^[3-4] for which the basic requirement is the ability to visualize the structures of interest (SoIs) in relation to the surrounding structures. An appropriate transfer function must be designed to visualize the SoIs in a 3D image^[5-13]. The appropriate transfer function can assign different voxels with different opacities and colors. So far many transfer functions for vascular and cardiac visualization have also been widely studied by many researchers^[14-23]. But the arteries, spine and heart are the closely adjacent structures in 3D computed tomography angiography (CTA) images, and they are usually occluded by each other in clinical visualization. These structures cannot be easily separated due to the partial volume effects (PVEs)^[24]. The previous transfer

functions usually fail in visualizing the arteries and the heart separately. Although Lan's method^[25] can separate and visualize the arteries and the heart in volume rendering, it faces the region selection problem in the scalar-gradient transfer function (SG-TF) space^[8]. Usually, it is done manually by the user through trial-and-error and is a tedious task. The other clinical problem is that the arteries and small vessels cannot be visualized simultaneously.

In this paper, we propose a new framework to greatly improve the region selection method in the SG-TF space and solve the mutual occlusion problem in clinical visualization for arteries and cardiac visualization. The proposed framework can provide user-friendly methods to select regions in the SG-TF space and extract the SoIs from the determined voxels. Here, we use the SG-TF space to determine the voxels of arteries and heart according to a priori knowledge and the visual feedback results. The distribution region of arteries or heart is the first step to be preselected in the SG-TF space with a priori knowledge, and then it is slightly adjusted according to the visual feedback results. The second step is to directly extract the arteries or the heart from the determined voxels by specifying the seed point in volume rendering. Compared with Lan's method^[25],

Received date: 2016-05-19

Foundation item: the National Basic Research Program (973) of China (No. 2013CB329401), the National Natural Science Foundation of China (No. 61375020), and the Cross Research Fund of Biomedical Engineering of Shanghai Jiao Tong University (No. YG2013ZD02)

***E-mail:** lswang@sjtu.edu.cn



Experimental and computational analysis of orthotic medial longitudinal arch support height

Haihua Ou ^a, Zeeshan Qaiser^a, Liping Kang^a and Shane Johnson^{a,b*}

^aShanghai Jiao Tong University, University of Michigan and Shanghai Jiao Tong University Joint Institute, Shanghai, China; ^bState Key Laboratory of Mechanical System and Vibration, Shanghai Jiao Tong University, Shanghai, China

(Received 11 January 2017; accepted 27 March 2017)

Keywords: foot; footwear; orthoses; arch support; plantar pressure; orthopaedic shoes

Introduction

Lower extremity injuries (LEI) in the foot and ankle region are the most common injuries experienced by physically active groups (including sports and military personnel). Classical treatment for LEI involves the fabrication of custom moulded or fitted foot orthoses. The arch height is a critical parameter for an orthosis at mid-stance. Typically, the standard procedure for fabricating a custom-made foot orthoses starts with using moulds or surface data captured in a neutral position of the foot based on Root's subtalar neutral theory (Root, 1973, 1997). More recent research (Laughton, Davis, & Williams, 2002), however, reported a significant difference in forefoot and rearfoot geometric measurements between different casting techniques (plaster cast, foam cast and laser scan), and arch height varied up to 2 cm among fabrication techniques.

A low arch height would lead to an orthosis with no functional orthotic benefits, and a high arch height would injure the subject instead of providing injury prevention or rehabilitation benefits. In all, an objective means of obtaining or forming orthotic shape has yet to be developed.

Purpose of the study

The purpose of the study is that we want to objectively determine the optimum range of orthotic arch height which controls navicular displacement and therefore the plantar pressure redistribution.

Methods

In this research a 3D finite element foot model is developed, including details of bones, soft tissue, ligament and cartilages. A series of virtual orthotic shape is obtained by

capturing the plantar foot surface profile when the foot is subjected to a portion of body weight under balance standing loading. The obtained virtual orthotic shapes are then integrated with the foot model and treated as rigid. Vertical navicular displacement during the loading serves as an indicator for determining the optimum orthotic arch height.

An adjustable arch height orthoses is developed. A fiberglass/epoxy orthosis is fabricated through the vacuum bagging method. A longitudinal cut-out is made just lateral to the first ray of the foot. The adjustment of flexible orthosis height is achieved by adjusting the length of the arch span through a lead screw mechanism under the hallux. An experimental study is performed on a range of individuals by varying the orthotic arch height. Displacement of the navicular is measured during balance standing with the orthotic changes. Plantar pressure redistribution is measured during walking by Novel plantar pressure measurement system for a range of walking speeds.

Results

The computational model gives the navicular displacement during balance standing versus orthotic height relation as shown in Figure 1.

Experimentally, the mean pressure in forefoot, mid-foot and rearfoot is evaluated and the mean mean pressure over the walking cycles is shown in Figure 2.


Discussion and conclusion

According to both the computation model and the experimental study, the navicular displacement and plantar pressure are sensitive to orthotic arch height. The navicular displaces vertically downward when the orthotic arch

*Corresponding author. Email: shane.johnson@sjtu.edu.cn

Thermoviscoelastic modeling of a nonpneumatic tire with a lattice spoke

Sairom Yoo¹, Md Salah Uddin², Hyeonu Heo²,
Jaehyung Ju² and Seok-Ju Choi³

Proc IMechE Part D:
J Automobile Engineering
2017, Vol. 231(2) 241–252
© IMechE 2016
Reprints and permissions:
sagepub.co.uk/journalsPermissions.nav
DOI: 10.1177/0954407016656287
journals.sagepub.com/home/pid


Abstract

Nonpneumatic tires made from materials with a low viscoelastic energy loss can be an option for developing tires with a low rolling resistance. For better fuel-efficient design of nonpneumatic tires, the rolling energy loss of the nonpneumatic tires may need to be analyzed at a component level. The objective of this study is to develop a numerical tool that can quantify the rolling energy loss and the corresponding internal heat generation of a nonpneumatic tire. We construct a thermomechanical model that covers the interaction between the deformation and the related heat generation in an elastomer material. We suggest, for various vehicle loads and various rolling speeds, a coupled thermoviscoelastic material model for a nonpneumatic tire with a hexagonal cellular spoke in order to investigate the temperature distribution of the nonpneumatic tire generated by hysteresis and convection loss to the air. Using a hyperviscoelastic material model developed from uniaxial (tension and compression) tests and dynamic mechanical analysis, a thermomechanical model is constructed by combining a shear-deformation-induced hysteresis and a cooling procedure when exposed to the air. The model of the temperature rise of the nonpneumatic tire is validated using temperature measurement with a thermal imaging camera during rolling of the nonpneumatic tire. The developed tool combining the viscoelastic material model with the aerodynamic heat loss quantifies well the hysteretic energy loss and the temperature distribution at each component of the nonpneumatic tire.

Keywords

Thermoviscoelastic model, nonpneumatic tire, heat generation, hyperelastic energy loss, polyurethane, lattice structures

Date received: 21 February 2015; accepted: 26 May 2016

Introduction

Non-pneumatic tires (NPTs) that use a compliant spoke to replace the air in pneumatic tires have received much attention because of their relatively simple manufacturing method, which enables them to expand their design space through a broader selection of materials including engineering thermoplastic elastomers, e.g. polyurethane (PU).^{1–5} The expanded selection of materials may enable engineers to have more freedom in the design of high-performance tires with functional enhancement. For example, thermoplastic PUs are environmentally friendly⁴ because they do not need the vulcanization process which is required in conventional tire-manufacturing processes. Moreover, thermoplastic PUs are known to have lower viscoelastic energy losses than natural and synthetic rubbers do, resulting in the production of tires with less rolling resistance.

The rolling energy loss of tires is a well-known phenomenon that occurs by thermal dissipation due to cyclic deformation of viscoelastic tire materials and is often

referred to as the hysteretic loss. The hysteretic loss is known to account for 90–95% of the rolling energy loss of tires⁶ under normal driving conditions. The remaining 5–10% is known to be attributed to the frictional contact loss between the tires and the road, the inertial distortions of the tires, and the aerodynamic drag.⁶

Thermomechanical models have been used to quantify the rolling energy loss of tires and the corresponding temperature rise of the tires.^{7–13} Simple analytical models^{6–8} and numerical models based on finite

¹School of Mechanical and Aerospace Engineering, Korea Aerospace University, Goyang City, Gyeonggi-do, Republic of Korea

²Department of Mechanical and Energy Engineering, University of North Texas, Denton, Texas, USA

³R&D Center, Hankook Tire Co. Ltd, Daejeon, Republic of Korea

Corresponding author:

Jaehyung Ju, Department of Mechanical and Energy Engineering, University of North Texas, 1155 Union Circle #311098, Denton, TX 76203-5017, USA.

Emails: jaehyung.ju@unt.edu, jaehyung.ju@gmail.com

Enhanced Coarse-Graining of Thermoplastic Polyurethane Elastomer for Multiscale Modeling

Md Salah Uddin

Department of Mechanical
and Energy Engineering,
University of North Texas,
3940 North Elm Street,
Denton, TX 76203-5017
e-mail: MdSalahUddin@my.unt.edu

Jaehyung Ju¹

Mem. ASME
Department of Mechanical
and Energy Engineering,
University of North Texas,
3940 North Elm Street,
Denton, TX 76203-5017
e-mails: jaehyung.ju@unt.edu;
jaehyung.ju@gmail.com

The objective of this work is to develop a multiscale modeling tool of copolymers with long chains. We propose an enhanced coarse-graining method of thermoplastic polyurethane (TPU) with three beads. The proposed coarse-graining provides an accurate molecular modeling tool to keep the molecular interaction together with computational efficiency. The coarse-grained model with three beads is further improved with pressure-correction of the force-field. The improved coarse-grained model holds similar properties of a bulk model of TPU—varying density with temperature, a close density value of TPU at 1 atm, and the phase separation. Equating potential energy densities of the coarse-grained model to the strain energy functions of the continuum model at volumetric and isochoric deformation modes, bulk and shear moduli of TPU are directly obtained and used to estimate Young's modulus and Poisson's ratio. The molecular simulation with the coarse-grained model of TPU demonstrates its much greater bulk modulus than the shear modulus, which is typically observed in elastomers. Modifying the coarse-grained model of TPU with hard and soft segments, we successfully demonstrated the material design of bulk modulus and Poisson's ratio by varying hard and soft segments at the molecular level. The proposed coarse-graining tool will pave a new way to explore the multiscale modeling of copolymers with long chains and can be directly applied to the multiscale modeling of other thermoplastic elastomers (TPE). [DOI: 10.1115/1.4034328]

Keywords: multiscale modeling, coarse-grained model, thermoplastic polyurethane elastomer (TPU), molecular dynamics, molecular mechanics

Introduction

To design macroscopic properties of materials, multiscale modeling with molecular simulations has been explored to investigate the structure–property relationship of the materials [1–3]. Multiscale modeling is especially challenged to predict unique properties of polymers and rubbers; e.g., their finite deformation and time-dependent properties. Several researchers have tried to estimate bulk properties of polymers and rubbers using the molecular simulation tools [4–10]. Theodorou and Suter investigated stresses of atoms for uniaxial and shear deformations [4]. They found that the chain topology strongly influences the atomic-level stresses with an active compensation effect of simulation at the atomic level [4]. Fan and Hsu applied a molecular simulation for a uniaxial loading, resulting in a good match of Young's modulus and thermal expansion coefficient but a poor match in Poisson's ratio due to the unavailability to apply Poisson's effect with molecular simulations under uniaxial loading [5].

Other research groups have developed mesoscale/coarse-grained models for polymers/elastomers to predict viscoelastic properties [6–8]. Valavala et al. developed a multiscale tool and used varying initial configurations for full-atomic simulations by setting up upper and lower limits of macroscopic properties [9]. Li et al. developed a constitutive model of a linear polymer using the dynamics of polymer chains at the molecular level, but did not bridge it with a continuum model [10]. A brief literature review of

molecular simulation for multiscale modeling of polymers and rubbers is presented in Table 1.

For a computationally viable molecular simulation, coarse-graining methods have been used. For complex structures such as TPE having a long chain with copolymers, we may need a coarse-graining method projecting molecular interaction while keeping computational efficiency.

The objective of this study is to develop an enhanced coarse-graining tool for multiscale modeling of TPU. A coarse-graining method with three beads is suggested with pressure-correction of the force-field. An equivalent continuum model is used to obtain the constitutive relations of TPU by equating the molecular potential energy to the strain energy. By the end of this study, we may answer the following research questions: (1) how sensitive are the iterative procedure and pressure-correction in the enhanced coarse-graining through molecular dynamics (MD) to the effective potentials through inverse Boltzmann method? (2) how useful is the molecular mechanics (MM) for constructing the equivalent energy model for an isochoric loading? and (3) how sensitive are the bulk modulus and Poisson's ratio with the addition of hard segments?

Enhanced Coarse-Grained Model

The representative volume element (RVE) of a molecular model of TPU is generated from an equilibrium molecular structure for a force-field. For a computationally viable modeling, we suggest an enhanced coarse-grained model of TPU with three beads constructed from a full-atomic model using the inverse Boltzmann method (IBM). MD simulations are conducted for the coarse-graining of TPU using the large-scale atomic/molecular

¹Corresponding author.

Contributed by the Materials Division of ASME for publication in the JOURNAL OF ENGINEERING MATERIALS AND TECHNOLOGY. Manuscript received January 28, 2016; final manuscript received July 8, 2016; published online September 2, 2016. Assoc. Editor: Harley Johnson.

GYNECOLOGY

Intraoperative cervix location and apical support stiffness in women with and without pelvic organ prolapse



Carolyn W. Swenson, MD; Tovia M. Smith, MD; Jiajia Luo, PhD; Giselle E. Kolenic, MA;
James A. Ashton-Miller, PhD; John O. DeLancey, MD

BACKGROUND: It is unknown how initial cervix location and cervical support resistance to traction, which we term “apical support stiffness,” compare in women with different patterns of pelvic organ support. Defining a normal range of apical support stiffness is important to better understand the pathophysiology of apical support loss.

OBJECTIVE: The aims of our study were to determine whether: (1) women with normal apical support on clinic Pelvic Organ Prolapse Quantification, but with vaginal wall prolapse (cystocele and/or rectocele), have the same intraoperative cervix location and apical support stiffness as women with normal pelvic support; and (2) all women with apical prolapse have abnormal intraoperative cervix location and apical support stiffness. A third objective was to identify clinical and biomechanical factors independently associated with clinic Pelvic Organ Prolapse Quantification point C.

STUDY DESIGN: We conducted an observational study of women with a full spectrum of pelvic organ support scheduled to undergo gynecologic surgery. All women underwent a preoperative clinic examination, including Pelvic Organ Prolapse Quantification. Cervix starting location and the resistance (stiffness) of its supports to being moved steadily in the direction of a traction force that increased from 0–18 N was measured intraoperatively using a computer-controlled servoactuator device. Women were divided into 3 groups for analysis according to their pelvic support as classified using the clinic Pelvic Organ Prolapse Quantification: (1) “normal/normal” was women with normal apical ($C < -5$ cm) and vaginal (Ba and Bp < 0 cm) support; (2) normal/prolapse had normal apical support ($C < -5$ cm) but prolapse of the anterior or posterior vaginal walls (Ba and/or Bp ≥ 0 cm); and (3) prolapse/prolapse had both apical and vaginal wall prolapse ($C > -5$ cm and Ba and/or Bp ≥ 0 cm). Demographics, intraoperative cervix locations, and apical support stiffness values were then compared. Normal range of cervix location during clinic examination and operative testing was defined by the total range of values observed in the normal/normal group. The proportion of women in each

group with cervix locations within and outside the normal range was determined. Linear regression was performed to identify variables independently associated with clinic Pelvic Organ Prolapse Quantification point C.

RESULTS: In all, 52 women were included: 14 in the normal/normal group, 11 in the normal/prolapse group, and 27 in the prolapse/prolapse group. At 1 N of traction force in the operating room, 50% of women in the normal/prolapse group had cervix locations outside the normal range while 10% had apical support stiffness outside the normal range. Of women in the prolapse/prolapse group, 81% had cervix locations outside the normal range and 8% had apical support stiffness outside the normal range. Similar results for cervix locations were observed at 18 N of traction force; however the proportion of women with apical support stiffness outside the normal range increased to 50% in the normal/prolapse group and 59% in the prolapse/prolapse group. The prolapse/prolapse group had statistically lower apical support stiffness compared to the normal/normal group with increased traction from 1–18 N (0.47 ± 0.18 N/mm vs 0.63 ± 0.20 N/mm, $P = .006$), but all other comparisons were nonsignificant. After controlling for age, parity, body mass index, and apical support stiffness, cervix location at 1 N traction force remained an independent predictor of clinic Pelvic Organ Prolapse Quantification point C, but only in the prolapse/prolapse group.

CONCLUSION: Approximately 50% of women with cystocele and/or rectocele but normal apical support in the clinic had cervix locations outside the normal range under intraoperative traction, while 19% of women with uterine prolapse had normal apical support. Identifying women whose apical support falls outside a defined normal range may be a more accurate way to identify those who truly need a hysterectomy and/or an apical support procedure and to spare those who do not.

Key words: apical support stiffness, cervix location, prolapse

Introduction

Pelvic organ prolapse is a common indication for gynecologic surgery, with the annual number of women undergoing these procedures projected to reach >190,000 by 2020.¹ While our

understanding of the pathophysiology of pelvic organ prolapse has improved over the last decade—especially the importance of apical support^{2,3}—much remains unknown regarding the biomechanical properties of the affected tissues and pelvic structures. A clinical evaluation of apical support is used to inform surgeons’ decision-making as to whether a hysterectomy is needed as part of surgery for prolapse. However, there is a 50% disagreement rate among gynecologic surgeons about the level of apical support, assessed under traction in the operating room, that indicates the need

for hysterectomy.⁴ Moreover, evidence about how to integrate Pelvic Organ Prolapse Quantification (POP-Q) and intraoperative findings in this assessment do not yet exist. At the heart of this issue is the fact that surgeons use their own assessment of whether the apical supports are normal under traction to make decisions about whether or not hysterectomy and/or apical suspension should be considered. An *objective* assessment of apical support stiffness along with outcome data could provide better information on which to base these important clinical decisions.

Cite this article as: Swenson CW, Smith TM, Luo J, et al. Intraoperative cervix location and apical support stiffness in women with and without pelvic organ prolapse. Am J Obstet Gynecol 2017;216:155.e1–8.

0002-9378/\$36.00

© 2016 Elsevier Inc. All rights reserved.

<http://dx.doi.org/10.1016/j.ajog.2016.09.074>

Heuristics-Enhanced Model Fusion Considering Incomplete Data Using Kriging Models

Anton v. Beek

University of Michigan-Shanghai Jiao Tong
University Joint Institute,
Shanghai Jiao Tong University,
Shanghai 200240, China
e-mail: mr.v.beek@sjtu.edu.cn

Mian Li¹

University of Michigan-Shanghai Jiao Tong
University Joint Institute,
Shanghai Jiao Tong University,
Shanghai 200240, China
e-mail: mianli@sjtu.edu.cn

Chao Ren

Corporate Technology of Siemens Ltd.,
Shanghai 200240, China
e-mail: chao.ren@siemens.com

Simulation models are widely used to describe processes that would otherwise be arduous to analyze. However, many of these models merely provide an estimated response of the real systems, as their input parameters are exposed to uncertainty, or partially excluded from the model due to the complexity, or lack of understanding of the problem's physics. Accordingly, the prediction accuracy can be improved by integrating physical observations into low fidelity models, a process known as model calibration or model fusion. Typical model fusion techniques are essentially concerned with how to allocate information-rich data points to improve the model accuracy. However, methods on subtracting more information from already available data points have been starving attention. Subsequently, in this paper we acknowledge the dependence between the prior estimation of input parameters and the actual input parameters. Accordingly, the proposed framework subtracts the information contained in this relation to update the estimated input parameters and utilizes it in a model updating scheme to accurately approximate the real system outputs that are affected by all real input parameters (RIPs) of the problem. The proposed approach can effectively use limited experimental samples while maintaining prediction accuracy. It basically tweaks model parameters to update the computer simulation model so that it can match a specific set of experimental results. The significance and applicability of the proposed method is illustrated through comparison with a conventional model calibration scheme using two engineering examples. [DOI: 10.1115/1.4038596]

1 Introduction

As science advances so does the complexity of engineering applications and the cost related to the experiments involved with their development. Subsequently, computer-based simulation models and computer simulation models have been widely adopted to replace experimental testing and ameliorate expense. However, the computational cost of some of these models as well as the uncertainty in the prediction can be undesirable, in particular for design optimization where a simulation has to be run for a large number of times. To address this challenge, multiple simplified low-fidelity models have been integrated with a limited amount of high-fidelity simulations or experimental samples giving rise to a specific class of computational efficient surrogate models, known as multimodel fusion [1–5]. Fidelity of simulation models can be regarded as the likelihood that a model prediction is within a certain bandwidth of accuracy. What is more, fidelity is a ubiquitous phenomenon that is propagated by epistemic uncertainty (e.g., model uncertainty) and/or by aleatory uncertainty (e.g., input uncertainty). Accordingly, the fusion of simulations with experimental data is a practical strategy that can significantly ameliorate the simulation cost and emend the model accuracy.

Model fusion is receiving a growing amount of interest, for which some prime examples are given in Refs. [6–8]. In general, the performance of these model fusion methods is scrutinized by their computational efficiency and simulation accuracy. In practice, the optimization of these properties in the available methods usually yields contradicting objectives. The computational efficiency can readily be quantified by time, yet quantifying the computational accuracy can be an arduous endeavor. Consequently, uncertainty quantification in prediction models has received many researchers' attention [9,10]. In addition, due to the complexity

and the interdisciplinary nature of contemporary systems, the quantification of model uncertainty has been extended to multidisciplinary systems [11,12]. These schemes are particularly applicable when dealing with engineering design optimization problems as they can be used to efficiently allocate resources to reduce model uncertainty [13]. Although uncertainty qualification can be a computational exhaustive effort, limiting its applicability to complex cases, it is still useful for applications in model fusion techniques due to the incorporate a spatial random process (SRP). One advantage of using SRPs is its intrinsic property of treating each prediction as a random variable, predicting the mean as well as its standard deviation [14,15]. Accordingly, model fusion techniques have been widely adopted in engineering applications because of their flexibility, computational efficiency, and prediction accuracy.

The work in this paper is concerned with incorporating prior knowledge of input parameters in model updating to ameliorate uncertainty. More accurately, the essence of this work is to make efficient use of current available data rather than using additional efforts to garner more. Moreover, methods in this area are growing in relevance as systems, and the data they produce are growing in complexity. Examples of similar work are given in Ref. [16], where prior identified simulation model bias is added to the baseline simulation model. An effort that is in contrast to the work of Gorguluarslan and Choi [17] and Rosen and Park [18] who attempt to improve the prediction of fine-scale heterogeneous simulations by substituting homogenized coarse-scale parameters while maintaining agreement between fine and coarse scale system response. Furthermore, for applications of model fusion techniques in design optimization problems [19], proposes a technique to avoid misinterpretation of stationary points, effectively reducing the computational cost involved in optimization.

For many typical engineering applications, the experienced users have a profound understanding of aleatory input uncertainty. In other cases input parameters are bounded by common sense. For example, the temperature at a specific latitude and longitude, or a design tolerance [20,21]. Accordingly, this information can

¹Corresponding author.

Contributed by the Design Automation Committee of ASME for publication in the JOURNAL OF MECHANICAL DESIGN. Manuscript received May 22, 2017; final manuscript received October 22, 2017; published online December 13, 2017. Assoc. Editor: Samy Missoum.



A key components-based heuristic modular product design approach to reduce product assembly cost

Junfeng Ma¹ · Gül E. Okudan Kremer² · Mian Li³

Received: 3 August 2017 / Accepted: 8 December 2017
© Springer-Verlag France SAS, part of Springer Nature 2017

Abstract

Nowadays, increasing awareness of sustainability and varied customer requirements have driven manufacturers to reconsider product development starting from the design phase. As one response to these concerns, modular product design (MPD) has attracted significant attention. Since the architecture of a product or a system can have implications on its assembly cost, MPD and product assembly should be investigated jointly. In this paper, a heuristic clustering algorithm with key components emphasis that will reduce assembly cost is offered to group components into modules. Key product/system components are those that afford competitiveness to a company. An MPD method that can decrease product assembly cost while accommodating key components strategically is the primary motivation for this research. Upon the foundation of extant works, we provide the details of the proposed methodology and illustrate its use via a coffee maker case study.

Keywords Modular product design · Heuristic search · Key components · Product assembly · Reduce cost

1 Introduction

One of the common ways to reduce complexity in a larger product or system is segmenting it into smaller subsystems. By applying this philosophy inversely to design engineering, MPD has evolved. Steward [41], who proposed the philosophy of system partition and testing, can be considered to propose the core idea of MPD. The MPD involves clustering simple and relevant product parts into more complex and larger subassemblies (called module), and then combining these subassemblies to create a complete product. In modular product architecture, each functional product com-

ponent is implemented in one subassembly (or module), with few interactions between subassemblies [46]. Many practical advantages of MPD have been explored in recent research. For example, MPD has been shown to increase manufacturing efficiency and effectiveness [28,36]; it can benefit the supply chain by reducing inventory cost and lead time [8,9,18]. It can also satisfy the demand for mass customization through practical and economical ways of increasing the set of product variants [11,12,23,29].

Assembly consideration in the design stage (a.k.a. design for assembly (DFA)), is a systematic process that primarily concentrates on reducing the assembly costs of a product in the design stage. DFA provides quantitative methods to evaluate cost and manufacturability during the design stage, and thereby provides suggestions for cost reduction. Many products have potential cost efficiencies as low as 20% before DFA analysis is implemented, and after DFA they achieve efficiencies higher than 70% [45]. DFA methods are developed under the assumption that the manufacturing/assembly costs are set in the design stage, before any manufacturing system analysis and tooling development are undertaken [3,34]. MPD can improve assembly performance [36,40]. Modular design tends to have fewer components for assembly; by increasing pre-assembly and using common interfaces, modularity decreases the cost of assembly [10]. Implementation of DFA in design engineering could reduce

✉ Junfeng Ma
ma@ise.msstate.edu

Gül E. Okudan Kremer
gkremer@iastate.edu

Mian Li
mianli@sjtu.edu.cn

¹ Dept. of Industrial and Systems Engineering, Mississippi State University, Mississippi State, MS 39762, USA

² Dept. of Industrial and Manufacturing Systems Engineering, Iowa State University, Ames, IA 50011, USA

³ University of Michigan-Shanghai Jiao Tong University Joint Institute, Shanghai Jiao Tong University, Shanghai 200240, China

Automated surface inspection for steel products using computer vision approach

JIAQI XI,¹ LIFENG SHENTU,¹ JIKANG HU,¹ AND MIAN LI^{2,*}

¹Department of Automation, Baosteel Research Institute, 885 Fu Jin Road, Shanghai 201900, China

²University of Michigan-Shanghai Jiao Tong University Joint Institute, Shanghai Jiao Tong University, Shanghai 200240, China

*Corresponding author: mianli@sjtu.edu.cn

Received 25 October 2016; revised 29 November 2016; accepted 29 November 2016; posted 5 December 2016 (Doc. ID 278939); published 3 January 2017

Surface inspection is a critical step in ensuring product quality in the steel-making industry. In order to relieve inspectors of laborious work and improve the consistency of inspection, much effort has been dedicated to the automated inspection using computer vision approaches over the past decades. However, due to non-uniform illumination conditions and similarity between the surface textures and defects, the present methods are usually applicable to very specific cases. In this paper a new framework for surface inspection has been proposed to overcome these limitations. By investigating the image formation process, a quantitative model characterizing the impact of illumination on the image quality is developed, based on which the non-uniform brightness in the image can be effectively removed. Then a simple classifier is designed to identify the defects among the surface textures. The significance of this approach lies in its robustness to illumination changes and wide applicability to different inspection scenarios. The proposed approach has been successfully applied to the real-time surface inspection of round billets in real manufacturing. Implemented on a conventional industrial PC, the algorithm can proceed at 12.5 frames per second with the successful detection rate being over 90% for turned and skinned billets. © 2017 Optical Society of America

OCIS codes: (150.3040) Industrial inspection; (150.0155) Machine vision optics.

<https://doi.org/10.1364/AO.56.000184>

1. INTRODUCTION

Surface inspection is an integral part of quality control in the steel-making industry. At present most of the inspection work is accomplished manually. It is usually repetitive and labor intensive in nature, and might also involve certain exposure to radiation [1]. In order to relieve inspectors of these heavy loads and improve the consistency of inspection, many vision-based systems have been integrated into the production line to assist in or partially replace the manual inspection. However, this poses new challenges. As is true of any vision-based approach, success in defect detection depends in large part on the image quality. Unfortunately, this can hardly be guaranteed due to poor lighting conditions at the worksites. More often than not, images are suffering from the degradation of non-uniform illumination, surface reflection, and environment reflection [2]. On occasions when continuous inspection is required, the blurring effect, caused by relative motion between the camera and the workpieces during exposure, can be another source of degradation [3]. Apart from these environmental factors, another major challenge is to discriminate the defect from the texture [4]. For some types of material, the difference between these two is too subtle to characterize properly even under

perfect lighting conditions. All these factors increase the difficulties of designing an effective and robust surface inspection algorithm.

Over the past decades a vast amount of work has been done in overcoming the difficulties mentioned above. Among them some efforts were dedicated to removing the surface texture under non-uniform illumination via image transformation [5–9]. By properly selecting sub-images at different decomposition levels for backward wavelet transform, Tsai and Hsiao successfully separated the local anomalies from regular texture patterns [5]. Then they used a simple threshold to extract the defective regions in the reconstructed image. In another work [6], Fourier transform was used to achieve the removal of statistical textures by attenuating the frequency components in the spectral space. Following the same line of reasoning, Li *et al.* eliminated the texture by manipulating the reconstructed coefficients of the inverse curvelet transform [7]. Then they segmented the reconstructed image based on statistics analysis. Yun *et al.* classified the surface defects into different groups and used undecimated wavelet transform for the detection of line defects [8]. It can be noted that with careful manipulation of the transformed image, these approaches can achieve

Ruixiang Zheng
University of Michigan—Shanghai Jiao Tong
University Joint Institute,
Shanghai Jiao Tong University,
Shanghai 200240, China

Mian Li¹
University of Michigan—Shanghai Jiao Tong
University Joint Institute,
Shanghai Jiao Tong University,
Shanghai 200240, China
e-mail: mianli@sjtu.edu.cn

Zhaoguang Wang
University of Michigan—Shanghai Jiao Tong
University Joint Institute,
Shanghai Jiao Tong University,
Shanghai 200240, China

Qiang Zhang
University of Michigan—Shanghai Jiao Tong
University Joint Institute,
Shanghai Jiao Tong University,
Shanghai 200240, China;
Department of Mechanical Engineering,
Aeronautics School of Engineering and
Mathematical Sciences,
City University London,
Northampton Square EC1V 0HB, London

Control of Blow-Down Wind Tunnel Using Combined Extended Kalman and Nonlinear Predictive Filters

A blow-down wind tunnel is a typical nonlinear time-varying system facing the coupling effects between the pressure and temperature during the short time test procedure. The control of blow-down wind tunnels has been discussed for a long time and a satisfactory general solution to this problem is still of interests. This paper aims to model the internal relationship of the state variables of the wind tunnel by using thermodynamic theories. With the developed model, a new control method combining extended Kalman filter (EKF) together with auxiliary nonlinear predictive filter (NPF) is proposed to improve the control performance of the blow-down wind tunnel controller, in terms of accuracy and robustness. The transient coupling effects between the pressure and temperature are fully considered in the proposed approach. The results from the simulation and experiments are consistent and demonstrate that the controller based on EKF combined together with NPF can work better than previously proposed EKF-based controller. [DOI: 10.1115/1.4035243]

Keywords: blow-down wind tunnel, nonlinear control, thermodynamic, EKF, NPF

1 Introduction

Supersonic wind tunnels are generally used as the testing platforms in area of aerodynamics, for both research and product development. There are different classifications of wind tunnels and the subcategory considered in this work is blow-down wind tunnels. Although they could only support short-time tests, because of their simpler structures, controlling profiles of blow-down wind tunnels would be easier to construct than those for other types, such as closed-circuit continuously driven wind tunnels. Blow-down wind tunnels have been widely used in the research area of gas turbine and aero-thermal, in both research institutes and gas turbine manufacturers [1–3]. The particular blow-down wind tunnel investigated in the present work has been used in the research for blade aero-thermal research [4–6].

The basic control target for blow-down wind tunnels is to maintain the total pressure in the test chamber as stable as possible. To achieve this goal, a controller taking the thermodynamic characteristics of the gas during the blow-down process into account should be developed. A main reason of using model-based control method is that the blow-down wind tunnel is a typical nonlinear time-varying system with coupling effects between control variables/parameters of interests (e.g., pressure, temperature, and mass, at the location of interests); and this property makes the state variables of vital importance in the control process. Based on this consideration, Xi et al. [7] proposed a control method for the blow-down wind tunnel based on EKF. Their results showed that the control process was satisfactory. However, the EKF-based controller for this application could be further improved in terms of accuracy and robustness, given the fact that EKF assumes each presented noise is white noise. Moreover, controlling the gas

temperature before the gas goes into the test chamber has not been considered in the previous work.

In this work, a new developed model-based control method, extended Kalman filter with auxiliary nonlinear predictive filter (NPF-EKF), is proposed to improve the control performance for the blow-down wind tunnel, in terms of issues mentioned above. This hybrid filter is developed to satisfy two important requirements in the wind tunnel system. First, the settling time of the pressure (i.e., the time elapsed between the starting of the test and when the pressure is stable around the set point with an acceptable error band) should be as short as possible to avoid wasting pressurized gas and to extend available testing duration. Second, and even more importantly, the overshoot should be strictly constrained since it could cause undesired temperature variation in the tunnel. In addition, a general method to assign proper values to the parameters of the NPF-EKF-based controller is also introduced in this work. The results from both simulation and experiments demonstrate that the proposed NPF-EKF-based controller achieves much better control performance, compared with the EKF based controller.

The rest of the paper is organized as follows: Section 2 provides the literature review and the experimental platform used in this work, and then, briefly discusses the background of EKF and NPF. Section 3 discusses the proposed NPF-EKF-based controller in details. Section 4 gives process modeling of the blow-down wind tunnels. The corresponding results are presented in Sec. 5, followed by the conclusion of this work in Sec. 6.

2 Background

This section provides the literature review, the experimental platform used in this work, as well as the introduction of EKF and NPF.

2.1 Literature Review. Early work in this research area can be traced back to 1980s when proportional-integral-derivative (PID) controllers were proposed to automatically tune the total

¹Corresponding author.

Contributed by the Fluids Engineering Division of ASME for publication in the JOURNAL OF FLUIDS ENGINEERING. Manuscript received November 17, 2015; final manuscript received October 27, 2016; published online February 8, 2017. Assoc. Editor: Mark F. Tachib.

Sequential Multi-Objective Optimization for Lubrication System of Gasoline Engines With Bilevel Optimization Structure

Jizhou Zhang

University of Michigan—Shanghai Jiao Tong
University Joint Institute,
Shanghai Jiao Tong University,
Shanghai 200240, China

Yu Qiu

SAIC Motor Technical Centre,
Shanghai 201804, China

Mian Li¹

University of Michigan—Shanghai Jiao Tong
University Joint Institute,
Shanghai Jiao Tong University,
Shanghai 200240, China;
National Engineering Laboratory for Automotive
Electronic Control Technology,
Shanghai Jiao Tong University,
Shanghai 200240, China
e-mail: mianli@sjtu.edu.cn

Min Xu

National Engineering Laboratory for Automotive
Electronic Control Technology,
Shanghai Jiao Tong University,
Shanghai 200240, China

The lubrication system is one of the most important subsystems in gasoline internal combustion engines (ICEs), which provides hydrodynamic lubrication for friction pairs. The performance of the lubrication system affects the performance of the engine directly. The objective of this work is to reduce the friction loss of the engine and the driven power of the oil pump through design optimization. Two most important oil consumers in the lubrication system are investigated using multibody dynamics (MBD) and elastohydrodynamics (EHD). Considering that MBD and EHD analyses are time-consuming, Kriging is applied to establish the approximation models for bearings. Multi-objective optimization of bearings based on approximation models is formulated and conducted. Given the difference among multiple cylinders in the engine, a bilevel optimization framework is used to perform bearing optimization. The oil consumption and the friction loss of the bearings are reduced within the entire speed range. After that, the pipe diameters of the lubrication system are optimized with optimized bearings to reduce the flow resistance. With the optimization of both bearings and lubrication pipes in a sequential manner, the oil pressure is maintained at the baseline level while the oil pump size is reduced, and the driven power is averagely dropped over the entire speed range. [DOI: 10.1115/1.4035493]

Keywords: lubrication system, multibody dynamics, elastohydrodynamics, multi-objective optimization, bilevel optimization

1 Introduction

The lubrication system is one of the most important subsystems in gasoline internal combustion engines (ICEs), which provides hydrodynamic lubrication for friction pairs in the engine. Starting from 1970s, research on lubrication systems that are used in the gasoline engines turned onto the system level when the lubrication system was considered as a kind of the complex network, consisting of different components and local structures connected [1]. The analysis of this system is very similar to the analysis in circuit design. After that, Chun et al. described the oil flow characteristics of key flow components (i.e., oil pump, oil filter, oil jet, bearings, and hydraulic tappet) in a four-cylinder gasoline engine [2,3]. The work of Klingebiel and Kahlstorf [4], Cehreli and Durgun [5], and Senatore et al. [6] were all applications of the network analysis method. The proposed network analysis method makes the optimization of the lubrication system possible. Tao even conducted robust optimization on the lubrication system where the smallest size of the oil pump and the diameter of the cylinder head throttle were obtained with the engine speed, oil temperature, and bearing clearances varying within a certain range [7]. Senatore also conducted the optimization on the lubrication system in order to decrease the size of the oil pump [6].

However, so far optimization for the lubrication system on the system level is still restricted since the components in the system are all simplified in those cases. It is well known that critical

components, especially bearings, can have great influence on the performance of the lubrication system. In this regard, optimization for the bearings, especially for the main bearings and conrod bigend bearings which are two types of the most important engine bearings, needs to be conducted first before the optimization of the entire system. Related work on bearing optimization has been reported in the literature. Dowson and Ashton described the process of bearing optimization and the selection of optimization algorithms [8,9]. They used conjugate gradient and Quasi-Newton methods to optimize cylinder bearings under constraints, and used more complex methods to optimize tilting pad thrust bearings. The bearing performance is always expressed by empirical equations in the optimization process considering the computational efficiency and convenience. However, those empirical equations are usually based on the classical hydrodynamics theory which considers that the friction surfaces are rigid and smooth. Moreover, the bearing is always considered as an independent object without the effect from other objects, such as conrod and cylinder block.

Elastohydrodynamics, EHD, is another bearing analysis theory that has been widely used nowadays. Based on the finite element method (FEM), the influence of both elastic deformation and surface roughness of the shell and journal on the bearing performance can be addressed. The results from EHD could be more accurate. To name a few, Poynton used SABRE-EHL to analyze conrod bigend bearings of a middle-speed diesel engine and investigated the influence of the groove position on the bearing performance [10]. Wang and Parker also used the same program to predict the oil flow rate of conrod bigend bearing where the EHD simulation results were very close to the experimental data, especially in the middle-speed range [11]. However, if the

¹Corresponding author.

Contributed by the Design Automation Committee of ASME for publication in the JOURNAL OF MECHANICAL DESIGN. Manuscript received April 3, 2016; final manuscript received December 8, 2016; published online January 5, 2017. Assoc. Editor: Massimiliano Gobbi.

SCIENTIFIC REPORTS

OPEN

Flexible Semiconductor Technologies with Nanoholes-Provided High Areal Coverages and Their Application in Plasmonic-Enhanced Thin Film Photovoltaics

Zhaozhao Wang¹, Linfa Peng¹, Zhongqin Lin¹, Jun Ni^{1,2}, Peiyun Yi¹, Xinmin Lai¹, Xiaolong He³ & Zeyu Lei³

Mechanical flexibility and advanced light management have gained great attentions in designing high performance, flexible thin film photovoltaics for the realization of building-integrated optoelectronic devices and portable energy sources. This study develops a soft thermal nanoimprint process for fabricating nanostructure decorated substrates integrated with amorphous silicon solar cells. Amorphous silicon (a-Si:H) solar cells have been constructed on nanoholes array textured polyimide (PI) substrates. It has been demonstrated that the nanostructures not only are beneficial to the mechanical flexibility improvement but also contribute to sunlight harvesting enhancement. The a-Si:H solar cells constructed on such nanopatterned substrates possess broadband-enhanced light absorption, high quantum efficiency and desirable power conversion efficiency (PCE) and still experience minimal PCE loss even bending around 180°. The PCE performance without antireflection coatings increases to 7.70% and it improves 40% compared with the planar devices. Although the advantages and feasibility of the schemes are demonstrated only in the application of a-Si:H solar cells, the ideas are able to extend to applications of other thin film photovoltaics and semiconductor devices.

Photovoltaic (PV) cells, which effectively convert sunlight into clean electrical power, provide virtually unlimited amounts of renewable energy. Silicon has been the material of choice for PV cells owing to low cost, earth abundance, non-toxicity, and the availability of mature processing technologies¹. However, the cost of current PV devices still needs to be substantially reduced so that large scale implementation of PV modules could be realized. Thin-film, second-generation solar cells of CdTe, amorphous Si, and CuInxGa1-xSe2 (CIGS) fabricated with absorbing layers of a few micrometers thick may provide a viable way towards this goal because of their small material assumption and low processing costs²⁻⁴. In addition, thin-film solar cells could be built to form mechanically flexible or even stretchable optoelectronic systems with inorganic materials. Some concepts integrating inorganic materials with organic substrates are now available for fabricating optoelectronic systems possessing a combinational effect of the mechanical robustness and superior light trapping^{5,6}.

Recent research exploits ways to build inorganic photovoltaic (PV) systems on flexible substrates, which could integrate excellent optoelectronic performances with mechanical flexibility. Compared to schemes built on planar, rigid substrates, such schemes enable various reversible deforming modes of inorganic optoelectronic systems, including bending, stretching, compressing or twisting, thereby expanding the potential applications from building-integrated optoelectronic devices to portable energy sources. There are a variety of choices of flexible substrates for flexible PV systems, such as metallic foils (Ti foils, Al foils, etc), thin glasses and membrane plastics⁷⁻¹⁰.

¹State Key Laboratory of Mechanical System and Vibration, Department of Mechanical Engineering, Shanghai Jiao Tong University, Shanghai, 200240, P.R. China. ²Department of Mechanical Engineering, University of Michigan, Ann Arbor, MI, 48109-2125, USA. ³University of Michigan-Shanghai Jiao Tong University Joint Institute, National Key Laboratory of Nano/Micro Fabrication Technology, Shanghai Jiao Tong University, Shanghai, 200240, P.R. China. Correspondence and requests for materials should be addressed to L.P. (email: penglinfa@sjtu.edu.cn) or J.N. (email: junni@umich.edu)



Contents lists available at ScienceDirect

Journal of Sound and Vibration

journal homepage: www.elsevier.com/locate/jsvi

Parametric instability of spinning elastic rings excited by fluctuating space-fixed stiffnesses

Chunguang Liu^a, Christopher G. Cooley^b, Robert G. Parker^{c,*}^a University of Michigan – Shanghai Jiao Tong University Joint Institute, Shanghai Jiao Tong University, Shanghai 200240, China^b Department of Mechanical Engineering and Energy Processes, Southern Illinois University Carbondale, Carbondale, IL 62901, USA^c Department of Mechanical Engineering, Virginia Tech, Blacksburg, VA 24061, USA

ARTICLE INFO

Article history:

Received 29 January 2017

Received in revised form

24 March 2017

Accepted 29 March 2017

Handling Editor: Ivana Kovacic

Available online 25 April 2017

Keywords:

Elastic ring

Gyroscopic systems

Parametric instability

Perturbation

Compliant gears

Mesh phasing

ABSTRACT

This study investigates the vibration of rotating elastic rings that are dynamically excited by an arbitrary number of space-fixed discrete stiffnesses with periodically fluctuating stiffnesses. The rotating, elastic ring is modeled using thin-ring theory with radial and tangential deformations. Primary and combination instability regions are determined in closed-form using the method of multiple scales. The ratio of peak-to-peak fluctuation to average discrete stiffness is used as the perturbation parameter, so the resulting perturbation analysis is not limited to small mean values of discrete stiffnesses. The natural frequencies and vibration modes are determined by discretizing the governing equations using Galerkin's method. Results are demonstrated for compliant gear applications. The perturbation results are validated by direct numerical integration of the equations of motion and Floquet theory. The bandwidths of the instability regions correlate with the fractional strain energy stored in the discrete stiffnesses. For rings with multiple discrete stiffnesses, the phase differences between them can eliminate large amplitude response under certain conditions.

© 2017 Elsevier Ltd. All rights reserved.

1. Introduction

Gears used in aerospace applications are designed to be thin to reduce weight. These thin, compliant gears experience large loads and operate at high rotation speeds, so elastic gear deformation is a substantial issue. Gear elastic vibrations are experimentally found in Refs. [1,2]. Excitation in geared systems comes from the changing contact conditions on the gear teeth as the gears rotate kinematically. In many dynamic models, this excitation is represented by fluctuating mesh stiffnesses. When the fluctuation frequency is near resonant gear speeds large dynamic response occurs, which leads to large dynamic loads, potential structural failure, and noise.

Gear weight reduction is achieved by using thin webs with large facewidths (for the large loads) or ring-like gears with no webs. Such lightweight gears are prone to deform elastically, and can be modeled geometrically as rings. The vibration of spinning, elastic rings has been intensively investigated in literature. Carrier [3] derived the governing equations of a rotating ring with in-plane flexural vibrations. General equations for the vibration of rotating bodies and the natural frequencies of a rotating ring were obtained by Johnson [4]. Bert and Chen [5] investigated the bending and twisting vibrations of rotating rings on a uniform elastic foundation. Their analysis included in-plane and out-of-plane deformations. Using

* Corresponding author.

E-mail address: r.parker@vt.edu (R.G. Parker).<http://dx.doi.org/10.1016/j.jsv.2017.03.043>

0022-460X/© 2017 Elsevier Ltd. All rights reserved.

Application of subharmonic resonance for the detection of bolted joint looseness

Mengyang Zhang · Yanfeng Shen · Li Xiao · Wenzhong Qu

Received: 17 November 2015 / Accepted: 3 January 2017 / Published online: 9 January 2017
© Springer Science+Business Media Dordrecht 2017

Abstract Bolted joint structures are prone to bolt loosening under environmental and operational vibrations, which may severely affect the structural integrity. This paper presents a bolt looseness recognition method based on the subharmonic resonance analysis. The bolted joint structure was simplified to a two-degree-of-freedom nonlinear model, and a multiple timescale method was used to explain the phenomenon of the subharmonic resonance and conditions for the generation of subharmonics. Numerical simulation predictions for the generation of the subharmonics and conditions for the subharmonics can be found with respect to the excitation frequency and the excitation amplitude. Experiments were performed on a bolt-joint aluminum beam, where the damage was simulated by loosening the bolts. Two surface-bonded piezoelectric transducers were utilized to generate continuous sinusoidal excitation and to receive corresponding sensing signals. The experimental results demonstrated that subharmonic components would appear in the response spectrum when the bolted structure was subjected to the excitation of twice its natural frequency. This sub-

harmonic resonance method was found to be effective on bolt looseness detection.

Keywords Bolt looseness detection · Structural health monitoring · Subharmonic · Method of multiple scales · Piezoelectric transducers

1 Introduction

Bolted joints are widely used in construction and mechanical industries to connect bear loading structures, and the loss of torque in one or more bolts can dramatically reduce the fatigue life of the mechanical parts [1]. For this reason, a quick assessment of the health status of bolted joints would elongate structural service life spans and prevent catastrophic failures in a variety of mechanical applications.

Among various inspection methods, nonlinear acoustic/ultrasonic techniques are drawing increasing attention within the structural health monitoring (SHM) community, due to their high sensitivity to incipient damage with distinctive nonlinear signal features [2]. In general, the appearance of contact surfaces in the wave paths contributes a significant increase in acoustic nonlinearity [3]. When a bolt becomes loose, a variation of contact stiffness at the interface exists under cyclic wave/vibration loading [4]. Several approaches have been investigated for the detection of bolt loosening, such as impedance method, electrical conductivity approach, and via vibration measurements [5–8]. Elastic waves propagating through the loosening bolted

M. Zhang · L. Xiao · W. Qu (✉)
Department of Engineering Mechanics, Wuhan University,
Wuhan 430072, China
e-mail: qwz@whu.edu.cn

Y. Shen
University of Michigan-Shanghai Jiao Tong University
Joint Institute, Shanghai Jiao Tong University,
800 Dongchuan Road, Shanghai 200240, China

Interaction of Lamb waves with rivet hole cracks from multiple directions

Md Yeasin Bhuiyan¹, Yanfeng Shen² and Victor Giurgiutiu¹

Proc IMechE Part C:
J Mechanical Engineering Science
2017, Vol. 231(16) 2974–2987
© IMechE 2017
Reprints and permissions:
sagepub.co.uk/journalsPermissions.nav
DOI: 10.1177/0954406216686996
journals.sagepub.com/home/pic


Abstract

This paper presents the interaction of Lamb waves with rivet hole cracks from multiple directions of incident using the finite element approach. Lamb waves undergo scattering and mode conversion after interacting with the damage. Shear horizontal waves appear in the scattered waves because of the mode conversion. Instead of analyzing the whole large structure, the local damage area is analyzed using finite element analyses and analytical formulation is used to analyze the whole structure. The scatter fields are described in terms of wave damage interaction coefficients that involve scattering and mode conversion of Lamb waves. Lamb wave mode (S_0 and A_0) hit the damage from multiple directions and corresponding wave damage interaction coefficients are obtained around the damage. Harmonic analysis has been performed over the fundamental frequency domain and “scatter cubes” of complex-valued wave damage interaction coefficients are formed. The scatter cube provides the information of relative amplitude and phase of scattered waves around the damage that can be used for designing the sensor installation. An application based on real time domain signal has been illustrated for the problem of multiple-rivet-hole cracks using the scatter cubes with the analytical framework.

Keywords

Lamb wave, shear horizontal wave, structural health monitoring, nondestructive evaluation, scatter cube, sensor design

Date received: 19 May 2016; accepted: 6 December 2016

Introduction

The most important field of structural health monitoring (SHM) and nondestructive evaluation (NDE) deals with the detection of faults in structures, such as cracks, disbonds, delamination, impact damage, and corrosion thinning. Development of corrosion and fatigue cracks at the rivet holes and fasteners in the aircraft structures is the most frequent problem faced in the maintenance of aircraft. The cracks can grow to a critical size and threaten the structural integrity if they remain undetected. Ultrasonic guided wave techniques can be used for the detection of the emanating cracks from the rivet holes fastly, accurately, and efficiently as compared to the laborious point-by-point inspection technique.

State of the art

The problem of the detection of rivet hole cracks has been analyzed by the researchers of the NDE and SHM research field over the recent years. In 2009, the probability of detection (POD) by model-assisted approach has been demonstrated for the fatigue crack growth in wing lap joint, wing skin fastener holes, and airframe fastener holes.^{1,2} In 2012, the use of the transfer function approach to the model-assisted

POD is investigated by Bode et al.³ through the inspection of a specimen of aircraft lap joint. However, the researchers emphasized the detection of fastener hole cracks mainly based on the nondestructive inspection (NDI) technique. In 2015, the SHM-based POD was obtained for the fatigue crack initiation in the lug with a wing attachment, which acted as a representative airplane component.⁴ The piezoelectric wafer active sensor (PWAS) was used for transmitting and receiving signals with the center frequency domain of 200 to 1000 kHz. In order to detect the crack, six receiver sensors and nine excitation center frequencies were used to compute the damage index for a different combination of sensor and center frequency pair.

¹Department of Mechanical Engineering, University of South Carolina, Columbia, SC, USA

²Department of Aerospace Engineering, University of Michigan, Ann Arbor, MI, USA

Corresponding author:

Md Yeasin Bhuiyan, Department of Mechanical Engineering, University of South Carolina, 300 Main Street, Room#A237, Columbia, SC 29208-0001, USA.

Email: yeasin85@gmail.com



Modeling of nonlinear interactions between guided waves and fatigue cracks using local interaction simulation approach



Yanfeng Shen, Carlos E.S. Cesnik*

Department of Aerospace Engineering, University of Michigan, Ann Arbor, MI 48109, USA

ARTICLE INFO

Article history:

Received 1 June 2016

Received in revised form 26 August 2016

Accepted 2 October 2016

Available online 6 October 2016

Keywords:

Ultrasonic guided waves

Fatigue crack

LISA

Damage detection

Structural health monitoring

Nonlinear ultrasonics

Contact model

ABSTRACT

This article presents a parallel algorithm to model the nonlinear dynamic interactions between ultrasonic guided waves and fatigue cracks. The Local Interaction Simulation Approach (LISA) is further developed to capture the contact-impact clapping phenomena during the wave crack interactions based on the penalty method. Initial opening and closure distributions are considered to approximate the 3-D rough crack microscopic features. A Coulomb friction model is integrated to capture the stick-slip contact motions between the crack surfaces. The LISA procedure is parallelized via the Compute Unified Device Architecture (CUDA), which enables parallel computing on powerful graphic cards. The explicit contact formulation, the parallel algorithm, as well as the GPU-based implementation facilitate LISA's high computational efficiency over the conventional finite element method (FEM). This article starts with the theoretical formulation and numerical implementation of the proposed algorithm, followed by the solution behavior study and numerical verification against a commercial finite element code. Numerical case studies are conducted on Lamb wave interactions with fatigue cracks. Several nonlinear ultrasonic phenomena are addressed. The classical nonlinear higher harmonic and DC response are successfully captured. The nonlinear mode conversion at a through-thickness and a half-thickness fatigue crack is investigated. Threshold behaviors, induced by initial openings and closures of rough crack surfaces, are depicted by the proposed contact LISA model.

© 2016 Elsevier B.V. All rights reserved.

1. Introduction

Fatigue cracks may exist in a broad range of engineering materials and are considered precursors to catastrophic failures. Effective detection of fatigue cracks at their early stages is of critical importance and particular interest [1]. However, unlike gross damage, the fatigue cracks are barely visible in their closed state, imposing considerable difficulty for the conventional ultrasonic techniques which are only sensitive to open cracks [2]. On the other hand, nonlinear ultrasonic techniques have shown much higher sensitivity to incipient structural changes with distinctive nonlinear features, such as higher/sub harmonic generation, DC response, mixed frequency modulation response (sideband effects), and various frequency/amplitude dependent threshold behaviors [3,4]. The integration of nonlinear ultrasonic techniques into guided wave based interrogation procedures is drawing increasing attention from the Structural Health Monitoring (SHM) and Non-destructive Evaluation (NDE) communities,

because such a practice inherits both the sensitivity from nonlinear NDE techniques and the large-area inspection capability from SHM guided waves [5].

In order to achieve the optimum design of nonlinear guided wave based SHM system and the effective interpretation of the sensing signals, efficient computational models are needed. Many theoretical work on nonlinear guided wave phenomena induced by material nonlinearity have been conducted. Deng investigated the generation and accumulation of higher harmonics of Lamb waves using analytical formulations [6,7]. Srivastava and di Scalea studied the existence of antisymmetric or symmetric Lamb waves at nonlinear higher harmonics via modal analysis approach and the method of perturbation [8]. Ohm and Hamilton derived a time-domain evolution equation for nonlinear Rayleigh waves in dispersive media [9]. Muller et al. investigated the second harmonic generation of Lamb waves in nonlinear elastic plates using the analytical solution through the use of a perturbation method [10]. Manktelow et al. used a finite-element based perturbation analysis to study the wave propagation in nonlinear periodic structures [11]. On the other hand, the simulation of localized nonlinear dynamics induced by fatigue cracks is also a challenging task; the

* Corresponding author.

E-mail address: cesnik@umich.edu (C.E.S. Cesnik).

Mapped finite element methods: High-order approximations of problems on domains with cracks and corners

Maurizio M. Chiaramonte^{1,2,*}, Yongxing Shen^{3,*} and Adrian J. Lew^{2,*}

¹*Department of Civil and Environmental Engineering, Princeton University, Princeton, NJ 08544, USA*

²*Department of Mechanical Engineering, Stanford University, Stanford, CA 94305, USA*

³*State Key Laboratory of Metal Matrix Composites, University of Michigan-Shanghai Jiao Tong University Joint Institute, Shanghai Jiao Tong University, Shanghai, 200240, China*

SUMMARY

Linear elasticity problems posed on cracked domains, or domains with re-entrant corners, yield singular solutions that deteriorate the optimality of convergence of finite element methods. In this work, we propose an optimally convergent finite element method for this class of problems. The method is based on approximating a much smoother function obtained by locally reparameterizing the solution around the singularities. This reparameterized solution can be approximated using standard finite element procedures yielding optimal convergence rates for any order of interpolating polynomials, without additional degrees of freedom or special shape functions. Hence, the method provides optimally convergent solutions for the same computational complexity of standard finite element methods. Furthermore, the sparsity and the conditioning of the resulting system is preserved. The method handles body forces and crack-face tractions, as well as multiple crack tips and re-entrant corners. The advantages of the method are showcased for four different problems: a straight crack with loaded faces, a circular arc crack, an L-shaped domain undergoing anti-plane deformation, and lastly a crack along a bimaterial interface. Optimality in convergence is observed for all the examples. A proof of optimal convergence is accomplished mainly by proving the regularity of the reparameterized solution. Copyright © 2016 John Wiley & Sons, Ltd.

Received 5 April 2016; Revised 23 November 2016; Accepted 24 November 2016

KEY WORDS: solid; crack problem; re-entrant corner; singularity

1. INTRODUCTION

In elliptic boundary value problems, such as linear elasticity and the Poisson problem, which can describe steady-state heat conduction, steady-state diffusion, or electrostatics, singularities in the solution may arise from non-smooth boundaries, discontinuous coefficients, or abrupt changes in boundary conditions. Problems with cracked domains, or those containing re-entrant corners, fall in the first category. The singularity of the solutions to this class of problems plagues the accuracy and convergence rate of standard (Lagrange) finite element methods. Concretely, finite element approximations of linear elasticity solutions in cracked domains converge in H^1 with order $1/2$, *regardless of the order of interpolating polynomials in each element*. To alleviate the shortcomings of standard finite element methods, several techniques have been proposed to address these singularities. These often provide a more accurate solution, but very few of them are capable of obtaining optimal rates of convergence for an arbitrary order of interpolating polynomials, which, as we show here, substantially reduce the computational time for a given desired accuracy.

*Correspondence to: Maurizio M. Chiaramonte, Department of Civil and Environmental Engineering, Princeton University, Princeton, NJ 08544, USA; Yongxing Shen, University of Michigan-Shanghai Jiao Tong University Joint Institute, Shanghai Jiao Tong University, Shanghai, China; Adrian J. Lew, Department of Mechanical Engineering, Stanford University, Stanford, CA 94305, USA.

†Email: chiaramonte@princeton.edu; yongxing.shen@sjtu.edu.cn; lewa@stanford.edu



Universal meshes for a branched crack

Yongxing Shen*, Can Wu, Yang Wan

State Key Laboratory of Metal Matrix Composites, University of Michigan-Shanghai Jiao Tong University Joint Institute, Shanghai Jiao Tong University, Shanghai, China



ARTICLE INFO

Keywords:

Branched crack
Universal meshes
Conforming mesh
Mesh deformation

ABSTRACT

We introduce an efficient approach to obtain conforming meshes for evolving branched cracks immersed in a fixed background mesh. The proposed approach is built on universal meshes (UM) proposed in Rangarajan et al. [34] which is able to construct conforming triangulations for a propagating simple crack. The UM functions by projecting certain nodes of the background mesh onto the crack and simultaneously relaxing their neighboring nodes to improve the quality of the resulting triangular mesh. The essence of the generalization to a branched crack is to determine which side of each branch to select nodes to move to the crack path. The choice is based on the consideration of minimizing mesh distortion. For the case of multiple junctions, we take into account the constraint that the nodes to be moved to the same crack branch must be on the same side of that branch. The proposed method inherits the main advantages of UM, including small perturbation to a fixed background mesh for a family of evolving cracks with no *a priori* conformity requirements. This advantage saves computational time compared with a brute-force mesh generation step. Numerical examples with one or multiple triple or quadruple junctions are provided.

1. Introduction

Dynamic crack analysis is essential in applications such as impact and explosion. Very often, an initially simple crack will bifurcate into two or more branches. Another scenario when bifurcation may occur is when the cracked material exhibits certain heterogeneity. Experimental and theoretical study of such phenomena has been an active field of research [1–9]. A typical example is hydraulic fracturing: when the hydraulic fracture intersects the natural fissures or layers, it may bifurcate into multiple branches, resulting in a complex fracture network [10].

Numerical analysis of crack propagation with the possibility of bifurcation allows gaining more insights of the process and more information for engineering designs. Such numerical methods can be roughly classified into two families: One explicitly taking into account the discrete crack paths, and the other adopting a smeared description of the cracks.

The smeared description of cracks is appealing since apparently the crack path evolution is obtained for free, without extra criteria for nucleation and bifurcation other than the evolution of the primary fields. Phase field methods for fracture are a typical kind of methods in this family [11–16], with [17] focused on branching. One of the drawbacks of such methods is, due to the *a priori* unknown crack path, the need to either employ a very fine mesh or an adaptively

refined mesh [18,19]. The gradient damage models [20] are another types of models of this kind.

In contrast, the discrete crack approaches generally simulate the crack evolution by obtaining the displacement, velocity and stress fields, calculating the crack increment and then updating the spatial discretization for the evolving crack. This requires two ingredients: An efficient solver for the elastic or elastoplastic field, and a branching criterion (including the critical crack speed and the directions of the new branches) such as that proposed by Katzav et al. [21]. For the first ingredient, distinction can be made on whether the spatial discretization needs to conform to the evolving cracked domain.

Employing a crack-independent mesh, the extended finite element method (XFEM) [22–24] approximates the displacement field via the introduction of Heaviside functions and leading terms of the near-tip asymptotic expansion. Nevertheless, XFEMs require processing elements divided by arbitrary crack paths, leading to complicated geometric programming, involved numerical integration, and possibly ill-conditioned stiffness matrix due to arbitrarily small pieces cut by the crack. Such disadvantages are overcome by various modifications of the method; however, if a conforming mesh is adopted, the aforementioned issues will disappear.

Several approaches can be used to obtain a conforming mesh for a propagating crack, or more generally, an evolving domain. A brute-force approach is to automatically mesh the cracked domain whenever

* Corresponding author.

E-mail addresses: yongxing.shen@sjtu.edu.cn (Y. Shen), pullding@sjtu.edu.cn (C. Wu), yang.wan@sjtu.edu.cn (Y. Wan).

<http://dx.doi.org/10.1016/j.finel.2016.12.003>

Received 1 September 2016; Received in revised form 21 November 2016; Accepted 12 December 2016

Available online 01 March 2017

0168-874X/ © 2016 Elsevier B.V. All rights reserved.



Research
Additive Manufacturing—Article

Modeling and Experimental Validation of the Electron Beam Selective Melting Process

Wentao Yan^{a,b}, Ya Qian^a, Weixin Ma^c, Bin Zhou^a, Yongxing Shen^c, Feng Lin^{a,*}

^a Department of Mechanical Engineering, Tsinghua University, Beijing 100084, China

^b Department of Mechanical Engineering, Northwestern University, Evanston, IL 60201, USA

^c State Key Lab of Metal Matrix Composites, Shanghai Jiao Tong University, Shanghai 200240, China

ARTICLE INFO

Article history:

Received 15 May 2017

Revised 25 September 2017

Accepted 27 September 2017

Available online 25 October 2017

Keywords:

Modeling

Electron beam

Additive manufacturing

Powder scale

ABSTRACT

Electron beam selective melting (EBSM) is a promising additive manufacturing (AM) technology. The EBSM process consists of three major procedures: ① spreading a powder layer, ② preheating to slightly sinter the powder, and ③ selectively melting the powder bed. The highly transient multi-physics phenomena involved in these procedures pose a significant challenge for *in situ* experimental observation and measurement. To advance the understanding of the physical mechanisms in each procedure, we leverage high-fidelity modeling and post-process experiments. The models resemble the actual fabrication procedures, including ① a powder-spreading model using the discrete element method (DEM), ② a phase field (PF) model of powder sintering (solid-state sintering), and ③ a powder-melting (liquid-state sintering) model using the finite volume method (FVM). Comprehensive insights into all the major procedures are provided, which have rarely been reported. Preliminary simulation results (including powder particle packing within the powder bed, sintering neck formation between particles, and single-track defects) agree qualitatively with experiments, demonstrating the ability to understand the mechanisms and to guide the design and optimization of the experimental setup and manufacturing process.

© 2017 THE AUTHORS. Published by Elsevier LTD on behalf of the Chinese Academy of Engineering and Higher Education Press Limited Company. This is an open access article under the CC BY-NC-ND license (<http://creativecommons.org/licenses/by-nc-nd/4.0/>).

1. Introduction

Electron beam selective melting (EBSM) is a promising additive manufacturing (AM) technology for metallic components. It is capable of manufacturing components with complex geometry, and opens up new avenues for locally manipulating chemical compositions and mechanical properties as well. For example, Yang et al. [1] manufactured auxetic lattice structures with negative Poisson's ratios, and Ge et al. [2–4] manufactured functionally graded Ti-TiAl materials.

There are three main fabrication procedures in EBSM [2], as shown in Fig. 1.

(1) Spread one layer of powder on a preheated platform or previous layer. The layer thickness can vary for different layers. For each

layer, the mixture ratio of the several different types of powder can be designed and tailored in order to allow the chemical compositions to be manipulated.

(2) Preheat the powder bed to make the powder slightly sintered. This helps prevent powder scattering, which may even lead to build failure.

(3) Selectively melt the powder bed. The beam power and scan speed are key factors that greatly influence the final part quality.

Although the basic principle of EBSM is rather straightforward, the actual processes consist of multiple physical phenomena such as powder particle packing, heat transfer, phase transformation, and fluid flow, and a number of factors influence the process and fabrication quality. There are a considerable number of fundamental physical mechanisms in each fabrication procedure to be understood

* Corresponding author.

E-mail address: linfeng@tsinghua.edu.cn

<http://dx.doi.org/10.1016/J.ENG.2017.05.021>

2095-8099/© 2017 THE AUTHORS. Published by Elsevier LTD on behalf of the Chinese Academy of Engineering and Higher Education Press Limited Company. This is an open access article under the CC BY-NC-ND license (<http://creativecommons.org/licenses/by-nc-nd/4.0/>).

Instability evolution of the viscous elliptic liquid jet in the Rayleigh regime

Shibo Gu, Lipo Wang,^{*} and David L. S. Hung

UM-SJTU Joint Institute, Shanghai Jiao Tong University, Shanghai, China

(Received 10 March 2017; published 21 June 2017)

For jet flow emanating from noncircular orifices, an unbalanced surface tension force leads to capillary instability, which is independent of influence from the ambient air in the Rayleigh regime. In the present article, the dynamic behavior of incompressible elliptical jets in the Rayleigh regime is investigated. Theoretically, with the consideration of the fluid viscosity, the solution of the Cosserat equation consists of a particular solution and a complementary solution. For the complementary solution the wave number of disturbance modes has two complex conjugate roots, which are responsible for the jet breakup. To match the nonzero particular solution, a spatial wave needs to be introduced, which is independent of external perturbations. Physically, such a spatial wave is interpreted as the axis-switching phenomenon. The predicted features of the axis-switching wavelength and the damping effect from the fluid viscosity have been successfully verified by experimental results. Moreover, the dispersion relations from the present theory suggest that the growth rate of spatial instability is influenced by orifice eccentricity, the Weber number, and the Ohnesorge number.

DOI: [10.1103/PhysRevE.95.063112](https://doi.org/10.1103/PhysRevE.95.063112)

I. INTRODUCTION

Liquid interface dynamics is of both fundamental and practical importance. For example, at the jet interface, the instability evolution, momentum, and species mixing are closely relevant to atomization and spray. Physically, once the instability modes, which may originate either from natural sources or forced perturbations imposed on the jet system, are strong enough, the jet breaks up. According to Reitz [1], there are four different jet instability and breakup regimes, which are the Rayleigh regime, first wind-induced regime, second wind-induced regime, and atomization regime. Such a classification depends on the relative dominance of the liquid inertia, surface tension, and aerodynamic forces acting on the jet, which can be summarized in the nondimensional Weber number $We_L = U^2 R \rho_L / \sigma$ for the liquid phase and $We_G = U^2 R \rho_G / \sigma$ for the gas phase, where U is the uniform jet velocity, R is the equivalent radius calculated from the jet cross-section area, ρ_L and ρ_G are the liquid and gas density, respectively, and σ is the surface tension coefficient. Under some conditions, the gravity force and liquid viscous forces are important as well.

The pioneering works on interface instability analysis include the study of liquid sheet dynamics [2] and interface instability [3–6]. For instance, Rayleigh studied the classic circular jet problem in the Rayleigh regime [4], where the effect of aerodynamics on the liquid jet can be neglected. Under the inviscid liquid assumption, the velocity potential satisfies the Laplacian equation. If the gravity effect is negligibly small, jet disintegration is mainly due to surface tension, referred to as capillary instability. The solution of the linearized equation for the axisymmetric disturbance component suggests that the liquid jet will break up when the disturbance wavelength exceeds the jet circumference. The linear Rayleigh theory developed for small perturbations is capable of a rather accurate prediction of the breakup time and length of capillary jets of low-viscosity liquids [7].

Besides the circular case, jets from different orifices are important as well, because of the advantages in mixing enhancement, faster breakup, and more freedom for design and control. In comparison with the aforementioned extensively studied circular jet problem, nonsymmetric jets are less understood, especially the axis-switching phenomenon, which originates from the imbalance between the capillary force and inertia force, leading to a change of the cross-section shape along the jet flow direction. Most of the existing results on nonsymmetric jet flows have been obtained either experimentally or numerically [8–10]. For example, the effects of the orifice aspect ratio and liquid viscosity on the axis-switching process of an elliptical jet were investigated experimentally [8]. It has been found that the breakup of an elliptical liquid jet is largely influenced by the shape of the orifice.

The relatively tractable elliptic configuration is of special interest for analysis. For the inviscid case, three-dimensional equations can be solved with the velocity potential method [4]. However, for the viscous case, an exact three-dimensional solution has not yet been obtained. Alternatively, one-dimensional Cosserat equations are derived to approximate the elliptical jet dynamics based on the assumption of a negligible cross-section variation [11,12]. For the circular case, when setting the semimajor and semiminor axes equal, the solution of such Cosserat equations agrees well with Rayleigh's results [4]. The mean velocity profile inside the elliptic jet was introduced and the propagation of different disturbances was analyzed in Refs. [13,14]. Bechtel and Bechtel *et al.* [15,16] studied the motion of inviscid and Newtonian elliptic jets directly from the Navier-Stokes equations. By integration over the cross section, one-dimensional equations with the same form as the Cosserat equations can be obtained. In addition, the effects of viscosity and gravity have been partly discussed. Amini *et al.* used the Cosserat model to study the growth rate of forced disturbances, and the dependence on different characteristic parameters [17,18]. Subsequently, the jet breakup property, together with experimental results, have been discussed, but the perturbation growth rate and cutoff wave number seem to have been significantly overpredicted [19]. For more complex cases, the three-dimensional

^{*}lipo.wang@sjtu.edu.cn

Cooling Injection Effect on a Transonic Squealer Tip—Part I: Experimental Heat Transfer Results and CFD Validation

H. Ma

University of Michigan-Shanghai
Jiao Tong University Joint Institute,
Shanghai 200240, China
e-mail: haitengma@gmail.com

Q. Zhang¹

Department of Mechanical Engineering
and Aeronautics,
School of Engineering
and Mathematical Sciences,
City, University of London,
Northampton Square,
London EC1V 0HB, UK
e-mail: Qiang.Zhang.1@city.ac.uk

L. He

Department of Engineering Science,
University of Oxford,
Oxford OX2 0ES, UK
e-mail: Li.He@eng.ox.ac.uk

Z. Wang

University of Michigan-Shanghai
Jiao Tong University Joint Institute,
Shanghai 200240, China
e-mail: wangzhaoguang1991@hotmail.com

L. Wang

University of Michigan-Shanghai
Jiao Tong University Joint Institute,
Shanghai 200240, China
e-mail: lipo.wang@sjtu.edu.cn

Recent studies have demonstrated that the aerothermal characteristics of turbine rotor blade tip under a transonic condition are qualitatively different from those under a low-speed subsonic condition. The cooling injection adds further complexity to the over-tip-leakage (OTL) transonic flow behavior and aerothermal performance, particularly for commonly studied shroudless tip configurations such as a squealer tip. However there has been no published experimental study of a cooled transonic squealer. The present study investigates the effect of cooling injection on a transonic squealer through a closely combined experimental and CFD effort. Part I of this two-part paper presents the first of the kind tip cooling experimental data obtained in a transonic linear cascade environment (exit Mach number 0.95). Transient thermal measurements are carried out for an uncooled squealer tip and six cooling configurations with different locations and numbers of discrete holes. High-resolution distributions of heat transfer coefficient and cooling effectiveness are obtained. ANSYS FLUENT is employed to perform numerical simulations for all the experimental cases. The mesh and turbulence modeling dependence is first evaluated before further computational studies are carried out. Both the experimental and computational results consistently illustrate strong interactions between the OTL flow and cooling injection. When the cooling injection (even with a relatively small amount) is introduced, distinctive series of stripes in surface heat transfer coefficient are observed with an opposite trend in the chordwise variations on the squealer cavity floor and on the suction surface rim. Both experimental and CFD results have also consistently shown interesting signatures of the strong OTL flow-cooling interactions in terms of the net heat flux reduction distribution in areas seemingly unreachable by the coolant. Further examinations and analyses of the related flow physics and underlining vortical flow structures will be presented in Part II. [DOI: 10.1115/1.4035175]

1 Introduction

The rotor blade tip is the most vulnerable part in high-pressure (HP) turbine. In addition to being a major contributor to the loss of turbine efficiency, the over-tip-leakage (OTL) flow introduces very high thermal load to the tip and casing. The tip cooling design has always been a challenging task due to the complex OTL flow behavior and its interaction with cooling injection.

Researches on the blade tip heat transfer have been carried out extensively in the past three decades. A thorough review was provided by Bunker [1] about 15 years ago. More understanding has been gained through the recent research efforts gradually moving from simplified low-speed condition to more engine-realistic high-speed environment.

The early work by Mayle and Metzger [2] measured the averaged heat transfer coefficient on a modeled flat tip in a low-speed condition. They also established the wisdom of pressure-driven mechanism for the tip gap flow. Bunker et al. [3] reported “central sweet spot” of low heat transfer within the thickest portion of the tip in their experiments ($M_{\text{exit}} = 0.75$). A complementary study by Ameri and Bunker [4] showed good comparison between the experimental data and the numerical results using a radius edge tip model. In a low-speed condition, Newton et al. [5] and Krishnababu et al. [6] showed that the maximum heat transfer coefficient occurs on the flow reattachment region near the pressure side rim.

The aerothermal behavior of the squealer tip has been widely studied, mostly under subsonic conditions. The effect of cavity depth was presented by Metzger et al. [7], Chyu et al. [8], and Bunker and Bailey [9]. They all found that increasing the cavity depth reduces the heat transfer on the cavity floor. The effects of tip gap height, squealer geometry arrangement on blade tip heat transfer were presented by Azad et al. [10,11] and Kwak et al. [12]. Their results showed that increasing the tip clearance would bring up the heat transfer level and the suction side squealer outperforms the full squealer in terms of decreasing the overall tip heat transfer. Another parametric study by Zhou and Hodson [13] found that thinner squealer rim could lower the average heat transfer coefficient on the tip.

The primary goal of the tip cooling is to reduce the heat load and help the tip survive the extremely hot gas temperature, as addressed by Bunker [14]. For a subsonic flat blade tip ($M_{\text{exit}} = 0.6$), Kwak and Han [15] found that higher blowing ratios would decrease the heat transfer coefficient and increase the film cooling effectiveness. The effect of tip gap height on the adiabatic effectiveness and heat transfer coefficient was evaluated by Christophel et al. [16,17]. Better cooling performance is achieved for smaller tip gap due to its larger adiabatic effectiveness value. The effect of cooling hole location was evaluated by Newton et al. [18], who reported that injecting coolant inside the separation bubble would bring higher net heat flux reduction compared with injecting at the reattachment region.

The squealer tip has to be effectively cooled, especially near the thin rim region. Kwak and Han [19] and Ahn et al. [20] reported that coolant injection from both tip and pressure side holes provides higher film cooling effectiveness compared to the injection from tip holes only. The parametric study by Mhetras

¹Corresponding author.

Contributed by the Structures and Dynamics Committee of ASME for publication in the JOURNAL OF ENGINEERING FOR GAS TURBINES AND POWER. Manuscript received July 14, 2016; final manuscript received October 8, 2016; published online January 10, 2017. Editor: David Wisler.

Cooling Injection Effect on a Transonic Squealer Tip—Part II: Analysis of Aerothermal Interaction Physics

H. Ma

University of Michigan-Shanghai Jiao Tong
University Joint Institute,
Shanghai Jiao Tong University,
Shanghai 200240, China
e-mail: haitengma@gmail.com

Q. Zhang¹

Department of Mechanical Engineering and
Aeronautics,
School of Engineering and Mathematical
Sciences,
City, University of London,
Northampton Square,
London EC1V 0HB, UK
e-mail: Qiang.Zhang@city.ac.uk

L. He

Department of Engineering Science,
University of Oxford,
Oxford OX2 0ES, UK
e-mail: Li.He@eng.ox.ac.uk

Z. Wang

University of Michigan-Shanghai Jiao Tong
University Joint Institute,
Shanghai Jiao Tong University,
Shanghai 200240, China
e-mail: wangzhaoguang1991@hotmail.com

L. Wang

University of Michigan-Shanghai Jiao Tong
University Joint Institute,
Shanghai Jiao Tong University,
Shanghai 200240, China
e-mail: lipo.wang@sjtu.edu.cn

A basic attribute for turbine blade film cooling is that coolant injected should be largely passively convected by the local base flow. However, the effective working of the conventional wisdom may be compromised when the cooling injection strongly interacts with the base flow. Rotor blade tip of a transonic high-pressure (HP) turbine is one of such challenging regions for which basic understanding of the relevant aerothermal behavior as a basis for effective heat transfer/cooling design is lacking. The need to increase our understanding and predictability for high-speed transonic blade tip has been underlined by some recent findings that tip heat transfer characteristics in a transonic flow are qualitatively different from those at a low speed. Although there have been extensive studies previously on squealer blade tip cooling, there have been no published experimental studies under a transonic flow condition. The present study investigates the effect of cooling injection on a transonic squealer tip through a closely combined experimental and computational fluid dynamics (CFD) effort. The experimental and computational results as presented in Part I have consistently revealed some distinctive aerothermal signatures of the strong coolant-base flow interactions. In this paper, as Part II, detailed analyses using the validated CFD solutions are conducted to identify, analyze, and understand the causal links between the aerothermal signatures and the driving flow structures and physical mechanisms. It is shown that the interactions between the coolant injection and the base over-tip leakage (OTL) flow in the squealer tip region are much stronger in the frontal subsonic region than the rear transonic region. The dominant vortical flow structure is a counter-rotating vortex pair (CRVP) associated with each discrete cooling injection. High HTC stripes on the cavity floor are directly linked to the impingement heat transfer augmentation associated with one leg of the CRVP, which is considerably enhanced by the near-floor fluid movement driven by the overall pressure gradient along the camber line (CAM). The strength of the coolant-base flow interaction as signified by the augmented values of the HTC stripes is seen to correlate to the interplay and balance between the OTL flow and the CRVP structure. As such, for the frontal subsonic part of the cavity, there is a prevailing spanwise inward flow initiated by the CRVP, which has profoundly changed the local base flow, leading to high HTC stripes on the cavity floor. On the other hand, for the rear high speed part, the high inertia of the OTL flow dominates; thus, the vortical flow disturbances associated with the CRVP are largely passively convected, leaving clear signatures on the top surface of the suction surface rim. A further interesting side effect of the strong interaction in the frontal subsonic region is that there is considerable net heat flux reduction (NHFR) in an area seemingly unreachable by the injected coolant. The present results have confirmed that this is due to the large reduction in the local HTC as a consequence of the upstream propagated impact of the strong coolant-base flow interactions. [DOI: 10.1115/1.4035200]

1 Introduction

In the development of new-generation gas turbine engines, the turbine inlet temperature keeps increasing to pursue higher efficiency. Advanced cooling technologies are crucial to ensure the survival of turbine blades in the extremely hot environment. Among all the surfaces of the high-pressure (HP) turbine blade, the tip region has the highest thermal load (Bogard and Thole [1]). The primary objective of tip cooling is to reduce surface heat flux with minimal coolant consumption while maintaining the

aerodynamic efficiency, and most blade tip cooling are achieved through experience (Bunker [2]).

Most of the tip cooling studies have been conducted at low-speed or high subsonic flow conditions. Thermal performance has been the main focus of these studies. Kwak and Han [3,4] found that higher blowing ratio produces lower heat transfer coefficient (HTC) and higher film cooling effectiveness on the flat and squealer tips. Christophel et al. [5,6] investigated the heat transfer characters of a cooled flat tip experimentally. Better cooling performance was reported for smaller tip gap height. Ahn et al. [7] carried out a parametric study regarding tip geometries, locations of the cooling holes, blowing ratios, and tip clearance. They found that the highest film cooling effectiveness was achieved by injecting coolant from only the pressure side (PS) for the flat tip case and from both the tip and pressure side for the squealer tip case.

¹Corresponding author.

Contributed by the Structures and Dynamics Committee of ASME for publication in the JOURNAL OF ENGINEERING FOR GAS TURBINES AND POWER. Manuscript received July 14, 2016; final manuscript received August 24, 2016; published online January 10, 2017. Editor: David Wisler.

Extremal-point density of scaling processes: From fractional Brownian motion to turbulence in one dimension

Yongxiang Huang (黄永祥),^{1,*} Lipo Wang (王利坡),² F. G. Schmitt,³ Xiaobo Zheng (郑小波),⁴
Nan Jiang (姜楠),⁴ and Yulu Liu (刘宇陆)⁵

¹State Key Laboratory of Marine Environmental Science, College of Ocean and Earth Sciences, Xiamen University, Xiamen 361102, China

²UM-SJTU Joint Institute, Shanghai JiaoTong University, Shanghai, 200240, China

³CNRS, Univ. Lille, Univ. Littoral Cote d'Opale, UMR 8187, LOG, Laboratoire d'Océanologie et de Géosciences, F 62 930 Wimereux, France

⁴Department of Mechanics, Tianjin University, 300072 Tianjin, China

⁵Shanghai Institute of Applied Mathematics and Mechanics, Shanghai University, Shanghai 200072, China

(Received 7 February 2017; revised manuscript received 19 May 2017; published 17 July 2017)

In recent years several local extrema-based methodologies have been proposed to investigate either the nonlinear or the nonstationary time series for scaling analysis. In the present work, we study systematically the distribution of the local extrema for both synthesized scaling processes and turbulent velocity data from experiments. The results show that for the fractional Brownian motion (fBm) without intermittency correction the measured extremal-point-density (EPD) agrees well with a theoretical prediction. For a multifractal random walk (MRW) with the lognormal statistics, the measured EPD is independent of the intermittency parameter μ , suggesting that the intermittency correction does not change the distribution of extremal points but changes the amplitude. By introducing a coarse-grained operator, the power-law behavior of these scaling processes is then revealed via the measured EPD for different scales. For fBm the scaling exponent $\xi(H)$ is found to be $\xi(H) = H$, where H is Hurst number, while for MRW $\xi(\mu)$ shows a linear relation with the intermittency parameter μ . Such EPD approach is further applied to the turbulent velocity data obtained from a wind tunnel flow experiment with the Taylor scale λ -based Reynolds number $Re_\lambda = 720$, and a turbulent boundary layer with the momentum thickness θ based Reynolds number $Re_\theta = 810$. A scaling exponent $\xi \simeq 0.37$ is retrieved for the former case. For the latter one, the measured EPD shows clearly four regimes, which agrees well with the corresponding sublayer structures inside the turbulent boundary layer.

DOI: 10.1103/PhysRevE.96.012215

I. INTRODUCTION

Multiscale statistics is recognized as one of the most important features of complex dynamical systems. Several methodologies have been put forward to characterize the multiscale property, such as structure function analysis proposed by Kolmogorov [1], wavelet-based approaches [2,3], the Hilbert-Huang transform [4,5], and multilevel segment analysis [6]. The local extremal point (see definition below) plays important roles in multiscale characterization [2,4–6]. For example, in the Hilbert-Huang transform, local extrema are used to construct the upper and lower envelope [4]; in multilevel segment analysis, a structure function is defined conditionally on the segments between consecutive extremal points [6]. Experimental results suggest that these two methods can overcome some potential shortcomings of the conventional structure function [6–8], such as scale mixing. The scale and the corresponding scaling or multifractal nature are embedded in the local extremal point statistics, which definitely deserves further studies.

The distribution of local extremal points is associated with the dynamical behavior of the considered process. For a discrete time series $x(t_i)$, $i = 1, 2, 3 \dots N$, and a sampling frequency f_s , the local extremal point (either local maxima or minima) satisfies the following relation:

$$x_t(t_{i+1})x_t(t_i) < 0, \quad (1)$$

where $x_t(t_i) = [x(t_{i+1}) - x(t_i)]/(t_{i+1} - t_i)$ is the local slope of $x(t_i)$. This property is used for direct counting of the number of extrema. Clearly the local extrema correspond to the zero-crossing of the first-order derivative of $x(t_i)$. If $x(t_i)$ acts as the turbulent velocity, $x_t(t_i)$ is then the acceleration. The local extreme is thus an indicator of the sign change of the acceleration and forcing, showing the dynamical property of $x(t_i)$ [6]. Theoretically, Rice [9] proved that for a stationary continuous process $x(t)$, if $x(t)$ and $x_t(t)$ are statistically independent and Gaussian distributed, then the zero-crossing ratio (ZCR) per second of $x(t)$, denoted as N_0 , can be expressed as

$$N_0 = \frac{1}{\pi} \left(\frac{\langle x_t^2(t) \rangle_t}{\langle x^2(t) \rangle_t} \right)^{1/2}, \quad (2)$$

where $\langle \rangle_t$ means the sample average with respect to t .

Similarly, ZCR of the first-order derivative, i.e., $x_t(t)$, denoted as N_1 can be written as [11]

$$N_1 = \frac{1}{\pi} \left(\frac{\langle x_{tt}^2(t) \rangle_t}{\langle x_t^2(t) \rangle_t} \right)^{1/2}, \quad (3)$$

where $x_{tt}(t)$ is the second-order derivative. The corresponding extremal-point-density (EPD), e.g., the ratio between number of extremal points and the total data length, is then written as

$$\mathcal{I} = \frac{N_1}{f_s} = \frac{1}{\pi f_s} \left(\frac{\langle x_{tt}^2(t) \rangle_t}{\langle x_t^2(t) \rangle_t} \right)^{1/2}, \quad (4)$$

where f_s is the sampling frequency of the discrete process. Later, Ylvisaker [12] showed that in Eq. (2) for any continuous

*yongxianghuang@gmail.com

Intrinsic flow structure and multifractality in two-dimensional bacterial turbulence

Lipo Wang (王利坡)^{1,*} and Yongxiang Huang (黄永祥)^{2,†}

¹UM-SJTU Joint Institute, Shanghai JiaoTong University, Shanghai 200240, People's Republic of China

²State Key Laboratory of Marine Environmental Science, College of Ocean and Earth Sciences, Xiamen University, Xiamen 361102, People's Republic of China

(Received 30 July 2016; revised manuscript received 31 March 2017; published 24 May 2017)

The active interaction between the bacteria and fluid generates turbulent structures even at zero Reynolds number. The velocity of such a flow obtained experimentally has been quantitatively investigated based on streamline segment analysis. There is a clear transition at about 16 times the organism body length separating two different scale regimes, which may be attributed to the different influence of the viscous effect. Surprisingly the scaling extracted from the streamline segment indicates the existence of scale similarity even at the zero Reynolds number limit. Moreover, the multifractal feature can be quantitatively described via a lognormal formula with the Hurst number $H = 0.76$ and the intermittency parameter $\mu = 0.20$, which is coincidentally in agreement with the three-dimensional hydrodynamic turbulence result. The direction of cascade is measured via the filter-space technique. An inverse energy cascade is confirmed. For the enstrophy, a forward cascade is observed when $r/R \leq 3$, and an inverse one is observed when $r/R > 3$, where r and R are the separation distance and the bacteria body size, respectively. Additionally, the lognormal statistics is verified for the coarse-grained energy dissipation and enstrophy, which supports the lognormal formula to fit the measured scaling exponent.

DOI: 10.1103/PhysRevE.95.052215

I. INTRODUCTION

In three-dimensional (3D) hydrodynamic turbulence, scale-invariant properties are inherited at different scales via the cascade process, i.e., the Richardson-Kolmogorov energy cascade, where energy is transferred from larger to smaller scales until dissipated to heat at viscosity scale [1]. It is generally believed that the energy injection is through the mean flow or the large-scale movement. To characterize such complex dynamics at different scales, the structure function based on velocity increment has been widely applied in different turbulent systems, including bacterial turbulence [2]. Conventionally the structure function is defined as

$$S_q(r) = \langle \Delta \mathbf{u}_r(\mathbf{x})^q \rangle_{\mathbf{x}} \sim r^{\zeta(q)}, \quad \Delta \mathbf{u}_r(\mathbf{x}) = \mathbf{u}(\mathbf{x} + \mathbf{r}) - \mathbf{u}(\mathbf{x}). \quad (1)$$

Here \mathbf{x} represents the spatial coordinate and $r = |\mathbf{r}|$ is the separation scale lying in the inertial range $\ell_v \ll r \ll L$, where ℓ_v is the Kolmogorov scale and L is the integral scale. The existing results [3–5] show that the aforementioned definition in Eq. (1) could mix information from different flow structures; thus, it is difficult to detect the scaling index $\zeta(q)$.

In general, the scale r is determined by the dynamic process itself, for instance the topology of the fluid structure. In recent years several new approaches have been proposed to overcome this difficulty, e.g., detrended fluctuation analysis [6], the Hilbert-Huang transform [7,8], and multilevel segment analysis [9]. For the hydrodynamic turbulent system, the measured $\zeta(q)$ is nonlinear with respect to q , which is termed multifractality. Physically, multifractality originates from the nonlinearity of the Navier-Stokes equation.

In active flows, living matter such as bacteria interacts with the fluid. Thus, the patterns of energy injection and dissipation

are different from the classic Navier-Stokes governed flows, raising more complexities to be investigated [10–12]. For example, in bacterial turbulence the energy injection scale is comparable to R , the body length scale of the microorganisms. R is often a few or dozens of micrometers, which is much smaller than the fluid dissipative scale ℓ_v . This interesting flow status has been redefined as “mesoscale turbulence” in living fluid [2,13]. Although the background flow has much smaller Reynolds numbers than that required for conventional fluid turbulence, under the self-propulsion action by the microorganisms, the flow still exhibits a turbulentlike movement even at zero Reynolds number [2,14–24]. Meanwhile the effects from the flow can be important not only for nutrient mixing, information passage, and thus the biological behavior but also for driving micromachines [25].

Experimentally the velocity field in bacterial turbulence can be measured in the Eulerian frame via the confocal particle image velocimetry (PIV) technique [18,19]. Flow visualization shows clearly that the collective motion of bacteria in the suspension exhibits coherent structures on a scale much larger than the individual body length, e.g., $10R$ [2]. This important property can be understood from a simplified picture of interaction between individual swimmers [15,16,21,23]. Theoretically there are different models to predict the active fluids by constructing the possible field governing equations, inevitably with some control parameters [2,12,20,22]. Numerical tests show that by adjusting these control parameters some of the measurement results can satisfactorily be reproduced, for instance, the large-scale coherent structure [13,20]. Wensink *et al.* [2] observed a dual-power-law behavior from the solution of a two-dimensional (2D) bacterial turbulence model equation. Recently, Qiu *et al.* [24] confirmed the intermittency correction in bacterial turbulence via a Hilbert-based methodology. From the observed dual-power-law behavior, it can be estimated that intermittency in the smaller-scale regime is stronger than that in the large-scale regime. In spite of these latest progresses, the

*lipo.wang@sjtu.edu.cn

†yongxianghuang@gmail.com

On the origin of intrinsic randomness of Rayleigh-Bénard turbulence

ZhiLiang Lin¹, LiPo Wang², and ShiJun Liao^{1,3*}

¹*School of Naval Architecture, Ocean and Civil Engineering, Shanghai Jiaotong University, Shanghai 200240, China;*

²*UM-SJTU Joint Institute, Shanghai Jiaotong University, Shanghai 200240, China;*

³*Ministry-of-Education Key Laboratory in Scientific and Engineering Computing, Shanghai 200240, China*

Received October 10, 2016; accepted November 10, 2016; published online November 28, 2016

It is of broad interest to understand how the evolution of non-equilibrium systems can be triggered and the role played by external perturbations. A famous example is the origin of randomness in the laminar-turbulence transition, which is raised in the pipe flow experiment by Reynolds as a century old unresolved problem. Although there exist different hypotheses, it is widely believed that the randomness is “intrinsic”, which, however, remains as an open question to be verified. Simulating the modeled Rayleigh-Bénard convection system by means of the so-called clean numerical simulation (CNS) with negligible numerical noises that are smaller even than thermal fluctuation, we verify that turbulence can be self-excited from the inherent thermal fluctuation without any external disturbances, i.e. out of nothing. This reveals a relationship between microscopic physical uncertainty and macroscopic randomness. It is found that in physics the system nonlinearity functions as a channel for randomness information, and energy as well, to transport microscopic uncertainty toward large scales. Such scenario can generally be helpful to understand the various relevant phenomena. In methodology, compared with direct numerical simulation (DNS), CNS opens a new direction to investigate turbulent flows with largely improved accuracy and reliability.

turbulence, chaos, thermal fluctuation, clean numerical simulation

PACS number(s): 47.20.Bp, 47.27.Cn, 47.27.er, 47.27.E-, 47.27.ek

Citation: Z. L. Lin, L. P. Wang, and S. J. Liao, On the origin of intrinsic randomness of Rayleigh-Bénard turbulence, *Sci. China-Phys. Mech. Astron.* **60**, 014712 (2017), doi: [10.1007/s11433-016-0401-5](https://doi.org/10.1007/s11433-016-0401-5)

1 Introduction

The evolution of non-equilibrium systems involves energy exchange through the system boundary with the surroundings. It is of broad interest to understand how such evolution can be triggered and what the function of external perturbation is. A famous example is the laminar-turbulent transition of the pipe flow first reported by Reynolds [1] from his pioneering experiment. The continuous devoted efforts [2-4] have greatly enriched our understanding. For example, by measuring the puff decay and splitting time the critical Rey-

nolds number in the 3D pipe flow can be numerically estimated (around 2040) [3,5,6]. Besides, with the help of direct numerical simulation (DNS) with very fine resolution, both spatially and temporally, Wu et al. [4] demonstrated the transition sensitivity to the pipe entrance condition. Physically laminar-turbulent transition is by nature closely relevant to disturbances, which can be both external and internal. It is widely believed that randomness is an intrinsic property in turbulence. However, till now our understanding of the origin and evolution mechanism of such intrinsic randomness is still unclear.

Numerically the Navier-Stokes (NS) equations can be solved by DNS with exactly the same initial/boundary conditions so as to exclude the external disturbances. Unfortu-

* Corresponding author (email: sjliao@sjtu.edu.cn)



Vorticity statistics based on velocity and density-weighted velocity in premixed reactive turbulence

Nilanjan Chakraborty^a, Lipo Wang^b, Ilias Konstantinou^a and Markus Klein^c

^aSchool of Mechanical and Systems Engineering, Newcastle University, Newcastle upon Tyne, UK; ^bUM-SJTU Joint Institute, Shanghai JiaoTong University, Shanghai, China; ^cFaculty for Aerospace Engineering, Universität der Bundeswehr München, Neubiberg, Germany

ABSTRACT

The local and non-local statistics of vorticity $\vec{\omega}$ (i.e. curl of velocity vector \vec{u}) and pseudo-vorticity $\vec{\omega}^*$ (i.e. curl of density-weighted velocity vector $\rho\vec{u}/\rho_0$) have been investigated in detail based on a direct numerical simulation (DNS) database of freely propagating statistically planar flames in different regimes of premixed turbulent combustion. It has been found that the relative orientation of $\vec{\omega}^*$ can be significantly different to that of $\vec{\omega}$ for small values of the Karlovitz number and large values of the Reynolds number. The vorticity $\vec{\omega}$ shows, depending on the case, considerable alignment with either the most extensive or compressive principal strain rate. In contrast, $\vec{\omega}^*$ has been found to align with the intermediate principal strain rate for all cases. The transport statistics of Reynolds averaged enstrophy (i.e. $\bar{\Omega} = \overline{\vec{\omega} \cdot \vec{\omega}}/2$) and pseudo-enstrophy (i.e. $\bar{\Omega}^* = \overline{\vec{\omega}^* \cdot \vec{\omega}^*}/2$) have been investigated in detail. The non-local vorticity statistics in turbulent premixed combustion have been investigated based on the vorticity line segment (VLS) structure, which is defined with respect to each grid point as the part of the (pseudo) vorticity line bounded by the two adjacent extremal points of the (pseudo) vorticity magnitude. VLS can be characterised by the segment length and the (pseudo) vorticity magnitude difference across the segment, i.e. $(\Delta\omega^*) \Delta\omega$. Strong dilatation effects tend to increase VLS length, whereas turbulent convection disturbs the flow field resulting in shorter VLS. The joint PDFs between the segment length and $(\Delta\omega) \Delta\omega^*$ are found to be symmetric, whereas the joint PDFs between the segment length and the pseudo-vorticity magnitude difference across the VLS in the flame normal direction show significant asymmetry, which is primarily determined by density variation across the flame front and turbulence intensity.

ARTICLE HISTORY

Received 15 September 2016
Accepted 19 May 2017

KEYWORDS

Vorticity; enstrophy; vorticity line segment; direct numerical simulations (DNS)

1. Introduction

Vorticity, $\vec{\omega}$ defined as curl of velocity vector (i.e. $\vec{\omega} = \nabla \times \vec{u}$), is a quantity of fundamental importance in turbulent flows. Its mathematical and topological features have been analysed extensively [1]. In complex turbulent flows, the regions of compression and stretching interact with each other, which leads to lumped distributions of vorticity $\vec{\omega}$. The

CONTACT Lipo Wang  Lipo.Wang@sjtu.edu.cn

© 2017 Informa UK Limited, trading as Taylor & Francis Group



Analysis of the filtered non-premixed turbulent flame

Lipo Wang

UM-SJTU joint institute, Shanghai JiaoTong University, Shanghai, China



ARTICLE INFO

Article history:

Received 28 February 2016

Revised 6 July 2016

Accepted 7 July 2016

Available online 26 July 2016

Keywords:

Non-premixed turbulent flame

Flamelet equation

Filtering

ABSTRACT

Results related to the filtered non-premixed turbulent flame statistics are presented. Considering non-premixed turbulent combustion modeling in the framework of large eddy simulations (LES), a turbulent flamelet equation is derived based on the filtered governing equations. Using a direct numerical simulation (DNS) data set, the statistical properties of two important parameters, the scalar dissipation and chemical source term, are analyzed in details. Numerical results show that for the scalar dissipation term, the probability density function (PDF) of the magnitude of the mixture fraction gradient changes is strongly dependent on the filter scale, whereas the PDF of the turbulent diffusivity is almost invariant. Theoretically from the scalar structure function a scaling law can be expected for the conditional mean of the difference between the filtered and nonfiltered scalars with respect to the filter scale, which is important for estimating the chemical source in the subgrid scale models.

© 2016 The Combustion Institute. Published by Elsevier Inc. All rights reserved.

1. Introduction

In reactive turbulence the interaction between the flame and flow is extremely complex. For problems with sufficiently high Reynolds numbers of practical interest, because of the large scale separation, both spatially and temporally, direction numerical simulations (DNS) are intractable. Thus models of the required relations need to be constructed. In non-premixed combustion simulation, the flamelet models originally developed by Williams [1] and Peters [2] play important roles. Physically if the flame scale is locally small compared with the turbulent dissipative scale, the flame structure remains to be laminar. Based on the flamelet equations, it is possible to largely reduce the dimensionality of the modeling parameters. The flamelet models have been widely applied [3–6] because of the clear physical meaning and high numerical efficiency. In recent years successful examples have been extended to various cases such as unsteady processes [7,8] and non-unity Lewis number effects [9]. The detailed budget analyses suggest that typically the flamelet assumption remains to be reasonable [10].

However, challenges in implementing the laminar flamelet models do exist. Especially in high Reynolds number turbulence the non-premixed flame structure is far away from being clearly defined, for instance unsteadiness and the strong influence from the premixed flame front associated with the triple flame [11,12]. When local extinction and re-ignition occur, premixed flame fronts

are present to bring both premixed and nonpremixed features, which can violate the laminar non-premixed flamelet assumption. Moreover, in pre- and post-extinction flames the local mixing is strong; thus the local timescale may be important as well [12]. Turbulence can also lead to complex topological structures of the non-premixed flame front, for instance the flame patch and extinction hole, both of which are associated with the flame edge [13]. It can reasonably be expected that the flame edge influence will be enhanced with the increase of turbulence intensity. Although for the unsteady flamelet models the additional time scale can be modeled [8,14], physically extra modeling complexity need to be further investigated.

Large eddy simulations (LES) are especially appealing in turbulence simulation. With the appropriate subgrid scale models, the large-scale turbulent structures can feasibly be calculated by LES. However, subgrid scale modeling of the non-premixed flame also suffers from the aforementioned complexities. Efforts in this area have made some important progresses. In the thickened flame models [15,16] the flame is artificially stretched to fit the numerical resolution, but the overall flame speed remains invariant. Such a scenario can be reasonably interpreted in the framework of LES, because the filtering operation alters the detailed flame structures, for instance the reduced chemical kinetics and the temperature field; however, the overall flame speed must be invariant because the kernel of the filtered flame overlaps the nonfiltered flame zone. In other words the thickened flame models address the field quantities at the coarse grid level at the cost of distorting the fine scale structures. A different modeling idea is the filtered tabulated chemistry for LES (F-TACLES) [17], where the unclosed terms are

E-mail address: lipo.wang@sjtu.edu.cn

Fangpan Zhong

State Key Laboratory for Turbulence and
Complex Systems,
College of Engineering,
Peking University,
Beijing 100871, China
e-mail: zhongfp@pku.edu.cn

Chao Zhou¹

State Key Laboratory for Turbulence and
Complex Systems,
College of Engineering,
Peking University,
Beijing 100871, China;
Collaborative Innovation Center of
Advanced Aero-Engine,
Beijing 100191, China
e-mail: czhou@pku.edu.cn

H. Ma

University of Michigan-Shanghai Jiao Tong Joint
Institute,
Shanghai Jiao Tong University,
UM-SJTU JI,
800 Dongchuan Road,
Minhang District,
Shanghai 200240, China
e-mail: haitengma@gmail.com

Q. Zhang²

University of Michigan-Shanghai
Jiao Tong Joint Institute,
Shanghai Jiao Tong University,
Shanghai 200240, China
e-mail: Qiang.Zhang.1@city.ac.uk

Heat Transfer of Winglet Tips in a Transonic Turbine Cascade

Understanding the heat transfer of winglet tips is crucial for their applications in high-pressure turbines. The current paper investigates the heat transfer performance of three different winglet-cavity tips in a transonic turbine cascade at a tip gap of 2.1% chord. A cavity tip is studied as the baseline case. The cascade operates at engine representative conditions of an exit Mach number of 1.2 and an exit Reynolds number of 1.7×10^6 . Transient infrared thermography technique was used to obtain the tip distributions of heat transfer coefficient for different tips in the experiment. The CFD results were validated with the measured tip heat transfer coefficients, and then used to explain the flow physics related to heat transfer. It is found that on the pressure side winglet, the flow reattaches on the top winglet surface and results in high heat transfer coefficient. On the suction side winglet, the heat transfer coefficient is low near the blade leading edge but is higher from the midchord to the trailing edge. The suction side winglet pushes the tip leakage vortex further away from the blade suction surface and reduces the heat transfer coefficient from 85% to 96% span on the blade suction surface. However, the heat transfer coefficient is higher for the winglet tips from 96% span to the tip. This is because the tip leakage vortex attaches on the side surface of the suction side winglet and results in quite high heat transfer coefficient on the front protrusive part of the winglet. The effects of relative endwall motion between the blade tip and the casing were investigated by CFD method. The endwall motion has a significant effect on the flow physics within the tip gap and near-tip region in the blade passage, thus affects the heat transfer coefficient distributions. With relative endwall motion, a scraping vortex forms inside the tip gap and near the casing, and the cavity vortex gets closer to the pressure side squealer/winglet. The tip leakage vortex in the blade passage becomes closer to the blade suction surface, resulting in an increase of the heat transfer coefficient. [DOI: 10.1115/1.4034208]

Introduction

In high-pressure turbines, tip clearances exist between the rotor blade tips and the casing to prevent rubbing. Hot gas goes through this tip gap, forming tip leakage flows. The tip leakage flow results in an undesirable loss of efficiency. It can also cause excessively high metal temperature on the blade tip.

Different tip geometries have been studied aiming to reduce the loss, such as flat, squealer, and winglet tips. Cavity tips have been widely studied and used in modern high-pressure turbines, and a lot of work showed that cavity tips produced lower loss than the flat tip (e.g., Kwak et al. [1] and Nho et al. [2]). With the additional design of tip winglets, the tip leakage loss was found to decrease further. In a low-speed linear cascade, Schabowski et al. [3] found that a winglet-cavity tip offered a 37% reduction in loss slope compared with a flat tip. Based on a cold flow high-speed rig, Harvey et al. [4] found that the tip leakage loss of a winglet tip was 45% lower than that of a flat tip. Winglet tips were also found to be able to reduce the tip leakage loss in a number of other studies, e.g., Patel [5], Yaras and Sjolander [6], and Zhou et al. [7].

To maintain the tip geometry and its aerodynamic performance, understanding the heat transfer of the blade tips is very important. There are quite a few studies about the thermal performance of

the flat or squealer tips, e.g., Newton et al. [8], Kwak and Han [9], Zhou and Hodson [10], Azad et al. [11], and Kwak et al. [12]. They all found that the thermal performance of the blade tips is determined by the flow physics within the tip gap. Fewer open publications discuss the thermal performance of winglet tips with experimental methods. In a linear cascade, Papa et al. [13] found that the use of a pressure side winglet reduced the tip heat transfer compared with the suction-side squealer tip. Saha et al. [14] studied combinations of a pressure-side winglet with a flat tip, a two-sided squealer tip, and a suction-sided squealer tip at a pressure ratio of 1.73 across the blade numerically. Their results showed that the pressure-side winglet reduced the tip area-averaged heat transfer coefficient by 7% and 1.5% for the flat tip and the suction-sided squealer tip, respectively, but there was no reduction for the two-sided squealer tip. Using numerical methods, Coull et al. [15] investigated a large number of winglet-flat tip designs at engine representative operating conditions. They found that the use of an early suction side winglet could achieve significant efficiency improvement with slight decrease in the overall heat transfer of the blade. O'Dowd et al. [16] measured the heat transfer on the tip and the near-tip wall region of a unique winglet tip design in a transonic turbine cascade condition. They found a region of higher Nusselt number close to the tip on the suction surface than the flat tip, while the Nusselt number at a lower span wise position of the winglet tip was lower. Most of the heat transfer studies related to winglet tips are conducted at low-speed conditions, and the studies at transonic conditions are very rare. However, the flow within a high-pressure turbine is often transonic, and very few data about heat transfer coefficient for different winglet tips at transonic conditions are available.

¹Corresponding author.

²Present address: Department of Mechanical Engineering and Aeronautics, City University London, Northampton Square EC1V 0HB, London.

Contributed by the Turbomachinery Committee of ASME for publication in the JOURNAL OF ENGINEERING FOR GAS TURBINES AND POWER. Manuscript received June 19, 2016; final manuscript received June 28, 2016; published online September 8, 2016. Editor: David Wisler.



Miniature all-optical probe for large synthetic aperture photoacoustic-ultrasound imaging

GUANGYAO LI,¹ ZHENDONG GUO,¹ AND SUNG-LIANG CHEN^{1,2,*}

¹University of Michigan-Shanghai Jiao Tong University Joint Institute, Shanghai Jiao Tong University, Shanghai 200240, China

²State Key Laboratory of Advanced Optical Communication Systems and Networks, Shanghai Jiao Tong University, Shanghai 200240, China

*sungliang.chen@sjtu.edu.cn

Abstract: A miniature all-optical probe for high-resolution photoacoustic (PA)-ultrasound (US) imaging using a large synthetic aperture is developed. The probe consists of three optical fibers for PA excitation, US generation, and detection of acoustic waves, respectively. The fiber for PA excitation has a large numerical aperture (NA) for wide-angle laser illumination. On the other hand, the fiber with a carbon black-polydimethylsiloxane composite coated on the end face of the optical fiber is used for wide-angle US transmission through laser-US conversion. Both the excited PA and backscattered US signals are detected by a fiber-tip Fabry-Perot cavity for wide-angle acoustic detection. The probe outer diameter is only ~2 mm. The synergy of the three optical fibers makes a large-NA synthetic aperture focusing technique for high-resolution PA and US imaging possible. High PA lateral resolutions of 104–154 μm and high US lateral resolutions of 64–112 μm over a depth range of > 4 mm are obtained. Compared with other existing miniature PA-US probes, to our knowledge, our probe achieves by far the best performance in terms of lateral resolutions and imaging depth range. The constructed probe has potential for endoscopic and intravascular imaging applications that require PA and US contrasts with high resolutions over a large depth range.

© 2017 Optical Society of America

OCIS codes: (170.5120) Photoacoustic imaging; (170.7170) Ultrasound; (120.2230) Fabry-Perot.

References and links

1. S. Jiao, M. Jiang, J. Hu, A. Fawzi, Q. Zhou, K. K. Shung, C. A. Puliafito, and H. F. Zhang, "Photoacoustic ophthalmoscopy for in vivo retinal imaging," *Opt. Express* **18**(4), 3967–3972 (2010).
2. A. Nair, B. D. Kuban, E. M. Tuzcu, P. Schoenhagen, S. E. Nissen, and D. G. Vince, "Coronary plaque classification with intravascular ultrasound radiofrequency data analysis," *Circulation* **106**(17), 2200–2206 (2002).
3. K. Jansen, A. F. W. van der Steen, H. M. M. van Beusekom, J. W. Oosterhuis, and G. van Soest, "Intravascular photoacoustic imaging of human coronary atherosclerosis," *Opt. Lett.* **36**(5), 597–599 (2011).
4. J. Mamou, O. Aristizabal, R. H. Silverman, J. A. Ketterling, and D. H. Turnbull, "High-frequency chirp ultrasound imaging with an annular array for ophthalmologic and small-animal imaging," *Ultrasound Med. Biol.* **35**(7), 1198–1208 (2009).
5. J. Xia and L. V. Wang, "Small-animal whole-body photoacoustic tomography: a review," *IEEE Trans. Biomed. Eng.* **61**(5), 1380–1389 (2014).
6. R. Nuster, N. Schmitner, G. Wurzing, S. Gratt, W. Salvenmoser, D. Meyer, and G. Paltauf, "Hybrid photoacoustic and ultrasound section imaging with optical ultrasound detection," *J. Biophotonics* **6**(6-7), 549–559 (2013).
7. K. Daoudi, P. J. van den Berg, O. Rabot, A. Kohl, S. Tisserand, P. Brands, and W. Steenbergen, "Handheld probe integrating laser diode and ultrasound transducer array for ultrasound/photoacoustic dual modality imaging," *Opt. Express* **22**(21), 26365–26374 (2014).
8. P. Subochev, A. Orlova, M. Shirmanova, A. Postnikova, and I. Turchin, "Simultaneous photoacoustic and optically mediated ultrasound microscopy: an in vivo study," *Biomed. Opt. Express* **6**(2), 631–638 (2015).
9. S.-Y. Hung, W.-S. Wu, B.-Y. Hsieh, and P.-C. Li, "Concurrent photoacoustic-ultrasound imaging using single-laser pulses," *J. Biomed. Opt.* **20**(8), 86004 (2015).
10. X. Bai, X. Gong, W. Hau, R. Lin, J. Zheng, C. Liu, C. Zeng, X. Zou, H. Zheng, and L. Song, "Intravascular optical-resolution photoacoustic tomography with a 1.1 mm diameter catheter," *PLoS One* **9**(3), e92463 (2014).

Photoacoustic microscopy *in vivo* using synthetic-aperture focusing technique combined with three-dimensional deconvolution

DE CAI,¹ ZHONGFEI LI,¹ YAO LI,¹ ZHENDONG GUO,¹ AND SUNG-LIANG CHEN^{1,2,*}

¹University of Michigan-Shanghai Jiao Tong University Joint Institute, Shanghai Jiao Tong University, Shanghai 200240, China

²State Key Laboratory of Advanced Optical Communication Systems and Networks, Shanghai Jiao Tong University, Shanghai 200240, China

*sungliang.chen@sjtu.edu.cn

Abstract: Acoustic-resolution photoacoustic microscopy (ARPAM) plays an important role in studying the microcirculation system of biological tissues with deep penetration. High lateral resolution of ARPAM is achieved by using a high numerical aperture acoustic transducer. The deteriorated lateral resolution in the out-of-focus region can be alleviated by synthetic aperture focusing technique (SAFT). Previously, we reported a three-dimensional (3D) deconvolution ARPAM to improve both lateral and axial resolutions in the focus region. In this study, we present our extension of resolution enhancement to the out-of-focus region based on two-dimensional SAFT combined with the 3D deconvolution (SAFT+Deconv). In both the focus and out-of-focus regions, depth-independent lateral resolution provided by SAFT, together with inherently depth-independent axial resolution, ensures a depth-independent point spread function for 3D deconvolution algorithm. Imaging of 10 μm polymer beads shows that SAFT+Deconv ARPAM improves the -6 dB lateral resolutions from 65–700 μm to 20–29 μm , and the -6 dB axial resolutions from 35–42 μm to 12–19 μm in an extended depth of focus (DOF) of ~ 2 mm. The signal-to-noise ratio is also increased by 6–30 dB. The resolution enhancement in three dimensions is validated by *in vivo* imaging of a mouse's dorsal subcutaneous microvasculature. Our results suggest that SAFT+Deconv ARPAM may allow fine spatial resolution with deep penetration and extended DOF for biomedical photoacoustic applications.

© 2017 Optical Society of America

OCIS codes: (170.3880) Medical and biological imaging; (170.5120) Photoacoustic imaging; (170.6900) Three-dimensional microscopy; (100.1830) Deconvolution.

References and links

1. L. V. Wang, "Multiscale photoacoustic microscopy and computed tomography," *Nat. Photonics* **3**(9), 503–509 (2009).
2. L. V. Wang and S. Hu, "Photoacoustic tomography: in vivo imaging from organelles to organs," *Science* **335**(6075), 1458–1462 (2012).
3. K. Maslov, H. F. Zhang, S. Hu, and L. V. Wang, "Optical-resolution photoacoustic microscopy for in vivo imaging of single capillaries," *Opt. Lett.* **33**(9), 929–931 (2008).
4. V. Ntziachristos, "Going deeper than microscopy: the optical imaging frontier in biology," *Nat. Methods* **7**(8), 603–614 (2010).
5. S.-L. Chen, Z. Xie, P. L. Carson, X. Wang, and L. J. Guo, "In vivo flow speed measurement of capillaries by photoacoustic correlation spectroscopy," *Opt. Lett.* **36**(20), 4017–4019 (2011).
6. T. J. Allen, A. Hall, A. P. Dhillon, J. S. Owen, and P. C. Beard, "Spectroscopic photoacoustic imaging of lipid-rich plaques in the human aorta in the 740 to 1400 nm wavelength range," *J. Biomed. Opt.* **17**(6), 0612091 (2012).
7. K. Jansen, A. F. Van Der Steen, H. M. van Beusekom, J. W. Oosterhuis, and G. van Soest, "Intravascular photoacoustic imaging of human coronary atherosclerosis," *Opt. Lett.* **36**(5), 597–599 (2011).
8. S. Sethuraman, J. H. Amirian, S. H. Litovsky, R. W. Smalling, and S. Y. Emelianov, "Spectroscopic intravascular photoacoustic imaging to differentiate atherosclerotic plaques," *Opt. Express* **16**(5), 3362–3367 (2008).
9. J.-M. Yang, C. Favazza, R. Chen, J. Yao, X. Cai, K. Maslov, Q. Zhou, K. K. Shung, and L. V. Wang, "Simultaneous functional photoacoustic and ultrasonic endoscopy of internal organs in vivo," *Nat. Med.* **18**(8), 1297–1302 (2012).
10. P. Wang, T. Ma, M. N. Slipchenko, S. Liang, J. Hui, K. K. Shung, S. Roy, M. Sturek, Q. Zhou, Z. Chen and J.-X. Cheng, "High-speed intravascular photoacoustic imaging of lipid-laden atherosclerotic plaque enabled by a 2-kHz barium nitrite Raman laser," *Sci. Rep.* **4**, 6889 (2014).

#281946

<http://dx.doi.org/10.1364/OE.25.001421>

Journal © 2017

Received 1 Dec 2016; revised 31 Dec 2016; accepted 4 Jan 2017; published 18 Jan 2017

Review

Review of Laser-Generated Ultrasound Transmitters and Their Applications to All-Optical Ultrasound Transducers and Imaging

Sung-Liang Chen ^{1,2}

¹ Electrical and Computer Engineering, University of Michigan-Shanghai Jiao Tong University Joint Institute, Shanghai Jiao Tong University, Shanghai 200240, China; sungliang.chen@sjtu.edu.cn; Tel.: +86-21-3420-6045

² State Key Laboratory of Advanced Optical Communication Systems and Networks, Shanghai Jiao Tong University, Shanghai 200240, China

Academic Editor: Kohji Masuda

Received: 19 November 2016; Accepted: 19 December 2016; Published: 28 December 2016

Abstract: Medical ultrasound is an imaging technique that utilizes ultrasonic signals as information carriers, and has wide applications such as seeing internal body structures, finding a source of a disease, and examining pregnant women. The most commonly used ultrasonic transducer today is based on piezoelectricity. The piezoelectric transducer, however, may have a limited bandwidth and insufficient sensitivity for reduced element size. Laser-generated ultrasound (LGUS) technique is an effective way to resolve these issues. The LGUS approach based on photoacoustic effect is able to greatly enhance the bandwidth of ultrasound signals and has the potential for high-resolution imaging. High-amplitude LGUS could also be used for therapy to accomplish high precision surgery without an incision. Furthermore, LGUS in conjunction with optical detection of ultrasound allows all-optical ultrasound imaging (i.e., ultrasound is generated and received optically). The all-optical platform offers unique advantages in providing high-resolution information and in facilitating the construction of miniature probes for endoscopic ultrasound. In this article, a detailed review of the recent development of various LGUS transmitters is presented. In addition, a recent research interest in all-optical ultrasound imaging, as well as its applications, is also discussed.

Keywords: ultrasound imaging; laser ultrasonics; laser-ultrasound transducer; laser-generated focused ultrasound; all-optical ultrasound imaging

1. Introduction

Ultrasound, defined as sound with frequencies from 20 kHz to several GHz, has demonstrated broad applications in medical imaging [1], material science, physics, chemistry, and nanotechnology. In classical medical ultrasound (also known as ultrasonography), an ultrasound pulse is transmitted into the body and the pulse is reflected due to the interfaces between tissues with different acoustic impedances as image contrast. The echo pulse carries back physiological and pathological information inside tissues. Especially, high-frequency ultrasound with frequencies >20 MHz is useful for high-resolution (<100 μm) biomedical applications such as endoscopic imaging [2], ophthalmology [3], intravascular imaging [4] and dermatology [5]. Magnetic resonance imaging (MRI) systems continue to enhance the resolution up to ~500 μm [6]. However, routine interventional procedures are restricted due to the high expense of MRI in both the initial investment and the upkeep. Furthermore, MRI has limited temporal resolution, which prohibits its use in fast imaging and rapid diagnosis. X-ray computed tomography is a relatively affordable modality with high resolution of ~400 μm [7], but it relies on ionizing radiation, making it unsafe for medical monitoring. Optical method is a promising approach for biomedical imaging [8]. Optical coherence tomography (OCT) is an optical technique



Synthetic aperture focusing technique for photoacoustic endoscopy

DE CAI,¹ GUANGYAO LI,¹ DONGQING XIA,¹ ZHONGFEI LI,¹
ZHENDONG GUO,¹ AND SUNG-LIANG CHEN^{1,2,*}

¹University of Michigan-Shanghai Jiao Tong University Joint Institute, Shanghai Jiao Tong University, Shanghai 200240, China

²State Key Laboratory of Advanced Optical Communication Systems and Networks, Shanghai Jiao Tong University, Shanghai 200240, China

*sungliang.chen@sjtu.edu.cn

Abstract: Photoacoustic endoscopy (PAE) is a promising tool for the detection of atherosclerotic plaque. In this work, we propose a novel design of a side-viewing PAE probe based on a synthetic aperture focusing technique (SAFT) to enable high transverse resolution over large depth of focus (DOF) along the radial direction. A point-like ultrasonic detector is used to ensure a wide detection angle and thus a large synthetic aperture for SAFT. We first perform numerical simulation to optimize the PAE probe design, which involves the placement of the point-like detector and the diameter of a reflection rod mirror. Then, experiments are conducted based on the optimized probe design. High transverse resolution of 115–190 μm over large DOF of 3.5 mm along the radial direction is experimentally obtained. The SAFT-based PAE holds promise for endoscopic imaging with a high transverse resolution for both the surface and deep regions of tissue.

© 2017 Optical Society of America

OCIS codes: (170.3880) Medical and biological imaging; (170.5120) Photoacoustic imaging; (170.2150) Endoscopic imaging; (100.0100) Image processing.

References and links

1. S. Tang, J. Chen, P. Samant, S. Kelly, and L. Xiang, "Transurethral photoacoustic endoscopy for prostate cancer: A simulation study," *IEEE Trans. Med. Imaging* **35**(7), 1780–1787 (2016).
2. J.-M. Yang, C. Favazza, R. Chen, J. Yao, X. Cai, K. Maslov, Q. Zhou, K. K. Shung, and L. V. Wang, "Simultaneous functional photoacoustic and ultrasonic endoscopy of internal organs in vivo," *Nat. Med.* **18**(8), 1297–1302 (2012).
3. C. Chen, Y. Zhao, S. Yang, and D. Xing, "Mechanical characterization of intraluminal tissue with phase-resolved photoacoustic viscoelasticity endoscopy," *Biomed. Opt. Express* **6**(12), 4975–4980 (2015).
4. S. Sethuraman, S. R. Aglyamov, J. H. Amirian, R. W. Smalling, and S. Y. Emelianov, "Intravascular photoacoustic imaging using an IVUS imaging catheter," *IEEE Trans. Ultrason. Ferroelectr. Freq. Control* **54**(5), 978–986 (2007).
5. B. Wang, J. L. Su, J. Amirian, S. H. Litovsky, R. Smalling, and S. Emelianov, "Detection of lipid in atherosclerotic vessels using ultrasound-guided spectroscopic intravascular photoacoustic imaging," *Opt. Express* **18**(5), 4889–4897 (2010).
6. K. Jansen, A. F. Van Der Steen, H. M. van Beusekom, J. W. Oosterhuis, and G. van Soest, "Intravascular photoacoustic imaging of human coronary atherosclerosis," *Opt. Lett.* **36**(5), 597–599 (2011).
7. X. Bai, X. Gong, W. Hau, R. Lin, J. Zheng, C. Liu, C. Zeng, X. Zou, H. Zheng, and L. Song, "Intravascular optical-resolution photoacoustic tomography with a 1.1 mm diameter catheter," *PloS one* **9**(3), e92463 (2014).
8. J.-M. Yang, C. Li, R. Chen, B. Rao, J. Yao, C.-H. Yeh, A. Danielli, K. Maslov, Q. Zhou, K. K. Shung and L. V. Wang, "Optical-resolution photoacoustic endomicroscopy in vivo," *Biomed. Opt. Express* **6**(3), 918–932 (2015).
9. J.-M. Yang, K. Maslov, H.-C. Yang, Q. Zhou, K. K. Shung, and L. V. Wang, "Photoacoustic endoscopy," *Opt. Lett.* **34**(10), 1591–1593 (2009).
10. J.-M. Yang, R. Chen, C. Favazza, J. Yao, C. Li, Z. Hu, Q. Zhou, K. K. Shung, and L. V. Wang, "A 2.5-mm diameter probe for photoacoustic and ultrasonic endoscopy," *Opt. Express* **20**(21), 23944–23953 (2012).
11. H. He, G. Wissmeyer, S. V. Ovsepian, A. Buehler and V. Ntziachristos, "Hybrid optical and acoustic resolution photoacoustic endoscopy," *Opt. Lett.* **41**(12), 2708–2710 (2016).
12. B. Dong, S. Chen, Z. Zhang, C. Sun, and H. F. Zhang, "Photoacoustic probe using a microring resonator ultrasonic sensor for endoscopic applications," *Opt. Lett.* **39**(15), 4372–4375 (2014).
13. C.-K. Liao, M.-L. Li, and P.-C. Li, "Optoacoustic imaging with synthetic aperture focusing and coherence weighting," *Opt. Lett.* **29**(21), 2506–2508 (2004).
14. M.-L. Li, H. F. Zhang, K. Maslov, G. Stoica, and L. V. Wang, "Improved in vivo photoacoustic microscopy based on a virtual-detector concept," *Opt. Lett.* **31**(4), 474–476 (2006).

A Broadband Fluorographene Photodetector

Sichao Du, Wei Lu, Ayaz Ali, Pei Zhao, Khurram Shehzad, Hongwei Guo, Lingling Ma, Xuemei Liu, Xiaodong Pi, Peng Wang, Hehai Fang, Zhen Xu, Chao Gao, Yaping Dan, Pingheng Tan, Hongtao Wang, Cheng-Te Lin, Jianyi Yang, Shurong Dong, Zhiyuan Cheng, Erping Li, Wenyan Yin, Jikui Luo, Bin Yu, Tawfique Hasan, Yang Xu, Weida Hu,* and Xiangfeng Duan*

High-performance photodetectors operating over a broad wavelength range from ultraviolet, visible, to infrared are of scientific and technological importance for a wide range of applications. Here, a photodetector based on van der Waals heterostructures of graphene and its fluorine-functionalized derivative is presented. It consistently shows broadband photoresponse from the ultraviolet (255 nm) to the mid-infrared (4.3 μm) wavelengths, with three orders of magnitude enhanced responsivity compared to pristine graphene photodetectors. The broadband photodetection is attributed to the synergistic effects of the spatial nonuniform collective quantum confinement of sp^2 domains, and the trapping of photoexcited charge carriers in the localized states in sp^3 domains. Tunable photoresponse is achieved by controlling the nature of sp^3 sites and the size and fraction of sp^3/sp^2 domains. In addition, the photoresponse due to the different photoexcited-charge-carrier trapping times in sp^2 and sp^3 nano-domains is determined. The proposed scheme paves the way toward implementing high-performance broadband graphene-based photodetectors.

Photodetectors as a class of optoelectronics device have been widely employed in diverse fields, including spectroscopy,^[1] telecommunication,^[2] astronomy,^[3] agriculture,^[4] pharmaceuticals,^[5] and environmental monitoring.^[6] In contrast to photodetectors operating at a specific wavelength range, broadband photodetectors with photoresponse to a much wider spectrum and spectrally distinctive are highly desirable, owing to their importance to a variety of applications.^[7,8] The wealth of sufficient information held in the broad spectral domain offers advantages over traditional panchromatic and multispectral imagery.^[9] Hence, hyperspectral imaging has been used as a powerful technique for global climate research, mapping of wetlands, mineral

Dr. S. Du, W. Lu, A. Ali, Dr. K. Shehzad, H. Guo, L. Ma, X. Liu, Prof. J. Yang, Prof. S. Dong, Prof. Z. Cheng, Prof. E. Li, Prof. W. Yin, Prof. J. Luo, Prof. Y. Xu
College of Information Science and Electronic Engineering
Zhejiang University
Hangzhou, Zhejiang 310027, China
E-mail: yangxu-isee@zju.edu.cn
Prof. P. Zhao, Prof. H. Wang
Institute of Applied Mechanics
Zhejiang University
Hangzhou, Zhejiang 310027, China
Dr. S. Du, Prof. Y. Xu, Prof. X. Pi
State Key Laboratory of Silicon Materials
College of Material Science
Zhejiang University
Hangzhou, Zhejiang 310027, China
P. Wang, H. Fang, Prof. W. Hu
National Laboratory for Infrared Physics
Shanghai Institute of Technical Physics
Chinese Academy of Sciences
Shanghai 200083, China
E-mail: wdhu@mail.sitp.ac.cn
Dr. Z. Xu, Prof. C. Gao
MOE Key Laboratory of Macromolecular
Synthesis and Functionalization
Zhejiang University
Hangzhou, Zhejiang 310027, China

DOI: 10.1002/adma.201700463

Prof. Y. Dan
University of Michigan - Shanghai Jiao Tong University Joint Institute
Shanghai Jiao Tong University
Shanghai 200240, China
Prof. P. Tan
State Key Laboratory of Superlattices and Microstructures
Institute of Semiconductors
Chinese Academy of Sciences
Beijing 100083, China
Prof. C.-T. Lin
Key Laboratory of Marine Materials and Related Technologies
Zhejiang Key Laboratory of Marine Materials and Protective
Technologies
Ningbo Institute of Materials Technology and Engineering
Chinese Academy of Sciences
Ningbo, Zhejiang 315201, China
Prof. B. Yu
College of Nanoscale Science and Engineering
State University of New York
New York, NY 12203, USA
Dr. T. Hasan
Department of Engineering
University of Cambridge
Cambridge CB3 0FA, UK
Prof. X. Duan
Department of Chemistry and Biochemistry
University of California
Los Angeles, CA 90095, USA

ARTICLE OPEN

A self-powered high-performance graphene/silicon ultraviolet photodetector with ultra-shallow junction: breaking the limit of silicon?

Xia Wan¹, Yang Xu^{1,2}, Hongwei Guo¹, Khurram Shehzad¹, Ayaz Ali¹, Yuan Liu², Jianyi Yang¹, Daoxin Dai¹, Cheng-Te Lin³, Liwei Liu⁴, Hung-Chieh Cheng², Fengqiu Wang⁵, Xiaomu Wang⁶, Hai Lu⁵, Weida Hu⁷, Xiaodong Pi⁸, Yaping Dan⁹, Jikui Luo^{1,10}, Tawfique Hasan¹¹, Xiangfeng Duan², Xinming Li¹², Jianbin Xu¹², Deren Yang⁸, Tianling Ren¹³ and Bin Yu^{1,14}

We present a self-powered, high-performance graphene-enhanced ultraviolet silicon Schottky photodetector. Different from traditional transparent electrodes, such as indium tin oxides or ultra-thin metals, the unique ultraviolet absorption property of graphene leads to long carrier life time of hot electrons that can contribute to the photocurrent or potential carrier-multiplication. Our proposed structure boosts the internal quantum efficiency over 100%, approaching the upper-limit of silicon-based ultraviolet photodetector. In the near-ultraviolet and mid-ultraviolet spectral region, the proposed ultraviolet photodetector exhibits high performance at zero-biasing (self-powered) mode, including high photo-responsivity (0.2 A W^{-1}), fast time response (5 ns), high specific detectivity (1.6×10^{13} Jones), and internal quantum efficiency greater than 100%. Further, the photo-responsivity is larger than 0.14 A W^{-1} in wavelength range from 200 to 400 nm, comparable to that of state-of-the-art Si, GaN, SiC Schottky photodetectors. The photodetectors exhibit stable operations in the ambient condition even 2 years after fabrication, showing great potential in practical applications, such as wearable devices, communication, and “dissipation-less” remote sensor networks.

npj 2D Materials and Applications (2017)1:4; doi:10.1038/s41699-017-0008-4

INTRODUCTION

Ultraviolet (UV) photodetectors could find a wide range of applications,^{1–8} such as environmental monitoring,³ biological and chemical analysis,⁴ flame detection,⁵ astronomical studies,⁸ internet-of-things sensors,⁹ and missile detection.¹⁰ Recently, wide band-gap (WBG) semiconductors (SiC,¹¹ GaN,¹² ZnO,¹³ TiO₂,¹⁴ etc.) have emerged as the candidates for UV photodetection, due to their high-strength chemical bonding structures and visible-blindness.^{15, 16} However, the performance of WBG semiconductor-based detectors is limited by relatively low-quality oxide layer and high surface states/defects,¹⁵ which causes slow recovery of photocurrent, hindering the practical applications for high-speed UV detection.

Silicon is a widely-used semiconductor material for UV detectors owing to its suitable bandgap, low-density surface states, high reliability, matured manufacturing, and high-speed detection.^{17–21} However, in the UV region, silicon photodetectors face the major challenge of low photo-responsivity (typically, less than 0.1 A W^{-1} for $\lambda < 400 \text{ nm}$) due to high reflection coefficient and shallow penetration depth of UV light in silicon. For example, a typical

silicon PN junction depth (X_j) is larger than 200 nm.²² As the penetration depth of UV light in Si is less than 20 nm for $\lambda < 370 \text{ nm}$,²³ the photo-generated carriers are primarily near the Si surface and need to diffuse ($\sim 100 \text{ nm}$ scale) into the junction region, resulting in significant carrier recombination and hence limiting the performance. Recently, techniques, such as delta doping are proposed to make shallow junction.^{24–27} The dead layer for mid-UV/far-UV absorption is still unavoidable. It was reported that the inversion-enhanced Si PN junction photodetector using fixed charges within oxide layer could alleviate the dead-layer problem, but the charges in oxide have stability issues.²³ In order to obtain high-performance silicon UV detectors, an ultra-shallow junction with charge separation/collection efficiency at fast-operating speed are required. Semi-transparent metal/Si Schottky structures can only partially satisfy the requirement, as a large proportion of UV light is reflected or absorbed by metal layer without contributing to the photocurrent, resulting in low photo-responsivity.²⁸

Graphene (Gr), a single-layer of carbon sheet, exhibits excellent electronic conductivity^{29–31} and optical transmittance^{32–34} with great potential to replace metals as transparent electrodes.^{35–42}

¹College of Information Science and Electronic Engineering and State Key Laboratory of Silicon Materials, Zhejiang University, Hangzhou 310027 Zhejiang, People's Republic of China; ²Department of Chemistry and Biochemistry, University of California at Los Angeles, Los Angeles 90095 CA, USA; ³Ningbo Institute of Industrial Technology, Chinese Academy of Sciences, Ningbo 315201, People's Republic of China; ⁴State Key Laboratory of Nanodevices and Applications at Chinese Academy of Sciences, Suzhou, People's Republic of China; ⁵State Key Laboratory of Microstructure and School of Electronics Science and Engineering, Nanjing University, Nanjing 210093, People's Republic of China; ⁶School of Engineering & Applied Science, Yale University, New Haven 06511 CT, USA; ⁷National Laboratory for Infrared Physics, Shanghai Institute of Technical Physics, Chinese Academy of Sciences, Shanghai 200083, People's Republic of China; ⁸State Key Laboratory of Silicon Materials, Zhejiang University, Hangzhou 310027 Zhejiang, People's Republic of China; ⁹University of Michigan-Shanghai Jiao Tong University Joint Institute, Shanghai 200240, People's Republic of China; ¹⁰Institute of Renewable Energy & Environ. Technol., University of Bolton, Bolton BL3 5AB, UK; ¹¹Department of Engineering, University of Cambridge, Cambridge CB3 0FA, UK; ¹²Department of Electronic Engineering, The Chinese University of Hong Kong, Shatin, Hong Kong SAR, People's Republic of China; ¹³Institute of Microelectronics, Tsinghua University, Beijing 10084, People's Republic of China and ¹⁴College of Nanoscale Science and Engineering, State University of New York, Albany 12203 NY, USA

Correspondence: Yang Xu (yangxu-isee@zju.edu.cn)

Received: 20 October 2016 Revised: 9 December 2016 Accepted: 6 January 2017

Published online: 11 April 2017

A silicon nanowire heater and thermometer

Xingyan Zhao¹ and Yaping Dan^{1,2,a)}

¹University of Michigan – Shanghai Jiao Tong University Joint Institute, Shanghai Jiao Tong University, Shanghai 200240, China

²School of Microelectronics, Xi'an Jiao Tong University, Xi'an, Shaanxi Province 710049, China

(Received 31 May 2017; accepted 11 July 2017; published online 24 July 2017)

In the thermal conductivity measurements of thermoelectric materials, heaters and thermometers made of the same semiconducting materials under test, forming a homogeneous system, will significantly simplify fabrication and integration. In this work, we demonstrate a high-performance heater and thermometer made of single silicon nanowires (SiNWs). The SiNWs are patterned out of a silicon-on-insulator wafer by CMOS-compatible fabrication processes. The electronic properties of the nanowires are characterized by four-probe and low temperature Hall effect measurements. The I - V curves of the nanowires are linear at small voltage bias. The temperature dependence of the nanowire resistance allows the nanowire to be used as a highly sensitive thermometer. At high voltage bias, the I - V curves of the nanowire become nonlinear due to the effect of Joule heating. The temperature of the nanowire heater can be accurately monitored by the nanowire itself as a thermometer. *Published by AIP Publishing.* [<http://dx.doi.org/10.1063/1.4985632>]

In search of high-performance thermoelectric materials and devices, the accurate measurement of thermal conductivity is the key.^{1–3} The widely used method for thermal conductivity measurements is to employ micro metal coils as the heater and thermometer.^{4–10} The thermal contact resistance between metal coils and the thermoelectric materials is difficult to quantify, which may lead to inaccurate or even artificial findings.^{6,7} If the heater and thermometer are made of the semiconducting thermoelectric material under test, then the potential contact resistance will be minimized.¹¹ What is more, a system made of homogeneous materials will significantly simplify fabrication and integration,¹² which may speed up the process of finding new high-performance thermoelectric materials and devices. Here, we demonstrate a heater and thermometer made of a single semiconducting silicon nanowire (SiNW). The SiNW thermometer relies on the thermal activation of dopants to sense the temperature, as a result of which we find that the nanowire thermometer is much more sensitive than the widely used commercial Pt thermometers. The nanowire can also act as a high-frequency heater at high power feed-through due to its nanoscale size. The temperature of the nanowire heater can be accurately monitored by the nanowire itself as a thermometer.

The silicon nanowires (SiNWs) used in this work were fabricated using the CMOS-compatible process on a silicon-on-insulator (SOI) substrate. The SOI wafer has a 200 nm thick device layer on 380 nm thick SiO₂. The device layer was boron doped at an average doping concentration of $\sim 1 \times 10^{18} \text{ cm}^{-3}$ by ion implantation. Electron beam lithography and thermal evaporation were first used to form a metal mask for patterning the device layer into the nanowires and micropads by reactive ion etch. A thin layer of the Au/Ti (200 nm/5 nm) film was deposited on the micropads by photolithography and metallization. Figure 1(a) shows a scanning electron microscopic (SEM) image of a silicon nanowire device. The nanowire is 24 μm long and 0.4 μm in

width. The 6 electrodes lying between the anode and cathode were designed for four-probe and Hall effect measurements.

Temperature dependent current measurements were conducted in the dark in a cryostat (ARS DE-202PI). The samples were placed on the cold finger of the cryostat. The temperature of the cold finger (called as background temperature below) was controlled by a temperature controller (Lakeshore 335). The dc voltage bias V_b is supplied between the anode and cathode by a sourcemeter (Keithley 2400) while the current I_d is monitored at the same time. The voltage V_{46} between electrodes 4 and 6 is also monitored by another sourcemeter at the same time in the four-probe measurements. The measured I_d - V_{46} curves of a single Si NW device at different temperatures under small voltage bias are plotted in Fig. 1(b). The four-probe measurements show that ohmic contacts are formed between the nanowire and metal electrodes and that the contact resistance is negligibly small compared to the nanowire resistance (see [supplementary material](#), Fig. S1). Hall effect measurements were conducted in a Physical Property Measurement System (PPMS EverCool-II). The Hall resistance R_H between electrodes 5 and 6 was measured as a function of magnetic field B at different temperatures, as shown in the inset of Fig. 1(c). The hole concentration p at different temperatures was extracted with the following equation:¹³

$$p = \frac{R_H}{Bqd}, \quad (1)$$

where q is the unit charge and d is the thickness of the nanowire. Figure 1(c) shows the measured hole concentration of a SiNW device as a function of temperature, from which the activation energy is extracted to be 0.043 eV, consistent with the boron ionization energy.¹⁴

As the voltage bias increases, the I_d - V_{46} curve is no longer linear but bent up at higher voltage bias, as shown in Fig. 2(a). This indicates an increase in the conductivity at higher voltage bias. The increase in conductivity is attributed to a higher concentration of holes, which is confirmed by the Hall measurements as shown in Fig. 2(b). A possible reason

^{a)}Author to whom correspondence should be addressed: yaping.dan@sjtu.edu.cn

SCIENTIFIC REPORTS

OPEN

Controlled doping by self-assembled dendrimer-like macromolecules

Haigang Wu^{1,2}, Bin Guan², Yingri Sun², Yiping Zhu³ & Yaping Dan²

Received: 01 August 2016

Accepted: 19 December 2016

Published: 01 February 2017

Doping *via* self-assembled macromolecules might offer a solution for developing single atom electronics by precisely placing individual dopants at arbitrary location to meet the requirement for circuit design. Here we synthesize dendrimer-like polyglycerol macromolecules with each carrying one phosphorus atom in the core. The macromolecules are immobilized by the coupling reagent onto silicon surfaces that are pre-modified with a monolayer of undecylenic acid. Nuclear magnetic resonance (NMR) and X-ray photoelectron spectroscopy (XPS) are employed to characterize the synthesized macromolecules and the modified silicon surfaces, respectively. After rapid thermal annealing, the phosphorus atoms carried by the macromolecules diffuse into the silicon substrate, forming dopants at a concentration of 10^{17} cm^{-3} . Low-temperature Hall effect measurements reveal that the ionization process is rather complicated. Unlike the widely reported simple ionization of phosphorus dopants, nitrogen and carbon are also involved in the electronic activities in the monolayer doped silicon.

Precisely placing individual dopants at arbitrary location is critical for single atom electronics¹ and sub-nanometer integrated circuits^{1,2}. Single-ion implantation technique^{2,3} and hydrogen lithography based on scanning tunneling microscopy (STM)^{4,5} have been successfully developed to control single dopants. However, these techniques are time-consuming serial processes in which dopants are placed one by one. A parallel process for control of individual dopants at large scale is required for industrial applications⁶. Self-assembled monolayer (SAM) doping might offer a promising solution if the dopant-carrier molecules can be individually controlled^{7,8}. Up to date, the SAM doping technique mostly uses small molecules for the purpose of achieving ultra-shallow junctions^{9,10}. It is extremely challenging to control the location of individual carrier molecules unless the molecule size is large enough. Recently, Popere *et al.* reported controlling the locations of dopants by using self-assembled block copolymers with dopants encapsulation¹¹. The self-assembled nature of block copolymers allows for placing dopants in a periodic array. Although the periodic distribution of dopants is useful in, for instance, minimizing the sub-threshold voltage fluctuation in deep nanoscale field-effect transistors², it cannot meet the requirements for circuit design that requires the individual dopants in single atom electronics to be placed at arbitrary locations.

To exclude any potential electrical interference, the best candidate for the carrier molecule is the one that is large (at least a few nanometer in diameter) to be comparable to the resolution of the most advanced lithography) and mostly importantly, only has C, O and H in addition to the dopant element such as P or B since C, O and H do not electrically dope silicon^{12,13}. Here, we demonstrate a novel monolayer doping approach by using the super-branched poly-glycerol molecules that are synthesized to carry only one phosphorus atom in the core (Fig. 1)^{14,15}. The synthesized macromolecules are then grafted onto the silicon substrate *via* the reaction with carboxyl-functionalized silicon surfaces. The electrical and secondary ion mass spectrometry (SIMS) measurements indicate that phosphorus dopants have successfully diffused into and electrically doped the silicon substrate after rapid thermal annealing. Low-temperature Hall effect measurements are employed to further investigate the ionization of the dopants in the samples.

Result and Discussion

Synthesis of Polyglycerol. To synthesize macromolecules with each carrying one phosphorus atom, we choose tris(4-methoxyphenyl)phosphine (TMP) as the core to initiate the polymerization with glycerol. Note

¹School of Biomedical Engineering, Shanghai Jiao Tong University, Shanghai, 200240, China. ²University of Michigan-Shanghai Jiao Tong University Joint Institute, Shanghai Jiao Tong University, Shanghai, 200240, China. ³Key Laboratory of Polar Materials and Devices, Ministry of Education, and Department of Electronic Engineering, East China Normal University, Shanghai 200241, China. Correspondence and requests for materials should be addressed to Y.D. (email: yaping.dan@sjtu.edu.cn)

Phosphorus ionization in silicon doped by self-assembled macromolecular monolayers

Haigang Wu,^{1,2} Ke Li,² Xuejiao Gao,² and Yaping Dan^{2,a}

¹*School of Biomedical Engineering, Shanghai Jiao Tong University, Shanghai 200240, China*

²*University of Michigan-Shanghai Jiao Tong University Joint Institute, Shanghai Jiao Tong University, Shanghai 200240, China*

(Received 7 August 2017; accepted 4 October 2017; published online 13 October 2017)

Individual dopant atoms can be potentially controlled at large scale by the self-assembly of macromolecular dopant carriers. However, low concentration phosphorus dopants often suffer from a low ionization rate due to defects and impurities introduced by the carrier molecules. In this work, we demonstrated a nitrogen-free macromolecule doping technique and investigated the phosphorus ionization process by low temperature Hall effect measurements. It was found that the phosphorus dopants diffused into the silicon bulk are in nearly full ionization. However, the electrons ionized from the phosphorus dopants are mostly trapped by deep level defects that are likely carbon interstitials. © 2017 Author(s). All article content, except where otherwise noted, is licensed under a Creative Commons Attribution (CC BY) license (<http://creativecommons.org/licenses/by/4.0/>). <https://doi.org/10.1063/1.4999232>

The precise control of individual dopants at arbitrary location is the key to developing atomic scale devices. Hydrogen lithography by scanning tunneling microscopy (STM)¹ and single ion implantation technique² have been demonstrated to manipulate single dopant atoms. However, these techniques are time-consuming serial processes and difficult to control atoms at large scale. Previously, we proposed to utilize the self-assembly of macromolecular dopant carriers to control single dopant atoms at large scale.³ However, the success of this process is hindered by the low activation rate of phosphorus dopants.^{3–5} Without a high activation rate, individual dopants, although controlled at large scale, will not function properly in electronic devices. Nitrogen is one of the main sources that lower the activation rate of phosphorus dopants.⁶ We have shown that nitrogen introduced by the carrier molecules or coupling reagents will significantly deactivate the P dopants in silicon.^{3,5}

In this work, we demonstrated a nitrogen-free macromolecule doping technique and investigated the phosphorus ionization process. Hyperbranched polyglycerols (hbPGs) that do not contain nitrogen were first synthesized. Each hbPG macromolecule carries one phosphorus atom. The hbPGs molecules were then grafted onto H-terminated silicon surfaces without using N-containing coupling reagents. Secondary ion mass spectroscopy and low temperature Hall effect measurements were employed to analyze the sample. It was found that the phosphorus dopants diffused into the silicon bulk are in nearly full ionization. However, the electrons ionized from the P dopants are mostly trapped by deep level defects that are likely carbon interstitials, resulting in a low nominal ionization rate of phosphorus dopants.

Hyperbranched polyglycerols (hbPGs) were synthesized by anionic ring-opening multibranching polymerization⁷ of glycerols (J&K Scientific) with diphenyl-phosphinyl hydroquinone (TCI (Shanghai) Development Co., Ltd) as the core to initiate the reaction. The monomer/core molar ratio is set at ~210 to produce high molecular weight hbPGs. After purified by dialysis bag (molecular weight cut-off > 50 kDa) in DI water, hbPGs were characterized by nuclear magnetic resonance (NMR) techniques (¹H NMR and ¹³C NMR) and dynamic light scattering (see the results in our previous work³). The results indicate that the number average molecular weight of hbPGs is approximately 84000 g/mol and the diameter of globular hbPGs is ~11 nm.

^aTo whom correspondence should be addressed: yaping.dan@sjtu.edu.cn.

Timing Acquisition and Error Analysis for Pulse-Based Terahertz Band Wireless Systems

Chong Han, *Member, IEEE*, Ian F. Akyildiz, *Fellow, IEEE*, and Wolfgang H. Gerstacker, *Senior Member, IEEE*

Abstract—Terahertz (THz) band communication is envisioned as a key technology to satisfy the increasing demand for ultra-broadband wireless systems, thanks to its ultrabroad bandwidth. Tailored for the unique properties of pulse-based communications in the THz band, two timing acquisition algorithms are proposed and analyzed thoroughly in this paper. First, a low-sampling-rate (LSR) synchronization algorithm is proposed, by extending the theory of sampling signals with finite rate of innovation in the communication context and exploiting the properties of the annihilating filter. The simulation results show that the timing accuracy at an order of ten picoseconds is achievable. In particular, the LSR algorithm has high performance with uniform sampling at $1/20$ of the Nyquist rate when the signal-to-noise ratio (SNR) is high (i.e., greater than 18 dB). Complementary to this, a maximum likelihood (ML) approach for timing acquisition is developed, which searches for the timing offsets by adopting a two-step acquisition procedure based on the ML criterion. The simulation results show that the ML-based algorithm is well suitable in the low SNR case with a half-reduced search space. For further evaluation, the error performance and the resulting bit-error-rate sensitivity to the timing errors in the LSR and the ML algorithms are both analytically and numerically studied. This paper provides very different and promising angles to efficiently and reliably solve the timing acquisition problem for pulse-based THz band wireless systems.

Index Terms—Terahertz band, timing acquisition, synchronization, low-sampling-rate, maximum likelihood approach.

I. INTRODUCTION

IN RECENT years, the wireless data traffic grew exponentially, further accompanied by an increasing demand for higher data rates. The data rates have doubled every eighteen months over the last three decades and are currently approaching the capacity of communication systems [1]. The (0.06–10) Terahertz band is identified as one of the promising spectrum

bands to address the spectrum scarcity and capacity limitations of current wireless systems [2]. The main benefit of the THz band comes from its ultra-broad bandwidth, which ranges from tens of GHz up to a few THz [3]. The use of this frequency band is envisioned to enable ultra-high-speed wireless communications, and boost a plethora of applications [4].

The huge bandwidth of the THz band comes at costs. First, a highly frequency- and distance-selective path loss, which causes severe distortion, including attenuation and temporal broadening effects, on the transmitted pulses [5]. Second, the digital synchronization, which has the advantages of cost-efficiency, full integration, and robustness [6], [7], requires multi-hundreds-Giga-samples-per-second (Gs/s) and even Tera-samples-per-second (Ts/s) sampling rates, while the fastest sampling rate to date does not exceed 100 Gs/s [8], [9]. Due to these reasons, timing errors as small as picoseconds can seriously degrade the system performance. As a result, timing acquisition, which is one part of the synchronization, constitutes an important but yet fully unexplored topic in the THz band system design to date.

To address the aforementioned challenges, two timing acquisition algorithms are proposed and evaluated for pulse-based THz band communications in this paper. First, in order to achieve efficient timing acquisition with reduced sampling rates, we extend the theory of sampling signals with finite rate of innovation [10]–[13] from compressive sampling in signal processing to the communication context. The first focus of this work is that we propose a *low-sampling-rate (LSR) algorithm* for timing acquisition in the THz band. In our LSR algorithm, we leverage the features of the annihilating filters which have been introduced in [14], [15] and apply them in the context of THz pulse-based communications. Moreover, we investigate the LSR algorithm in the THz band by considering the communication parameters, which include the antenna gain, the distance, the number of frames per symbol and the pulse width. However, the proposed LSR works well when the signal-to-noise ratio (SNR) is high and appears to be not suitable when the SNR is below 18 dB [16]. Therefore, the second focus of this work is that a *maximum likelihood (ML)* approach for timing acquisition is proposed in the low SNR case for THz band communications, complementary to the LSR approach. This algorithm adopts a two-step acquisition procedure to derive the timing acquisition solutions based on the ML criterion [17]–[19].

Furthermore, we analytically and numerically evaluate the LSR and the ML timing acquisition algorithms, in comparison with the Cramer-Rao lower bound (CRLB). In addition, we perform an analysis on the bit-error-rate (BER) sensitivity to the acquisition errors for the two algorithms. Then, extensive evaluations on the performance of the proposed two approaches are carried out via simulations, with the variation of the THz communication parameters, including the antenna gain, the distance,

Manuscript received April 9, 2017; revised August 2, 2017; accepted September 6, 2017. Date of publication September 11, 2017; date of current version November 10, 2017. This work was supported in part by the U.S. National Science Foundation under Grant ECCS-1608579, and in part by the Alexander von Humboldt Foundation through Prof. Akyildiz's Humboldt Research Prize in Germany. The review of this paper was coordinated by Prof. S.-H. Leung. (Corresponding author: Chong Han.)

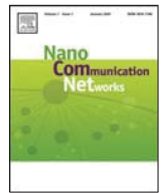
C. Han is with the University of Michigan–Shanghai Jiao Tong University Joint Institute, Shanghai Jiao Tong University, Shanghai 200240, China (e-mail: chong.han@sjtu.edu.cn).

I. F. Akyildiz is with the Broadband Wireless Networking Laboratory, School of Electrical and Computer Engineering, Georgia Institute of Technology, Atlanta, GA 30332 USA (e-mail: ian@ece.gatech.edu).

W. H. Gerstacker is with the Institute for Digital Communications, Friedrich-Alexander-University Erlangen-Nuernberg, Erlangen 91058, Germany (e-mail: gersta@LNT.de).

Color versions of one or more of the figures in this paper are available online at <http://ieeexplore.ieee.org>.

Digital Object Identifier 10.1109/TVT.2017.2750707



MA-ADM: A memory-assisted angular-division-multiplexing MAC protocol in Terahertz communication networks



Chong Han^{a,b,*}, Wenqian Tong^a, Xin-Wei Yao^c

^a University of Michigan–Shanghai Jiao Tong University Joint Institute, Shanghai Jiao Tong University, Shanghai, 200240, China

^b Shenzhen Institute of Terahertz Technology and Innovation, Shenzhen, 518101, China

^c College of Computer Science and Technology, Zhejiang University of Technology, Hangzhou, 310023, China

ARTICLE INFO

Article history:

Received 31 July 2017

Accepted 3 August 2017

Available online 14 August 2017

Keywords:

Terahertz band

Medium access control

Angular-division-multiplexing

Quantized angular space

ABSTRACT

Terahertz band communication is envisioned as a key technology to satisfy the increasing demand for ultra-high-speed wireless links and enable interconnections in a nanonetwork. In this paper, a memory-assisted medium access control (MAC) protocol with angular-division-multiplexing (ADM) is proposed for THz communication networks. The service region of an access point (AP) is divided into multiple angular slots by exploiting the 3D quantized angular space. For efficient service discovery and communications, a node equips with (i) the omni-directional antennas at the service discovery phase, and (ii) directional antennas for message transmissions. Moreover, the memory is leveraged in the ADM scheme to assist the AP to skip the unregistered angular slots to improve the network performance. Based on the proposed MAC protocol, the analytical models of the interference, SINR, outage probability, throughput and the delay in the THz network are derived respectively. According to the simulation and numerical analysis, the results show that our proposed MAC protocol can effectively improve the throughput by over 15% and substantially reduce the delay, in comparison with the ADM scheme without the memory guidance.

© 2017 Elsevier B.V. All rights reserved.

1. Introduction

The Terahertz (0.1–10 THz) band provides wireless communication devices with an unprecedentedly large bandwidth, ranging from several tens of GHz up to a few THz, which can satisfy the increasing demand of 100 Gbps and even 1 Tbps data rates within the next decade [1]. The use of this frequency band is envisioned to address the spectrum scarcity and capacity limitations of current wireless systems, and boost a plethora of applications, including ultra-high-speed indoor wireless links (e.g., for virtual reality and augmented reality), and wireless backhaul and access in small cell networks [2]. In addition to macro/micro-scale applications, the THz band will also enable wireless communication among nanoscale machines or nanomachines [3]. The state of the art in nanoscale transceivers and antennas points to the THz band as their frequency range of operation [4]. Applications that are enabled by the nanomachines range from advanced health monitoring systems to chemical attack prevention systems, wireless networks on chip to the Internet of Nano-things [5].

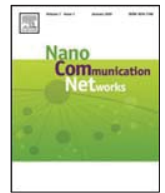
Thanks to the very small wavelength at THz frequencies, very large antenna arrays realizing *ultra-massive MIMO* [6] can be used

to enable directional transmissions in the THz network, to overcome the very high path loss and the limited communication distance. The highly directional and the ultra-high-speed links in the network design introduce the following challenges that motivate this work. First, the focus of the network solutions needs to shift from access contention to coordination and scheduling. Furthermore, the coordination and scheduling should be compatible with the very high data rates, the unique channel and physical properties of the THz band. Second, the interference models that were studied for omni-directional transmissions need to be revisited in the THz network. Third, although directional links can substantially improve the system performance, the difficulty for network discovery increases and the associated deafness problem [7] might arise. Therefore, the efficiency and performance between the service discovery and the data communication need to be balanced.

In this work, we focus on the fundamental problem of the network design: *medium access control (MAC)*, in a centralized network. We exploit the *quantized angular space* and propose a *memory-assisted MAC protocol with angular-division-multiplexing (ADM)* for THz communication networks. The distinctive features of our work are summarized as follows. First, we present the centralized THz network architecture, in which there are one access point (AP) and multiple nodes. The directional links between the AP and the nodes are confined into a number of angular slots. Based on the THz communication models, we propose a memory-assisted MAC protocol with ADM. A flowchart for the protocol is

* Corresponding author at: University of Michigan–Shanghai Jiao Tong University Joint Institute, Shanghai Jiao Tong University, Shanghai, 200240, China

E-mail addresses: chong.han@sjtu.edu.cn (C. Han), light123star@sjtu.edu.cn (W. Tong), xwyao@zjut.edu.cn (X.-W. Yao).



Stochastic geometry analysis of interference and coverage in Terahertz networks

Xin-Wei Yao^{a,*}, Chao-Chao Wang^a, Wan-Liang Wang^a, Chong Han^{b,*}

^a College of Computer Science and Technology, Zhejiang University of Technology, Hangzhou, 310023, China

^b University of Michigan-Shanghai Jiao Tong University Joint Institute, Shanghai Jiao Tong University, Shanghai, 200240, China

ARTICLE INFO

Article history:

Received 10 February 2017

Received in revised form 19 May 2017

Accepted 22 June 2017

Available online 30 June 2017

Keywords:

Terahertz band communication

Interference

Coverage probability

Beamforming technology

ABSTRACT

Terahertz (THz) band communication has been envisioned as a key wireless technology for providing unprecedented high data rates. However, due to the severe path loss, the transmission distance in THz band is very limited. Therefore, the beamforming techniques are explored to enlarge the communication range in THz networks, particularly employed at Access Points (APs). Interference is a critical factor affecting the performance of THz networks. In this paper, the interference and the coverage probability are investigated for the THz band communications with beamforming APs. First, based on the Line-of-Sight (LoS) and Non-Line-of-Sight (NLoS) ray propagation models of THz signals, the interferences from neighboring users and beamforming APs are modeled in closed forms based on stochastic geometry methods. Then, the Signal-to-Interference-plus-Noise-Ratio (SINR) and the coverage probabilities are further derived based on the THz channel and interference model. Extensive simulations are carried out to evaluate the interference and coverage for the THz band communications with beamforming APs, for the different system parameters, which include SINR threshold, density of APs, transmission frequency, gain of beamforming AP, density of users and radius of interference area. Learning from the simulation results, high density of APs with a small beam-width and the transmission at THz frequencies with low absorption efficient, such as 0.67 THz, are recommended to mitigate the interference and achieve a better coverage performance.

© 2017 Elsevier B.V. All rights reserved.

1. Introduction

The explosive growth in data traffic in the past decades requires higher data rates for wireless communications. In particular, the data rates have doubled every eighteen months over the past three decades, and will reach Terabit-per-second (Tps) within the next ten years [1]. However, for wireless network applications, such as indoor wireless communications and mobile communications, existing technologies cannot achieve Tps data rates with the traditional transmission frequencies, or even with the latest millimeter wave (mm-Wave) at 60 Gigahertz (GHz), as result of the limited bandwidth [2]. Therefore, new spectral bands are demanded to support these ultra-fast wireless communications. Among others, THz band is envisioned as a key wireless technology for providing unprecedented data rates [3].

So far, the study of THz band communications becomes more systematic and varies from the fundamental peculiarities [4], to channel modeling [5] and MAC protocols [6,7]. All of these are

driving THz band communications to become more realistic. However, there is few analysis on interference and coverage probability in THz band communications, which are critical to analyze the performance of the communications and measure the quality of wireless connections. The challenges to characterize the interference and the coverage are described as follows. On the one hand, due to the high path loss in THz band which limits the transmission range [8,9], beamforming techniques are studied to extend the transmission distance and increase the network throughput [10,11]. Meanwhile, the beamforming AP increases the transmission power inside the main lobe of the beamforming antenna where has a high antenna gain, while mitigating the transmission power outside the main lobe in networks [12]. On the other hand, owing to the high frequency of THz band, the wavelength ranges from micrometer to millimeter. The surfaces classified as smooth in traditional band are classified as rough in THz band. Hence, the interference from NLoS ray propagations should be taken into consideration [13].

Some related works have made an effort in this regard. Two types of interference associated with multi-wideband transmission, namely, Inter-Symbol Interference (ISI) and Inter-band Interference (IBI) have been proposed in [14]. This analysis of

* Corresponding authors.

E-mail addresses: xwyao@zjut.edu.cn (X.-W. Yao), ccwang@zjut.edu.cn (C.-C. Wang), wwl@zjut.edu.cn (W.-L. Wang), chong.han@sjtu.edu.cn (C. Han).

<http://dx.doi.org/10.1016/j.nancom.2017.06.002>

1878-7789/© 2017 Elsevier B.V. All rights reserved.

Three-Dimensional End-to-End Modeling and Analysis for Graphene-Enabled Terahertz Band Communications

Chong Han, *Member, IEEE*, and Ian F. Akyildiz, *Fellow, IEEE*

Abstract—Terahertz (0.1–10 THz) band communication is envisioned as a key technology to satisfy the increasing demand for ultra-high-speed wireless links. In this paper, a 3-D end-to-end model in the THz band is developed that includes the graphene-based reflectarray antenna response and the 3-D multipath propagation phenomena. In particular, the architecture of a graphene-based reflectarray antenna is investigated, and the 3-D radiation pattern is modeled. Moreover, a 3-D THz channel model based on ray tracing techniques is developed as a superposition of the line-of-sight (LoS), reflected, and scattered paths. By using the developed end-to-end model, an in-depth analysis on the 3-D channel characteristics is carried out. Specifically, the gain at the main beam of the graphene-based reflectarray antenna is 18 dB, and the 3-dB beamwidths in the elevation and the azimuth planes are 7° and 10° , respectively. The use of the reflectarray leads to a decrease of the delay spread from 1.23 to 0.099 ns, which suggests that the resulting coherence bandwidth reaches 2 GHz. Moreover, the root mean square (rms) angular spread in the elevation plane is less than 0.12° , which is one tenth of that without beamforming. Furthermore, the wideband channel capacity at THz frequencies is characterized, which can be enhanced with a larger transmit power, a lower operating frequency, a larger bandwidth, and a higher beamforming gain. Finally, the beamforming gain enabled by the reflectarray antenna is compromised at the cost of the strict beam alignment, and the deviation needs to be smaller than 11° . The provided analysis and the channel physical parameters lay out the foundation and are particularly useful for realizing reliable and efficient ultra-high-speed wireless communications in the THz band.

Index Terms—Graphene, reflectarray antenna, terahertz (THz) band, 3-D channel, wideband.

I. INTRODUCTION

IN RECENT years, the wireless data traffic grew exponentially, further accompanied by an increasing demand for higher data rates. The data rates have doubled every 18 months

over the last three decades and are currently approaching the capacity of wireless systems [1]. Following this trend, wireless data rates of 100 Gb/s and even 1 Tb/s will become reality within the next decade [2]. In addition to many proposed solutions for next generation advanced cellular systems, the Terahertz (THz) band, i.e., 0.1–10 THz, is considered as one of the most promising spectrum bands to support ultra-high-speed wireless communications in the future [3]. With its ability to offer an ultrabroad bandwidth and very high data rates, the use of the THz band is envisioned to address the spectrum scarcity and capacity limitations of current wireless systems, and boost a plethora of applications, including ultra-high-speed wireless backhaul to the small cells, and ultra-high-speed data transfers among proximal devices [4]. Furthermore, related to vehicular networks, THz band communications [5] can be applied in intelligent transport systems for intravehicle, intervehicle, and vehicle-to-roadside wireless ultrabroadband links.

For the realization of efficient wireless communication networks in the THz band, it is imperative to develop an accurate 3-D channel model which accurately characterizes the Terahertz spectrum peculiarities in both the elevation and the azimuth planes. In realistic application scenarios, the multipath rays arrive at the receiver from both the azimuth and the elevation planes, which is the result of the 3-D radiation diagram of the antennas and the 3-D propagation of the electromagnetic waves in the channel. These facts introduce an angular spread in the elevation plane and influence the channel physical peculiarities. The first model that recognizes the elevation coordinate in a 3-D model was proposed in [6], in which the author assumed that the arriving signals were uniformly distributed in the azimuth plane and nonuniformly distributed in the elevation plane. Further development provides analytical solutions of the power spectral density of the received signal in the three dimensions and produces the desired spatiotemporal characteristics of a 3-D wireless channels as studied in [7] and [8]. However, these models for lower frequency bands do not capture the behavior of the THz band, such as the very high molecular absorption loss or the very high reflection loss. Existing THz band channel models in [9]–[12] are developed for 2-D cases, which fail to describe signal variations in the elevation plane. Furthermore, THz antenna responses are not included in these models. Consequently, there is a need for an end-to-end model that captures the antenna response and the 3-D multipath propagation and investigates the resulting channel characteristics.

Manuscript received February 21, 2016; revised August 11, 2016; accepted September 26, 2016. Date of publication September 28, 2016; date of current version July 14, 2017. This work was supported in part by the U.S. National Science Foundation under Grant ECCS-1608579 and in part by Alexander von Humboldt Foundation through Dr. I. F. Akyildiz's Humboldt Research Prize in Germany. The review of this paper was coordinated by Dr. S. Mumtaz.

C. Han is with the University of Michigan–Shanghai Jiao Tong University Joint Institute, Shanghai Jiao Tong University, Shanghai 200240, China (e-mail: chong.han@sjtu.edu.cn).

I. F. Akyildiz is with the Broadband Wireless Networking Laboratory, School of Electrical and Computer Engineering, Georgia Institute of Technology, Atlanta, GA 30332 USA (e-mail: ian@ece.gatech.edu).

Color versions of one or more of the figures in this paper are available online at <http://ieeexplore.ieee.org>.

Digital Object Identifier 10.1109/TVT.2016.2614335

Design of a short nonuniform acquisition protocol for quantitative analysis in dynamic cardiac SPECT imaging — a retrospective ^{123}I -MIBG animal study

Yunlong Zan

School of Biomedical Engineering, Shanghai Jiao Tong University, Shanghai, China

School of Medicine, Department of Nuclear Medicine, Rui Jin Hospital, Shanghai Jiao Tong University, Shanghai, China

University of Michigan – Shanghai Jiao Tong University Joint Institute, Shanghai Jiao Tong University, Shanghai, China

Yong Long

University of Michigan – Shanghai Jiao Tong University Joint Institute, Shanghai Jiao Tong University, Shanghai, China

Kewei Chen

Image Analysis and Research Lab., Banner Good Samaritan Medical Center, Phoenix, AZ, USA

Biao Li

School of Medicine, Department of Nuclear Medicine, Rui Jin Hospital, Shanghai Jiao Tong University, Shanghai, China

Qiu Huang^{a)}

School of Biomedical Engineering, Shanghai Jiao Tong University, Shanghai, China

School of Medicine, Department of Nuclear Medicine, Rui Jin Hospital, Shanghai Jiao Tong University, Shanghai, China

Grant T. Gullberg

Life Science Division, Lawrence Berkeley National Laboratory, Berkeley, CA, USA

Radiology and Biomedical Imaging, University of California, San Francisco, CA, USA

(Received 16 September 2016; revised 29 March 2017; accepted for publication 30 March 2017; published 26 May 2017)

Purpose: Our previous works have found that quantitative analysis of ^{123}I -MIBG kinetics in the rat heart with dynamic single-photon emission computed tomography (SPECT) offers the potential to quantify the innervation integrity at an early stage of left ventricular hypertrophy. However, conventional protocols involving a long acquisition time for dynamic imaging reduce the animal survival rate and thus make longitudinal analysis difficult. The goal of this work was to develop a procedure to reduce the total acquisition time by selecting nonuniform acquisition times for projection views while maintaining the accuracy and precision of estimated physiologic parameters.

Method: Taking dynamic cardiac imaging with ^{123}I -MIBG in rats as an example, we generated time activity curves (TACs) of regions of interest (ROIs) as ground truths based on a direct four-dimensional reconstruction of experimental data acquired from a rotating SPECT camera, where TACs represented as the coefficients of B-spline basis functions were used to estimate compartmental model parameters. By iteratively adjusting the knots (i.e., control points) of B-spline basis functions, new TACs were created according to two rules: accuracy and precision. The accuracy criterion allocates the knots to achieve low relative entropy between the estimated left ventricular blood pool TAC and its ground truth so that the estimated input function approximates its real value and thus the procedure yields an accurate estimate of model parameters. The precision criterion, via the D-optimal method, forces the estimated parameters to be as precise as possible, with minimum variances. Based on the final knots obtained, a new protocol of 30 min was built with a shorter acquisition time that maintained a 5% error in estimating rate constants of the compartment model. This was evaluated through digital simulations.

Results: The simulation results showed that our method was able to reduce the acquisition time from 100 to 30 min for the cardiac study of rats with ^{123}I -MIBG. Compared to a uniform interval dynamic SPECT protocol (1 s acquisition interval, 30 min acquisition time), the newly proposed protocol with nonuniform interval achieved comparable (K_1 and k_2 , $P = 0.5745$ for K_1 and $P = 0.0604$ for k_2) or better (Distribution Volume, DV , $P = 0.0004$) performance for parameter estimates with less storage and shorter computational time.

Conclusion: In this study, a procedure was devised to shorten the acquisition time while maintaining the accuracy and precision of estimated physiologic parameters in dynamic SPECT imaging. The procedure was designed for ^{123}I -MIBG cardiac imaging in rat studies; however, it has the potential to be extended to other applications, including patient studies involving the acquisition of dynamic SPECT data. © 2017 American Association of Physicists in Medicine [https://doi.org/10.1002/mp.12288]

Key words: dynamic SPECT imaging, nonuniform acquisition interval, shorten acquisition time

LOW DOSE CT IMAGE RECONSTRUCTION WITH LEARNED SPARSIFYING TRANSFORM

Xuehang Zheng¹, Zening Lu¹, Saiprasad Ravishankar², Yong Long^{*1}, Jeffrey A. Fessler²

¹University of Michigan - Shanghai Jiao Tong University Joint Institute,
Shanghai Jiao Tong University, Shanghai, China

²Department of Electrical Engineering and Computer Science, University of Michigan, MI, USA

ABSTRACT

A major challenge in computed tomography (CT) is to reduce X-ray dose to a low or even ultra-low level while maintaining the high quality of reconstructed images. We propose a new method for CT reconstruction that combines penalized weighted-least squares reconstruction (PWLS) with regularization based on a sparsifying transform (PWLS-ST) learned from a dataset of numerous CT images. We adopt an alternating algorithm to optimize the PWLS-ST cost function that alternates between a CT image update step and a sparse coding step. We adopt a relaxed linearized augmented Lagrangian method with ordered-subsets (relaxed OS-LALM) to accelerate the CT image update step by reducing the number of forward and backward projections. Numerical experiments on the XCAT phantom show that for low dose levels, the proposed PWLS-ST method dramatically improves the quality of reconstructed images compared to PWLS reconstruction with a nonadaptive edge-preserving regularizer (PWLS-EP).

Index Terms— Low dose CT, Sparsifying transform learning, Statistical image reconstruction, Sparse representation, Dictionary learning

1. INTRODUCTION

A major challenge in computed tomography (CT) is to reduce X-ray dose to a low or even ultra-low level while maintaining the high quality of reconstructed images. Low dose CT (LDCT) scans that still provide good image quality could significantly improve the benefits of CT scans and open up numerous entirely new clinical applications.

Currently, most commercial CT scanners use a technique called filtered back-projection (FBP) for image reconstruction. FBP requires undesirably high doses of radiation to produce high-quality diagnostic images. Model-based image reconstruction (MBIR) methods, also known as statistical

image reconstruction methods, produce high-quality and accurate images, while reducing patient radiation exposure. Weighted-least squares (WLS) estimation is commonly used for CT [1]. WLS estimation with proper weighting that gives less weight to measurements that are noisier and more weight to the more reliable data reduces noise in the reconstructed image. Penalized weighted-least squares (PWLS) reconstruction with added regularization based on prior knowledge of the underlying unknown object improves image quality in LDCT reconstruction [2]. Thus, MBIR with better image priors is a promising way to develop improved reconstruction methods for achieving high quality LDCT imaging.

Prior information extracted from big datasets of CT images could potentially enable dramatic improvements in image reconstruction from LDCT measurements. It is well known that natural signals are sparse in certain transform domains, such as wavelets and discrete gradient domain. A sparsifying transform (ST) converts signals into these domains where they can be represented using a few non-zero coefficients. Ravishankar and Bresler [3, 4] proposed a generalized analysis dictionary learning method, called transform learning, to efficiently find sparse representations of data. The transform learning method avoids optimization of highly non-convex or NP-hard cost functions involved in both synthesis [5, 6] and previous analysis [7] dictionary learning methods, and shows promising performance and speed-ups over the popular synthesis K-SVD [6] algorithm in applications such as image denoising.

Xu et al. [8] first applied dictionary learning to CT image reconstruction by proposing a PWLS approach with regularization based on a redundant synthesis dictionary. Their method uses a global dictionary trained from image patches extracted from one normal-dose FBP image, or an adaptive dictionary jointly estimated with the low-dose image. Pfister and Bresler [2, 9] proposed a model-based iterative reconstruction method with adaptive sparsifying transforms to jointly estimate the ST and the image, showing the promise of PWLS reconstruction with ST regularization. Existing CT image reconstruction methods based on dictionary/transform learning have two common downsides. Firstly, the dictionary is often learned from a very small number of prior images or from the current measurements themselves, which does not

This work was supported in part by SJTU-UM Collaborative Research Program, NSFC (61501292), Shanghai Pujiang Talent Program (15PJ1403900), NIH grant U01 EB018753, ONR grant N00014-15-1-2141, DARPA Young Faculty Award D14AP00086, and ARO MURI grants W911NF-11-1-0391 and 2015-05174-05.
*Yong Long (email: yong.long@sjtu.edu.cn).

Statistical image-domain multimaterial decomposition for dual-energy CT

Yi Xue

Sir Run Run Shaw Hospital, Zhejiang University School of Medicine, Institute of Translational Medicine, Zhejiang University, Hangzhou, Zhejiang 310009, China

Key Laboratory of Biomedical Engineering of Ministry of Education, Zhejiang University, Hangzhou, Zhejiang 310009, China

Ruoshui Ruan

University of Michigan–Shanghai Jiao Tong University Joint Institute, Shanghai Jiao Tong University, Shanghai 200240, China

Xiuhua Hu

Sir Run Run Shaw Hospital, Zhejiang University School of Medicine, Institute of Translational Medicine, Zhejiang University, Hangzhou, Zhejiang 310009, China

Yu Kuang

Department of Medical Physics, University of Nevada, 4505 S Maryland Pkwy, Box 453037, Las Vegas, NV 89154-3037, USA

Jing Wang

Sir Run Run Shaw Hospital, Zhejiang University School of Medicine, Institute of Translational Medicine, Zhejiang University, Hangzhou, Zhejiang 310009, China

Yong Long^{a)}

University of Michigan–Shanghai Jiao Tong University Joint Institute, Shanghai Jiao Tong University, Shanghai 200240, China

Tianye Niu^{a)}

Sir Run Run Shaw Hospital, Zhejiang University School of Medicine, Institute of Translational Medicine, Zhejiang University, Hangzhou, Zhejiang 310009, China

Key Laboratory of Biomedical Engineering of Ministry of Education, Zhejiang University, Hangzhou, Zhejiang 310009, China

(Received 2 October 2016; revised 12 December 2016; accepted for publication 27 December 2016; published 21 February 2017)

Purpose: Dual-energy CT (DECT) enhances tissue characterization because of its basis material decomposition capability. In addition to conventional two-material decomposition from DECT measurements, multimaterial decomposition (MMD) is required in many clinical applications. To solve the ill-posed problem of reconstructing multi-material images from dual-energy measurements, additional constraints are incorporated into the formulation, including volume and mass conservation and the assumptions that there are at most three materials in each pixel and various material types among pixels. The recently proposed flexible image-domain MMD method decomposes pixels sequentially into multiple basis materials using a direct inversion scheme which leads to magnified noise in the material images. In this paper, we propose a statistical image-domain MMD method for DECT to suppress the noise.

Methods: The proposed method applies penalized weighted least-square (PWLS) reconstruction with a negative log-likelihood term and edge-preserving regularization for each material. The statistical weight is determined by a data-based method accounting for the noise variance of high- and low-energy CT images. We apply the optimization transfer principles to design a serial of pixel-wise separable quadratic surrogates (PWSQS) functions which monotonically decrease the cost function. The separability in each pixel enables the simultaneous update of all pixels.

Results: The proposed method is evaluated on a digital phantom, Catphan®600 phantom and three patients (pelvis, head, and thigh). We also implement the direct inversion and low-pass filtration methods for a comparison purpose. Compared with the direct inversion method, the proposed method reduces noise standard deviation (STD) in soft tissue by 95.35% in the digital phantom study, by 88.01% in the Catphan®600 phantom study, by 92.45% in the pelvis patient study, by 60.21% in the head patient study, and by 81.22% in the thigh patient study, respectively. The overall volume fraction accuracy is improved by around 6.85%. Compared with the low-pass filtration method, the root-mean-square percentage error (RMSE(%)) of electron densities in the Catphan®600 phantom is decreased by 20.89%. As modulation transfer function (MTF) magnitude decreased to 50%, the proposed method increases the spatial resolution by an overall factor of 1.64 on the digital phantom, and 2.16 on the Catphan®600 phantom. The overall volume fraction accuracy is increased by 6.15%.

Conclusions: We proposed a statistical image-domain MMD method using DECT measurements. The method successfully suppresses the magnified noise while faithfully retaining the quantification accuracy and anatomical structure in the decomposed material images. The proposed method is practical and promising for advanced clinical applications using DECT imaging. © 2017 American

A 6.78 MHz Multiple-Receiver Wireless Power Transfer System With Constant Output Voltage and Optimum Efficiency

Minfan Fu¹, Member, IEEE, He Yin, Member, IEEE, Ming Liu, Member, IEEE, Yong Wang², Member, IEEE, and Chengbin Ma¹, Member, IEEE

Abstract—This paper develops a 6.78 MHz multiple-receiver wireless power transfer system driven by a Class E power amplifier. Constant output voltage is achieved for each receiver with optimized overall efficiency. A novel one-receiver model is built to analyze the overall power-efficiency characteristics. The loads and input voltage are then designed as two control variables. Through tuning the loads, constant output voltage is achieved by independent controllers at the receiver side. Then, the efficiency is optimized by tuning the input voltage at the transmitter side. Finally, the theoretical analysis and control scheme are validated using a three-receiver system. It shows that different constant output voltages, 5, 9, and 12 V can be achieved independently for different receivers. When the load resistance, real coupling, and number of receivers change, the voltage can be quickly regulated, and the overall optimum system efficiency is 66.6%.

Index Terms—Class E power amplifier (PA), constant output voltage, efficiency optimization, multiple receivers (RXs), wireless power transfer (WPT).

I. INTRODUCTION

WIRELESS power transfer (WPT) has attracted an increasing attention among industrial and academic sectors. One of its unique advantages is to simultaneously charge multiple receivers (RXs), such as wearable devices, cellphones, and household appliances. At the same time, it also presents challenges on the system analysis and control, especially considering the change of coupling, loads, and number of RXs. Such issues have been well studied in the conventional one-RX systems. Examples of the efforts include the design of power am-

plifier (PA) and rectifier [1], [2]; analysis of coupling coils [3], [4]; tunable circuits [5]; and feedback-based control [6].

Parallel with the one-RX systems, many research groups have also shown strong interests in multiple-RX systems. Fundamental works were carried out to evaluate the power transfer characteristics between the coupling coils [7]–[9]. With these basic findings on coil performance, efforts are placed on developing practical systems by including more control freedoms and power stages. For example, multiple frequencies are used in [10]–[13] to charge several devices. Impedance matching networks are proposed to adjust the power distribution among RXs [14]–[16]. Additional coils can be used to manage the power flow among multiple RXs [17], [18]. Multiple-transmitter (multiple-TX) multiple-RX system configuration is also developed in [19]–[21]. Omnidirectional power transfer is achieved by using three-dimensional coils and cavity [22], [23]. All these fundamental works show the variety of possible solutions for multiple-RX applications, and well contribute the progress on the research on multiple-RX systems. However, their ideas were validated by the open-loop measurements. In applications more practical issues should be considered, such as the output power regulation, efficiency optimization, control complexity, and hardware implementation. Furthermore, a multiple-RX system should work robustly under various uncertainties, which are mainly caused by the change of coupling, load resistance, and number of RXs. Therefore, it is important to develop a feedback-based system with a suitable design and control scheme.

In planar charging applications, it is practical to use single transmitter to charge multiple portable devices. A MHz WPT system is promising for such small-power applications thanks to its improved spacial freedom. A MHz system usually uses a Class E PA, i.e., dc/ac, to drive the TX coil due to the high efficiency of the PA. For each RX, a rectifier and a dc/dc converter are respectively used for ac/dc conversion and control purposes (voltage regulation or efficiency optimization). This four-stage (dc/ac, ac/ac, ac/dc, and dc/dc) configuration has been adopted by the A4WP standard and applied in the control of WPT systems [24], [25]. In [24], the system efficiency is optimized to 71% based on a tracking mechanism. However, the output voltage is not regulated. Although the regulation of the output voltage is discussed in [25], the efficiency significantly varies from 66% to 48% under loading and coupling variations. For the

Manuscript received February 26, 2017; revised May 19, 2017; accepted June 30, 2017. Date of publication July 12, 2017; date of current version February 22, 2018. This work was supported by Shanghai Natural Science Foundation under Grant 16ZR1416300. Recommended for publication by Associate Editor C. T. Rim. (Corresponding author: Chengbin Ma.)

M. Fu is with the Center for Power Electronics Systems, Virginia Polytechnic Institute and State University, Blacksburg, VA 24061 USA (e-mail: minfanfu@vt.edu).

H. Yin, M. Liu, and C. Ma are with the University of Michigan–Shanghai Jiao Tong University Joint Institute, Shanghai Jiao Tong University, Shanghai 200240, China (e-mail: yyy@sjtu.edu.cn; mikeliu@sjtu.edu.cn; chbma@sjtu.edu.cn).

Y. Wang is with the Department of Electrical Engineering, Shanghai Jiao Tong University, Shanghai 200240, China (e-mail: wangyong75@sjtu.edu.cn).

Color versions of one or more of the figures in this paper are available online at <http://ieeexplore.ieee.org>.

Digital Object Identifier 10.1109/TPEL.2017.2726349

A High-Efficiency/Output Power and Low-Noise Megahertz Wireless Power Transfer System Over a Wide Range of Mutual Inductance

Ming Liu, *Student Member, IEEE*, Shuangke Liu, *Student Member, IEEE*, and Chengbin Ma, *Member, IEEE*

Abstract—Wireless power transfer (WPT) systems working at several megahertz (MHz) are widely considered as a promising solution for a mid-range transfer of a medium amount of power. The soft-switching-based Class E power amplifier (PA) and rectifier are known to be suitable for high-frequency applications, which may potentially improve the performance of the MHz WPT systems. Meanwhile, the efficiency and output power of the Class E PA are sensitive to its loading condition, particularly when there is variation in the relative position of the coupling coils, namely a changed mutual inductance between the coils. Thus the purpose of this paper is to propose and discuss circuit and design improvements that maintain a high efficiency and output power of the MHz WPT systems over a wide range of mutual inductance, when the Class E PA and the Class E rectifier are employed. Besides, the suppression of the harmonic contents, i.e., the electromagnetic interference problem, is also considered in the circuit design. Both the simulation and experimental results show that the newly added and optimally designed π matching network obviously improves the drops of the efficiency and output power of the Class E PA and the overall WPT system when the mutual inductance varies. The reduction of the total harmonic distortion in the input voltage of the coupling coils is also significant, from the original 52.9% to 9.6%. The circuit and design improvements discussed in this paper could serve as a general and practical solution for building high-performance MHz WPT systems.

Index Terms—Efficiency, harmonics, matching network, megahertz (MHz) wireless power transfer (WPT), output power.

I. INTRODUCTION

WIRELESS power transfer (WPT) is receiving considerable attention from both academia and industry due to a dramatic need to wirelessly charge various electronic devices (e.g., cellphones, laptop computers, wearable devices, medical implant devices, and so on) and the systems requiring much higher power (e.g., electric vehicles and robots). Now the near-field WPT is popular such as through the inductive resonance coupling working at either kilohertz (kHz) or several megahertz (MHz), 6.78 and 13.56 MHz at industrial, scientific, and medical (ISM) band [1]. The kHz WPT systems are particularly superior to high-power applications thanks to the new development of power electronics [2]–[7]. Meanwhile,

in terms of spatial freedom, namely a longer transfer distance and higher tolerance to coupling coil misalignment, the WPT at MHz is advantageous. Besides, higher the operating frequency, more compact and lighter a WPT system [8], [9]. These aspects are especially useful for mid-range and low-power applications such as charging a consumer electronic device. Efforts have been made to build high-efficiency MHz WPT systems through compensation of coils, high-efficiency power amplifiers (PAs) and rectifiers, tunable circuits, frequency tuning, optimal load tracking, and so on [10]–[15].

A practical challenge for MHz WPT is the high switching loss when using conventional hard-switching-based PAs and rectifiers such as the full-bridge ones. Recently, the soft-switching-based ones have begun to be applied in the WPT systems, particularly the MHz WPT systems [16]–[20]. For instance, the Class E PA and the Class E rectifier were originally developed for general high-frequency applications thanks to their soft-switching properties. Using the Class E half-wave rectifier in WPT was first investigated in [17]. A high efficiency of the rectifier (94.43%) was reported when working at 800 kHz. Liu *et al.* [20] developed a system-level optimization procedure for a 6.78-MHz WPT system, which used both a Class E PA and a Class E half-wave rectifier, i.e., a so-called Class E² dc–dc converter. An 84% dc-to-dc efficiency was achieved with loosely coupled coils (mutual inductance coefficient $k = 0.1327$) and at a power level of 20 W. In such systems, the performance of the Class E PA is important for providing a high efficiency and output power of the overall MHz WPT system. This type of PA is known to be a promising high-frequency ac power source due to its simple topology and zero-voltage switching (ZVS)/zero-voltage-derivation switching (ZVDS) properties [21]. Meanwhile, difficulties arise from the uncertainties, such as possible variation in the relative position of the coupling coils (i.e., the mutual inductance), which could be common in real applications. This problem is especially challenging for a WPT system driven by a Class E PA due to the high load sensitivity of the PA [19]. The Class E PA using a finite (ac) choke has been investigated to improve the PA efficiency under a varying PA load [22], [23]. However, its design solution cannot be analytically represented, which makes it difficult to perform optimized parameter design. Thus, this paper focuses on the Class E PA using an infinite (dc) choke. Besides, it should also be noted that another potential problem is the electromagnetic interference (EMI). This issue is particularly crucial for building a practical WPT system working at MHz.

Manuscript received December 19, 2016; accepted March 26, 2017. Date of publication April 27, 2017; date of current version November 3, 2017. This work was supported by the Shanghai Natural Science Foundation under Grant 16ZR1416300. (Corresponding author: Chengbin Ma.)

The authors are with the University of Michigan–Shanghai Jiao Tong University Joint Institute, Shanghai Jiao Tong University, Shanghai 200240, China (e-mail: mikeliu@sjtu.edu.cn; liushuangke@sjtu.edu.cn; chbma@sjtu.edu.cn).

Color versions of one or more of the figures in this paper are available online at <http://ieeexplore.ieee.org>.

Digital Object Identifier 10.1109/TMTT.2017.2691767

0018-9480 © 2017 IEEE. Personal use is permitted, but republication/redistribution requires IEEE permission.

See http://www.ieee.org/publications_standards/publications/rights/index.html for more information.

Analysis and Design of A Robust Class E^2 DC–DC Converter for Megahertz Wireless Power Transfer

Ming Liu, *Student Member, IEEE*, Yue Qiao, Shuangke Liu, *Student Member, IEEE*, and Chengbin Ma, *Member, IEEE*

Abstract—Wireless power transfer (WPT) working at megahertz (MHz) is widely considered a promising technology for midrange and low-power applications. A Class E^2 dc–dc converter is composed of a Class E power amplifier (PA) and a Class E rectifier. It is attractive for applications in MHz WPT due to the soft-switching properties of both the PA and the rectifier. Using the existing design, the Class E^2 dc–dc converter can only achieve optimal performance such as a high efficiency under a fixed operating condition. Meanwhile, in real applications variations in the coil relative position and the final load are common. The purpose of this paper is to analyze and develop a general design methodology for a robust Class E^2 dc–dc converter in MHz WPT applications. Component and system efficiencies are analytically derived, which serve as the basis for the determination of the design parameters. The classical matching network of the Class E PA is also improved that provides the required impedance compression capability. Then, a robust parameter design procedure is developed. Both the experimental and calculated results show that proposed design approach can significantly improve the robustness of the efficiency of the Class E^2 dc–dc converter against variations in coil relative position and final load. Finally, the experiments show that the range of variation of the system efficiency is narrowed from 47.5%–85.0% to 73.3%–83.7% using the proposed robust design.

Index Terms—Class E^2 dc–dc converter, efficiency, matching network, robust analysis and design, wireless power transfer (WPT).

NOMENCLATURE

Z_0	Input impedance of matching network.
Z_{in}	Input impedance of coupling coils.
Z_{rec}	Input impedance of Class E rectifier.
C_S	Shunt capacitor of Class E power amplifier.
C_0	Series capacitor of matching network.
C_1	Shunt capacitor of matching network.
C_{rx}	Compensation capacitor of receiving coil.
C_r	Parallel capacitor of Class E rectifier.
V_{pa}	DC input voltage of Class E power amplifier.
P_{in}	Input power of Class E power amplifier.

P_o	Output power of Class E rectifier.
D	Duty cycle of diode in Class E rectifier.
k	Mutual inductance coefficient.
d	Distance between coupling coils.
R_L	Final dc load.

I. INTRODUCTION

IN recent years wireless power transfer (WPT) using inductive resonance coupling has become increasingly popular. The technology is now being applied to charge cellphones, wearable devices, and even electric vehicles, etc. [1], [2]. For large-power applications, WPT working at kilohertz (kHz) is making rapid progress particularly in terms of coil design and control [3]–[5]. At the same time, in order to further improve the spatial freedom of WPT, i.e., a longer transfer distance and a higher tolerance to the coil misalignment, it is desirable to increase the operating frequency to several megahertz (MHz) such as 6.78 and 13.56 MHz [2], [6]. Designs with higher operating frequencies result in more compact and lighter WPT systems. However, a major limitation is the insufficient power capability of the present switching devices when working in the MHz frequency band. Therefore, the MHz WPT is usually considered to be suitable for midrange and low-power applications [2], [7]–[9]. This presents a technical challenge because high switching loss occurs when the conventional hard-switching-based power amplifiers (PA) and rectifiers are operated in the MHz range. The soft-switching-based PAs and rectifiers are promising candidates to build high-efficiency MHz WPT systems, such as the Class E PA and rectifier.

The Class E PA was first introduced for high-frequency applications in [10]. It has been applied in MHz WPT systems thanks to its high efficiency and simple structure [11]–[14]. The Class E PA can achieve a very high efficiency when it satisfies zero-voltage switching (ZVS) and zero-voltage-derivative switching (ZVDS) conditions. Similarly, the Class E rectifier has also been proposed for high-frequency rectification [15]. Various topologies of the Class E rectifier were developed later such as current-/voltage-driven and half-/full-wave ones [16]–[21]. The application of the Class E rectifier in WPT was first investigated in [22]. As mentioned previously, a high-efficiency (94.43%) rectifier was reported at an 800-kHz operating frequency. Thus both the Class E PA and rectifier can be applied to achieve high-efficiency WPT systems working at MHz, namely the so-called Class E^2 dc–dc converters. A state-space-based analysis of a Class E^2 dc–dc converter is provided for a 200-kHz WPT application in [23]. Initial discussion on the Class E^2 dc–dc converter for MHz WPT can be found in [24]. Meanwhile, as to the knowledge of the authors, studies on a system-level

Manuscript received February 8, 2016; revised May 1, 2016; accepted May 16, 2016. Date of publication May 27, 2016; date of current version January 20, 2017. This work was supported by the Shanghai Natural Science Foundation under Grant 16ZR1416300. Recommended for publication by Associate Editor M. Duffy.

M. Liu and S. Liu are with University of Michigan-Shanghai Jiao Tong University Joint Institute, Shanghai Jiao Tong University, Shanghai 200240, China (e-mail: mikeliu@sjtu.edu.cn; liushuangke@sjtu.edu.cn).

C. Ma is with the University of Michigan-Shanghai Jiao Tong University Joint Institute and School of Mechanical Engineering, Shanghai Jiao Tong University, Shanghai 200240, China (e-mail: chbma@sjtu.edu.cn).

Y. Qiao is with GE AVIC Civil Avionics Systems Company Limited, Shanghai 200241, China (e-mail: chimmy@sjtu.edu.cn).

Color versions of one or more of the figures in this paper are available online at <http://ieeexplore.ieee.org>.

Digital Object Identifier 10.1109/TPEL.2016.2573839

Battery Charging Profile-Based Parameter Design of a 6.78-MHz Class E^2 Wireless Charging System

Ming Liu, *Student Member, IEEE*, Chen Zhao, Jibin Song, *Student Member, IEEE*, and Chengbin Ma, *Member, IEEE*

Abstract—Wireless power transfer (WPT) working at several megahertz (MHz), 6.78 or 13.56 MHz, is widely considered to be a promising candidate for charging electronic devices. The so-called Class E^2 converters combining the soft-switching-based Class E power amplifier (PA) and Class E rectifier are known to be suitable for high-frequency applications with improved efficiency. However, the charging of batteries usually need to follow a specific profile, in which battery voltage and charging current vary over time. The input reactance of the Class E rectifier also becomes obvious at megahertz. This nonneglectable and varying reactance significantly lowers system efficiency and complicates parameter design. In this paper, a systematic design approach is developed that minimizes the energy loss of a 6.78-MHz Class E^2 wireless charging system during the entire battery charging cycle. A LC matching network is added to improve the loading conditions of the Class E PA and coupling coils, and provides new degrees of freedom in the parameter design. Average power loss is defined based on analytically derived system efficiency and a discretized battery charging profile. It serves as an objective function that is minimized through the proposed battery charging profile-based parameter design. In final experiments, the proposed design achieves a 24.5% reduction of the average power loss when comparing with that through the conventional design.

Index Terms—Battery charging system, charging profile, efficiency, lithium-ion battery, megahertz wireless power transfer.

I. INTRODUCTION

IN RECENT years, wireless power transfer (WPT) through inductive resonance coupling became popular to charge various electronic devices (e.g., cellphones, laptop computers, wearable devices, medical implant devices) and even electric vehicles [1], [2]. For high-power applications, WPT working at

kilohertz (kHz) is making rapid progress in terms of coil design, compensation topologies, control strategies, etc., [3]–[6]. At the same time, in order to reduce size and weight of WPT systems, it is preferred to further increase the operating frequency to several megahertz (MHz) such as 6.78 and 13.56 MHz. A higher operating frequency also helps to improve spatial freedom, namely a longer transfer distance and higher tolerance to coupling coil misalignment, which is particularly beneficial for charging mobile devices. However, the power capability of the present switching devices is insufficient when operating at MHz. At present, the MHz WPT is usually considered to be suitable for mid-range and low-power applications [2], [7]–[9].

A practical challenge for the MHz WPT is the high switching loss when using conventional hard-switching-based power amplifiers (PAs) and rectifiers. Class E PA and rectifier are promising candidates to build high-efficiency MHz WPT systems because of their soft-switching properties. The Class E PA was first introduced for high-frequency applications in [10]. It has been applied in MHz WPT systems and shown improvements thanks to its high efficiency and simple topology [11]–[14]. Similarly, the Class E rectifier has also been proposed for high-frequency rectification [15]. Its application in WPT was first investigated in [16]. A high efficiency of the rectifier 94.43% was reported at an 800-kHz operating frequency. Thus, the combination of both Class E PA and rectifier, i.e., a Class E^2 converter, is expected to enable a high-efficiency wireless charging system working at MHz.

Lithium-ion batteries are now widely used in consumer electronic devices mostly due to its high energy density [17], [18]. A typical charging profile of the lithium-ion batteries usually consists of two modes, constant current (CC) mode and constant voltage (CV) mode. The battery is first charged in CC mode. When its voltage reaches a nominal value, the charging system enters the CV mode, in which the charging current rapidly drops. In order to prolong the battery cycle-life, a wireless charging system must supply current and voltage accurately following a specific battery charging profile [19]. In real applications, the charging profiles can be tracked through either the input voltage control of the charging system or the regulation circuit between the charger and batteries.

In the conventional Class E^2 converter for WPT applications, the system parameters are optimized targeting on only a single

Manuscript received September 1, 2016; revised December 30, 2016; accepted January 29, 2017. Date of publication March 14, 2017; date of current version July 10, 2017. This work was supported by the Shanghai Natural Science Foundation under Grant 16ZR1416300.

M. Liu, J. Song, and C. Ma are with the University of Michigan-Shanghai Jiao Tong University Joint Institute, Shanghai Jiao Tong University, Minhang, Shanghai 200240, China (e-mail: mikeliu@sjtu.edu.cn; jibinsong@sjtu.edu.cn; chbma@sjtu.edu.cn).

C. Zhao is with United Automotive Electronic Systems Co., Ltd., Pudong, Shanghai 201206, China (e-mail: chen.zhao3@uaes.com).

Color versions of one or more of the figures in this paper are available online at <http://ieeexplore.ieee.org>.

Digital Object Identifier 10.1109/TIE.2017.2682017

Efficiency Optimization and Power Distribution Design of a Megahertz Multi-receiver Wireless Power Transfer System

Jibin Song, Ming Liu, Chengbin Ma,
Univ. of Michigan-Shanghai Jiao Tong Univ. Joint Institute,
Shanghai Jiao Tong University, Shanghai, P. R. China

Abstract—It is attractive to achieve multi-receiver wireless power transfer (WPT) through a megahertz operating frequency. However, the power distribution among receivers can be a difficult task due to the different load characteristics, i.e., power requirement, receiver size, and coupling coefficient. This paper proposes a general design methodology of efficiency optimization and power distribution of a MHz multi-receiver WPT System. A Class E rectifier is introduced in the MHz multi-receiver WPT system to provide the design freedom for the power distribution and efficiency optimization. Based on the fundamental analysis and analytical derivations of the Class E rectifier and coupling coils, a numerical optimization problem is formulated to achieve the power distribution and maximized efficiency simultaneously. Finally, an example 6.78-MHz three-receiver WPT system is built to verify the proposed design methodology. The experimental results show that the proposed design can meet the power requirement of loads within 5% error and achieve system efficiency of 90% at a power level of 25W.

Index Terms—multi-receiver, megahertz Wireless power transfer, Class E rectifier, power distribution

I. INTRODUCTION

Megahertz (MHz) wireless power transfer (WPT) is now being considered a promising candidate for the mid-range transfer of a medium amount of power [1], [2]. A higher operating frequency (such as 6.78 and 13.56 MHz) is desirable for a more compact and lighter WPT system with a longer transfer distance and make it possible to charge multiple receivers simultaneously. Lots of researches have been done on the design and optimization of one-receiver WPT systems [3]–[7], however, there are still many unsolved problems to apply these techniques for a multiple-receiver system due to the different power requirement and charging condition among loads. For the multi-receiver WPT system, most of works focus on efficiency, resonance frequency, or cross coupling analysis [8]–[10]. However, there are few works addressing power distribution among receivers. Further research work is needed to address the most critical problem in the multi-receiver WPT system for real applications.

Initial discussions about the power distribution for a two-receiver WPT system can be found in [11], where the equivalent series resistance (ESR) of coils are ignored and the proposed model is too complicated to analyze the WPT system with more receivers. In [12] a power distribution control method is discussed by adjusting the load impedance of the receivers. However, an additional hardware is required for the

load impedance adjustment. Ref. [13] proposed an impedance matching and power division method utilizing impedance inverters at the receiver sides. Generally, the additional control circuits or the impedance inverters will increase the system complexity and power loss in the real application. In [14], [15], a frequency-shifting based method was investigated to realize the power control in a multi-receiver WPT system. Band pass filters or certain resonance circuits were used to implement frequency selection among the multiple receivers. However, the complicated power transmitter and filtering circuits of the frequency shifting method make it difficult to charging multiple receivers simultaneously. Furthermore, frequency shifting or frequency tuning is impractical in megahertz WPT applications due to the ISM band limitation.

Based on power distribution and efficiency optimization, this paper proposes a novel design method for a multi-receiver WPT system with simple topology and fixed components. Firstly, the input impedance and efficiency of the Class E rectifiers is given and serve as the basis to analyze the coupling coils. Then the efficiency of the coupling coils is derived and formulated. Then the basic principals of power distribution among receivers and the overall system efficiency is analyzed and formulated. Based on the analytical derivations, the whole system design is formulated as an optimization problem to achieve the power distribution and efficiency optimization. Finally, a 6.78-MHz WPT system with three receivers is built to validate the proposed design method. The experimental results shows that the WPT system using the proposed optimization design method can meet the power requirement of each load and achieve the system efficiency of 90%.

II. MODELING AND ANALYSIS

The entire configuration of a MHz multi-receiver WPT system is demonstrated in Fig. 1 (a), including a power transmitter TX and n receivers $RX_i (i \in [1, \dots, n])$. i is always used to denote different receivers. The TX consists of a MHz power source and a transmitting coil. The transmitting coil is fully resonant with the compensation capacitor C_{tx} to achieve an unit power factor. Each RX_i consists of a receiving coil, a current driven Class E rectifier and a DC load. The receiving coils are also compensated by a series-connected capacitor $C_{rx,i}$. In the following subsection, the efficiencies of the Class E rectifier and coupling coils are formulated

Low-Harmonic-Contents and High-Efficiency Class E Full-Wave Current-Driven Rectifier for Megahertz Wireless Power Transfer Systems

Ming Liu, *Student Member, IEEE*, Minfan Fu, *Student Member, IEEE*, and Chengbin Ma, *Member, IEEE*

Abstract—Wireless power transfer (WPT) working at megahertz (MHz) is now being widely considered a promising candidate for the midrange transfer of a medium amount of power. Efforts have been made to build high-efficiency MHz WPT systems via both component- and system-level approaches. However, so far there have been few discussions on high-frequency rectifier for MHz WPT applications. The soft-switching-based rectifiers, such as the Class E rectifiers, are one of the promising candidates for MHz rectification. This paper investigates the application of a Class E full-wave current-driven rectifier, for the first time, in WPT systems. A procedure is also developed to optimize the design of the rectifier and the MHz WPT system. For comparison purposes, the performances of both the Class E rectifier and the conventional full-bridge rectifier are investigated in terms of total harmonic distortion (THD), efficiency, power factor, voltage/current stresses, and voltage/current transfer functions, when being applied in an example 6.78-MHz WPT system. The simulation and experimental results show that the input voltage THD of the Class E full-wave rectifier is reduced to one-fourth of the THD of the full-bridge rectifier. In the optimally designed MHz WPT system, efficiencies of both the rectification (over 91%) and the overall system (around 80%) are obviously improved compared to the system using the conventional full-bridge rectifier.

Index Terms—Class E full-wave current-driven rectifier, efficiency, low-harmonic contents, megahertz wireless power transfer (MHz WPT).

I. INTRODUCTION

THERE is now a dramatic need in charging various electronic devices (e.g., cellphones, laptop computers, wearable devices, medical implant devices, etc.) and other high-power systems, especially electric vehicles. This need makes the wireless power transfer (WPT) using inductive resonance coupling, i.e., the so-called inductive coupling and magnetic resonance coupling, increasingly popular in recent years [1], [2]. Currently WPT working at kilohertz (kHz) is making

significant progress in power level, system design, and applications [3]–[7]. Meanwhile, for medium- and low-power applications, further increasing the resonance frequency such as to several megahertz (MHz) brings a higher level of spatial freedom, namely a longer transfer distance and higher tolerance to coupling coil misalignment, and is desirable for building more compact and lighter WPT systems [2], [8]. Now WPT working at MHz is being widely considered a promising candidate for the midrange transfer of a medium amount of power. Meanwhile, in MHz WPT systems, ultrahigh-speed logic gates are required to drive the MOSFET switches. This leads to increased gate power dissipation and cost. The soft-switching operation of the power amplifier (PA) and the rectifier is also expected to reduce the increased switching losses [9], [10]. Besides, generally the parasitic resistances of the ac inductors including the coupling coils increase at MHz. It is especially desirable to use high-Q (quality factor) inductors and coupling coils for conduction loss reduction [11]. Moreover, the impedance characteristics of circuits working at MHz are much more complicated than those at kHz. For instance, at MHz, the influence of the parasitic and/or parallel capacitors of the diodes becomes significant. This causes nonnegligible reactance of the rectifier that could lower the efficiency and power transfer capability of the system [12]. In addition, electromagnetic interference (EMI) problem in the MHz WPT systems is also more challenging. In order to improve the overall performance of the MHz WPT systems, it is important to introduce new topologies of the circuits, and conduct comprehensive analysis and optimization.

Efforts have been made to build high-efficiency MHz WPT systems via both component- and system-level approaches focusing on the improvements in coupling coils [13]–[17], PA [18]–[21], and load control [22]–[24]. At the same time, so far there have been few discussions on high-frequency rectifier for MHz WPT applications. Most existing MHz WPT systems use conventional hard-switching-based rectifiers such as the full-bridge rectifier. Due to the hard-switching operation, there is significant switching loss from the full-bridge rectifier when operating at MHz. In addition, the hard switching also leads to high-voltage harmonic contents in WPT systems due to the square-wave input voltage in the full-bridge rectifier. For a high-frequency rectification at MHz, the soft-switching-based rectifiers, such as the Class E rectifiers, are one of the promising candidates. Meanwhile, care should be taken to use proper diodes due to the higher diode voltage stress in the Class E rectifiers [25]. The Class E rectifier was first proposed for a high-frequency dc–dc converter in 1988 [26]. Various Class E

Manuscript received September 30, 2015; revised January 16, 2016; accepted March 28, 2016. Date of publication April 6, 2016; date of current version November 11, 2016. This work was supported by Shanghai Natural Science Foundation under Grant 16ZR1416300. Recommended for publication by Associate Editor M. A. E. Andersen.

M. Liu and M. Fu are with the University of Michigan-Shanghai Jiao Tong University Joint Institute, Shanghai Jiao Tong University, Minhang, Shanghai 200240, China (e-mail: mikeliu@sjtu.edu.cn; fuminfan@sjtu.edu.cn).

C. Ma is with the University of Michigan-Shanghai Jiao Tong University Joint Institute, Shanghai Jiao Tong University, Shanghai 200240, China, and also with the School of Mechanical Engineering, Shanghai Jiao Tong University, Shanghai 200240, China (e-mail: chbma@sjtu.edu.cn).

Color versions of one or more of the figures in this paper are available online at <http://ieeexplore.ieee.org>.

Digital Object Identifier 10.1109/TPEL.2016.2551288

Megahertz Multiple-Receiver Wireless Power Transfer Systems With Power Flow Management and Maximum Efficiency Point Tracking

Minfan Fu, *Member, IEEE*, He Yin, *Student Member, IEEE*, and Chengbin Ma, *Member, IEEE*

Abstract—This paper presents systematic analysis and design of a megahertz multiple-receiver (RX) wireless power transfer (WPT) system driven by a Class E power amplifier. Both circuit-level and system-level analyses are conducted to discuss the characteristics of the WPT system. In order to simultaneously manage the power flow and maximize the overall system efficiency, a new control scheme is proposed that combines maximum efficiency point tracking and time-division multiplexing. Through the proposed scheme, RXs with different loading and coupling conditions can be charged by the same transmitter with simplified design and control strategy. Finally, the proposed control scheme is validated using an example 6.78-MHz three-RX WPT system. The experimental results show that various power requirements can be quickly and stably satisfied, and the overall average system efficiency can reach as high as 71.7%.

Index Terms—Analysis and design, maximum efficiency point tracking (MEPT), multiple receivers (RXs), time-division multiplexing (TDM), wireless power transfer (WPT).

I. INTRODUCTION

WIRELESS power transfer (WPT) through inductive coupling became increasingly popular during the past years [1]. Besides the noncontacting power delivery, another unique advantage of WPT is the possibility to charge multiple receivers (RXs), such as wearable devices, cellphones, and household appliances, namely, multiple-RX WPT systems. There are fundamental works focusing on the analysis of multiple coupling coils under basic compensations [2]–[4]. Meanwhile, various coil configurations and circuits have been developed to improve the transfer characteristics, such as multiple transmitters (TXs) [5], impedance matching networks [6]–[8], and relay coils [9], [10]. Using dual-band or multiple-band concept, it is possible to charge multiple devices with different resonant frequencies [11]–[13]. Several recently published papers discuss the 3-D charging by using orthogonal coils or cavities [14]–[16]. A new technology called MultiSpot can even charge the devices, which are worn or carried by

the users [17]. All the above-mentioned works help to speed up the transition from laboratory systems to real multiple-RX applications. However, there are still many unsolved challenges for practical multiple-RX systems, particularly the system controllability and stability under variations in load and coupling. It is important to specifically develop a suitable configuration and a control scheme for multiple-RX systems.

In the conventional design, usually all the RXs are powered at the same time. The control methods implemented at the TX side (frequency tracking, load-independent source, automatic impedance matching, and so on) can hardly be used to manage the power flow among RXs, because they only affect the overall performance [18]–[20]. In a multiple-RX WPT system, uncertainties caused by the loading and coupling variations may dramatically increase due to the varied number of RXs. The interactive relationships among RXs, such as the cross coupling, also further affect the coil efficiency and make the power distribution unpredictable [4]. New design and control schemes are required to achieve power flow management and maintain high overall system efficiency at the same time in multiple-RX systems.

In order to simplify the system design and control, a well-known communication technology, time-division multiplexing (TDM), has been introduced in WPT applications [21]. The TDM-based WPT system does not require all the RXs to be simultaneously powered. This significantly reduces the system uncertainties and totally avoids the adverse effects of the cross coupling [4]. TDM can be directly combined with the existing control approaches originally developed for the one-RX systems. In high-power applications, an early example is the combination of frequency tuning and TDM to maintain the system stability [22]. TDM-based WPT systems have also been developed to charge low-power devices. A real TDM-based WPT system is briefly explained in [23] without details in analysis and implementation. Through having different resonant frequencies, one designated device among multiple devices can be selectively and exclusively charged [24]. Meanwhile, the discussion mainly focuses on the coupling coils in the multiple-RX system. A TDM-based TX was built to charge arbitrarily distributed devices in a medical application with a power level of several milliwatts and an average efficiency of 5.8% at the worst case of 90° coil misalignment [25]. A TDM-based power control is applied in a three-orthogonal-coil TX [16]. The purpose is to focus the power flow directionally toward the targeted areas. The improvement of efficiency is not fully discussed.

Manuscript received October 1, 2016; revised December 22, 2016; accepted March 6, 2017. Date of publication April 12, 2017; date of current version November 3, 2017. This work was supported by the Shanghai Natural Science Foundation under Grant 16ZR1416300. (Corresponding author: Chengbin Ma.)

M. Fu is with the Center for Power Electronics Systems, Virginia Polytechnic Institute and State University, Blacksburg, VA 24061 USA (e-mail: minfanfu@vt.edu).

H. Yin and C. Ma are with the University of Michigan–Shanghai Jiao Tong University Joint Institute, Shanghai Jiao Tong University, Shanghai 200240, China (e-mail: yyy@sjtu.edu.cn; chbma@sjtu.edu.cn).

Color versions of one or more of the figures in this paper are available online at <http://ieeexplore.ieee.org>.

Digital Object Identifier 10.1109/TMTT.2017.2689747

0018-9480 © 2017 IEEE. Personal use is permitted, but republication/redistribution requires IEEE permission. See http://www.ieee.org/publications_standards/publications/rights/index.html for more information.

A Novel Design Methodology for High-Efficiency Current-Mode and Voltage-Mode Class-E Power Amplifiers in Wireless Power Transfer systems

Shuangke Liu, *Student Member, IEEE*, Ming Liu, *Student Member, IEEE*, Songnan Yang, Chengbin Ma, *Member, IEEE*, and Xinen Zhu, *Member, IEEE*

Abstract—The high-efficiency current-mode (CM) and voltage-mode (VM) Class-E power amplifiers (PAs) for MHz wireless power transfer (WPT) systems are first proposed in this paper and the design methodology for them is presented. The CM/VM Class-E PA is able to deliver the increasing/decreasing power with the increasing load and the efficiency maintains high even when the load varies in a wide range. The high efficiency and certain operation mode are realized by introducing an impedance transformation network with fixed components. The efficiency, output power, circuit tolerance, and robustness are all taken into consideration in the design procedure, which makes the CM and the VM Class-E PAs especially practical and efficient to real WPT systems. 6.78-MHz WPT systems with the CM and the VM Class-E PAs are fabricated and compared to that with the classical Class-E PA. The measurement results show that the output power is proportional to the load for the CM Class-E PA and is inversely proportional to the load for the VM Class-E PA. The efficiency for them maintains high, over 83%, when the load of PA varies from 10 to 100 Ω , while the efficiency of the classical Class-E is about 60% in the worst case. The experiment results validate the feasibility of the proposed design methodology and show that the CM and the VM Class-E PAs present superior performance in WPT systems compared to the traditional Class-E PA.

Index Terms—Current-mode (CM) Class-E power amplifier (PA), high-efficiency, impedance-transformation network, load-pull analysis, voltage-mode (VM) Class-E PA, wireless power transfer (WPT).

I. INTRODUCTION

WIRELESS charging technology for portable electric devices has received intensive attention and realized commercialization by the lunch of Qi standard [1], [2]. It makes the power transfer more flexible and provides a comfortable user experience. This technology has been constantly improving and lots of efforts have been paid to pursue larger charging freedom, higher efficiency, and better performance for concurrent mul-

tiple charging (a technique that transmits power concurrently to multiple receiving coils) [3]–[8]. However, most of them have been focusing on the coupling coils and research on the high-frequency high-efficiency power source for wireless power transfer (WPT) is lacked [6]–[11].

The majority of power sources that have been used in WPT systems are inverters [12], [13]. They require at least four switches and usually work at tens to hundreds of kilohertz. For the requirements of smaller circuit size and larger charging freedom, a new operating frequency, 6.78 MHz for WPT, has received more and more attention [14], [15]. It belongs to the industrial, scientific, and medical (ISM) band and has been adopted by Rezence standard proposed by the Alliance for Wireless Power. The switch loss of inverters become considerably large at this frequency and thus a high-performance power source working at 6.78 MHz is required. The power source should maintain a high efficiency under the dynamic charging environment, i.e., the misalignment of coil coupling and the change of number of charging devices [16], [17]. Besides, it is expected that the power source is able to work in a certain mode, i.e., work as a current source or a voltage source [18], [19], for which the relationship of the output power and the load is predetermined. The power source with a certain operation mode is especially valuable to concurrent multiple charging systems, where the output power of source should adapt to the power requirements of charging devices. For instance, the load of power source in [16] increases as the number of charging device goes up, which indicates that the power source in this system should work as a current source, providing increasing output power with increasing load.

The Class-E power amplifier (PA) is a good candidate for MHz WPT systems due to its simple topology and high efficiency [20]–[22]. It is designed under zero voltage switching (ZVS) and zero voltage derivative switching (ZVDS) conditions, which result in a 100% efficiency theoretically [23], [24]. The achievable efficiencies of the Class-E PAs are known to be about 90% when they operate at several to tens of MHz and deliver power of several to tens of watts [21], [25]. However, the ZVS and ZVDS conditions make the Class-E PA sensitive to the load variation, which is inevitable in real WPT systems due to the misalignment of coil coupling and the change of the number of receivers [16], [17]. The efficiency drops quickly when the load of PA deviates from the optimum value [26]. Besides, the

Manuscript received April 20, 2016; revised June 23, 2016; accepted August 2, 2016. Date of publication August 15, 2016; date of current version February 11, 2017. Recommended for publication by Associate Editor Regan Zane.

S. Liu, M. Liu, C. Ma, and X. Zhu are with the University of Michigan—Shanghai, Jiao Tong University Joint Institute, Shanghai Jiao Tong University, Minhang, Shanghai 200240, China (e-mail: liushuangke@sjtu.edu.cn; mike-liu@sjtu.edu.cn; chbma@sjtu.edu.cn; zhuxinen@sjtu.edu.cn).

S. Yang is with Intel Corporation, Santa Clara, CA 95054-1549 USA (e-mail: songnan.yang@intel.com).

Color versions of one or more of the figures in this paper are available online at <http://ieeexplore.ieee.org>.

Digital Object Identifier 10.1109/TPEL.2016.2600268

0885-8993 © 2016 IEEE. Personal use is permitted, but republication/redistribution requires IEEE permission.

See http://www.ieee.org/publications_standards/publications/rights/index.html for more information.

Tunable Class E^2 DC-DC Converter with High Efficiency and Stable Output Power for 6.78 MHz Wireless Power Transfer

Shuangke Liu, *Student Member, IEEE*, Ming Liu, *Member, IEEE*, Songyang Han, *Student Member, IEEE*, Xinen Zhu, *Member, IEEE*, Chengbin Ma, *Member, IEEE*

Abstract—Class E^2 dc-dc converter composed of Class E power amplifier (PA) and rectifier is a promising candidate for MHz wireless power transfer (WPT). It is soft-switching based and able to achieve high efficiency at MHz frequency. However, the converter implemented through traditional static design is sensitive to the variations of operation condition. Its performance gets deteriorated when dc load and coil coupling deviate from their respective optimum values. This paper demonstrates that the degradation of system efficiency is mostly due to the mismatch of PA load, and the efficiency drop can be efficiently improved by adding a L-type impedance matching network (IMN) after PA. A fixed IMN is sufficient to maintain a high efficiency, while a tunable IMN is required to ensure stable output power when operation condition dramatically changes. Key techniques, particularly system-level optimization, are discussed in this paper that ensure high efficiency over a wide range of variation in operation condition and also with reduced capacitor/inductor tuning ranges in the IMN. The 6.78 MHz Class E^2 dc-dc converters with and without the fixed/tunable IMN are fabricated and measured for validation purposes. The experimental results show that both high efficiency ($>66\%$) and stable output power (around 9 W) are maintained for the tunable converter when there are variations in the dc load and coil coupling.

Index Terms—Tunable Class E^2 dc-dc converter, megahertz wireless power transfer, high-efficiency, stable output power, tunable impedance matching network.

I. INTRODUCTION

WIRELESS power transfer systems working at MHz have been receiving increasing research attention in recent years due to their advantages of larger spatial freedom and compact circuit size [1], [2]. However, the switching loss occurred in MOSFET and diode could also become considerably large at high frequencies. The traditional hard-switching based inverters and rectifiers, such as the full bridge

inverter and rectifier used in kHz WPT systems, are usually not suitable for being directly applied in the MHz systems. Class E^2 dc-dc converter, composed of soft-switching based Class E PA and Class E rectifier, is a promising solution for a high-efficiency operation in MHz WPT applications.

The Class E PA was first proposed in 1975 [3]. It has been widely used thanks for its simple topology and high efficiency [4], [5]. The drain voltage of an ideal Class E PA reaches zero prior to turn on of the MOSFET, which theoretically results in zero switching loss. High efficiency of the Class E PA up to 94% at MHz frequency has been observed in experiments [4]. The Class E rectifier applied in WPT systems was initially presented in [6], in which an efficiency of 94% at 800 KHz was achieved. In the rectifier, a capacitor is connected in parallel with the diode such that the diode turns on and off with low dv_D/dt (v_D is the voltage across the diode), namely reduced switching loss. Due to the soft-switching property of the Class E PA and rectifier, the Class E^2 dc-dc converter is able to achieve high efficiency in MHz WPT applications [7]–[9]. Traditional design of Class E^2 dc-dc converter is a static one. The dc load and coupling coefficient are assumed to be constant. The circuit parameters are then designed to let each subsystem of the dc-dc converter (i.e., PA, coupling coils, and rectifier) operate under optimum conditions [8], [9]. However, in real applications, a WPT system may work under a changing operation condition. The coupling coefficient may change due to the coil misalignment. The load of rectifier could also vary over time such as when charging a battery. Ref. [10] shows that the system efficiency ranges from 15% to 90% when the ratio of transfer distance to coil diameter changes from 0.2 to 1.4. The system efficiency drop caused by the coil misalignment is due to both the deteriorated coil performance and the load mismatch of power source [11]. In [12], a robust Class E^2 WPT system is designed, in which the coupling coefficient and dc load change from 0.1 to 0.4 and 15 to 45 Ω , respectively. The system efficiency itself is improved significantly when the coil coupling and dc load vary. However, at the same time, the output power varies dramatically from about 2.5 to 18 W. The existing design of the Class E^2 WPT system still can not fully adapt to the varying operation conditions, particularly its incapability of maintaining stable output power.

Many solutions have been proposed to improve system efficiency through subsystem-level optimization and optimum load tracking. In [13]–[16], the duty cycle of driving signal,

Manuscript received January 4, 2017; revised April 27, 2016; accepted September 26, 2017 (*Corresponding author: Chengbin Ma*). This work was supported by the Shanghai Natural Science Foundation under Grant 16ZR1416300.

S. Liu, and S. Han are with University of Michigan-Shanghai Jiao Tong University Joint Institute, Shanghai Jiao Tong University, 800 Dongchuan Road, Minhang, Shanghai 200240, P. R. China (e-mail: liushuangke@sjtu.edu.cn; hansongyang@sjtu.edu.cn).

M. Liu is with Department of Electrical Engineering, Princeton University, Princeton, NJ 08544, USA (e-mail: ml45@princeton.edu).

X. Zhu is with Shanghai Industrial μ Technology Research Institute, 235 Chengbei Road, Jiading, Shanghai 201800, P. R. China (e-mail: alfred.zhu@sitigroup.com).

C. Ma is with the University of Michigan-Shanghai Jiao Tong University Joint Institute, Shanghai Jiao Tong University, 800 Dongchuan Road, Minhang, Shanghai 200240, P. R. China (e-mail: chbma@sjtu.edu.cn).



Contents lists available at ScienceDirect

INTEGRATION, the VLSI journal

journal homepage: www.elsevier.com/locate/vlsi

A high-accuracy approximate adder with correct sign calculation

Junjun Hu, Zhijing Li, Meng Yang, Zixin Huang, Weikang Qian*

University of Michigan-Shanghai Jiao Tong University Joint Institute, Shanghai Jiao Tong University, Shanghai, China

ARTICLE INFO

Keywords:

Approximate adder
Approximate computing
Low relative error
Sign error correction
Low-power design

ABSTRACT

Conventional precise adders take long delay and large power consumption to obtain accurate results. Exploiting the error tolerance of some applications such as multimedia, image processing, and machine learning, a number of recent works proposed to design approximate adders that generate inaccurate results occasionally in exchange for reduction in delay and power consumption. However, most of the existing approximate adders have a large relative error. Besides, when applied to 2's complement signed addition, they sometimes generate a wrong sign bit. In this paper, we propose a novel approximate adder that exploits the generate signals for carry speculation. Furthermore, we introduce a low-overhead module to reduce the relative error and a sign correction module to fix the sign error. Compared to the conventional ripple carry adder and carry-lookahead adder, our adder with block size of 4 reduces power-delay product by 66% and 32%, respectively, for a 32-bit addition. Compared to the existing approximate adders, our adder significantly reduces the maximal relative error and ensures correct sign calculation with comparable area, delay, and power consumption. We further tested the performance of our adders with and without the sign error correction module in three real applications, mean filter, edge detection, and k-means clustering. The experimental results demonstrated the importance of reducing the relative error and ensuring the correct sign calculation for 2's complement signed additions. The outputs produced using our adder with the sign error correction module are very close to those produced using accurate adder.

1. Introduction

As CMOS devices are scaled into the sub-nanometer regime, power consumption has become a major bottleneck in sustaining Moore's law. Thus, energy efficiency has become a critical concern in designing VLSI circuits. At the same time, with the prevalence of mobile computing, there is an increasing demand for signal processing, multimedia, machine learning, and pattern recognition applications [1]. These applications are essentially error tolerant due to various reasons such as limitation of human perception, redundancy in the input signal, and lack of a unique golden answer [2]. As a result, an inaccurate computation result may still lead to an output with acceptable quality. The relaxation of the accuracy requirement for these applications potentially enlarges the design space, which may contain some solutions with smaller area, delay, and power consumption than those targeted for accurate computation. This leads to a new design paradigm, known as *approximate computing*, which deliberately sacrifices a small amount of accuracy to achieve improvement in performance and power consumption [3].

In this work, we focus on designing approximate adder. As adders

are key building blocks in many applications that are suitable for approximate computing, many previous works propose various designs of approximate adders [4–7] (A detailed review of several existing representative approximate adders can be found in Section 2). These adders have smaller areas, delays, and power consumption compared to the accurate ones. Many of them also have small error rates. However, most of them cannot guarantee a small relative error in their outputs. As a result, they may degrade the output quality for some applications. Furthermore, these approximate adders are subject to sign calculation error when doing signed addition for 2's complement numbers.

In this paper, to address the above problems of the existing approximate adders, we propose a novel approximate adder design. It exploits the generate signals to produce the speculated carry signals. This approach leads to a simplified circuitry to calculate carry, resulting in a dramatic reduction in adder area and power consumption compared to the accurate adders. To reduce the maximal relative error, we introduce a low-overhead error reduction module. Furthermore, to eliminate the potential sign error in 2's complement signed addition, we introduce a lightweight sign error correction

* Corresponding author.

E-mail addresses: wujunjun_sh@hotmail.com (J. Hu), liuyuedtian@sjtu.edu.cn (Z. Li), yangm.meng@sjtu.edu.cn (M. Yang), zxhuang14@sjtu.edu.cn (Z. Huang), qianwk@sjtu.edu.cn (W. Qian).

<http://dx.doi.org/10.1016/j.vlsi.2017.09.003>

Received 5 May 2017

0167-9260/ © 2017 Elsevier B.V. All rights reserved.

A Reconfigurable Architecture with Sequential Logic-Based Stochastic Computing

M. HASSAN NAJAFI, University of Minnesota

PENG LI, Intel Corporation

DAVID J. LILJA, University of Minnesota

WEIKANG QIAN, University of Michigan-Shanghai Jiao Tong University Joint Institute

KIA BAZARGAN and MARC RIEDEL, University of Minnesota

Computations based on stochastic bit streams have several advantages compared to deterministic binary radix computations, including low power consumption, low hardware cost, high fault tolerance, and skew tolerance. To take advantage of this computing technique, previous work proposed a combinational logic-based reconfigurable architecture to perform complex arithmetic operations on stochastic streams of bits. The long execution time and the cost of converting between binary and stochastic representations, however, make the stochastic architectures less energy efficient than the deterministic binary implementations. This article introduces a methodology for synthesizing a given target function stochastically using finite-state machines (FSMs), and enhances and extends the reconfigurable architecture using sequential logic. Compared to the previous approach, the proposed reconfigurable architecture can save hardware area and energy consumption by up to 30% and 40%, respectively, while achieving a higher processing speed. Both stochastic reconfigurable architectures are much more tolerant of soft errors (bit flips) than the deterministic binary radix implementations, and their fault tolerance scales gracefully to very large numbers of errors.

Categories and Subject Descriptors: B.6.1 [Logic Design]: Design Styles—Sequential Circuits; B.8.1 [Performance and Reliability]: Reliability, Testing and Fault-Tolerance

General Terms: Design, Performance, Reliability

Additional Key Words and Phrases: Stochastic computing, finite-state machine, polynomial arithmetic

ACM Reference Format:

M. Hassan Najafi, Peng Li, David J. Lilja, Weikang Qian, Kia Bazargan, and Marc Riedel. 2017. A reconfigurable architecture with sequential logic-based stochastic computing. *J. Emerg. Technol. Comput. Syst.* 13, 4, Article 57 (June 2017), 28 pages.

DOI: <http://dx.doi.org/10.1145/3060537>

This work was supported in part by the National Science Foundation, under grant no. CCF-1241987 and CCF-1408123, and National Natural Science Foundation of China (NSFC) under Grant No. 61472243 and 61204042. Any opinions, findings, and conclusions or recommendations expressed in this material are those of the authors and do not necessarily reflect the views of the NSF. Portions of this work were presented in the 2012 IEEE/ACM International Conference on Computer-Aided Design [Li et al. 2012], in the 17th Asia and South Pacific Design Automation Conference [Li et al. 2012], and in the 30th IEEE International Conference on Computer Design [Li et al. 2012].

Authors' addresses: M. H. Najafi, D. J. Lilja, K. Bazargan, and M. Riedel, Department of Electrical and Computer Engineering, University of Minnesota, Minneapolis, MN, 55455; emails: {najaf011, lilja, kia, mriedel}@umn.edu; P. Li, Intel Corporation, 2111 NE 25th Ave., Hillsboro, OR, 97124 (most of the research work presented in this article was completed when the author was pursuing his Ph.D. in the Department of Electrical and Computer Engineering at University of Minnesota, Twin Cities); email: lipeng@umn.edu; W. Qian, University of Michigan-Shanghai Jiao Tong University Joint Institute, Shanghai, China, 200240; email: qianwk@sjtu.edu.cn.

Permission to make digital or hard copies of part or all of this work for personal or classroom use is granted without fee provided that copies are not made or distributed for profit or commercial advantage and that copies show this notice on the first page or initial screen of a display along with the full citation. Copyrights for components of this work owned by others than ACM must be honored. Abstracting with credit is permitted. To copy otherwise, to republish, to post on servers, to redistribute to lists, or to use any component of this work in other works requires prior specific permission and/or a fee. Permissions may be requested from Publications Dept., ACM, Inc., 2 Penn Plaza, Suite 701, New York, NY 10121-0701 USA, fax +1 (212) 869-0481, or permissions@acm.org.

© 2017 ACM 1550-4832/2017/06-ART57 \$15.00

DOI: <http://dx.doi.org/10.1145/3060537>

Cyclewise Operation of Printed MoS₂ Transistor Biosensors for Rapid Biomolecule Quantification at Femtomolar Levels

Byunghoon Ryu,^{†,§} Hongsuk Nam,^{†,§} Bo-Ram Oh,[†] Yujing Song,[†] Pengyu Chen,[†] Younggeun Park,[†] Wenjie Wan,[‡] Katsuo Kurabayashi,[†] and Xiaogan Liang^{*,†,§}

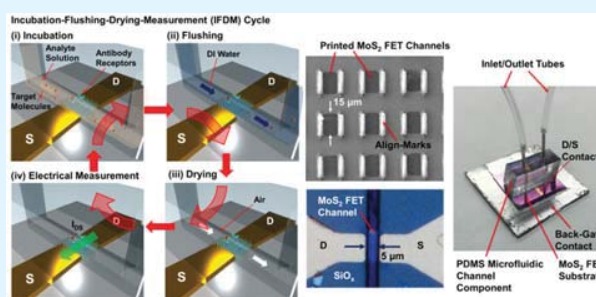
[†]Mechanical Engineering, University of Michigan, Ann Arbor, Michigan 48109, United States

[‡]University of Michigan-Shanghai Jiao Tong University Joint Institute and Department of Physics and Astronomy, Shanghai Jiao Tong University, Shanghai 200240, China

S Supporting Information

ABSTRACT: Field-effect transistors made from MoS₂ and other emerging layered semiconductors have been demonstrated to be able to serve as ultrasensitive biosensors. However, such nanoelectronic sensors still suffer seriously from a series of challenges associated with the poor compatibility between electronic structures and liquid analytes. These challenges hinder the practical biosensing applications that demand rapid, low-noise, highly specific biomolecule quantification at femtomolar levels. To address such challenges, we study a cyclewise process for operating MoS₂ transistor biosensors, in which a series of reagent fluids are delivered to the sensor in a time-sequenced manner and periodically set the sensor into four assay-cycle stages, including incubation, flushing, drying, and electrical measurement. Running multiple cycles of such an assay can acquire a time-dependent sensor response signal quantifying the reaction kinetics of analyte-receptor binding. This cyclewise detection approach can avoid the liquid-solution-induced electrochemical damage, screening, and nonspecific adsorption to the sensor and therefore improves the transistor sensor's durability, sensitivity, specificity, and signal-to-noise ratio. These advantages in combination with the inherent high sensitivity of MoS₂ biosensors allow for rapid biomolecule quantification at femtomolar levels. We have demonstrated the cyclewise quantification of Interleukin-1 β in pure and complex solutions (e.g., serum and saliva) with a detection limit of ~ 1 fM and a total detection time ~ 23 min. This work leverages the superior properties of layered semiconductors for biosensing applications and advances the techniques toward realizing fast real-time immunoassay for low-abundance biomolecule detection.

KEYWORDS: biosensor, transistor, transition metal dichalcogenide, nanoelectronics, semiconductor, streptavidin



Field-effect transistor (FET) biosensors made from emerging layered transition metal dichalcogenides (TMDCs), such as MoS₂ and WSe₂, have exhibited attractive characteristics, such as high biodetection sensitivity, low limit-of-detection (LOD), and good compatibility with planar nanofabrication processes, potentially enabling multiplexing sensor arrays. Specifically, Wang et al. and Sarkar et al. demonstrated MoS₂ FET biosensors with femtomolar (fM)-level detection limits.^{1,2} Nam et al. established the device physics for calibrating the sensor response signals measured from MoS₂ FET sensors with insulating layers and preliminarily demonstrated the fabrication of MoS₂ FET arrays.^{3,4} Lee et al. demonstrated that antibody receptors can be directly grafted on MoS₂ FET channels without using insulating layers, which is due to the hydrophobicity of the MoS₂ surface.⁵ Such an insulating-layer-free sensor structure can significantly lower the fabrication complexity and cost of MoS₂ biosensors. Nam et al. further found that insulating-layer-free MoS₂ sensors exhibit a higher sensitivity than insulating-layer-coated ones.⁶ This was attributed to the fact that two mechanisms, target-molecule-

induced electrostatic doping and target-molecule-induced surface scattering of carriers, synergistically affect the response signal of an insulating-layer-free sensor, but only target-molecule-induced electrostatic doping contributes to the response signal of an insulating-layer-coated sensor.^{6,7} Nam et al. also demonstrated that WSe₂ FET sensors exhibit a higher sensitivity than MoS₂ FET sensors, which is attributed to the ambipolar transfer characteristics of WSe₂ FETs.⁷

In spite of the progress mentioned above, MoS₂ and other TMDC-based FET biosensors still suffer seriously from a series of challenges that hinder their practical biosensing applications. Especially, a FET sensor needs to be continuously exposed to a liquid reagent environment for quantifying the time-dependent reaction kinetics of analyte-receptor binding. Such a time-dependent detection capability is a key to realize rapid

Received: December 8, 2016

Accepted: January 26, 2017

Published: January 26, 2017

Femtosecond OPO based on MgO:PPLN synchronously pumped by a 532 nm fiber laser

Jianjun Cao¹, Dongyi Shen², Yuanlin Zheng², Yaming Feng², Yan Kong¹ and Wenjie Wan^{2,3}

¹ School of Science, Jiangnan University, Wuxi 214122, People's Republic of China

² MOE Key Laboratory for Laser Plasmas and Collaborative Innovation Center of IFSA, Department of Physics and Astronomy, Shanghai Jiao Tong University, Shanghai 200240, People's Republic of China

³ The State Key Laboratory of Advanced Optical Communication Systems and Networks, University of Michigan-Shanghai Jiao Tong University Joint Institute, Shanghai Jiao Tong University, Shanghai 200240, People's Republic of China

E-mail: jianjuncao@jiangnan.edu.cn and wenjie.wan@sjtu.edu.cn

Received 30 December 2016

Accepted for publication 22 February 2017

Published 23 March 2017



CrossMark

Abstract

With the rapid progress in fiber technologies, femtosecond fiber lasers, which are compact, cost-effective and stable, have been developed and are commercially available. Studies of optical parametric oscillators (OPOs) pumped by this type of laser are demanding. Here we report a femtosecond optical parametric oscillator (OPO) at 79.6 MHz repetition rate based on MgO-doped periodically poled LiNbO₃ (MgO:PPLN), synchronously pumped by the integrated second harmonic radiation of a femtosecond fiber laser at 532 nm. The signal delivered by the single resonant OPO is continuously tunable from 757 to 797 nm by tuning the crystal temperature in a poling period of 7.7 μm . The output signal shows good beam quality in TEM₀₀ mode profile with pulse duration of 206 fs at 771 nm. Maximum output signal power of 71 mW is obtained for a pump power of 763 mW and a low pumping threshold of 210 mW is measured. Moreover, grating tuning and cavity length tuning of the signal wavelength are also investigated.

Keywords: femtosecond optical parametric oscillator, fiber lasers, quasi-phase-matched material, ultrafast nonlinear optics

(Some figures may appear in colour only in the online journal)

1. Introduction

Synchronously pumped optical parametric oscillators (OPOs) have made great contribution to various applications, such as coherent anti-Stokes Raman scattering (CARS) microscope [1–3], time-domain spectroscopy [4] and frequency metrology [5, 6], by delivering ultrafast pulses at continuously tunable wavelengths over a wide range. Nowadays, femtosecond OPOs pumped by the fundamental or second-harmonics of Ti:sapphire lasers have been extensively developed and are commercially available, covering spectral regions including ultraviolet, visible, near-infrared (NIR) and mid-infrared [7–11]. At the same time, the rapid progress in fiber lasers has

led to the emergence of OPOs pumped by this type of ultrafast lasers, showing advantages of significantly reduced size, less expensiveness, cost-effectiveness, increased reliability and stability compared with OPOs pumped by the conventional Ti:sapphire laser.

To date, femtosecond fiber-laser-based green-pumped OPOs that produce NIR wavelengths have been demonstrated using the birefringent nonlinear crystal LiB₃O₆ (LBO). For high-power OPOs, LBO is preferred due to its high optical damage threshold, broadband transparency and noncritical phase-matching capability. Based on such a material, a femtosecond OPO pumped by a frequency-doubled Yb-fiber laser-amplifier system and tunable across 780–940 nm (signal)

Optical velocimeter by second order correlation

Yaji Suo¹, Yaming Feng¹, Da-xiao Xu¹ and Wenjie Wan^{1,2}

¹ The State Key Laboratory of Advanced Optical Communication Systems and Networks, Collaborative Innovation Center of IFSA, Department of Physics and Astronomy, Shanghai Jiao Tong University, Shanghai 200240, People's Republic of China

² MOE Key Laboratory for Laser Plasmas, University of Michigan-Shanghai Jiao Tong University Joint Institute, Shanghai Jiao Tong University, Shanghai 200240, People's Republic of China

E-mail: wenjie.wan@sjtu.edu.cn

Received 13 February 2017

Accepted for publication 17 April 2017

Published 10 May 2017



Abstract

Motional information can be buried inside the temporal statistics of scattering light. Here we explore the second order correlation of scattering light to trace back the transverse velocity of objects, verifying the inverse relationship between the coherence time and the velocity. Based on this principle, a new type of optical velocimeter is demonstrated, which has been further applied to study the fluid flow inside a microfluidic channel. This new noninvasive and easy-to-implement velocimeter may offer a new avenue in many applications.

Keywords: second order correlation, fluid flow, velocimeter, coherence time

(Some figures may appear in colour only in the online journal)

1. Introduction

Optical based velocimetry provides a convenient and non-invasive scheme to measure the fluid's flow with high spatial and temporal resolution, enabling many practical applications in turbulent flow studies, microfluidic flow and medical blood flow [1]. Currently, by exploring light's properties such as scattering, fluorescence, Doppler effect and holograph, many velocimetry methods have been realized, including particle image velocimetry [2], laser-induced fluorescence velocimetry [3], Doppler velocimeter [4, 5], and holographic velocimetry [6]. However, the former two methods are limited by the camera's imaging speed, while the Doppler velocimeter can only detect the motional velocity along the longitudinal direction, so that an angled beam must be implemented in order to read out the beating signal light from the particles with transverse motion. This causes some inconvenience in some applications where the angle relation between the incident laser and the particles movement is hard to access, for example, using Doppler velocimeter *in vivo* to measure blood flow under the skin surfaces [7]. On the other hand, pseudo-thermal light sources have been widely used in ghost imaging applications, i.e. a 2D spatial revolved imaging method by utilizing the transverse

second-order correlation of the speckle patterns [8–12]. But the temporal aspect of second order correlation in pseudo-thermal light is underappreciated on the fact that it depends on the relative transverse rotation velocity of diffusers, i.e. speckle pattern generator [13], such dependence is important to determine the original transverse movement from scattered light's correlation measurement, hence, it can be expected to provide another useful alternative in an optical based velocimeter applications.

In this paper, we introduce a new optical velocimetry method capable of measuring transverse velocity by exploring the second order correlation of scattering light. By simply recording the temporal intensity fluctuations of scattering light, we experimentally exam the inverse relationship between the coherence time of the second order statistics and the transverse velocity of a rotating diffuser. We also doubly confirm the current velocimetry method by comparing to another one through direct-intensity modulation. Furthermore, we demonstrate a proof-of-principle experiment to utilize this new velocimeter to measure fluid flow inside a microfluidic channel. Our method can noninvasively measure the flow velocity at user-specified locations in highly scattering media with a relative simple setup which may find various applications in fluid dynamics, automation, biomedical science.



Subwavelength imaging by a nonlinear negative refraction lens through four wave mixing

JIANJUN CAO,^{1,4} YAN KONG,¹ SHUMEI GAO,^{1,5} AND WENJIE WAN^{2,3}

¹Jiangsu Provincial Research Center of Light Industrial Optoelectronic Engineering and Technology, School of Science, Jiangnan University, Wuxi 214122, China

²MOE Key Laboratory for Laser Plasmas and Collaborative Innovation Center of IFSA, Department of Physics and Astronomy, Shanghai Jiao Tong University, Shanghai 200240, China

³The State Key Laboratory of Advanced Optical Communication Systems and Networks, University of Michigan-Shanghai Jiao Tong University Joint Institute, Shanghai Jiao Tong University, Shanghai 200240, China

⁴jianjuncao@jiangnan.edu.cn

⁵gaosm@jiangnan.edu.cn

Abstract: We propose a new approach for subwavelength imaging using a nonlinear negative refraction lens based on four wave mixing process. Here a thin metal film is implemented as the nonlinear negative refraction lens to bend the incident signal waves to negatively refracted FWM ones according to the partial phase matching along its surface. The imaging process can be described by the nonlinear optical transfer function over the entire spatial spectra including the evanescent ones. Analytical calculations and numerical simulations are performed to demonstrate the capability of such imaging. Compared with the existing techniques, our method works on non-resonant condition over a broad range of spectrum, therefore, it may open up a new avenue for super-resolution imaging applications.

© 2017 Optical Society of America

OCIS codes: (100.6640) Superresolution; (190.4380) Nonlinear optics, four-wave mixing; (190.4360) Nonlinear optics, devices; (260.2110) Electromagnetic optics.

References and links

1. J. B. Pendry, "Negative refraction makes a perfect lens," *Phys. Rev. Lett.* **85**(18), 3966–3969 (2000).
2. R. A. Shelby, D. R. Smith, and S. Schultz, "Experimental verification of a negative index of refraction," *Science* **292**(5514), 77–79 (2001).
3. A. Grbic and G. V. Eleftheriades, "Overcoming the diffraction limit with a planar left-handed transmission-line lens," *Phys. Rev. Lett.* **92**(11), 117403 (2004).
4. N. Fang, H. Lee, C. Sun, and X. Zhang, "Sub-diffraction-limited optical imaging with a silver superlens," *Science* **308**(5721), 534–537 (2005).
5. V. M. Shalaev, "Optical negative-index metamaterials," *Nat. Photonics* **1**(1), 41–48 (2007).
6. X. Zhang and Z. Liu, "Superlenses to overcome the diffraction limit," *Nat. Mater.* **7**(6), 435–441 (2008).
7. Z. Shi, V. Kochergin, and F. Wang, "193nm Superlens Imaging Structure for 20nm Lithography Node," *Opt. Express* **17**(14), 11309–11314 (2009).
8. C. P. Moore and R. J. Blaikie, "Experimental characterization of the transfer function for a Silver-dielectric superlens," *Opt. Express* **20**(6), 6412–6420 (2012).
9. Q. Jiang, J. Chen, B. Liang, Y. Wang, J. Hu, and S. Zhuang, "Direct measurement of the negative Goos-Hänchen shift of single reflection in a two-dimensional photonic crystal with negative refractive index," *Opt. Lett.* **42**(7), 1213–1216 (2017).
10. Y. Xu, Y. Fu, and H. Chen, "Electromagnetic wave propagations in conjugate metamaterials," *Opt. Express* **25**(5), 4952–4966 (2017).
11. S. Maslovski and S. Tretyakov, "Phase conjugation and perfect lensing," *J. Appl. Phys.* **94**(7), 4241–4243 (2003).
12. J. B. Pendry, "Time reversal and negative refraction," *Science* **322**(5898), 71–73 (2008).
13. H. Harutyunyan, R. Beams, and L. Novotny, "Controllable optical negative refraction and phase conjugation in graphite thin films," *Nat. Phys.* **9**(7), 423–425 (2013).
14. P. Y. Chen and A. Alù, "Subwavelength imaging using phase-conjugating nonlinear nanoantenna arrays," *Nano Lett.* **11**(12), 5514–5518 (2011).
15. S. Palomba, S. Zhang, Y. Park, G. Bartal, X. Yin, and X. Zhang, "Optical negative refraction by four-wave mixing in thin metallic nanostructures," *Nat. Mater.* **11**(1), 34–38 (2011).

A Game With Randomly Distributed Eavesdroppers in Wireless Ad Hoc Networks: A Secrecy EE Perspective

Younggap Kwon, Xudong Wang, *Senior Member, IEEE*, and Taewon Hwang [✉], *Senior Member, IEEE*

Abstract—We study energy-efficient secure communication using the combined approach of game theory and stochastic geometry in a large-scale wireless network, where legitimate transmitters (Alice nodes) and eavesdroppers (Eve nodes) are randomly distributed in space. We consider the following two scenarios according to the Eve tier's strategy: I) the Eve tier activates all its nodes to maximally eavesdrop the confidential messages of the Alice tier; and II) the Eve tier activates only a portion of its nodes to maximize its energy efficiency (EE) in eavesdropping according to the Alice tier's node activation. In Scenario I, we propose an alternating optimization scheme that maximizes the secrecy EE of the Alice tier by controlling the node-activation probability, the confidential message rate, the redundancy rate, and the number of active antennas. Simulation result shows that the proposed scheme can achieve the optimal secrecy EE. In Scenario II, we study an energy-efficient node activation game between the Alice tier and the Eve tier, where the former and the latter control their node-activation probabilities to maximize the secrecy EE and the eavesdropping EE, respectively. We show that the node activation game admits a unique Nash equilibrium. The node-activation probabilities of the Alice tier and the Eve tier at the Nash equilibrium can be used to estimate their network lifetimes, which are important information for the energy-efficient secure network design. Simulation result shows that the best-response dynamics converges to the Nash equilibrium within a few iterations.

Index Terms—Game theory, physical layer security, secrecy energy efficiency, stochastic geometry.

I. INTRODUCTION

DUE to the broadcast characteristic of the wireless medium, ensuring the security is an important issue in wireless communications. Traditionally, the security in communications has

been achieved by using cryptographic schemes at the application layer. For example, the works in [1] and [2] proposed secure vehicular ad hoc networks (VANETs), where confidential messages are encrypted by key-based cryptographic schemes. The work in [1] proposed a security system for VANETs to achieve privacy desired by vehicles and traceability required by law enforcement authorities. In the security system, the vehicles encrypt their messages using a cryptographic scheme. The work in [2] proposed RescueMe, location-based secure and dependable VANETS for disaster rescue. The RescueMe securely stores user location information and reliably retrieves such information for disaster rescue. Here, the user location information is encrypted by a cryptographic scheme. However, the security level achieved by the cryptographic approach could be compromised as the computational capabilities of eavesdroppers (Eve nodes) continuously improve [3]. Contrary to the cryptographic approach, physical layer security, or information-theoretic security, can guarantee perfect secure transmission even though the Eve nodes have unlimited computational capabilities [4]. It exploits the physical properties of the wireless channels to prevent the Eve nodes from acquiring confidential information of legitimate transmitters (Alice nodes). In [4], it is shown that perfect secrecy can be achieved in the simple three-node system consisting of an Alice node, a legitimate receiver (Bob node), and an Eve node if the Bob node experiences better channel conditions than the Eve node. Many works have developed the physical layer security schemes for multi-antenna systems [5], [6], relay networks [7], [8], and cognitive radio networks [9]. On the other hand, achieving high energy efficiency (EE), defined as the number of reliably transmitted bits per energy consumption, has drawn much attention for wireless communications. Most of the wireless devices are battery-driven. Long battery lifetime is essential for the battery-driven wireless devices especially when they are deployed in harsh environments such as deep underwater, earthquake zones, and battlefields, where recharging the batteries is inconvenient or even impossible. However, the improvement in battery technology has not kept up with the increasing energy-supply demands of the wireless devices. For this reason, many efforts have been put to develop energy-efficient communication schemes [10], [11].

From above, improving secrecy EE, defined as the number of reliably and securely transmitted bits per energy consumption, is an important research issue for future wireless network design

Manuscript received August 18, 2016; revised April 18, 2017; accepted July 17, 2017. Date of publication July 26, 2017; date of current version November 10, 2017. This work was supported by Basic Science Research Program through the National Research Foundation of Korea funded by the Ministry of Education (2016R1D1A1A09916968). The review of this paper was coordinated by Prof. J. Sun. (Corresponding author: Taewon Hwang.)

Y. Kwon was with the School of Electrical and Electronic Engineering, Yonsei University, Seoul 120-749, South Korea. This work was done while he was with Yonsei University. He is now with the Agency for Defense Development, Daejeon 305-600, South Korea (e-mail: thingap@yonsei.ac.kr).

X. Wang is with the University of Michigan–Shanghai Jiao Tong University (UM-SJTU) Joint Institute, Shanghai Jiao Tong University, Shanghai 200240, China (e-mail: wxudong@sjtu.edu.cn).

T. Hwang is with the School of Electrical and Electronic Engineering, Yonsei University, Seoul 120-749, South Korea (e-mail: twhwang@yonsei.ac.kr).

Color versions of one or more of the figures in this paper are available online at <http://ieeexplore.ieee.org>.

Digital Object Identifier 10.1109/TVT.2017.2731983

Scheduling of Electric Vehicle Charging via Multi-Server Fair Queueing

Xudong Wang[✉], Senior Member, IEEE, Yibo Pi, and Aimin Tang

Abstract—Charging electric vehicles (EVs) at home is attractive to EV users. However, when the penetration level of EVs becomes high, a distribution grid suffers from problems such as under-voltage and transformer overloading. EV users also experience a fairness problem, i.e., the limited capacity is unfairly shared among EVs. To solve these problems, a physical fair-queueing framework is established for EV charging. In this framework, a distribution sub-grid is first mapped to a multi-server queueing system, and then a fluid-model based queueing scheme called physical multi-server generalized processor sharing (pMGPS) is designed. pMGPS ensures perfect fairness but cannot be used practically due to its nature of fluid model. To this end, a packetized scheme called physical start-time fair queueing (pSTFQ) is developed to schedule tasks of EV charging. The fairness performance of the pSTFQ scheduling scheme is characterized by the ratio of energy difference between pSTFQ and pMGPS. This critical performance metric is studied through theoretical analysis and is also evaluated via simulations. Performance results show that the pSTFQ scheduling scheme achieves an energy difference ratio of less than 4 percent in various scenarios without causing under-voltage and transformer overloading problems.

Index Terms—Electric vehicle charging, distribution grid, multi-server fair queueing

1 INTRODUCTION

ELECTRIC vehicles (EVs) have been considered as an alternative to conventional vehicles. As predicted in [1], by 2050 the penetration level of EVs will reach 62 percent in the US. Compared to the supercharging and battery swap services at public charging stations, charging EVs at home is also very attractive. EV users can have their EVs charged immediately after they arrive home. However, unlike public charging stations that are deliberately designed for EV charging, charging stations at homes are distributed and pose threats to the existing distribution grid.

Generally, EVs consume much larger power than home appliances like air conditioners and heaters. For an individual user, charging an EV at home can be easily achieved by installing an outlet with high power rating. However, from the perspective of an entire distribution grid, if a large number of EVs are to be charged simultaneously, the peak load is expected to increase abruptly. Since the capacity of existing transformers is planned without considering the additional peak load from such EVs [2], these transformers can easily experience an *overloading problem*. EV charging also increases the current flowing through transmission feeders, which results in severe voltage drop along these feeders,

especially in rural areas with long transmission feeders [3]. Voltage below the operation range leads to an *under-voltage problem*, which can damage home appliances. In this paper, we call both problems the *physical problems* of power grid.

Reinforcing the existing distribution grid by upgrading the transformers and feeders can solve the above problems, but it is costly. Thus, a preferable and practical approach is to shift EV charging in peak-load time to non-peak-load time. Following this approach, so far both offline and online schemes have been proposed. Offline schemes [4], [5], [6] usually formulate the load-shifting task as an optimization problem, subject to the constraints of EV energy requirements and grid safety. The energy requirement of an EV is said to be satisfied if its required energy can be charged before deadline. Based on a solution to the optimization problem, the on/off time of each EV can be determined. Offline methods share several common issues. First, the load profiles of homes need to be forecast, but it may be much different from the real value. Charging decisions based on erroneous forecast profiles can still cause transformer overloading or under-voltage problems. Second, offline schemes assume the grid capacity is sufficient to charge all EVs by deadlines. Third, each EV has to follow a pre-specified deadline strictly, which is not practical for EV users. For example, an EV arriving at 6 pm sets a deadline of 12 pm, its charging period may be scheduled between 10 to 12 pm. In case it departs at 10 pm, it awaits 4 hours for nothing.

So far online schemes [7], [8] have been developed to avoid forecast errors by using updated status data of power grid. However, in the case of arbitrary early departure of EVs or occurrence of the physical problems, these schemes cannot ensure EVs to be charged in a fair way. Thus, a *fairness problem* arises. The schemes in [9], [10] consider the physical problems, but the fairness problem is still not addressed.

- X. Wang and A. Tang are with the University of Michigan-Shanghai Jiao Tong University Joint Institute, Shanghai 200240, China. E-mail: wxudong@ieee.org, tangaiming@sjtu.edu.cn.
- Y. Pi was with the University of Michigan-Shanghai Jiao Tong University Joint Institute, Shanghai 200240, China and is now with the University of Michigan, Ann Arbor, MI 48109. E-mail: piyibo@gmail.com.

Manuscript received 9 Apr. 2016; revised 15 May 2017; accepted 18 May 2017. Date of publication 1 June 2017; date of current version 11 Oct. 2017.

(Corresponding author: Xudong Wang.)

Recommended for acceptance by M. M. Hayat.

For information on obtaining reprints of this article, please send e-mail to: reprints@ieee.org, and reference the Digital Object Identifier below.

Digital Object Identifier no. 10.1109/TPDS.2017.2710197

Cooperative Full Duplex Device to Device Communication Underlying Cellular Networks

Aimin Tang, *Student Member, IEEE*, Xudong Wang, *Senior Member, IEEE*, and Chi Zhang

Abstract—Recently, device-to-device (D2D) communication and full duplex communication are both considered key technologies for 5G networks. In this paper, two novel cooperative modes are developed for full duplex D2D communication underlying cellular networks: the network MU-MIMO based mode (N-mode) and the sequential forwarding mode (S-mode). In the N-mode, two D2D users work as network MIMO to forward the data to cellular users and thus leverage the channel diversity. In the S-mode, the spatial distribution of D2D users and cellular users is explored to improve the transmission rate. Based on these modes, two D2D users share the downlink resources with two nearby cellular users simultaneously to achieve both proximity gain and reuse gain. Moreover, these modes are well suited for edge cellular users. To optimize the performance of the two modes, optimal power allocation is conducted by considering the influence of residual self-interference at full duplex radios and the requirements of the minimum transmission rate for both cellular users and D2D users. Simulation results show that, compared with the dedicated mode, the sum rate of cooperative modes in the perfect self-interference cancellation case can achieve 32% overall improvement and about 70% improvement in the scenario with non-edge D2D users and edge cellular users. With residual self-interference at a full duplex radio, the overall performance improvement is reduced to 15%. However, the cooperative modes can still achieve 40% improvement in the scenario with non-edge D2D users and edge cellular users.

Index Terms—Device to device communication, full duplex, MIMO, power allocation.

I. INTRODUCTION

A. Background of D2D and Full Duplex Communication

IN RECENT years, the proliferation of smart phones, tablets, and other wireless devices has stimulated wide spreading of social networking and multimedia content sharing, which leads to an explosive growth of wireless data traffic. As a result, the base station (BS) suffers a heavy burden. To meet the enormously increasing demands of data traffic, device to device (D2D) communication underlying cellular

networks has been proposed as a key feature in 4G and 5G networks [1]–[5]. D2D communication cannot only alleviate the burden of a BS, but it can also improve the spectrum efficiency.

So far, three modes have been designed for D2D communication underlying cellular networks: cellular mode, dedicated mode, and reuse mode [6], [7]. In the cellular mode, the BS is acting as a relay for D2D users. In the dedicated mode and the reuse mode, the D2D users share orthogonal and non-orthogonal resources with a cellular user, respectively. Based on the above three modes, several resource allocation schemes have been developed [6]–[8]. In [9], a D2D user is utilized as a relay to help the downlink transmission. A two-way-relay D2D communication protocol is proposed in [10], where one of the D2D users acts as a two-way-relay between a cellular user and the BS. In the aforementioned research work, only half duplex communication is considered. However, full duplex communication has become practical in recent years [11]–[14], which is also considered as a promising technology in 5G networks [5]. In [12], a balanced RF circuit is designed to conduct analog self-interference cancellation at the front-end, which can achieve 60dB self-interference cancellation. A prototype for full duplex WiFi radio is implemented via one antenna in [13] and can achieve 110 dB self-interference cancellation so that the residual self-interference is lower than noise floor. Moreover, their experimental results show: 1) the received signal suffers negligible SNR loss regardless of the received SNR; 2) their prototype supports all WiFi modulation schemes and bandwidths with low SNR loss. In [14], a real-time full duplex prototype is implemented for LTE systems, which can achieve 1.9 times higher throughput than half duplex system. Thus, it is necessary to consider how to effectively combine full duplex and D2D communication for 5G networks. So far, a few papers have considered the combination of full duplex and D2D communication [15]–[18]. The applications of full duplex D2D communication for heterogeneous networks are discussed in [15]. In [16], a fixed relay is considered as a full duplex radio and all the clients are half duplex radios. The relay is used to send data to a client and relays the downlink data from BS to another client simultaneously. In [17], [18], the D2D users are considered as full duplex radios. However, these papers directly use the existing three modes, in which the capability of the full duplex radio is not fully utilized.

Manuscript received July 15, 2016; revised December 24, 2016, March 23, 2017, and July 22, 2017; accepted September 7, 2017. Date of publication September 22, 2017; date of current version December 8, 2017. The associate editor coordinating the review of this paper and approving it for publication was S. Mukherjee. (Corresponding author: Xudong Wang.)

A. Tang and X. Wang are with the University of Michigan–Shanghai Jiao Tong University Joint Institute, Shanghai Jiao Tong University, Shanghai 200240, China (e-mail: wxudong@ieee.org).

C. Zhang is with Huawei Technologies Corporation, Shanghai 201206, China.

Color versions of one or more of the figures in this paper are available online at <http://ieeexplore.ieee.org>.

Digital Object Identifier 10.1109/TWC.2017.2753785

Enhanced resolution for amplitude object in lensless inline holographic microscope with grating illumination

Shaodong Feng, Mingjun Wang, and Jigang Wu*

Shanghai Jiao Tong University, University of Michigan—Shanghai Jiao Tong University Joint Institute, Biophotonics Laboratory, Shanghai, China

Abstract. In a compact digital lensless inline holographic microscope (LIHM), where the sample-to-sensor distance is short, the imaging resolution is often limited by sensor pixel size instead of the system numerical aperture. We propose to solve this problem by applying data interpolation with an iterative holographic reconstruction method while using grating illumination in the LIHM system. In the system setup, the Talbot self-image of a Ronchi grating was used to illuminate the sample, and the inline hologram was recorded by a CMOS imaging sensor located behind the sample. The hologram was then upsampled by data interpolation before the reconstruction process. In the iterative holographic reconstruction, the sample support was defined by the bright areas of the grating illumination pattern and was used as constraint. A wide-field image can also be obtained by shifting the grating illumination pattern. Furthermore, we assumed that the sample was amplitude object, i.e., no obvious phase change was caused by the sample, which provided additional constraint to refine the interpolated data values. Besides improved resolution, the iterative holographic reconstruction also helped to reduce the twin-image background. We demonstrated the effectiveness of our method with simulation and imaging experiment by using the USAF target and polystyrene microspheres with 1 μm diameter as the sample.

© 2017 Society of Photo-Optical Instrumentation Engineers (SPIE) [DOI: [10.1117/1.OE.56.9.093107](https://doi.org/10.1117/1.OE.56.9.093107)]

Keywords: compact lensless imaging; digital holography; phase retrieval.

Paper 171139P received Jul. 21, 2017; accepted for publication Sep. 13, 2017; published online Sep. 28, 2017.

1 Introduction

In recent years, the digital lensless inline holographic microscope (LIHM) has become a promising microscopic imaging solution for compact and portable applications because of its unique advantages, including compactness, low cost, and wide-field-of-view compared to a conventional lens-based microscope.^{1–5} The principle of a LIHM is based on Gabor's holography,⁶ and the setup is very simple, which consists of an illumination source, the sample, and an imaging sensor located right behind the sample to record the inline holograms. Without using lenses, the sample-to-sensor distance can be very small, usually around 1 to 10 mm, and thus greatly reduces the system size. Furthermore, the short sample-to-sensor distance also means that the imaging field of view is limited by the imaging sensor size, which can be much larger than conventional microscope. For comparison, the size of an 1/3" CMOS imaging sensor is 4.8×3.6 mm, whereas the field-of-view of a conventional microscope is usually less than 1 mm for 10 \times objective, and even less when using high magnification objectives. Compared to the lensless shadow imaging techniques,^{7,8} the LIHM provides more flexibility on the sample-to-sensor distance and allows the imaging sensor to be reusable for different samples.

Despite its advantages, the LIHM has two major disadvantages, i.e., twin-image disturbance and relatively low resolution compared to conventional microscope. The twin-image disturbance is a well-known problem because of the loss of phase information while recording the inline holograms by the imaging sensor. On the other hand, the low resolution is caused by the sampling process during recording because of the finite pixel size of the imaging sensor.

The twin-image issue has attracted considerable attention since the invention of holography by Gabor.⁶ Although the off-axis holography configuration can be used to eliminate the twin-image background by spatial separation,^{9,10} the mechanical complexity because of the requirement of reference wave prevents the imaging system to be built compact. Generally, the inline holography scheme has to be used in order to achieve system compactness, which also makes the system more robust. In conventional inline holographic reconstruction (will be called "direct reconstruction" hereinafter), the sample image is acquired by backpropagating the inline hologram to the sample plane using scalar diffraction formula. Because of the loss of phase information, the twin-image background will be imposed to the reconstructed sample images and affect the imaging quality especially for short sample-to-sensor distance in the LIHM. Many methods have been proposed to overcome the twin-image problem in inline holography.^{11–20} Among these methods, the phase retrieval methods,^{14–18} especially the iterative phase retrieval methods are widely used, where the phase information of the optical field is retrieved iteratively by recording multiple intensity measurements in different planes^{21,22} or only one intensity measurement with certain constraints in the sample plane.^{23,24} The sample image without twin-image disturbance can then be reconstructed with the additional phase information. Obviously, the iterative holographic reconstruction methods with constraints in the sample plane are more suitable for real-time imaging and mechanically more stable. In our previous paper,²⁵ we proposed to apply Talbot grating illumination on the sample to define the sample support, which acts as the constraint in the sample plane in the

*Address all correspondence to: Jigang Wu, E-mail: jigang.wu@sjtu.edu.cn



Contents lists available at ScienceDirect

Optics Communications

journal homepage: www.elsevier.com/locate/optcom

Enhanced resolution in lensless in-line holographic microscope by data interpolation and iterative reconstruction

Shaodong Feng, Mingjun Wang, Jigang Wu *

Biophotonics Laboratory, University of Michigan—Shanghai Jiao Tong University Joint Institute, Shanghai Jiao Tong University, Shanghai 200240, China

ARTICLE INFO

Keywords:

Compact lensless imaging
Digital holography
Phase retrieval

ABSTRACT

In a compact lensless in-line holographic microscope, the imaging resolution is generally limited by the sensor pixel size because of the short sample-to-sensor distance. To overcome this problem, we propose to use data interpolation based on iteration with only two intensity measurements to enhance the resolution in holographic reconstruction. We did numerical simulations using the U.S. air force target as the sample and showed that data interpolation in the acquired in-line hologram can be used to enhance the reconstruction resolution. The imaging resolution and contrast can be further improved by combining data interpolation with iterative holographic reconstruction using only two hologram measurements acquired by slightly changing the sample-to-sensor distance while recording the in-line holograms. The two in-line hologram intensity measurements were used as a priori constraint in the iteration process according to the Gerchberg–Saxton algorithm for phase retrieval. The iterative reconstruction results showed that the iteration between the sample plane and the sensor planes can refine the interpolated data and thus further improve the resolution as well as the imaging contrast. Besides numerical simulation, we also experimentally demonstrated the enhancement of imaging resolution and contrast by imaging the U.S. air force target and a microscope slide of filamentous algae.

© 2017 Elsevier B.V. All rights reserved.

1. Introduction

Compact microscopic imaging techniques are very attractive for many potential applications in healthcare and biology because of their low-cost and portable system design [1–6]. Among the reported techniques, digital lensless in-line holographic microscope (LIHM) [7–10] has the advantages of achieving wide field-of-view imaging with flexible sample-to-sensor distance and the capability of acquiring multilayer sample images simultaneously. Conventional in-line holographic reconstruction (will be called “direct reconstruction”, as opposed to “iterative reconstruction” below) based on scalar optical field propagation generally has two issues that affect the imaging resolution and image quality, i.e., twin-image background caused by the loss of phase information and the reduced resolution in the sampling process of the imaging sensor.

Many methods have been proposed to eliminate or reduce the twin-image background [11–24]. Iterative phase retrieval techniques [11,12] are among the most popular solutions, where the phase information of the optical field is retrieved iteratively according to multiple intensity measurements [14–16,19,22] or one intensity measurement [17,21,23,24]. Once both intensity and phase information of the

light field are known, the holographic reconstruction will be free of twin-image and thus have better SNR and image contrast.

On the other hand, the imaging resolution in LIHM is mainly determined by two factors: the detection numerical aperture (NA) and the sensor pixel size (Δ). Physically, the ultimate resolution limit will be the Abbe diffraction limit, i.e., $\sim 0.61 \lambda / \text{NA}$ in Rayleigh criterion, where λ is the wavelength of illumination light. Thus the resolution can be improved by enlarging the NA of the optical system when the wavelength is fixed [25–29]. For compact in-line holography setup, the sample-to-sensor distance is very small (~ 5 mm in our experiment) and the sensor size is relatively large (5.7×4.3 mm in our experiment), so the NA will be large enough to achieve submicron resolution according to the Abbe diffraction limit. However, the pixel size (Δ) of the commercially available imaging sensor is generally larger than $1.2 \mu\text{m}$ because of fabrication and sensitivity requirements. So the resolution in LIHM will be limited by the pixel size of the sensor because there is almost no magnification for short sample-to-sensor distance. To overcome the sampling issue caused by the relatively large sensor pixel size, researchers proposed many effective techniques, for example, the optofluidic microscope (OFM) [30–34], where the sampling distance

* Corresponding author.

E-mail address: jigang.wu@sjtu.edu.cn (J. Wu).<http://dx.doi.org/10.1016/j.optcom.2017.05.059>Received 15 March 2017; Received in revised form 19 May 2017; Accepted 21 May 2017
Available online 4 July 2017

0030-4018/© 2017 Elsevier B.V. All rights reserved.

SCIENTIFIC REPORTS

OPEN

Multilayer pixel super-resolution lensless in-line holographic microscope with random sample movement

Mingjun Wang, Shaodong Feng & Jigang Wu

We report a multilayer lensless in-line holographic microscope (LIHM) with improved imaging resolution by using the pixel super-resolution technique and random sample movement. In our imaging system, a laser beam illuminated the sample and a CMOS imaging sensor located behind the sample recorded the in-line hologram for image reconstruction. During the imaging process, the sample was moved by hand randomly and the in-line holograms were acquired sequentially. Then the sample image was reconstructed from an enhanced-resolution hologram obtained from multiple low-resolution in-line holograms by applying the pixel super-resolution (PSR) technique. We studied the resolution enhancement effects by using the U.S. Air Force (USAF) target as the sample in numerical simulation and experiment. We also showed that multilayer pixel super-resolution images can be obtained by imaging a triple-layer sample made with the filamentous algae on the middle layer and microspheres with diameter of 2 μm on the top and bottom layers. Our pixel super-resolution LIHM provides a compact and low-cost solution for microscopic imaging and is promising for many biomedical applications.

Lensless in-line holographic microscope (LIHM)^{1–6} provides a promising alternative to conventional microscope in application areas such as personal healthcare and telemedicine that requires compact and low-cost microscopic imaging systems. To achieve compactness in LIHM, short sample-to-sensor distance is usually required in the process of recording the holograms. In this case, the resolution of the reconstructed sample image is limited by the finite pixel size of the imaging sensors instead of the numerical aperture of the imaging system. To overcome this resolution limit, researchers have resorted to the pixel super-resolution (PSR) technique which was widely used to improve imaging resolution in photography⁷, holography⁸ and microscopy^{9–11}. In LIHM, PSR technique has been successfully applied to reconstruct sub-pixel resolution image from multiple holograms acquired with different light illumination angles^{9,10}. In the reported method, a high-resolution hologram was first obtained from multiple low-resolution holograms by the PSR technique, then the high-resolution sample image can be reconstructed from the high-resolution holograms. Nevertheless, this technique requires multiple illumination sources and corresponding control circuits which increase the complexity of the system. This issue can be resolved by using the PSR technique with shifting samples instead of changing the illumination angle. PSR imaging technique with shifting samples has been reported in shadow imaging microscopic techniques^{11–13} and also the holographic opto-fluidic microscopy (HOM)¹⁴, which is a variation of the LIHM. In the shadow imaging technique, the sample must be attached to or very close to the sensor so as to maintain the microscopic resolution, which limited its applications. In contrast, the HOM solved this problem by using holographic reconstruction. Recently, resolution-enhanced techniques using wavelength scanning was also reported^{15,16} with the additional requirement of a tunable light source or several light sources with different wavelengths.

In the HOM¹⁴, we notice that the PSR is achieved with sample movement in the microfluidic channel, so the wide field-of-view and multilayer imaging capability of the LIHM is not fully utilized. In this paper, we propose to apply the PSR technique with shifting samples in LIHM for wide field-of-view and multilayer imaging. In our PSR-LIHM system, the shifting sample on a microscope slide is illuminated by a laser beam and the in-line

Biophotonics Laboratory, University of Michigan - Shanghai Jiao Tong University Joint Institute, Shanghai Jiao Tong University, 800 Dong Chuan Road, Shanghai, 200240, China. Correspondence and requests for materials should be addressed to J.W. (email: jigang.wu@sjtu.edu.cn)



Resolution enhancement method for lensless in-line holographic microscope with spatially-extended light source

SHAODONG FENG AND JIGANG WU*

Biophotonics Laboratory, University of Michigan – Shanghai Jiao Tong University Joint Institute, Shanghai Jiao Tong University, Shanghai 200240, China

*jigang.wu@sjtu.edu.cn

Abstract: We propose a resolution enhancement method for lensless in-line holographic microscope (LIHM) with spatially-extended light source, where the resolution is normally deteriorated by the insufficient spatial coherence of the illumination. In our LIHM setup, a light-emitting diode (LED), which was a spatially-extended light source, directly illuminated the sample, and the in-line hologram were recorded by a CMOS imaging sensor located behind the sample. In our holographic reconstruction process, the in-line hologram was first deconvolved with a properly resized image of the LED illumination area, and then back-propagated with scalar diffraction formula to reconstruct the sample image. We studied the hologram forming process and showed that the additional deconvolution process besides normal scalar diffraction reconstruction in LIHM can effectively enhance the imaging resolution. The resolution enhancements capability was calibrated by numerical simulations and imaging experiments with the U.S. air force target as the sample. We also used our LIHM to image the wing of a green lacewing to further demonstrate the capability of our methods for practical imaging applications. Our methods provide a way for LIHM to achieve satisfactory resolution with less stringent requirement for spatial coherence of the source and could reduce the cost for compact imaging system.

© 2017 Optical Society of America

OCIS codes: (090.1995) Digital holography; (110.0180) Microscopy; (100.1830) Deconvolution.

References and links

1. A. Greenbaum, W. Luo, T. W. Su, Z. Göröcs, L. Xue, S. O. Isikman, A. F. Coskun, O. Mudanyali, and A. Ozcan, "Imaging without lenses: achievements and remaining challenges of wide-field on-chip microscopy," *Nat. Methods* **9**(9), 889–895 (2012).
2. E. Serabyn, K. Liewer, C. Lindensmith, K. Wallace, and J. Nadeau, "Compact, lensless digital holographic microscope for remote microbiology," *Opt. Express* **24**(25), 28540–28548 (2016).
3. S. Feng, M. Wang, and J. Wu, "Lensless in-line holographic microscope with Talbot grating illumination," *Opt. Lett.* **41**(14), 3157–3160 (2016).
4. M. Sanz, J. A. Picazo-Bueno, L. Granero, J. García, and V. Micó, "Compact, cost-effective and field-portable microscope prototype based on MISHELF microscopy," *Sci. Rep.* **7**, 43291 (2017).
5. H. J. Kreuzer, M. H. Jericho, I. A. Meinertzhagen, and W. Xu, "Digital in-line holography with photons and electrons," *J. Phys. Condens. Matter* **13**, 10729–10741 (2001).
6. U. Schnars and W. P. O. Jüptner, "Digital recording and numerical reconstruction of holograms," *Meas. Sci. Technol.* **13**, R85–R101 (2002).
7. W. Xu, M. H. Jericho, H. J. Kreuzer, and I. A. Meinertzhagen, "Tracking particles in four dimensions with in-line holographic microscopy," *Opt. Lett.* **28**(3), 164–166 (2003).
8. Y. Hao and A. Asundi, "Resolution analysis of a digital holography system," *Appl. Opt.* **50**(2), 183–193 (2011).
9. H. Meng, W. L. Anderson, F. Hussain, and D. D. Liu, "Intrinsic speckle noise in in-line particle holography," *J. Opt. Soc. Am. A* **10**, 2046–2058 (1993).
10. P. Picart, "Speckle noise in digital holographic images: genesis and reduction methods," in *Digital Holography and Three-Dimensional Imaging*, OSA Technical Digest (online) (Optical Society of America, 2017), paper Th1A.1.
11. L. Repetto, E. Piano, and C. Pontiggia, "Lensless digital holographic microscope with light-emitting diode illumination," *Opt. Lett.* **29**(10), 1132–1134 (2004).
12. C. Oh, S. O. Isikman, B. Khademhosseini, and A. Ozcan, "On-chip differential interference contrast microscopy using lensless digital holography," *Opt. Express* **18**(5), 4717–4726 (2010).

Second-order distributed-feedback surface plasmon resonator for single-mode fiber end-facet biosensing

Zeyu Lei,^{1,a)} Xin Zhou,^{1,a)} Jie Yang,¹ Xiaolong He,² Yalin Wang,² and Tian Yang^{1,b)}

¹State Key Laboratory of Advanced Optical Communication Systems and Networks, Key Laboratory for Thin Film and Microfabrication of the Ministry of Education, UM-SJTU Joint Institute, Shanghai Jiao Tong University, Shanghai 200240, China

²Xu Yuan Biotechnology Company, 1180 Xingxian Road, Shanghai 201815, China

(Received 6 March 2017; accepted 9 April 2017; published online 26 April 2017)

Integrating surface plasmon resonance (SPR) devices upon single-mode fiber (SMF) end facets renders label-free biosensing systems that have a dip-and-read configuration, high compatibility with fiber-optic techniques, and *in vivo* monitoring capability, which however meets the challenge to match the performance of free-space counterparts. We report a second-order distributed feedback (DFB) SPR cavity on an SMF end facet and its application in protein interaction analysis. In our device, a periodic array of nanoslits in a gold film is used to couple fiber guided lightwaves to surface plasmon polaritons (SPPs) with its first order spatial Fourier component, while the second order spatial Fourier component provides DFB to SPP propagation and produces an SPP bandgap. A phase shift section in the DFB structure introduces an SPR defect state within the SPP bandgap, whose mode profile is optimized to match that of the SMF to achieve a reasonable coupling efficiency. We report an experimental refractive index sensitivity of 628 nm RIU^{-1} , a figure-of-merit of 80 RIU^{-1} , and a limit of detection of $7 \times 10^{-6} \text{ RIU}$. The measurement of the real-time interaction between human immunoglobulin G molecules and their antibodies is demonstrated. Published by AIP Publishing. [<http://dx.doi.org/10.1063/1.4982625>]

Surface plasmon resonance (SPR) devices have been implemented in many label-free biosensing applications due to their convenient surface wave configuration and capability to optically detect biomolecule surface binding with a high uniformity between different experiments.^{1–4} On this ground, it has long been desired to integrate SPR devices upon single-mode fiber (SMF) end facets, in order to achieve fiber-optic biosensing systems which are much more compact than free-space prism coupled ones, to adopt the dip-and-read configuration and replace the microfluidic flow cells which require complicated operation by specialists, to facilitate *in vivo* monitoring by fitting fibers into tiny spaces and to consume less samples.^{5–14} However, most of the studies reported that SMF end-facet SPR devices suffer from broad and shallow resonance spectra due to the SMF guided mode's diffraction, which results in poor refractive index sensing performance, and a number of works focused on enhanced Raman scattering instead.^{5,8,15–18} To mitigate the diffraction of fiber guided lightwaves, in a number of reports, the SMF was replaced by a large core multi-mode fiber (MMF) and the fundamental guided mode was used, which nevertheless lost the immunity to mechanical perturbation and the flexibility of SMF systems.^{5,6,13,19–22} In Ref. 14, we reported the first SMF end-facet SPR device that has a limit-of-detection (LOD) at the 10^{-6} refractive-index-unit (RIU) level. This device is a plasmonic crystal cavity with separate surface plasmon polariton (SPP) coupling and confinement regions, the coupling region being a grating coupled SPR periodic structure, and the confinement region being a

distributed Bragg reflector (DBR).^{23,24} In this paper, we study a different SPR cavity that also has a LOD at the 10^{-6} RIU level, which is a second order distributed feedback (DFB) structure with a phase shift section in the center of the cavity. Measurement of the real-time interaction processes between human immunoglobulin G (hIgG) molecules and their antibodies at fiber tip is also demonstrated. Analogous to the history of development of photonic crystal cavities, we believe that studies on a variety of new cavity concepts and designs are critical to the research field and may lead to substantial performance improvement in the future.

In this paper, the refractive index sensitivity is defined as the shift in the SPR wavelength divided by the change in the refractive index (nm RIU^{-1}), figure-of-merit (FOM) is defined as sensitivity divided by the full-width-half-maximum (FWHM) linewidth of the SPR spectrum (RIU^{-1}), and LOD is defined as three times the root-mean-square (RMS) noise of refractive index measurement results (RIU).^{2,14}

In our device design, we first numerically obtained the SPP band diagram of a two-dimensional (2D) periodic array of gold nanoslits on top of a SiO_2 substrate which is immersed in water, as illustrated in Fig. 1(a). The width of the nanoslit d is 50 nm, and the period p of the array is 645 nm. The thickness t of the gold film is 55 nm. The permittivity of gold is taken from Ref. 25. The refractive index of SiO_2 is taken to be 1.445 and that of water is taken to be 1.333. The calculation was done by the finite-difference time-domain (FDTD) method using Lumerical FDTD Solutions, with Bloch boundary conditions along x and perfectly matched layer (PML) boundary conditions along y . A mesh grid size of 3 nm (x) \times 5 nm (y) is used inside and near the gold array. The band diagram was calculated by using five pulsed dipole sources that were randomly

^{a)}Z. Lei and X. Zhou contributed equally to this work.

^{b)}Author to whom correspondence should be addressed. Electronic mail: tianyang@sjtu.edu.cn.

Converting State of Polarization With a Miniaturized Metasurface Device

Zeyu Lei and Tian Yang, *Member, IEEE*

Abstract—We have designed and experimentally demonstrated a radial and azimuthal polarization converter, which is a plasmonic metasurface with a radius of not more than $5\ \mu\text{m}$. The metasurface is composed of an array of metal–insulator–metal gap plasmon resonators, each of which reflects the incident local electric field to a predesignated polarization angle. The simulation results show effective polarization conversion within a broad band from 700 to 930 nm.

Index Terms—Metamaterials, plasmonics, polarization.

I. INTRODUCTION

LIGHTWAVES with unconventional states of polarization (SOP) have been studied extensively in the last ten years or so [1]. Three of the widely concerned SOPs are linear polarization (LP), radial polarization (RP) and azimuthal polarization (AP). The latter two exhibit unique cylindrically symmetric polarization distributions. This has led to intriguing phenomena, e.g. focusing beyond diffraction limit and strong axial electric component, and has found interesting applications, such as optical trapping [2], scanning microscopy [3], and Raman spectroscopy [4]. A variety of polarization converters to convert the LP state into RP or AP have been demonstrated, including the liquid crystal (LC) [5], the spatially varying retardation plate [6] and the anisotropic dielectric waveguide array [7]. Meanwhile, converting SOP with miniaturized devices is a less investigated subject [8]–[10], which shall be interesting for they can be integrated into an array so as to process multiple fiber outputs in parallel or quickly switch between SOPs by microscale mechanic motions, and at the same time they can be produced at significantly reduced costs. The challenge with using a miniaturized device is that to ensure high conversion efficiency and high beam quality, the local polarization needs to be manipulated accurately at a deep sub-wavelength scale. For this purpose, the fast development of metasurfaces in recent years provides a powerful tool for subwavelength wavefront manipulation. In particular, the work on gap

plasmon resonator (GPR) based metasurfaces, especially the demonstration of quarter- and half-wave plates, set a foundation for our work here [11]–[15].

In this work, we design and experimentally demonstrate a $5\ \mu\text{m}$ radius metasurface device that converts two orthogonal LP states into RP and AP, respectively, in the reflection mode. The metasurface consists of an array of GPRs in which each GPR rotates the local polarization with only a slight change in the relative field amplitude between different spatial positions. In addition to miniaturization, simulation shows that the working bandwidth of our device can be optimized to as broad as from 700 nm to 930 nm, while commercial LC devices are limited by the bandwidth of a π -phase shifter to compensate for the discontinuity in LC molecule orientation. We note that similar device designs have been used to control the phase of local reflection by working with circular polarizations, including the demonstrations of holograms [16] and metalens [17], showing the versatile functionality from the basic idea of rotating the GPR to control the local field.

II. DESIGN OF LOCAL POLARIZATION ROTATORS

The local polarization of an RP (AP) beam is aligned along the radial (azimuthal) direction. In order for converting an LP input beam into an RP or AP output beam, the metasurface must rotate the local polarization by an angle that matches the difference between the input and output which varies by up to 360° . In this work, we employ the GPR as a polarization rotation component, while the change in field amplitude doesn't vary much with the rotation angle in order to minimize coupling to higher order SOPs. The geometry of the GPR unit cell is shown in Fig. 1(a). A gold nanobrick with length L_x , width L_y , and thickness t is at the top. The middle layer is a continuous silicon dioxide spacer with thickness t_s . The bottom layer is an optically thick gold film. The incident lightwave is normal to the metal surface. An (x, y) coordinate system is defined in Fig. 1. The GPR at a predetermined angle, α , rotates the local incident linear electric field at an angle θ , E^{inc} , to a local reflected linear electric field at an angle of $\beta = 180^\circ - \theta + 2\alpha$, E^{refl} , as shown in Fig. 1(b). The rotation of local electric field and the design principles are explained as follows. The major axes of the nanobrick are denoted by x' and y' . To find E^{refl} , we decompose E^{inc} into its projections onto the x' and y' axes, $E_{x'}^{inc}$ and $E_{y'}^{inc}$, each being resonantly reflected by the GPR to $E_{x'}^{refl}$ and $E_{y'}^{refl}$, which combine into the total local reflected electric field, E^{refl} . The GPR is configured such that the amplitude reflection coefficients for $E_{x'}$ and $E_{y'}$ have

Manuscript received November 5, 2016; revised January 30, 2017; accepted February 23, 2017. Date of publication March 1, 2017; date of current version March 14, 2017. This work was supported in part by the National Science Foundation of China under Grant 61275168 and Grant 11204177 and in part by the National High Technology Research and Development Program of China (863 Program) under Grant 2015AA020944. (Corresponding author: Tian Yang.)

The authors are with the State Key Laboratory of Advanced Optical Communication Systems and Networks, Key Laboratory for Thin Film and Microfabrication of the Ministry of Education, UM-SJTU Joint Institute, Shanghai Jiao Tong University, Shanghai 200240, China (e-mail: leizeyu@sjtu.edu.cn; tianyang@sjtu.edu.cn).

Color versions of one or more of the figures in this letter are available online at <http://ieeexplore.ieee.org>.

Digital Object Identifier 10.1109/LPT.2017.2675453

1041-1135 © 2017 IEEE. Personal use is permitted, but republication/redistribution requires IEEE permission.

See http://www.ieee.org/publications_standards/publications/rights/index.html for more information.

A Quantum Hamiltonian Identification Algorithm: Computational Complexity and Error Analysis

Yuanlong Wang, Daoyi Dong, *Senior Member, IEEE*, Bo Qi, Jun Zhang, *Senior Member, IEEE*,
Ian R. Petersen, *Fellow, IEEE*, Hidehiro Yonezawa

Abstract—Quantum Hamiltonian identification is important for characterizing the dynamics of quantum systems, calibrating quantum devices and achieving precise quantum control. In this paper, an effective two-step optimization (TSO) quantum Hamiltonian identification algorithm is developed within the framework of quantum process tomography. In the identification method, different probe states are inputted into quantum systems and the output states are estimated using the quantum state tomography protocol via linear regression estimation. The time-independent system Hamiltonian is reconstructed based on the experimental data for the output states. The Hamiltonian identification method has computational complexity $O(d^6)$ where d is the dimension of the system Hamiltonian. An error upper bound $O(\frac{d^2}{\sqrt{N}})$ is also established, where N is the resource number for the tomography of each output state, and several numerical examples demonstrate the effectiveness of the proposed TSO Hamiltonian identification method.

Index Terms—Quantum system, Hamiltonian identification, process tomography, computational complexity.

I. INTRODUCTION

AS quantum technology develops, there is an increasing demand for characterizing an unknown quantum process since it is vital to verify and benchmark quantum devices for quantum computation, communication and metrology [1]. The standard solution to characterizing a quantum process is Quantum Process Tomography (QPT), wherein usually known input quantum states (probe states) are applied to the process and the output states are measured to reconstruct the quantum process [2]–[4]. Hamiltonian identification for closed quantum systems is a special class of QPT that corresponds to a unitary

quantum process and is an essential component to characterize the dynamics of a quantum system.

System identification has been widely investigated in classical (non-quantum) systems and control theory, and many identification algorithms have been developed to estimate unknown dynamical parameters of linear or nonlinear input-output systems [5]–[7]. In recent years, the problem of quantum system identification has attracted more and more attention due to the rapid development of emerging quantum technology [8], [9] and increasing demand of characterizing quantum devices. For example, a framework for quantum system identification has been established in [10] to classify how much knowledge about a quantum system is attainable from a given experimental setup. Guță and Yamamoto [11] considered a class of passive linear quantum input-output systems, and investigated the problem of identifiability and how to optimize the identification precision by preparing good input states and performing appropriate measurements on the output states.

In this paper, we focus on the problem of quantum Hamiltonian identification (QHI), which is a key task in characterizing the dynamics of quantum systems and achieving high-precision quantum control. There exist some results on QHI and various aspects of QHI have been investigated [12]–[15]. For example, a symmetry-preserving observer has been developed for the Hamiltonian identification of a two-level quantum system [16]. The identifiability problem for a Hamiltonian corresponding to a dipole moment has been investigated [17] and the question of how to utilize quantum control to identify such Hamiltonian has been addressed [18]. Closed-loop learning control has been presented to optimally identifying Hamiltonian information [19] and compressed sensing has been proposed to enhance the efficiency of identification algorithms for Hamiltonian with special structures [20], [21]. Several Hamiltonian identification algorithms have been developed using only measurement in a single fixed basis [22]–[24]. Wang *et al.* [25] utilized dynamical decoupling to identify Hamiltonians for quantum many-body systems with arbitrary couplings. Cole *et al.* [26] discussed the estimation error in identifying a two-state Hamiltonian and Zhang *et al.* [27] presented a QHI protocol using measurement time traces. Most of these existing results have limitations for practical applications (e.g., estimating a single parameter [24], [28], identifying special Hamiltonian [22], [26]), and there are few theoretical results on the analysis of computational complexity and upper bounds on estimation errors. This paper presents an identification algorithm for general time-independent Hamil-

This work was supported by the Australian Research Council's Discovery Projects funding scheme under Project DP130101658, Laureate Fellowship FL110100020, the Air Force Office of Scientific Research under agreement number FA2386-16-1-4065, Centres of Excellence CE110001027 and the National Natural Science Foundation of China under Grant Nos. 61374092, 61621003, 61227902, 61174086 and 61533012.

Y. Wang and H. Yonezawa are with the School of Engineering and Information Technology, University of New South Wales, Canberra, ACT 2600, Australia, and also with the Centre for Quantum Computation and Communication Technology, Australian Research Council, Canberra, ACT 2600, Australia (e-mail: yuanlong.wang.qc@gmail.com; h.yonezawa@adfa.edu.au).

D. Dong is with the School of Engineering and Information Technology, University of New South Wales, Canberra, ACT 2600, Australia (e-mail: daoyidong@gmail.com).

B. Qi is with the Key Laboratory of Systems and Control, Academy of Mathematics and Systems Science, Chinese Academy of Sciences, Beijing 100190, China (e-mail: qibo@amss.ac.cn).

J. Zhang is with the Joint Institute of UM-SJTU, Shanghai Jiao Tong University, Shanghai 200240, China (e-mail: zhangjun12@sjtu.edu.cn).

I. R. Petersen is with the Research School of Engineering, The Australian National University, Canberra, ACT 2601, Australia (e-mail: i.r.petersen@gmail.com).



Reliability of analog quantum simulation

Mohan Sarovar^{1*}, Jun Zhang^{2*} and Lishan Zeng²

*Correspondence:

mnsarov@sandia.gov;

zhangjun12@sjtu.edu.cn

¹Digital & Quantum Information Systems, Sandia National Laboratories, Livermore, CA 94550, USA

²Joint Institute of UMich-SJTU, Key Laboratory of System Control and Information Processing (MOE), Shanghai Jiao Tong University, Shanghai, 200240, China

[†]Equal contributors

Abstract

Analog quantum simulators (AQS) will likely be the first nontrivial application of quantum technology for predictive simulation. However, there remain questions regarding the degree of confidence that can be placed in the results of AQS since they do not naturally incorporate error correction. Specifically, how do we know whether an analog simulation of a quantum model will produce predictions that agree with the ideal model in the presence of inevitable imperfections? At the same time there is a widely held expectation that certain quantum simulation questions will be robust to errors and perturbations in the underlying hardware. Resolving these two points of view is a critical step in making the most of this promising technology. In this work we formalize the notion of AQS reliability by determining sensitivity of AQS outputs to underlying parameters, and formulate conditions for robust simulation. Our approach naturally reveals the importance of model symmetries in dictating the robust properties. To demonstrate the approach, we characterize the robust features of a variety of quantum many-body models.

Quantum simulation is an idea that has been at the center of quantum information science since its inception, beginning with Feynman's vision of simulating physics using quantum computers [1]. A quantum simulator is a tunable, engineered device that maintains quantum coherence among its degrees of freedom over long enough timescales to extract information that is not efficiently computable using classical computers. The modern view of quantum simulation differentiates between *digital* and *analog* quantum simulations. Specifically, the former performs simulation of a quantum model by using discretized evolutions (*i.e.*, gates) [2–4] whereas the latter uses a physical mimic of the model to infer its properties [5]. A crucial issue is that while quantum error correction can be naturally incorporated into digital quantum simulation, this does not seem to be possible for AQS, which are essentially special-purpose hardware platforms built to model systems of interest. However, digital quantum simulators are extremely challenging to build, whereas AQS are more feasible in the near future, with several experimental candidates already under study [6–10]. Thus a critical question for the quantum simulation field is: as AQS become more sophisticated and begin to model systems that are not classically simulable, can one verify or certify the accuracy of results from systems that are inevitably affected by noises and experimental imperfections [11]?

In response to this challenge, we develop a technique for analyzing the robustness of an AQS to experimental imperfections. We specialize to AQS that prepare ground or thermal

Physical Models of Planar Spiral Inductor Integrated on the High-Resistivity and Trap-Rich Silicon-on-Insulator Substrates

Shuangke Liu, *Student Member, IEEE*, Lei Zhu, *Student Member, IEEE*, Frederic Allibert, *Member, IEEE*, Ionut Radu, *Member, IEEE*, Xinen Zhu, *Member, IEEE*, and Yumin Lu

Abstract—High-resistivity (HR) silicon-on-insulator (SOI) substrates provide low substrate loss, so planar spiral inductors integrated on them presenting higher quality factor (Q) than those on traditional Si substrates. However, the parasitic surface conduction (PSC) effect in the SOI substrate constitutes a conductive layer underneath the buried oxide layer, which deteriorates the inductors performance. This effect can be effectively eliminated by introducing a trap-rich layer. In this paper, physical models that can accurately characterize the behavior of inductors integrated on the HR and radio frequency enhanced signal integrity (RFeSI) SOI substrates are presented, and the analysis and evaluation of PSC effect on the performance of inductors, i.e., the inductance, the quality factor, the self-resonant frequency, and the frequency, where Q peaks, are shown. Planar spiral inductors integrated on HR and RFeSI SOI substrates are fabricated and measured, validating the feasibility of the models we use. The experiment results show that the value of Q and the frequency where it peaks can be improved significantly by eliminating the PSC effect. The temperature effects are also explored, showing that the PSC effect gets worse with rising temperature and accelerates the degradation rate of Q.

Index Terms—High-resistivity silicon-on-insulator (HR-SOI) substrate, parasitic surface conduction (PSC) effect, physical model, planar spiral inductor, radio frequency enhanced signal integrity (RFeSI) SOI, trap rich (TR).

Manuscript received December 6, 2016; revised February 7, 2017, March 16, 2017, and April 19, 2017; accepted April 24, 2017. Date of publication May 26, 2017; date of current version June 19, 2017. The review of this paper was arranged by Editor G. Niu. (*Corresponding author: Shuangke Liu.*)

S. Liu is with the University of Michigan-Shanghai Jiao Tong University Joint Institute, Shanghai Jiao Tong University, Shanghai 200240, China (e-mail: liushuangke@sjtu.edu.cn).

L. Zhu is with the State Key Laboratory of Functional Materials for Informatics, Shanghai Institute of Microsystem and Information Technology, Chinese Academy of Science, Shanghai 200050, China, and also with the School of Physical Science and Technology, ShanghaiTech University, Shanghai 200031, China (e-mail: ray.zhu@sitigroup.com).

F. Allibert and I. Radu are with Soitec Company, 38190 Bernin, France (e-mail: frederic.allibert@soitec.com; ionut.radu@soitec.com).

X. Zhu and Y. Lu are with the Shanghai Industrial μ Technology Research Institute, Shanghai 201800, China (e-mail: alfred.zhu@sitigroup.com; yumin.lu@sitigroup.com).

Color versions of one or more of the figures in this paper are available online at <http://ieeexplore.ieee.org>.

Digital Object Identifier 10.1109/TED.2017.2700022

I. INTRODUCTION

HIGH-RESISTIVITY silicon-on-insulator (HR-SOI) substrates have received intensive attention for growing demands of Si-based integrated circuits, thanks to its low substrate loss, high isolation, and low cost [1]–[4]. The resistivity of its handle wafer is high, usually larger than $1000 \Omega \cdot \text{cm}$, and the buried oxide (BOX), an insulating SiO_2 layer, isolates the active layer from the HR substrate. Thus, passive components integrated on HR-SOI, such as transmission lines and inductors, present superior performance to those on the traditional bulk silicon substrate [5], [6]. However, the BOX layer has a fixed positive charge density of an order of 10^{11} cm^{-2} . The positive charges are caused by the structural defects in the oxide layer near to the Si/SiO₂ interface and are inevitable in the SOI process [7], [8]. These charges attract free carriers near the SiO₂/HR-Si interface and constitute a conductive layer, which is known as the parasitic surface conduction (PSC) effect. When the signal propagates through the devices integrated on the SOI substrate, the longitudinal electric field acts on the attracted carriers and leakage current passing through the PSC layer is produced. The PSC effect is temperature- and process-dependent, and it has an adverse impact on the RF performance, including attenuation, harmonic distortion, and crosstalk, referring to [6] and [9]. Thus, it is expected that the PSC effect can be accurately scaled and modeled, so that the performance of components integrated on HR-SOI substrates can be predicted and optimized precisely.

The PSC effect on the transmission line has been fully studied and can be characterized through the effective resistivity [10]. The effective resistivity of HR-SOI substrate varies with passivation processes and operating temperature [11]–[14]. In addition, the PSC effect can be deteriorated when the CMOS process is applied, leading to added transmission loss, as shown in [15]. It has been proved that the PSC effect can be suppressed by introducing a trap-rich (TR) layer under the oxide layer [16]. The TR layer holds the free charges effectively, making the substrate virtually lossless. The transmission lines integrated on the radio frequency enhanced signal integrity RFeSI-SOI substrate (an enhanced HR-SOI substrate, introducing a TR layer below the SiO₂ to trap free charges) present a low attenuation coefficient

ARTICLE

DOI: 10.1038/s41467-017-01772-1

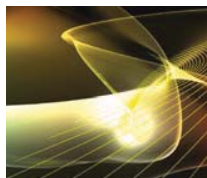
OPEN

High magnesium mobility in ternary spinel chalcogenides

Pieremanuele Canepa^{1,2}, Shou-Hang Bo^{1,2,5}, Gopalakrishnan Sai Gautam^{1,2,3}, Baris Key⁴, William D. Richards², Tan Shi³, Yaosen Tian³, Yan Wang², Juchuan Li¹ & Gerbrand Ceder^{1,2,3}

Magnesium batteries appear a viable alternative to overcome the safety and energy density limitations faced by current lithium-ion technology. The development of a competitive magnesium battery is plagued by the existing notion of poor magnesium mobility in solids. Here we demonstrate by using ab initio calculations, nuclear magnetic resonance, and impedance spectroscopy measurements that substantial magnesium ion mobility can indeed be achieved in close-packed frameworks ($\sim 0.01\text{--}0.1\text{ mS cm}^{-1}$ at 298 K), specifically in the magnesium scandium selenide spinel. Our theoretical predictions also indicate that high magnesium ion mobility is possible in other chalcogenide spinels, opening the door for the realization of other magnesium solid ionic conductors and the eventual development of an all-solid-state magnesium battery.

¹Materials Science Division, Lawrence Berkeley National Laboratory, Berkeley, CA 94720, USA. ²Department of Materials Science and Engineering, Massachusetts Institute of Technology, Cambridge, MA 02139, USA. ³Department of Materials Science and Engineering, University of California Berkeley, Berkeley, CA 94720, USA. ⁴Chemical Sciences and Engineering Division, Argonne National Laboratory, Argonne, IL 60439, USA. ⁵Present address: University of Michigan—Shanghai Jiao Tong University Joint Institute, Shanghai Jiao Tong University, 800 Dong Chuan Road, Minhang District, Shanghai 200240, China. Pieremanuele Canepa and Shou-Hang Bo contributed equally to this work. Correspondence and requests for materials should be addressed to University of Michigan—Shanghai Jiao Tong University Joint Institute, Shanghai Jiao Tong University, 800 Dong Chuan Road, Minhang District, Shanghai 200240 China P.C. (email: pcanepa@lbl.gov) or to S.-H.B. (email: shouhang.bo@sjtu.edu.cn) or to G.C. (email: gceder@berkeley.edu)



COMMENTARY

Protons and the hydrogen economy

Qianli Chen, State Key Laboratory of Metal Matrix Composites, University of Michigan–Shanghai Jiao Tong University Joint Institute, Shanghai Jiao Tong University, Shanghai 200240, China

Artur Braun, Laboratory for High Performance Ceramics, Empa, Swiss Federal Laboratories for Materials Science and Technology, CH-8600 Dübendorf, Switzerland; and Department of Mechanical Engineering, Biomedical & Energy Systems Laboratory, Yonsei University, Seoul 120-749, Republic of Korea

Address all correspondence to Artur Braun at artur.braun@alumni.ethz.ch

(Received 9 August 2017; accepted 15 November 2017)

ABSTRACT

As materials science is becoming components development and systems technology, hydrogen economy is approaching your porch. Welcome!

Hydrogen mobility can now be purchased from the shelf. Fuel cell electric vehicles from various well-known car manufacturers are now available. The number of hydrogen filling stations in Europe is increasing at a rate that long-distance tours become less and less adventurous. The efforts of fuel cell researchers have paid off. Suppliers of components and systems for hydrogen infrastructure are anticipating business. Meanwhile, basic science in electrochemistry and materials research is continuing, with surprises such as the discovery of a proton polaron which are adding to the progress in fundamental understanding of energy materials in operation. Has the long awaited hydrogen economy finally arrived?

Keywords: hydrogenation; energy storage; neutron scattering

DISCUSSION POINT

- Hydrogen economy is not impeded by scientific or technological shortcomings. The challenge is only one of political, social, and ultimately mental nature. Competition against traditional energy carriers is the challenge.

Introduction

Hydrogen is, still, the most abundant matter in the universe. Unimaginably, astronomically long times warrant that physical processes with extremely small probability such as proton tunneling eventually manifest in the proton–proton reaction where two hydrogen nuclei approach each other so close that they melt into a deuterium nucleus and further react to a helium nucleus. Subsequent chain reactions cause radiative energy release in the MeV range.^{1,2}

Our sun is a hotspot, one hundred million miles away in safe distance from the Earth, where the proton–proton reaction has taken place for 4 billion years and will continue so for the next 4 billion years to come. About 95% of our energy

supply today on our planet derives from the energy which we receive from the sun.³

Given this size of the matter, is there any doubt that our current Terawatt Challenge⁴ can be met?

Access to energy is a precondition for economical welfare and for social welfare. While fossil fuels and nuclear power dominate world energy supply, renewable energy has an increasing share in the energy mix. Fear for global warming with gross scenarios such as a new mass extinction of species⁶ or flooding and droughts has helped increase efforts in sustainable development, and peer pressure by the sustainability movement helped to turn the direction.⁷ The world energy consumption is to 20% electric energy. The other 80% are provided by all kinds of fuels. With increasing electrification in our modern world, an increase of the share of electric energy to >20% is anticipated.⁵ Such growth would be good news for the photovoltaic industry and business, and for wind and hydropower.

Would not it be great if still the 80% of fuels (fossil, nuclear, biomass) could be produced by renewable energy? The idea of the hydrogen energy economy is almost 100 years old⁸ and is based on the calculation that transporting energy as H₂ gas

ARTICLE

Received 28 Oct 2016 | Accepted 8 May 2017 | Published 14 Jun 2017

DOI: 10.1038/ncomms15830

OPEN

Experimental neutron scattering evidence for proton polaron in hydrated metal oxide proton conductors

Artur Braun^{1,*} & Qianli Chen^{1,2,3,*}

Hydration of oxygen-deficient metal oxides causes filling of oxygen vacancies and formation of hydroxyl groups with interstitial structural protons, rotating around the oxygen in localized motion. Thermal activation from 500 to 800 K triggers delocalization of the protons by jumping to adjacent oxygen ions, constituting proton conductivity. We report quantitative analyses of proton and lattice dynamics by neutron-scattering data, which reveal the interaction of protons with the crystal lattice and proton-phonon coupling. The motion for the proton trapped in the elastic crystal field yields Eigen frequencies and coupling constants, which satisfy Holstein's polaron model for electrons and thus constitutes first experimental evidence for a proton polaron at high temperature. Proton jump rates follow a polaron model for cerium-oxygen and hydroxyl stretching modes, which are thus vehicles for proton conductivity. This confirms that the polaron mechanism is not restricted to electrons, but a universal charge carrier transport process.

¹Modern Materials and Surfaces, Laboratory for High Performance Ceramics Empa, Swiss Federal Laboratories for Materials Science and Technology, Überlandstrasse 129, Dübendorf 8600, Switzerland. ²Department of Physics, ETH Zürich, Zürich 8057, Switzerland. ³State Key Laboratory of Metal Matrix Composites, University of Michigan-Shanghai Jiao Tong University Joint Institute, Shanghai Jiao Tong University, Shanghai 200240, China. * These authors contributed equally to this work. Correspondence and requests for materials should be addressed to A.B. (email: artur.braun@alumni.ethz.ch) or to Q.C. (email: qianli.chen@sjtu.edu.cn).

Article

Defect-Free Large-Area (25 cm²) Light Absorbing Perovskite Thin Films Made by Spray Coating

Mehran Habibi, Amin Rahimzadeh, Inas Bennouna and Morteza Eslamian *

University of Michigan-Shanghai Jiao Tong University Joint Institute, Shanghai 200240, China; mhabibi82@sjtu.edu.cn (M.H.); amin.rahimzadeh@sjtu.edu.cn (A.R.); inas.bennouna@etu.univ-nantes.fr (I.B.)

* Correspondence: Morteza.Eslamian@sjtu.edu.cn or Morteza.Eslamian@gmail.com; Tel.: +86-213-420-7249; Fax: +86-213-420-6525

Academic Editor: Alessandro Lavacchi

Received: 20 January 2017; Accepted: 9 March 2017; Published: 12 March 2017

Abstract: In this work, we report on reproducible fabrication of defect-free large-area mixed halide perovskite (CH₃NH₃PbI_{3-x}Cl_x) thin films by scalable spray coating with the area of 25 cm². This is essential for the commercialization of the perovskite solar cell technology. Using an automated spray coater, the film thickness and roughness were optimized by controlling the solution concentration and substrate temperature. For the first time, the surface tension, contact angle, and viscosity of mixed halide perovskite dissolved in dimethylformamide (DMF) are reported as a function of the solution concentration. A low perovskite solution concentration of 10% was selected as an acceptable value to avoid crystallization dewetting. The determined optimum substrate temperature of 150 °C, followed by annealing at 100 °C render the highest perovskite precursor conversion, as well as the highest possible droplet spreading, desired to achieve a continuous thin film. The number of spray passes was also tuned to achieve a fully-covered film, for the condition of the spray nozzle used in this work. This work demonstrates that applying the optimum substrate temperature decreases the standard deviation of the film thickness and roughness, leading to an increase in the quality and reproducibility of the large-area spray-on films. The optimum perovskite solution concentration and the substrate temperature are universally applicable to other spray coating systems.

Keywords: mixed halide perovskite; large area perovskite; spray coating; perovskite solution physical properties; perovskite film optimization

1. Introduction

Within the past few years, a tremendous effort has been made to increase the power conversion efficiency (PCE) of perovskite solar cells (PSCs). In spite of achieving remarkable PCEs in the research labs, as high as 22.1% [1], two main obstacles still hinder the development of this technology: The device instability and the lack of knowledge and experience for large scale and large area device fabrication. Development of commercial methods for the fabrication of large area PSCs is one of the prerequisites for their commercialization, and it is as important as stabilizing the PSC performance. It is generally expected that, by increasing the film surface area, the defect and pinhole density would increase; therefore, research on the development of large area solar cells is essential. An ideal perovskite film must have a fully-covered monocrystalline structure with high uniformity and low roughness. Obtaining such ideal films is challenging if not impossible, due to the special behavior of the halide perovskite materials, which is the tendency to crystallize in a polycrystalline structure upon deposition, making the resulting thin films prone to dewetting due to crystallization (crystallization dewetting), and, therefore, the emergence of pinholes [2]. Perovskite crystal growth in all directions, including the direction normal to the film, tends to shrink and disintegrate the film, resulting in a decrease in the film coverage and an increase in the roughness. An ideal perovskite film must have a thickness

Development of multiple-droplet drop-casting method for the fabrication of coatings and thin solid films

Morteza Eslamian , Firuze Soltani-Kordshuli

© American Coatings Association 2017

Abstract Spray coating is a commercial and low-cost technique for the fabrication of large-area coatings and thin films, but it is a stochastic process that is hard to control, as far as the fabrication of thin coatings and solid films is concerned. On the other hand, drop-casting is a facile and more controllable coating technique than spray coating, but its application is limited to small-area thin solid films and coatings. The objective of this work is, therefore, to study the feasibility of impinging an array of droplets, rather than just one droplet, to fabricate polymeric and other solution-processed thin films with larger surface areas than those produced by conventional drop-casting. To this end, in this study, four droplets of poly(3,4-ethylenedioxythiophene)-polystyrene sulfonate (PEDOT:PSS) solution are released simultaneously and impinged on the four vertices of a square on a wettable solid surface to make a thin film. The effect of the substrate texture on the spreading and the film formation process is studied. As a novel idea, the substrate is excited by ultrasonic vibration to improve the droplet spreading and coalescence. It is shown that as time elapses, the impinged droplets successfully coalesce and make a thin film. Surface morphology and roughness of the resulting PEDOT:PSS thin solid films show that, except on the edges, the resulting thin solid films are uniform. This leads us to conclude that the application of equal-sized and equally-spaced multiple droplets released simultaneously and impinged on vibrating substrates could be considered as a new coating technique, which has some of the benefits of the spray coating, but it is much more controllable than spray coating.

M. Eslamian (✉), F. Soltani-Kordshuli
University of Michigan - Shanghai Jiao Tong University
Joint Institute, Shanghai 200240, China
e-mail: Morteza.Eslamian@sjtu.edu.cn;
Morteza.Eslamian@gmail.com

Keywords Drop-casting, Multiple-droplet impact, Ultrasonic substrate vibration, PEDOT:PSS, Coatings, Thin solid films

Introduction

Coatings and thin solid films may be deposited from the vapor or liquid phases, depending on the nature of the precursors and the desired functionality and expectations of the resulting films. The vapor-phase methods, which are categorized under either physical or chemical vapor deposition routes, require a well-controlled atmosphere and are usually performed in a vacuum, using expensive equipment and energy intensive processes. Therefore, highly ordered and defect-free thin films and coatings are usually deposited from the vapor phase. This paper focuses on the deposition of materials that could form a liquid solution or a fine emulsion or ink at room temperature, such as organic materials. The liquid-phase methods for the deposition of solution-processed or colloidal mixtures are less expensive, but are also less controllable. Therefore, it is highly desirable to perform basic research and develop new ideas to make the solution-processed deposition methods more precise, reliable, and reproducible.¹

Solution-processed thin solid films and coatings are obtained by the drying of thin liquid films or liquid patches or islands (e.g., impinged droplets in spray coating). The thin liquid films or liquid patches are formed on the substrates based on two main methodologies. In slot-die coating, blade coating, spin coating, and other similar methods, a continuous thin liquid film is cast on the substrate. In contrast, in drop-casting, inkjet printing, and spray coating, the process is based on the release, impact, spreading and deposition of one or more droplets.² The impinged droplets may form a continuous liquid film before drying or may dry individually to make a thin solid film comprised of



Effects of Self-Assembled Monolayer Modification of Nickel Oxide Nanoparticles Layer on the Performance and Application of Inverted Perovskite Solar Cells

Qin Wang,^[a, c] Chu-Chen Chueh,^[a] Ting Zhao,^[a] Jiaqi Cheng,^[d] Morteza Eslamian,^{*,[c]} Wallace C. H. Choy,^[d] and Alex K.-Y. Jen^{*,[a, b]}

Entirely low-temperature solution-processed ($\leq 100^\circ\text{C}$) planar p-i-n perovskite solar cells (PSCs) offer great potential for commercialization of roll-to-roll fabricated photovoltaic devices. However, the stable inorganic hole-transporting layer (HTL) in PSCs is usually processed at high temperature ($200\text{--}500^\circ\text{C}$), which is far beyond the tolerant temperature ($\leq 150^\circ\text{C}$) of roll-to-roll fabrication. In this context, inorganic NiO_x nanoparticles (NPs) are an excellent candidate to serve as the HTL in PSCs, owing to their excellent solution processability at room temperature. However, the low-temperature processing condition is usually accompanied with defect formation, which deteriorates the film quality and device efficiency to a large extent. To suppress this setback, we used a series of benzoic acid self-assembled monolayers (SAMs) to passivate the surface defects

of the NiO_x NPs and found that 4-bromobenzoic acid could effectively play the role of the surface passivation. This SAM layer reduces the trap-assisted recombination, minimizes the energy offset between the NiO_x NPs and perovskite, and changes the HTL surface wettability, thus enhancing the perovskite crystallization, resulting in more stable PSCs with enhanced power conversion efficiency (PCE) of 18.4%, exceeding the control device PCE (15.5%). Also, we incorporated the above-mentioned SAMs into flexible PSCs (F-PSCs) and achieved one of the highest PCE of 16.2% on a polyethylene terephthalate (PET) substrate with a remarkable power-per-weight of 26.9 W g^{-1} . This facile interfacial engineering method offers great potential for the large-scale manufacturing and commercialization of PSCs.

Introduction

The intriguing perovskite solar cells (PSCs) have aroused tremendous interest owing to their excellent optoelectronic properties, long charge-carrier lifetime, low-temperature solution processability, and relatively low fabrication cost, with a remarkable certified power conversion efficiency (PCE) of 22.1%,

which could now compete with the commercialized silicon solar cells, if the device stability can be improved.^[1] Generally speaking, the current state-of-the-art PSCs adopt a planar heterojunction architecture that could be fabricated with either n-i-p or p-i-n structure, due to the ambipolar transport property of the perovskite light harvesters.^[2] However, the n-i-p type suffers from severe hysteresis setback owing to the unbalanced charge distribution in the perovskite layer.^[3] Considering the fact that the electron-diffusion length in perovskites is relatively longer than the hole-diffusion length, the p-i-n structure is more advantageous to obtain a reasonably stable device performance.^[4,5] Employing a suitable hole-transporting layer (HTL) is a prerequisite for developing a high-performance p-i-n PSC, because the HTL not only facilitates effective hole collection but also minimizes the interfacial charge recombination.^[6]

The most frequently used HTL in PSCs is poly(3,4-ethylenedioxythiophene):polystyrene sulfonate (PEDOT:PSS) and nickel oxide (NiO_x). Although PEDOT:PSS is a commercialized and standard HTL material, it suffers from several intrinsic problems such as hygroscopicity, acidity-induced instability, and large potential loss due to unmatched energy level with the adjacent layers in the PSC structure.^[7] In contrast, p-type NiO_x is advantageous due to its large band gap (3.5–3.9 eV),^[8] deep valence band (5.1–5.4 eV),^[9–11] high mobility ($\approx 10^{-3}\text{ cm}^2\text{ V}^{-1}\text{ s}^{-1}$)^[12,13] induced by the large doping of Ni^{3+} ion,^[13] and its superior stability^[14] resulting from its inorganic nature, which brings about a longer device lifetime.^[15] To date,

[a] Q. Wang, Dr. C.-C. Chueh, T. Zhao, Prof. A. K.-Y. Jen
Department of Materials Science and Engineering
University of Washington
Seattle, WA, 98105 (USA)
E-mail: ajen@uw.edu

[b] Prof. A. K.-Y. Jen
Department of Materials Science & Engineering
City University of Hong Kong
Kowloon, Hong Kong (SAR China)

[c] Q. Wang, Prof. M. Eslamian
University of Michigan-Shanghai Jiao Tong University Joint Institute
Shanghai, 200240 (P. R. China)
E-mail: Morteza.Eslamian@sjtu.edu.cn

[d] J. Cheng, Prof. W. C. H. Choy
Department of Electrical and Electronic Engineering
The University of Hong Kong
Pokfulam, Hong Kong (SAR China)

Supporting Information and the ORCID identification number(s) for the author(s) of this article can be found under:
<https://doi.org/10.1002/cssc.201701262>.

This publication is part of dual Special Issues on "Perovskite Optoelectronics", published in *ChemSusChem* and *Energy Technology*. Please visit the *ChemSusChem* issue at <http://doi.org/10.1002/cssc.v10.19>, and the companion issue of *Energy Technology* at <http://dx.doi.org/10.1002/ente.v5.10>.



Review

Excitation by acoustic vibration as an effective tool for improving the characteristics of the solution-processed coatings and thin films



Morteza Eslamian*

University of Michigan-Shanghai Jiao Tong University Joint Institute, Shanghai, 200240, China

State Key Laboratory for Composite Materials, School of Materials Science and Engineering, Shanghai Jiao Tong University, Shanghai, 200240, China

ARTICLE INFO

Keywords:

Thin liquid films
Thin solid films
Organic coatings
Acoustic vibration
Ultrasonic vibration
Thin film devices

ABSTRACT

Solution-processed thin films and coatings have received tremendous attention in recent years, as a substitute for vapor-phase grown films, to develop low-cost devices, such as thin film solar cells, displays, sensors, etc. The challenge, however, is to overcome the lack of adequate controllability and reproducibility of solution-processed thin films which inherently contain excessive pinholes and other defects, particularly when processed at low temperatures. In this review, it is substantiated that imposed sound and ultrasound vibrations could result in significant improvements in the nanostructure, uniformity, and functionality of the resulting thin solid films. Using a wealth of information in the fluid dynamics literature, it is demonstrated that the acoustic excitation results in creation of fluid flow, such as streaming, microstreaming, and surface waves, as well as enhanced heat transfer, causing improvement in the quality and characteristics of the thin films prepared by vibration-assisted techniques, even though the vibration tends to destabilize the liquid films. In addition, the pertinent works that have exploited this effect to prepare high performance materials are critically reviewed and the results are discussed and interpreted in the framework of fluid dynamics. A brief review on the effect of imposing other external fields including electric and magnetic fields on the fabrication process and characteristics of the thin films is also provided.

1. Introduction

Thin solid films and some emerging devices incorporating thin solid films, such as thin film transistors and displays, solar cells, organic light emitting diodes (OLED), thermoelectric devices, sensors and actuators, are currently at the forefront of research and development in various areas of nanotechnology and renewable energy [1]. A thin solid film may be processed and deposited from the vapor phase, using physical or chemical vapor deposition or from liquid solutions or colloidal mixtures also in a physical or chemical route, using casting and printing methods [2], such as drop casting, spin coating, blade coating, gravure, slot-die coating, screen-printing, inkjet printing and spray coating, as shown in Fig. 1 [3]. The solution-processed methods are cheaper in terms of capital, energy, and operating costs, and therefore are desirable, but generally suffer from the lack of controllability and reproducibility of the resulting products, which may also contain manufacturing defects in micro- and nano- scales. Addressing and resolving the aforementioned setbacks is a prerequisite for the fabrication of high performance solution-processed thin film devices in a high volume and industrial scale.

From a fluid mechanics point of view, the solution-processed casting and printing methods may be categorized as either those based on immediate formation of a thin liquid film or those based on the formation of many impinged droplets on the substrate. To elaborate, in methods such as spin coating, slot-die coating, and blade coating, a thin liquid film of the solution forms directly, whereas in spray coating and inkjet printing, the impinged droplets may form a continuous liquid film before drying or may dry individually to yield a thin solid film comprised of dried liquid islands that usually overlap with one another. The latter scenario (overlapped dried islands) is hard to control; thus, for obtaining a high quality and uniform thin solid film or coating, particularly an ultrathin film, it is desirable to have a continuous liquid film formed first, followed by a drying stage to yield a defect-free and smooth thin solid film or coating [4].

Most applications, particularly emerging molecular semiconductor thin film devices, require fabricating defect-free, homogenous, and uniform thin solid films for satisfactory performance of the ensuing devices. For this reason, the thin solid films made using well-controlled vapor and vacuum-based methods are currently more desirable than the solution-processed methods, as far as the device performance is

* Corresponding author at: State Key Laboratory for Composite Materials, School of Materials Science and Engineering, Shanghai Jiao Tong University, Shanghai, 200240, China.
E-mail addresses: Morteza.Eslamian@sjtu.edu.cn, Morteza.Eslamian@gmail.com.

<http://dx.doi.org/10.1016/j.porgcoat.2017.08.008>

Received 18 June 2017; Received in revised form 6 August 2017

Available online 31 August 2017

0300-9440/ © 2017 Elsevier B.V. All rights reserved.



Experimental study on the evaporation of sessile droplets excited by vertical and horizontal ultrasonic vibration



Amin Rahimzadeh, Morteza Eslamian*

University of Michigan-Shanghai Jiao Tong University Joint Institute, Shanghai 200240, China

ARTICLE INFO

Article history:

Received 23 April 2017

Received in revised form 19 June 2017

Accepted 22 June 2017

Available online 3 July 2017

Keywords:

Sessile droplet

Ultrasonic vibration

Droplet evaporation

Droplet oscillation

Contact angle

Stick-slip

ABSTRACT

Interaction between sessile droplets and solid surfaces is a fundamental science and engineering problem, with ubiquitous presence in various applications. In this paper, we study the effect of imposing vertical and horizontal ultrasonic vibration (40 kHz) on dynamics (oscillations) and evaporation of sessile droplets of dimethylformamide (DMF), isopropyl alcohol (IPA) and water on Teflon and glass substrates. There is no or very few works considering dynamics and evaporation aspects of excited droplets, simultaneously. The theory concerning the force balance and pinning/depinning in pristine and excited sessile droplet systems is elucidated. Time varying left and right contact angles and contact radius are measured for the duration of the droplet lifetime, where the stick-slip phenomena are observed and interpreted for various liquids. Imposing substrate vibration results in significant decrease in droplet lifetime and affects the behavior of the stick-slip mechanism. Droplets excited by horizontal vibration have the shortest lifetime. It is also experimentally shown that in the case of vertical vibration, the left and right contact angles oscillate in-phase, whereas in the case of horizontal vibration, there is 180° phase difference between left and right contact angles.

© 2017 Elsevier Ltd. All rights reserved.

1. Introduction

Sessile droplets have ubiquitous presence in nature and have numerous applications, such as in droplet-based coating methods, as well as in emerging microfluidic and micro/nano devices, e.g. [1]. Analysis of sessile droplets involves surface science, thermodynamics, hydrodynamics, and heat transfer, making them an interesting but complex research topic. The present study focuses on dynamics (oscillations) and evaporation of ultrasonically-excited sessile droplets. Therefore, first the literature concerning evaporation and then dynamics and oscillation of excited droplets is reviewed to substantiate the novelty and demand for this work.

Numerous studies have been performed on behavior of evaporating sessile droplets on a substrate. Erbil [2] and Kovalchuk et al. [3] have reviewed and discussed some works pertinent to the basic theory and some special topics related to droplet evaporation. Evaporation of a sessile droplet in the most general case is a complex problem, due to possible internal liquid motion, gas phase motion, and heat transfer between solid, liquid and gas phases. However, based on some assumptions, various simplified evaporation models have been developed, as discussed in Ref. [4]. For

instance, in the case of a sessile droplet evaporating in a stagnant surrounding gas, based on the diffusion-controlled model [5], droplet evaporation rate is controlled by diffusion rate of the liquid vapor in the surrounding gas. The evaporation rate varies with the droplet size and density, substrate temperature and substrate thermal properties [6–9], the choice of the ambient gas and pressure, which affect the diffusion coefficient [10], the vapor concentration in the ambient, and hydrophobicity of the substrate (contact angle) [11,12]. Obviously, if convective effects are present, the diffusion-controlled model is not sufficient to predict the experimental data [3], and more sophisticated multiphase flow models are needed [13–15]. Murisic and Kondic [4,13] provide a clear picture of the underlying physics and modeling of evaporation of sessile droplets with moving contact lines under various conditions and assumptions. They considered two commonly used evaporative models based on either the liquid phase or the vapor phase [13]. Of relevance to the present work is their simulation on the behavior of various liquids, where it was shown that the time variation of the base radius significantly changes with the choice of the liquid, as our experimental data also corroborate. In another comprehensive numerical study, Saenz et al. [14] presented a coupled two-phase model based on the diffuse-interface method to conduct three-dimensional direct numerical simulations of deformed evaporating droplets. The stick-slip modes, to

* Corresponding author.

E-mail addresses: Morteza.Eslamian@sjtu.edu.cn, Morteza.Eslamian@gmail.com (M. Eslamian).

<http://dx.doi.org/10.1016/j.ijheatmasstransfer.2017.06.099>

0017-9310/© 2017 Elsevier Ltd. All rights reserved.



Impact dynamics and deposition of pristine and graphene-doped PEDOT:PSS polymeric droplets on stationary and vibrating substrates



Firuze Soltani-Kordshuli, Morteza Eslamian*

University of Michigan - Shanghai Jiao Tong University Joint Institute, Shanghai 200240, China

ARTICLE INFO

Keywords:

Droplet impact dynamics
PEDOT:PSS
Graphene
Ultrasonic substrate vibration
Drop casting
Polymeric solutions

ABSTRACT

In this work, using high speed imaging, the impingement of water as the reference liquid, polymeric PEDOT:PSS and graphene-doped PEDOT:PSS droplets onto bare glass and FTO-coated glass substrates with varying contact angles (surface energy) is studied, in an attempt to understand the process of drop casting, spray coating and inkjet printing frequently used for the fabrication of polymeric thin films in thin film devices. The effect of imposing lateral and vertical ultrasonic vibration on the substrate on impinging droplets and deposition is also studied, and unprecedented results are obtained, and discussed. It is concluded that, when the substrate is fully cleaned and exposed to UV light, droplet contact angle significantly decreases because of an increase in the surface energy, resulting in an effective deposition process and suppression of receding. It is also demonstrated that imposing vertical ultrasonic vibration on the substrate increases spreading of PEDOT:PSS-based droplets. The enhanced spreading as a result of surface treatment and imposed vibration is of great importance for the fabrication of solution-processed thin films by droplet-based coating methods. It is also observed that imposed ultrasonic vibration results in a decrease in the roughness of the resulting thin solid films.

1. Introduction

Droplet impact on solid and wet surfaces is a fundamental fluid dynamic problem with numerous applications, such as in spray surface cooling, spray painting, direct fuel injection combustion engines, and a wide range of coating and printing methods, such as drop casting, inkjet printing, and spray coating [1]. The emergence of solution-processed thin film devices, such as thin film solar cells, has opened up new windows of opportunity for the application of such coating and printing methods [2]. Many researchers have studied various aspects of droplet impact dynamics of simple fluids, such as water on various substrates, identifying various phenomena including spreading, splashing, receding, rebounding and bouncing, e.g., [3–24], among others. Some aspects of droplet impact dynamics of more complex liquids and liquid solutions used for coating, printing, or device fabrication purposes have been studied, as well, e.g., [25–41], to name a few. This paper investigates the effects of substrate treatment (surface energy) and excitation by vibration on spreading of polymeric solutions, less studied before, to be elaborated in the following.

When a droplet impinges on a substrate with a high velocity normal to the surface, its momentum creates a radial flow tangent to the surface, which results in the formation of a liquid disk (lamella). Consequently, a rim will form and the liquid radial velocity pushes the

liquid towards the rim, while the droplet is spreading on the surface. Meanwhile, if the inertial kinetic energy is much larger than the surface tension force, it may cause drop splashing and breakup and ejection of smaller droplets. On the other hand, if the droplet highly spreads on a wettable surface without splashing and receding, the phenomenon is called deposition, which is desirable for coating and printing purposes. All factors that control the spreading process are present in the droplet Weber (We) and Reynolds (Re) numbers at the time of impact and the contact angle and surface physical and chemical characteristics, where We and Re numbers are affected by droplet size and velocity, as well as liquid surface tension, viscosity, and density, and contact angle is controlled by the wetting behavior of the liquid on a particular substrate, e.g. [10,42,43]. Every spreading droplet experiences an advancing phase in which its diameter increases, until reaching its maximum diameter (d_{max}), followed by a possible receding phase, if the droplet has overspread due to its excess kinetic energy, while the surface energy is not high enough to pin the liquid to the substrate to balance the three mutual interfacial forces. On an ideal and smooth surface, the Young-Laplace equation defines the droplet equilibrium shape and contact angle as follows:

$$\gamma_{SL} + \gamma \cos \theta_{eq} = \gamma_{SV} \quad (1)$$

in which γ_{SL} , γ_{SV} , and θ_{eq} are interfacial tension between solid and

* Corresponding author.

E-mail addresses: Morteza.Eslamian@sjtu.edu.cn, Morteza.Eslamian@gmail.com (M. Eslamian).

<http://dx.doi.org/10.1016/j.expthermflusci.2017.08.019>

Received 24 September 2016; Received in revised form 16 June 2017; Accepted 18 August 2017

Available online 19 August 2017

0894-1777/ © 2017 Elsevier Inc. All rights reserved.

REVIEW

Inorganic and Organic Solution-Processed Thin Film Devices

Morteza Eslamian^{1,2}

Received: 20 July 2016 / Accepted: 16 August 2016 / Published online: 8 September 2016
© The Author(s) 2016. This article is published with open access at Springerlink.com

Abstract Thin films and thin film devices have a ubiquitous presence in numerous conventional and emerging technologies. This is because of the recent advances in nanotechnology, the development of functional and smart materials, conducting polymers, molecular semiconductors, carbon nanotubes, and graphene, and the employment of unique properties of thin films and ultrathin films, such as high surface area, controlled nanostructure for effective charge transfer, and special physical and chemical properties, to develop new thin film devices. This paper is therefore intended to provide a concise critical review and research directions on most thin film devices, including thin film transistors, data storage memory, solar cells, organic light-emitting diodes, thermoelectric devices, smart materials, sensors, and actuators. The thin film devices may consist of organic, inorganic, and composite thin layers, and share similar functionality, properties, and fabrication routes. Therefore, due to the multidisciplinary nature of thin film devices, knowledge and advances already made in one area may be applicable to other similar areas. Owing to the importance of developing low-cost, scalable, and vacuum-free fabrication routes, this paper focuses on thin film devices that may be processed and deposited from solution.

Keywords Organic electronics · Photovoltaics · Thin film transistors · Thermoelectric devices · Organic light-emitting diodes · Smart materials · Sensors and actuators · Solution-processed methods

1 Background

A thin solid film usually refers to a layer of material ranging from few nanometers to several micrometers in thickness. Thin solid films may be divided into two categories of passive and active films. Passive thin films including coatings are used for aesthetic and decoration purposes, or protection of the underlying surfaces, against moisture, oxygen, high temperature, and mechanical forces

to avoid corrosion, surface damage, etc. On the other hand, active thin films can in fact respond to specific triggering effects, such as light, heat, and contact with gases and biological analytes and generate a response for energy conversion, sensing, mechanical actuation, etc. Therefore, the combination of one or more active thin films, and perhaps some passive thin films, can make a thin film device, such as thin film solar cells (SCs), transistors, thermoelectric devices, sensors, and actuators, to name a few. Various types of thin film devices may share similar principles of operation or fabrication processes, and therefore advances in one device may provide new windows of opportunity for the development of other devices. As an example, molecular semiconductors, such as perovskites developed for perovskite SCs, may be used in other devices, such as thin film transistors. Or most of the thin film devices employ graphene and carbon nanotubes in their structures, and advances in one field may be utilized in other fields, as well.

✉ Morteza Eslamian
Morteza.Eslamian@sjtu.edu.cn;
Morteza.Eslamian@gmail.com

¹ Photovoltaics Lab, University of Michigan-Shanghai Jiao Tong University Joint Institute, Shanghai Jiao Tong University, Shanghai 200240, China

² State Key Lab of Composite Materials, School of Materials Science and Engineering, Shanghai Jiao Tong University, Shanghai 200240, China



On evaporation of thin liquid films subjected to ultrasonic substrate vibration



Amin Rahimzadeh, Morteza Eslamian *

University of Michigan-Shanghai Jiao Tong University Joint Institute, Shanghai, 200240, China

ARTICLE INFO

Available online 22 March 2017

Keywords:

Thin film evaporation
Ultrasonic vibration
Convection heat transfer
Thin film instability

ABSTRACT

Theoretical and experimental studies on evaporation of thin and ultrathin liquid films (all volatile or liquid solutions) are desirable, but scarce. In this context, excitation of thin liquid films by (ultrasonic) vibration is also an interesting theoretical and applied research direction affecting the hydrodynamics, stability, and evaporation of thin liquid films. In this study, the evaporation history of drop-cast stationary and excited thin liquid films subjected to vertical and horizontal ultrasonic vibration is studied, and unprecedented results are obtained and discussed. The evaporation history of two model thin liquid films is captured using video camera and high precision digital balance. Since evaporation of excited thin films by substrate vibration resembles forced convection, the convective heat transfer coefficient and consequently the evaporation rate of the excited thin films are expected to increase compared to those of non-excited thin films. Experimental results substantiate this hypothesis. It is further shown and discussed that the films excited by horizontal ultrasonic substrate vibration evaporate faster than those excited by vertical vibration.

© 2017 Elsevier Ltd. All rights reserved.

1. Introduction

Evaporation from the free surface of a liquid exposed to surrounding gas may be realized in various natural phenomena and practical applications. Depending on the characteristic lengths, the problem may be treated differently. For instance, estimating liquid evaporation rate in thick or deep liquid layers, such as swimming pools, ponds and lakes, is a classic design problem, e.g. [1–3]. For very shallow layers of liquids or simply thin liquid films, interaction between the liquid-gas and solid-liquid interfaces and the disjoining pressure as a result of intermolecular forces may affect the evaporation, although the shallow depth assumptions may bring about some major simplifications to governing equations [4–6]. Evaporation from the surface of thin liquid films has existing and potential applications, such as in heat pipes and evaporators [7,8]. And, if a thin film of a liquid solution is used instead of a completely volatile liquid, the solvent evaporation and solute precipitation leaves behind a thin solid film. This is a favorable process for the fabrication of thin solid films in the field of solution-processed thin film devices with ubiquitous presence in existing and emerging technologies, such as thin film organic electronics and photovoltaics [9]. Understanding the physics of thin liquid film evaporation is therefore essential for achieving desired device or process performance, by

controlling the evaporation rate. Application of multicomponent solvents with different boiling points [10], anti-solvent to accelerate solvent evaporation [11], suppression of dewetting in crystalline films, such as perovskites [12], employing patterned substrates with a gradient in thermal conductivity, to prepare patterned films [13,14], and imposing ultrasonic vibration to control the film structure and evaporation rate [15–19] are some of the attempts made to control the drying and morphology of the ensuing thin solid films. The abovementioned works concern the development of advanced materials and device fabrication, without particular focus on transport phenomena associated with liquid film evaporation in microscale. This work addresses the problem of thin film evaporation from a fluid and thermal point of view.

To establish the argument and to justify the need for the present work, we start with some notable researches performed on deep liquids subjected to natural convection, and then most relevant works on evaporation of thin liquid films are reviewed. Numerous works have been performed on natural and forced convection over a deep layer of liquid. For instance, Bower and Saylor [1–3] studied evaporative natural convection over liquid surface in a walled container and obtained correlations between the Sherwood (Sh) and Rayleigh (Ra) numbers in the form of $Sh = BSc^{1/3}Ra^\alpha$, where B and α are constants. In the correlation developed by Bower and Saylor $B = 0.230$ and $\alpha = 0.321$. These simple correlations may be used to estimate the evaporation rate. Unfortunately, in the case of thin liquid films, there is no such correlation, due to the presence of other important variables, as discussed above. There are very few experimental works that consider evaporation of thin liquid

* Corresponding author.

E-mail addresses: Morteza.Eslamian@sjtu.edu.cn, Morteza.Eslamian@gmail.com (M. Eslamian).

Optimization of spray coating for the fabrication of sequentially deposited planar perovskite solar cells

Mehran Habibi,^a Mohammad-Reza Ahmadian-Yazdi,^a and Morteza Eslamian^{a,b,*}

^aUniversity of Michigan–Shanghai Jiao Tong University Joint Institute, Shanghai, China

^bShanghai Jiao Tong University, State Key Laboratory for Composite Materials, School of Materials Science and Engineering, Shanghai, China

Abstract. We use facile coating techniques including spray coating and drop casting to fabricate methylammonium lead iodide perovskite solar cells through a two-step sequential deposition approach. In the first step, for the deposition of the lead iodide, spray coating substitutes for the commonly used lab-scale spin coating, while the operating parameters of the former process are optimized to achieve a fully covered and uniform film of lead iodide. In the second step, to deposit methylammonium iodide atop the lead iodide layer to form methylammonium lead iodide perovskite, dip-coating process is replaced by the touch-free drop casting and scalable pulsed-spray coating. It is found that the performance of the perovskite films and devices made by pulsed-spray coating and drop casting is similar to those prepared by dip coating, while the large-scale production capabilities of such methods beside the low material consumptions of drop casting prove their potential to replace dip coating in large-scale manufacturing of perovskite solar cells. The champion devices fabricated by spray-drop and spin-drop techniques demonstrated power conversion efficiencies of 6.92% and 9.48%, respectively. It is expected that device fabrication in a low-humidity environment using the optimized parameters and optimization of other layers will result in higher efficiencies. © The Authors. Published by SPIE under a Creative Commons Attribution 3.0 Unported License. Distribution or reproduction of this work in whole or in part requires full attribution of the original publication, including its DOI. [DOI: [10.1117/1.JPE.7.022003](https://doi.org/10.1117/1.JPE.7.022003)]

Keywords: perovskite solar cells; sequential deposition; drop casting; spray coating; pulsed-spray coating; optimization.

Paper 17036SS received Mar. 24, 2017; accepted for publication May 10, 2017; published online Jun. 1, 2017.

1 Introduction

Inorganic (e.g., chalcogenide), organic (e.g., polymeric), mixed inorganic-organic (e.g., perovskite), and quantum-dot thin film solar cells (SCs) are in the forefront of research and development in energy and nanotechnology fields to secure a renewable and cost-effective source of electrical energy based on the photovoltaic (PV) effect.^{1,2} The aforementioned PV SCs have the potential to be fabricated using low-cost vacuum-free techniques, such as processing and casting from solutions. Organometallic perovskite SCs (PVSCs) are currently the most attractive in the abovementioned list with compelling efficiencies over 20%,³ and therefore are the focus of this work. A recent review of the structure and advances in PVSCs is found in Ref. 2.

The perovskite light harvesting layer in a PVSC may be formed using a two-step sequential deposition strategy^{4,5} or a one-step approach.^{6,7} In the two-step sequential deposition, the perovskite layer, e.g., methylammonium lead iodide ($\text{CH}_3\text{NH}_3\text{PbI}_3$), is prepared in two steps. First, the PbI_2 precursor solution is deposited on the substrate by a casting method, preparing a thin layer composed of PbI_2 crystals. Then, this layer is exposed to the solution of $\text{CH}_3\text{NH}_3\text{I}$ (MAI) to form perovskite crystals in a film. In the one-step approach, a mixture of PbI_2 and $\text{CH}_3\text{NH}_3\text{I}$ dissolved in appropriate solvents is directly deposited on the substrate. Grätzel

*Address all correspondence to: Morteza Eslamian, E-mail: morteza.eslamian@gmail.com

Article

Photocatalytic Graphene-TiO₂ Thin Films Fabricated by Low-Temperature Ultrasonic Vibration-Assisted Spin and Spray Coating in a Sol-Gel Process

Fatemeh Zabihi ^{1,2}, Mohammad-Reza Ahmadian-Yazdi ¹ and Morteza Eslamian ^{1,3,*}

¹ University of Michigan-Shanghai Jiao Tong University Joint Institute, Shanghai 200240, China; fzabihi@dhu.edu.cn (F.Z.); 1143709026@sjtu.edu.cn (M.-R.A.-Y.)

² State Key Laboratory for Modification of Chemical Fibers and Polymer Materials, College of Materials Science and Engineering, Donghua University, Shanghai 201620, China

³ State Key Laboratory for Composite Materials, School of Materials Science and Engineering, Shanghai Jiao Tong University, Shanghai 200240, China

* Correspondence: morteza.eslamian@sjtu.edu.cn or morteza.eslamian@gmail.com; Tel.: +86-21-3420-7249; Fax: +86-21-3420-6525

Academic Editors: Vladimiro Dal Santo and Alberto Naldoni

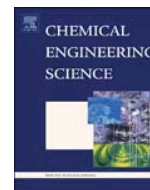
Received: 29 March 2017; Accepted: 27 April 2017; Published: 2 May 2017

Abstract: In this work, we communicate a facile and low temperature synthesis process for the fabrication of graphene-TiO₂ photocatalytic composite thin films. A sol-gel chemical route is used to synthesize TiO₂ from the precursor solutions and spin and spray coating are used to deposit the films. Excitation of the wet films during the casting process by ultrasonic vibration favorably influences both the sol-gel route and the deposition process, through the following mechanisms. The ultrasound energy imparted to the wet film breaks down the physical bonds of the gel phase. As a result, only a low-temperature post annealing process is required to eliminate the residues to complete the conversion of precursors to TiO₂. In addition, ultrasonic vibration creates a nanoscale agitating motion or microstreaming in the liquid film that facilitates mixing of TiO₂ and graphene nanosheets. The films made based on the above-mentioned ultrasonic vibration-assisted method and annealed at 150 °C contain both rutile and anatase phases of TiO₂, which is the most favorable configuration for photocatalytic applications. The photoinduced and photocatalytic experiments demonstrate effective photocurrent generation and elimination of pollutants by graphene-TiO₂ composite thin films fabricated via scalable spray coating and mild temperature processing, the results of which are comparable with those made using lab-scale and energy-intensive processes.

Keywords: photocatalysis; spray coating; ultrasonic vibration; graphene-TiO₂; sol-gel; microstreaming

1. Introduction

A photocatalyst performs catalytic activity using incident photons as the driving force for a chemical reaction, without being consumed or chemically altered as a result of the reaction. Photocatalysts are low-cost, efficient and environmentally-favored alternatives to commonly used industrial catalysts [1–3]. Photocatalyst works based on oxidative surface decomposition of the reactants are typically used for the removal of residual oils and solvents and for inhibiting the growth of microorganisms on the surface [2–4]. Some metal oxides, such as TiO₂, with inherent resistance to oxidation and hydration exhibit photocatalytic properties at room temperature [4–6]. TiO₂ is a large band gap semiconductor that absorbs high energy UV photons to generate electron and hole pairs. As Figure 1a depicts, the holes may react with the hydroxyl ions from the adsorbed surface water molecules to form highly reactive but neutral hydroxyl radicals. Airborne or aqueous pollutants



Stability of thin liquid films subjected to ultrasonic vibration and characteristics of the resulting thin solid films



Amin Rahimzadeh, Morteza Eslamian*

University of Michigan - Shanghai Jiao Tong University Joint Institute, Shanghai 200240, China

ARTICLE INFO

Keywords:

Thin liquid film instability
Thin solid films
Ultrasonic vibration
Dewetting
Thin film devices

ABSTRACT

Thin solid films have ubiquitous presence in many existing and emerging technologies. Solution-processed thin solid films may be fabricated by casting a thin liquid film followed by a drying step. It has been shown that by imposing a low-amplitude ultrasonic vibration on the substrate, the physical and structural characteristics of the resulting thin solid films is improved, significantly. Therefore, in this study, to investigate and rationalize the aforementioned findings, the evolution and stability of thin and ultrathin films of Newtonian liquid solutions, subjected to vertical and horizontal ultrasonic vibration is studied, using the long-wave approximation and negligible inertia forces. An explicit criterion is obtained for the film instability. Consistent with established theories, it is found that the vertical vibration tends to destabilize the thin liquid film, although for ultrasonic vibrations with low-amplitude, the term contributing to the perturbation growth rate decays rapidly with time and the film may remain stable. However, the vertical ultrasonic vibration is found as a significant destabilizing force, if the film thickness is near a critical value in which case the destabilizing van der Waals and stabilizing gravity and surface tension forces balance one another. To validate the model, experiments on thin liquid films of dilute polymeric solutions are performed. It is found that while imposing ultrasonic vibration may potentially destabilize and breakup the thin film, imposing a low-power vibration can significantly improve the homogeneity, electrical properties, and uniformity of the film, whereas a large-amplitude vibration may have a detrimental effect, because of excessive mixing and agitation of the liquid film or cracking of the resulting thin solid film.

1. Introduction

The field of thin liquid films and its associated phenomena, such as the formation of surface waves and patterns, wetting/dewetting and instability, is indeed one of the most fascinating areas of fluid mechanics with practical applications (Bonn et al., 2009; Craster and Matar, 2009; Oron et al., 1997). The application of thin liquid films is now extended to emerging solution-processed thin film devices, such as polymer and perovskite thin film solar cells, transistors, sensors, and displays, which incorporate functional thin and ultrathin solid films. The layers of such devices are usually deposited using a casting method to form thin or ultrathin liquid films, which subsequently dry to form functional thin solid films (Eslamian, 2016). However, the common issue in solution-processed thin solid films is the occurrence of undesired phenomena, such as dewetting and pinhole formation, which arise during casting and drying of thin liquid films. At small thicknesses required for such applications, the intermolecular forces may contribute to instability of thin liquid films. In an effort to improve the intactness, uniformity and nanostructure of the solution-processed thin

solids films, Eslamian et al. (Zabihi and Eslamian, 2015; Wang and Eslamian, 2016) imposed ultrasonic vibration on thin films of dilute polymer solutions, where remarkable improvement was achieved in almost all characteristics of the resulting thin solid films, as well as in the performance of the solar cells incorporating such thin films (Eslamian and Zabihi, 2015; Xie et al., 2016; Zabihi et al., 2016). This improvement was rather surprising, given that it is known that the vertical vibration has a destabilizing effect on liquid films, albeit under certain conditions such as amplitudes larger than a critical value, on the basis of the Faraday's experiments (Faraday, 1831), also revisited by others in various liquid solutions from inviscid flows to non-Newtonian liquid solutions (Benjamin and Ursell, 1954; Edwards and Fauve, 1994; Miles and Henderson, 1990; Kumar, 1996, 1999; Kumar and Matar, 2002; Matar et al., 2004; Raynal et al., 1999; Sharma, 1993). Then, further experiments showed that indeed if the amplitude of the imposed vertical vibration is excessively large, the resulting thin solid film will be ruptured (Habibi et al., 2016). Others have also used ultrasonic vibration to improve the process or device performance, e.g. Kim et al., 2010; Diemer et al., 2013. Beside vertical

* Corresponding author.

E-mail addresses: Morteza.Eslamian@sjtu.edu.cn, Morteza.Eslamian@gmail.com (M. Eslamian).

<http://dx.doi.org/10.1016/j.ces.2016.11.006>

Received 15 August 2016; Received in revised form 2 November 2016; Accepted 3 November 2016

Available online 05 November 2016

0009-2509/ © 2016 Elsevier Ltd. All rights reserved.



Contents lists available at ScienceDirect

Materials Today Energy

journal homepage: www.journals.elsevier.com/materials-today-energy/

Enhancing efficiency of perovskite solar cells by reducing defects through imidazolium cation incorporation

Qin Wang^{a, b}, Francis Lin^a, Chu-Chen Chueh^a, Ting Zhao^a, Morteza Eslamian^b, Alex K.-Y. Jen^{a, c, d, *}

^a Department of Materials Science and Engineering, University of Washington, Seattle, WA, 98105, USA

^b University of Michigan–Shanghai Jiao Tong University Joint Institute, Shanghai, 200240, China

^c Department of Chemistry, City University of Hong Kong, Kowloon, Hong Kong

^d Department of Materials Science & Engineering, City University of Hong Kong, Kowloon, Hong Kong

ARTICLE INFO

Article history:

Received 18 July 2017

Received in revised form

3 September 2017

Accepted 10 September 2017

Available online xxx

Keywords:

Imidazolium cation

Perovskite solar cells

Defect passivation

Photovoltaic performance

Tolerance factor

ABSTRACT

Regarding the polycrystalline nature of the solution-processed organic/inorganic hybrid perovskite (ABX₃) thin films, how to enhance the crystallinity of the prepared perovskite films has become the most critical issue for realizing high-performance perovskite solar cells. Recently, A-site cation engineering has been reported to effectively modulate the perovskite crystallization. Nevertheless, owing to the limited tolerance space of three-dimensional (3D) perovskite, the suitable A-site cations are extremely restrained to methylammonium (MA), formamidinium (FA), or Cesium (Cs) cations. We herein described a new A-site cation engineering for CH₃NH₃PbI₃ by utilizing imidazolium (IA) cation that affords a tolerance factor of 1 to modulate the perovskite crystallization. The mixed MA_{0.95}IA_{0.05}PbI₃ film was revealed to possess an improved film quality and crystallinity as compared to the pristine MAPbI₃ film, which thereby enables a much increased carrier lifetime as a result of the reduced defect density. Consequently, its derived solar cell device yields both enhanced efficiency (17%) and stability, outperforming the control MAPbI₃ device showing an inferior efficiency of 15.7%.

© 2017 Published by Elsevier Ltd.

1. Introduction

The current state-of-the-art perovskite solar cell (PVSC) has reached a certified power conversion efficiency (PCE) of 22.1%, rivaling the commercialized silicon solar cells [1]. Such high PCE is enabled by the exceptional semiconducting properties of organic/inorganic hybrid perovskite materials, which can effectively generate photo-excited carriers for extraction at room temperature. Generally, the prototype metal halide perovskite has a formula of ABX₃, where A is monovalent cation [methylammonium (MA), formamidinium (FA), or cesium (Cs)], B is a divalent metal cation (Pb²⁺ or Sn²⁺), and X is halide anion (Cl[−], Br[−], or I[−]). In principle, the A cation not only acts as an essential role responsible for neutralizing the electrons but also influences the symmetry of perovskite lattice and associated phase transformation, while both B⁺ and X[−] ions constitute the electronic band structures of derived

perovskites and primarily govern their resultant electronic structures [2,3].

It has been well documented that the most critical issue in developing high-performance PVSCs is rooted in the effective suppression of defect density of the fabricated perovskite films [4]. The simple solution-based deposition techniques inevitably engender the polycrystalline nature of the prepared perovskite films, for which concomitant crystallographic defects and structural disorder [5] will be thus formed to incur severe charge recombination and deteriorate the resulting device performance [4,6]. As considering the influence of perovskite composition in relation to the derived lattice and overall crystallinity, it is therefore feasible to engineer perovskite composition to improve the film quality and resulting opto-physical properties for further device optimization.

Lately, A-site cation engineering of the 3D CH₃NH₃PbI₃ regime has been vigorously investigated to ameliorate the device performance since this modulation imposes the minimal impacts on its pristine superior semiconducting properties [7]. Fundamentally, the adaptability of an A-site cation for a 3D perovskite structure can

* Corresponding author. Department of Materials Science and Engineering, University of Washington, Seattle, WA, 98105, USA.
E-mail address: ajen@uw.edu (A.K.-Y. Jen).

<http://dx.doi.org/10.1016/j.mtener.2017.09.007>
2468-6069/© 2017 Published by Elsevier Ltd.

Low-cost transparent graphene electrodes made by ultrasonic substrate vibration-assisted spray coating (SVASC) for thin film devices

Fatemeh Zabihi¹ · Morteza Eslamian¹ 

Received: 12 January 2017 / Revised: 6 February 2017 / Accepted: 17 February 2017 / Published online: 2 March 2017
© Springer International Publishing Switzerland 2017

Abstract In an attempt to replace expensive and rigid transparent conductive oxides, used as electrodes in thin film devices, in this study, transparent graphene electrodes (TGEs) are fabricated by conventional spray coating and ultrasonic substrate vibration-assisted spray coating. Systematic characterizations of the TGEs and indium tin oxide (ITO) demonstrate comparable and even better surface and morphological characteristics, film coverage, surface potential distribution and suitable work function of the spray-on TGEs compared to those of the reference ITO electrode. A lower transmittance, electrical conductivity and charge quenching potential are observed in the TGEs compared to those of the reference ITO, which may be further improved by process optimization. As a proof of concept, the TGE was incorporated into a perovskite solar cell, where power conversion efficiency of 3.54% was achieved, which is promising given that the developed graphene electrode was fabricated using scalable and low-cost spray coating.

Keywords Transparent graphene electrode · Perovskite solar cells · Spray coating · ITO-free solar cells · Ultrasonic substrate vibration · Large scale

Electronic supplementary material The online version of this article (doi:10.1007/s41127-017-0003-8) contains supplementary material, which is available to authorized users.

✉ Morteza Eslamian
Morteza.Eslamian@sjtu.edu.cn;
Morteza.Eslamian@gmail.com

¹ University of Michigan-Shanghai Jiao Tong University Joint Institute, 800 Dongchuan Road, Minhang, Shanghai 200240, China

1 Introduction

In both inorganic and organic thin film solar cells (SCs) and photonic-based thin film devices, one of the electrodes has to be transparent, usually a thin film of a transparent conductive oxide (TCO), to allow for transmission of sunlight into the device. The material used for TCO is usually indium-doped thin oxide (ITO) or fluorine-doped thin oxide (FTO), sputtered on glass substrates [1, 2]. However, the high materials and fabrication costs, limited resources of the constituting elements such as indium, and the rigid and rough nature of TCO electrodes hinder the low-cost and sustainable development of thin film devices that need transparent electrodes [3]. Beside the high cost and rigidity, undesired chemical reactions between TCO and adjacent layers may cause additional complications [4, 5].

Emerging conducting polymers, such as poly(3,4-ethylenedioxythiophene) polystyrene sulfonate (PEDOT:PSS), usually doped with nanoparticles or graphene, are alternatives to TCO electrodes [6]. Another feasible option to replace TCO electrodes is to employ carbon-based materials, such as carbon nanotubes and graphene, because of their suitable and tunable band energies, acceptable transparency, high electrical conductivity, chemical stability, solution processability and flexibility. Thus, this work focuses on the application of spray coating, as a scalable method, to fabricate transparent graphene electrodes (TGEs). Graphene nanosheets dispersed in proper solvents may be readily sprayed, in contrast to carbon nanotubes, which may cause clogging of the spray nozzle, because of their large aspect ratios [7].

TGEs have been implemented in a variety of solar cells and other thin film devices, such as amorphous silicon SCs, e.g., [8], quantum-dot SCs, e.g., [9], dye-sensitized SCs,

Self-Healing Shape Memory PUPCL Copolymer with High Cycle Life

Hafeez Ur Rehman, Yujie Chen,* Mikael S. Hedenqvist, Hua Li, Wenchao Xue, Yunlong Guo, Yiping Guo, Huanan Duan, and Hezhou Liu*

New polyurethane-based polycaprolactone copolymer networks, with shape recovery properties, are presented here. Once deformed at ambient temperature, they show 100% shape fixation until heated above the melting point, where they recover the initial shape within 22 s. In contrast to current shape memory materials, the new materials do not require deformation at elevated temperature. The stable polymer structure of polyurethane yields a copolymer network that has strength of 10 MPa with an elongation at break of 35%. The copolymer networks are self-healing at a slightly elevated temperature (70 °C) without any external force, which is required for existing self-healing materials. This allows for the new materials to have a long life of repeated healing cycles. The presented copolymers show features that are promising for applications as temperature sensors and activating elements.

1. Introduction

Stimuli-sensitive materials have received a great interest in the scientific community for applications ranging from microactuators in micro-electromechanical systems,^[1] and light weight structures in space to biomedical applications such as intelligent medical devices or controlled drug delivery systems in human daily life. Shape memory alloys, shape memory polymers (SMPs), and their composites are group of promising materials that have the ability to undergo stable predefine shape shifts and perform controllable activation to recover their original shape.^[2] SMPs based implants materials can be inserted in compact shapes in ergonomic products like shape memory fab-

rics, Simply Immaculate suits (SI suits), ergonomic computer input devices,^[3] biomedical devices like clit removal devices, catheters, programmable sutures^[4] and actuators like McKibbin type pneumatic actuators, artificial muscles actuators, and morphing air craft.^[5] Increasing applications demand SMP materials having abilities to maintain stabilized deformed shapes and perform work against external load upon shape recovery.^[6] This leads toward multifunctional SMP materials which combine shape memory capability, load bearing ability, and biodegradability that can reduce cost in space and aircraft industry and avoid explantation of device in human body as a 2nd surgery.^[2,7]

Thermosensitive SMPs are polymers obtained through programming process in which polymer is deformed and fixed in secondary shape that remains unchanged until heat is applied resulting in recovery of original shape. For the programming process heat–deformation–cooling cycle is employed, where deformation is performed above T_{trans} (transition temperature) of SMPs switching segments and fixation of temporary shape is achieved by cooling to temperature below T_{trans} , while holding the material under the same deformation stress. Finally reheating the materials above responsive temperature actuates materials, which results in shape memory effect.^[2,8] This programming cycle of heat–deformation–cooling can be repeated several times. In order to offer shape memory behavior, polymers must present permanent domains formed by chemically cross-linked structures and switching domains to response to external stimulus. The most widely used stimulus is temperature, which impacts dependents on the actual amorphous or crystalline nature of the switching phase. Here the transition temperatures are the glass transition temperature and/or the melting temperature.^[9]

To date numerous SMPs based on various structures have been developed, including polyurethanes (PUs), polycaprolactone (PCL), polystyrene copolymers, and epoxy based polymers. Among these, self-healable thermal induced shape memory PUs have been used mostly in practice. Because of their competitive mechanical and shape memory properties, they exhibit high specific strength, high degrees of shape fixation, self-healing, and shape recovery, with a transition temperature that can be tuned approximately to human body temperature. Shape memory polyurethanes (SMPUs) are segmented polymers of hard and soft segments. Hard

H. Ur Rehman, Dr. Y. Chen, W. Xue, Prof. Y. Guo, Prof. Y. Guo, Dr. H. Duan
State Key Laboratory of Metal Matrix Composites
School of Material Science and Engineering
Shanghai Jiao Tong University
Shanghai 200240, P. R. China
E-mail: yujiechen@sjtu.edu.cn

Prof. M. S. Hedenqvist
KTH Royal Institute of Technology
School of Chemical Science and Engineering
Fibre and Polymer Technology
SE-100, 44 Stockholm, Sweden

Prof. H. Li, Prof. H. Liu
Collaborative Innovation Center for Advanced Ship and Deep-Sea Exploration
Shanghai Jiao Tong University
Shanghai 200240, P. R. China
E-mail: hzhliu@sjtu.edu.cn

DOI: 10.1002/adfm.201704109



Short Communication: Material Behaviour

Features of structural relaxation in diblock copolymers



Mingchao Ma^{a, b}, Tianju Xue^{a, b}, Shenyue Chen^{a, b}, Yunlong Guo^{a, b, c, *}, Yujie Chen^{b, c},
Hezhou Liu^{b, c}

^a The State Key Lab of Metal Matrix Composites, Shanghai Jiao Tong University, Shanghai 200240, China

^b University of Michigan – Shanghai Jiao Tong University Joint Institute, Shanghai Jiao Tong University, Shanghai 200240, China

^c School of Materials Science and Engineering, Shanghai Jiao Tong University, Shanghai 200240, China

ARTICLE INFO

Article history:

Received 8 November 2016

Received in revised form

17 February 2017

Accepted 27 February 2017

Available online 1 March 2017

Keywords:

Structural relaxation

Diblock copolymers

Enthalpy recovery

Calorimetry

ABSTRACT

Time- and temperature-dependent structural relaxation (physical aging) of poly (styrene-*b*-methyl methacrylate) (PS-*b*-PMMA) block copolymers was investigated by calorimetry. Our study reveals the interplay of the relaxation responses of the two components of the copolymer in an intermediate temperature regime. That is, when the testing temperature is closely below the glass transition temperatures of PS and PMMA, structural relaxation in these polymer phases takes place concurrently, the corresponding thermogram displays partially superposed dual endothermic peaks as a feature of physical aging in the diblock copolymers. The aging response for each component is identified from a curve fitting method and analyzed by the relaxation of enthalpy. Comparing with the homopolymer analogs, the PS and PMMA in diblock copolymers show enhanced aging rate.

© 2017 Elsevier Ltd. All rights reserved.

1. Introduction

Block copolymers usually serve as templates and scaffolds in fabrication of patterned or hierarchical structures down to nanometer scale, so that design and self-assembly of structures from copolymers by phase separation have received vast research interests in last two decades [1–6]. Many procedures to create complicated architectures ranging from uniform ordered planar nanostructures [7] to three-dimensional hierarchical structures [8] have been developed. While the smart design and processing utilizing copolymers have attracted a great deal of attention, the naturally time-dependent instability of the material, including physical aging which affects the physical properties of the chemically immiscible blocks, especially how the properties evolve in the relaxation process, and how they interact each other during aging, remain to be elucidated.

Below the glass transition temperature (T_g), polymeric materials often fall into non-equilibrium state, the conformation of disordered molecules alter with time, toward a lower position in the potential energy landscape. This evolution process is referred to as structural relaxation, or physical aging [9,10]. Many physical

properties of polymers such as specific volume, mechanical moduli, gas permeability, and thermal conductivity change concurrently in the process of physical aging.

Physical aging is of highly technological importance, however, to the best of our knowledge, structural relaxation of copolymers has not been systematically investigated, although a lot of research effort exists for homopolymers [9,11–13]. To date the majority of literature related to physical aging of copolymers focuses on particular engineering properties of the material, for instance, a few studies reported the influence of processing on mechanical behavior [14–16] or free volume change [17] in copolymers during aging, and several others examined the physical aging of blends of homopolymer and copolymer, regarding dynamic mechanical response or mechanical strength and elasticity [18,19]. Lack of fundamental understanding and systematic characterization of physical aging of copolymers would bottleneck applications of the material in the aforesaid emerging fields.

Experimentally, due to its high sensitivity and low amount need of materials, thermal analysis is a routine means to characterize aging response from enthalpy recovery, and it has been widely applied to capture aging effect of homopolymers [13]. In contrast, for copolymers, this method has not been adequately exploited to describe structural relaxation of the materials [20].

We systematically investigated the structural relaxation of copolymers using a differential scanning calorimeter (DSC). Here we

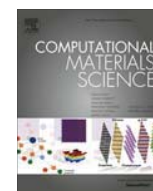
* Corresponding author. The State Key Lab of Metal Matrix Composites, Shanghai Jiao Tong University, Shanghai 200240, China.

E-mail address: yunlong.guo@sjtu.edu.cn (Y. Guo).



Contents lists available at ScienceDirect

Computational Materials Science

journal homepage: www.elsevier.com/locate/commatsci

Formation of iron hydride in α -Fe under dislocation strain field and its effect on dislocation interaction

Yanguang Cui^{a,b}, Dongyue Xie^a, Ping Yu^a, Yunlong Guo^b, Yonghua Rong^a, Guozhen Zhu^{a,*}, Mao Wen^a^a State Key Laboratory of Metal Matrix Composites, School of Material Science & Engineering, Shanghai Jiaotong University, Dongchuan Road 800, Shanghai 200240, China^b UM-SJTU Joint Institute, Shanghai Jiaotong University, Dongchuan Road 800, Shanghai 200240, China

ARTICLE INFO

Article history:

Received 7 March 2017

Received in revised form 23 August 2017

Accepted 18 September 2017

Available online 5 October 2017

Keywords:

Hydrogen embrittlement

Iron hydride

Dissociation of dislocation

Monte Carlo simulation

ABSTRACT

Atomistic simulation of hydride formation under dislocation strain field piled up at inclusions in α -Fe was performed using a new Finnis–Sinclair-type embedded atom method potential. Two $1/2 [111] (10\bar{1})$ edge dislocations were introduced in BCC α -Fe to study the effects of dislocation interaction on the formation of hydride. Our simulation demonstrated that the interaction of dislocation-inclusion could produce ultrahigh stress that resulted in the formation of iron hydride. In addition, the dissociation of one of the two $1/2 [111]$ edge dislocations into $[001] + 1/2 [11\bar{1}]$ two perfect dislocations can occur under a large applied shear (5%) or smaller shear (0.5%) when a hydride plate forms, despite the dissociation not satisfying the energy condition of dislocation reaction. The $[001]$ perfect dislocation is usually considered the origin of cleavage on $\{100\}$ planes, which is not stable without large applied load or hydrogen. In our model, the densities of both dislocation and inclusion on the glide plane could be changed to correspond to the dislocation density and inclusion (carbide) density in real martensitic steels. The results indicated that low dislocation density and small size of inclusions could prevent the formation of hydride. From these findings, tempering was suggested as a measure of preventing hydrogen embrittlement because proper tempering can effectively reduce the residual stress caused by quenching, precipitate dispersive and fine carbides (inclusion) and, in addition, decrease dislocation density in quenching and tempering martensitic steels.

© 2017 Elsevier B.V. All rights reserved.

1. Introduction

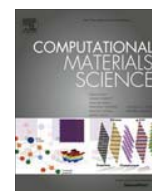
Hydrogen embrittlement (HE), which usually results in a catastrophic failure of various metals, has received considerable attention for over a century [1]. In particular, in steels, the HE sensitivity increases with the increase in strength [2,3]. Therefore, the growing market for high-strength steels strongly demands techniques for preventing HE in steels. Understanding the HE mechanism is a prerequisite for this goal. So far, several HE mechanisms have been proposed and are categorized as follows: (1) hydride formation and cleavage [4,5], (2) hydrogen-enhanced decohesion [6], and (3) hydrogen-enhanced local plasticity (HELP) [7,8]. Hydride formation is seldom considered the leading mechanism of HE in steels because iron hydride is unstable at normal pressure, and thus, no hydride was experimentally detected in their fracture microstructure [9]. HELP is usually considered the most important mechanism of HE in steels because the fracture surface of hydrogen-embrittled specimen is plastic in nature [10],

and dislocation multiplication is always observed in grains of subfracture surface [11]. Sofronis proposed the hydrogen shielding effect on the basis of hydrogen-induced volume and elastic moduli changes [12]. In-situ observation of dislocations in the environment by using a transmission electron microscope revealed that higher dislocation piling-up density and mobility in the presence of hydrogen support Sofronis' theory and HELP mechanism. However, the results of atomistic simulation conflicted with both hydrogen-enhanced dislocation mobility and hydrogen shielding effect [13].

Hirth calculated the Fermi–Dirac atmosphere of hydrogen at a stressed crack tip in Fe and showed that the saturation occurs at room temperature [14,15], indicating the probability of formation of iron hydride. As is well known, the high strength of steels results from the high densities of dislocations and carbides in the iron matrix. It can be assumed that the saturation of hydrogen or even the formation of hydride may occur within the strain field in the surrounding of dislocations and carbides in high-strength steels, and such a phenomenon may lead to the catastrophic performance of the material. However, little attention has been focused on this issue. It remains a great challenge to resolve the site occupation of

* Corresponding author.

E-mail address: zhugz@sjtu.edu.cn (G. Zhu).



Origin of the modulus anomaly over a wide temperature range of $\text{Mn}_{0.70}\text{Fe}_{0.25}\text{Cu}_{0.05}$ alloy



Yanguang Cui^a, Yunlong Guo^a, Yangxin Li^b, Jianfeng Wan^{b,*}, Jihua Zhang^b, Yonghua Rong^b, Nailu Chen^b, Dong Wang^c, Yunzhi Wang^d

^a UM-SJTU Joint Institute, Shanghai Jiaotong University, Dongchuan Road 800, Shanghai 200240, China

^b School of Material Science & Engineering, Shanghai JiaoTong University, Shanghai 200240, China

^c Center for Computational Study of Microstructure Evolution in Materials and Multi-Disciplinary Materials Research Center, Frontier Institute of Science and Technology, State Key Laboratory for Mechanical Behavior of Materials, Xi'an Jiaotong University, Xi'an 710049, China

^d Department of Materials Science and Engineering, The Ohio State University, 2041 College Road, Columbus, OH 43210, USA

ARTICLE INFO

Article history:

Received 28 June 2017

Received in revised form 23 August 2017

Accepted 24 August 2017

Available online 15 September 2017

Keywords:

Modulus anomaly

Antiferromagnetic transition

Phase-field method

ABSTRACT

To reveal the origin of modulus anomaly over a wide temperature range (about 240 K) observed in $\text{Mn}_{0.70}\text{Fe}_{0.25}\text{Cu}_{0.05}$ alloy, a phase-field model considering antiferromagnetic (AF) transition with doping Fe was established, in which the average modulus is considered as a functional of order parameter. Simulation reveals that the pinning effect by doping Fe leads to the increase of low spin non-collinear AF domain walls (LS), meanwhile, the LS domain walls gradually evolve to high spin collinear AF domains (HS) with lowering temperature, accompanying the growth of HS domains and the decrease of modulus, and vice versa. Such a dynamic antiferromagnetic domain size (DAFDZ) effect gives rise to modulus anomaly, while the proper volume ratio of LS and HS is a crucial factor for the wide temperature range of modulus anomaly.

© 2017 Elsevier B.V. All rights reserved.

1. Introduction

Since discovery of Invar and Elinvar alloys by Guillaume, who was awarded the Nobel Prize of Physics in 1920 [1], physical properties of materials with abnormal temperature dependence have stimulated extensive experimental and theoretical studies for more than a century [2–10]. A lot of models have been suggested. Amongst these models, the 2γ -state model considering coexistence of two spin states is the most promising one, whose key idea was proposed by Weiss in 1963 [2]. In the theory, there are two possible states for FCC γ -Fe: the ferromagnetic high volume state and the antiferromagnetic low volume state. Thermal excitations between these two states are supposed to compensate for the usual lattice expansion related to anharmonic effects of the lattice vibrations. In the following decades, further development on various magnetic theories and models has been accelerating the step of research. Endoh and Ishikawa [11] proposed two spin structures in antiferromagnetic γ -FeMn alloy: collinear spin structure and non-collinear spin structure and roughly determined the Mn content range corresponding to the exchange of two spin structures.

Besides, two antiferromagnetic (AF) states mentioned above existing in Mn-Ni alloys were reported [12,13]. Meanwhile, elastic modulus anomaly with wide temperature range was observed in these alloys [14]. In 1999, Schilfsgaarde et al. presented *ab initio* calculations of the volume dependences of magnetic and thermodynamic properties for the most typical Invar system, in which non-collinear (canted) spin alignments lead to an anomalous volume dependence of the binding energy [6]. It is worthy to point out that non-collinear (canted) spin structure can have various spin directions and magnitude, which is different from non-collinear structure and unique spin state proposed by Endoh and Ishikawa [11]. Owing to the limited capability of *ab initio* calculations on larger scale, compositional fluctuation has not yet been considered in models reported. Although Elinvar effect was discovered in Invar alloy with doping 12Cr by Guillaume a century ago, the origin of modulus anomaly as a base of Elinvar effect has not been clarified from the viewpoint of magnetism, even though it has long been realized that the Elinvar effect is related to magnetism like Invar effect. Recently, a mechanism being independent magnetism was proposed by Cui and Ren [15], and they observed the Elinvar effect in Co-doped TiNi strain glass alloys and proposed the origin of Elinvar effect resulting from the coupling of dynamic size effect and size dependence of elastic modulus, in which strain glass transition between the critical temperature (T_{nd}) and glass temperature (T_g)

* Corresponding author.

E-mail addresses: jfwan0909@hotmail.com, jfwan@sjtu.edu.cn (J. Wan).

<http://dx.doi.org/10.1016/j.commatsci.2017.08.040>

0927-0256/© 2017 Elsevier B.V. All rights reserved.

Spatially Distributed Rheological Properties in Confined Polymers by Noncontact Shear

Mithun Chowdhury,^{†,⊥} Yunlong Guo,^{†,§,⊥} Yucheng Wang,[†] Weston L. Merling,^{||} Jayachandra H. Mangalala,^{||} David S. Simmons,^{*,||} and Rodney D. Priestley^{*,†,⊥}

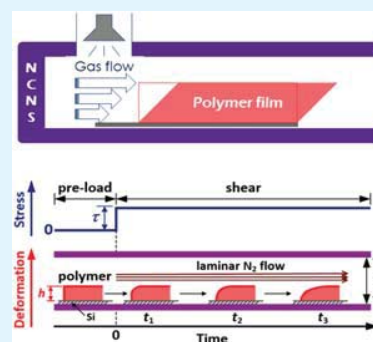
[†]Department of Chemical and Biological Engineering and [‡]Princeton Institute for the Science and Technology of Materials, Princeton University, Princeton, New Jersey 08544, United States

[§]University of Michigan – Shanghai Jiao Tong University Joint Institute, Shanghai Jiao Tong University, Shanghai 200240, P. R. China

^{||}Department of Polymer Engineering, University of Akron, Akron, Ohio 44325, United States

S Supporting Information

ABSTRACT: When geometrically confined to the nanometer length scale, a condition in which a large portion of the material is in the nanoscale vicinity of interfaces, polymers can show astonishing changes in physical properties. In this investigation, we employ a unique noncontact capillary nanoshearing method to directly probe nanoresolved gradients in the rheological response of ultrathin polymer films as a function of temperature and stress. Results show that ultrathin polymer films, in response to an applied shear stress, exhibit a gradient in molecular mobility and viscosity that originates at the interfaces. We demonstrate, via molecular dynamics simulations, that these gradients in molecular mobility reflect gradients in the average segmental relaxation time and the glass-transition temperature.



The confinement of polymeric materials to the nanoscale has enabled the development of new materials^{1–3} and functional devices^{4,5} that impact a myriad of emerging technologies^{2–4} and challenge our fundamental understanding of materials' behavior.^{6–14} In geometrically confined polymers, as the confining dimension (e.g., thickness for thin films^{12,13,15–17} or interparticle spacing for nanocomposites^{8,14,18}) is reduced, an increasingly large portion of the polymeric material is in close proximity to an interface.⁶ The presence of supporting interfaces can affect the molecular mobility of polymers through the formation of nonequilibrium states,^{19–21} for instance, the formation of an irreversibly adsorbed polymer layer.^{6,22} In these confined states, in which interfacial effects can perturb mean structure and dynamics,^{6,9,16,17,19,21,23} astonishing changes in material properties have been reported, including in the glass-transition temperature (T_g),^{6,9,13,15,16,22,24–28} fracture toughness,¹⁰ viscosity,^{12,13,20,29–33} modulus,^{11,12,34,35} and compliance.³⁶ It has been shown that these interfacial effects can reflect a spatial gradient in T_g that correlates well with its size-dependent changes.^{15,17} A broader perspective on the origin of gradients in molecular mobility of confined polymers has been very recently addressed.⁶ However, it remains unclear whether shifts in T_g , diffusion, and viscosity are correlated in nanoconfined polymers.¹³ While several experiments have been designed to measure the viscoelastic properties of confined polymers,^{12,19,21,33,35–37} they have generally directly measured

only average properties, with spatial distributions indirectly inferred based on layer-model interpretations of average mechanical responses.^{13,30} While several techniques are capable of directly measuring viscoelastic properties at the free surface of confined polymers,^{12,37,38} direct depth-resolved analysis still remains a challenge. Direct access to spatially resolved rheological properties in confined polymers would provide fundamental insights into how interfaces and finite-size effects combine to modify viscoelastic functions,^{23,25,27} allow for the identification of correlations between spatially distributed properties,^{15,17} and aid in the development of novel processing routes to generate nanostructured polymers.²

It has been recognized for over a decade that there is an important “need to understand how the mechanical properties of matter are changed by the proximity of interfaces”.¹⁶ To enable a direct experimental probe of this issue, we introduce a noncontact capillary nanoshearing (NCNS) method that allows for the measurement of spatially resolved time-dependent viscoelastic functions of ultrathin polymer films supported atop a substrate. We focus our study on low-molecular-weight ($M_w = 2.5$ kDa) polystyrene (PS) because its average viscosity has been characterized in the thin-film geometry.^{30,31,33} We show that NCNS reports the depth-resolved thermoviscoelastic

Received: January 27, 2017

Accepted: February 21, 2017

Published: March 3, 2017



ACS Publications

© 2017 American Chemical Society

1229

DOI: 10.1021/acs.jpclett.7b00214
J. Phys. Chem. Lett. 2017, 8, 1229–1234

Enhancing the Photocatalytic Hydrogen Evolution Performance of a Metal/Semiconductor Catalyst through Modulation of the Schottky Barrier Height by Controlling the Orientation of the Interface

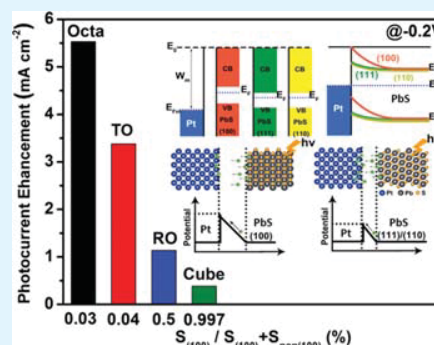
Yang Liu,^{†,§} Xin Gu,^{†,§} Wen Qi,^{†,‡} Hong Zhu,^{*,†,‡} Hao Shan,[†] Wenlong Chen,[†] Peng Tao,[†] Chengyi Song,[†] Wen Shang,[†] Tao Deng,^{*,†} and Jianbo Wu^{*,†,§}

[†]State Key Laboratory of Metal Matrix Composites, School of Materials Science and Engineering and [‡]University of Michigan–Shanghai Jiao Tong University Joint Institute, Shanghai Jiao Tong University, 800 Dongchuan Road, Shanghai 200240, P. R. China

§ Supporting Information

ABSTRACT: Construction of a metal–semiconductor heterojunction is a promising method to improve heterogeneous photocatalysis for various reactions. Although the structure and photocatalytic performance of such a catalyst system have been extensively studied, few reports have demonstrated the effect of interface orientation at the metal–semiconductor junction on junction-barrier bending and the electronic transport properties. Here, we construct a Pt/PbS heterojunction, in which Pt nanoparticles are used as highly active catalysts and PbS nanocrystals (NCs) with well-controlled shapes are used as light-harvesting supports. Experimental results show that the photoelectrocatalytic activities of the Pt/PbS catalyst are strongly dependent on the contacting facets of PbS at the junction. Pt/octahedral PbS NCs with exposed PbS(111) facets show the highest photoinduced enhancement of hydrogen evolution reaction activity, which is ~14.38 times higher than that of the ones with only PbS(100) facets (Pt/cubic PbS NCs). This enhancement can further be rationalized by the different energy barriers of the Pt/PbS Schottky junction due to the specific band structure and electron affinity, which is also confirmed by the calculations based on density functional theory. Therefore, controlling the contacting interfaces of a metal/semiconductor material may offer an effective approach to form the desired heterojunction for optimization of the catalytic performance.

KEYWORDS: photocatalysis, hydrogen evolution reaction, Schottky junction, energy bending, interface control



1. INTRODUCTION

With the rapid development of modern society, it is imperative to search for new energy sources to replace traditional energy sources, such as fossil, gas, and coal. Among all kinds of renewable energy, solar energy can be exploited as an alternative to meet the ever-increasing needs due to its cleanliness and sustainability. However, solar-light harvesting must be coupled with efficient energy-storage mechanisms to maintain a constant energy supply during periods of low sunlight irradiation or at night.¹ Hydrogen can be used as an excellent energy carrier to store solar energy through water splitting because it can be utilized as an economic fuel to supply electric power whenever needed. Developing an efficient catalyst for the photoelectrochemical hydrogen evolution reaction (HER) as a part of water splitting is the key to constructing such sustainable and clean solar energy conversion systems.

It is well known that the most effective and widely used electrocatalytic HER catalysts are platinum (Pt) and Pt-based alloys, which facilitate HERs at low overpotentials to generate large cathodic current densities in the highly acidic solutions

that are used for water electrolysis.² However, Pt-based HER catalysts are limited in their use for large-scale applications due to their scarcity and high cost. Many efforts have been devoted to developing earth-abundant, low-cost, and highly efficient HER catalysts through the development of bimetallic nanocrystals (NCs), with different structures and atomic distributions in the form of core-shells, alloys, and dendrites, by combining Pt with a secondary metal that is more abundant and/or less expensive, with an aim of overcoming the aforementioned limitations.^{3–13} Previous studies have shown that some transition metal sulfides of tungsten, cobalt, nickel, iron, etc. are catalytically active in the HER.¹⁴ Nonetheless, current studies are still not ready to be applied practically for hydrogen generation on a large scale.⁸ Recently, a few works have focused on replacing the carbon support with semiconductors to construct a metal–semiconductor heterojunction to utilize solar energy to improve the electrocatalysis.^{15,16} The

Received: January 29, 2017

Accepted: March 23, 2017

Published: March 23, 2017

ARTICLE OPEN

Effective mass and Fermi surface complexity factor from ab initio band structure calculations

Zachary M. Gibbs¹, Francesco Ricci², Guodong Li³, Hong Zhu⁴, Kristin Persson⁵, Gerbrand Ceder^{4,5}, Geoffroy Hautier², Anubhav Jain⁵ and G. Jeffrey Snyder³

The effective mass is a convenient descriptor of the electronic band structure used to characterize the density of states and electron transport based on a free electron model. While effective mass is an excellent first-order descriptor in real systems, the exact value can have several definitions, each of which describe a different aspect of electron transport. Here we use Boltzmann transport calculations applied to ab initio band structures to extract a density-of-states effective mass from the Seebeck Coefficient and an inertial mass from the electrical conductivity to characterize the band structure irrespective of the exact scattering mechanism. We identify a Fermi Surface Complexity Factor: $N_v^* K^*$ from the ratio of these two masses, which in simple cases depends on the number of Fermi surface pockets (N_v^*) and their anisotropy K^* , both of which are beneficial to high thermoelectric performance as exemplified by the high values found in PbTe. The Fermi Surface Complexity factor can be used in high-throughput search of promising thermoelectric materials.

npj Computational Materials (2017)3:8; doi:10.1038/s41524-017-0013-3

INTRODUCTION

The calculation of electronic band structures using density functional theory (DFT) is now so routine that it is becoming faster to compute certain physical properties than make samples and measure them—inspiring the materials genome initiative efforts worldwide. Ab initio calculations are important from a materials' design perspective in that they provide insight into the underlying electronic states that give rise to experimentally measurable properties. Dielectric, optical and transport properties such as electrical conductivity, Hall effect, and thermoelectric power (Seebeck effect) require knowledge not only of the electronic structure readily available from ab initio calculations, but may also require an assumption about the scattering. Using a constant relaxation time approximation, very precise predictions of transport properties that depend on fine details of the band structure can be made, however, the electrical conductivity predicted for instance can be greatly misleading because the relaxation time is approximated, often to an arbitrary constant. A recent study performed by the authors demonstrated that while Seebeck coefficient was reproduced fairly well across a variety of compounds (provided that the band gap was not severely underestimated), the experimental values on conductivities can be highly inaccurate using a constant relaxation time.¹ While some scattering mechanisms can now be calculated using ab initio methods, they are far from routine and require special algorithms. The goal of this study is to extract transport information from band structure calculations that does not depend on any scattering assumption.

In the common free-electron approximation lexicon of electronic and optical properties we typically describe charge carriers as having an effective mass m^* and a relaxation or scattering time τ . Combining with the density of carriers n , the electrical

conductivity $\sigma = ne^2\tau/m^*$ and drift mobility $\mu_d = e\tau/m^*$ can also be expressed. This description, while not exact, has proven immensely helpful in the understanding and engineering of electronic materials that have profoundly changed our civilization. This representation already separates transport into electronic structure (through the m^*) and scattering (τ) terms as well as allowing the flexibility of varying n (through doping, for example). It is, therefore, natural to expect that knowledge of electronic structure should reveal the appropriate effective mass for various values of n but not necessarily the scattering-dependent transport properties (such as σ and μ_d) until the scattering is known.

The free-electron description has been integral to semiconductor physics despite many examples of profound deviations. In the free-electron model the electronic structure is represented by a single, isotropic Fermi surface described by particle with mass and charge of an electron. A free-electron like description is only helpful to describe real semiconductors if we allow multiple (N_v) free-electron like pockets to describe the Fermi surface and that each pocket may be anisotropic (described by anisotropy term K) with effective mass m^* that differs from free-electron mass. Because of the multiple pockets the total density of electronic states will be N_v times that of a single pocket.

In thermoelectrics, for example, these and other material parameters are helpful to predict the promise of a material for use in a thermoelectric device.^{2–4} For typical semiconductor transport where the electrons are scattered by acoustic phonons (deformation potential scattering)⁵ the thermoelectric quality factor B , given by:

$$B = \frac{2k_B^2\hbar}{3\pi} \frac{N_v}{m_c^*} \frac{C_l}{\kappa_L} T \quad (1)$$

¹California Institute of Technology, Division of Chemistry and Chemical Engineering, Pasadena, CA, USA; ²Institute of Condensed Matter and Nanosciences (IMCN), Université catholique de Louvain, Chemin des étoiles 8, bte L7.03.01, Louvain-la-Neuve, Belgium; ³Department of Materials Science and Engineering, Northwestern University, 2220 Campus Drive, Evanston, IL, USA; ⁴Department of Materials Science and Engineering, Massachusetts Institute of Technology, 77 Massachusetts Avenue, Massachusetts, MA, USA and ⁵Lawrence Berkeley National Lab, 1 Cyclotron Road, Berkeley, CA, USA

Correspondence: G. Jeffrey Snyder (jeff.snyder@northwestern.edu)

Received: 30 October 2016 Revised: 13 January 2017 Accepted: 25 January 2017

Published online: 23 February 2017

6

Making the Case for Political Anthropology: Understanding and Addressing the Backlash Against Liberalism

Rockwell F. Clancy

6.1 Introduction

This chapter outlines the concept and contemporary importance of political anthropology, attempting to understand and address the backlash against inclusive liberal values on this basis. “Political anthropology” refers to an understanding of political activities and notions belonging to the political sphere—such as “justice,” “rights,” etc.—on the basis of philosophical anthropology, classically conceived in terms of conceptions of human nature. Although classic and modern thought has traditionally grounded its analyses of the political with reference

This chapter is based on the conceptual framework developed and materials included in R. Clancy, *Towards a Political Anthropology in the Work of Gilles Deleuze: Psychoanalysis and Anglo-American Literature*, Leuven, Leuven University Press, 2015 and “Civil religion as an antidote to political conservatism and religious fundamentalism? Navigating the course between inclusive universalism and exclusive particularism,” *Europeana*, forthcoming.

R.F. Clancy (✉)

University of Michigan-Shanghai Jiao Tong Joint Institute, Shanghai, China

© The Author(s) 2016

R. Winkler (eds.), *Identity and Difference*,

DOI 10.1007/978-3-319-40427-1_6

129

ORIGINAL ARTICLE

Using the Unified Theory of Acceptance and Use of Technology model to analyze cloud-based mHealth service for primary care

Fatema Khatun^{1,2*}, Md. Jahir U. Palas³, Pradeep K. Ray^{2,4}

¹Health Systems and Population Studies Division, International Centre for Diarrhoeal Disease Research, Bangladesh (icddr,b), Dhaka, Bangladesh, ²WHO Collaborating Centre on eHealth, The University of New South Wales, Kensington, NSW, Australia, ³Department of Banking and Insurance, Faculty of Business Studies, University of Dhaka, Dhaka, Bangladesh, ⁴Centre For Entrepreneurship, University of Michigan-Shanghai Jiao Tong University Joint Institute, China

ABSTRACT

Background and Objectives: Cloud-based mHealth services have the potential to make quality healthcare available in remote locations in the world. A practical deployment will involve medicolegal issues involving physicians and patients in different within and across countries. However, the first step is to evaluate such a cloud-based mHealth (MyOnlineClinic). This study aimed to understand and find out the factors that influence the end-user intention to use this new technology in Australia. **Materials and Methods:** We surveyed 167 end-users in 2015 and performed a Structural Equation Model analysis using Smart PLS to identify the intention to use the system among the participants. **Results:** The study revealed that the Unified Theory of Acceptance and Use of Technology construct, particularly facilitating condition (FC) ($\beta = 0.355$, $P = 0.002$), has yielded a significant influence on the behavioral intention to use MyOnlineClinic. However, the relationships between performance expectancy and behavioral intention ($\beta = 0.162$, $P = 0.141$), effort expectancy and behavioral intention ($\beta = -0.004$, $P = 0.971$), and social influences and behavioral intention ($\beta = 0.164$, $P = 0.100$) were insignificant. Further, age showed moderating effect on these variables. The majority of the respondents agreed or strongly agreed that technological issues such as sound (92.2%), video qualities (88.6%), and interaction with doctor (89.8%) are good. **Conclusion:** The end-users' intentions to use MyOnlineClinic system were particularly influenced by FCs such as hardware, software, and the information technology knowledge/familiarity of users. These factors may get further accentuated when these systems are deployed across countries with different languages, technological infrastructures, and medicolegal environments. Therefore, cloud-based mHealth would help in removing some barriers, such as differences in software versions and interoperability problems of systems at physician and patient ends.

Keywords: Cloud-based mHealth service, MyOnlineClinic, telehealth, Unified Theory of Acceptance and Use of Technology

INTRODUCTION

Worldwide telehealth has expanded and targeted to meet the

health-care needs for rural and remote habitants.^[1] Telehealth is important to leverage health-care gap when it is necessary and urgent.^[2-3] This new technology creates huge opportunity for both users and health-care service providers. In Australia, MyOnlineClinic, a telehealth services has been serving since 2015 as a pilot phase (<http://myonlineclinic.com.au>). Cloud-based mHealth (healthcare enabled by mobile phones) opens up a new dimension in the deployment of telehealth

*Address for correspondence:

Dr. Fatema Khatun, WHO Collaborating Centre on eHealth, The University of New South Wales Sydney, Kensington, NSW 2052, Australia and Health Systems and Population Studies Division, International Centre for Diarrhoeal Disease Research, Bangladesh (icddr,b), Dhaka 1212, Bangladesh.
E-mail: fkfatem@icddr.org

Access this article online	
Quick Response Code	Website: www.digitmedicine.com
	DOI: 10.4103/digm.digm_21_17

This is an open access article distributed under the terms of the Creative Commons Attribution-NonCommercial-ShareAlike 3.0 License, which allows others to remix, tweak, and build upon the work non-commercially, as long as the author is credited and the new creations are licensed under the identical terms.

For reprints contact: reprints@medknow.com

How to cite this article: Khatun F, Palas MU, Ray PK. Using the Unified Theory of Acceptance and Use of Technology model to analyze cloud-based mHealth service for primary care. Digit Med 2017;3:69-75.

A Systematic Literature Review of the Application of Information Communication Technology for Visually Impaired People

Md Mahfuz Ashraf,¹ Najmul Hasan,² Lundy Lewis,³ Md Rashadul Hasan,⁴ and Pradeep Ray⁵

¹ School of Public Health and Community Medicine, University of New South Wales, Australia,

² MRC Bangladesh Ltd, Dhaka, Bangladesh,

³ Southern New Hampshire University, United States of America,

⁴ Brainstorm Bangladesh Ltd, Dhaka, Bangladesh

⁵ WHO Collaborating Centre on e-Health, University of New South Wales, Australia

Technological advancement in general is providing better and cheaper solutions to assist the visually impaired (VI) community. Although information communication technology (ICT) has great potential to support the inclusion of VI people in educational, social and workforce settings, there are far fewer ICT projects for VI people compared to other projects. This systematic literature review provides our findings on the existing state of ICT projects and describes outstanding issues in ICT support of VI people. Based on our findings, we suggest increased collaboration among healthcare professionals, caregivers, programmers, engineers, as well as policy makers; and adoption of policies in future ICT projects for VI people. A wide search of seven journal databases found a relevant cross-section of articles that were published between 2010 and 2015. Software Zotero Standalone and EndNote were used to screen and maintain metadata. After the initial screening of 6993 titles, 683 abstracts were scrutinised, from which 55 full text articles were selected for final review. We analysed and synthesised 37 articles. Our findings show the progress, awareness, interest, and issues in ICT integration to improve the quality of life for VI people. Three emergent topics for VI people are (a) assistive technology, (b) e-accessibility, and (c) virtual interfaces. Our findings suggest that ICT-aided applications can bring positive changes for VI people. We advance several issues that should be addressed and further developed, collaboratively, to spread awareness and invoke new policies aimed to improve the quality of life of VI people.

Keywords: information communication technology (ICT), visually impaired (VI) people, systematic literature review, thematic analysis

According to the most recent survey by the World Health Organization (WHO), the number of visually impaired (VI) people in the world is 285 million, where approximately 39 million people are blind (Mariotti, 2012). Visual impairment includes both low vision and blindness (WHO, 2007). The majority of people with visual impairment (about 90%) live in developing countries and about 65% are aged 50 or above (Mothiravally, Ang, Baloch, Kulampallil, & Geetha, 2014). Only 14% to 20% of people in developed countries suffer from disabilities in general, and these people have greater opportunities to take advantage of ICT-aided tools (Hogan, Kyaw-Myint, Harris, & Denronden, 2012).

Numerous studies have been conducted focusing on people with disabilities from a sociological point of view. McAnaney and Williams (2010) suggest using action research methods for disability management. Hogan et al. (2012) contend that people with disabilities face significant inequity of remuneration, globally, due to the perception of a lack of skills and employment accommodations for particular roles. Niehaus and Marfels (2010) identify the key competencies of disabled people by using factor analysis and investigate the scope of their integration into the workforce and mainstream society. However, there are insufficient studies in the specific domain of ICT applications for VI people

Address for correspondence: Md Mahfuz Ashraf, Lecturer, School of Public Health and Community Medicine, University of New South Wales, Australia. E-mail: md.ashraf@unsw.edu.au

PoDMan: Policy Deviation Management

Aishwarya Bakshi

University of New South Wales

Amir Talaei-Khoei

University of Nevada, Reno

University of Technology Sydney

atalaeikhoei@unr.edu

Pradeep Ray

University of Michigan–Shanghai Jiao Tong University Joint Institute,

Shanghai Jiao Tong University, China

Terje Solvoll

Norwegian Centre for Integrated Care and Telemedicine

University Hospital of North Norway

Abstract

Whenever an unexpected or exceptional situation occurs, complying with the existing policies may not be possible. The main objective of this work is to assist individuals and organizations to decide in the process of deviating from policies and performing a non-complying action. The paper proposes utilizing software agents as supportive tools to provide the best non-complying action while deviating from policies. The article also introduces a process in which the decision on the choice of non-complying action can be made. The work is motivated by a real scenario observed in a hospital in Norway and demonstrated through the same settings.

Keywords: Agent; Policy; Deviation

1 Introduction

While policy based systems have largely been successful in controlling and managing cooperative work environments, one of its weaknesses lies in the fact that there is always the risk of exceptions, where following the policy rule might result in non-optimal outcomes and at worst lead to completely devastating consequences. Many studies have proposed the use of adaptive policies to counter the changing environmental circumstances, thereby reducing the risk of exception. As it is humanly not possible to envision all possible exceptions, there is a need to introduce procedures whereby the user is given the decision making support and flexibility to deviate from a policy when absolutely needed. While many decision support systems have been suggested for CSCW systems (Chau 2003, Benbasat 1990, Shum 2011), this paper aims to introduce a method which allows greater flexibility to CSCW systems by assisting in the decision making process of deviating from policies, making sure that the deviations take place in a controlled manner when such exceptions arise. In order to address the problem, the study proposes a methodology called PoDMan (Policy deviation management) which uses software agents to detect policy violations and if required, assist users in the decision making process of deviating from the policy in a controlled manner.

The rest of this paper is organized in the following way: Section 2 illustrates the motivation behind this work by providing a real scenario observed in the wireless communication system in a hospital in Norway. Section 3 presents background and defines different concepts being used in this research. Section 4 proposes the PoDMan methodology that consists of a framework of definitions and semantics as well as a stepwise process for policy deviation deployed in the framework. Section 5 demonstrates PoDMan through the wireless communication scenario introduced in Section 2. Section 6 presents a simulation for evaluating PoDMan. Section 7 concludes the study and discusses the implications and limitations of the work.

Financing Universal Health Coverage: A Systematic Review

Md. Jahir Uddin Palas

*Department of Banking and Insurance, University of Dhaka
Email: jahir@du.ac.bd*

Mahfuz Ashraf

School of Public Health and Community Medicine, University of New South Wales

Pradeep Kumar Ray

*Centre for Entrepreneurship, Joint Institute- University of Michigan-Shanghai Jiao Tong University (SJTU), China
School of Public Health and Community Medicine, University of New South Wales*

Abstract

Across the globe, a significant portion of the population lacks the essential healthcare services due to the rising cost of such services. To ensure healthcare for all, the idea of universal health coverage has evolved but affordability and equity of health services have become the major concerns in this regard. This paper presents a systematic review that offers a detailed picture of diverse issues of universal healthcare financing. Eight popular databases were thoroughly searched with appropriate keywords for finding relevant articles published within 1980 to 2016. After four constructive iterations with logical constraints, 24 articles were finally selected for finding significant research themes in universal healthcare finance arena. The characteristics of the studies were presented graphically from different aspects such as fields of publication, research approaches, geographic distribution etc. The themes, so found in the review, have been categorized into four broad themes with respective sub-themes. The broad themes were namely A) financing options for healthcare B) medical expenses C) inequality in healthcare finance, and D) development of healthcare finance. This systematic review analyzed the studies, discussed avenues, and concluded with gaps for future research in universal healthcare finance. The synthesis of multifarious concepts in the prevalent literature on financing universal healthcare offered profound insights of universal healthcare arena.

Keywords: Universal Health Coverage, Financing Healthcare, Systematic Review, Health Service Costs, Financial Policy Design for Healthcare

1. Introduction

Declaration of health as a fundamental human right in World Health Organization's (WHO) constitution of 1948 and the agenda of Health for All by Alma-Ata declaration of 1978 were instrumental behind universal health coverage. Equity in healthcare has been marked as the prime element in marking healthcare progress within different groups of a nation and across the national population [1]; [2]. While tracking the progress of universal healthcare coverage, World Health Organization (WHO) conducted a survey in 37 countries and published a report within the time frame of 2002 and 2012 which has been the first of its kind. According to the report published by World Bank and WHO, about 400 million

people do not have access to essential health services around the globe [3]. From clean water to pregnancy care, these people lack proper access to one out of seven important health services, in the least severe case [3]. Although the number of people getting into the healthcare coverage is increasing, the coverage gap is also ever enhancing among world population [4]; [5]. The incidence of catastrophic health spending has been quite alarming as about 2 percent of the surveyed population experienced such catastrophic expenditure, which exceeded the 25% of their household expenditures [3]. Due to unaffordable healthcare costs, a significant portion (6%) of the population has fallen below the extreme poverty line (\$1.25 per day) and the percentage

Original Paper

Tablet-Based Well-Being Check for the Elderly: Development and Evaluation of Usability and Acceptability

Pradeep Ray^{1,2*}, PhD; Junhua Li^{3*}, PhD; Arni Ariani², PhD; Vasvi Kapadia², MPH

¹Centre For Entrepreneurship, University of Michigan Joint Institute, Shanghai Jiao Tong University, Shanghai, China

²WHO Collaborating Centre on eHealth, School of Public Health and Community Medicine, UNSW (University of New South Wales), Sydney, Australia

³Hammondcare, Sydney, Australia

*these authors contributed equally

Corresponding Author:

Pradeep Ray, PhD

Centre For Entrepreneurship

University of Michigan Joint Institute

Shanghai Jiao Tong University

800 Dong Chuan Road Minghang District

Shanghai,

China

Phone: 86 18616734596

Fax: 86 21 34206045

Email: p.ray@unsw.edu.au

Abstract

Background: Many elderly people prefer to live at home independently. One of the major concerns raised by the family members is the safety and well-being of their elderly family members when living independently in a home environment. To address this issue, assistive technology solutions have been available in the market. Despite their availability and proliferation, these types of solutions are not popular with the elderly due to their intrusive nature, privacy-related issues, social stigma, and fear of losing human interaction. This study shares the experience in the development of a digital photo frame system that helps family members to check the well-being of the elderly, exploiting their desire to remain socially connected.

Objectives: The aim of this study was to iteratively design, implement, and assess the usability, user friendliness, and acceptability of a tablet-based system to check the well-being of the elderly.

Methods: Our study methodology comprises three separate stages: initial system development, contextual assessment, and comparative case study evaluation.

Results: In the first stage, requirements were elicited from the elderly to design a well-being check prototype. In the second stage, areas for improvements (eg, privacy features) were identified. Also, additional features (such as medication prompts or food reminders) were suggested to help aged and health care service providers with effective but subtle monitoring of the elderly. These would lower their operating cost by reducing visits by care providers to the homes of the elderly. In the third stage, the results highlighted the difference (between users in India and Australia) in the levels of familiarity of the elderly with this technology. Some elderly participants at the Kalyani Institute for Study, Planning and Action for Rural Change, India latched onto this technology quickly while a few refused to use the system. However, in all cases, the support of family members was crucial for their willingness to use the technology.

Conclusions: This project has three major outcomes. First, a picture frame prototype was tested with the elderly to leverage the benefits of social communication. Second, the project helped us test and implement the “Silvercare” model for supporting the elderly through young retired people residing in the area. Finally, the project helped formalize the agile three-stage design methodology to develop information technology solutions for the elderly. Also, the project contributed to an ongoing European Union Project called Victoryahome, which involves more than 50 sites across 5 countries (Norway, Sweden, Netherlands, Portugal, and Australia) to assess the use of telepresence robots, wearable fall detectors, and medication dispensers for the elderly living independently.

(JMIR Hum Factors 2017;4(2):e12) doi:[10.2196/humanfactors.7240](https://doi.org/10.2196/humanfactors.7240)

Social business as an entrepreneurship model in emerging economy

Systematic review and case study

Md Mahfuz Ashraf, Mohammed Abdur Razzaque and
Siaw-Teng Liaw

UNSW (University of New South Wales) Sydney, Australia

Pradeep Kumar Ray

*University of Michigan, Ann Arbor, Michigan, USA and
Shanghai Jiao Tong University (SJTU), Shanghai, China, and*

Md Rashadul Hasan

Brainstorm Bangladesh, Dhaka, Bangladesh

Social business
in emergin
economy

Received 19 April 2017
Revised 15 September 2017
8 November 2017
Accepted 16 November 2017

Abstract

Purpose – Despite its immense potentials as a sustainable and innovative means to solve specific social problems, the basic concept of the social business model (SBM) advanced by Professor Muhammad Yunus remains unclear to many. There exists no literature that objectively compares this model from empowerment and economic growth perspectives with other seemingly similar concepts, such as social enterprise, non-governmental organization (NGO) and corporate social responsibility. Although many NGOs have been showing increasing interest towards the adoption of the SBM to minimize social problems sustainably, lack of conceptual clarity of the model limits the scope of its adoption in addressing social issues. The paper aims to discuss these issues.

Design/methodology/approach – This study is based on a systematic search, analysis and review of literature. It has made use of narrative synthesis of relevant literature on a diverse range of socially oriented models, frameworks and interventions.

Findings – This study identified five key aspects of social business, namely: business's mission and outcomes, characteristics, operation, resource utilization and environmental considerations. Based on these five key aspects one may like to infer that unlike other social interventions, the alignment of SBM is specific to empowerment of disadvantaged people leading to sustainable economic growth. Analyzing a range of social business interventions in a developing country, Bangladesh, through the lens five key aspects demonstrates that social business is the most efficient way to sustainably maximize the social benefits and minimize specific social issues poverty of the people affected.

Originality/value – This study discusses the scopes of adopting SBM for the socially responsible organizations for sustainable empowerment and economic growth in emerging economies.

Keywords Social enterprise, Entrepreneurship, Corporate social responsibility (CSR), Non-governmental organization, Emerging economy, Muhammad Yunus, Social business

Paper type Literature review

Background

A major limitation of the business enterprises in the market economy is that they are not intended to solve social problems; they may actually worsen the issues of poverty, pollution, corruption, and inequality (Yunus, 2007). Even in the USA, the most industrially advanced nation of the world, the number of people living in poverty has increased in the last two decades; level of social deprivation and inequality there is rather unsatisfactory. While social issues are not the concerns of traditional businesses, it is the government that is primarily held responsible to represent the interests of society



Management Decision
© Emerald Publishing Limited
0025-1747
DOI 10.1108/MD-04-2017-0343

Simulated Kinetics and Chemical and Physical Properties of a Four-Component Diesel Surrogate Fuel

Qiaoling Wang and C. P. Chen*

University of Michigan–Shanghai Jiao Tong University Joint Institute, Shanghai Jiao Tong University, Shanghai 200240, People's Republic of China

ABSTRACT: Real diesel fuels are mixtures composed of hundreds to thousands of components; thus, developing surrogate fuels composed of a few representative hydrocarbon components is essential for multidimensional computational fluid dynamics spray combustion simulation purposes. Surrogates that can characterize the thermophysical properties and evaporation processes of real fuel are the “physical” surrogates. Surrogates that are able to mimic fuel chemical-kinetics-related properties are viewed as the “chemical” surrogate models. For spray combustion modeling, fuels experience thermophysical (heating and evaporation) and chemical kinetics (ignition and combustion) processes. To model the multiphase spray combustion process, a “unified” diesel surrogate, which can emulate both the physical and chemical (kinetics) properties of the real diesel fuel, is proposed in this study. A group of hydrocarbon species was selected, using an inversed batch distillation methodology, to match the experimental distillation curve of standard diesel blends. For the chemical kinetics target, a detailed reaction mechanism of 352 species with 13 264 reactions was used for gas-phase ignition delay time predictions and a reduced reaction mechanism of 200 species with 6907 reactions was used for laminar flame speed simulations. On the basis of the hydrocarbon class concentrations of typical diesel fuels of normal/isoalkanes, cycloalkanes and aromatics, this study identified the four-component surrogate fuel for diesel fuel as 1,2,4-trimethylbenzene (C_9H_{12}), *trans*-decalin ($C_{10}H_{18}$), heptamethylnonane ($iC_{16}H_{34}$), and *n*-hexadecane ($C_{16}H_{34}$) with mole fraction 0.262:0.065:0.365:0.308. Important thermophysical and chemical targets, including molecular weight, lower heating value, cetane number, hydrogen/carbon mass ratio, density, kinematic viscosity, surface tension, and specific heat, are also predicted using this surrogate. In addition, chemical kinetics characteristics, including ignition delay times as well as laminar flame speeds, are used to validate the proposed surrogate fuel.

1. INTRODUCTION

During the last few decades, diesel engines have become important energy-supplying sources for various industrial sectors, including transportation and manufacturing. Although diesel engines have better combustion and thermal efficiencies when compared to gasoline engines, issues related to emissions and cold starts require further improvement. Engine performance depends highly upon the fuel type and the subsequent fuel atomization, fuel droplet breakup, vaporization, mixing, and combustion processes. Multidimensional computational fluid dynamics (CFD) methods have been routinely used to gain insight of complex phenomena associated with spray combustion involving real transportation fuels. Real diesel fuels are mixtures composed of hundreds to thousands of components; thus, it is not possible to perform real fuel spray combustion simulations, even with high-performance computing. Therefore, in developing surrogate fuels composed of only a few representative hydrocarbon components, it is essential that they mimic the properties of real fuel.

Component selection for surrogate fuels is closely related to the targeted applications. Surrogates that can characterize the thermophysical properties and evaporation processes of real fuel are called “physical” surrogates,¹ and surrogates that are capable of mimicking fuel chemical kinetics-related phenomena (for example, gas-phase ignition delay times, laminar flame speed, etc.) are considered as “chemical” surrogate models.² In the previous research, much emphasis has been put on gas-phase chemical kinetics. Therefore, the suggested surrogates usually focus on a single-phase gas combustion process.

However, some of the chemical surrogates are not able to match physical properties, including fuel volatility or distillation curve, and, thus, are not suitable for characterizing the complex process of droplet heating and evaporation. In many cases, surrogate development and validation studies predict the distillation curve, evaporation process, and chemical kinetics separately. For spray combustion modeling, fuels experience thermophysical (heating and evaporation) and chemical kinetics (ignition and combustion) processes. To model the multiphase spray combustion process, a “unified” diesel surrogate that can emulate the physical, chemical, and combustion (kinetics) properties of the real diesel fuel is highly desirable.

Research activities on developing surrogate diesel fuels have been active for the past few decades. Recent proposed multicomponent-based surrogates are summarized in Table 1. Table 1a summarizes the surrogates based on physical and chemical property predictions, while Table 1b summarizes surrogates focused on chemical kinetics properties of diesel predictions. Luo et al.³ uses a three-component surrogate to simulate ignition delay and combustion phenomenon in a simplified engine. This surrogate, however, shows high discrepancy in physical properties, such as density and C/H mass ratio. Liang et al.⁴ uses two different surrogates for engine

Received: July 6, 2017

Revised: November 8, 2017

Published: November 9, 2017

FEDSM2017-69499

MODELING OF CAVITATION INDUCED FUEL ATOMIZATION AND BREAKUP PROCESSES

Bolin Zhao and C. P. Chen*

University of Michigan-Shanghai Jiao Tong University Joint Institute
Shanghai Jiao Tong University
Shanghai, China

ABSTRACT

Recent experimental and modeling studies have indicated that turbulence and cavitation behaviors within a realistic fuel injector have significant effects on the liquid atomization and spray processes. In addition to the breakup process induced by aerodynamic force at the liquid/gas interface, the effects of flow characteristics including turbulence and cavitation inside the injector nozzle on atomization have been shown to be important. The cavitation within the injector is complicated by the turbulent flow under large pressure gradient and geometry of the injector orifice. We have previously developed the “T-blob” and “T-TAB” model, for liquid fuel primary and secondary breakup predictions respectively, to account for liquid turbulence effects within the injector. The objective of this study is to further account for the cavitation effect in the atomization process of a cylindrical liquid jet. In the primary breakup model, the level of the turbulence effect on the liquid breakup depends on the characteristic scales and the initial flow conditions. These scales are further modified to include the cavitation effect. The drop size formed is estimated based on the energy distribution among wave, turbulence and cavitation modes. This paper describes theoretical development of the current model. Both non-evaporating and evaporating spray cases will be investigated to validate the newly developed cavitation-induced atomization model.

INTRODUCTION

In diesel powered engines, the liquid fuel is injected into the engine cylinder after a compression stroke. The fuel issuing from the injector nozzle will experience atomization and vaporization processes. After mixing with air, it will be ignited and provide energy to power the vehicle. The nozzle shape and

initial spray conditions including injection pressure, initial injection temperature and flow characteristics [1-4] would influence the spray properties and the mixing rate between fuel and air. For a fixed nozzle shape and given initial conditions, spray properties that can be obtained from most experiments are limited to macroscopic features such as liquid jet penetration lengths, fuel mass fraction distributions, spray angle and velocity of particles. To better understand the droplet breakup and atomization processes in the near nozzle regions, it still depends on atomization modeling and simulations. Recent experimental and modeling studies have indicated that turbulence and cavitation behaviors within a realistic fuel injector have significant effects on the liquid atomization and spray processes. The cavitation within the injector is complicated by the internal turbulent flow subject to large pressure gradient and injector orifice geometry. Previously, the so-called T-blob/T-TAB model has been developed to account for liquid turbulence effect in primary and secondary breakup predictions [5].

The primary objective of this study is to further account for the cavitation effect in the atomization process of a cylindrical liquid jet. The proposed model is based on the existing features of atomization models including the KH (Kelvin-Helmholtz) model and the T-blob model. In addition, the new model would improve performance such as particle radius estimation and the switch mechanism of primary and secondary breakup. In the past, liquid turbulence has been used in the modification of breakup mechanism. However, the methods, used to combine the wave perturbation and turbulence, vary in the previous modeling approaches [6-8]. In most methods, the characteristic length and time scales proposed by Huh et al. [6] are applied, which is deduced from the original k-epsilon turbulence model by referring to a 1D nozzle flow model. In this study, this assumption will also be used. Based on this baseline, the cavitation effect will be added.

*Previously affiliated with University of Alabama in Huntsville

Distortion Mapping Correction of In-Cylinder Flow Field Measurements through Optical Liner Using Gaussian Optics Model

2017-01-0615

Published 03/28/2017

Penghui Ge, Fengnian Zhao, and David Hung

University of Michigan - SJTU Joint Institute

Hujie Pan and Min Xu

Shanghai Jiao Tong University

CITATION: Ge, P., Zhao, F., Hung, D., Pan, H. et al., "Distortion Mapping Correction of In-Cylinder Flow Field Measurements through Optical Liner Using Gaussian Optics Model," SAE Technical Paper 2017-01-0615, 2017, doi:10.4271/2017-01-0615.

Copyright © 2017 SAE International

Abstract

Combustion efficiency of internal combustion engine is closely influenced by the air flow pattern in the engine cylinder. Some researchers use high-speed particle image velocimetry to visualize and measure the temporally and spatially resolved in-cylinder velocity flow fields in the optically assessable engine. However, the transparent cylindrical liner makes it difficult to accurately determine the particle displacements inside the cylinder due to the optically distorted path of scattering light from seeding particles through the curved liner. To correct for the distortion-induced error in the seeding particle positions through the optical liner, the distortion mapping function is modeled using the Gaussian optics theory. Two artificial flow patterns with 5 by 5 vectors were made to illustrate the mapping correction. Distortion-induced error of velocity vectors was precisely mapped in six different planes inside the cylinder. In addition, the in-cylinder PIV measurements in these six planes were applied to illustrate the distortion-induced error. Results show that velocity fields in the center plane did not exhibit much distortion-induced effect. However, the relative distortion-induced error percentage of ensemble velocity magnitude near the cylinder liner could reach as much as 2.1%, indicating that it is necessary to correct for optical distortion in this location. The distortion mapping function used in this study can provide an effective way to correct the distortion-induced error in the planar in-cylinder flow field measured through the transparent liner.

Introduction

The air-fuel mixing process plays a critical role in combustion efficiency, especially in direct-injected spark-ignition engine. Since flows inside an engine cylinder are highly transient and can change abruptly cycle by cycle, maintaining a good stability of fuel-air mixture with low cycle-to-cycle variations is needed for consistent power output. A common practice to understand the cycle-to-cycle variations is to apply high-speed particle image velocimetry (PIV) to measure the transient in-cylinder flow fields in multiple engine cycles

because it can provide spatially and temporally (crank-angle) resolved flow field data. Extensive studies have been conducted to improve PIV measurement accuracy in engine flow applications [1, 2]. While the setting of PIV parameters such as seeding density and laser pulse separation may introduce measurement uncertainty, the curved surface of liner used in optical engine normally leads to apparent errors when Mie scattering rays pass through the transparent cylindrical wall. Some researchers are aware that optical distortion makes it difficult to measure the flow fields accurately in the engine cylinder [3, 4]. Reuss [3] studied the possible factors including the camera noise, particle image aberrations, light transmission variations near the cylinder liner and image focusing that induces uncertainties in the in-cylinder PIV measurement. The important factors are the poor focusing induced by image aberrations and low light transmission near the cylinder wall, which shows that optical distortion in the cylinder can cause some more uncertainties in the PIV measurement. Figure 1 depicts the use of a calibration board with uniform spacing (5×5 mm) to illustrate optical path distortion through the cylinder liner. This board is placed at three different positions inside the optical liner whose inner diameter is 86 mm with a thickness of 13 mm. The BB plane which is along the center of the cylinder. The other two planes are AA and CC positioned at +19.4 mm and -19.4 mm, respectively, away from BB plane. These two planes cut through the axis of intake and exhaust valves which are important for the investigation of valve motion effect on in-cylinder flow field. Since the camera is only positioned at about 45 cm to the liner axis, the board size appears slightly larger when the plane is closer to the camera. It is clear that positions of some crosses are distorted when imaging through the liner. For all three planes, the spacing between any horizontal lines does not change, but the spacing between the vertical lines changes with different magnitude on various planes. The spacing on each plane increases progressively from the centerline to the vicinity of liner. For the center plane BB, the largest change of spacing is 0.13 mm. Away from the cylinder axis, the largest spacing change in AA is increased by 0.50 mm (10% larger than original spacing), while the most change in CC is reduced

Experimental Investigation of Fuel Film Characteristics of Ethanol Impinging Spray at Ultra-Low Temperature

2017-01-0851

Published 03/28/2017

Hujie Pan and Min Xu

Shanghai Jiao Tong University

David Hung and Huijia Lv

University of Michigan-SJTU Joint Institute

Xue Dong

Shanghai Jiao Tong University

Tang-Wei Kuo, Ronald O. Grover, and Scott E. Parrish

General Motors Company

CITATION: Pan, H., Xu, M., Hung, D., Lv, H. et al., "Experimental Investigation of Fuel Film Characteristics of Ethanol Impinging Spray at Ultra-Low Temperature," SAE Technical Paper 2017-01-0851, 2017, doi:10.4271/2017-01-0851.

Copyright © 2017 SAE International

Abstract

Increasing the injection pressure in DISI engine is an efficient way to obtain finer droplets but it will also potentially cause spray impingement on the cylinder wall and piston. Consequently, the fuel film sticking on the wall can dramatically increase the soot emission of the engine especially in a cold start condition. On the other hand, ethanol is widely used as an alternative fuel in DI engine due to its sustainable nature and high octane number. In this study, the fuel film characteristics of single-plume ethanol impinging spray was investigated. The experiments were performed under ultra-low fuel/plate temperature to simulate the cold start condition in cold areas. A low temperature thermostatic bath combined with specially designed heat exchangers were used to achieve ultra-low temperature for both the impinging plate and the fuel. Laser induced fluorescence (LIF) technique was employed to measure the thickness of fuel film deposited on the impinging plate. Rhodamine 6G was resolved into ethanol as the tracer, which can be excited by 532 nm laser and fluorescence at 560-590 nm. A low speed imaging system was used to capture the film characteristics. The LIF signal was converted to film thickness following a known height calibration approach. It was found that, with the decrease of plate temperature, the average film became thicker and the adhered mass increased although the wetted area became smaller due to the larger viscosity. Moreover, lower fuel temperature leads to thicker film and more adhered mass. The wetted areas are close to each other under different fuel temperatures.

Introduction

In a Direct-Injection Spark-Ignition (DISI) engine, the fuel is injected directly into the combustion chamber and it needs rapid atomization of spray to produce better air-fuel mixture. Increasing the injection

pressure is an efficient way to obtain finer fuel droplets. However, at least in the range of 20 MPa to 100MPa, which covers today's applied pressure in DISI engine, the spray penetration increases with the injection pressure [1]. This will potentially cause the spray impingement on the cylinder wall and the piston. Moreover, engine downsizing with boosting technologies is applied to achieve higher fuel efficiency and lower emission, which will decrease the distance between the injector tip and the wall. The impingement will consequently be easier to occur compared to the traditional DI engine.

Spray-wall interaction plays an important role in fuel-air mixture formation and consequently influences the engine performance. On the one hand, finer droplets are produced and air entrainment is enhanced during the impingement process [2]. On the other hand, more unburned HC and soot are generated due to poor vaporization of the liquid film adhered on the surfaces. The drawbacks of impinging spray become more severe under cold start conditions, Sherry Zhang *et al.* found that PM mass and numbers emission are the highest during engine cold start [3]. When in a cold region, the temperature of the piston and the cylinder wall could be as low as -10 °C to -20 °C which may cause higher PM emission compare to the normal temperature such as 20°C. However, the fuel film characteristics under ultra-low fuel/plate temperature have never been experimentally investigated. In the meantime, the existing spray impingement model was validated with the experimental results performed on room/high temperature plate [4], which results in inaccurate prediction of spray impingement under cold conditions. Therefore, it is essential to study the fuel film characteristics under ultra-low temperature conditions, not only to better understand the impinging behavior, but also to extend the database for developing accurate spray impingement models.

Uncertainty Quantification of Spray Wall Impingement Simulation

Cao Jingjing¹, *Xu Min¹, David L.S. Hung^{1,2}, Pan Hujie¹, Dong Xue¹

1. School of Mechanical Engineering, Shanghai Jiao Tong University, National Engineering

Laboratory for Automotive Electronic Control Technology, Shanghai, China

2. University of Michigan-Shanghai Jiao Tong University Joint Institute, Shanghai Jiao Tong University

Key Words: Spray/Wall Interactions, CFD, Ultra-Low Temperature Plate

ABSTRACT

Wall wetting phenomenon in direct-injection spark-ignition (DISI) engine has been demonstrated to increase both the fuel consumption and soot emissions. The drawbacks of impinging spray become more severe under cold start conditions. However, the accuracy of the existing fuel impingement model is limited under cold condition, as the current models were only validated under high and room temperature. Therefore, this paper presents a parametric study of the spray impingement model with an aim to improve its accuracy under cold conditions. Experimental validation was performed under ultra-low plate temperature to simulate the cold start condition in cold areas. The spray structure was characterized with 2D particle image velocimetry (PIV) system. Also, laser induced fluorescence (LIF) technique was employed to measure the thickness of fuel film deposited on the impinging plate. Simulations were performed using a commercial software CONVERGE. The free spray pattern, velocity distribution of the spray and the wall film thickness are compared qualitatively and quantitatively to assess the current impingement model.

INTRODUCTION

In a direct-injection spark-ignition (DISI) engine, the fuel is injected directly into the combustion chamber, thus requiring rapid atomization and sufficient fuel-air mixing. To achieve this, the injection pressure is being elevated to much higher level. However, at least in the range of 20 MPa to 100MPa, which covers today's applied pressure in DISI engine, the spray penetration increases with the injection pressure[1]. Moreover, engines are downsized with boosting technologies to achieve higher fuel efficiency and lower emissions. Therefore, higher spray penetration speed in small combustion cylinder makes spray impingement in DISI engine a serious and unavoidable issue.

Spray/wall interaction has a significant impact on the in-cylinder fuel-air mixture formation and consequently influences the engine combustion performance. On the one hand, finer droplets are produced and air entrainment is enhanced during the impingement process[2]. On the other hand, more unburned HC and soot are generated due to poor vaporization of the liquid fuel film adhered on the surfaces. Moreover, the liquid film on the piston may also lead to lubricating oil dilution. The drawbacks of impinging spray become more severe under cold start conditions, Hwang J. *et al.* found that PM mass and numbers emission are the highest during engine cold start[3]. When in a cold region, the temperature of the

ANALYSIS OF CRANK ANGLE-RESOLVED VORTEX CHARACTERISTICS UNDER HIGH SWIRL CONDITION IN A SPARK-IGNITION DIRECT-INJECTION ENGINE

Fengnian Zhao, Penghui Ge, Hanyang Zhuang, David L.S. Hung
University of Michigan-Shanghai Jiao Tong University Joint Institute
Shanghai Jiao Tong University
Shanghai, China

ABSTRACT

In-cylinder air flow structure makes significant impacts on fuel spray dispersion, fuel mixture formation, and flame propagation in spark ignition direct injection (SIDI) engines. While flow vortices can be observed during the early stage of intake stroke, it is very difficult to clearly identify their transient characteristics because these vortices are of multiple length scales with very different swirl motion strength. In this study, a high-speed time-resolved 2D particle image velocimetry (PIV) is applied to record the flow structure of in-cylinder flow field along a swirl plane at 30 mm below the injector tip. First, a discretized method using flow field velocity vectors is presented to identify the location, strength, and rotating direction of vortices at different crank angles. The transients of vortex formation and dissipation processes are revealed by tracing the location and motion of the vortex center during the intake and compression strokes. In addition, an analysis method known as the wind-rose diagram, which is implemented for meteorological application, has been adopted to show the velocity direction distributions of 100 consecutive cycles. Results show that there exists more than one vortex center during early intake stroke and their fluctuations between each cycle can be clearly visualized. In summary, this approach provides an effective way to identify the vortex structure and to track the motion of vortex center for both large-scale and small-scale vortices.

INTRODUCTION

Better engine performance and lower engine emissions are constantly pursued by automobile manufacturers around the world. The stringent regulations mandated by government and environmental protection agencies provide ample opportunities for further improvements of internal combustion engines to meet these targets. According to the review by Sick *et al.* [1, 2], the intake air flow fields play one of the most important roles in affecting the spray structure, air-fuel mixing process, and flame propagation inside the cylinder. The spark-ignition direct-injection (SIDI) engine is proven to be an effective technology

enabling the targets of better fuel economy, higher power output, and lower emissions to be met. In SIDI engine, the flexibility of directly injecting gasoline liquid fuel into cylinder provides the additional tailoring ability to improve the fuel-air mixture formation. Therefore, most improvements of engine combustion and emissions can be achieved through the research conducted inside an engine cylinder.

With the development of various optical diagnostics techniques, the in-cylinder engine processes can be clearly and thoroughly visualized by researchers. Particle Image Velocimetry (PIV), as one of the most commonly used optical diagnostic techniques, can reveal the development of in-cylinder flow fields by taking crank angle-resolved images with high spatial and temporal resolutions. During intake stroke of the SIDI engine under homogeneous mode, the air fuel mixing is affected mostly since the fuel droplets and vapor are carried by the intake air flow. Strong flow motions (swirl and tumble flows) normally lead to different air-fuel mixture distributions inside the cylinder. For both swirl- and tumble-flow conditions, flow vortices are generated gradually from the intake stroke. At early stage of intake stroke, it is difficult to clearly identify the characteristics of these flow vortices since the flow field is very complicated, and the vortices of multiple length scales with different swirl motion strengths may co-exist at the same time. As for compression stroke, some researchers analyzed the flow fields and concluded that there was a dominant vortex motion during compression stroke and small cycle-to-cycle variations were present [3, 4, 5].

Since vortices do exist inside the cylinder after the intake stroke, many researchers have developed vortex center identification algorithms to identify the vortex center location [5, 6, 7, 8]. They used various methods to detect the vortex center, such as the velocity directions of vortex center's neighboring points, streamlines and vorticity contour lines of the flow field, etc. Based on existing vortex center identification algorithms, some researchers show how the vortex motion moves and changes in the swirl or tumble plane [3, 4, 9]. The movement

Transient structure and footprint of iso-octane impinging spray under room and low temperature

Hujie Pan¹, Di Xiao¹, Min Xu^{1*}, David Hung^{1,2}, Xue Dong¹

¹ School of Mechanical Engineering, Shanghai Jiao Tong University, China

² University of Michigan-Shanghai Jiao Tong University Joint Institute, Shanghai Jiao Tong University, China

Corresponding author: Min Xu, Email: mxu@sjtu.edu.cn

Keywords: Spray impingement, Cold start, Macroscopic structure, Fuel film, Transient behavior, Iso-octane spray

1. Introduction

Soot is one of the most significant pollutant emissions of today's internal combustion (IC) engine, especially in diesel and gasoline direct injection (GDI) engines. Since the fuel is injected directly into the combustion chamber with a high injection pressure, wall wetting could occur, potentially followed by poor evaporation of fuel film on piston and cylinder wall, especially under cold start condition. Peckham *et al.* found that more than half of the soot particles were emitted within the first 200 seconds of the start of the cycle [1]. This indicates that wall wetting during the cold start has a strong relationship with soot emission. Furthermore, the cold start temperature varies in a wide range and it could be as low as -20°C in certain cold areas, which is expected to have more severe impact on the PM emission during engine cold start. However, the study of the impinging spray under extremely cold start condition is limited.

So far, not much effort has been put on the study of spray impingement and fuel film measurement. Akop *et al.* studied the influence of impingement area, incident angle, droplet weber number and ambient pressure on diesel impinging spray and adhered mass [2-4]. Wang *et al.* investigated the microscopic behavior of impinging droplets of the spray by decreasing the number density using a slit [5]. As to the wall film measurement, Refractive Index Matching (RIM) and Laser Induced Fluorescence (LIF) are two of the most widely used techniques [6, 7]. For RIM method, the measurable range of film thickness is limited by the surface roughness of the plate. In contrast, LIF method requires a polished plate and a proper selection of the tracer but has a much larger measurable range compared to RIM method. The author's group has successfully applied LIF method to study the characteristics of fuel film under extreme

cold start condition [8]. However, the study of transient behavior of the footprint combined with macroscopic structure is still limited.

In this study, simultaneous measurements of macroscopic structure (side view) and its corresponding footprint (bottom view) of impinging spray have been conducted under room and extreme low temperature mimicking cold start engine condition. The transient behavior of impinging spray, including structure and footprint of impinging spray, is analyzed qualitatively and quantitatively.

2. Apparatus and Operating Conditions

2.1 Experimental Setup

Fig. 1 shows the experimental setup of simultaneous measurement of macroscopic structure and footprint of impinging spray. A polished sapphire plate was used as the impinging plate in the test and it was placed at 50 mm below the injector tip. The temperature of the plate and holder was controlled by changing the temperature of the coolant flowing in and out of the holder. A robust low temperature thermostatic bath was utilized to regulate the temperature of the coolant to as low as -60°C. The maximum temperature difference at different points on the plate was verified to be no more than 3°C. The 60 mm hole at the center of the holder provides the access for the bottom view of the sapphire plate.

The fuel used in the test was iso-octane blended with 10% ethanol by volume to dissolve the dopant, Rhodamine 6G. A high speed Nd:YLF laser was employed to excite the dopant and a high speed camera 1 (Phantom V7.3) equipped with a bandpass filter was utilized to capture the fluorescence from the fuel film. A red light LED array was used to

Validation of Spray Evaporation Model via Simultaneous Measurements of Liquid and Vapor Concentration of a Single Plume Spray

Zhe Sun, Xue Dong, Peng Yin, Tianyun Li, Min Xu*

School of Mechanical Engineering, Shanghai Jiao Tong University

Corresponding author: Min Xu, Email: mxu@sjtu.edu.cn

Keywords: Evaporation model, LIEF, vapor concentration, Numerical simulation, Experiment validation

1. Introduction

In a gasoline direct injection (GDI) engine, the air-fuel mixture characteristics have profound effects on the engine combustion performance. Commercial computational fluid dynamics (CFD) software is usually applied in the development of engine combustion system, where the simulation of spray plays a key role. One of the targets of advanced spray strategies is optimizing the mixture formation in the chamber. Many studies were performed to verify that the vapor of the fuel could affect the in-cylinder homogeneity, which consequently influences the engine combustion performance. And in the current studies, the macroscopic structure of a spray in the constant volume bomb could be measured so that the penetration and the particle size distribution of the spray could be used to calibrate the spray model. In addition, the role of the evaporation also has an impact on the mixing especially in the spray modelling, which make a difference at the distribution of liquid phase and vapor phase of fuel. Ho Teng did a series of researches to analyze the impact of the distribution of the droplet and rate of evaporation on the engine air-fuel mixing. [1] Q. Chen et al gave a rigorous mathematical model for spray model. [2] And various models based on single droplet were designed for different application environments. Such as the stationary droplet evaporation model considering about the influence of natural convection, Chungen Yin developed a model fully addressing the circulation, heat transfer and mass transfer in droplets and Zhi-Fu Zhou et al designed a model using 3rd order polynomial profile assumption to reflect the internal temperature distribution within the droplet. [3, 4, 5]

In the study, laser induced exciplex fluorescence

(LIEF) technology was utilized in the constant volume chamber to measure the vapor concentration of the spray. And CFD model was set up to simulate the vaporization of the spray. Then comparison between the experimental and simulation results were made.

2. Methodology

2.1 Experiments

The experimental system is shown in Figure X. laser induced exciplex fluorescence (LIEF) technique was utilized to simultaneously quantify the distribution of vapor and liquid phase of the spray. Constant volume chamber was used to provide controlled ambient environment. The ambient pressure for the spray could be regulated from 20KPa (absolute) to 2MPa using the vacuum pump and the high-pressure nitrogen gas charging system. A water jacket and a heat exchanger were assembled around the injector to control the fuel temperature. An accumulator charging with high-pressure nitrogen was utilized to generate a spray pressure of up to 20Mpa. Nd: YAG laser at 266nm was employed as the excitation light source. The laser beam was formed in to a laser sheet by means of a series of optical lens. For LIEF technique, the two types of tracers were added to the fuel, namely fluorobenzene (FB) and Diethyl-Methyl-Amine (DEMA). The base fuel in this study is n-hexane. The volume ratio of n-hexane/FB/DEMA is 89/2/9. The fluorescence signals of the fuel were captured by a CCD camera at 1 Hz. An image intensifier was installed to magnify the fluorescence intensity. The resolution in this study was set to 1376×1040 Pixels. Because of the spectral overlap between fluorescence spectra of the two phases, a correction processing was done by two optical band-pass filters.

SUPPRESSED PROMPT ATOMIZATION OF FLASH-BOILING SPRAY BY ELEVATING INJECTION PRESSURE

QINGLIN XU¹, MIN XU^{1,*}, DAVID L. S. HUNG^{1, 2}, TIANYUN LI¹ and XUE DONG¹

¹ School of Mechanical Engineering, Shanghai Jiao Tong University, China

² University of Michigan-Shanghai Jiao Tong University Joint Institute, Shanghai Jiao Tong University, China

Corresponding author: Min Xu, Email: mxu@sjtu.edu.cn

Keywords: superheat degree, injection pressure, penetration, dispersion

1. Introduction

In a direct injection spark ignition (DISI) engine, the mixing time of the fuel with intake air in the cylinder is limited, thus quicker atomization and evaporation are desired [1]. In general, there are two viable ways to promote these processes. One of them is by increasing the injection pressure, which has always been the key technology adopted by automobile manufacturers to improve the engine performance and meet the emission regulations. While high-pressure injection is already applied in most of the DISI engines, it has been reported that further increase of injection pressure is still beneficial on fuel efficiency and emissions reduction [2, 3]. In addition to this, flash-boiling is also regarded as an effective way to improve fuel atomization and evaporation with the potential to reduce fuel consumption and emissions [4, 5].

Existing research on flash-boiling spray mainly focuses on the multi-hole injector. Its plume-to-plume interaction phenomenon, as called “collapse”, has been thoroughly studied. Its benefits on atomization and evaporation have been proved [6, 7]. However, limited work has been done on the flash-boiling spray of a single-hole injector. Its breakup mechanism and movement behavior need to be further studied. Moreover, the study of high pressure gasoline spray beyond 35 MPa is also limited, especially at flash-boiling conditions. The effects of injection pressure on flash-boiling spray is still unrevealed. Therefore, the objective of this work is to study the influence of the superheat degree and injection pressure on the spray penetration and dispersion of a single-hole injector.

2. Experiment Method and Conditions

The experiments were conducted in a constant volume chamber. The ambient pressure was regulated from 20 kPa to 100 kPa (absolute pressure) by compressed nitrogen and a vacuum pump. Fuel temperature was regulated from 20°C to 60°C by a heat exchanger surrounding the injector. Water bath was used as the heating source of the heat exchanger. Fuel injection pressure was regulated from 20 MPa to 55 MPa by a high-pressure pneumatic-driven liquid pump.

Backlit macroscopic imaging method was used to capture the far-field liquid spray behavior. Fig. 1 shows its optical setup. Back illumination was provided by a Xenon arc lamp. This arrangement provided a homogeneous illumination behind the window. A high-speed camera with imaging frequency of 100 kHz was used to capture the macroscopic images.

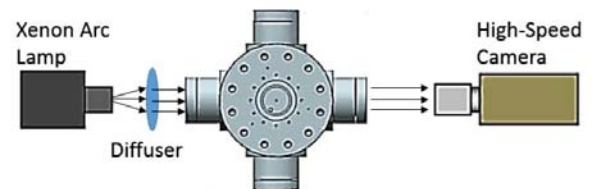


Fig. 1. Optical configuration of backlit macroscopic imaging

Similarly, backlit microscopic imaging method was used to capture the near-nozzle spray behavior. Its setup was similar to the setup of backlit macroscopic imaging. The only difference was that its lens was replaced by a microscopic lens.

Table. 1 shows test conditions in this study. An injector with a vertically oriented single-hole nozzle,

Detecting Outliers in Crank Angle Resolved Engine Flow Field Datasets for Proper Orthogonal Decomposition Analysis

2017-01-0612

Published 03/28/2017

Li Shen, Kwee-Yan Teh, Penghui Ge, Yusheng Wang, and David L.S. Hung

UM-SJTU JI, Shanghai Jiao Tong University

CITATION: Shen, L., Teh, K., Ge, P., Wang, Y. et al., "Detecting Outliers in Crank Angle Resolved Engine Flow Field Datasets for Proper Orthogonal Decomposition Analysis," SAE Technical Paper 2017-01-0612, 2017, doi:10.4271/2017-01-0612.

Copyright © 2017 SAE International

Abstract

Proper Orthogonal Decomposition (POD) is a useful statistical tool for analyzing the cycle-to-cycle variation of internal combustion engine in-cylinder flow field. Given a set of flow fields (also known as snapshots) recorded over multiple engine cycles, the POD analysis optimally decomposes the snapshots into a series of flow patterns (known as POD modes) and corresponding coefficients of successively maximum flow kinetic energy content. These POD results are therefore strongly dependent on the kinetic energy content of the individual snapshots, which may vary over a wide range. However, there is as yet no algorithm in the literature to define, detect, and then remove outlier snapshots from the dataset in a systematic manner to ensure reliable POD results. In this paper, one such outlier detection algorithm is proposed: A snapshot is considered an outlier if it has excessively high kinetic energy content as well as relevance index (a measure of flow pattern similarity) versus a particular POD mode. An analytical expression is derived to relate these two parameters and provide the statistical and physical underpinnings for the outlier detection algorithm. The algorithm is applied to two sets of crank angle-resolved engine in-cylinder flow fields in the middle tumble plane that were obtained experimentally using high-speed particle image velocimetry techniques, and improvements in POD results obtained after the removal of outlier snapshots are discussed.

Introduction

Cycle-to-cycle variation of in-cylinder flow field is a key feature of internal combustion (IC) engine operation, leading to variations in fuel and air mixing, ignition, and combustion. It limits stable operation of an engine within a narrow range, especially when running in low-temperature, high-dilution, or stratified combustion mode, beyond which combustion instabilities may degrade the engine fuel economy, increase its emissions, or even damage the engine. The flow fields may vary in macroscopic scale, i.e., on the order of the engine cylinder dimensions, entailing significant deviation in magnitude and direction

from the mean, as opposed to velocity fluctuations in small scales about that mean, underlying the classical Reynolds-averaged-Navier-Stokes (RANS) turbulence modeling framework.

Proper orthogonal decomposition (POD) was originally proposed by Lumley [1] as an alternative technique to analyze turbulent flows. The earliest studies applied the technique to canonical turbulent flows — in a channel [2], over a flat plate [3], during the development of an axisymmetric jet [4], etc. — with the goal of identifying large-scale patterns of “organized” fluid motion (known as “coherent structures”) that dominate, and therefore serve as bases for low-order description of those flows. The POD analysis technique has since been extended to the study of IC engine in-cylinder behaviors, whereby the coherent structures are used to explain larger scale variations in scalar fields [5, 6] and vector fields [7, 8, 9, 10], whereas what remained unexplained are deemed smaller scale turbulence or noise within the those fields.

Proper orthogonal decomposition has its roots in the fields of optimization and multivariate statistics. When an ensemble of flow field samples is considered as a multivariate dataset with the velocity components defined on individual grid points of the flow fields being the random variables, the result of the POD analysis of the ensemble is a series of flow patterns (known as POD modes) that successively maximize the sample variance in statistical terms and, equivalently, the average flow kinetic energy content in physical terms. It is on the basis of this property of optimality that the first several lower POD modes are identified as the coherent structures dominating the flow fields within the ensemble.

Viewed from another perspective, which has yet to be considered in the literature, the kinetic energy maximizing property of the POD analysis technique implies that each POD mode will tend to bear closer resemblance to the flow patterns of those members of the ensemble with high kinetic energy at that stage of the analysis. For instance, Abraham et al. [11] reported POD results upon combining two sets of velocity fields in the engine tumble plane, obtained separately from large eddy simulation (LES) computation and particle image velocimetry (PIV) experiment using virtual versus real engines of identical geometry and

Diesel Spray Characterization at Ultra-High Injection Pressure of DENSO 250 MPa Common Rail Fuel Injection System

2017-01-0821

Published 03/28/2017

Qinglin Xu and Min Xu

Shanghai Jiao Tong University

David Hung

UM-SJTU JI - Shanghai Jiao Tong University

Shengqi Wu and Xue Dong

Shanghai Jiao Tong University

Hiroaki Ochiai, Zhisong Zhao, Caixia Wang, and Kaiyue Jin

DENSO (China) Investment Co., Ltd.

CITATION: Xu, Q., Xu, M., Hung, D., Wu, S. et al., "Diesel Spray Characterization at Ultra-High Injection Pressure of DENSO 250 MPa Common Rail Fuel Injection System," SAE Technical Paper 2017-01-0821, 2017, doi:10.4271/2017-01-0821.

Copyright © 2017 SAE International

Abstract

High fuel injection pressure has been regarded as a key controlling factor for internal combustion engines to achieve good combustion performance with reduced emissions and improved fuel efficiency. For common-rail injection system (CRS) used in advanced diesel engines, fuel injection pressure can often be raised to beyond 200 MPa. Although characteristics of diesel spray has been thoroughly studied, little work has been done at ultra-high injection pressures. In this work, the characteristics of CRS diesel spray under ultra-high injection pressure up to 250 MPa was investigated. The experiments were conducted in an optically accessible high-pressure and high-temperature constant volume chamber. The injection pressure varied from 50 MPa to up to 250 MPa. Both non-evaporating condition and evaporating condition were studied. A single-hole injector was specially designed for this investigation. High-speed Mie-scattering imaging and Schlieren imaging were used to capture the global structure of the liquid and vapor sprays. In addition, high-speed microscopic back-lit imaging was used to obtain detailed information of sprays near the nozzle. Results show that, the increase of injection pressure from 50 MPa to 250 MPa decreases the injection response time and cut time by 58% and 49% respectively. A correlation of injection rate and the velocity of initial spray was observed. The initial spray experiences a quick accelerating to its maximum velocity, then quickly slows down, and higher injection pressure results in shorter accelerating time and higher maximum velocity. In addition, spray liquid penetration increases as injection pressure increases under non-evaporating conditions. However, under evaporating conditions, the increase of injection pressure from 50 MPa to 250 MPa results in about 15% decrease of liquid penetration but increase of vapor penetration.

Introduction

Diesel engines are widely used in the medium and heavy duty vehicles, due to its high torque and good thermal efficiency. However, higher nitrogen oxide (NO_x) and particulate matter (PM) emissions have always been the barriers that hinder the development of diesel engines. Meanwhile, the fuel consumption regulations are becoming more stringent. In order to meet these challenges, researchers from academic and industrial institutions have conducted extensive investigations on improving fuel system design and performance. Among all factors influencing the performance of diesel engines, elevating the fuel injection pressure would be considered as one of the most effective ways to overcome these challenges [1, 2]. Over the last two decades, commercial fuel injection systems of diesel engine have been upgraded from mechanical pump system to high pressure common-rail system, and the injection pressure has also gone up from 50 MPa to 200 MPa, and in some cases even to an ultra-high level of reaching 250 MPa. For instance, DENSO's 4th generation of common rail system is capable of operating at fuel injection pressure up to 300 MPa [3, 4].

It is well known that optimal spray characteristics have contributed to the improvement of fuel atomization, fuel air mixing improvement, combustion efficiency, and emissions reduction in diesel engines. In light of this important attribute, fundamental studies on spray characteristics, such as tip penetration, spray angle and Sauter mean diameter (SMD), are essential to evaluate injector performance, validate spray models, and design combustion cylinder profile, etc. [5]. Up to now, extensive studies have been conducted on diesel spray characteristics at injection pressure typically below 200 MPa, resulting in a multitude of empirical

DETC2017-67677

CONCENTRIC HELICAL AXIAL SPRING TUNABLE STIFFNESS MECHANISM: ANALYTICAL MODELING, DESIGN OPTIMIZATION AND EXPERIMENTAL VALIDATION

Zeeshan Qaiser

University of Michigan and Shanghai Jiao Tong
University Joint Institute
Shanghai, China 200240

Shane Johnson Ph.D.

State Key Laboratory of Mechanical Systems and
Vibration
University of Michigan and Shanghai Jiao Tong
University Joint Institute
Shanghai, China 200240

Liping Kang

University of Michigan and Shanghai Jiao Tong
University Joint Institute
Shanghai, China 200240

ABSTRACT

The human foot modulates its stiffness in different anatomical regions in order to attain greater efficiency and performance. The purpose of this study is to develop an adaptable robotic foot by biomimicking the human foot's arch, horizontal tie and its ability of varying its stiffness. In this research we describe the design, modeling, development and optimization of the robotic foot with a novel Tunable Stiffness Mechanism (TSM) which acts as a horizontal tie. The TSM is made up of two concentric helical springs and the tunable stiffness feature is obtained by changing the parallel/series configuration of these springs. A flexible fiberglass composite arch is selected, and Multiobjective Design Optimization (MDO) is used to maximize the stiffness range and effectiveness of the system. Analytical modeling results closely match the experimental validation of both the tunable axial stiffness behavior of the TSM and tunable stiffness foot.

NOMENCLATURE

A	Cross sectional area
C	Non-dimensional Spring index
d_1	Wire diameter on inner spring
d_2	Wire diameter on outer spring
D_1	Mean diameter on inner spring
D_2	Mean diameter on outer spring
D_{TSM}	Extension in the horizontal tie (TSM)

E	Young's Modulus of the spring
EI	Arch stiffness
F_1	Force in the horizontal tie
F_{max}	Maximum force in the spring
F_{min}	Minimum force in the spring
G	Shear Modulus of the spring
I	Moment of inertia
K_{TSM}	Stiffness of the TSM
$K_{1,outer}$	Effective stiffness of the outer spring
$K_{2,inner}$	Effective stiffness of the lower inner spring
$K_{3,inner}$	Effective stiffness of the upper inner spring
$K_{total,parallel}$	Total stiffness of arch+TSM system in parallel configuration
$K_{total,inner}$	Total stiffness of arch+TSM system in inner spring only configuration
$K_0^{fatigue,yield}$	Coefficients in fatigue and yield calculation
M_i, M_{ij}	Material coefficients for Tsai-Wu failure criterion
M_o	Bending moment in reference straight beam
N_{total}	Total number of coils in a spring
N_a	Number of active coils
M_P	Bending moment due to loading P
N_P	Axial force due to loading P
P	Loading at the apex of arch
$P_{parallel}$	Force in the TSM in parallel only configuration
P_{inner}	Force in the TSM in the inner spring only configuration

DETC2017-67346

OPTIMIZATION FOR LARGE OR LINEAR TUNABLE STIFFNESS CONTROL WITH A CONCENTRIC CIRCULAR TAPERED BEAM DESIGN

Shane Johnson, Ph.D.

State Key Laboratory of Mechanical Systems and
Vibration
University of Michigan and Shanghai Jiao Tong
University Joint Institute
Shanghai, China 200240

Anton Van Beek

University of Michigan and Shanghai Jiao Tong
University Joint Institute
Shanghai, China 200240

Zeeshan Qaiser

University of Michigan and Shanghai Jiao Tong
University Joint Institute
Shanghai, China 200240

Liping Kang

University of Michigan and Shanghai Jiao Tong
University Joint Institute
Shanghai, China 200240

ABSTRACT

Most examples of structure controlled Tunable Stiffness Mechanisms (TSM) systems have two predefined settings of stiffness, e.g. bi-stiffness behavior, or they have a low range in tunable stiffness. In this research, this problem of control is overcome through optimization of a novel concentric circular tapered spring beam design with the novel design concept of changing the mode of deformation from bending to axial or shear. A Monte Carlo (MC) function is used with an analytical model - the unit load method of virtual work, to determine the optimum shape of two concentric tapered beams where the minimum stiffness is set, and the objective is to achieve linear and/or large stiffness change control. Three optimum designs were 3D printed, tested, and the stiffness vs. loading angle of control was validated with excellent correlation. The optimum design was obtained by changing the dominant loading modes.

NOMENCLATURE

a, c	Coefficients of the linear function
b	Thickness of the beam
E	Young's Modulus of the spring
El	Arch stiffness
G	Shear Modulus of the spring
h	Height of cross section
h_i	Section height of the inner spring
h_o	Section height of the outer spring
$h_{o,max}$	Maximum section height of the outer spring
I	Moment of inertia

f_1	Linearity error objective function
f_2	Stiffness range objective function
k	Stiffness of the system
k_{min}	Minimum stiffness of the system
L	Length of the beam
m_1	Moment product in unit loaded structure
M_o	Bending moment in an arch
P	Loading at the apex of arch
Q_o	Shear force in the reference straight beam
R_i	Radius of the inner spring
R_o	Inner radius of the outer circular arch
κ	Form factor
θ_o	Angle measured from the free end of the beam
θ	Angle with an origin at the free end of the beam
δ_o	Bending deformation in outer circular beam
δ_i	Bending deformation in inner circular beam
$\delta_{i,v}$	Shear deformation in the inner circular beam
$\delta_{o,v}$	Shear deformation in the outer circular beam
δ_s	Bending deformation in the strut
δ_a	Axial deformation in the strut
σ	Stresses at any point in the beam

INTRODUCTION

TSMs are used in a wide variety of robotic and structural applications such as industrial and biomechanics where humans are interacting with machines [1-3] or in structural systems where key design considerations include shock absorption, storage and reuse of mechanical energy [2, 4].

IMECE2017-70854

2D MOTION STRUCTURES OF N-FOLD ROTATIONAL SYMMETRY

Zhiming Cui

UM-SJTU Joint Institute
Shanghai Jiao Tong University
Shanghai 200240, China
zhiming.cui@sjtu.edu.cn

Jaehyung Ju

UM-SJTU Joint Institute
Shanghai Jiao Tong University
Shanghai 200240, China
jaehyung.ju@sjtu.edu.cn

ABSTRACT

Kinematic motion structures having a reconfigurable property appear to be a potential candidate for the programmable matter. Motion structures with N-fold rotational symmetry show a reconfigurable pattern transformation, resulting in providing tunable mechanical properties, which deserves to explore more for their unique properties of transformation and the corresponding structural behaviors. The objective of this work is to synthesize motion structures from a bar-and-joint framework, investigating their transformability, linear structural properties - modulus and Poisson's ratio, and nonlinear structural behaviors with kinematic bifurcation. Two-dimensional (2D) motion structures are synthesized by central scissor links with revolute joints, connected with binary links in the radial direction. They possess an N-fold rotational symmetry (MS-N), and their transformed patterns are investigated. Five 2D motion structures - MS-4, MS-6, MS-8, MS-10, and MS-12, are generated for investigating their mechanical properties together with their transformability. Analytical models of the motion structures are constructed for obtaining relative density, moduli, Poisson's ratios, volume at each transformed state, and the strain energy required to transform from one state to another. This study integrates kinematics and structural mechanics, expanding the design space of light-weight structural materials with pattern transformation.

Keywords: motion structures, programmable matter, deployable structures, pattern transformation

1. INTRODUCTION

Programmable matter is a material whose shapes and properties can be tunable to achieve desired densities with volume change, shapes or mechanical properties; e.g., stiffness, strength, Poisson's ratio, etc., upon command. Cellular materials are widely used in nature, such as wood, bone, plant stems, and bird beaks [1]. Compared to dense solids, they are lightweight, yet adequately stiff and strong. Microstructures play a significant role in cellular solids' performance; e.g., Maxwell criteria tells that trigon in 2D and tetrahedron in 3D

structures provide stretching dominated stiff properties, yet tetragon and other polygons in 2D and cube in 3D generate bending dominated compliant structural properties for an axial loading condition [2-4].

The bending dominated structural properties are often explained by the mobility criteria [5]. For example, the tetragon structures are a four-bar linkage having the mobility of one degree-of-freedom (DOF), which is possibly used for motion structures. Motion structures are a deployable structure made up of kinematic linkages, possessing multiple mechanical properties with transformation [6, 7]. The applications of motion structures range from toys, e.g., the Hoberman sphere, to satellite solar panels. There are two ways to design motion structures [7]. One is the integration of a small number of moving bodies whose motions are synchronized by electronic means [8]. The other is the selection of conventional mechanisms as necessary building blocks, followed by assembly of these blocks together while retaining the degrees of freedom of each mechanism. The second method has been investigated due to its convenience in designing new structures. You and Pellegrino introduced a generalized method for the design of two-dimensional foldable structures utilizing angulated rods connected by scissor hinges, which gives more freedom in the range of shapes that can be achieved [9]. Mao et al. developed the theory of planar closed double chain linkages consisting of a series of scissor-like pairs connected by hinges [10]. Kiper et al. proposed a methodology for designing linkages with slider assemblies for scaling polygonal and polyhedral shapes [11]. It is interesting for motion structures to generate transformable patterns, yet the implementation of cellular structures has not been actively explored: only several studies have been reported [12-14].

Some motion structures show an auxetic behavior; i.e., being laterally expanded when longitudinally stretched [15], which is typically observed in the re-entrant hexagonal honeycombs [16, 17]. Auxetics have been fabricated by modifying the internal microstructure of foams and microporous polymers [18, 19]. Several structural materials with auxetic behavior have also been proposed [12, 13, 20, 21]. Grima and Evans proposed an arrangement of rigid squares

IMECE2017-70858

TUNABLE TRIANGULAR CELLULAR STRUCTURES BY PNEUMATIC CONTROL OF DUAL CHANNEL ACTUATORS

Zhihao Yuan
UM-SJTU Joint Institute
Shanghai Jiao Tong University
Shanghai 200240, China
myindex@sjtu.edu.cn

Jaehyung Ju
UM-SJTU Joint Institute
Shanghai Jiao Tong University
Shanghai 200240, China
jaehyung.ju@sjtu.edu.cn

ABSTRACT

Programmable matter, a material whose properties can be programmed to achieve desired density with volume change, shapes or structural properties (stiffness, strength, Poisson's ratio, etc.) upon command, is an important technology for intelligent materials. Recently emerging soft robotics-based pneumatic control can be potentially used for the design of programmable matter due to its several advantages – quick response for actuation, stiffening effect with internal air pressure, easy to manufacture, inexpensive materials, etc. The objective of this work is to construct programmable two-dimensional (2D) cellular structures with pneumatic actuators, investigating the effect of local deformation of the pneumatic actuators on the macroscopic pattern generation and mechanical properties of cellular structures. We synthesize 2D soft triangular structures with pneumatic actuators embedding dual air channels wrapped with fiber reinforcement. The local deformation modes provide different macroscopic deformations of cellular structures. We build an analytical model integrating the deformation of a single actuating member with nonlinear deformation of cellular structures. Finite element based simulations and experimental validation are followed. This study integrates soft robotics with cellular structures for intelligent materials design, expanding the design space of materials with programming. The fast response of the tunable soft cellular structures may be an ideal for the application of acoustic metamaterials with tunable band gaps.

Keywords: soft pneumatic actuator, programmable matter, mesostructures, cellular solids, soft robotics

1 INTRODUCTION

Programmable matter is a general term for the materials whose physical performance (density, shape, color, etc.) and mechanical properties (modulus, Poisson's ratio, etc.) can be modified or controlled by user input without any additional reprocessing. This technology has developed during the past few decades. Some recent studies which aim at recreating the

essential features of the materials, such as self-folding origami structures [1] and the 'Catoms' [2] which can cooperatively rearrange themselves to achieve different functions, are some examples. However, both of them lack the ability to scale down to their elements. David and his coworkers found a new approach to design programmable materials which aim at modifying the effective properties of the material rather than the gross shape of a piece of material [3], but the input was difficult to control.

In this work, we implement a programmable function to cellular structures. Cellular structures having low density have widely been used for light weight sandwich beams, panels, or energy absorption and structural protection. The stretching dominant triangular structures were a popular choice for the light-weight structural design. However, they are likely to buckle when subjected to an in-plane compressive load, which limits their strength. Previous work about cellular structures has mainly focused on the hexagonal cell structure with low relative densities [4-6]. Wang and McDowell [7] laid the foundation for the theoretical analysis of a series of cellular structures. They estimated the stiffness and Poisson's ratio and approximated the buckling strength of these cellular structures with a simplified beam model under uniaxial compression. Later, Fan et al. [8] have used a beam-column approach to estimate the uniaxial buckling strength more precisely. Recently, Haghpanah et al. [9] provided a formula for the in-plane buckling under a general stress state. Although the critical load has been well studied, the buckling patterns, especially the macroscopic shapes, are still hard to determine due to the random behavior of the cell walls during buckling. Some researchers try to find the buckling induced microstructural deformation by post-buckling analysis [10-11], Kang et al. [12] also find that the porosity can determine the buckling patterns with periodic boundary conditions under biaxial compression. In this study, we are interested in the triangular cellular structures having a local buckling mode, exploring the effect of pneumatic actuation on the buckling behaviors.

There are several ways of actuating programmable matter-mechanical [13], electrical [14], thermal [15], pneumatic [16]

Article

First View

Understanding the shape memory behavior of thermoplastic polyurethane elastomers with coarse-grained molecular dynamics simulations

Md Salah Uddin ^(a1) and Jaehyung Ju ^(a2) DOI: <https://doi.org/10.1557/adv.2017.11> Published online: 12 January 2017

Abstract

We perform molecular dynamics (MD) simulations to understand thermally triggered shape memory behavior of a thermoplastic polyurethane (TPU) elastomer with an enhanced coarse-grained (CG) model. Hard and soft phases of shape memory polymers (SMPs) are known as fixed and reversible phase, respectively. Fixity depends on the content of hard segments due to their restricted mobility. On the contrary, recovery depends on the dynamic motion of the soft segments as well the degree of cross-linking, which is also affected by the quantity of hard segment. Several CG models of the TPU are constructed varying the weight percentage of soft segments to observe their effects on shape recovery and fixity. All of the models are equilibrated at 300K (above glass transition, T_g : 200-250 K) and deformed under uniaxial loading with NPT (isothermal-isobaric) ensembles. The deformed state is cooled to 100K (below T_g) and further equilibrated to estimate the shape fixity. Shape recovery is predicted by heating and equilibrating the structures back to 300K. By the end of this study, we may answer how much the shape fixities and recoveries are changed for varying concentration of hard segments from thermomechanical cycles with CGMD simulations.

DETC2017-67291

**ROBUST OPTIMIZATION WITH PARAMETER AND MODEL UNCERTAINTIES USING GAUSSIAN
PROCESSES WITH LIMITED SAMPLES**

Yanjun Zhang and Mian Li*

University of Michigan – Shanghai Jiao Tong University Joint Institute
Shanghai Jiao Tong University, Shanghai, China 200240

ABSTRACT

Uncertainty is inevitable in engineering design. The existence of uncertainty may change the optimality and/or the feasibility of the obtained optimal solutions. In simulation-based engineering design, uncertainty could have various types of sources, such as parameter uncertainty, model uncertainty, and other random errors. To deal with uncertainty, robust optimization (RO) algorithms are developed to find solutions which are not only optimal but also robust with respect to uncertainty. Parameter uncertainty has been taken care of by various RO approaches. While model uncertainty has been ignored in majority of existing RO algorithms with the hypothesis that the simulation model used could represent the real physical system perfectly. In the authors' earlier work, a RO framework was proposed to consider both parameter and model uncertainties using the Bayesian approach with Gaussian processes (GP), where metamodeling uncertainty introduced by GP modeling is ignored by assuming the constructed GP model is accurate enough with sufficient training samples. However, infinite samples are impossible for real applications due to prohibitive time and/or computational cost. In this work, a new RO framework is proposed to deal with both parameter and model uncertainties using GP models but only with limited samples. The compound effect of parameter, model, and metamodeling uncertainties is derived with the form of the compound mean and variance to formulate the proposed RO approach. The proposed RO approach will reduce the risk for the obtained robust optimal designs considering parameter and model uncertainties becoming non-optimal and/or infeasible due to insufficiency of samples for GP modeling. Two test examples with different degrees of complexity are utilized to demonstrate the applicability and effectiveness of the proposed approach.

KEYWORDS: Robust Optimization, Parameter Uncertainty, Model Uncertainty, Gaussian Process, Metamodeling Uncertainty

1. INTRODUCTION

Real engineering applications unavoidably involve uncertainty, which may result in variations in objectives and/or constraints. The former may degrade the designed performance while the latter can even change the feasibility of optimal solutions obtained using deterministic formulations. To deal with uncertainty, robust design was first proposed by Taguchi to improve the quality of a product through minimizing the effect of uncontrollable uncertainty [1]. Thereafter robust design has been developed to obtain an optimum design being insensitive to variations. Numerous theories and approaches of robust design have been proposed in various design areas, only a small part of which are listed in [2-13] as examples.

Simulation models, implemented by computer codes and therefore also termed as computer models, are mathematical representations of real physical systems. Since physical experiments can be either too expensive or time-consuming, simulation models have been widely used to simulate and analyze real systems in many fields, including robust optimization (RO). Majority of existing simulation-based RO approaches assume that the simulation model used could always provide identical outputs given the same inputs. However, it cannot be true since no simulation model is perfect due to various sources of uncertainty [14], such as, parameter uncertainty, model uncertainty, metamodeling uncertainty, and other random errors. Parameter uncertainty refers to uncontrollable variations in parameters and/or design variables, which can be either aleatory or epistemic [15]. The former refers to the inherent variation associated with the physical system or environment [16], while the latter reflects the lack of knowledge or information about the nature of physical systems [17]. A parameter with aleatory uncertainty is usually treated as a random variable following a specific probability distribution [18]. Epistemic parameter uncertainty has been widely represented by intervals on the contrary. On the other hand, model uncertainty is associated with lack of knowledge or information of the underlying true physics [14], which is also called model discrepancy, bias, or inadequacy. Model

DETC2017-68101

A NORMALIZED CIRCLE INTERSECTION METHOD FOR BI-OBJECTIVE OPTIMIZATION PROGRAMMING

Jianhua Zhou^{1*}, Tingting Xia², Mian Li^{1,2}, and Min Xu¹

¹ National Engineering Laboratory for the Automotive Electronic Control Technology

² University of Michigan-Shanghai Jiao Tong University Joint Institute
Shanghai Jiao Tong University, Shanghai, China 200240

ABSTRACT

Multi-objective optimization (MOO) problems are encountered in many applications and a number of approaches have been proposed to deal with this kind of problems. Despite the computational efforts, the quality of the Pareto front is also a considerable issue. An evenly distributed Pareto front is desirable for developing analytical expressions. In this paper, a brand new approach called Normalized Circle Intersection (NCI) is proposed, which is able to efficiently generate a Pareto front with evenly-distributed Pareto points for bi-objective problems, no matter the feasible boundary is convex or not. Firstly, the anchor points are computed using an existing sequential MOO (SMOO) approach. Then in the normalized objective space, a circle with a radius of r centering at one of the anchor points or the latest obtained Pareto point is drawn. The intersection of the circle and the feasible boundary, which exists for sure, can be determined whether it is a Pareto point or not. For a convex or concave feasible boundary, the intersection is exactly the Pareto point to be found, while for a non-convex boundary the intersection can provide useful information for searching the true Pareto point even if it self is not a Pareto point. A novel MOO formulation is proposed for NCI correspondingly. Four examples, including two numerical and two engineering examples, are provided to demonstrate the applicability of the proposed method. Comparison of the computational results with WS, NNC and SMOO shows the effectiveness of the proposed method.

1 INTRODUCTION

One substantial portion of real-world optimization problems belongs to multi-objective optimization (MOO). Conflicts always exist among multiple objectives in this type of problems, thus trade-offs have to be made by decision makers. A solution

is in the Pareto set only if any improvement of one objective requires sacrificing at least one of the other objectives, that is, no Pareto point is objectively better than the others. MOO is an important research topic since there are still some open questions in this area. Existing methods in literature for solving MOO problems can be divided into three categories: scalarization algorithm, heuristic algorithm and hybrid algorithm.

Scalarization algorithms transform MOO problems into SOO (single-objective optimization) ones by forming an aggregate objective function (AOF) either using weights or transforming other objectives into constraints. AOF is a scalar substitute function that aggregates the objectives. For example, the multi-objective compound scaling (MCS) algorithm [1] can obtain only part of the Pareto set with the difficulty to get the pseudo-target value by which the unchosen objectives are treated as additional constraints. The weighted sum (WS) method is a linear combination of design objectives, which is easy to implement but fails to capture the solutions located on the non-convex region of the Pareto frontier. Prior assessment of the weight for each objective is required and an even distribution of the numerical weights in the AOF cannot guarantee to generate an evenly spaced set of Pareto solutions [2, 3]. Since weight-based approaches typically require many iterations to choose different weights, physical programming (PP) [4] was proposed to eliminate the need for iterative weight setting and thus substantially reducing the computational intensity. Generating an evenly spread Pareto frontier for both convex and concave regions using PP has been compared with WS in [5]. Another method to obtain an even spread of Pareto solutions is the normal-boundary intersection (NBI) approach, however, the Pareto points found by NBI may not be globally Pareto optimal for some cases [6]. Inspired by the ε -constrained method, the

* Corresponding author, email: zhoujhjane@sjtu.edu.cn, phone: +86-13761721419

Multi-Objective Tolerance Optimization Considering Friction Loss for Internal Combustion Engines

2017-01-0250

Published 03/28/2017

Jizhou Zhang, Jianhua Zhou, Mian LI, and Min Xu

Shanghai Jiao Tong University

CITATION: Zhang, J., Zhou, J., LI, M., and Xu, M., "Multi-Objective Tolerance Optimization Considering Friction Loss for Internal Combustion Engines," SAE Technical Paper 2017-01-0250, 2017, doi:10.4271/2017-01-0250.

Copyright © 2017 SAE International

Abstract

Manufacturing of the internal combustion engines (ICEs) has very critical requirements on the precision and tolerance of engine parts in order to guarantee the engine performance. As a typical complex nonlinear system, small changes in dimensions of ICE components may have great impact on the performance and cost of the manufacturing of ICEs. In this regard, it is still necessary to discuss the optimization of the tolerance and manufacturing precision of the critical components of ICEs even though the tolerance optimization in general has been reported in the literature. A systematic process for determining optimal tolerances will overcome the disadvantages of the traditional experience-based tolerance design and therefore improve the system performance. A novel multi-objective tolerance design optimization problem considering the friction loss in two important systems, the piston and the crankshaft, is proposed and solved in this work, since nearly 70% mechanical loss of an engine is caused by the piston and the crankshaft systems and friction loss is an important factor to affect the performance of the ICEs. The simulation models of the piston and crankshaft system are built using AVL Excite Piston & Ring® and Power Unit®, respectively. An analysis model used in the optimization is set up using the Gaussian Process with the corresponding simulation data. Finally, the multi-objective tolerance design optimization problem is formulated and solved using a newly developed sequential multi-objective optimization (S-MOO) method.

Introduction

Nowadays, the gas internal combustion engine (ICE) is still the most important and popular core component of the power unit of vehicles. Given the ICE is a complex engineering system, precision manufacturing is always required during the manufacturing of ICEs. With the development of precision manufacturing, the performance of the ICEs has been improved significantly, but is still considered as a difficult question since a small variation in the dimensions of key components may have great impact on the performance and cost of the ICEs. In this regard, the manufacturing precision of the critical components should be more rigorous.

Tolerance design is critical to precision manufacturing as the machining tolerance and manufacturing precision are determined in this process before actual manufacturing. If the tolerances of the components cannot reach the required standards, for example, they are too large, the performance of the system may fluctuate widely and the reliability of the system will become too low. However, reducing the tolerance always increases the costs and rejection rates during the manufacturing. From this perspective, the tolerances should be assigned properly to ensure the performance and to reduce the manufacturing cost as well.

The traditional experience-based tolerance design have many disadvantages. Without a systematic and global analysis of the tolerances, the designer may not understand the impact of the tolerances on the system performance comprehensively. The ICE is a typical complex system with a large number of components. The designer has to face a high risk of misusing a substandard tolerance based on his/her own experience. To avoid the substandard design, a more conservative way is often used. From this insight, experience-based tolerance design will either lead to unexpected system performance or wasted manufacturing cost. In addition, the tolerance design will become more complex when the system includes multiple subsystems. It is important to select critical components and have a systematic analysis on the relationship between the system performance and their corresponding tolerances. However, seldom research on the optimization of tolerance design has been reported in the literature since it is very difficult, if not impossible, to analyze and estimate the impact of the tolerances on system performance by traditional methods. The verification of the optimized tolerance design by experiments can cost too much too. It is even worse for a multi-objective optimization problem since the complexity of tolerances usually increases sharply when the number of the components increases. Considering these challenges, this work aims to apply multi-objective optimization on the tolerance design of an ICE majorly considering both piston and crankshaft subsystems based on simulation and analysis models.

IMECE2016-68197

EFFICIENT MODELING OF NONLINEAR SCATTERING OF ULTRASONIC GUIDED WAVES FROM FATIGUE CRACKS USING LOCAL INTERACTION SIMULATION APPROACH

Yanfeng Shen
UM-SJTU Joint Institute
Shanghai Jiao Tong University
Shanghai, China

Carlos E.S. Cesnik
Department of Aerospace Engineering
University of Michigan
Ann Arbor, Michigan, USA

ABSTRACT

This paper presents an efficient modeling technique to study the nonlinear scattering of ultrasonic guided waves from fatigue damage. A Local Interaction Simulation Approach (LISA) is adopted, which possesses the versatility to capture arbitrary fatigue crack shapes. The stick-slip contact dynamics is implemented in the LISA model via the penalty method, which captures the nonlinear interactions between guided waves and fatigue cracks. The LISA framework achieves remarkable computation efficiency with its parallel implementation using Compute Unified Device Architecture (CUDA) executed on GPUs. A small-size LISA model is tailored for the purpose of extracting the guided wave scattering features. The model consists of an interior damage region and an exterior absorbing boundary. The interior damage region captures various types of fatigue crack scenarios, while the exterior absorbing boundary surrounds the damage model to eliminate boundary reflections. Thus, the simulation of guided wave scattering in an infinite media can be achieved utilizing a small-size local LISA model. Due to the parallel CUDA implementation and the small-size nature, this local LISA model is highly efficient. Selective mode generation is achieved by coupling/decoupling excitation profiles with certain wave mode shapes, which allows the study of sensitivity of different wave modes to a certain fatigue damage situation. At the sensing locations, mode decomposition is performed on the scattering waves, which enables the study of mode conversion at the damage. Fourier analysis allows the extraction of scattering features at both fundamental and higher harmonic frequencies. A numerical case study on nonlinear scattering of guided waves from a fatigue crack is given. The higher harmonic generation and mode conversion phenomena are presented using the wave damage interaction coefficients (WDIC), from which the sensitive detection directions can be inferred to place sensors. This study can provide guidelines for

the effective design of sensitive SHM systems using nonlinear ultrasonic guided waves for fatigue crack detection.

INTRODUCTION

Guided-wave Structural Health Monitoring (SHM) systems generally identify damage by detecting the scattering waves. The effectiveness and sensitivity of an SHM sensor array depends on whether the sensors can receive sufficient damage-scattered wave energy at the sensing locations. Thus, it is important to understand the scattering features of ultrasonic guided waves from structural damage such as wave mode sensitivity, interrogation frequency influence, scattering amplitude and directionality, mode conversion effects, etc. Nonlinear ultrasonic techniques are drawing increasing attention in SHM applications due to their sensitivity to incipient fatigue cracks in structures. However, the nonlinear scattering features are quite complex with distinctive phenomena such as harmonic generation and mode conversion.

The fundamentals of wave damage interaction have been investigated analytically. Approximate solutions using Kirchhoff, Mindlin, Kane-Mindlin plate theory have been reported in the literature [1]. Moreau et al. applied 3D elasticity solution or exact Lamb wave solution to solve the wave scattering problem from cavities and flat-bottomed damage with irregular shapes [2]. Although these analytical methods manage to offer fast parametric studies, they are only possible for simple damage types. To solve guided wave scattering from arbitrary damage, Moreau et al. further developed small-size local finite element models (FEM) with absorbing boundaries [3]. Such local FEM can provide efficient predictive results of wave scattering from complex structural damage due to its light computational burden and frequency domain harmonic solution scheme. This technique has been used to provide the wave damage interaction information for the analytical wave

Guided Wave Generation and Propagation in Piezoelectric Composite Plates for Establishing Structural Self-awareness

YANFENG SHEN and JUNZHEN WANG

ABSTRACT

This paper presents a numerical investigation of guided wave generation, propagation, interaction with damage, and reception in piezoelectric composite plates for the purpose of establishing structural self-awareness. This approach employs piezoelectric composite materials as both load bearing structure and sensing elements. To understand the wave propagation characteristics in piezoelectric composite plates, finite element modal analysis of a plate cell with Bloch-Floquet condition is performed. A comparative study is carried out between a standard composite plate and a piezoelectric composite plate to highlight the influence of piezoelectricity on guided wave dispersion relations. Subsequently, a transient dynamic coupled-field finite element model is constructed to simulate the procedure of guided wave generation, propagation, interaction with damage, and reception in a piezoelectric composite plate. Active sensing array is designed to capture the structural response containing the damage information. Three engineering scenarios are considered to demonstrate the ultrasonic sensing capability of the piezoelectric composite system: a pristine case, a one-damage-location case, and a two-damage-location case. Finally, time-reversal method is utilized to locate and image the damage zones. This research shows that piezoelectric composite material possesses great potential to establish structural self-awareness, if it serves both as the load bearing and structural sensing component.

INTRODUCTION

Piezoelectric materials can be made into both actuation and sensing device due to their inverse and direct piezoelectric properties. For example, Piezoelectric Wafer Active Sensors (PWAS) have been widely adopted as enablers for generating and receiving ultrasonic guided waves [1]. On the other hand, composite materials have been increasingly used in mechanical and aerospace structural design, serving as load

Yanfeng Shen, University of Michigan-Shanghai Jiao Tong University Joint Institute, Shanghai Jiao Tong University, Shanghai, 200240, China, yanfeng.shen@sjtu.edu.cn
Junzhen Wang, University of Michigan-Shanghai Jiao Tong University Joint Institute, Shanghai Jiao Tong University, Shanghai, 200240, China

Numerical Investigation of Nonlinear Interactions between Multimodal Guided Waves and Delamination in Composite Structures

Yanfeng Shen*

University of Michigan-Shanghai Jiao Tong University Joint Institute, Shanghai Jiao Tong University, Shanghai, 200240, China

ABSTRACT

This paper presents a numerical investigation of the nonlinear interactions between multimodal guided waves and delamination in composite structures. The elastodynamic wave equations for anisotropic composite laminate were formulated using an explicit Local Interaction Simulation Approach (LISA). The contact dynamics was modeled using the penalty method. In order to capture the stick-slip contact motion, a Coulomb friction law was integrated into the computation procedure. A random gap function was defined for the contact pairs to model distributed initial closures or openings to approximate the nature of rough delamination interfaces. The LISA procedure was coded using the Compute Unified Device Architecture (CUDA), which enables the highly parallelized computation on powerful graphic cards. Several guided wave modes centered at various frequencies were investigated as the incident wave. Numerical case studies of different delamination locations across the thickness were carried out. The capability of different wave modes at various frequencies to trigger the Contact Acoustic Nonlinearity (CAN) was studied. The correlation between the delamination size and the signal nonlinearity was also investigated. Furthermore, the influence from the roughness of the delamination interfaces was discussed as well. The numerical investigation shows that the nonlinear features of wave delamination interactions can enhance the evaluation capability of guided wave Structural Health Monitoring (SHM) system. This paper finishes with discussion, concluding remarks, and suggestions for future work.

Keywords: structural health monitoring, guided waves, nonlinear ultrasonics, composite structures, LISA, delamination, higher harmonics

1. INTRODUCTION

The prompt detection and quantification of delamination in composite structures is critical for the prevention of catastrophic failures. Ultrasonic guided waves have been investigated as a promising interrogation tool to achieve real-time passive and active structural sensing. When guided waves interact with the delamination, Contact Acoustic Nonlinearity (CAN) may arise due to the clapping of the delamination interfaces, which may introduce distinctive signal features such as higher harmonics and side-band frequency components. Thus, the nonlinear ultrasonic phenomena possess great potential to improve the delamination evaluation capability of current Structural Health Monitoring (SHM) systems.

The evolution of damage in composite structures undergoes several stages, such as matrix cracking, matrix-fiber debonding, delamination, and fiber breakage. During such a procedure, the damage are mostly hidden underneath the laminate surface and are hard to notice. Conventional linear ultrasonic inspection techniques are only sensitive to relatively large size damage. On the other hand, nonlinear ultrasonic techniques have shown much higher sensitivity to incipient structural changes with distinctive nonlinear features, such as sub/higher harmonic generation, DC response, mixed frequency modulation response (sideband effects), and various frequency/amplitude dependent threshold behaviors [1]. The integration of nonlinear ultrasonic techniques into guided wave based inspection procedures is drawing increasing attention from the SHM and Nondestructive Evaluation (NDE) communities, because such a practice inherits both the sensitivity from nonlinear techniques and the large-area inspection capability from guided waves [2]. Many researchers have explored using guided waves for delamination detection. Utilizing the linear information of guided waves and scanning laser vibrometry, delamination was detected with advanced signal processing techniques [3, 4]. Research efforts aiming at taking advantage of the nonlinear information during wave delamination interaction have been reported as well. Soleimanpour et al. investigated the higher harmonic generation at the delamination and utilized nonlinear guided waves to locate the delamination zones in laminated composites [5, 6]. Yelve et al. also conducted finite element modeling and experiments to apply nonlinear ultrasonic methods to detect delamination [7, 8].

*yanfeng.shen@sjtu.edu.cn, Phone: +86-21-34206524, Fax: +86-21-34206525

Structural Health Monitoring of High-speed Railways Using Ultrasonic Guided Waves

YANFENG SHEN, JUNFANG WANG and YI-QING NI

ABSTRACT

This paper presents a damage detection strategy for high-speed railways using piezoelectric active sensors. Multimodal ultrasonic guided waves generated by a piezoelectric transmitter propagate along the rail track, undergo dispersion, interact with the damage zone, and are finally picked up by the sensors. First, numerical investigations are carried out to understand the guided wave features and their interaction mechanism with typical damage scenarios in the railways. The modal analysis of a finite element scheme with Bloch-Floquet condition is conducted to obtain the dispersion characteristics and the mode shapes of the rail track guided waves. Optimum wave generation location and frequency were explored using a small-size local coupled field finite element model. Further, a Local Interaction Simulation Approach (LISA) model was developed to achieve efficient simulation of elastic wave propagation in railway structures. The LISA procedure was coded using the Compute Unified Device Architecture (CUDA), which enables the highly parallelized computing on powerful Graphics Processing Units (GPUs). This transient dynamic analysis reveals the influence of rail track features and damage signature on the sensing signals. Finally, full-scale experiments on a BS 90A rail track with embedded piezoelectric sensors are carried out to compare with the numerical investigations. This study shows that the active sensing system possess promising potential for the in-situ health monitoring of railway structures.

INTRODUCTION

High-speed railways are prone to develop various types of damage, such as cracks and corrosion, during their service. The prompt detection and in-situ monitoring of damage zones is becoming a critical demand to ensure the operation safety of railway

Yanfeng Shen, University of Michigan-Shanghai Jiao Tong University Joint Institute, Shanghai Jiao Tong University, Shanghai, 200240, China, yanfeng.shen@sjtu.edu.cn

Junfang Wang, Department of Civil and Environmental Engineering, the Hong Kong Polytechnic University, Kowloon, Hong Kong, junfang-flora.wang@polyu.edu.hk

Yi-Qing Ni, Department of Civil and Environmental Engineering, the Hong Kong Polytechnic University, Kowloon, Hong Kong, yiqing.ni@polyu.edu.hk

AN EFFICIENT MODELING STRATEGY FOR LINEAR AND NONLINEAR GUIDED WAVE PROPAGATION IN COMPLEX STRUCTURES

Yanfeng Shen

(*UM-SJTU Joint Institute, Shanghai Jiao Tong University, Shanghai 200240, China*)

Abstract: This paper presents a Local Interaction Simulation Approach (LISA) based on the Finite Difference (FD) method and Sharp Interface Model (SIM) for the efficient modeling of ultrasonic guided wave propagation and nonlinear interaction with damage in complex structures. Case studies and experimental verifications are carried out to demonstrate LISA's prowess for wave modeling tasks. First, the case study for ultrasonic guided wave propagation in anisotropic carbon fiber composite panels are presented. The simulation results are compared with experimental measurements using Scanning Laser Doppler Vibrometry (SLDV). Then, the case study on guided wave propagation in complex structures and nonlinear wave damage interactions is presented. It addresses the wave propagation in a rail track with a fatigue crack. This research shows that LISA is a highly efficient modeling technique for guided wave simulations and possesses great application potential in structural health monitoring (SHM) for system design and sensing signal interpretation.

Key words: ultrasonic guided waves, nonlinear ultrasonics, structural health monitoring, local interaction simulation approach, complex structure

Detecting Outliers in Crank Angle Resolved Engine Flow Field Datasets for Proper Orthogonal Decomposition Analysis

2017-01-0612

Published 03/28/2017

Li Shen, Kwee-Yan Teh, Penghui Ge, Yusheng Wang, and David L.S. Hung

UM-SJTU JI, Shanghai Jiao Tong University

CITATION: Shen, L., Teh, K., Ge, P., Wang, Y. et al., "Detecting Outliers in Crank Angle Resolved Engine Flow Field Datasets for Proper Orthogonal Decomposition Analysis," SAE Technical Paper 2017-01-0612, 2017, doi:10.4271/2017-01-0612.

Copyright © 2017 SAE International

Abstract

Proper Orthogonal Decomposition (POD) is a useful statistical tool for analyzing the cycle-to-cycle variation of internal combustion engine in-cylinder flow field. Given a set of flow fields (also known as snapshots) recorded over multiple engine cycles, the POD analysis optimally decomposes the snapshots into a series of flow patterns (known as POD modes) and corresponding coefficients of successively maximum flow kinetic energy content. These POD results are therefore strongly dependent on the kinetic energy content of the individual snapshots, which may vary over a wide range. However, there is as yet no algorithm in the literature to define, detect, and then remove outlier snapshots from the dataset in a systematic manner to ensure reliable POD results. In this paper, one such outlier detection algorithm is proposed: A snapshot is considered an outlier if it has excessively high kinetic energy content as well as relevance index (a measure of flow pattern similarity) versus a particular POD mode. An analytical expression is derived to relate these two parameters and provide the statistical and physical underpinnings for the outlier detection algorithm. The algorithm is applied to two sets of crank angle-resolved engine in-cylinder flow fields in the middle tumble plane that were obtained experimentally using high-speed particle image velocimetry techniques, and improvements in POD results obtained after the removal of outlier snapshots are discussed.

Introduction

Cycle-to-cycle variation of in-cylinder flow field is a key feature of internal combustion (IC) engine operation, leading to variations in fuel and air mixing, ignition, and combustion. It limits stable operation of an engine within a narrow range, especially when running in low-temperature, high-dilution, or stratified combustion mode, beyond which combustion instabilities may degrade the engine fuel economy, increase its emissions, or even damage the engine. The flow fields may vary in macroscopic scale, i.e., on the order of the engine cylinder dimensions, entailing significant deviation in magnitude and direction

from the mean, as opposed to velocity fluctuations in small scales about that mean, underlying the classical Reynolds-averaged-Navier-Stokes (RANS) turbulence modeling framework.

Proper orthogonal decomposition (POD) was originally proposed by Lumley [1] as an alternative technique to analyze turbulent flows. The earliest studies applied the technique to canonical turbulent flows — in a channel [2], over a flat plate [3], during the development of an axisymmetric jet [4], etc. — with the goal of identifying large-scale patterns of “organized” fluid motion (known as “coherent structures”) that dominate, and therefore serve as bases for low-order description of those flows. The POD analysis technique has since been extended to the study of IC engine in-cylinder behaviors, whereby the coherent structures are used to explain larger scale variations in scalar fields [5, 6] and vector fields [7, 8, 9, 10], whereas what remained unexplained are deemed smaller scale turbulence or noise within the those fields.

Proper orthogonal decomposition has its roots in the fields of optimization and multivariate statistics. When an ensemble of flow field samples is considered as a multivariate dataset with the velocity components defined on individual grid points of the flow fields being the random variables, the result of the POD analysis of the ensemble is a series of flow patterns (known as POD modes) that successively maximize the sample variance in statistical terms and, equivalently, the average flow kinetic energy content in physical terms. It is on the basis of this property of optimality that the first several lower POD modes are identified as the coherent structures dominating the flow fields within the ensemble.

Viewed from another perspective, which has yet to be considered in the literature, the kinetic energy maximizing property of the POD analysis technique implies that each POD mode will tend to bear closer resemblance to the flow patterns of those members of the ensemble with high kinetic energy at that stage of the analysis. For instance, Abraham et al. [11] reported POD results upon combining two sets of velocity fields in the engine tumble plane, obtained separately from large eddy simulation (LES) computation and particle image velocimetry (PIV) experiment using virtual versus real engines of identical geometry and

Cycle-to-Cycle Variation of In-Cylinder Tumble Flow by Moment Normalization

2017-01-2214

Published 10/08/2017

Kwee-Yan Teh, Penghui Ge, Yusheng Wang, and David Hung

UM-SJTU JI - Shanghai Jiao Tong Univ.

CITATION: Teh, K., Ge, P., Wang, Y., and Hung, D., "Cycle-to-Cycle Variation of In-Cylinder Tumble Flow by Moment Normalization," SAE Technical Paper 2017-01-2214, 2017, doi:10.4271/2017-01-2214.

Copyright © 2017 SAE International

Abstract

The large-scale rotating flow structure in an engine cylinder exhibits features that can be described in generic terms of tumble and swirl. The structural details, nevertheless, vary from cycle to cycle due to fluctuating initial and boundary conditions of the flow. Typical analysis of the flow field cyclic variability - by simple root-mean-square, or additional spatial or temporal filtering, or proper orthogonal decomposition - is based on *pointwise* deviation of the instantaneous velocity from the ensemble mean. However, that analysis approach is not amenable to the evaluation of spatial variation of the flow structure, in position and orientation, within the flow field. To this end, other studies in the past focused instead on quantifying the variation of the vortex center for the dominant tumble or swirl pattern within the flow field. Yet there is no attempt in the literature to analyze both translational and *rotational* variations of more complex in-cylinder flow patterns, such as a counter-rotating tumble vortex pair generated during intake. In this paper, the technique of complex moment normalization from pattern recognition applications is extended to enable such an analysis. The algebraic properties of complex moments are introduced and related to the geometric and physical properties of two-dimensional flow fields. Complex moment normalization is then used to analyze a set of in-cylinder flow fields obtained by high-speed particle image velocimetry in the middle tumble plane of an optical engine. The cycle-to-cycle variation of the large-scale tumble flow structure - in magnitude, position, and orientation - are quantified and discussed.

Introduction

The large-scale rotating flow structure found within an internal combustion engine cylinder can be described generically in terms of tumble about an axis perpendicular to the axis of the engine cylinder, and swirl about an axis parallel to the cylinder axis [1]. The rotating flow is produced by design, with the aim of enhancing mixing and subsequent combustion of fuel with air [2]. That being the case, cycle-to-cycle variations of the flow structure would also lead to cyclic variability of the combustion process. This in turn limits stable

operation of the engine within a narrow range, beyond which combustion instabilities may degrade the engine fuel economy, increase its emissions, or even damage the engine.

It has been well recognized that cycle-to-cycle flow field variations cannot be analyzed simply as pointwise deviation of instantaneous velocity vectors from the ensemble mean velocity field (recorded at the same location within the cylinder and at the same phase of the engine cycle, averaged over multiple cycles) following the classical Reynolds decomposition approach [3, 4]. The so-called fluctuating velocity field that results from Reynolds decomposition may exhibit high intensity, whether expressed in terms of Reynolds stress tensor components [4] or two-dimensional fluctuating "kinetic energy" [5]. However, one cannot discern solely through the result of the velocity decomposition the nature of the flow field variation, whether it is due to turbulence in the classical sense (random variation of flow field that develops under the exact same boundary and initial conditions), or due to cyclic, and not entirely random, variation in the overall large-scale flow pattern (which arises under varying boundary or initial conditions). Yet such distinction is important to clarify their respective influences on the engine performance - whereas cyclic variability of the in-cylinder flow field is deemed detrimental to ignition and subsequent flame kernel development, turbulent fluctuations of the flow is understood to enhance combustion and flame propagation [2].

This immediate shortcoming is addressed in past studies via some form of filtering of the fluctuating velocity field: spatially [3], temporally [6], or according to kinetic energy via proper orthogonal decomposition (POD) [7, 8]. The low-pass filtered velocity or the velocity component of low POD modes is associated with larger-scale cyclic variation from the ensemble mean, whereas the high-pass filtered velocity or the velocity component of higher POD modes that remain is considered smaller-scale turbulence. Of course, the issue then turns to the lack of a physics-based justification for demarcating cyclic variation from flow turbulence by a single cutoff frequency or POD mode number. More crucially, each of the filtered velocity vector is still interpreted in a pointwise manner, with little regard for

Flame-Wall Interaction in Premixed Reactive Turbulence

Peipei Zhao and Lipo Wang
UM-SJTU Joint Institute, Shanghai Jiaotong University
Shanghai 200240, China

Nilanjan Chakraborty
Newcastle University, Newcastle-Upon-Tyne, UK

1 Introduction

The modern combustors are often made smaller in size for the sake of increasing the energy-density and improving the compactness but the flame-wall interaction (FWI) becomes a limiting factor. Such interaction may strongly affect the flame structure and the wall cooling. Especially local quenching close to the wall boundary adversely affects the efficiency of the combustors. Therefore, better understanding and rational modeling of FWI are necessary to the engineering design of modern combustion equipments.

In recent years, many efforts have been devoted to the relevant studies. One of the popular FWI configurations is shown in Fig. 1 (a), where the premixed flame propagates toward the cold wall and finally quenches. Based on this configuration, important results, for instance the quenching distance and maximum wall heat flux for both the laminar and turbulent cases, have been obtained [1–3]. Moreover, the local or even global

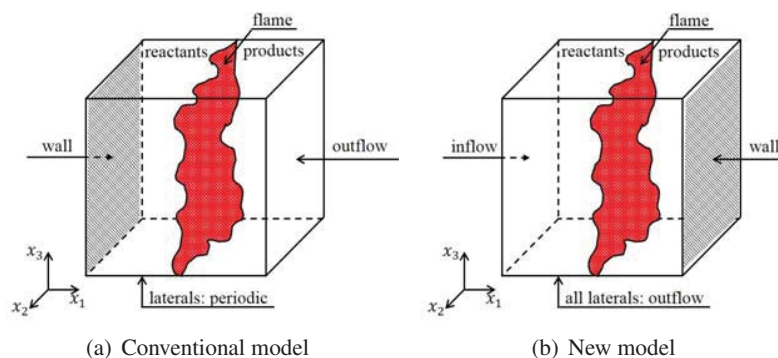


Figure 1: The configuration for FWI.

EXPERIMENTAL EVIDENCE OF TEMPERATURE RATIO EFFECT ON TURBINE BLADE TIP HEAT TRANSFER

H. Jiang
University of Michigan-Shanghai
Jiao Tong University Joint Institute,
Shanghai Jiao Tong University
jianghm188@163.com
Shanghai, China

Q. Zhang
City University London
Qiang.Zhang.1@city.ac.uk
London, UK

L. He
University of Oxford
li.he@eng.ox.ac.uk
Oxford, UK

S. Lu
School of Aeronautics and
Astronautics,
Shanghai Jiao Tong University
lusp@sjtu.edu.cn
Shanghai, China

L. Wang
University of Michigan-
Shanghai Jiao Tong
University Joint Institute,
Shanghai Jiao Tong
University
lipo.wang@sjtu.edu.cn
Shanghai, China

J. Teng
School of Aeronautics and
Astronautics,
Shanghai Jiao Tong University
tjf@sjtu.edu.cn
Shanghai, China

ABSTRACT

Determination of a scalable Nusselt number (based on “adiabatic heat transfer coefficient”) has been the main research objective of most existing heat transfer experimental researches for turbine blade tip. They were mostly carried out at near adiabatic condition without matching the engine realistic wall-to-gas low Temperature Ratio (TR). This practice is based on the assumption that the wall thermal boundary conditions do not affect the over-tip-leakage (OTL) flow field, the aerodynamics and heat transfer can be studied separately. Recent numerical studies raised a question on the validity of this conventional practice. Due to the relatively low thermal inertia of the leakage fluids contained within the thin clearance, the fluids transport properties vary greatly with the wall thermal boundary condition and the two-way coupling between OTL aerodynamics and heat transfer cannot be neglected. The issue could become more severe when the gas turbine manufacturers are making effort to achieve much tighter clearance. However, there has been no experimental evidence to back up these numerical findings. In this study, transient thermal measurements were conducted in a high-temperature linear cascade rig for a range of tip clearances (0.3%, 0.4%, 0.6% and 1%). Surface temperature history was captured by Infrared Thermography at a range of wall-to-gas TRs. Heat Transfer Coefficient (HTC) distributions were obtained based on a conventional data processing technique. The profound influence of tip surface thermal boundary condition on heat transfer and OTL

flow was revealed by the first-of-its-kind experimental data obtained in the present study.

INTRODUCTION

Most experimental research in gas turbine heat transfer community was carried out at near adiabatic condition without matching the engine realistic wall-to-gas Temperature Ratio (TR). The underlying assumption is that the wall thermal boundary condition does not affect the flow field, the aerodynamics and heat transfer can be studied separately. Therefore, the data obtained in the “cold experiment” could be scaled to the engine operating condition. Very recently, the coupling effect between aerodynamics and heat transfer received more attention. There have been increasingly debates on whether the conventional convection-only approach still works over the rotor blade tip, considering the complex Over-Tip-Leakage (OTL) flow and the ongoing effort from the gas turbine manufacturers to achieve much tighter clearance.

The convective heat transfer coefficient (HTC) was defined as a fluid mechanical property in the Newton’s law of cooling.

$$q = HTC \times (T_d - T_w) \quad (1)$$

where T_w is local wall surface temperature, and T_d is the local fluid driving temperature. For low speed flow, it can be assumed to be the freestream temperature, while for high

GT2017-64422

ON SCALING METHOD TO INVESTIGATE HIGH-SPEED OVER-TIP-LEAKAGE FLOW AT LOW-SPEED CONDITION

Hongmei Jiang

University of Michigan-Shanghai Jiao Tong
University Joint Institute, Shanghai Jiao Tong
University, Shanghai, China

Li He

University of Oxford
Oxford, UK

Qiang Zhang

City, University of London
London, UK

Lipo Wang

University of Michigan-Shanghai Jiao Tong
University Joint Institute, Shanghai Jiao Tong
University, Shanghai, China

ABSTRACT

Modern High Pressure Turbine (HPT) blades operate at high speed conditions. The Over-Tip-Leakage (OTL) flow, which plays a major role in the overall loss generation for HPT, can be high-subsonic or even transonic. In practice from the consideration of problem simplification and cost reduction, the OTL flow has been studied extensively in low speed experiments. It has been assumed a redesigned low speed blade profile with a matched blade loading should be sufficient to scale the high speed OTL flow down to the low speed condition.

In this paper, the validity of this conventional scaling approach is computationally examined. The CFD methodology was firstly validated by experimental data conducted in both high and low speed conditions. Detailed analyses on the OTL flows at high and low speed conditions indicate that, only matching the loading distribution with a redesigned blade cannot ensure the match of the aerodynamic performance at the low speed condition with that at the high-speed condition. Specifically, the discrepancy in the peak tip leakage mass flux can be as high as 22.2%, and the total pressure loss at the low speed condition is 10.7% higher than the high speed case.

An improved scaling method is proposed hereof. As an additional dimension variable, the tip clearance can also be “scaled” down from the high speed to low speed case to match the cross-tip pressure gradient between pressure and suction surfaces. The similarity in terms of the overall aerodynamic loss and local leakage flow distribution can be improved by adjusting the tip clearance, either uniformly or locally. The limitations of this proposed method are also addressed in this paper.

INTRODUCTION

The Over-Tip-Leakage (OTL) flow has a significant impact on the overall turbine aerodynamic performance. Many

experimental studies have been carried out to study its complex flow physics and to validate various tip design concepts. During the design process of these experiments, the key flow conditions in the real engine have to be carefully scaled and matched, although there has always been a compromise between experimental accuracy and cost.

As a reasonable simplification which requires few compromises to represent the real blade structure [1], low speed linear cascades rigs have been widely used. The advantage of these rigs are relatively low experimentation costs and excellent spatial resolution [1, 2]. In addition to match the Reynolds number and key geometry parameters, the blade profile employed in these low speed tests has to be redesigned to compensate the influence of compressibility at the high speed condition, so the blade loading could also be closely matched.

The scaling method related to the blade profile redesign has been well-studied in the literature. Wisler [3-5] studied pressure loss reduction in axial-flow compressors through Low-Speed Model Testing (LSMT) of GE-E3. The idea is to modify the incidence angles, the chordwise camber distributions, and the thickness distributions of the low-speed airfoils until these airfoils achieve the same normalized surface velocity distributions as the high-speed airfoils. The low-speed airfoils require leading edge camber line bending and somewhat thicker shape in order to match the velocity distributions. Low speed experiments by Lyes et al. [6-8] focused on the fourth stage of a five-stage high pressure compressor C147. The low speed blading was designed for same enthalpy rise across the rotor, and same non-dimensional axial velocity and absolute flow angle for the inlet to the rotor. A drawback is that the De Haller number (the blade exit-to-inlet velocity ratio) cannot be maintained. However, by designing the blade sections to produce the same distributions of normalized local velocity, the blade surface static

GT2017-64293

ROTATING EFFECT ON TRANSONIC SQUEALER TIP COOLING PERFORMANCE

D. Zhu

University of Michigan-Shanghai Jiao Tong
University Joint Institute
Shanghai, China

S. Lu

School of Aeronautics and Astronautics, Shanghai
Jiao Tong University
Shanghai, China

H. Ma

University of Michigan-Shanghai
Jiao Tong University Joint
Institute
Shanghai, China

Q. Zhang

City University London
London, UK

J. Teng

School of Aeronautics and
Astronautics, Shanghai Jiao
Tong University
Shanghai, China

ABSTRACT

The aerothermal behavior of turbine blade tip has been studied for decades, mostly using stationary linear cascade. The blade rotation effect still remains unclear to the tip research community. This paper investigates two squealer tip cooling configurations with the effect of relative casing movement. The numerical method was validated against thermal measurement obtained in a transonic wind tunnel. Further analysis is presented for cases with relative casing motion. Dramatic changes in aerodynamics and heat transfer were observed, mostly due to the strong interactions between the over tip leakage flow and the coolant injection. The need to consider the rotating effect into future experimental validation is highlighted.

1. INTRODUCTION

A higher thermal efficiency and a larger power generation of aircraft turbine engine have long been pursued by researchers. To achieve this target, the turbine inlet temperature must be raised. Gas turbines are operated at around 1800 degree Celsius now and definitely will be higher than 2000 degree Celsius someday. This temperature induces excessive thermal stresses on the turbine blade, thus the possibility of thermal failure is enhanced.

The thermal failure problem is even more serious on rotor blade tip and near tip regions. For unshrouded blade, tip leakage flow is formed and accelerated due to the pressure difference between the pressure side and the suction side of the blade, causing a higher heat transfer rate and more complex heat transfer distributions on the tip surface and near tip regions.

To prevent turbine blade from thermal failure, cooling techniques are required. The blade tip and near tip region are more difficult to cool because the heat transfer distribution varies significantly with different tip geometries and different aerothermal conditions. Han [1] has summarized the heat transfer research topics and cooling techniques.

Film cooling is commonly used in turbine blade. Coolant from the compressor is ejected from inside of the blade through slots or discrete holes on the surface of the blade. The high temperature mainstream flow is pushed away from the surface and a low temperature film is formed over the surface. Thus, the temperature difference between the solid and the fluid is decreased.

To achieve effective cooling system designs, a large amount of work has been done to help understand the heat transfer mechanisms in the tip gap. Bunker [2] presented a review of the publicly available knowledge concerning subsonic turbine blade tip heat transfer before 2001. Yang et al. [3] employed CFX 5.7 to simulate the flow fields in the tip gap of stationary case, casing moving case and blade rotating case. They found that, on the flat tip, the heat transfer difference between casing moving case and blade rotating case was small, and it was even smaller on a squealer tip. Viridi et al. [4] used an IR camera to observe the heat transfer on the blade tip and used this experimental result to validate their numerical simulation with casing motion. Their numerical flow visualization showed relative casing motion moved the cavity vortex in a squealer tip closer to the pressure side rim, causing a high heat transfer strip on this location. Zhou [5] also found this flow structure change using numerical method. And he also found relative casing

Combined synthetic aperture focusing technique and three-dimensional deconvolution for resolution enhancement in photoacoustic microscopy

De Cai^a, Zhongfei Li^a, Yao Li^a, Zhendong Guo^a, and Sung-Liang Chen^{a,b,*}

^aUniversity of Michigan-Shanghai Jiao Tong University Joint Institute, Shanghai Jiao Tong University, Shanghai 200240, China

^bState Key Laboratory of Advanced Optical Communication Systems and Networks, Shanghai Jiao Tong University, Shanghai 200240, China

*sungliang.chen@sjtu.edu.cn

ABSTRACT

Acoustic-resolution photoacoustic microscopy (ARPAM) is a promising tool for deep imaging of biological tissues. Synthetic aperture focusing technique (SAFT) can improve the degraded lateral resolution in the out-of-focus region of ARPAM when using a high numerical aperture acoustic transducer. We previously reported a three-dimensional (3D) deconvolution technique to improve both lateral and axial resolutions in the focus region of ARPAM. In this work, we extended resolution enhancement of ARPAM to the out-of-focus region based on two dimensional SAFT combined with the 3D deconvolution (SAFT+Deconv). In both the focus and out-of-focus regions, depth-independent lateral and axial resolution after SAFT ensures a depth-independent point spread function for 3D deconvolution algorithm. In an extended depth of focus (DOF) of ~ 2 mm, SAFT+Deconv ARPAM improves the -6 dB lateral resolutions from $65\text{--}700\text{ }\mu\text{m}$ to $20\text{--}29\text{ }\mu\text{m}$, and the -6 dB axial resolutions from $35\text{--}42\text{ }\mu\text{m}$ to $12\text{--}19\text{ }\mu\text{m}$. The signal-to-noise ratio is also increased by $6\text{--}30$ dB. The enhanced resolution in extended DOF by SAFT+Deconv ARPAM may enable important applications in biomedical photoacoustic imaging.

Keywords: Photoacoustic imaging, Three-dimensional microscopy, Synthetic aperture focusing technique, Deconvolution

1. INTRODUCTION

Photoacoustic (PA) imaging can achieve high resolution with deep penetration in biological tissues.^{1,2} High-resolution of PA microscopy (PAM) can be implemented either by optical-resolution PAM (ORPAM)^{3,4} or acoustic-resolution PAM (ARPAM).⁵⁻⁷ The lateral resolution of several micrometers or even sub-micrometer in ORPAM has been reported by tight optical focusing, which is limited in only ~ 1 mm below the surface of biological tissues.¹ By utilizing focused ultrasonic transducers with high center frequency and high numerical aperture (NA), ARPAM can usually achieve tens of micrometers in lateral resolution with deeper penetration. A penetration depth of 6 mm in ARPAM has been demonstrated⁸ because the scattering of ultrasound in tissues is 2–3 orders of magnitude weaker than that of light. High-resolution ARPAM still faces two challenges: (1) higher-frequency ultrasound waves attenuate sharply in biological tissues; (2) depth-of-focus (DOF) shrinks quickly with increased NA for focused transducer. High lateral resolution is therefore guaranteed only in limited focus region.

Synthetic aperture focusing technique (SAFT) can improve the degraded lateral resolution of ARPAM in the out-of-focus region. SAFT in PA imaging was first proposed by Liao *et al.*, using a needle hydrophone, to improve the resolution and the signal-to-noise ratio (SNR).⁹ Virtual-point detector (VPD) SAFT for focused transducer was then developed by Li *et al.*¹⁰ Afterwards, two-dimensional (2D) SAFT was naturally extended by Deng *et al.* to yield isotropic lateral resolution.¹¹ More recently, SAFT with weighting from spatial impulse response (SIR) of a transducer was introduced so that SAFT can be applied to the focus region.¹² Depth-independent lateral resolution was demonstrated in SAFT both for ultrasound imaging¹³ and PA imaging.^{10,14} The inherently depth-independent axial resolution of ARPAM is determined by the bandwidth of an ultrasonic transducer.

Ultrasound detection with surface plasmon resonance on fiber end-facet

Xin Zhou¹, De Cai¹, Xiaolong He^{1,2}, Sung-Liang Chen¹, Xueding Wang³ and Tian Yang^{1*}

¹State Key Laboratory of Advanced Optical Communication Systems and Networks, Key Laboratory for Thin Film and Microfabrication of the Ministry of Education, UM-SJTU Joint Institute, Shanghai Jiao Tong University, Shanghai 200240, China.

²Xu Yuan Biotechnology Company, 1883 South Huicheng Road, Shanghai 201821, China.

³Department of Biomedical Engineering, University of Michigan, 2200 Bonisteel Blvd, Ann Arbor, MI 48109, USA.

E-mail: tianyang@sjtu.edu.cn

Abstract: A surface plasmon resonance cavity on an optical fiber end-facet is designed and demonstrated for ultrasound detection. A noise equivalent pressure of 25 KPa over 20 MHz, almost omni-directional response and stable performance are reported.

OCIS codes: (130.3120) Integrated optics devices; (230.1040) Acousto-optical devices; (240.6680) Surface plasmons.

1. Introduction

The development of invasive ultrasound imaging demands ultrasound detectors that have a small size, a flexible configuration, a flat angular response as well as a satisfactory combination of sensitivity and bandwidth. In the case of piezoelectric detectors, in order to achieve high sensitivity, a large size of the piezoelectric material has to be used to reap enough ultrasound energy, which in turn limits the bandwidth and angular response. In addition, to detect high frequency ultrasound, the piezoelectric material has to be thinner than the acoustic wavelength, which presents a challenging fabrication task. A few optical detection methods have been reported which show noise equivalent pressure (NEP) values from 105 Pa to 3.3 KPa under bandwidths of more than 100 MHz, e.g. microring devices [1] and prism-coupled surface plasmon resonance (SPR) [2], but whose configurations can't be straightforwardly integrated with in vivo applications. By integrating a Fabry-Perot cavity on the end-facet of a single-mode optical fiber (SMF), Beard's group has demonstrated NEP values as low as a few Pa's and broad working bandwidths [3]. The SMF platform offers an ideal combination of small size, flexible configuration and easy optical transmission. In this work, we report an SPR cavity device on the end-facet of a SMF, which shows a NEP of 25 KPa and an almost omni-directional angular response, which at the same time shall have a broader bandwidth than any of the above-mentioned detectors in principle, and which is fabricated at a low cost and high yield.

2. Experiments

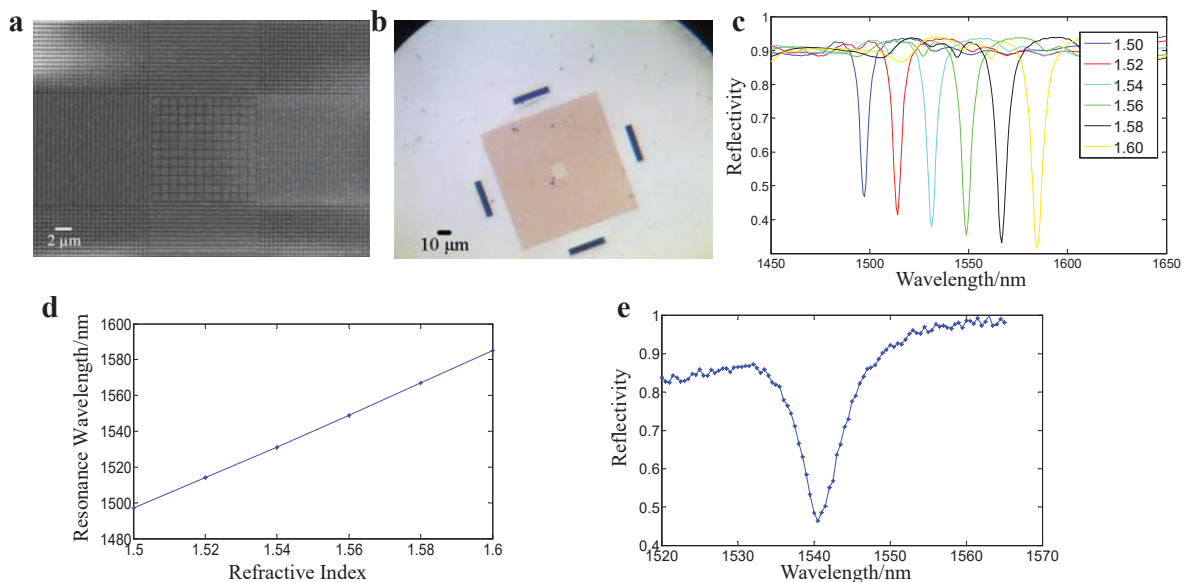


Fig. 1(a) Scanning electron micrograph of an SPR cavity. (b) The transferred device on a fiber end-facet under an optical microscope. (c) Simulated reflection spectra with different refractive indices of glue. (d) The linear relationship between the SPR resonance wavelength and the

A Memory-Assisted MAC Protocol with Angular-Division-Multiplexing in Terahertz Networks

Chong Han, Wenqian Tong, and Xinyi Wu

University of Michigan–Shanghai Jiao Tong University Joint Institute

Shanghai Jiao Tong University, Shanghai 200240, China

Email: {chong.han, light123star, slogger}@sjtu.edu.cn

Abstract—Terahertz band communication is envisioned as a key technology to satisfy the increasing demand for ultra-high-speed wireless links. In this paper, a memory-assisted medium access control (MAC) protocol with angular-division-multiplexing (ADM) is proposed for the service discovery and communications in the THz network. In particular, the efficiency balance is achieved by equipping the nodes with (i) the omni-directional antennas at the service discovery phase, and (ii) directional antennas for message transmissions. Moreover, the memory is leveraged in the ADM scheme to assist the access point (AP) to skip the unregistered angular slots to improve the network performance. Based on the proposed MAC protocol, the analytical models of the interference, SINR, outage probability, throughput and the delay in the THz network are derived respectively. According to the simulation and numerical analysis, the results show that our proposed MAC protocol can effectively improve the throughput by over 15% and substantially reduce the delay, in comparison with the ADM scheme without the memory guidance.

I. INTRODUCTION

The Terahertz (0.1 - 10 THz) band provides wireless communication devices with an unprecedentedly large bandwidth, ranging from several tens of GHz up to a few THz, which can satisfy the increasing demand of 100 Gbps and even 1 Tbps data rates within the next decade [1]. The use of this frequency band is envisioned to address the spectrum scarcity and capacity limitations of current wireless systems, and boost a plethora of applications, including wireless backhaul to the small cells, and ultra-high-speed data transfers among proximal devices [2].

Thanks to the very small wavelength at THz frequencies, very large antenna arrays realizing *ultra-massive MIMO* [3] can be used to enable directional transmissions in the THz network, to overcome the very high path loss and the limited communication distance. The highly directional and the ultra-high-speed links in the network design introduce the following challenges that motivate this work. First, the focus of the network solutions needs to shift from access contention to coordination and scheduling. Furthermore, the coordination and scheduling should be compatible with the very high data rates, the unique channel and physical properties of the THz band. Second, the interference models that were studied for omni-directional transmissions need to be revisited in the THz network. Third, although directional links can substantially improve the system performance, the difficulty for network discovery increases and the associated deafness problem [4]

might arise. Therefore, the efficiency and performance between the service discovery and the data communication need to be balanced.

In this work, we focus on the fundamental problem of the network design: medium access control (MAC). Existing MAC solutions for the relevant millimeter-wave [5], [6] and the THz band [7] so far have not addressed the aforementioned challenges. The very recent THz MAC design in [8] relies on the one-way receiver-initiated handshake method. However, the effectiveness of the receiver initiation, the service discovery and the multi-user interference have not been addressed.

The distinctive features of our work are summarized as follows. First, we present the centralized THz network architecture, in which there are one access point (AP) and multiple nodes. The directional links between the AP and the nodes are confined into a number of angular slots. Based on the THz communication models, we propose a memory-assisted MAC protocol with angular-division-multiplexing (ADM). A flowchart for the protocol is presented, which consists of four steps, namely, service discovery, angle determination and network association, memory-guided message transmission and fairness reset. The novelties of the proposed design are twofold. The efficiency balance is achieved by equipping the nodes with (i) the omni-directional antennas at the service discovery phase, and (ii) directional antennas for message transmissions. Additionally, the memory is leveraged in the ADM scheme that directs the AP to skip the unregistered angular slots, which can improve the network performance.

Furthermore, we analyze the interference and signal-to-interference-plus-noise ratio (SINR) in the THz network. In light of these physical parameters and the proposed MAC protocol, we proceed with analytical models for the outage probability, the throughput, and the delay. According to the extensive simulation and numerical analysis, the results show that our proposed MAC protocol can effectively improve the throughput and substantially reduce the delay, in comparison with the ADM scheme without the memory guidance.

The remainder of the paper is organized as follows. In Sec. II, the THz network is described. The proposed memory-assisted MAC protocol with ADM is detailed in Sec. III. In Sec. IV, the critical parameters including the interference, SINR, outage probability, throughput and the delay based on the proposed MAC protocol in the TH network are modeled. Simulation and numerical results are presented in Sec. V.

Interference and Coverage Analysis for Terahertz Band Communication in Nanonetworks

Chao-Chao Wang, Xin-Wei Yao

and Wan-Liang Wang

College of Computer Science and Technology

Zhejiang University of Technology

Hangzhou 310023, China

Email: {ccwang, xwyao, zjutwwl}@zjut.edu.cn

Chong Han^{*†}

^{*}University of Michigan-Shanghai Jiao Tong University Joint Institute

Shanghai Jiao Tong University

Shanghai 200240, China

[†]Shenzhen Institute of Terahertz Technology and Innovation

Shenzhen 518101, China

Email: chong.han@sjtu.edu.cn

Abstract—Interference and coverage is a critical factor affecting the performance of nanonetworks in the terahertz (THz) band. In this paper, on the basis of THz channel model, the interferences from surrounding omnidirectional nanosensors (NSs) and beamforming Base Stations (BSs) are derived in closed forms by using stochastic geometry methods respectively. Furthermore, the corresponding Signal-to-Interference-plus-Noise-Ratio (SINR) and the coverage probabilities are investigated based on the proposed interference model. Simulation results, observed from the spectral windows at 1.0 THz, 4.5 THz and 9.1 THz, demonstrate that high density of BSs, beamforming antenna with small beam-width and low density of NSs are recommended to mitigate the interference and improve the coverage performance. Moreover, low frequency in THz band with low absorption coefficient is advocated to guarantee the correct reception with enough high received signal strength.

I. INTRODUCTION

A Nanonetwork is a kind of network composed by extremely small nanointerface and nanosensors (NSs), etc. It is driven by nanotechnology and enables new applications in biomedical, environmental and military fields, such as intra-body health monitoring systems, air pollution control, and military defense system [1]. Two main alternatives for communications in nanonetworks are based either on ElectroMagnetic (EM) communication or molecular communication. In this paper, we focus on the EM communication. Due to the extremely limited size of NSs, high transmission frequencies have to be introduced for communication. Following this trend, THz band are recommended overcome this limitation [2].

For the time being, the studies of THz band communications and nanonetworks become more systematic and vary from the fundamental peculiarities [3] [4], to channel modeling [5] and design of upper layer protocols [6]. All of these are driving nanonetworks to be more realistic. However, there is few analysis on interference and coverage for THz band communication in nanonetworks which are critical to analyze the performance of THz communications and measure the quality of wireless connections of nanonetworks. In [7], two types of interference associated with multi-wideband transmission, namely, Inter-Symbol Interference (ISI) and Inter-band Interference (IBI) have been considered. This analysis of interference was studied between a transmitter and a receiver,

instead of the perspective of network. In this direction, [8] presented an analytical model for interference from omnidirectional NSs and SINR assessment in dense THz networks. But the interference from BSs was not considered and the coverage probability was not analyzed. However, due to the very limited transmission distance as a result of high path loss in THz band and limited transmission power at nano-devices, the BSs become intensive. Meanwhile, beamforming and massive Multiple Input Multiple Output (MIMO) [9] technologies are introduced, particularly to be deployed at BSs. These features in nanonetworks make the existing interference models unsuitable, which necessitates new framework for the analysis of interference and coverage performance.

Stochastic geometry has been widely utilized for modeling and analysis in the conventional communication networks, especially for interference and coverage analysis in lower frequency bands and millimeter-wave systems [10]. Also, [8] applied a stochastic geometry method to investigate the interference in dense THz networks. Accordingly, in this paper, the interference from omnidirectional NSs and beamforming BSs are comprehensively investigated by using stochastic geometry methods for nanonetworks in the THz band. Moreover, with the features of THz communication and the proposed interference model, the corresponding SINR and coverage probabilities are presented. Through the simulations with the spectral windows at 1.0 THz, 4.5 THz and 9.1 THz, frequency with low absorption loss, beamforming antenna with small beam-width and low density of NSs can significantly improve the coverage performance. Increasing the number of BSs appropriately is an option to improve the coverage probability when the density of NSs increases. Moreover, low frequency in THz band with low absorption coefficient is advocated to guarantee the correct reception with enough high received signal strength.

The remainder of the paper is organized as follows. In Sec. II, we introduce the nanonetwork model. The detailed analysis of interference is conducted in Sec. III. Sec. IV presents the SINR and the coverage probability based on the interference models. Simulation results are presented in Sec. V. Finally, we conclude the paper in Sec. VI.

A Three-Dimensional Time-Varying Channel Model for 5G Indoor Dual-Mobility Channels

Shuai Nie*, Chong Han[†], and Ian F. Akyildiz*

*Broadband Wireless Networking (BWN) Laboratory

School of Electrical and Computer Engineering

Georgia Institute of Technology, Atlanta, GA 30332, USA

{shuainie, ian}@ece.gatech.edu

[†]University of Michigan – Shanghai Jiao Tong University Joint Institute

Shanghai Jiao Tong University, Shanghai, China

chong.han@sjtu.edu.cn

Abstract—This paper presents a time-varying channel model in three-dimensional environments for the 5G wireless system. Using the continuous-time Markov chain, the proposed model captures the statistical movement of the transceiver, the transition between line-of-sight and non-line-of-sight propagation scenarios, and the dynamic variation of propagation parameters. Moreover, a novel frequency-dependent factor that describes the dynamic path behavior is described in this model. According to the simulation results based on ray-tracing techniques and field measurements from the literature, the proposed time-varying channel model is validated at 5.2, 10, and 60 GHz. Furthermore, under realistic 5G device-to-device communication scenario, the simulation results and time-varying channel characteristics are highlighted, including the number of paths, path gain, delay spread, delay variation, Rician K -factor, and coherence bandwidth.

Index Terms—3D channel modeling, spatial consistency, ray-tracing, dual-mobility, continuous-time Markov chain

I. INTRODUCTION

The fifth-generation (5G) wireless systems require new modeling approaches that characterize the propagation channel accurately. Most 4G wireless communication systems are deploying channel models based on the assumption of a stationary or quasi-stationary channel. The stationary channel models reduce time complexity to channels with fixed links. However, due to the nature of mobility in wireless channels and the growing popularity in the device-to-device (D2D) communications with both terminals in movement, the demand of characterizing the rapid time-varying non-stationary channel to optimize modeling accuracy is increasing [1]. The current standards in 3GPP only describe the time-varying Doppler shift in the channel, however, a more detailed study is needed to include random movements of objects in environment as well as dual mobility of both transmitter and receiver.

In addition to the D2D communication scenario, the three-dimensional (3D) channel modeling approach is necessary in characterizing propagation channel because of an extra degree of freedom in the elevation plane [2]. With techniques of diversity and spatial multiplexing utilized in a multiple antenna system, the 3D channel model is crucial for leveraging the capacity of wireless communication systems [3]. The QuaDRiGa channel model, which depicts a 3D multi-cell

channel model with time evolution, has been validated by outdoor measurements in downtown Berlin [4]. So far, only a few indoor measurements capturing the mobility of transceivers are reported. At 60 GHz, continuous-route measurements have been conducted in a hallway and an office to study the shadowing and angular statistics of a channel with mobility [5]. A wideband dynamic directional channel model is extracted from measurements at 5.2 GHz which demonstrates that the time-varying channel can be characterized using an M-step four-state Markov process [6]. Although the measurements capture a full-dimensional view of the channel, the proposed directional model is based on 2D statistics that cannot fully reflect the channel properties in the elevation plane, and causes a mismatch between simulated and measured number of paths.

We propose a new channel model in indoor environments that describes the time-varying nature of a wireless channel using a continuous-time Markov chain. By combining the stochastic modeling and the ray-tracing method, our proposed model can accurately characterize the dual-mobility scenario in the 5G system. Specifically, we use the ray-tracing method to model the deterministic channel parameters at the initial time step and utilize a birth-death process derived from a continuous-time Markov chain to describe the dynamic behavior of paths. We validate the model by comparing the simulated results with existing measurements in the literature. Furthermore, we highlight the critical characteristic parameters under realistic 5G D2D communication scenario, which include the number of paths, path gain, delay spread, delay variation, Rician K -factor, and coherence bandwidth.

II. 3D TIME-VARYING CHANNEL MODEL

In signal processing and wireless communications [7], the output signal of a propagation channel is a function of the channel impulse response $h(t, \tau)$ and an input signal $x(t)$, plus some random noise $n(t)$, as shown in the following equation,

$$y(t) = \int_{-\infty}^{\infty} x(t - \tau) \cdot h(t, \tau, f_d, \phi, \theta) d\tau + n(t). \quad (1)$$

The channel impulse response (CIR) in a time-varying channel can be further expressed as a function of delay τ , Doppler

MRA-MAC: A Multi-Radio Assisted Medium Access Control in Terahertz Communication Networks

Wenqian Tong¹ and Chong Han^{1,2}

¹University of Michigan–Shanghai Jiao Tong University Joint Institute
Shanghai Jiao Tong University, Shanghai 200240, China
Email: {light123star, chong.han}@sjtu.edu.cn

²Shenzhen Institute of Terahertz Technology and Innovation, Shenzhen, 518101, China

Abstract—Terahertz (THz) communication is envisioned as one of the key technologies to satisfy the increasing demand for higher-speed wireless communication networks. Thanks to the very small wavelengths at THz frequencies, the very large antenna array can be equipped to enable beamforming, which can effectively overcome the very high path loss and improve the communication distance. However, directional transmissions, as well as the peculiarities of the THz channel and physical layer, increase the difficulties of medium access control (MAC) design. In this paper, a multi-radio assisted (MRA-MAC) protocol in the distributed THz network is proposed and analyzed. The key idea is to enable 2.4/5 GHz omni-directional radio for control signaling and THz beamforming for data transmissions. A flowchart of the protocol and detailed operations are presented. Based on the models of THz pulse waveform and the THz channel with beamforming, the delay, the outage probability, and the network throughput are analytically investigated, supported by extensive simulation and numerical evaluations.

I. INTRODUCTION

The Terahertz (0.1 – 10 THz) band has an unprecedentedly large bandwidth, ranging from several tens of GHz up to a few THz, which can satisfy the increasing demand for 100 Gbps and even 1 Tbps data rates within the next decade [1]. The use of this frequency band is envisioned to address the spectrum scarcity and capacity limitations of current wireless systems, and boost a plethora of applications [2]. To overcome the very high path loss and the resulting limited communication distance, very large antenna arrays forming *ultra-massive MIMO* [3] can be realized, thanks to the very small wavelength at THz frequencies. Coupled with beamforming techniques, pencil-sharp beams can be generated to enable highly directional transmissions in THz networks.

Although directional links can substantially improve the link data rate and extend the coverage, the difficulties for network discovery and Medium Access Control (MAC) largely increase. Particularly in a distributed network without central coordination, the most critical challenge is the deafness problem, which occurs when a transmitter tries to communicate with a receiver but fails because the receiver beamforms towards a direction away from the transmitter [4]. Available MAC solutions for lower-frequency systems cannot directly be utilized in the THz paradigm, mainly because they do not capture the peculiarities of the THz channel or the capabilities of THz communications and devices. An attractive and novel

approach for the MAC design in broadband networks is to decouple the control plane and data plane by separating their operating frequencies, owing to the advancement of multi-radio transceiver technologies. This idea has been exploited for millimeter-wave communications [5], [6], and THz systems [7]. However, the dual-band TAB-MAC protocol in [7] strictly relies on anchor nodes to track accurate geographic location. Also, this scheme does not consider the absence of line-of-sight (LoS) between the transmitter and the receiver. To overcome these restrictions and further improve the effectiveness of protocol operation, we propose a *multi-radio assisted medium access control (MRA-MAC)* design in distributed THz networks in this work.

The distinctive contributions are summarized as follows. First, we separate the control plane and data plane in two phases, by leveraging multi-radio transceiver technologies. In Phase 1, nodes use the omni-directional low-GHz radio (e.g., at 2.4 or 5 GHz) to exchange control information and establish a network association. In Phase 2, based on processing angle-of-arrival (AoA), nodes start ultra-high-rate data transmissions by utilizing beamforming techniques in the THz band using the best AoA path. Second, a flowchart of the protocol with detailed operations is presented. Moreover, the redundant overhead in the existing low-GHz control signaling is further reduced in our design. Third, in light of the models of THz pulse waveform and THz channel with beamforming, we provide analytical models for the signal-to-interference-plus-noise ratio (SINR), delay, the outage probability, and the network throughput, supported by numerical evaluations.

The remainder of the paper is organized as follows. In Sec. II, the distributed THz network and the capabilities of multi-radio transceivers are described. In Sec. IV, the models for the THz pulse waveform and the THz channel with beamforming, and SINR are provided. The proposed MRA-MAC protocol is numerically evaluated in Sec. V. Finally, the paper is concluded in Sec. VI.

II. TERAHERTZ NETWORK MODEL

In this section, the THz network model based on a distributed architecture is presented. In particular, multi-radio transceivers are considered, which can enable 2.4/5 GHz omni-directional radio for control signaling and THz beamforming

Accelerating Separable Footprint (SF) Forward and Back Projection on GPU

Xiaobin Xie^{a,b}, Madison G. McGaffin^c, Yong Long^d, Jeffrey A. Fessler^c, Minhua Wen^b, and James Lin^b

^aDepartment of Computer Science and Engineering, Shanghai Jiao Tong University, Shanghai, 200240, China

^bCenter for High Performance Computing, Shanghai Jiao Tong University, Shanghai, 200240, China

^cDepartment of Electrical Engineering and Computer Science, University of Michigan, Ann Arbor, MI 48109 USA

^dUniversity of Michigan - Shanghai Jiao Tong University Joint Institute, Shanghai Jiao Tong University, Shanghai, 200240, China

ABSTRACT

Statistical image reconstruction (SIR) methods for X-ray CT can improve image quality and reduce radiation dosages over conventional reconstruction methods, such as filtered back projection (FBP). However, SIR methods require much longer computation time. The separable footprint (SF) forward and back projection technique simplifies the calculation of intersecting volumes of image voxels and finite-size beams in a way that is both accurate and efficient for parallel implementation. We propose a new method to accelerate the SF forward and back projection on GPU with NVIDIA's CUDA environment. For the forward projection, we parallelize over all detector cells. For the back projection, we parallelize over all 3D image voxels. The simulation results show that the proposed method is faster than the acceleration method of the SF projectors proposed by Wu and Fessler.¹³ We further accelerate the proposed method using multiple GPUs. The results show that the computation time is reduced approximately proportional to the number of GPUs.

Keywords: Statistical image reconstruction (SIR), X-ray CT, forward and back projection, separable footprint (SF), GPU, CUDA

1. INTRODUCTION

Statistical image reconstruction (SIR) methods for X-ray CT improve the ability to produce high-quality and accurate images, while greatly reducing radiation dosages. However, SIR methods operate with one major drawback. They need long computation time to process the scanned data and reconstruct a diagnostically useful image. SIR methods iteratively find the image that best fits the measurement, according to the system physical model, the measurement statistical model and prior information about the object.

Most SIR methods require one forward projection and one back projection in each iteration. These operations are the primary computational bottleneck in SIR methods, especially in 3D image reconstruction. Accelerating forward and back projection is crucial to fast implementation of SIR methods. Numerous approaches have been proposed to accelerate the forward and back projection using Graphics Processing Unit (GPU). Gao proposed fast and highly parallelizable algorithms for X-ray transform and its adjoint for the infinitely narrow beam in both 2D and 3D, but only extended these fast algorithms to the finite-size beam in 2D.¹ To extend these fast algorithms to the finite-size beam in 3D, an efficient 3D formula to compute the intersection volume of the finite-size beam with each nontrivially intersecting voxel needs to be supplied.¹ Xie et al.² proposed a Fixed Sampling Number Projection (FSNP) strategy to ensure the operation synchronization in ray-driven forward

Further author information: (Send correspondence to Yong Long)

Yong Long: E-mail: yong.long@sjtu.edu.cn

Sparse-View X-Ray CT Reconstruction Using ℓ_1 Regularization with Learned Sparsifying Transform

Il Yong Chun, Xuehang Zheng, Yong Long*, and Jeffrey A. Fessler

Abstract—A major challenge in X-ray computed tomography (CT) is to reduce radiation dose while maintaining high quality of reconstructed images. To reduce the radiation dose, one can reduce the number of projection views (sparse-view CT); however, it becomes difficult to achieve high quality image reconstruction as the number of projection views decreases. Researchers have shed light on applying the concept of learning sparse representations from (high-quality) CT image dataset to the sparse-view CT reconstruction. We propose a new statistical CT reconstruction model that combines penalized weighted-least squares (PWLS) and ℓ_1 regularization with learned sparsifying transform (PWLS-ST- ℓ_1), and an algorithm for PWLS-ST- ℓ_1 . Numerical experiments for sparse-view CT show that our model significantly improves the sharpness of edges of reconstructed images compared to the CT reconstruction methods using edge-preserving hyperbola regularizer and ℓ_2 regularization with learned ST.

I. INTRODUCTION

Radiation dose reduction is a major challenge in X-ray computed tomography (CT). Sparse-view CT reduces dose by acquiring fewer projection views [1], [2]. However, as the number of projection views decreases, it becomes harder to achieve high quality (high resolution, contrast, and signal-to-noise ratio) image reconstruction. There have been extensive studies for sparse-view CT reconstruction with total variation [3], [4] or other sparsity promoting regularizers [1], [2]. This paper investigates learned sparsifying transforms for regularization.

Learning prior information from big datasets of CT images and exploiting it for CT reconstruction is a fascinating idea. In particular, patch-based sparse representation learning frameworks [5], [6] have been successfully applied to improve low-dose CT reconstruction [7], [8]. However, CT reconstruction with a ℓ_2 regularizer using a learned sparsifying transform (ST) had difficulty in reconstructing sharp edges [8].

This paper proposes 1) a new (statistical) CT reconstruction model that combines penalized weighted-least squares (PWLS) and ℓ_1 regularization with learned ST (PWLS-ST- ℓ_1) and 2) a corresponding algorithm based on Alternating Direction Method of Multipliers (ADMM) [9]. Numerical experiments with the XCAT phantom show that, for sparse-view CT, the proposed PWLS-ST- ℓ_1 model significantly improves

the edge sharpness of reconstructed images compared to a PWLS reconstruction method with an edge-preserving (EP) hyperbola regularizer (PWLS-EP) and to ℓ_2 regularization with a learned ST (PWLS-ST- ℓ_2 [8]).

II. METHODS

A. Offline Learning Sparsifying Transform

We pre-learn a ST by solving the following problem [6]:

$$\min_{\substack{\Psi \in \mathbb{R}^{n \times n}, \\ \{\mathbf{z}'_j \in \mathbb{R}^n\}}} \sum_{j=1}^{J'} \|\Psi \mathbf{x}'_j - \mathbf{z}'_j\|_2^2 + \gamma' \|\mathbf{z}'_j\|_0 + \tau (\xi \|\Psi\|_F^2 - \log |\det \Psi|) \quad (1)$$

where $\Psi \in \mathbb{R}^{n \times n}$ is a square ST, $\{\mathbf{x}'_j \in \mathbb{R}^n : j = 1, \dots, J'\}$ is a set of patches extracted from training data, $\mathbf{z}'_j \in \mathbb{R}^n$ is the sparse code corresponding to the j th patch \mathbf{x}'_j , J' is the total number of the image patches, and $\gamma', \tau, \xi \in \mathbb{R}$ are regularization parameters. The ℓ_0 function $\|\cdot\|_0$ counts the nonzero elements in a vector.

B. CT Reconstruction Model Using ℓ_1 -Regularization with Learned Sparsifying Transform: PWLS-ST- ℓ_1

To reconstruct a linear attenuation coefficient image $\mathbf{x} \in \mathbb{R}^N$ from post-log measurement $\mathbf{y} \in \mathbb{R}^m$ [2], [10], we solve the following non-convex optimization problem using PWLS and the ST Ψ learned via (1):^a

$$\min_{\mathbf{x}, \mathbf{z} \in \mathbb{R}^{n \times J}} \frac{1}{2} \|\mathbf{y} - \mathbf{A}\mathbf{x}\|_{\mathbf{W}}^2 + \lambda \|\tilde{\Psi}\mathbf{x} - \mathbf{z}\|_1 + \gamma \|\mathbf{z}\|_0, \quad (2)$$

where

$$\tilde{\Psi} = \begin{bmatrix} \Psi \mathbf{P}_1 \\ \vdots \\ \Psi \mathbf{P}_J \end{bmatrix} \quad \text{and} \quad \mathbf{z} = \begin{bmatrix} \mathbf{z}_1 \\ \vdots \\ \mathbf{z}_J \end{bmatrix}.$$

Here, $\mathbf{A} \in \mathbb{R}^{m \times N}$ is a CT scan system matrix, $\mathbf{W} \in \mathbb{R}^{m \times m}$ is a diagonal weighting matrix with elements $\{W_{l,l} = \rho_l^2 / (\rho_l + \sigma^2) : l = 1, \dots, m\}$ based on a Poisson-Gaussian model for the pre-log measurements $\boldsymbol{\rho} \in \mathbb{R}^m$ with electronic readout noise variance σ^2 [2], [12], $\mathbf{P}_j \in \mathbb{R}^{n \times N}$ is a patch-extraction operator for the j th patch, $\mathbf{z}_j \in \mathbb{R}^n$ is unknown sparse code for the j th patch, J is the number of extracted patches, and $\lambda, \gamma \in \mathbb{R}$ are regularization parameters.

The term $\|\tilde{\Psi}\mathbf{x} - \mathbf{z}\|_1$ denotes an ℓ_1 -based sparsification error [13]. We expect ℓ_1 to be more robust to model mismatch than the ℓ_2 -based sparsification error used in [8]. In particular,

^aIn [11], a similar approach is introduced with a “dictionary” (or synthesis) perspective and solved by a reweighted- ℓ_2 minimization. Here we directly attack ℓ_1 minimization—see Section II-C.

The first two authors contributed equally to this work. This work is supported in part by UM-SJTU Collaborative Research Program, NSFC (61501292), Shanghai Pujiang Talent Program (15PJ1403900), and NIH Grant U01 EB018753. Asterisk indicates the corresponding author.

Il Yong Chun and Jeffrey A. Fessler are with the Department of Electrical Engineering and Computer Science, The University of Michigan, Ann Arbor, MI 48109 USA (email: {iyichun, fessler}@umich.edu). Xuehang Zheng and Yong Long are with the University of Michigan - Shanghai Jiao Tong University Joint Institute, Shanghai Jiao Tong University, Shanghai 200240, China (email: {zhxhang, yong.long}@sjtu.edu.cn).

Union of Learned Sparsifying Transforms Based Low-Dose 3D CT Image Reconstruction

Xuehang Zheng, Saiprasad Ravishankar, Yong Long*, and Jeffrey A. Fessler

Abstract—We propose a new penalized weighted-least squares (PWLS) reconstruction method that exploits regularization based on an efficient Union of Learned TRANSforms (PWLS-ULTRA). The union of square transforms is pre-learned from numerous 3D patches extracted from a dataset of CT volumes. The proposed PWLS-based cost function is optimized by alternating between a CT image reconstruction step, and a sparse coding and clustering step. The CT image reconstruction step is accelerated by a relaxed linearized augmented Lagrangian method with ordered-subsets that reduces the number of forward and backward projections. Simulations with 3D axial CT scans of the XCAT phantom show that for low-dose levels, the proposed method significantly improves the quality of reconstructed images compared to PWLS reconstruction with a nonadaptive edge-preserving regularizer (PWLS-EP). PWLS with regularization based on a union of learned transforms leads to better image reconstructions than using a single learned square transform.

I. INTRODUCTION

The development of computed tomography (CT) image reconstruction methods that significantly reduce patient radiation exposure while maintaining high image quality is an important area of research in low-dose CT (LDCT) imaging.

The analytical filtered back-projection (FBP) image reconstruction method typically produces unacceptable image quality when the radiation dose is reduced. Model-based image reconstruction (MBIR) methods, aka statistical image reconstruction methods, can provide high-quality reconstructions from low-dose scans. In MBIR methods, penalized weighted-least squares (PWLS) cost functions with a statistically weighted quadratic data-fidelity term and a penalty term (regularizer) modeling prior knowledge of the underlying unknown object are commonly used [1].

Extracting prior information from big datasets of regular dose CT images has great potential to enable MBIR methods to produce improved reconstructions from LDCT measurements. For example, dictionary learning has been recently applied to CT image reconstruction and was shown to have better performance over total variation-based PWLS method [2]. The sparse coding step in both synthesis dictionary learning and analysis [3] dictionary learning is NP-Hard and methods such

as K-SVD [4], [5] involve expensive computations. Recently, Ravishankar et al. [6], [7] proposed a generalized analysis dictionary learning approach, called sparsifying transform learning, to more efficiently learn a square transform (ST). Pfister et al. [8] showed the promise of PWLS reconstruction with ST based regularization by combining the MBIR technique with an adaptive ST based regularizer, to jointly estimate the ST and the image. More recently, Wen et al. extended the single ST learning method to learning an overcomplete transform with block cosparsity (OCTOBOS) [9]. This approach jointly learns a union of square transforms and a clustering of image patches or textures.

Incorporating the OCTOBOS model, we propose a new PWLS reconstruction method with regularization based on a Union of Learned TRANSforms (PWLS-ULTRA) for 3D (e.g., cone beam) LDCT reconstruction. The union of square transforms is pre-learned from numerous 3D patches extracted from a dataset of CT volumes. Experiments with 3D axial CT scans of the XCAT phantom show that for low-dose levels, the proposed PWLS-ULTRA method significantly improves the quality of reconstructed images compared to PWLS reconstruction with a nonadaptive edge-preserving regularizer (PWLS-EP). While we recently proposed a PWLS method based on a pre-learned ST (PWLS-ST) for 2D CT [10], here we study its extension to 3D CT reconstruction. PWLS-ULTRA that uses a union of learned transforms is shown to lead to better image reconstructions than PWLS-ST that uses a learned ST. The image reconstruction step of the proposed PWLS based methods is accelerated by a relaxed linearized augmented Lagrangian method with ordered-subsets (relaxed OS-LALM) [11].

II. PROBLEM FORMULATION

We reconstruct an image volume $\mathbf{x} \in \mathbb{R}^{N_p}$ from noisy sinogram data $\mathbf{y} \in \mathbb{R}^{N_d}$ using a union of K pre-learned square transform matrices $\{\mathbf{\Omega}_k \in \mathbb{R}^{l \times l}, k = 1, \dots, K\}$, by solving the following optimization problem:

$$\min_{\mathbf{x} \in \mathcal{C}} \frac{1}{2} \|\mathbf{y} - \mathbf{A}\mathbf{x}\|_{\mathbf{W}}^2 + \beta R(\mathbf{x}) \quad (\text{P0})$$

where the regularizer $R(\mathbf{x})$ is based on a union of sparsifying transforms, and is defined as

$$R(\mathbf{x}) \triangleq \min_{\{\mathbf{z}_j, C_k\}} \sum_{k=1}^K \left\{ \sum_{j \in C_k} \left\{ \|\mathbf{\Omega}_k \mathbf{P}_j \mathbf{x} - \mathbf{z}_j\|_2^2 + \gamma^2 \|\mathbf{z}_j\|_0 \right\} \right\} \\ \text{s.t.} \quad \{C_k\} \in \mathcal{G}, \quad (1)$$

This work was supported in part by the SJTU-UM Collaborative Research Program, NSFC (61501292), Shanghai Pujiang Talent Program (15PJ1403900), NIH grant U01 EB018753, ONR grant N00014-15-1-2141, DARPA Young Faculty Award D14AP00086, and ARO MURI grants W911NF-11-1-0391 and 2015-05174-05.

X. Zheng and *Y. Long are with the University of Michigan - Shanghai Jiao Tong University Joint Institute, Shanghai Jiao Tong University, Shanghai 200240, China (email: yong.long@sjtu.edu.cn)

S. Ravishankar and J. A. Fessler are with the Department of Electrical Engineering and Computer Science, University of Michigan, Ann Arbor, MI, 48109 USA

Image-domain multi-material decomposition for dual-energy CT based on correlation and sparsity of material images

Qiaoqiao Ding

School of Mathematical Sciences, Shanghai Jiao Tong University, 800, Dongchuan Road, Shanghai, 200240, China

Tianye Niu

Sir Run Run Shaw Hospital and Institute of Translational Medicine, Key Laboratory of Biomedical Engineering of Ministry of Education, Zhejiang University, Hangzhou, Zhejiang, 310009, China

Xiaoqun Zhang

School of Mathematical Sciences and Institute of Natural Sciences, Shanghai Jiao Tong University, 800, Dongchuan Road, Shanghai, 200240, China

Yong Long^{a)}

University of Michigan-Shanghai Jiao Tong University Joint Institute, Shanghai Jiao Tong University, 800 Dongchuan Road, Shanghai, 200240, China

(Dated: 20 October 2017)

Purpose: Dual energy CT (DECT) enhances tissue characterization because it can produce images of basis materials such as soft-tissue and bone. DECT is of great interest in applications to medical imaging, security inspection and nondestructive testing. Theoretically, two materials with different linear attenuation coefficients can be accurately reconstructed using DECT technique. However, the ability to reconstruct three or more basis materials is clinically and industrially important. Under the assumption that there are at most three materials in each pixel, there are a few methods that estimate multiple material images from DECT measurements by enforcing sum-to-one and a box constraint ($[0 \ 1]$) derived from both the volume and mass conservation assumption. The recently proposed image-domain multi-material decomposition (MMD) method introduces edge-preserving regularization for each material image which neglects the relations among material images, and enforced the assumption that there are at most three materials in each pixel using a time-consuming loop over all possible material-triplet in each iteration of optimizing its cost function. We propose a new image-domain MMD method for DECT that considers the prior information that different material images have common edges and encourages sparsity of material composition in each pixel using regularization.

Method: The proposed PWLS-TNV- ℓ_0 method uses penalized weighted least-square (PWLS) reconstruction with three regularization terms. The first term is a total nuclear norm (TNV) that accounts for the image property that basis material images share common or complementary boundaries and each material image is piecewise constant. The second term is a ℓ_0 norm that encourages each pixel containing a small subset of material types out of several possible materials. The third term is a characteristic function based on sum-to-one and box constraint derived from the volume and mass conservation assumption. We apply the Alternating Direction Method of Multipliers (ADMM) to optimize the cost function of the PWLS-TNV- ℓ_0 method.

Result: We evaluated the proposed method on a simulated digital phantom, Catphan©600 phantom and patient's pelvis data. We implemented two existing image-domain MMD methods for DECT, the Direct Inversion²² and the PWLS-EP-LOOP method³⁶. We initialized the PWLS-TNV- ℓ_0 method and the PWLS-EP-LOOP method with the results of the Direct Inversion method and compared performance of the proposed method with that of the PWLS-EP-LOOP method. The proposed method lowered bias of decomposed material fractions by 84.47% in the digital phantom study, by 99.50% in the Catphan©600 phantom study, and by 99.64% in the pelvis patient study, respectively, compared to the PWLS-EP-LOOP method. The proposed method reduced noise standard deviation (STD) by 52.21% in the Catphan©600 phantom study, and by 16.74% in the patient's pelvis study, compared to the PWLS-EP-LOOP method. The proposed method increased volume fraction accuracy by 6.04%, 20.55% and 13.46% for the digital phantom, the Catphan©600

ADAPTIVE SPARSE MODELING AND SHIFTED-POISSON LIKELIHOOD BASED APPROACH FOR LOW-DOSE CT IMAGE RECONSTRUCTION

*Siqi Ye¹, Saiprasad Ravishankar², Yong Long^{*1}, Jeffrey A. Fessler²*

¹University of Michigan - Shanghai Jiao Tong University Joint Institute,
Shanghai Jiao Tong University, Shanghai, China

²Department of Electrical Engineering and Computer Science, University of Michigan, MI, USA

ABSTRACT

Recent research in computed tomographic imaging has focused on developing techniques that enable reduction of the X-ray radiation dose without loss of quality of the reconstructed images or volumes. While penalized weighted-least squares (PWLS) approaches have been popular for CT image reconstruction, their performance degrades for very low dose levels due to the inaccuracy of the underlying WLS statistical model. We propose a new formulation for low-dose CT image reconstruction based on a shifted-Poisson model based likelihood function and a data-adaptive regularizer using the sparsifying transform model for images. The sparsifying transform is pre-learned from a dataset of patches extracted from CT images. The nonconvex cost function of the proposed penalized-likelihood reconstruction with sparsifying transforms regularizer (PL-ST) is optimized by alternating between a sparse coding step and an image update step. The image update step deploys a series of convex quadratic majorizers that are optimized using a relaxed linearized augmented Lagrangian method with ordered-subsets, reducing the number of (expensive) forward and backward projection operations. Numerical experiments show that for low dose levels, the proposed data-driven PL-ST approach outperforms prior methods employing a nonadaptive edge-preserving regularizer. PL-ST also outperforms prior PWLS-ST approach at very low X-ray doses.

Index Terms— Transform learning, low-dose CT, shifted-Poisson statistical model, sparse representations, machine learning

1. INTRODUCTION

X-ray Computed Tomography (CT) is a popular imaging technique in modern medical diagnosis and treatment. However, X-ray radiation can be harmful to human health, so there has been growing interest in techniques that enable reduced radiation dose without compromising image quality.

Two common strategies to reduce dose include decreasing the photon intensity at the X-ray source, and acquiring fewer projection views (angles) aka sparse-view CT. Both approaches yield degraded projection data, for which the conventional algebraic filtered back-projection (FBP) image reconstruction method yields poor image quality. In these settings, statistical image reconstruction (SIR) methods have been proposed and are popular.

This work was supported in part by the SJTU-UM Collaborative Research Program, NSFC (61501292), Shanghai Pujiang Talent Program (15PJ1403900), NIH grant U01 EB018753, ONR grant N00014-15-1-2141, DARPA Young Faculty Award D14AP00086, and ARO MURI grants W911NF-11-1-0391 and 2015-05174-05. *Yong Long (email: yong.long@sjtu.edu.cn)

Most SIR methods involve optimizing a cost composed of a data-fidelity term accounting for the statistical model of the measurement data and a regularization term modeling prior knowledge or expected characteristics of the target image. Often a Poisson + Gaussian model is used for the CT measurements, where the Poisson distribution models photon counting statistics and the electronic noise at the detector is assumed Gaussian. However, the associated likelihood function in this case lacks an elegant form. An approximate alternative but popular SIR method is penalized (or regularized) weighted least-squares (PWLS), where the logarithm of the measurements is modeled as a linear function of the image, up to additive Gaussian noise with projection view-dependent variance (hence WLS).

While PWLS works well at regular X-ray doses, it becomes inapplicable for very low-dose or noisy cases, when measurements need not be positive, and their logarithm would not exist. Techniques to resolve this problem include applying zero-weighting (in PWLS) on the non-positive measurements [1], replacing the non-positive components by some artificial positive values [2], or corrections using some recursive mean-preserving operations [3] and interpolation by sinogram smoothing or denoising [4, 5] to eliminate non-positive values. Nevertheless, these methods would introduce bias in the reconstructed image, and the spatial resolution of the reconstruction would be heavily degraded when the CT dose is ultra-low. Moreover, the correction of non-positive values and the non-linearity of the logarithm create challenges for estimation of the weighting parameters in PWLS. To address these challenges, a more robust statistical model for the CT (pre-log) measurements, the shifted-Poisson model that better approximates the Poisson + Gaussian model was proposed recently [6–8].

The quality of reconstructed images for SIR methods also depends highly on the efficacy of the image prior (regularizer) in modeling CT image properties. While total variation regularization has been successfully exploited for low-dose CT image reconstruction, there has been increasing interest in designing data-driven regularizers. The parameters of such image priors can be effectively learned from big data sets. Xu et al. [9] proposed a PWLS approach with a regularizer promoting sparsity of image patches in a redundant learned synthesis dictionary. An alternative approach uses a sparsifying transform model for image patches, wherein the patches are assumed approximately sparse in a learned transform domain. In contrast to the often non-convex and NP-hard synthesis dictionary learning problems [10, 11] and expensive learning algorithms, efficient methods have been proposed for learning sparsifying transforms (ST) with good convergence properties [12–14]. Moreover, sparse coding in the ST model involves simple thresholding, which is

A Flexible Distributed Approach to Energy Management of an Isolated Microgrid

Songyang Han, He Yin, Amro Alsabbagh, Chengbin Ma*

University of Michigan-Shanghai Jiao Tong University Joint Institute,
Shanghai Jiao Tong University, Shanghai, P. R. China

Email: hansongyang@sjtu.edu.cn, yyy@sjtu.edu.cn, amro.alsabbagh@sjtu.edu.cn, chbma@sjtu.edu.cn

Abstract—This paper studies an energy management problem for an isolated microgrid including photovoltaic panels, wind turbines, batteries and ultracapacitors. A normal form game is proposed for the energy management to maximize the energy utilization ratio of renewable energy sources, extend the battery life and keep the ultracapacitors able to compensate the dynamic variations. The solution of this game represented by Nash equilibrium is analytically derived and proved to be the existing and unique. A simulation platform using data in second is established to study the energy management approach based on probability distribution functions. In simulation, the game theory based approach has a comparable performance against the rule based control, while the pre-knowledge of the load demands and weather information is not required. Also the game theory based approach is more flexible than rule based approach under the influence of uncertain weather.

Index Terms—Game theory, isolated microgrid, photovoltaic panel, wind turbine, Nash equilibrium.

I. INTRODUCTION

The microgrid is a networked group consisting of different distributed energy sources, such as photovoltaic panels (PVs), wind turbines (WTs), and energy storage devices [1]. The network of microgrids can operate either in grid connected mode or in isolated mode [2]. The isolated microgrids are worth being studied because isolated microgrids have some distinct applications such as in avionic, automotive, marine industries and remote rural areas [3]. There are many problems to be solved in isolated microgrids. One of them is to find a proper energy management approach due to the existence of substantial energy sources and demand fluctuations. This paper introduces a flexible distributed approach to energy management of an isolated microgrid.

Before looking at the energy management approaches, the system configuration is first introduced clearly. The studied system includes PVs, WTs, battery pack and ultracapacitor (UC) pack, which are connected to the DC bus. The power suppliers include two renewable energy sources due to the complementary behavior of solar irradiance and wind speed patterns [4]. Since batteries have high energy density while ultracapacitors have high power density, the hybrid energy storage system (HESS) consists of a battery pack and a UC pack. Each device has its own distributed controller that can determine its power flow autonomously.

As the HESS is one important part of this isolated microgrid, the energy management approaches of HESSs can

become good references. In fact, many approaches have been proposed to control the battery-ultracapacitor HESSs [5]–[7]. The multi-objective optimization is used to determine the trade-off between the energy loss minimization and the battery protection [5]. In the ideal situation, the batteries satisfy the average load demand (ALD), while the UCs meet the rest dynamic load demands [6]. To implement the ALD-based control, the load demands should be known in advance and the capacity of the UCs should meet the dynamic load requirement. In [7], the optimization problem is solved by Karush-Kuhn-Tucker conditions, whose results have a comparable performance with ALD-based control without the pre-knowledge of the load demands.

In terms of energy management approaches in isolated microgrids, many technologies have already been studied [8]–[10]. A fixed control strategy is proposed in [8] for a hybrid WT/PV reverse osmosis desalination microgrid. But only operating constraints and power balance are considered in this approach. An optimal approach for the isolated wind-diesel microgrid in [9] is used to optimize energy of the storage system and operation cost of the microgrid. However, the prediction of WT output power and load demands should be known in advance. In [10], the supervisor control is proposed to determine the power distribution between PVs, WTs and storage system. In this approach, the WTs have priority to provide power compared with PVs, and the battery will start to discharge if the renewable energy sources can not meet the load demands. This approach may be influenced by uncertain weather.

This paper is organised as follows. Section II describes the environment data, the system topology, devices modeling and sizing. To implement the normal form game, the utility functions of all the devices are defined in section III. Then, the detail normal form game is presented in section IV. In section V, the simulation is conducted under the comparison with rule based approach. Finally, the conclusion is given in section VI.

II. ISOLATED MICROGRID MODELING

This section introduces the environment, system topology, the simulation models and sizings of all the devices.

A. Environment

The hourly wind speed, solar irradiance, temperature and load profiles are obtained on Feb. 2nd of San Diego Lindbergh

A Novel Switched Capacitor Circuit for Battery Cell Balancing Speed Improvement

Yandong Wang, He Yin, Songyang Han, Amro Alsabbagh, Chengbin Ma*

University of Michigan - Shanghai Jiao Tong University Joint Institute, Shanghai, China

E-mail: wangyd@sjtu.edu.cn, yyy@sjtu.edu.cn, hansongyang@sjtu.edu.cn, amro.alsabbagh@sjtu.edu.cn, chbma@sjtu.edu.cn

Abstract—To improve battery cell balancing speed, a novel switched capacitor (SC) circuit combining the conventional SC circuit and the optimized SC circuit is proposed in this paper. It has the advantage that the balancing speed is independent of number increase as well as initial voltage variation of battery cells. The equivalent model of the proposed circuit is developed and analyzed in this paper. Compared with the optimized SC circuit, the balancing speed of the proposed circuit is doubled. Simulation comparisons with the conventional SC circuit and the optimized SC circuit under different numbers and initial voltages of battery cells are carried out in PSIM environment. Simulation results show 82% and 50% decrement in the balancing time averagely compared with the conventional SC circuit and the optimized SC circuit, respectively.

Index Terms—Cell balancing, capacitor based circuits, equivalent model, PSIM.

I. INTRODUCTION

Due to the high power and energy density, lithium-ion batteries are widely used in various applications such as electric vehicles (EVs) and renewable energy storage systems [1]. In most applications, the battery pack consists of hundreds of lithium-ion battery cells in order to meet high voltage and high power demands [2]. However, owing to manufacturing inconsistencies, environmental variances, capacity degradation with aging, and difference in self-discharge rates, there is imbalance between battery cell voltages or state of charge (SOCs) [3]. Furthermore, as the batteries are charged and discharged with time, the voltage or SOC imbalance tends to become more and more severe. As a result, the available capacity and lifecycle of the battery pack are reduced and safety hazards such as fire or explosion may even happen because of the overcharge of battery cells [4]. Consequently, the battery management system (BMS) is essential to protect the battery pack from these hazards and maintain the safety and reliability conditions of the battery pack. The main functions of the BMS are measurement of battery voltage, current and temperature, estimation of battery state of charge (SOC) and state of health (SOH), battery cell balancing, safety and thermal management. Among these functions, battery cell balancing is the key function to improve the cell voltage imbalance [5].

Several cell balancing techniques have been proposed, which are usually classified into dissipative and nondissipative methods [6]. The dissipative cell balancing is the simplest cell balancing method. It usually uses the resistive elements to consume the excessive energy of higher voltage battery

cells. The main defects of this method are low energy conversion efficiency and high temperature rise [7]. In order to overcome the defects of dissipative cell balancing method, some nondissipative cell balancing methods have been studied. These nondissipative cell balancing circuits are usually implemented based on switched capacitors, inductors/transformers or DC/DC converters [8]. On one hand, due to the usage of inductors, transformers, or DC/DC converters, the inductor/transformer based circuit or DC/DC converter based circuit has the disadvantages of high control complexity, high cost, and large size. On the other hand, capacitor based cell balancing circuit employs capacitors as the energy transfer elements, it has the advantages of low control complexity, low cost and small size [9]. Compared with other circuits, the capacitor based cell balancing circuit is more promising [10].

For the capacitor based cell balancing circuit, some topologies have been proposed. The conventional switched capacitor (SC) circuit [11] as shown in Fig. 1(a) is the basic one among all the capacitor based cell balancing circuits. In the conventional SC circuit, charge is only exchanged between two adjacent battery cells through one capacitor within one switching period [11]. When there are only two cells in the battery string, the balancing speed is fast. However, as the battery cell number increases, the balancing speed will decrease significantly. In order to improve the balancing speed, a double-tiered SC (DTSC) circuit [12] and a chain structure of SC circuit [13] are developed. These two methods increase the balancing speed by adding more charge transfer paths. However, charge is still not able to be exchanged between any two cells directly. The balancing speed still decreases as the battery cell number increases. To overcome these problems, a series-parallel SC voltage equalizer [14] and an automatic SC cell balancing circuit [15] are proposed. By connecting the capacitors in parallel with the corresponding battery cells and all the capacitors in parallel periodically, any two battery cells can exchange charge directly in these two circuits [14], [15]. Therefore the balancing speed is improved significantly. However, the disadvantage is that the number of switches is twice of that in the conventional SC circuit. To decrease switch number, an optimized SC circuit as shown in Fig. 1(b) is proposed in [16] and a switched coupling capacitor equalizer is developed in [17]. In these two methods, charge can also be exchanged between any two cells directly, therefore the balancing speed of these two methods is the same as that of

Design Procedure of A Class E^2 DC-DC Converter for Megahertz Wireless Power Transfer Based on A Compact Class E Current-Driven Rectifier

Xinhong Fu, Ming Liu, Zefan Tang, Chengbin Ma*

University of Michigan - Shanghai Jiao Tong University Joint Institute, Shanghai, China

E-mail: xinhongfu@sjtu.edu.cn, mikeliu@sjtu.edu.cn, zftang@sjtu.edu.cn, chbma@sjtu.edu.cn

Abstract—This paper presents a design procedure of a Class E^2 DC-DC converter for megahertz wireless power transfer. The design formulas are analytically derived based on the input impedance of the Class E rectifier. A 6.78 MHz Class E^2 DC-DC converter is designed and implemented by means of those formulas. The power-level of the converter is 15W. The experiments are provided to verify the proposed design procedure and evaluate the performance of the converter. The experiment results show that the Class E^2 converter for loosely coupled wireless power transfer can achieve a very high efficiency, 85% for the best case, over a wide load and varying mutual inductance. Finally, the well agreement between the experimental results and design specifications indicates the validity of the proposed design procedure.

Index Terms—Wireless power transfer, Class E^2 DC-DC converter, Class E power amplifier, Compact Class E rectifier.

I. INTRODUCTION

In recent years, the wireless power transfer (WPT) becomes more and more attractive due to the convenient and safe non-contacting charging. Generally speaking, WPT system can be classified into two types: inductive coupling [1] and magnetic coupling [2]. The magnetic resonance coupling working at megahertz (MHz) is being widely considered a promising candidate for the mid-range transfer of a medium amount of power [2] [3]. It is because generally a higher operating frequency (such as several megahertz) is desirable for a more compact and lighter WPT system with a longer transfer distance. In order to build a well-performed MHz WPT system, most of researches focus on the design and optimization for the resonant coupling coils [4] [5] and the optimal load control for coupling coils [6] [7]. However, there are few works on high-efficiency power amplifiers and rectifiers for MHz WPT applications. Because the traditional hard-switching based inverters and rectifiers will have significant switching loss when working at MHz, it is desirable to apply the soft-switching techniques for MHz WPT system. Due to the resonant structures, the Class E power amplifier (PA) and Class E rectifier are suitable candidates to meet to the requirement.

The Class E PA was first introduced in [8]. It is attractive to be used in MHz WPT system for its high efficiency and simple structure [9]–[11]. The Class E PA achieves high efficiency, approaching 100% theoretically, when the circuit satisfies zero

voltage switching (ZVS) condition and zero voltage derivative (ZDS) condition. The Class E rectifier was first presented and used for very high frequency rectification in [12] at 1988. Then various Class E topologies have been developed, such as half-wave, full-wave, and mixed-mode rectifiers [13]. The application of the Class E rectifier in WPT system was first investigated and an efficiency of 94.43% was reported in [14] at 800 kHz operating frequency. Since the Class E PA and rectifier can achieve a high efficiency for the high frequency applications, it is attractive to introduce the Class E^2 DC-DC converter for MHz WPT, i.e., a Class E PA and a Class E rectifier. Paper [15] presents a state-space-based analysis of a Class E^2 converter for wireless power systems based on the inductive link. However, those systems are still working at frequencies below 1 MHz. Initial discussions about MHz Class E^2 converter for WPT can be found in [16], where the simulation-based analysis is introduced. Generally, the existence of the equivalent reactance of the rectifier will detune the receiving coil and lead to lower efficiency and weaker power transfer capacity. Meanwhile, the performance of Class E PA will be affected by the undesirable input impedance of coupling coils caused by the rectifier impedance. Thus, based on the rectifier's impedance, this paper proposed a design procedure for the MHz Class E^2 WPT system. In this procedure, the reactance of the rectifier is used to compensate the receiving coil. Then the input impedance of coupling coil is designed to be the optimal load for Class E PA by means of the resistance of the rectifier.

This paper is organized as follows. It first gives the circuit configuration of the proposed Class E^2 DC-DC converter and defines the efficiency of each part. Then the design procedure is shown with respect to the three subsystem, i.e., the Class E rectifier, coupling coils, and the Class E PA. A design case is provided to explain the design process of a Class E^2 WPT system using the proposed procedure. Finally, a 6.78 MHz Class E^2 WPT system is implemented and the experiments are carried out to verify the design procedure and evaluate its performance.

II. CLASS E^2 DC-DC CONVERTER FOR WPT

Fig. 1 (a) shows the circuit configuration of a MHz Class E^2 DC-DC converter for loosely coupled WPT. It consists of

Optimal Design of Megahertz Wireless Power Transfer Systems for Biomedical Implants

Siyu Peng, Ming Liu, Zefan Tang
Univ. of Michigan-Shanghai Jiao Tong
Univ. Joint Institute,
Shanghai Jiao Tong University,
Shanghai, P. R. China
Email: psy618@sjtu.edu.cn
mikeliu@sjtu.edu.cn
zftang@sjtu.edu.cn

Chengbin Ma^{*1,2}
1. Univ. of Michigan-Shanghai Jiao Tong
Univ. Joint Institute,
2. School of Mechanical Engineering,
Shanghai Jiao Tong University,
Shanghai, P. R. China
Email: chbma@sjtu.edu.cn

Abstract—Wireless power transfer (WPT) working at megahertz (MHz) is widely considered a promising technology for the mid-range transfer of low power. In the biomedical implantable WPT systems, the receiving coil is small. Meanwhile, in real applications, the required transfer distance is large. Thus, the coupling coefficient k is low. For the applications of large load, the low coupling coefficient k and large load R_L deteriorate the system efficiency largely. This paper proposes an optimal design method of MHz WPT systems for biomedical implants. A capacitive L-matching network is inserted in the conventional MHz Class E^2 WPT system to enlarge the reflected impedance of the receiving coil on the transmitting side, i.e., improve the power transfer capability and efficiency of the coupling coils. Then the input impedance of the matching network and efficiency of the proposed MHz WPT system are derived and serves as the basis of the proposed parameter design procedure. Based on the circuit improvement and analytical derivations, a numerical optimization design method is proposed to optimize the design parameters of the MHz WPT system. The final experiment verifies the feasibility of the design procedure. With loosely coupled coils (coupling coefficient $k=0.035$, distance of the coupling coils=1.5 cm, diameter of receiving coil=1.5 cm), the system efficiency can achieve 36.43% under a 0.5 W power transfer.

Keywords—Megahertz wireless power transfer, system efficiency, matching network, optimal design.

I. INTRODUCTION

Wireless power transfer (WPT) systems provide a convenient non-contacting charging method for devices that require electrical power, and there has been a growing demand for wireless charging in recent years. The magnetic resonance coupling working at megahertz (MHz) is being widely considered a promising technology for the mid-range transfer and low-power applications [1], [2]. It is because generally a higher operating frequency (such as 6.78 and 13.56 MHz) is desirable for a more compact and lighter WPT system with a longer transfer distance. Lots of research has been done on the design and optimization of WPT systems both at component and system levels, including the improvements on coupling coils [3]–[7], and power amplifier (PA) [8]–[11].

It is known that the soft-switching-based PAs are promising candidates to build high-efficiency MHz WPT systems, such

as the Class E PA. The Class E PA was first introduced for high-frequency applications in [12]. It has been applied in MHz WPT systems thanks to its high efficiency and simple structure [8], [9], [13]. The Class E rectifier was first proposed for high-frequency DC-DC converter applications in 1988 [14]. Various Class E topologies were later developed, such as voltage-driven, current-driven, and full-wave ones.

Implantable biomedical devices, especially cardiac pacemakers and nerve stimulators, are playing more and more significant roles in curing many kinds of diseases [15]. However, energy depletion in the battery of the biomedical implantable devices eventually forces the patient to accept reimplantation of the device, adding extra ordeal to the patient and increasing the risk of surgery failure. Accordingly, an urgent solution is in vitro wireless energy supply that provides uninterrupted power supply for implantable devices. It has attracted the attention of professionals in medical and engineering fields [16].

However, the size of implants is much smaller compared with non-implantable devices. Therefore, the size of the receiving coil should be small, leading to the very weak coupling between transmitting and receiving coils and eventually the low system efficiency. What's more, in real applications for medical implants, the required transfer distance is large (usually more than 1 cm). In that case, the very small size and relative large transfer distance are the common challenges existing in the wireless power transfer system for biomedical implants.

In this paper, a capacitive L-matching network is added between the rectifier and the receiving coil. Basically, the newly added capacitive matching network will not enlarge the system size and involve more power loss. Based on the improved circuits, a system level design methodology is proposed to optimize the efficiency and power transfer of the WPT systems in the biomedical implant applications. For applications in real life, the changes in the distance and misalignment of the coupling coils are very common. The simulation and experiment results of system efficiencies under different distances and misalignments are also presented to demonstrate the change tendency of system efficiency under

Two-level Energy Management Strategy for a Fuel Cell-Battery-Ultracapacitor Hybrid System

Chen Zhao, He Yin

Univ. of Michigan-Shanghai Jiao Tong Univ. Joint Institute,
Shanghai Jiao Tong University,
Shanghai, P. R. China
Email: zc437041363@sjtu.edu.cn
yyy@sjtu.edu.cn

Chengbin Ma^{*1,2}

1. Univ. of Michigan-Shanghai Jiao Tong Univ. Joint Institute,
2. School of Mechanical Engineering,
Shanghai Jiao Tong University,
Shanghai, P. R. China
Email: chbma@sjtu.edu.cn

Abstract—This paper provides a two-level energy management strategy for a fuel cell-battery-ultracapacitor (UC) hybrid system. In the proposed strategy, the battery and UC packs are seen as an energy storage system (ESS) at the first level and the equivalent consumption minimization strategy is used to distribute load power between this ESS and the fuel cell system. The penalty factor is tuned based on estimated average load power and SOC of the ESS. At the second level, the power distribution between the battery and UC packs is determined using the equivalent series resistance-based control strategy to minimize the energy loss. Then, the performance of the proposed two-level energy management strategy is analyzed in simulation under a realistic load profile. Finally, detailed comparison results show that the two-level energy management strategy can achieve lower hydrogen consumption, compared with the rule-based method.

Index Terms—Battery, Energy management strategy, Fuel cell, Hybrid system, Ultracapacitor

I. INTRODUCTION

With the rapid increase in greenhouse gas emission, the fuel cell technology can be seen as a good candidate to replace the internal combustion engine (ICE) due to its high efficiency and zero emission [1]. Due to the slow response time of the fuel cell system, fast changing load demand would lead to fuel starvation phenomenon, which will shorten its lifespan [2]. One of common solutions is to use an energy storage system (ESS) as a buffer to isolate the fuel cell system from the dynamic load demand [3]. Therefore, the fuel cell system can be designed to supply the constant average power at its high-efficiency region with low fuel consumption and long lifespan [4].

Batteries and ultracapacitors (UCs) can be seen as two promising energy storage devices in the fuel cell based hybrid system [4]–[6]. Experimental results show that the efficiency and specific power density of the fuel cell-battery hybrid system is higher than that of the fuel cell system alone [7]. Because UCs have higher power density and longer cycle life than batteries, the fuel cell-UC hybrid system shows a lower cost compared to the fuel cell-battery hybrid system [8], [9]. However, due to the limited energy density of UCs, the fuel cell-UC hybrid system may malfunction during the fuel cell start-up time [4]. Therefore, the battery-UC hybrid system is proposed as the ESS to assist the fuel cell system [4], [9], [10].

The comparative studies show that the fuel cell-battery-UC hybrid system has higher fuel economy than fuel cell-battery and fuel cell-UC hybrid systems [5], [6].

In the fuel cell-battery-UC hybrid system, many energy management strategies have been proposed. A set of operation states are defined to determine the output power of each device [11], [12]. Model predictive control is proposed to restrict the current slope of fuel cell and stabilize the dc bus voltage based on its linearized state-space model [13], [14]. A power sharing strategy based on fuzzy logic and wavelet transform is proposed to distribute load demand among different energy devices based on their response times [15]. For a better fuel economy, the equivalent consumption minimization strategy (ECMS) is proposed to minimize the equivalent fuel consumption in the fuel cell based hybrid system [16]. Since it is a realization of the Pontryagin's minimum principle (PMP) for on-line implementation purposes, ECMS with well-tuned parameters guarantees a near-optimal performance [17]. The ECMS is first used in the fuel cell-battery-UC hybrid system to determine the power of the fuel cell system [18]. Since the SOC of UCs is simply controlled to the predefined value, the proposed strategy in [18] does not guarantee an overall optimal performance.

In this paper, a two-level energy management strategy is proposed for the fuel cell-battery-UC hybrid system. In the proposed two-level energy management strategy, the load power is distributed between the fuel cell system and the battery-UC hybrid system using the ECMS to minimize the total hydrogen consumption at the first level. At the second level, the power flow between battery and UC packs is determined using the equivalent series resistance (ESR)-based method. Then, the performance of the two-level energy management strategy is analyzed in simulations. Finally, the proposed energy management strategy is compared with the rule-based strategy in terms of the hydrogen consumption.

II. FUEL CELL-BATTERY-UC HYBRID SYSTEM

A. Fuel Cell System

In the proposed hybrid system, a 100 W proton exchange membrane fuel cell (PEMFC) system from Heliocentris is used, in which 20 cells with active surface area (A) of 25

A Decentralized Energy Management for A Multiple Energy System with Fault Tolerance Analysis

He Yin, Chen Zhao, and Amro Alsabbagh
Univ. of Michigan-Shanghai Jiao Tong
Univ. Joint Institute,
Shanghai Jiao Tong University,
Shanghai, P. R. China
Email: yyy@sjtu.edu.cn
chenzhaosjtu@gmail.com
amro.alsabbagh@hotmail.com

Chengbin Ma^{*1,2}
1. Univ. of Michigan-Shanghai Jiao Tong
Univ. Joint Institute,
2. School of Mechanical Engineering
Shanghai Jiao Tong University,
Shanghai, P. R. China
Email: chbma@sjtu.edu.cn

Abstract—This paper discusses a decentralized energy management for an engine-generator/battery/ultracapacitor (UC) hybrid energy system with fault tolerance analysis. The energy management problem among the energy suppliers and the load is formed into a non-cooperative power distribution game where the engine-generator, the battery pack, the UC pack, and the load are modeled as independent and related players. Each player has a unique objective, i.e., reducing fuel consumption, prolonging battery cycle life, maintaining UC state of charge and satisfying the load demands, represented by different second order polynomial function based utility functions. In this game, a Nash equilibrium is reached at each control instant to give a balanced solution among players. The weight coefficients in the utility functions can be determined through the parato optimal solution a multi-objective genetic algorithm. The fault tolerance analysis based simulation shows that the proposed energy management has a flexible and reconfigurable performance under six different case studies.

Index Terms—Multiple energy system; Game theory; Nash equilibrium; Fault tolerance analysis;

I. INTRODUCTION

Thanks to the rising interests in the renewable energy vehicles, i.e., hybrid electric vehicles (HEVs) and electric vehicles (EVs), hybrid energy systems (HESs), serving as the main energy supplier, are widely discussed [1]. The applications of HESs can also be extended to smart houses, micro grids, and smart grids [2]. A typical HES consists of multiple energy suppliers such as fuel cells, batteries, and internal combustion engines together with assistive devices, e.g., ultracapacitors (UC) and flywheels [3]. Due to the complicated characteristics of each energy suppliers, it is a challenging task to model and manage the energy flow inside a HES. This paper focuses on the energy management and fault tolerance analysis of an engine-generator/battery/UC pack HES.

The energy management problems of HESs have been widely discussed in recent years. Basically, there are two kinds of energy management, i.e., the centralized energy managements and the decentralized energy managements. For

centralized energy managements, [4] applies a rule based energy management for a series-parallel plug-in hybrid electric bus. The parameters in the rules-table is optimized by dynamic programming. [5] discusses the fuzzy-logic energy management together with the rule based control applied on EVs with battery and UC HES. An adaptive fuzzy logic controller is applied to tune the membership function based on the previous driving conditions. [6] solves the energy management problem for a battery and UC HES through Karush-Kuhn-Tucker (KKT) conditions. This paper tries to optimize the battery cycle life and maintain the UC capacity. [7] applies an optimal control through using Neural Networks for a HEV. In addition to the centralized energy managements, decentralized energy management, on the other hand, can also be applied on HESs [8]. Among the decentralized managements, game theory is a famous approach to solve the trade-offs among self-interested players and predict their choices which is also widely discussed in the energy management problem in HESs. [9] discusses a game theoretic energy management on an engine-generator/battery/UC HES. The Nash equilibrium is determined at each control instant to solve the power distribution problem. [10] also discusses a game theoretic energy management for a HES together with renewable energy system. It focuses on the coalition among the energy suppliers. Comparing with the centralized energy managements, decentralized energy managements are more flexible, reconfigurable, and fault-tolerant [11]. Since the application background of this paper is a series electric vehicle, the fault tolerance should be considered for safety purposes [12]. The fault tolerance analysis for two five-phase permanent magnetic synchronous machines (PMSM) in a fuel cell/ultracapacitor HES has been discussed [13]. Their strategy focuses on dealing with the situation that one or two phases of the PMSM is failed. To the knowledge of the authors, there is a lack of research focusing on the fault tolerance analysis on multiple source energy system. In this paper, the situation that one or two

Approximate Logic Synthesis for FPGA by Wire Removal and Local Function Change

Yi Wu, Chuyu Shen, Yi Jia, and Weikang Qian

University of Michigan-Shanghai Jiao Tong University Joint Institute
Shanghai Jiao Tong University, Shanghai, China

Email: {eejessie, ericolivier, yvonne222, qianwk}@sjtu.edu.cn

Abstract— Approximate computing is a new design paradigm targeting at error-tolerant applications. By allowing a little amount of inaccuracy in the computation, it could significantly reduce circuit area and power consumption. Several logic synthesis methods for approximate computing were proposed recently. However, these methods are mainly aimed at ASIC designs. In this work, we propose a novel approximate logic synthesis method targeting at the FPGA design. We exploit the flexibility of look-up tables and propose a method that combines wire removal and local function change. The experimental results showed that our method produces better results than the state-of-the-art approximate logic synthesis method adapted to FPGA designs. Moreover, it can be combined with the state-of-the-art method to further improve the design quality.

I. INTRODUCTION

As modern VLSI designs become more complex and CMOS devices have reached nanoscale, reducing power consumption of the circuits becomes a critical mission in VLSI design. Meanwhile, more and more applications used today exhibit an inherent error tolerance. For example, applications in machine learning, data mining, and pattern recognition demonstrate significant algorithmic resilience to errors, because most of these applications have redundancies in their input data sets and some of them have no golden answers [1]. Given this context, a new computing paradigm called approximating computing was proposed recently which exploits the application-level error tolerance to improve the power consumption and performance of digital circuits [2]. The basic idea of approximate computing is to change the function properly so that a much simpler design can be achieved while still satisfying the error specification. The effectiveness of this idea has been demonstrated in many previous works at different design levels ranging from architecture, logic, to transistor [3–5].

In order to quantify the error, two types of error measurements are used in practice [2]. One is error rate and the other is error magnitude. Error rate is defined as the ratio of input vectors that cause an output error. Error magnitude is generally applied to arithmetic circuits of which the outputs are treated as a numerical value. It is defined as the error of the encoded numerical value. In this work, we focus on approximate computing under error rate constraint.

A number of earlier works in approximate computing studied the manual design of approximate arithmetic circuits, such as adders and multipliers [6–9]. More recently, several approximate logic synthesis (ALS) methods were proposed [4, 10–16]. These methods explore the design space in a systematic way to synthesize a low-cost approximate circuit subject to given error constraints. However, all these ALS methods target at the ASIC design. When the design target shifts to FPGA, although these methods can still be applied with proper modifications,

they fail to fully exploit the special characteristics of FPGA to further improve the synthesis results. One important feature that can be further exploited is the functional flexibility of the look-up tables (LUTs), which are the basic components of modern FPGA.

In this work, we propose a novel ALS method for FPGA designs under error rate constraint. The main idea of our method exploits the functional flexibility of the LUTs in FPGA, i.e., a k -input LUT can implement any k -input Boolean function. Based on this feature, we propose to derive an approximation of a local sub-network by removing one of its inputs and simultaneously reconfiguring the function. By removing an input of a local sub-network, the number of LUTs needed to cover the network is likely to be reduced. Meanwhile, by properly configuring the function, we can minimize the induced error rate.

The main contributions of our work are as follows.

- We proposed a novel ALS technique which simultaneously removes an input of a local sub-network and changes its function. The technique is highly suitable for FPGA designs, since it exploits the functional flexibility of the LUTs in FPGA.
- We proposed a practical flow to apply the basic technique to the synthesis of FPGA designs. It applies the basic technique to local sub-networks in FPGA and derives candidate transformations. Then it formulates an ILP problem to determine which transformations should be selected to maximize the area reduction.
- We explored the combination of our method with the state-of-the-art method. Experimental results showed that this combined method can further improve the design quality.

The rest of the paper is organized as follows. In Section II, we discuss the related works. In Section III, we introduce some preliminaries that will be used later. In Section IV, we present the basic idea and the detailed techniques of the proposed method. In Section V, we show the overall flow which applies the proposed techniques. In Section VI, we show the experimental results on a set of benchmarks. Finally, in Section VII, we conclude the paper.

II. RELATED WORKS

Several previous works have proposed approximate logic synthesis methods. The works [10] and [11] studied ALS for two-level circuits under the error rate constraint. The work [12] further proposed a two-level ALS algorithm considering both the error rate and error magnitude constraints. Several later works [4, 13–16] studied ALS for multi-level circuits, which

Approximate Disjoint Bi-decomposition and Its Application to Approximate Logic Synthesis

Yue Yao, Shuyang Huang, Chen Wang, Yi Wu and Weikang Qian

University of Michigan-Shanghai Jiao Tong University Joint Institute

Shanghai Jiao Tong University, Shanghai, China

Email: {patrickyao, King_hsy, wangchen_2011, eejessie, qianwk}@sjtu.edu.cn

Abstract— Approximate computing is an emerging design paradigm targeting at error-tolerant applications. The area, delay, and power consumption of a circuit can be improved by sacrificing a reasonable amount of accuracy. Approximate logic synthesis (ALS) aims at automatically synthesizing an approximate circuit for a given target circuit. In this paper, we propose to approximate a target function by a maximally disjoint bi-decomposable function, which can significantly reduce the implementation cost. We propose novel techniques to effectively generate such an approximation with low error rate. We further integrate this approximation technique into a systematic ALS flow. Experiment results showed the effectiveness of our proposed ALS flow in producing approximate circuits with reduced areas.

Index Terms—approximate logic synthesis, approximate computing, inexact circuit, Boolean function decomposition

I. INTRODUCTION

As the level of integration for VLSI designs increases, the power consumption of a design also dramatically grows. This calls for technologies that simplify the circuit without affecting their effectiveness in their application context. Meanwhile, many recent applications tolerate errors by their nature. Given this context, a new computing paradigm called *approximate computing* [1][2] was proposed. This paradigm sacrifices accuracy in hope of generating a much simpler circuit so that both its area and power consumption can be reduced. Many studies employed this idea at different design levels, including algorithm, architecture, logic, and transistor level, and demonstrated the effectiveness of this design paradigm [2].

One challenging problem in designing approximate circuits is to find the optimal circuit that approximates the target design. In previous works, researchers have either manually derived an approximate circuit [3][4][5][6], or developed algorithms to synthesize one. The latter option is known as *approximate logic synthesis* (ALS) [7][8]. This strategy aims at designing algorithms that automatically simplify a given target circuit by introducing a small amount of approximation to the original function. There are some ALS approaches for two-level circuits [7][9] and some for multilevel circuits [10][11][12].

In traditional logic synthesis, functional decomposition is a widely-used technique for synthesizing circuits with smaller areas [13][14][15]. A general decomposition method decomposes a large function into a combination of smaller functions, and hence could reduce the implementation cost. A special type of decomposition is the disjoint bi-decomposition (DBD), which represents a function $f(X)$ as $D(g_1(X_1), g_2(X_2))$, where X is the input set of f , D , g_1 , and g_2 are Boolean functions, and X_1 and X_2 form a bipartition of the set X [16]. If the functions g_1 and g_2 can be recursively disjoint bi-decomposed, then the Boolean function f can be maximally disjoint bi-decomposed (MDBDed). As a result, it can be realized by a tree of logic gates, which significantly reduces its implementation cost. Unfortunately, most Boolean functions cannot be MDBDed. However, in the approximate computing context, since error is

allowed, it is possible to approximate the target function by another one that can be MDBDed. Previous works proposed a few efficient bi-decomposition algorithm, including the BDD-based algorithm in [17] and the spectral method in [18]. However, these methods can only produce a decomposition when the function is bi-decomposable. In contrast, our work tries to produce a bi-decomposition that is closest to the target function even if the function is not bi-decomposable. Toward this end, we first study the necessary and sufficient condition for a function to be disjoint bi-decomposed. Then, based on that result, we develop a method to find a disjoint bi-decomposable function that is closest to the target function. Based on this technique, we further develop a method that can find a Boolean function that can be maximally disjoint bi-decomposed and is closest to the target function. Finally, a systematic ALS flow incorporating the proposed technique is proposed. The experimental results demonstrated that our ALS flow can produce approximate circuits with significantly reduced areas.

To evaluate the error resulted from approximation, two major metrics are commonly used. The first is *error rate*, which is the percentage of input patterns that result in an inaccurate output. The second is *error magnitude*, which is the maximal numerical difference of the output by treating all the output bits encoding a binary number. In this study, we choose error rate instead of error magnitude as the error constraint, since for many logic circuits, the error magnitude may not be well-defined.

The rest of the paper is organized as follows. In Section II, we introduce the concept of disjoint bi-decomposition. In Section III, we elaborate our proposed approach to perform approximate disjoint bi-decomposition. In Section IV, we describe our proposed method to perform approximate maximum disjoint bi-decomposition (AMDBD). In Section V, we present the ALS flow that exploits the AMDBD technique. In Section VI, we show the experiment results. Finally, in Section VII, we conclude the paper.

II. DISJOINT BI-DECOMPOSITION

In this work, we propose techniques to perform approximate disjoint bi-decomposition. First, we introduce a few definitions.

Definition 1: Let the set of input variables be $X = \{x_1, x_2, \dots, x_n\}$. If two non-empty subsets X_1 and X_2 satisfy that $X_1 \cup X_2 = X$ and $X_1 \cap X_2 = \emptyset$, then (X_1, X_2) is a **bipartition** of X [19]. \square

Definition 2: Let $F(X) : \mathbf{B}^n \mapsto \mathbf{B}$ be a Boolean function and (X_1, X_2) be a bipartition of X . The **decomposition chart (DC)** of F over the bipartition (X_1, X_2) is a table of $2^{|X_1|}$ columns and $2^{|X_2|}$ rows, with columns labeled by all the binary combinations of the variables in X_1 , rows by all the binary combinations of the variables in X_2 , and the intersection of each row and each column by the value of F on the corresponding combination of inputs specified by the column and the row [19]. \square

Design of Accurate Stochastic Number Generators with Noisy Emerging Devices for Stochastic Computing

Meng Yang¹, John P. Hayes², Deliang Fan³, and Weikang Qian⁴

^{1,4}University of Michigan-Shanghai Jiao Tong University Joint Institute, Shanghai Jiao Tong University, Shanghai, China

²Department of Electrical Engineering and Computer Science, University of Michigan, Ann Arbor, U.S.A.

³Department of Electrical and Computer Engineering, University of Central Florida, Orlando, U.S.A.

Email: {¹yangm.meng, ⁴qianwk}@sjtu.edu.cn, ²jhayes@eecs.umich.edu, ³dfan@ucf.edu

Abstract—Stochastic computing (SC) is an unconventional computing paradigm that operates on stochastic bit streams. It has gained attention recently because of the very low area and power needs of its computing core. SC relies on stochastic number generators (SNGs) to map input binary numbers to stochastic bit streams. A conventional SNG comprises a random number source (RNS), typically an LFSR, and a comparator. It needs far more area and power than the SC core, offsetting the latter's main advantages. To mitigate this problem, SNGs employing emerging nanoscale devices such as memristors and spintronic devices have been proposed. However, these devices tend to have large errors in their output probabilities due to unpredictable variations in their fabrication processes and noise in their control signals. We present a novel method of exploiting such devices to design a highly accurate SNG. It is built around an RNS that generates uniformly distributed random numbers under ideal (nominal) conditions. It also has a novel error-cancelling probability conversion circuit (ECPCC) that guarantees very high accuracy in the output probability under realistic conditions when the RNS is subject to errors. An ECPCC can also be used to generate maximally correlated stochastic streams, a useful property for some applications.

I. INTRODUCTION

Stochastic computing (SC) was introduced in 1960s as an unconventional computing paradigm [1]. Its main difference from traditional “binary” computing is that it operates on stochastic bit streams that encode data values as the probabilities of 1’s occurring in the bit streams. For example, the bit stream “01001100” represents 3/8. Due to this uniformly weighted encoding, SC is very tolerant of bit-flip errors. Moreover, its probabilistic nature allows very simple circuits to realize complex arithmetic operations. A notable example is multiplication, which can be realized by an AND gate, as shown in Fig. 1(a). Arithmetic circuits like this with stochastic bit streams as inputs and outputs are referred to here as the *SC core*. Because of the core’s low area and power requirements, SC has been applied successfully in several application domains, including image processing [5], low-density parity-check (LDPC) decoding [2], and artificial neural networks [4].

SC relies on stochastic number generators (SNGs) to generate input stochastic bit streams of the desired probabilities. A widely used SNG is composed of a random number source (RNS) and a comparator, as shown in Fig. 2(a). (More details will be given in Section II.) This SNG has a linear feedback shift register (LFSR) as its RNS, and usually consumes far more area and power than the SC core. Furthermore, to guar-

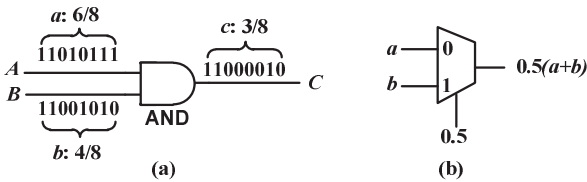


Fig. 1. Examples of stochastic computing elements: (a) An AND gate used to multiply two numbers encoded by stochastic bit streams; (b) A 2-to-1 multiplexer (MUX) implementing scaled addition.

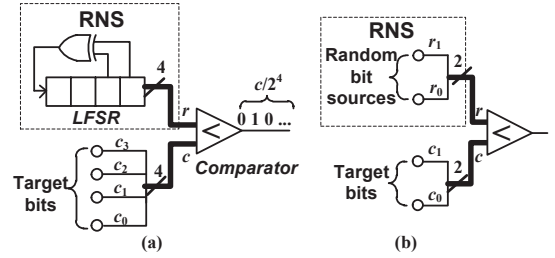


Fig. 2. Stochastic number generators composed of an RNS and a comparator: (a) the RNS is an LFSR; (b) the RNS is composed of $k = 2$ random bit sources.

antee the SC core’s correct functionality, its input bit streams should be mutually independent or uncorrelated, which means the number of SNGs must equal the number of inputs to the core.

To reduce the area and power needs of the SNGs in a stochastic circuit, several solutions have been proposed. One proposal is to share a single LFSR among multiple SNGs. For example, circular shifting of the output bits of the LFSR is suggested in [6] to produce stochastic bit streams with low correlation. In [7], the insertion of delay elements into the circuit is proposed to decorrelate the stochastic bit streams. However, these solutions cannot guarantee perfect mutual independence among the input streams; hence, errors may remain in the final result. A deterministic method for SC is proposed in [8] to reduce the cost of generating input streams. However, it is only applicable when the input precision is low.

A very different approach is to exploit the special properties of emerging technologies such as memristors [9][10] and spintronic devices [13][14]. These nanoscale devices have two different stable states that can be mapped into binary values. For example, a memristor has high- and low-impedance states, which can be switched by applying a programming pulse. Recent studies showed that the state switching can be random and the switching probability can be controlled by an input signal [9]. For example, the switching probability of a memristor is

$$P(t) = 1 - e^{-t/\tau}, \quad (1)$$

where t is the width of the programming pulse and τ is a constant determined by the device itself and the amplitude of the programming pulse. Therefore, by changing the value of t , a stochastic bit stream of arbitrary probability can be generated. Previous studies show that SNGs based on these emerging devices have much smaller area and power consumption than conventional CMOS-based SNGs. For example, the power needed by a memristor-based design can be 16x lower than that of a CMOS SNG [9], while a design based on spintronic devices can achieve a 7x power reduction [13].

However, these emerging devices are nanoscale and subject to noise due to manufacturing parameter variations and run-time signal variations. They may also be subject to quantum-mechanical effects like tunneling that are inherently probabilistic [11]. In the memristor case, for example, Eq. (1) implies that its switching probability is vulnerable to noise in the programming pulse [12] and variations in its device parameters. Consequently, the bit streams produced by conventional SNG designs that employ such devices may have probability values that deviate significantly from the expected ones. To take advantage of these noisy

Design of Reliable Stochastic Number Generators Using Emerging Devices for Stochastic Computing

Meng Yang and Weikang Qian

University of Michigan-Shanghai Jiao Tong University Joint Institute

Shanghai Jiao Tong University, Shanghai, China

Email: {yangm.meng, qianwk}@sjtu.edu.cn

Abstract—Stochastic computing (SC), an unconventional computing paradigm that operates on stochastic bit streams, gains more and more attention recently because of the low area and power consumption of its computing core. SC relies on stochastic number generators (SNGs) to generate input stochastic bit streams. An SNG is composed of a random number source (RNS) and a comparator. However, conventional SNGs, which use linear feedback shift register (LFSR) as the RNS, consume much more area and power than the SC core, offsetting the small area and the low power advantages of the SC core. To mitigate this issue, some emerging devices, such as memristor and spintronic devices, were proposed to build SNGs. However, due to the large process variation in fabricating these devices, these SNGs are unreliable: their output probabilities could have a large error than the desired values. In this paper, we propose a general method to design reliable SNGs that use emerging device-based RNS's. Experimental results showed that our design is effective in improving the reliability.

Keywords—stochastic computing; novel nanoscale devices; stochastic number generator (SNG)

I. INTRODUCTION

Stochastic computing (SC) was first introduced in 1960s as an unconventional computing paradigm [1]. Its biggest difference from traditional binary computing is that it operates on stochastic bit streams that encode real values through the probabilities of 1s in the streams. For example, the bit stream “01001100” represents 3/8. Due to the uniformly weighted encoding, SC has strong fault tolerance to bit flip errors. Moreover, the probabilistic way of encoding data allows very simple digital circuits to realize complex arithmetic operations. One notable example is that multiplication can be realized by an AND gate, as shown in Fig. 1(a). These circuits taking stochastic bit streams as inputs and outputs are referred to as *SC core*.

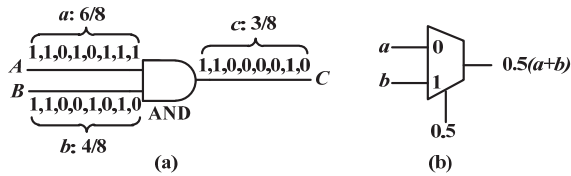


Fig. 1. Examples of stochastic computing elements. (a) Multiplication of the numbers encoded by stochastic bit streams can be realized by an AND gate; (b) Scaled addition of the numbers encoded by stochastic bit streams can be realized by a 2-to-1 multiplexer.

Because of its low area and power consumption, SC has been applied in many application domains, such as image processing

[2][7], low-density parity-check (LDPC) decoding [3], artificial neural networks [6], and digital filters [5].

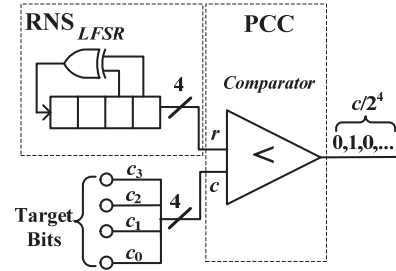


Fig. 2. A stochastic number generator composed of an LFSR and a comparator.

SC relies on stochastic number generators (SNGs) to generate input stochastic bit streams of the desired probabilities. A widely used SNG is composed of a pseudo random number source, such as a linear feedback shift register (LFSR), and a comparator, as shown in Fig. 2 (more details on it will be discussed in Section II). However, it consumes much more area and power than the SC core. Furthermore, to guarantee the correct functionality, the input stochastic bit streams should be mutually independent, which means the number of SNGs is equal to the number of inputs of the SC core. As a result, the existence of the large and power-hungry SNGs significantly mitigates the advantages of the SC core in area and power consumption.

To reduce the area and power consumption of the SNGs in a stochastic circuit, several solutions were proposed. One method is to share a single LFSR among multiple SNGs. For example, in [14], the circular shift of the output bits of the LFSR was proposed to produce stochastic bit streams with low correlation. In [15], the insertion of delay elements into the circuit was proposed to decorrelate the stochastic bit streams. However, these solutions cannot guarantee the perfect mutual independence of the input streams and hence, could introduce error to the output result.

Another method is to leverage the emerging devices, such as memristors [8][10] and spintronic devices [9][11][12]. These novel nanoscale devices usually have two different stable states that can be converted into binary values. For example, the memristor has a high-impedance state and a low-impedance state, which can be switched by applying a programming pulse to the device. Recent studies showed that the state switching of some emerging devices is random and the switching probability could be controlled by an input signal [8]. For example, the state switching probability of a memristor is

$$P(t) = 1 - e^{-t/\tau}, \quad (1)$$

Observation of Transient Nonlinear Dynamics of Optical Frequency Comb in a Microcavity

Yuanlin Zheng¹, Tian Qin², Jianfan Yang², Li Ge³ and Wenjie Wan^{1,2*}

¹Department of Physics and Astronomy, Shanghai Jiao Tong University, Shanghai 200240, China

²The University of Michigan-Shanghai Jiao Tong University Joint Institute, Shanghai Jiao Tong University, Shanghai 200240, China

³Department of Engineering Science and Physics, College of Staten Island, CUNY, NY 10314, United States of America
e-mail: wenjie.wan@sjtu.edu.cn

Abstract: We experimentally observe gain spiking and nonlinear optical beating induced by nonlinear phase modulations during the transient regime of optical comb generation in a microcavity. We exam its basic nonlinear properties by external modulations.

OCIS codes: (140.3945) Microcavities; (190.3270) Kerr effect; (190.5940) Self-action effects

Optical frequency combs, combining thousands of ultra-sharp laser lines over a wide frequency spectrum, enable ultrashort laser pulsing for important applications in precision spectroscopy, optical metrology, microwave generation, optical clock. Traditional optical frequency combs based on mode-locked femtosecond laser technology such as Ti:Sapphire solid state or Er/Yb doped fiber based lasers, are bulky and lack of robustness. Recent advancements of optical frequency combs in micro-resonators base on nonlinear Kerr effect have promising futures for a compact and stable comb generations[1]. Unlike frequency combs in conventional optical gain medium, such optical frequency combs in microresonators rely on nonlinear Kerr effects to provide parametric gains. These nonlinear gains usually company with other nonlinear processes complicating the comb generations, e.g. Raman, four-wave mixing, nonlinear phase modulation, modulation instability, soliton, which are yet well studied. However, they are as important as the original parametric gain regulating comb generations: like its counterpart in lasers, where nonlinear gain saturation can limit multimode lasing, cause laser spiking effect, which finally lead to the idea of mode-locked pulse laser. Here these important nonlinear processes will also play a major role in optical comb generation in microresonators, especially in the transient regime, where the next emerging area will explore the possibility of experimenting mode-locked or pulsed laser operations in such compact platforms. Hence, it's essential to understand how these nonlinear processes behave during optical frequency comb generation in microcavities. Here we study these nonlinear phase modulations' effect on gain spiking during the transient regime of optical comb generation in a microcavity, and show the self-stabilization of optical frequency comb due to such nonlinear phase modulation. Furthermore, by externally adding a probe beam, we observe nonlinear optical beating between the signals and the idlers of optical combs. Our experimental observations here confirm the importance of nonlinear phase modulations in the transient regime, enabling further applications in temporal pulsing operations with this compact platform.

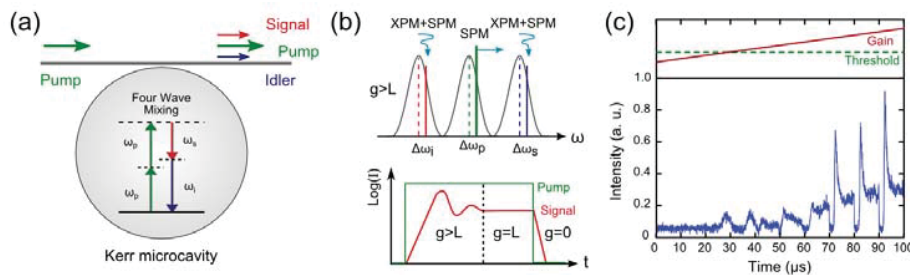


Fig. 1. (a) Principle of Kerr frequency combs in a resonator. (b) NPMs on signal/idler shifts their detunings, leading to the spiking effect observed in the time trace. (c) The intensity of signal as pump intensity crosses the threshold of parametric oscillation.

OFCs arise from Kerr-enabled four wave mixings inside whispering-gallery-Mode (WGM) microresonators[2]: this cavity-enhanced parametric processes simultaneously convert two of incoming pump photons into one “signal” and another “idler”, when the intensities of these generated photons build up, they successively cascade into next generations of photon pairs. In the meantime, a rigid phase matching conditions must be met to fulfill the momentum conversion. However, such phase matching conditions are affected by nonlinear phase modulations (NPM including SPM and XPM), which effectively alter the effective path lengths photons undergo inside the

Digital in-line holographic microscope based on the grating illumination with improved resolution by interpolation

Shaodong Feng, Mingjun Wang, and Jigang Wu*

Biophotonics Laboratory, University of Michigan – Shanghai Jiao Tong University Joint Institute,
Shanghai Jiao Tong University, 800 Dongchuan Road, Shanghai, China

*jigang.wu@sjtu.edu.cn

ABSTRACT

High resolution is always a pursuing target in the imaging field, as a new prospective technique in imaging applications, digital in-line holography has become a very active field for compactness, more information and low-cost. However, for compact system, the resolution is often limited by sensor pixel size. To overcome this problem, we propose an iterative reconstruction method with data interpolation based on the grating illumination. In our method, the Talbot self-image of a Ronchi grating is exerted in the sample plane as a priori constraint which lead to the convergence of the iteration, the iteration between the sample plane and the sensor plane can provide some extra information with interpolation in the sensor plane based on the a priori constraint, furthermore, the iteration reconstruction can also eliminates the twin-image to improve the image quality. Numerical simulation has been conducted to show the effectiveness of this method. In order to make a further verification, we have developed a lensless in-line holographic microscope with a compact and wide field-of-view design. In our setup, the sample was under the Talbot image illumination of the Ronchi grating, which was illuminated by a collimated laser beam, and holograms were recorded by a digital imaging sensor. We can shift the grating laterally to get a wide-field image. We demonstrated the resolution of our imaging system by using the USAF resolution target as a sample, and the results shown the resolution improvement of the image.

Keywords: digital holography, grating illumination, interpolation, high resolution

1. INTRODUCTION

High resolution is always the pursuing target in the imaging field, especially in the microscopic applications[1-4]. As a new emerging field in imaging applications, digital holography microscopy has become a very active part in the imaging field for their advantages, such as: compactness, more information and low cost[5-8]. However the low resolution has become largest limitation;

In digital holography, the resolution is decided by mainly two factors: numerical aperture (NA) and sensor pixel size. The resolution limitation by the NA is diffraction limited resolution. The only two methods to overcome this limitation include shorten the wavelength of the light wave and enlarge the NA of the optical system[7, 9-14], there are many ways to increasing the NA of the setup, such as using oil-immersed setup at the specific reconstruction distance[9], adopting synthetic aperture technique[10], expanding the size of the hologram by self-extrapolating[11-13]. For the compact digital setup, the distance between sensor and sample is very small, so the resolution limitation caused by NA is not a decisive factor, In general, the pixel size of the commercial sensor is about several micrometers, it is larger than many details in microorganism. So the sensor pixel size dominates the resolution of the system.

Many efforts have been made to achieve high-resolution imaging to overcome the resolution limits caused by the pixel size of sensor, such as: Optofluidic microscopy(OFM)[15, 16], sub-pixel shifting method[13, 17]. These methods are very effective but complicated, the OFM system needs the sensor covered by metallic layer with small aperture and the distance between the sensor and sample is very close. Furthermore, it needs work with the microfluidic channel; The sub-pixel shifting method needs high-precision shifting device. A possible method to enhance the resolution is interpolation[18], but the additional information introduced by the interpolation is not reliable.

In this article, we make use of the iteration reconstruction method with grating illumination to enhance the resolution by hologram interpolation. It's not hard to see the interpolation of hologram can provide more information, but the extra

Iterative holographic reconstruction based on the grating illumination with improved resolution by interpolation

Shaodong Feng, Mingjun Wang, Jigang Wu,*

*Biophotonics Laboratory, University of Michigan—Shanghai Jiao Tong University Joint Institute,
Shanghai Jiao Tong University, Shanghai 200240, China*

**Corresponding author: jigang.wu@sjtu.edu.cn*

Abstract: we proposed an iterative holographic reconstruction method with data interpolation based on grating illumination with improved resolution. Using the U.S. air force target as the sample, simulation and experiments prove the feasibility of this method.

OCIS codes: (180.0180) Microscopy; (100.5070) Phase retrieval; (170.3880) Medical and biological imaging.

1. Introduction

Digital in-line holography microscopy (DIHM) has become a promising imaging field for the inherent advantages: free of optical aberrations[1,2], compactness, low cost[3] and three-dimensional information[4]. The resolution of digital holography is decided by numerical aperture (NA) and sensor pixel size. For the compact DIHM system, the pixel size of the sensor becomes the dominated factor of the resolution. However, for the reason that the pixel size of digital sensor always larger than the silver bromide particles, digital hologram has lower resolution than the analog holography[5]. So obtain the high resolution of the digital holography is an urgent demand.

Many efforts have been made to achieve high-resolution imaging to overcome the resolution limits caused by the pixel size of sensor, such as: Optofluidic microscopy[6,7], sub-pixel shifting method[8]. These methods are effective but complicated. Decreasing the pixel size by data interpolation is an effective and low cost way to get the high resolution images.

In this article, we make use of the iteration reconstruction method with data interpolation under grating illumination to improve the resolution. The grating illumination is to provide the constraints in object plane[9]. The data interpolation is aim to decreasing the pixel size to enhance the resolution. The iterative phase retrieval algorithm is iteratively propagated between the sensor and sample plane by numerical computation.

2. Principle and Methods

The resolution limits caused by diffraction limits can be calculated by the Rayleigh Criterion as below:

$$R = \frac{1.22\lambda z}{N\Delta} \quad (1)$$

where λ is the wavelength, z presents the reconstruction distance, N is the number of the pixels of the sensor and Δ is the pixel size. The $N\Delta$ is sensor size and also is the aperture size of the digital holography system. A simple calculation can give the result that resolution limits caused by diffraction limits is always smaller than pixel size for the compact DIHM system.

For the transfer function of DIHM can be regarded as the linear filter with a finite bandwidth. So the propagation of the light wave from the sample to sensor is a filtering process, which filters the high frequency components. Proper propagation distance is an effective filtering process, which make sure the sampling meets Nyquist-Shannon sampling theorem. The interval in sample plane is same as the pixel size of the sensor according to the inherent property of angular spectrum, so smaller details can't be recognized in the reconstructed images. So, in this situation, decreasing the pixel size by data interpolation is effective.

However, the additional information introduced by data interpolation is just an approach to estimate the new data points within the range of a discrete set of known data points, so the new information should be corrected by phase retrieval method. The grating illumination provides the constraints in sample plane, in order to provide tight constraints, the phase constraints in sample plane are necessary, phase constraints are also reasonable for thin and average samples. The iterative phase retrieval method not only can get high resolution, also can eliminate the twin-image disturbance.

3. Simulation and Experimental results

Pixel Super-resolution in Digital In-line holography

Mingjun Wang, Shaodong Feng, Jigang Wu*

Biophotonics Laboratory, University of Michigan – Shanghai Jiao Tong University Joint Institute,
Shanghai Jiao Tong University, 800 Dongchuan Road, Shanghai, China

*jigang.wu@sjtu.edu.cn

ABSTRACT

We report a new holographic microscope using pixel super-resolution algorithm. In our method, a sequence of low resolution images are acquired by a complementary metal oxide semiconductor (CMOS) sensor in digital inline holography system and the resolution is limited by the sensor pixel size. Then the super-resolution algorithm is applied to the low resolution images to get the image with much higher resolution that beyond the Nyquist criteria.

We perform both numerical simulation and experiments to demonstrate our method with US Air Force Target used as the sample. The sample is randomly moved in the sample plane and a set of holograms are captured by the camera in inline holographic system. We use two methods to reconstruct the sample image. In the first method, super-resolution algorithm is applied with the low resolution holograms to get the high resolution hologram. Then the high resolution hologram is reconstructed using auto-focusing algorithm to get the high resolution sample image. In the second method, the raw holograms are directly reconstructed to get a set of low resolution sample images, then the super-resolution algorithm is applied to get the high resolution sample image. We observed that the above mentioned two methods can get similar results in both numerical stimulation and experiments. We believe that the combination of pixel super-resolution algorithm and digital in-line holography can be very useful to implement a compact low-cost microscope with high resolution.

Keywords: Super-resolution, digital in-line holography, image resolution

1. INTRODUCTION

Optical microscope has developed for several hundred years and been widely used in many aspect our life and research. However the precise instruments need bulky lens, big body and expensive cost which limit the use of microscope. Recent rapid development technique and great effort has made CMOS imaging sensor cheap and high density chip, which lead to rise of new microscopic design. These developments use imaging sensor as the receiver, making it easy to combine with computational calculation and analysis. For instance, the on-chip microscope makes difference with the classical microscope [5,6]. It avoids bulky size and use of lens to make it smaller and less-cost, its capability of test cell or microorganism morphology makes it more popular and promising in healthcare diagnosis in remote devises. However, there is a significant characteristic of these kind of electrical receiver, the resolution is greatly determined by the pixel size of imaging sensor, which means that the resolution of images will be limited by the sensor parameter. Recently the most common pixel size of imaging sensor is 2.2 μm or larger, to achieve even higher resolution would lead to much funding, which hinder the development of lens-less on -chip microscope. Digital in-line holography is a example of lens-less microscope[1-7]. This technique is capable to recover the 3 dimensional images of object with the use of phase information.

Herein, to get high resolution go beyond the Niquist criteria and satisfy the cost-less and portable function, computer algorithms are more suitable for lens-less on-chip microscope. We introduce a new digital in-line holographic microscope making use of super-resolution algorithm [8-11]. Nowadays super-resolution has been used in many image enhancement technique, such as optifluidic microscope [12,13]. The core concept of this algorithm is to generate one or several high resolution images with one or several low resolution images. It takes advantage of precise subpixel movement between subsequent low resolution images. With the calculated motion vector to generate larger image frame. The result shows that it can achieve even higher resolution which can reach $\sim 1\mu\text{m}$. Geometrically the setup of our method is very simple, which has only several devices and can work without lens, as shown in Fig 1. The coherent light through fiber and pin hole works as the light source. After a distance of propagation, the light comes to the sample plane. Some coherent light wave partially gets scattered and absorbed and the rest directly go across the glass, acting as

Efficient Four-Wave Mixing in Loaded Nanoscale Plasmonic Hotspots

Xiaodan Wang, Hui Yi and Tian Yang*

State Key Laboratory of Advanced Optical Communication Systems and Networks, Key Laboratory for Thin Film and Microfabrication of the Ministry of Education, University of Michigan - Shanghai Jiao Tong University Joint Institute, Shanghai Jiao Tong University, Shanghai 200240, China.

* Email: tianyang@sjtu.edu.cn

Abstract: Gold nanosphere-plane antennas, with a monolayer of graphene in the junction gaps and wrapped by aluminum oxide, show over 10% frequency conversion efficiencies by four-wave mixing under femtosecond laser pumping.

OCIS codes: (190.4380) Nonlinear optics, four-wave mixing; (250.5403) Plasmonics; (350.4238) Nanophotonics and photonic crystals.

1. Introduction

Nonlinear plasmonics has become a subject of intense interest in recent years thanks to the fast progress of the field of plasmonics and the sub-diffraction limit confinement of electromagnetic fields that greatly enhances high order processes [1]. Among them, the third order nonlinear nanoscale plasmonic devices are an essential category, but have been limited to high pump laser powers and extremely low frequency conversion efficiencies, due to the small third order susceptibilities of available Kerr nonlinear materials (KNM) and the short light-matter interaction distances [2-6]. However, in previous experiments, usually only three of the four mixed waves have their wavelengths match the localized surface plasmon resonance (LSPR), which leaves a significant space for improvement in quadruple enhanced efficiency. In addition, the plasmonic enhancement factor of the electric field in the KNM can be further enhanced, for example, to as high as the nanometer size plasmonic hotspots in surface enhanced Raman scattering [7]. In this work, we pump the gold nanosphere-plane antennas with a femtosecond laser, which have a monolayer of graphene in the junction gaps as loaded KNM, and which are wrapped by aluminum oxide. The combination of quadruple enhancement and high intensity hotspots of the four-wave mixing (FWM) process results in significant linewidth broadening of the scattered light, which corresponds to a frequency conversion efficiency of over 10% by comparing to a theoretical model.

2. Experiment

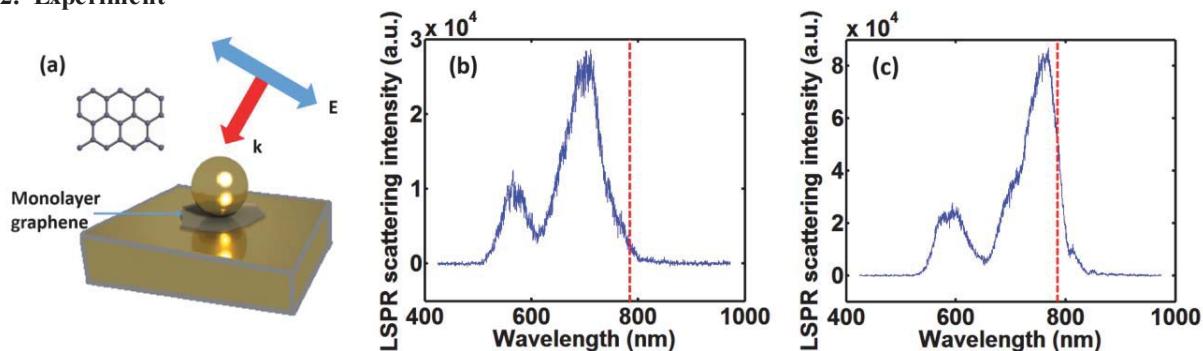


Fig. 1. (a) A schematic diagram of the nanosphere-plane antenna under linearly polarized focused excitation. The mirror image of the nanosphere is also plotted. (b) The LSPR spectrum of an antenna before deposition of aluminum oxide. (c) The LSPR spectrum of the same antenna after deposition of 25 nm aluminum oxide. The femtosecond laser's central wavelength, 785 nm, is labeled as a red dashed line.

A schematic illustration of our structure is shown in Fig. 1a. A 100 nm diameter gold nanosphere is on top of a 200 nm thick atomically flat gold plane. A monolayer of graphene lies in the gap between the nanosphere and the plane as a subnanometer (0.34 nm) spacer. The nanosphere and its image form a vertically oriented optical antenna [7]. A pulsed laser centered at 785 nm with a pulse width of 100 fs and a repetition rate of 80 MHz is focused by an objective with a numerical aperture (NA) of 0.9 onto the sample, then experiences four-wave mixing in the antenna junction loaded with graphene and possibly also aluminum oxide, and has its scattering spectrum measured which

Stepwise Quantum Phonon Pumping in Surface-Enhanced Raman Scattering

Tian Yang*, Jing Long and Xiaodan Wang

State Key Laboratory of Advanced Optical Communication Systems and Networks, Key Laboratory for Thin Film and Microfabrication of the Ministry of Education, UM-SJTU Joint Institute, Shanghai Jiao Tong University, Shanghai 200240, China.
 tianyang@sjtu.edu.cn

Abstract: Theory and experiments show that, in extremely intense plasmonic hotspots, the quantum nature of molecular vibration results in stepwise pumping of phonons and a complicated nonlinear Raman scattering intensity versus laser power relation.

OCIS codes: (020.5580) Quantum electrodynamics; (190.5890) Scattering, stimulated; (240.6695) Surface-enhanced Raman scattering

Raman scattering is usually taken for granted to be a linear process, whose intensity is linearly proportional to the laser power. However, in plasmon-enhanced situations, including surface-enhanced Raman scattering (SERS) and tip-enhanced Raman scattering (TERS), the strong coupling between elementary excitations bring the system out of the linear regime of weak interactions. Particularly, when the molecular vibrations are Stokes excited to contain a finite number of phonons, stimulated emission of phonons and amplification of vibration by cavity opto-mechanical feedback turn on, which lead to the recently discovered nonlinear Raman phenomenon [1-5]. Such complicated and strong interactions in the ultra-intense and nanometer-size plasmonic hotspots are key to understanding the mechanisms behind SERS and TERS, and to controlling and utilizing these techniques for applications that require ultimate accuracy and precision, for example, single molecule detection and single chemical event tracking.

In this work, by quantization of the molecular vibration coherent state into phonon number states, and by incorporating different Raman activities for different Stokes transitions, we theoretically predict a multi-step phonon pumping phenomenon for resonant Raman molecules, which includes a saturation step and a stimulated phonon emission step. Previous models have assumed a homogeneous Raman activity for all these states, which actually reduces the problem to a single-step spontaneous and stimulated phonon emission scenario [4,5].

A schematic illustration of our experiment is shown in Fig. 1(a), which was described in [3] in details. A 60 nm gold nanosphere is on top of an atomically flat gold plane, and a radially polarized He-Ne laser beam at 633 nm is focused by an objective with a numerical aperture of 0.9 to excite the nanosphere. A monolayer of malachite green isothiocyanate molecules is coated on the surface of the nanosphere. The nanosphere pairs with its mirror image to form a vertical optical antenna, which contains a $\sim 9 \text{ nm}^2$ hotspot in its junction gap. Raman scattering off molecules in the hotspot is collected by the same objective. Such an experimental scheme has been reported to produce reproducible ultrahigh enhancement in individual deterministic hotspots under low laser powers [3]. Figure 1(b) shows a typical surface enhanced Raman scattering (SERS) spectrum.

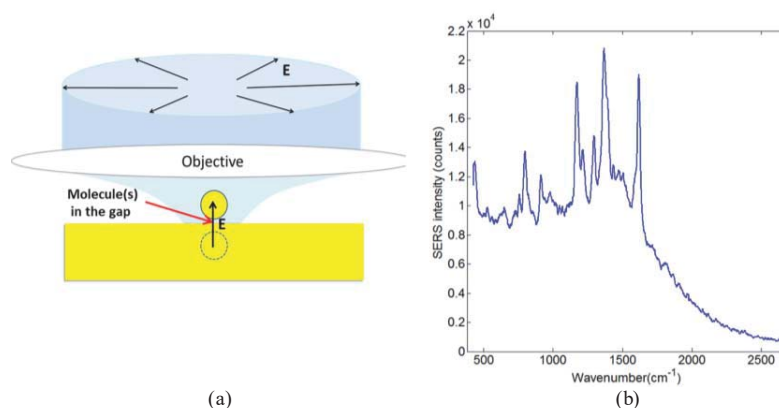


Fig. 1. (a) Schematic illustration of the SERS experiment. (b) A typical SERS spectrum.

Ultrasound detection with surface plasmon resonance on fiber end-facet

Xin Zhou¹, De Cai¹, Xiaolong He^{1,2}, Sung-Liang Chen¹, Xueding Wang³ and Tian Yang^{1*}

¹State Key Laboratory of Advanced Optical Communication Systems and Networks, Key Laboratory for Thin Film and Microfabrication of the Ministry of Education, UM-SJTU Joint Institute, Shanghai Jiao Tong University, Shanghai 200240, China.

²Xu Yuan Biotechnology Company, 1883 South Huicheng Road, Shanghai 201821, China.

³Department of Biomedical Engineering, University of Michigan, 2200 Bonisteel Blvd, Ann Arbor, MI 48109, USA.

E-mail: tianyang@sjtu.edu.cn

Abstract: A surface plasmon resonance cavity on an optical fiber end-facet is designed and demonstrated for ultrasound detection. A noise equivalent pressure of 25 KPa over 20 MHz, almost omni-directional response and stable performance are reported.

OCIS codes: (130.3120) Integrated optics devices; (230.1040) Acousto-optical devices; (240.6680) Surface plasmons.

1. Introduction

The development of invasive ultrasound imaging demands ultrasound detectors that have a small size, a flexible configuration, a flat angular response as well as a satisfactory combination of sensitivity and bandwidth. In the case of piezoelectric detectors, in order to achieve high sensitivity, a large size of the piezoelectric material has to be used to reap enough ultrasound energy, which in turn limits the bandwidth and angular response. In addition, to detect high frequency ultrasound, the piezoelectric material has to be thinner than the acoustic wavelength, which presents a challenging fabrication task. A few optical detection methods have been reported which show noise equivalent pressure (NEP) values from 105 Pa to 3.3 KPa under bandwidths of more than 100 MHz, e.g. microring devices [1] and prism-coupled surface plasmon resonance (SPR) [2], but whose configurations can't be straightforwardly integrated with in vivo applications. By integrating a Fabry-Perot cavity on the end-facet of a single-mode optical fiber (SMF), Beard's group has demonstrated NEP values as low as a few Pa's and broad working bandwidths [3]. The SMF platform offers an ideal combination of small size, flexible configuration and easy optical transmission. In this work, we report an SPR cavity device on the end-facet of a SMF, which shows a NEP of 25 KPa and an almost omni-directional angular response, which at the same time shall have a broader bandwidth than any of the above-mentioned detectors in principle, and which is fabricated at a low cost and high yield.

2. Experiments

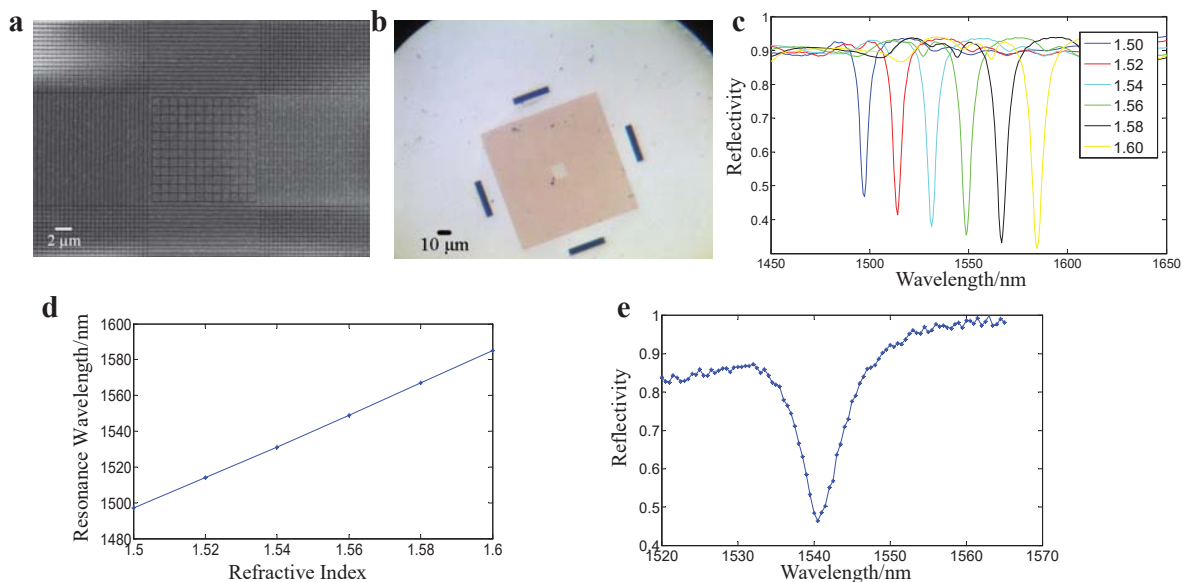


Fig. 1(a) Scanning electron micrograph of an SPR cavity. (b) The transferred device on a fiber end-facet under an optical microscope. (c) Simulated reflection spectra with different refractive indices of glue. (d) The linear relationship between the SPR resonance wavelength and the

An Approximate Algorithm for Quantum Hamiltonian Identification with Complexity Analysis[★]

Yuanlong Wang^{*,**} Daoyi Dong^{*} Ian R. Petersen^{***} Jun Zhang^{****}

^{*} School of Engineering and Information Technology, University of New South Wales, Canberra, ACT 2600, Australia (e-mail: yuanlong.wang.qc@gmail.com; daoyidong@gmail.com)

^{**} Centre for Quantum Computation and Communication Technology, Australia Research Council, Canberra, ACT 2600, Australia

^{***} Research School of Engineering, Australian National University, Canberra, ACT 0200, Australia (e-mail: i.r.petersen@gmail.com)

^{****} Joint Institute of UM-SJTU, Shanghai Jiao Tong University, Shanghai 200240, China (e-mail: zhangjun12@sjtu.edu.cn)

Abstract: Identification of the Hamiltonian is vital for characterizing the dynamical evolution of a quantum system. The dimension of a multi-qubit system increases exponentially with the qubit number, which usually leads to daunting computational complexity for general Hamiltonian identification algorithms. In this paper, we design an efficient quantum Hamiltonian identification method based on periodical sampling. The computational complexity is $O(M^2 + MN^2)$, where M is the number of unknown parameters to be identified in the Hamiltonian and N is the length of the sampling data. Numerical results with different data lengths demonstrate the effectiveness of the proposed identification algorithm.

© 2017, IFAC (International Federation of Automatic Control) Hosting by Elsevier Ltd. All rights reserved.

Keywords: Quantum systems, Hamiltonian identification, sampling data.

1. INTRODUCTION

Recent decades have witnessed the fast development of a series of different branches of quantum technology, such as quantum computation, quantum communication and quantum metrology (Nielsen and Chuang (2000)). To control or utilize a quantum system, it is necessary to extract enough information about the system through estimating the parameters we are interested in.

To fully characterize an unknown static quantum state, some quantum state tomography methods such as maximum likelihood estimation (Hradil (1997); Řeháček et al. (2001, 2007)), Bayesian mean estimation (Blume-Kohout (2010)) and linear regression estimation (Qi et al. (2013); Hou et al. (2015, 2016); Qi et al. (2015)) have been developed. For estimating an dynamic quantum state, quantum filtering theory has been well established (Bouten et al. (2007); Gao et al. (2016)).

Some process tomography methods have been presented to characterize a quantum process (Nielsen and Chuang (2000)). An important class of quantum processes are unitary processes, where the evolution is fully governed by the system Hamiltonian. Hamiltonian identification is an important research problem to characterize quantum dynamics. There have been some results for Hamiltonian identification in quantum systems. For

example, Burgarth and Yuasa (2012) established a general framework to quantify the amount of knowledge attainable for a quantum system under a given experimental setup. Bonnabel et al. (2009) proposed a symmetry-preserving observer-based Hamiltonian identification algorithm and presented an exponential convergence result. Bris et al. (2007) proved well-posedness in identifying the field free Hamiltonian and/or the dipole moment of a quantum system, and proposed a numerical identification algorithm. Geremia and Rabitz (2002) used a closed-loop learning control method to optimally identify quantum Hamiltonian information. Franco et al. (2009) proposed a scheme to determine the coupling parameters in a spin chain without requiring state initialization or prior knowledge of the system state. Cole et al. (2005) developed a Hamiltonian estimation method for two-state systems and gave uncertainty bounds on the estimation result. Schirmer and Oi (2009) proposed a Bayesian-based Hamiltonian estimation method for two-qubit systems using only initialization and measurement in a single fixed basis. Ferrie et al. (2012) derived an adaptive Hamiltonian estimation protocol based on Bayesian experimental design techniques and showed an exponential enhancement in estimation accuracy for a single two-level quantum system under strong measurement. Wang et al. (2016) proposed an iterative method to identify a general quantum Hamiltonian based on matrix differentiation.

For general Hamiltonian identification algorithms, the computational complexity is usually high for systems consisting of a large number of qubits. One possible solution is to design

[★] This work was supported by the Australian Research Council's Discovery Projects funding scheme under Project DP130101658, Laureate Fellowship FL110100020, AFOSR under grant FA2386-16-1-4065 and the National Natural Science Foundation of China under Grant Nos. 61174086 and 61533012.

Swiss team discovers how protons move through fuel cell

Researchers at Empa – the Swiss Federal Laboratories for Materials Science and Technology – have decoded the movement of hydrogen ions in crystals, which is seen as a key step towards more efficient energy conversion using hydrogen.

Electrons and ions play the leading role in electrochemical energy storage and conversion devices such as batteries and fuel cells, carrying charge through the device. Proton conductivity is crucial in fuel cells, since protons (i.e. positively charged hydrogen ions) are formed from hydrogen, and used to power the fuel cell. Empa physicist Artur Braun and Qianli Chen, a doctoral student at ETH Zürich (now with Shanghai Jiao Tong University in China), conducted neutron scattering experiments using the Swiss Spallation Neutron Source (SINQ) at the Paul Scherrer Institute (PSI), to study the mobility of protons in the crystal lattice. They observed that the proton movements in ceramic fuel cells obey far more complex laws than had previously been assumed: the movement of the protons takes place according to the so-called 'polaron model'. The research was recently reported in *Nature Communications*.^[1]

The polaron model

The polaron theory, developed by the Russian physicist and Nobel Prize-winner Lev Landau in 1933, was for a long time only applied to electrons.^[2] The model describes how electrons 'worm' their way through a dielectric crystal and force 'interfering' atoms out of position, which slows down the electrons. In other words, polarons are waves of movement in the crystal, the spread of which can be described as the trajectory of a particle – and they can be deflected and reflected.

The electron polaron has long been a pillar of theoretical physics, and the basis for applied model calculations. By contrast, the existence of a hydrogen polaron – i.e. a hydrogen ion that 'hops' from one position to the next – had only been a speculative theory. Although biologists have used the model of hopping hydrogen atoms to explain certain metabolic processes, solid-state physicists did not regard hydrogen polarons as a valid explanatory model.

This could now change. Based on experiments using hydrated yttrium-doped barium cerate ($\text{BaCe}_{0.8}\text{Y}_{0.2}\text{O}_{3-\delta}$, or BCY20) and barium zirconium oxide ($\text{BaZr}_{0.9}\text{Y}_{0.1}\text{O}_3$, or BZY10) perovskite crystals, Braun and Chen

proved the existence of the proton polaron. In a dry state, these crystals are non-conductive. But if they are exposed to a steam atmosphere, OH groups form inside the crystal structure. Released protons can then move in a wavelike fashion, and the oxide becomes ionically conductive.

Heat and high pressure confirm hydrogen ions

Braun and Chen found evidence of hydrogen ion waves by studying the crystals under different high pressure conditions and at temperatures up to 600°C. The samples were X-rayed on PSI's neutron source, and the high pressure experiments on the crystals were conducted in conjunction with researchers in the Faculty of Geosciences/Geography at Goethe University Frankfurt in Germany.

This work found that at temperatures between 220 and 520°C, the conductivity increases to exactly the same extent as predicted in model calculations for the lattice vibrations of the crystal. The protons are therefore initially bound in the crystal lattice, and begin to hop through the crystal from one OH group to another in the concert of lattice vibrations when heated. If the crystal is exposed to high pressure with a special compactor, there is less

space for the proton leaps, and the conductivity drops again. This proves that the polaron model applies to both electrons and protons.

'And who knows, perhaps the theory also holds true for other ions such as lithium,' speculates Artur Braun.

The Empa researchers' findings could soon yield vital information on the choice of materials for fuel cells and hydrogen storage systems. The behaviour of ceramic insulators can now also be gauged more effectively, such as whether they still insulate well at high temperatures in humid outside air, or whether current leakages develop that can be attributed to polaron conduction. Braun and Chen's project, which was funded by the Swiss National Science Foundation (SNSF), has allowed some materials science riddles to be solved.

References

1. Artur Braun and Qianli Chen: Experimental neutron scattering evidence for proton polaron in hydrated metal oxide proton conductors, *Nature Communications* **8** (14 June 2017) 15830, <http://dx.doi.org/10.1038/ncomms15830> (Open Access).
2. Polaron (on Wikipedia): <https://en.wikipedia.org/wiki/Polaron>

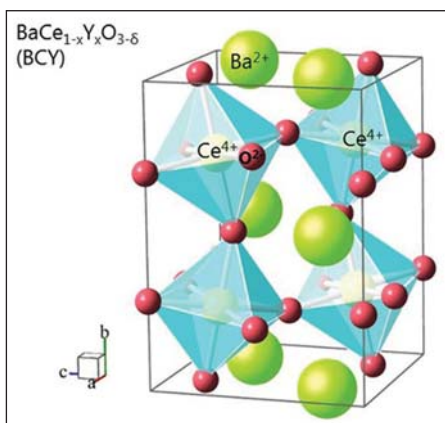
More information

Dr Artur Braun, Modern Materials and Surfaces, Laboratory for High Performance Ceramics, Empa Swiss Federal Laboratories for Materials Science and Technology, Dübendorf, Switzerland. Tel: +41 58 765 4850, Email: artur.braun@empa.ch, Web: www.empa.ch/web/s201

Dr Qianli Chen, State Key Laboratory of Metal Matrix Composites, University of Michigan-Shanghai Jiao Tong University Joint Institute, Shanghai Jiao Tong University, Shanghai, China. Email: qianli.chen@sjtu.edu.cn, Web: <http://en.smse.sjtu.edu.cn/index.asp>

Paul Scherrer Institute, Swiss Spallation Neutron Source: www.psi.ch/sinq

Goethe University Frankfurt, Faculty of Geosciences/ Geography: www.goethe-university-frankfurt.de/45572377/fb11



Artur Braun and Qianli Chen conducted experiments with barium cerate, whose crystal is non-conductive in a dry state – but when moisture enters, the protons form OH bonds and move through the crystal. [Image: Empa]

ROLE OF THE FABRICATION TECHNIQUE IN THE STABILITY OF CH₃NH₃PbI₃ PEROVSKITE THIN FILMS

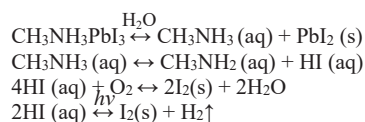
Mehran Habibi, Morteza Eslamian

University of Michigan-Shanghai Jiao Tong University Joint Institute
800 Dongchuan Road, Minhang District, Shanghai, 200240, China
Email: mhabibi82@sjtu.edu.cn, morteza.eslamian@sjtu.edu.cn

ABSTRACT: Despite the high power conversion efficiency of the state-of-the-art halide perovskite solar cells, their poor stability against humidity, oxygen, temperature, and light has hindered their commercialization. In this work, it is shown that the nature of the deposition method, and its attributes, is an important parameter that affects the stability of the perovskite films. To this end, the stability of the CH₃NH₃PbI₃ perovskite films deposited by spray and blade coating, as two scalable and commercially viable techniques, and spin coating, as a lab scale technique are compared. To achieve a uniform and defect-free film made by spray and blade coating, the substrate temperature was raised during the deposition process, whereas the anti-solvent treatment was performed in the case of the spin-coated films. It is shown that the perovskite stability is influenced by the morphology of the film which is in turn controlled by the dynamics of the coating process. The stability analysis was performed by obtaining the SEM and XRD graphs of the films exposed to a humid environment (35-60%). Comparison of the ratio of the XRD peak intensity of the lead iodide (PbI₂) to perovskite after 10 days revealed that the blade-coated samples are the most stable films. The spray- and spin-coated counterparts, on the other hand, are rough and prone to decomposition. It is also observed that the fabrication of a fully-covered and smooth perovskite film through the anti-solvent engineering can prolong the stability of the spin-coated films. In conclusion, a smooth film with fewer number of gap-free grain boundaries is found to be more stable. In this context, the blade-coated samples and then the spin-coated samples treated by anti-solvent (toluene) showed the best stability.

1 INTRODUCTION

The global energy demand in near future is predicted to be near 1 GW per day [1]. Photovoltaic solar cells as a clean, renewable, and affordable source of energy are expected to have a major contribution in the energy sector to meet the future energy demand. Perovskite solar cell, as an emerging member of the family of the solution-processed solar cells, has proved its potential to be an efficient and cheap source of energy, although it suffers from poor stability and inadequate lifetime [2]. Instability is originated from sensitivity of the perovskite structure to moisture, oxygen, temperature, UV light and solution processing [3]. The methylammonium lead iodide CH₃NH₃PbI₃ (MAPbI₃) is the common perovskite light harvester, which contains a hygroscopic amine component. Due to the presence of this part, the MAPbI₃ may decompose to the perovskite precursors, i.e., PbI₂ and CH₃NH₃I, upon exposure to water and oxygen. After that, a series of chemical reactions may occur resulting in the formation of H₂O, I₂ and H₂, according to the following reactions [4]:



To avoid or delay the decomposition of the perovskite structure, several approaches have been reported, to date. Some works have tried to intrinsically stabilize the perovskite active layer by changing its components. For instance, substituting the I ions with the Br ions to tune the stoichiometry of the mixed halide CH₃NH₃Pb(I_{1-x}Br_x)₃ perovskites can significantly improve the stability [5]. Also, replacing the methylammonium (MA) cation with formamidinium (FA) cation has shown an improvement in the thermal stability of the perovskite structure [6].

Some attempts have been made to encapsulate the

entire device or the perovskite layer. Various encapsulating techniques and materials have been reported in some comprehensive reports [7-9]. In some papers, it is argued that the interface engineering has an encapsulating effect [10-13]. In fact, some interlayers engineered between the electron transporting layer and the metal electrode, e.g., PEIE polymer [12], fullerene amine interlayer (PCBDAN) [11], and MoO_x [13], or between the perovskite and the hole transporting layer, e.g., zinc phthalocyanine (ZnPc) [10], not only enhance the electrical performance of the device, but they also protect the perovskite layer against decomposition.

Beside the abovementioned considerations, the fabrication method, through its attributes, is another important parameter that affects the stability. It has been reported that manipulating the process parameters or using alternative casting techniques may alter the thermal and air stability of the perovskite solar cells. Kim and coworkers [14] modified the sequential deposition technique in the fabrication of the MAPbI₃ perovskite layer, by changing the steps and duration of the dipping time. Through a two-step CH₃NH₃I (MAI) dipping process they showed that the thermal stability of the devices can enhance. In another work, hybrid chemical vapor deposition was applied which resulted in stable devices. In this case, the fabrication was performed in high temperature, which led to better stability. This was ascribed to the complete evaporation of the excess MAI and water in hybrid chemical vapor deposition [15]. Therefore, in this work to further investigate the aforementioned approach, blade coating, spray coating and spin coating with and without anti-solvent engineering are employed to fabricate the MAPbI₃ perovskite films and examine their stability.

2 MATERIALS AND METHODS

Lead iodide (PbI₂, 98.5%), dimethylsulfoxide (DMSO, 99.5 %), γ -butyrolactone (GBL) and toluene (98.8%) were purchased from Sigma-Aldrich, USA.

EVAPORATION OF DMF SESSILE DROPS ON STATIONARY AND VIBRATING SUBSTRATES

Amin Rahimzadeh and Morteza Eslamian*.

*Author for correspondence

University of Michigan-Shanghai Jiao Tong University Joint Institute,
Shanghai, 200240, China

E-mail: Morteza.eslamian@sjtu.edu.cn

ABSTRACT

Contact and interaction between droplet and solid surface is a fundamental transport phenomena problem, with ubiquitous presence in various applications. In this paper, we study the effect of imposing vertical and horizontal ultrasonic vibration on dynamics and evaporation of sessile droplets of dimethylformamide (DMF), a pure volatile model solvent. Droplet contact angle and contact radius are the two main parameters that may change during evaporation. Hence, droplet evaporation may be categorized into different modes: constant angle (CA), constant radius (CR), and a complex combination of CA and CR modes. Imposing substrate vibration affects the evaporation rate and mode by changing the thermodynamics and hydrodynamics of the sessile droplet on the substrate. The former happens by changing the heat transfer coefficient and the latter by pinning or unpinning the droplet from the substrate. Experimental analysis using an optical tensiometer has been conducted for a small DMF sessile drop on a Teflon substrate. Among our results, it is observed that the DMF droplet on a Teflon substrate evaporates in the CR mode until it reaches its receding contact angle. Then, its contact radius recedes to the next equilibrium position. Imposing vertical ultrasonic vibration pins the droplet to the substrate and reduces the receding contact angle, while horizontal ultrasonic vibration unpins it. Furthermore, imposing vibration accelerates the evaporation rate more than 5 times higher than that of the natural convection. The increase is more significant for the horizontal vibration.

INTRODUCTION

Numerous studies have been performed on spreading, deposition, and surface wetting of evaporating liquid droplets on a substrate, e.g. Anderson and Davis [1], Burelbach et al. [2], and Ajaev [3], among others. One influential study that has shed light on the research path in evaporation of sessile droplets is a study conducted by Picknett and Bexon [4], in which two extreme modes of evaporation are identified: constant contact angle (CA) and constant radius (CR) evaporation. Based on their investigation, droplet mass varies linearly with time in the CR mode, while it changes with a power law in the CA mode. In addition, droplet lifetime in the CR mode is shorter unless the contact angle is greater than 140° [4], i.e. the droplet lifetime is affected by the hydrophobicity of the substrate [5]. In reality, droplet evaporation proceeds based on a combination of multiple CR and CA modes, also called stick-slip modes, where stick

refers to the CR mode and slip usually denotes the CA mode [6]. The duration and sequence of the CA and CR modes in stick-slip evaporation mechanism is hard to predict and varies with the choice of the liquid and substrate, as well as the ambient conditions [7]. In other words, liquid properties, substrate physiochemical characteristics, as well as the substrate temperature are important parameters that identify the wetting, evaporation, and other phenomena associated with sessile droplets [8-12]. In some cases, after a period of CR evaporation, the droplet may quickly slip or jump to a new position, in lieu of the CA mode. Therefore, the so-called CA, CR, and stick-slip modes only provide qualitative description of sessile droplet evaporation.

Erbil [13] reviewed and discussed some works pertinent to the basic theory and some special topics related to droplet evaporation. Erbil et al. [14] investigated the CA mode of evaporation of sessile droplets of various organic solvents, and Birdi et al. investigated evaporation of sessile droplets of water on smooth substrates, which was found to follow the CR mode [15]. The evaporation rate varies with droplet size, however more recent studies consider other effects, such as substrate temperature and substrate thermal properties [16, 17], and the choice of the ambient gas and pressure [18]. Sefiane et al. [18] showed that by reducing the ambient pressure, water vapor diffusion coefficient increases leading to an increase in evaporation rate [6].

As mentioned above, the CR, CA, or stick-stick modes of droplet evaporation could be quite complex. A theoretical work has analyzed modes of water droplet evaporation on a hydrophobised substrate [19], and some experimental works have demonstrated the existence of these complex modes in most real cases, e.g. [20-22]. For instance, Strauber et al. [22] showed that the lifetime of droplet may not be always constrained by the lifetime in the extreme modes. In other words, since the time of evaporation in CA and CR modes are different, and since the real stick-slip behavior of an evaporating droplet is a combination of CA and CR extreme modes, one may conclude that the lifetime of an evaporating droplet would be in between of those of the extreme modes. However, Strauber et al. showed that this may not be necessarily the case, simply because an evaporating

Ultrasonic assisted solution deposition of graphene based nano-composite thin films; Highly-efficient functional component for opto-electrical devices

F. Zabihi^{(1)*}, M. Eslamian⁽²⁾

⁽¹⁾ ¹State Key Laboratory for Modification of Chemical Fibers and Polymer Materials, College of Materials Science and Engineering, Donghua University, Shanghai, 201620, China, fzabihi@dhu.edu.cn

⁽²⁾ ²University of Michigan-Shanghai Jiao Tong University Joint Institute, Shanghai 200240, China, morteza.eslamian@sjtu.edu.cn

* Corresponding Author e-mail: fzabihi@dhu.edu.cn

Keywords: Photo-catalysis, spray coating, ultrasonic, thin film

Abstract: Carbon family has shown great potentials in numerous applications such as coating, membrane and electrical junctions. Traditional forms of carbon i.e. fibers and CNT¹ are frequently used in batteries, capacitors and transistors but functional and operational limitations have led the attentions to an atom-thick architecture, graphene [1-2]. Unique band structure, fast charge mobility and photo-response, abundant and low price are the main reasons for popularity of graphene. Literature report on graphene preparation through costly processes e.g. liquid-phase exfoliation (LPE), chemical vapor deposition (CVD), molecular beam epitaxy (MBE) [3], which are limited to lab scale. Our recent publications report on incorporation of an efficient technology (Substrate Vibration Assistance) into solution deposition technologies i.e. Spray coating [2-3]. Results show the remarkable enhancement of the structure and opto-electrical performance of functional thin films, when the substrate ultrasonic vibration affects is applied in solution deposition. Here we use this subtle technology within a roll-to-roll procedure (spray coating) to prepare TiO₂-graphene hybrid thin film, which serves as transparent photo-active layer in many opto-electrical devices such as photo-catalysis and photo-sensors [2-3]. Schematic 1 illustrates the experimental procedures and apparatus used for casting TiO₂ doped graphene.



Schematic 1-Ultrasonic vibration assisted spray coating, ultrasonic vibration equipment, thin film formation mechanism

In this method the severe thermal processing and the chemical reactions are simply replaced by a single-step mechanical treatment. The issuing combined thin film was characterized by visual and opto-electrical probations such as SEM, Atomic Force Microscopy, Raman spectroscopy, UV-visible transmission spectroscopy and surface potential analysis. We suggest substrate ultrasonic vibration assisted spray coating is a promising idea for solution deposition and can be replaced for costly, chemical based, high temperature and multi-step conventional methods.

[1] F.D. Hardcastle, J. Arkansas Academy of Science, **65** (2011) 43–48.

[2] F. Zabihi, M.R. Ahmadian-Yazdi, M. Eslamian, Nano-scale Res. Lett. **11**, 71 (2016)

[3] M. Eslamian, F. Zabihi, Nanoscale Research Letters **10** (2015) 462.

¹ Carbon nano-tube

Observation of the Coating Process in Spray Coating

Jianchi Huang, Zhihao Yuan, Siyi Gao, Jianshan Liao, Morteza Eslamian¹
University of Michigan-Shanghai Jiao Tong University Joint Institute
Shanghai, 200240, China

Abstract

Spray coating is a facile coating and deposition process with numerous existing and emerging applications. However, it is a stochastic process comprising impingement of many droplets, which upon impact on a heated substrate may dry individually or coalesce first to make a thin liquid film and then dry to make a thin solid film. There is very limited knowledge on how this process occurs; therefore in this work, high speed imaging is used to visualize the spray coating process. Two model solutions including food-dye with properties similar to those of water, and PE-DOT:PSS, a polymeric solution, are sprayed onto glossy paper and regular glass substrates. Substrates are kept at room temperature and elevated temperature of 80 °C. In some cases, a vertical ultrasonic vibration is imposed on the substrate to study its effect on the coating process. In conclusion, it is observed that the spray coating process is highly random and stochastic. A higher substrate temperature results in better coating process. Imposed vibration in the case of glossy paper substrates results in better droplet spreading and a more uniform coating, whereas in the case of glass substrate results in droplet “walking” on the substrate. Further systematic study is required to better understand the process.

¹ Corresponding author: Morteza.Eslamian@sjtu.edu.cn & Morteza.Eslamian@gmail.com

Title: Ultrasonic Vibration Imposed on Thin Liquid Solution Films as an Effective Tool for Improved Characteristics of Ensuing Thin Solid Films

Authors: [Eslamian, Morteza](#); [Zabihi, Fatemeh](#); [Rahimzadeh, Amin](#); [Wang, Qin](#); [Habibi, Mehran](#); [Xie, Yu](#)

Affiliation: AA(University of Michigan-Shanghai Jiao Tong University Joint Institute), AB(University of Michigan-Shanghai Jiao Tong University Joint Institute), AC(University of Michigan-Shanghai Jiao Tong University Joint Institute), AD(University of Michigan-Shanghai Jiao Tong University Joint Institute), AE(University of Michigan-Shanghai Jiao Tong University Joint Institute), AF(University of Michigan-Shanghai Jiao Tong University Joint Institute)

Publication: APS March Meeting 2017, abstract id. A35.012

Publication Date: 00/2017

Origin: [APS](#)

Bibliographic Code: [2017APS..MARA35012E](#)

Abstract

Thin solid films have ubiquitous presence in various existing and emerging technologies. Solution-processed thin solid films may be fabricated by casting a liquid solution film followed by a drying step. We have developed a method in which by imposing ultrasonic vibration on the substrate, characteristics of the resulting thin solid films and the performance and reproducibility of the ensuing thin film devices, such as perovskite and polymer solar cells, are improved. To explain this, we have studied the evolution of thin liquid films, subjected to ultrasonic vibration. It is found that the vertical vibration tends to destabilize the thin liquid film, however, in low-amplitude ultrasonic vibration, the term contributing to the perturbation growth rate due to vibration, decays rapidly. Vertical vibration is found as a destabilizing force, only if the film thickness is near a critical thickness in which the destabilizing van der Waals and stabilizing gravity and surface tension forces balance one another. It is substantiated that the lateral vibration does not promote instability. In summary it is found that while imposing ultrasonic vibration may destabilize and breakup the thin liquid film, a mild and controlled vibration significantly improves the homogeneity and uniformity of the ensuing thin solid film.

[Bibtex entry for this abstract](#)
[Preferences](#)

[Preferred format for this abstract](#) (see

Which Factors are Correlated with Engineering Students' Expectations of Ethical Issues?

Dr. Rockwell Franklin Clancy III, University of Michigan, Shanghai Jiao Tong Joint Institute

Rockwell F. Clancy is a lecturer in engineering ethics and philosophy at the University of Michigan-Shanghai Jiao Tong Joint Institute, Shanghai Jiao Tong University, and has acted as a long-term educational, setting up a course and writing a corresponding textbook with Heinz Luegenbiehl on global moral issues for engineers. His research and teaching interests include engineering ethics, philosophy of technology, Chinese philosophy, political philosophy, and science, technology, and society studies. Rockwell completed his PhD at Purdue University, West Lafayette, MA at the Katholieke Universiteit, Leuven, Belgium, and BA at Fordham University, New York.

Dr. Joanna Ruth Sessford, The Sino-British College, USST

Dr Joanna Sessford is an engineering lecturer at the Sino-British College, University of Shanghai for Science and Technology. She completed both her PhD and BEng at The University of Liverpool, UK. She was awarded a Graduate Certificate in Tertiary Teaching from Curtin University of Technology, Australia.

Longfei An, Shanghai Jiao Tong University, China

Longfei An is currently a PhD student in Business Management (Media Management) from Laboratory of Social Cognitive and Decision-making Studies, Institute of Arts and Humanities, Shanghai Jiao Tong University, China. He received his B.S. Degree in Applied Psychology from Jiangsu Second Normal University, and M.A. Degree in Applied Psychology from Hangzhou Normal University. His research interests include Social Cognition and Cultural Psychology by methods of Cognitive Neuroscience.

Dr. Yan Ge, Shanghai Jiao Tong University, China

PhD from University of Pittsburgh

Distinguished Professor, Shanghai Jiao Tong University

Director, Laboratory of Social Cognitive and Decision-making Studies, Institute of Arts and Humanities, Shanghai Jiao Tong University

Professor, School of Media and Design, Shanghai Jiao Tong University

Professor, Institute of Social Cognitive and Behavioral Science, Shanghai Jiao Tong University

Role of Entrepreneurship in Universal Health Coverage (UHC) using mHealth

Pradeep K. Ray and Congfei Zhang

Joint Institute of University Michigan-Shanghai Jiao Tong University
pradeep.ray@sjtu.edu.cn

Abstract—Healthcare is now the largest business sector that involves trillions of dollars of business all over the world. Declaration of health as a fundamental human right in World Health Organization's (WHO) constitution of 1948 and the agenda of Health for All by Alma-Ata declaration of 1978 were instrumental behind Universal Health Coverage (UHC). The World Health Organization (WHO) has identified e-Health (Healthcare using Internet technologies) as of prime importance for the access of healthcare to the population all over the world. Thanks to the rapid proliferation of mobile wireless technology (e.g., cellular phones and PDAs) especially in developing countries, mHealth (healthcare services based on mobile wireless technology) can play a major role in achieving the UHC. This is only sustainable through entrepreneurship in mHealth services through mobile apps and various wireless technologies. This paper examines entrepreneurship in mHealth through a systematic review.

Keywords—Universal Health Coverage; eHealth; mHealth; entrepreneurship; sustainability of mHealth, systematic review

I. INTRODUCTION

eHealth involves the application of Information and Communication Technologies (ICT) in healthcare. The Global Health Assembly organized by WHO has resolved that eHealth is important for reaching to masses all over the world thanks to the proliferation of mobile phones (mHealth) in many remote locations in the world [4]. mHealth will help developing countries overcome the obstacle of inadequate technological infrastructure in reaching healthcare all population [8]. This universal access to healthcare is now being enabled through the globally accepted objective of Universal Health coverage (UHC) that seeks to overcome inequality in tackling the service provision gap and financial gap that populations face. It may not be possible to realize UHC mainly due to the scarcity of funds and growing healthcare costs all over the world. Perhaps mHealth helps overcome the problem to some extent. However, financing UHC is still a major problem that may be partially overcome by encouraging social entrepreneurship in eHealth/mHealth based services [7]. This paper carries out a systematic literature survey of entrepreneurship in mHealth.

The paper starts with a review of barriers to eHealth in modern healthcare environment. This is followed by a systematic survey of published literature. The paper concludes with a discussion of the literature on mHealth and entrepreneurship as evidenced through the systematic survey.

II. UHC AND ROLE OF EHEALTH

The use of ubiquitous technology such as mobile electronic devices to support medical or public health practice and health systems has been embraced as the new frontier of ICT that will improve efficiency and effectiveness of health care, especially for the majority of the world's population that live in low and middle income countries. It has been predicted that by 2017 there will be "more mobile phones than people" on the planet, and currently three-quarters of the world's population have access to a mobile phone [1,10]. "Mobile communication devices, in conjunction with Internet and social media, present opportunities to enhance disease prevention and management by extending health interventions beyond the reach of traditional care—an approach referred to as mHealth" [2]. The World Health Organization (WHO) has announced [4] that m-health has the "potential to transform the face of health service delivery across the globe".

In view of this emphasis on mHealth, many of the current developments in eHealth are actually focused on mHealth. Here are some important issues of mHealth that need innovation and entrepreneurship to make mHealth useful for UHC. These issues were arrived at during 2015 annual meeting of 300 eHealth professionals organised by the Asia eHealth Information Network (www.AeHIN.org), an NGO promoted by the WHO, ADB and health ministries of countries in Asia-Pacific.

A. Sustainability

Recently in Mark Tomlinson and colleagues [3] highlighted the proliferation of m-health pilots in many countries and identified the issue of "pilotitis". Tomlinson and colleagues state that few pilots move forward to scale-up, and there be little evidence to inform whether, when, and how, pilots might expand countrywide. They also raise concerns regarding the increasing interest in m-health from industry, which is likely to have very different motivations than would patients or those responsible for safeguarding public health [1]. It is important to note that all stakeholders have different

Global eHealth, Social Business and Citizen Engagement: A Natural Convergence?

Siaw-Teng Liaw^{a, b, c, d}, Alvin Marcelo^{d, e}, Padmanesan Narasimhan^a,
Md Mahfuz Ashraf^a, Pradeep Ray^{a, d}

^a UNSW Medicine School of Public Health & Community Medicine
(including WHO Collaborating Centre on eHealth & Yunus Social Business Health Hub), Randwick, NSW, Australia

^b Ingham Institute of Applied Medical Research, Liverpool, NSW, Australia

^c SW Sydney Local Health District, Liverpool, NSW, Australia

^d Asia eHealth Information Network

^e University of the Philippines, Manila

Abstract

This paper draws on the vision, mission and experience with the WHO Collaborating Centre on eHealth (WHOCC-eHealth) and Yunus Social Business Health Hub (YSBHH) based at UNSW Australia, and the Asia electronic Health Information Network (AeHIN). Global eHealth aims to provide equitable access to ICT and health care, particularly to the poor, vulnerable and disadvantaged. Social business aims to solve social and economic problem. Its best known product is microcredit financial services for the poor which are small loans that enable them to “produce something, sell something, earn something to develop self-reliance and a life of dignity”. Citizen engagement and community participation is integral to both constructs within the context of global partnerships for Integrated People-Centred Health Services (IPCHS) and Sustainable Development Goals (SDGs). The eHealth dimension is consumer health informatics, social media, mHealth and the Internet of Things. The convergence is multidimensional, mutually beneficial and requires good governance and leadership.

Keywords:

Commerce; Community Participation; Goals

Introduction

The World Health Organization Collaborating Centre (WHOCC) in eHealth was established in The University of New South Wales (UNSW) Medicine in 2013, with its designated activities being evidence-based evaluation, assessment of eHealth and scoping eHealth solutions[1], including the Internet of Things (IoT) [2]. The Asia eHealth Information Network (AeHIN), a group of eHealth advocates in the Asia-Pacific region with an intent on using the peer learning approach to solve their eHealth challenges, is a longstanding collaborator (<http://aehin.org/Home.aspx>). The UNSW Yunus Social Business Health Hub (YSBHH) was established in 2015 to establish, conceive, and promote social business eHealth initiatives.

The scope includes implementation and evaluation of integrated information systems and data, mobile health (mHealth) and working towards an IoT for health. The WHO and the International Telecommunication Union (ITU) sponsored National eHealth Strategy Toolkit is a guiding document that promotes seven strategies for successful implementation of eHealth programs [3]. The vision is global partnerships for Integrated People-Centred Health Services

(IPCHS) [4], United Nations Millennium Development Goals (MDGs) [5, 6], Sustainable Development Goals (SDGs) [7] and health and eHealth workforce [8].

With more than 400 million people globally lacking access to essential health care, the SDGs remain aspirational, like the MDGs. To achieve universal health coverage and equitable access to timely health services, the IPCHS Framework proposes five critical shifts that need to happen (Figure 1): Coordinating services within and across sectors; Re-orienting the model of care; Strengthening governance and accountability; Empowering and engaging people; and Creating an enabling environment.

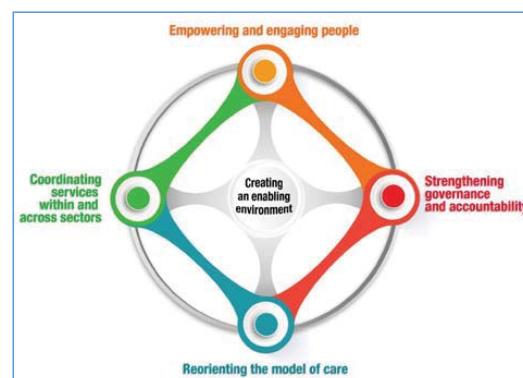


Figure 1 – Five critical shifts required to achieve timely Integrated People Centred Health Services (©WHO 2016)

Developing more integrated people-centred care systems has the potential to generate significant benefits for the health and health care of all people. There is no perfect combination nor a “one size fits all” solution. The right solution will depend on a country’s unique context and needs, as well as local considerations [4].

The MDGs aim to eradicate extreme poverty and hunger, achieve universal primary education, promote gender equality and empower women, reduce child mortality, improve maternal health, combat HIV/AIDS, malaria, and other diseases, ensure environmental sustainability and develop a global partnership for development. The 17 SDGs replaced the MDGs in 2016, with goals relevant to health and well-being:

- SDG#3: Ensure healthy lives and promote well-being for all, at all ages;

Editorial Section > Information Technology (<https://www.asianhbm.com/information-technology>)

Patient-Physician Communication by Using Mobile Technology in Developing Countries

Yasmin Jahan, Graduate school of Biomedical and Health Sciences, Hiroshima University, Japan

Md Moshir Rahman, Institute of Biomedical and Health Sciences, Hiroshima University, Japan

Prof. Pradeep Kumar Ray, Engineering Research Centre on Digital Medicine and Clinical Translation (DMCT), Shanghai Jiao Tong University, China

Michiko Moriyama, Institute of Biomedical and Health Sciences, Hiroshima University, Japan

The positive outcomes of a successful patient-physician communication are widespread considering the health related aspects. The rapid proliferation of mobile technology has facilitated the healthcare system to provide better support and establish sustainable implication of standard procedures in a broader range of healthcare services.

Patient-Physician communication is one of the foremost important part in patient care, given the godlike stature of physicians in many countries. This is critical for every physician to deliver a high-quality healthcare. Patient health outcomes depend on effective communication with the physician. Many physicians encourage open communication and complete information for getting more accurate diagnosis, proper counselling, improving treatment plans and better health outcome.

The Institute of Medicine (IoM), allied with American College of Obstetricians and Gynecologists, has identified the use of information and communication technology (ICT) as one of the perilous forces obligatory for improving the quality of healthcare in the developed countries. Currently, more physicians are becoming handy in using mobile health technology for keeping health records and web messaging to communicate with their patients. The South-East Asia region still has some barriers to implement mobile health technology including policy, technical knowledge and expertise and service costs for implementation of such services. To make mobile healthcare technology more effective and user friendly, our understanding is, that it is essential to improve the way of implementation from top to bottom.

A Successful Joint Venture for International Engineering Education

Dr. Gang Zheng, University of Michigan-Shanghai Jiao Tong University Joint Institute

Dr. Gang Zheng currently is the Associate Dean for Undergraduate Education of the University of Michigan-Shanghai Jiao Tong University Joint Institute. He is also a faculty member of Electrical and Computer Engineering. He has been working with the Joint Institute since 2009, leading advancement in various aspects of the institute. He has led the initial ABET accreditation for both engineering programs of the institute. Previously, Dr. Zheng was an Assistant Professor in the Department of Electrical & Computer Engineering at Gannon University in the US. He received his Ph.D. from the University of Colorado, Colorado Springs in 2005. His research interests include embedded systems, rapid prototyping with FPGA, biometrics, and engineering education.

Dr. Yanchun Yang, University of Michigan-Shanghai Jiao Tong University Joint Institute

Yanchun Yang is the director for Academic Affairs Division of UM-SJTU Joint Institute. His division supports the academic mission of the UM-SJTU Joint Institute, helping students fulfill the requirements of the JI, reach the optimal level in personal and professional development, and achieve their academic and career goals. Yanchun has rich experience in Sino-foreign cooperative education, he joined the JI in 2007, he was the Manager of Student Affairs from 2007 to 2010, and he was the first President of JI Honor Council. Yanchun earned his Ph.D. in Mechanical Manufacturing from Shanghai Jiaotong University, concentrating in computer aided design and Virtual Reality technology (2009). He earned his B.S. in Mechatronics at Shanghai Jiaotong University (2002).



University of Michigan-Shanghai Jiao Tong University Joint Institute
800 Dongchuan Road, Shanghai 200240, China

Tel: +86-21-3420-6045

Fax: +86-21-3420-6525

<http://ji.sjtu.edu.cn/>